

**Investigating The Role Of
Imprinted Genes As Master
Regulators Of Placental
Hormones Using Trophoblast
Stem Cells**

Alice Margaret Chibnall

A thesis submitted for the degree of
Doctor of Philosophy

Cardiff University

April 2025

Summary

The placental programming hypothesis coupled with placental endocrine insufficiency describes the complex mechanisms surrounding placental hormone's role in preparing the pregnant female for motherhood and complications resulting in maternal mental health issues. This thesis focusses on imprinted genes which regulate placental hormones.

In human, *PEG3* and *PHLDA2* have been associated with varying levels of human placental lactogen hormone, whilst not being directly linked. In mouse, *Peg3* and *Phlda2* have previously demonstrated the ability to regulate the mouse placental hormone capacity by acting on the development of the endocrine compartment on the mouse placenta, the junctional zone. This thesis used four genetically modified mouse models to further investigate their regulatory capabilities. These were a loss of imprinting model of *Phlda2*, knockout models of *Peg3* (*Peg3^{KO}*) and *Phlda2* (*Phlda2^{KO}*) and finally a double knockout (DKO) model of both *Peg3* and *Phlda2*. The latter model was to specifically determine the antagonistic behaviour between *Peg3* and *Phlda2*. To establish if the function of these genes is conserved across species, trophoblast stem cell knockout models were generated for both mouse and human and their endocrine capacity was assessed.

Elaborating on previous characterisation of the *Phlda2* loss of imprinting model, this thesis documented a reduction in placenta weight, junctional zone area and hormone production which was more acutely presented in female placentas and not male. In the placenta assessment of *Peg3* and *Phlda2* knockout models, *Peg3^{KO}* placentas demonstrated a male only reduction in junctional zone size and placental hormone production where *Phlda2^{KO}* placentas demonstrated an increase in both metrics for both sexes. The assessment of the double knockout model revealed the correction to a wild type phenotype in the junctional zone but not in the labyrinth. Mouse trophoblast stem cell models revealed that *Peg3* regulates *Phlda2* expression and human trophoblast stem cell assessment discovered long elusive causative evidence that *PHLDA2* directly regulates human placental lactogen, with the *PHLDA2^{KO}* human trophoblast stem cell lines demonstrating an increase in human placental lactogen expression.

In summary, this thesis contributed to the knowledge surrounding imprinted genes regulation of placental hormones and emphasised the sexually dimorphic characteristic of this action.

Table of Contents

SUMMARY	I
TABLE OF CONTENTS	II
LIST OF ABBREVIATIONS	VI
LIST OF FIGURES	XI
LIST OF TABLES	XIV
LIST OF EQUATIONS	XVII
DECLARATION	XVIII
ACKNOWLEDGMENTS OF ASSISTANCE RECEIVED:	XVIII
DATA PRODUCED JOINTLY	XIX
DATA/MATERIALS PROVIDED BY SOMEONE ELSE	XIX
FUNDING	XX
ACKNOWLEDGEMENTS	XXI
CHAPTER 1: INTRODUCTION	1
1.1 IMPRINTED GENES: DISCOVERY, MECHANISM, AND FUNCTION	1
1.2 EVOLUTION OF THE PLACENTA	3
1.3 IMPRINTED GENES: EVOLUTIONARY PERSPECTIVES AND THEORIES OF COADAPTATION AND PARENTAL CONFLICT	5
1.4 PLACENTAL DEVELOPMENT, STRUCTURE AND FUNCTION: HUMAN VERSUS MOUSE	8
1.5 PLACENTAL HORMONES PRIME MATERNAL RESOURCES	18
1.6 THE IMPORTANCE OF STUDYING PLACENTAL LINEAGES: THE PLACENTAL PROGRAMMING HYPOTHESIS AND PLACENTAL ENDOCRINE INSUFFICIENCY	21
1.7 THE REAL-WORLD IMPACT: MATERNAL ANXIETY AND DEPRESSION	25
1.8 IMPRINTED GENES REGULATION OF THE PLACENTA	28
1.8.1 <i>IC1/IC2 Domain and KvDMR1: Imprinting control regions</i>	28
1.8.2 <i>Pleckstrin homology like domain family A member 2 (Phlda2)</i>	30
1.8.3 <i>Paternally expressed gene 3 (Peg3)</i>	36
1.9 ANTAGONISTIC FUNCTION: PEG3 VERSUS PHLDA2	41
1.10 TROPHOBLAST STEM CELLS	45
1.11 SEXUAL DIMORPHISM	48
1.12 SUMMARY	49
1.12.1 <i>Aims and objectives</i>	50
CHAPTER 2: METHODS	52
2.1 MOUSE MODEL AND HUSBANDRY	52
2.1.1 <i>Phlda2^{+/+BACx1(BL6)}: A Phlda2 loss of imprinting mouse model</i>	52
2.1.2 <i>Phlda2^{KO} mouse model</i>	53
2.1.3 <i>Peg3^{KO} mouse model</i>	54
2.1.4 <i>Animal husbandry</i>	55
2.1.5 <i>Breeding schemes and generation of experimental tissues</i>	55
2.1.6 <i>Dissection</i>	57
2.2 GENOTYPING	58
2.2.1 <i>DNA extraction</i>	58
2.2.2 <i>Polymerase chain reaction (PCR)</i>	58
2.2.3 <i>Gel electrophoresis</i>	62
2.2.4 <i>Weight data</i>	62
2.3 RNASCOPE	62

2.3.1	<i>Tissue generation for sections</i>	62
2.3.2	<i>Tissue mounting and sectioning (E7.5, E9.5, E14.5 and E16.5)</i>	63
2.3.3	<i>RNAscope staining protocol</i>	63
2.4	SLIDE SCANNER AND CONFOCAL IMAGING	65
2.4.1	<i>Program details</i>	65
2.5	E9.5 PARIETAL TROPHOBLAST GIANT CELL COUNTING	67
2.6	CELL COUNTING WITH ZEN PROGRAM.....	67
2.6.1	<i>Image processing</i>	68
2.6.2	<i>Cell Counting</i>	69
2.6.3	<i>Data processing</i>	72
2.6.4	<i>Parietal trophoblast giant cell identification and quantification</i>	73
2.6.5	<i>Decidua area measurement</i>	73
2.7	GENERAL TISSUE CULTURE METHODS	73
2.7.1	<i>Mycoplasma testing</i>	73
2.7.2	<i>Foetal bovine serum inactivation</i>	75
2.7.3	<i>Mouse embryonic feeders (MEF)</i>	75
2.7.4	<i>Conditioned media</i>	76
2.8	MOUSE TROPHOBLAST STEM (MTS) CELLS	77
2.8.1	<i>Generation of mTS cells</i>	77
2.8.2	<i>mTS cell genotyping</i>	80
2.8.3	<i>mTS Cell differentiation assay</i>	80
2.8.4	<i>TS cell counting proliferation analysis</i>	80
2.9	HUMAN TROPHOBLAST STEM CELLS	81
2.9.1	<i>Training in Japan and acquiring human trophoblast stem cells</i>	81
2.9.2	<i>Maintenance of human trophoblast stem cells</i>	81
2.9.3	<i>Passaging of hTS cells</i>	82
2.9.4	<i>Freezing human trophoblast stem cells</i>	82
2.9.5	<i>Preparing human trophoblast stem cell KO lines</i>	83
2.9.6	<i>Single cell cloning</i>	85
2.9.7	<i>Differentiation assay</i>	86
2.10	QUANTITATIVE REVERSE TRANSCRIPTION POLYMERASE CHAIN REACTION (qRT-PCR)	87
2.10.1	<i>RNA extraction</i>	87
2.10.2	<i>DNase treatment</i>	88
2.10.3	<i>cDNA synthesis and sample validation</i>	89
2.10.4	<i>qRT-PCR</i>	90
2.10.5	<i>Primer design</i>	90
2.10.6	<i>Plate preparation</i>	90
2.11	PROTEIN ANALYSIS.....	95
2.12	ENZYME-LINKED IMMUNOSORBENT ASSAY	95
2.13	WESTERN BLOTTING.....	95
2.14	STATISTICAL ANALYSIS.....	97
2.15	FIGURES.....	98

CHAPTER 3: CHARACTERISING THE SEXUALLY DIMORPHIC EFFECT OF TWO-FOLD *PHLDA2* MODELLING LOSS OF IMPRINTING ON THE DEVELOPING MOUSE PLACENTA 99

3.1	OVERVIEW	99
3.2	AIMS.....	100
3.3	RESULTS	101
3.3.1	<i>Placental weight reduced in $Phlda2^{+/-BACx1(BL6)}$</i>	101
3.3.2	<i>$Phlda2^{+/-BACx1(BL6)}$ impacts female placentas more significantly than males</i>	103
3.3.3	<i>Pooled sex qRT-PCR analysis masks impact on female placentas placental hormone and lineage marker RNA expression</i>	114
3.4	DISCUSSION.....	119

3.4.1	<i>Analysis of foetal and placental weights demonstrate sexual dimorphism in Phlda2^{+/+}BACx1(BL6) placenta</i>	119
3.4.2	<i>Automated RNAscope program demonstrates reductions in functional endocrine output of Phlda2^{+/+}BACx1(BL6) placentas</i>	120
3.4.3	<i>Sexually dimorphic gene expression alterations reflect impacts on junctional zone and labyrinth structures of Phlda2^{+/+}BACx1(BL6) placenta</i>	124
3.5	LIMITATIONS	126
3.6	SUMMARY	127
CHAPTER 4: CHARACTERISATION OF PEG3 AND PHLDA2 ANTAGONISM IN THE DEVELOPING MOUSE PLACENTA130		
4.1	OVERVIEW	130
4.2	AIMS	131
4.3	RESULTS	131
4.3.1	<i>Confirming co-expression: RNAscope multiplexing at E7.5 and E9.5 for Peg3, Phlda2 and key lineage markers</i>	131
4.3.2	<i>RNAscope on E9.5 samples of each genotype do demonstrate expression of knockout targets</i>	144
4.3.3	<i>P-TG cell counting of E9.5 samples to assess phenotype establishment timeline</i>	147
4.3.4	<i>E16.5 Placental and foetal impacts from KO models</i>	148
4.3.5	<i>RNAscope automated counting program demonstrates more significant impact on male KO placentas</i>	149
4.4	DISCUSSION	162
4.4.1	<i>Peg3 and Phlda2 co-expression with key endocrine regulators in placental lineage progenitors</i>	162
4.4.2	<i>Evaluation of the effectiveness of Peg3 and Phlda2 knockouts on E9.5 placentas: Insights from RNAscope multiplexing</i>	165
4.4.3	<i>Assessing early phenotype development: P-TG cell variations in Peg3^{KO}, Phlda2^{KO} and DKO placentas</i>	167
4.4.4	<i>Sexual dimorphism in foetal and placental weights of E16.5 KO placentas</i>	167
4.4.5	<i>E16.5 placental region and cell type alterations: Genotypic and sexually dimorphic effects on junctional zone and labyrinth structures</i>	169
4.5	LIMITATIONS	174
4.6	SUMMARY	175
CHAPTER 5: PEG3 AND PHLDA2 KNOCKOUT IN HUMAN AND MOUSE TROPHOBLAST STEM CELLS 179		
5.1	OVERVIEW	179
5.2	AIMS	180
5.3	RESULTS	180
5.3.1	<i>Mouse trophoblast stem cells</i>	180
5.3.2	<i>Human trophoblast stem cells</i>	187
5.4	DISCUSSION	196
5.4.1	<i>Mouse TS cells</i>	196
5.4.2	<i>Human TS cells</i>	203
5.5	LIMITATIONS	205
5.6	SUMMARY	206
CHAPTER 6: GENERAL DISCUSSION 208		
6.1	OVERVIEW	208
6.1.1	<i>Main findings</i>	208
6.1.2	<i>Sex specific sensitivities in imprinting: Exploring offspring sensitivities to imprinted genes from parent of the same sex</i>	211
6.1.3	<i>Differential roles of Peg3 and Phlda2: Antagonistic interactions in the junctional zone versus unbalances roles in the labyrinth</i>	212

6.2	LIMITATIONS AND FUTURE DIRECTIONS OF RESEARCH	214
6.3	CONCLUDING REMARKS	216
REFERENCES.....		218
APPENDIX:		259

List of Abbreviations

Abbreviation	Definition
129	129S2/SvHsD mouse strain
A	Adenine
ADHD	Attention deficit/ hyperactivity disorder
AKT	Protein kinase B
AR	Arginine
<i>Ascl2</i>	Achaete-scute complex homolog 2
B	Restriction enzyme site Bgl II
<i>B</i> -ME	<i>B</i> -mercaptoethanol
BH	Restriction enzyme site BamHI
bHLH	Basic helix–loop–helix
BLAST(P)	Basic local alignment search tool (protein)
BMP	Bone Morphogenetic Protein
C-TG (Cell)	Canal trophoblast giant cell
CBWC	Custom birth weight centiles
<i>Cdkn1c</i>	Cyclin-dependent kinase inhibitor 1C
Ch-TG (Cell)	Channel trophoblast giant cell
CI-MPR	Cation-independent mannose 6-phosphate receptor
CP	Crossover point
CT	Cytotrophoblast
DEPC	Diethylpyrocarbonate
dH ₂ O	Distilled water
DKO	Double knockout (<i>Phlda2</i> ^(+/-) ; <i>Peg3</i> ^(-/+))
DS	Downstream probe
DSM	The Diagnostic and Statistical Manual of Mental Disorders
E	Embryonic day
EDTA	Ethylenediaminetetraacetic acid
EGF	Epidermal growth factor
EGFR	Epidermal growth factor receptor

ELISA	Enzyme-linked immunosorbent assay
Epc	Ectoplacental cone
EPDS	Edinburgh postnatal depression scale
<i>ERBB2</i>	Erythroblastosis oncogene B
ES Cells	Embryonic stem cells
EST	Expressed sequences tag
EVT	Extravillous cytotrophoblast
ExE	Extraembryonic ectoderm
F	Forward
F1	Filial (F)1
FBS	Foetal bovine serum
FGF4	Fibroblast growth factor-4
FISH	Fluorescent in situ hybridization
<i>Flk1/Kdr</i>	Kinase insert domain protein receptor
<i>Flt1</i>	FMS-like tyrosine kinase 1
G	Guanine
G0/G1 phase	Gap (0/1) phase
<i>Gbe1</i>	1,4- α -glucan branching enzyme
<i>Gcm1</i>	Glial cell missing 1
GDM	Gestational diabetes mellitus
GH	placental growth hormone
DMRs	Differentially methylated regions
<i>Gjb3</i>	Gap junction protein beta 3
GlyT	Glycogen
Gyg	Glycogenin
H	Histidine
H & E	Haematoxylin and eosin
H ₂ O ₂	Hydrogen peroxide
<i>Hand1</i>	Heart and neural crest derivatives expressed transcript 1
hCG	Human chorionic gonadotropin
HDAC	Histone deacetylase

HIII	Restriction enzyme site Hind III
<i>hPL</i>	Human Placental Lactogen
hTS	Human trophoblast stem (cells)
ICs	Imprinting centre
ICM	Inner cell mass
<i>IGF1</i>	Insulin-like growth factor 1
<i>Igf2</i>	Insulin-like growth factor 2
<i>Igf2r</i>	Insulin-like growth factor 2 receptor
IPD	Ischemic placental disease
<i>IPL</i>	Imprinted in placenta and liver
ITS-X	Insulin-Transferrin-Selenium-Ethanolamine
IUGR	Intrauterine growth restriction
K	Carrying capacity
KI	Restriction enzyme site <i>kpnI</i>
KO	Knockout
KvDMR1	KCNQ1OT1 transcript Voluntary differentially methylated region 1
LGA	Large for gestational age
LoxP	Restriction enzyme site <i>LoxP</i>
Ltd	Limited
Lz:Jz	Labyrinth to junctional zone area ratio
MCS	Multiple cloning site
MEF	Mouse embryonic fibroblasts
MetOH	Methanol
MMC	Mitomycin C
mTS	Mouse trophoblast stem cells
NaCl	Sodium chloride
Neo	(P _{gk})-Neomycin (Neo)
OD	Optical density
P-TG (Cell)	Parietal trophoblast giant cell
PAM	Protospacer adjacent motifs
PBS	Phosphate-buffered saline

PBS (-)	PBS Without Calcium and Magnesium
PCR	Polymerase chain reaction
<i>Peg3</i>	Paternally expressed gene 3
<i>Peg3</i> ^{KO}	<i>Peg3</i> ^(-/+) ; <i>Phlda2</i> ^(+/+)
PFA	Paraformaldehyde
<i>Phlda2</i>	Pleckstrin homology like domain family A member 2
<i>Phlda2</i> ^{KO}	<i>Phlda2</i> ^(+/-) ; <i>Peg3</i> ^(+/+)
PI3K	Phosphatidylinositol 3-kinase
Pod	Placenta and embryo are contained with the decidua
<i>PRL</i>	Prolactin
<i>Prl3b1</i>	Placental lactogen II
<i>Prl3d</i>	Placental lactogen I
<i>Prl8a8</i>	Prolactin family 8 subfamily A member 8
PVDF	Polyvinylidene fluoride
qRT-PCR	Quantitative reverse transcription polymerase chain reaction
R	Reverse
RFLP	Restriction fragment length polymorphism
RFM	Reduced foetal movement
RNP	Ribonucleoprotein
ROCK	Rho-associated protein kinase
RPKM	Reads per kilobase per million reads placed
RT	Room temperature (20-25 °C)
RT-	Reverse transcriptase negative
RT+	Reverse transcriptase positive
S phase	Synthesis phase
S-TG (Cell)	Sinusoidal trophoblast giant cell
SCC	Saline sodium citrate
SDS	Sodium dodecyl sulfate
SpA-TG (Cell)	Spiral artery trophoblast giant cell
SpT/GlyT	Spongiotrophoblast cell to glycogen cell ratio
STAI	State-trait anxiety inventory

STB	Syncytiotrophoblast
<i>Syna</i>	Syncytin-A
<i>Synb</i>	Syncytin-B
SynT-I	Syncytiotrophoblast layer 1
SynT-II	Syncytiotrophoblast layer 2
TAE	Tris-acetate-EDTA
TB1x	Transfer buffer
Tg	<i>Phlda2</i> ^{+/+BACx1(BL6)}
TGC	Trophoblast giant cell
TGF- β	Transforming growth factor β 1
<i>Tpbpa</i>	Trophoblast specific protein alpha
TS	Trophoblast stem (cell)
TSSC3	Tumour suppressor STF cDNA3
UK	United Kingdom
US	Upstream probe
VCT	Villous cytotrophoblast
VPA	Valproic Acid
Wnt	Wingless/integrated (Wnt) signalling pathway
WT	Wild type
Xb	Restriction enzyme site Xba I
Xh	Restriction enzyme site Xho

List of Figures

Figure 1: Mechanisms and function of genomic imprinting.	3
Figure 2: The evolution of the placenta and genomic imprinting, and the relationship between parental investment.....	6
Figure 3: Mouse placental structures.....	15
Figure 4: Placental lineages.	17
Figure 5: Placental programming hypothesis and placental endocrine insufficiency.....	24
Figure 6: Schematic of KvDMR1 imprinting control region.....	29
Figure 7: PHLDA2 protein structure.....	31
Figure 8: PEG3 protein structure.	38
Figure 9: Genomic imprinting adjusts maternalisation or paternalisation	42
Figure 10: Imprinted genes regulation of placental endocrine lineages. .	43
Figure 11: Functional roles of <i>Peg3</i> and <i>Phlda2</i> in the placental programming hypothesis.	44
Figure 12: Location and isolation of trophoblast stem cells.....	46
Figure 13: Genomic map of the IC2 region distal mouse chromosome 7.	52
Figure 14: Schematic of <i>Phlda2</i> ^{KO} generation.	53
Figure 15: Schematic of <i>Peg3</i> ^{KO} generation.....	54
Figure 16: Breeding scheme to generate experimental materials for <i>Phlda2</i> ^(+/+) WT and <i>Phlda2</i> ^{+/+BACx1(BL6)} transgenic (Tg) tissues.	56
Figure 17: Breeding scheme to generate experimental materials for WT, <i>Peg3</i> ^{KO} , <i>Phlda2</i> ^{KO} and DKO tissues.	57
Figure 18: E9.5 pod with P-TG cells counted.	67
Figure 19: Diagram of photon release and detection. Fluorophore (F). ..	69
Figure 20: Defined region for counting with area value presented.....	70
Figure 21: Zen program using counting program showing signal deemed to be nuclei in purple.	71
Figure 22: Image showing Cy5 signal in the perimeter of a cell in yellow within the junctional zone.....	71
Figure 23: Image showing Cy5 signal in the perimeter of a cell in yellow within the labyrinth.....	72
Figure 24: Phases of mouse trophoblast stem cell derivation.....	79
Figure 25: Haemocytometer used for counting cells.	81
Figure 26: qRT-PCR temperature amplification program.	94
Figure 27: Foetal and placental weight data for WT and Tg.	101
Figure 28: Foetal and placental weight data for WT and Tg.	102
Figure 29: Area of placental subsections for WT and Tg.....	103
Figure 30: Area of placental sub-sections split by sex for WT and Tg...	105
Figure 31: Cell counts for WT and Tg junctional zone.	107
Figure 32: Cell counts for sex split WT and Tg junctional zone.....	108
Figure 33: Labyrinth zone cell counts for WT and Tg placenta.	109

Figure 34: Labyrinth cell counts for sex split WT and Tg placenta.	110
Figure 35: Total placental cell counts for WT and Tg placenta.....	111
Figure 36: Total cell counts for sex split WT and Tg placenta.....	112
Figure 37: Representative RNAscope images of WT and Tg.	113
Figure 38: qRT-PCR analysis of Prl family members for WT and Tg.	114
Figure 39: qRT-PCR analysis of Prl family members for WT and Tg split by sex.	116
Figure 40: qRT-PCR analysis of labyrinth related genes WT and Tg.	117
Figure 41: qRT-PCR analysis of labyrinth related genes for WT and Tg split by sex.....	118
Figure 42: Duo-plex detection identifies co-localisation of <i>Peg3</i> and <i>Phlda2</i> expression.....	132
Figure 43: Multi-plex detection identifies co-localisation of <i>Peg3</i> , <i>Phlda2</i> and <i>Prl3b1</i> expression.....	134
Figure 44: Multi-plex detection identifies co-localisation of <i>Peg3</i> , <i>Tpbpa</i> and <i>Pcdh12</i> expression.....	136
Figure 45: Multi-plex detection identifies co-localisation of <i>Pcdh12</i> , <i>Phlda2</i> and <i>Tpbpa</i> expression.	138
Figure 46: Multi-plex detection identifies co-localisation of <i>Ascl2</i> , <i>Phlda2</i> and <i>Cdkn1c</i> expression.	140
Figure 47: Multi-plex detection identifies co-localisation of <i>Pcdh12</i> , <i>Ascl2</i> , and <i>Tpbpa</i> expression.	142
Figure 48: Multi-plex detection identifies co-localisation of <i>Tpbpa</i> , <i>Cdkn1c</i> and <i>Pcdh12</i> expression.....	143
Figure 49: Representative images of multi-plex detection identifying co-localisation of RNA expression of <i>Peg3</i> , <i>Phlda2</i> and <i>Tpbpa</i>	146
Figure 50: E9.5 P-TG cell counts for <i>WT</i> , <i>Peg3^{KO}</i> , <i>Phlda2^{KO}</i> and <i>DKO</i> . ..	147
Figure 51: Foetal and placental weight data for <i>WT</i> , <i>Peg3^{KO}</i> , <i>Phlda2^{KO}</i> and <i>DKO</i> at E16.5.....	148
Figure 52: Area of placental subsections for <i>WT</i> , <i>Peg3^{KO}</i> , <i>Phlda2^{KO}</i> and <i>DKO</i>	151
Figure 53: Region ratios for <i>WT</i> , <i>Peg3^{KO}</i> , <i>Phlda2^{KO}</i> and <i>DKO</i> placentas.	152
Figure 54: Junctional zone cell counting parameters for <i>WT</i> , <i>Peg3^{KO}</i> , <i>Phlda2^{KO}</i> and <i>DKO</i>	154
Figure 55: Cell counts within E16.5 labyrinth region for <i>WT</i> , <i>Peg3^{KO}</i> , <i>Phlda2^{KO}</i> and <i>DKO</i>	157
Figure 56: Total cell counts of E16.5 placenta for <i>WT</i> , <i>Peg3^{KO}</i> , <i>Phlda2^{KO}</i> and <i>DKO</i>	159
Figure 57: Representative images of E16.5 placenta for male and female, <i>WT</i> , <i>Peg3^{KO}</i> , <i>Phlda2^{KO}</i> and <i>DKO</i> placentas.	161
Figure 58: Example of validation techniques for mouse trophoblast stem cells.....	181
Figure 59: ELISA for Prl3d1 and Prl3b1 on 10-day differentiated mTS cells compared to E9.5 and E14.5 mouse placenta.	182

Figure 60: Representative images of differentiation trial for WT, <i>Peg3</i> ^{KO} , <i>Phlda2</i> ^{KO} and DKO mouse trophoblast stem cells.	183
Figure 61: Proliferation assay of WT, <i>Peg3</i> ^{KO} , <i>Phlda2</i> ^{KO} and DKO mouse trophoblast stem cells.	184
Figure 62: Knockout targets <i>Peg3</i> and <i>Phlda2</i> RNA expression in WT, <i>Peg3</i> ^{KO} , <i>Phlda2</i> ^{KO} and DKO in 10-day differentiated mTS cells.....	185
Figure 63: qRT-PCR of 10-day differentiated WT, <i>Peg3</i> ^{KO} , <i>Phlda2</i> ^{KO} and DKO mouse trophoblast stem cells.....	186
Figure 64: <i>PHLDA2</i> CRISPR design and trophoblast stem cell line knockouts.....	188
Figure 65: <i>PEG3</i> CRISPR design.	189
Figure 66: Gel confirmation of <i>PHLDA2</i> ^{KO} results for four combinations of gRNAs.....	190
Figure 67: Genotype results of single cell colonies after <i>PHLDA2</i> ^{KO} sgRNA combination 1-1.	191
Figure 68: Representative images of differentiation trial of WT and <i>PHLDA2</i> ^{KO} hTS cells.....	193
Figure 69: Western blot analysis of differentiated WT and <i>PHLDA2</i> ^{KO} hTS cells.....	194
Figure 70: qRT-PCR of five day differentiated WT and <i>PHLDA2</i> ^{KO} and hTS cells.....	195
Figure 71: Updated figure of placental programming hypothesis.....	210
Figure 72: Hypothetical gendered offspring sensitivity to imprinted gene dosage.	212

List of Tables

Table 1: Scale of extra embryonic investment and genomic imprinting. “?” indicates the predicted status of X chromosomes in monotremes. Based on table from Reik and Lewis (2005).....	6
Table 2: Table of cell type makers and cellular process markers	14
Table 3: Relationships between <i>Phlda2</i> expression levels, placenta structure, hormone concentrations, foetal weight, and maternal behaviour for both human and mouse models.....	35
Table 4: Relationships between <i>Peg3</i> expression levels,	41
Table 5: Reaction mix for PCR.....	59
Table 6: Reaction mix for PCR with betain.	59
Table 7: Primer details. Forward primer (F), Reverse primer (R).....	60
Table 8: Standard PCR program.	61
Table 9: <i>Peg3</i> 64 PCR program.....	61
Table 10: DTAQ PCR program.	61
Table 11: TAE buffer mix.	62
Table 12: Details of probes used for RNAscope.....	65
Table 13: Light intensity parameters.....	66
Table 14: Light intensity and exposure times.	66
Table 15: Mycoplasma testing primer set sequences, GC percentages and melting temperatures.....	74
Table 16: Mycoplasma PCR program.	74
Table 17: Cell densities for producing conditioned media.	77
Table 18: Inactive MEFs co-culture plating densities.	77
Table 19: TS media additives and concentrations.	78
Table 20: TS+1.5X F4H media recipe.	78
Table 21: hTS basal media recipe.	81
Table 22: hTS media recipe.	82
Table 23: Freezing media for hTS cells.	83
Table 24: CRISPR sequences.	83
Table 25: RNP complex recipe.....	84
Table 26: Nucleofection solution recipe.	84
Table 27: Primer sequences for hTS knockout confirmation.....	85
Table 28: Differentiation media recipe.....	87
Table 29: DNase treatment reagent recipe.....	89
Table 30: cDNA mastermix.	89
Table 31: Primer working mix.	90
Table 32: List of qRT-PCR primers.	93
Table 33: Master-mix for qRT-PCR plates.	94
Table 34: Recipe for western blotting gel.	96
Table 35: Primary and secondary information for westerns.	97
Table 36: Comparison between manual and automatic counting	106

Table 37: Key findings of Chapter 3.	128
Table 38: Key sexually dimorphic impacts of <i>Phlda2</i> ^{+/+BACx1(BL6)}	128
Table 39: Summary of key findings for Chapter 4.	176
Table 40: Sexually dimorphic findings from Chapter 4.	177
Table 41: Summary of mouse trophoblast stem cell derivations.	180
Table 42: Summary of the number of successfully banked cell lines of each genotype.	180
Table 43: Key findings from Chapter 5.	206
Table 44: Summary of key findings.	209
Table 45: Group sizes for weight data analysis.	259
Table 46: Group sizes for <i>Prl3b1</i> stained cell counted placenta.	260
Table 47: Sample numbers used for qRT-PCR.	260
Table 48: Weight data for WT and Tg comparison results	261
Table 49: Sex split weight data for WT and Tg comparison results	262
Table 50: Placental area measurements for WT and Tg comparison	263
Table 51: Placental area measurements for WT and Tg split by sex.	264
Table 52: Cell counts of the junctional zone for WT and Tg comparison	265
Table 53: Cell counts of the junctional zone for sex split WT and Tg.	267
Table 54: Cell counts of the labyrinth for WT and Tg comparison	267
Table 55: Cell counts of labyrinth for sex split WT and Tg comparison .	268
Table 56: Cell counts of whole placenta for WT and Tg comparison	269
Table 57: Cell counts of whole placenta for sex split WT and Tg	269
Table 58: <i>Prl</i> family qRT-PCR values for WT and Tg.	270
Table 59: <i>Prl</i> family qRT-PCR values for sex split WT and Tg (\pm SEM). .	271
Table 60: <i>Prl</i> family comparison <i>P</i> values for qRT-PCR.	271
Table 61: Labyrinth related qRT-PCR values for WT and Tg (\pm SEM) with <i>P</i> values for ANCOVA analysis. Significant <i>P</i> values in bold.	272
Table 62: Labyrinth related qRT-PCR values for sex split WT and Tg ...	272
Table 63: Labyrinth related qRT-PCR comparison <i>P</i> values for qRT-PCR.	273
Table 64: Group sizes for morphological analyses.	273
Table 65: Group sizes for <i>Prl3b1</i> counted placenta.	274
Table 66: Group averages and SEMs for placental and foetal weight. ..	276
Table 67: Genotype <i>P</i> values for placental and foetal weight.	276
Table 68: Sex <i>P</i> values for placental and foetal weight data.	276
Table 69: Group averages and SEMs for placental region area measurements (μm^2).	278
Table 70: Genotype comparison <i>P</i> values for placental region area measurements. Significant <i>P</i> values in bold.	278
Table 71: Sex comparison <i>P</i> values for placental region area measurements. Significant <i>P</i> values in bold.	278
Table 72: Group averages and SEMs for placental region area measurements (μm^2).	279

Table 73: Genotype comparison <i>P</i> values for placental region area measurements.	279
Table 74: Sex comparison <i>P</i> values for placental region area measurements.	280
Table 75: Group averages and SEMs for junctional zone cell counts. ...	281
Table 76: Genotype <i>P</i> values for junctional zone cell counts.	281
Table 77: Sex comparison <i>P</i> values for junctional zone cell counts.	282
Table 78: Group averages and SEMs for labyrinth cell counts.	283
Table 79: Genotype comparison <i>P</i> values for labyrinth cell counts.	283
Table 80: Sex comparison <i>P</i> values for labyrinth cell counts.	283
Table 81: Group averages and SEMs for total cell counts.	285
Table 82: Genotype comparison <i>P</i> values for total cell counts.	285
Table 83: Sex comparison <i>P</i> values for total cell counts.	286
Table 84: Group averages and SEMs for ELISA results.	288
Table 85: Sample type comparison <i>P</i> values for ELISA results.	288
Table 86: Genotype averages and SEMs for proliferation assay.	289
Table 87: Genotype comparison <i>P</i> values for proliferation assay.	289
Table 88: Group averages and SEMs qRT-PCR results of 10-day differentiation mTS cells.	290
Table 89: Genotype comparison <i>P</i> values for RNA expression in 10-day differentiated mouse trophoblast stem cells.	290
Table 90: Group averages and SEMs qRT-PCR results of 10-day differentiation mouse trophoblast stem cells.	291
Table 91: Genotype comparison <i>P</i> values for RNA expression in 10-day differentiated mouse trophoblast stem cells.	291
Table 92: Group averages and SEMs for expression in five day differentiated hTS stem cells.	292
Table 93: Genotype comparison <i>P</i> values for expression in five day differentiated hTS cells.	292
Table 94: qRT-PCR primer blast results and off target details.	301

List of Equations

Equation 1: Excel formula to consolidate parent of origin cell number. ..	72
Equation 2: Excel formula to identify Cy5 signal within each cell.....	73
Equation 3: Cell number calculation.	80
Equation 4: Effect size calculation (Cohens d).	97

Declaration

Acknowledgments of assistance received:

Professor Rosalind John: Training for mouse trophoblast stem cell work and maintenance support, mouse husbandry, dissections, superovulation injections, along with project design and guidance, statistical analysis guidance, and general advice.

Professor Nicholas Allen: Guidance for CRISPR targeting of *PEG3* and guidance around human trophoblast stem cell maintenance.

Dr David Harrison: Mouse husbandry, dissections, general guidance, and mentoring.

Susan Hunter: Mouse husbandry, dissections, and genotyping.

Dr Mathew Higgs: Automatic counting program design and recommendations to apply automatic counting to placenta analysis. Automatic counting troubleshooting. Automatic counting data generation advice and statistical advice.

Dr Ekaterina Lysikova: Protein extraction from mouse trophoblast stem cell samples. Training, guidance and troubleshooting for western blotting analysis of both mouse and human trophoblast stem cell samples. Help with cell maintenance.

Dr Ryan Sixtus: Animal husbandry dissections and superovulation injections. General guidance and advice. Statistical analysis guidance and advice.

Mrs Bridget Allen: Advice and guidance around work with stem cells and using CRISPR. Training and help with CRISPR targeting in human trophoblast stem cells. FACS and picking of human trophoblast stem cells.

Miss Mariia Melinoshevska: Trophoblast stem cell maintenance and help with differentiation assay for mice. Attempts at targeting *PEG3* in human trophoblast stem cells in female and male cells, including colony picking and maintenance. Animal husbandry and genotyping.

Professor Hiroaki Okae: Guidance and advice around *PHLDA2* and *PEG3* targeting using CRISPR in human trophoblast stem cells. Oversaw laboratory project which derived *PHLDA2^{KO}* human trophoblast stem cells.

Dr Asato Sekiya: CRISPR design and targeting of *PHLDA2* in human trophoblast stem cells. Training for general cell maintenance, knockout

derivation, and single cell colony generation of *PHLDA2^{KO}* line in human trophoblast stem cells. Postage of human trophoblast stem cell lines from Kumamoto Japan to Cardiff University and sharing of general maintenance protocols.

Dr Raquel Boque Sastre: RNAscope training and slide scanner training.

Dr Anthony Hayes: Training and technical assistance with confocal imaging of E7.5 and E9.5 multiplexing images.

Cardiff University Bioimaging Hub Core Facility,

RRID:SCR_022556: Sectioning and H & E staining of E7.5, E9.5, E14.5 and E16.5 placental samples.

Data produced jointly

With thanks to:

Dr Anthony Hayes: Some confocal imaging for multiplexing of E7.5 and E9.5 in Chapter 4, specifically the E9.5 63X magnification image (J) used in Figure 45: Multi-plex detection identifies co-localisation of *Pcdh12*, *Phlda2* and *Tpbpa* expression. Also, all E9.5 images of ectoplacental cones for WT, *Peg3^{KO}*, *Phlda2^{KO}* and DKOs in Figure 49: Representative images of multi-plex detection identifying co-localisation of RNA expression of *Peg3*, *Phlda2* and *Tpbpa*.

Dr Ryan Sixtus: Generation of E9.5 foetal-placental pods for trophoblast giant cell counting (Chapter 4).

Data/materials provided by someone else

With thanks to:

Professor Hiroaki Okae: Providing human trophoblast stem cells.

Dr Asato Sekiya: Providing *PHLDA2* CRISPR guide RNAs, *PHLDA2^{KO}* confirmation primers and *PHLDA2^{KO}* human trophoblast stem cells.

Miss Amelia Stoddart: Blind manual counting of wild type and *Phlda2^{+/+BACx1(BL6)}* mouse placenta during the development of the automatic counting program.

Dr Ekaterina Lysikova: Performing and analysing ELISA on mouse trophoblast stem cell proteins.

Mr Mark Bishop: FACS of human trophoblast stem cells.

Funding

This research was funded BBSRC grants BB/P008623/1 "Exposing the link between placental endocrine dysfunction and offspring behavioural outcomes" and BB/V014765/1 "Imprinted genes as master regulators of placental hormones".

Acknowledgements

Firstly, I would like to thank my supervisors Professor Rosalind John and Professor Nicholas Allen. Ros, thank you for having me as a part of your team for the last five years and for the opportunity to progress my career with this PhD. Nick, thank you for your support surrounding all things cell work and CRISPR. I would also like to thank my second supervisor Claire Hughes for her helpful pep talks.

I could not have completed this project without the incredible support of the wider Pregnancy Epigenetics team. To Hannah, Sam and Raquel, thank you for support during my early time in the team and for the encouragement to do a PhD. To Harri, thank you for endless project and emotional support and much needed reassurance. Thank you to Matt and Anna, for our reciprocal RNAscope relationship, particularly to Matt for the therapy sessions.

Additionally, I would like to acknowledge the support and efforts of the newer Pregnancy Epigenetics team members, Ryan, Mariia and Kate. Thank you to Ryan, for tackling the grant project with me and for the encouragement to see the PhD over the finish line. To Mariia, my fellow laboratory technician, for the enthusiasm and support around the cell work and general laboratory maintenance. To Kate, for the support around general laboratory functioning, troubleshooting experimental issues and all the time spent training and helping me with protein work, but mainly for the optimism and positivity.

To the people that supported my internship in Japan, this project would not have been achievable without, Professor Hiroaki Okae who accepted me into the program and supported my work. Dr Asato Sekiya who trained me and guided me, along with welcoming me into Japanese culture. Koga Aiko who made sure everything was going smoothly throughout my internship and Lusu Mwahlilino for taking me out and showing me around Kumamoto.

To my personal supporters, I have been incredibly fortunate to have many women in my life who encourage me and inspire me to work harder for the greater female cause, Lauren, Stef, Amy, Amanda, Sophie, Taylor, my sister Grace and my Mum Rachel, thank you for the drive to push forward. I am thankful to my dad for starting my obsession with science and for believing in me that I could go this far. I would like to thank my Scottish family, the Cranston's, for their continued support throughout the many ups and downs of this process. I would also like to thank my Grandad, who, although quite morbid, conveniently timed his death to

coincide with the International Federation of Placenta Associations conference in New Zealand in 2023.

Finally, I would like to acknowledge the unwavering encouragement of my husband Jonny. Thank you for supporting me in my return to being a student and for the staunch belief that I could do this.

Chapter 1: Introduction

1.1 Imprinted genes: Discovery, mechanism, and function

Mendelian inheritance is the established framework in which genetic inheritance is understood. Until the late twentieth century this mechanism was thought to follow a relatively predictable model. However, it has recently been discovered that some mammalian genes have a more complex pattern of expression than previously understood (Ferguson-Smith & Surani, 2001; Reik & Walter, 2001; Surani, 1998). Mono-parental embryo studies identified that although each parent contributes half of the alleles to the offspring, those halves are not equal. Maternally derived mono-parental embryos are fatal at embryonic day (E)10 after progressively worsening growth restriction. Paternally derived genomes are fatal at E8.5 after growth restriction, developmental delays, and surplus extraembryonic tissues (McGrath & Solter, 1984; Surani & Barton, 1983; Surani et al., 1987). Further studies into maternal and paternal disomy revealed specific chromosomes to be lethal when both are from the same parent, suggesting that these chromosomes house locus of parent of origin functionality (Cattanach & Kirk, 1985). These are clusters of differentially methylated regions (DMRs) known as imprinting centres (ICs). These are grouped by maternal or paternal expression (Barlow & Bartolomei, 2014; Ferguson-Smith, 2011; Ferguson-Smith & Bourc'his, 2018).

This mode of expression was termed 'genomic imprinting' (McGrath & Solter, 1984; Surani et al., 1984). Genomically imprinted genes are those that are expressed based on the parent of origin. During either oogenesis or spermatogenesis these ICs are methylated or not depending on which parent is deriving them (Surani, 1998)(Figure 1). When the gametes are combined, the diploid zygote contains two alleles, one of the alleles is genomically silenced while the other is expressed. Modes of expression are either paternally imprinted and maternally expressed or maternally imprinted and paternally expressed. This imprinting pattern is then maintained in the offspring except in the primordial germ cells, where global demethylation allows maternal or paternal pattern of imprinting to be applied to the new gametes according to the sex of the embryo (SanMiguel & Bartolomei, 2018; Surani, 1998).

Imprinted genes are abundant in placental development (Carrion et al., 2023; Fowden et al., 2006; Frost & Moore, 2010). There is a consistent pattern across imprinted genes with their imprinted parent of origin and their function. Genes that are silenced by the maternal genome are often

growth promoters, suggesting that the mother is trying to limit her investment into the foetus in favour of maintaining her own fitness. Paternally silenced genes, are often those that constrain growth, suggesting that the male is trying to present a genome which will produce maximum investment in the offspring, giving each offspring maximal chance for survival (Haig & Graham, 1991; John, 2013)(Figure 1). This fine tuning performed by each sex, utilises the imprinted gene mechanism as a regulator of gene dosage. As these genes are functionally related to growth, imprinted genes are used as a mechanism for manipulating parental investment (Cassidy & Charalambous, 2018; John, 2022; Monk, 2015) which is facilitated through the placenta. Genomic imprinting is the molecular arena in which the resource conflict battle rages between the mother and the foetus/father. The placenta is the platform to execute each party's influence. This thesis's research project has selected one gene of each imprinted mode of expression and has produced a double knockout of both modes simultaneously. This investigated each genes interaction with each other to understand if each genetic model produces its phenotype through the same mechanism. It also allowed insight into if the two genes behave antagonistically.

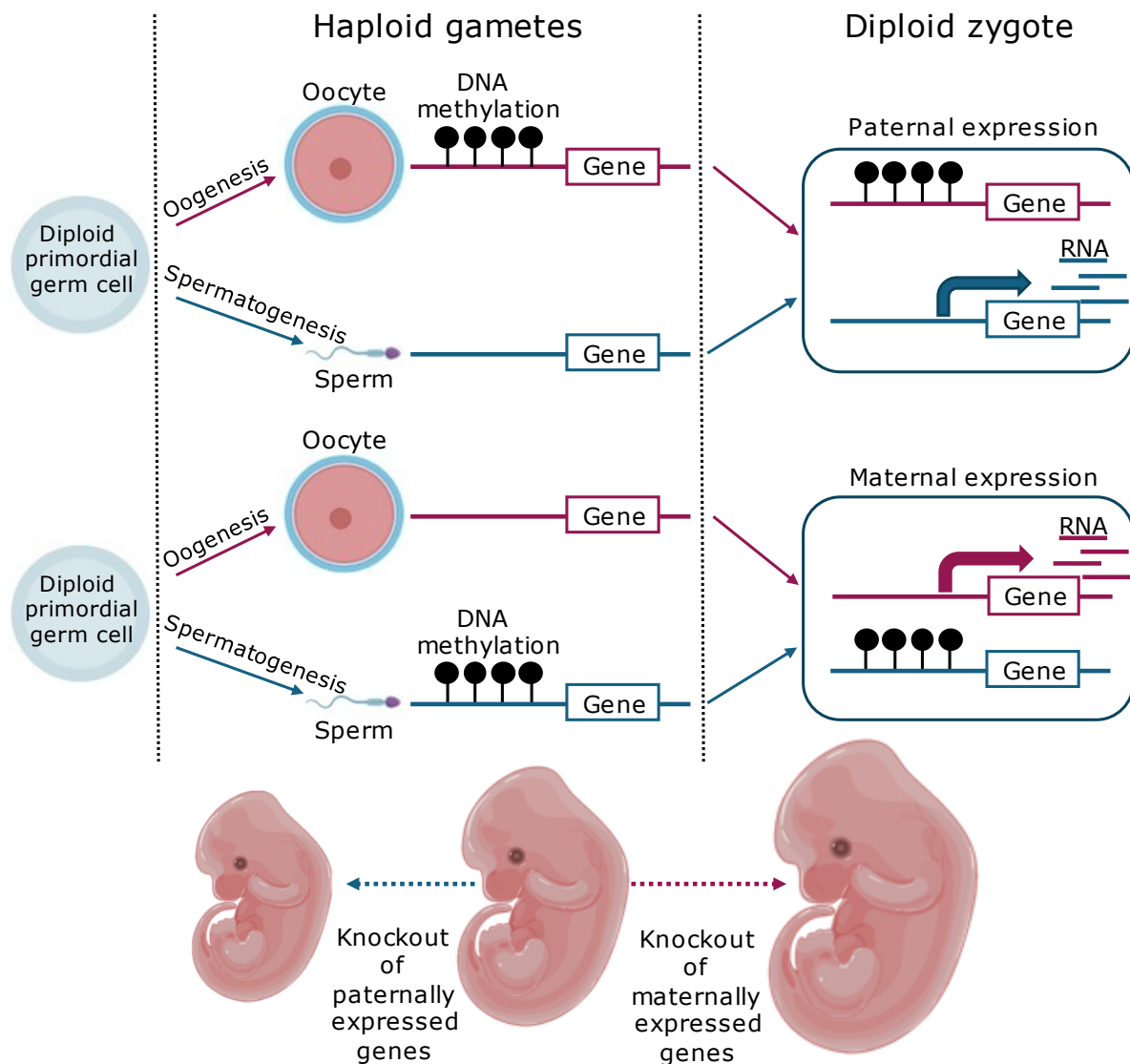


Figure 1: Mechanisms and function of genomic imprinting.
Adapted from John (2013) and Baran et al. (2015).

1.2 Evolution of the placenta

The evolution of viviparity has taken place independently multiple times across the animal kingdom (Blackburn, 2015; Kalinka, 2015). This progression begins with the retention of the embryo within the reproductive tract rather than spawning or egg laying. In spawning the parental investment post spawn is near zero (Clutton-Brock & Scott, 1991). In egg laying, the foetus is nutritionally supported by the egg initially and the parental investment is demonstrated by egg protection. These parental relationships are often monogamous and have equal investment from both the father and the mother (Clutton-Brock & Scott, 1991)(Figure 2). Post hatching the parental investment is also varied.

Some animals provide parental investment by feeding young whereas others are not present (Doody et al., 2013). Once the egg is retained within the mother, the parental investment is altered significantly and immediately, unbalancing the investment between parents. Initial consequences are a reduction in fecundity. Moving the animal from a R-type (rate of reproduction (R)) to a K-type (carrying capacity (K)) parental investment mode (MacArthur & Wilson, 1967). This reduction in number of offspring places a higher value on each individual offspring, therefore increasing the need for each individual offspring to be successful, in turn requiring more investment per offspring (MacArthur & Wilson, 1967).

There are many physiological changes that need to occur in the maternal body between oviparity and viviparity. Monotremes, are the most evolutionarily primitive version of the mammalian model. The egg is retained within the mother for a prolonged period, in which the egg does receive nutrients from the mother (Figure 2). The monotremes hatch in a foetal like state and are then nourished by the mother via lactation through mammary glands in openings on their skin (Tyndale-Biscoe, 1979). The next transitional phase of the mammal is the marsupial. Marsupials diverged from eutherian mammals 160 million years ago (Renfree et al., 2013). Marsupials have live births to a foetal like pup after a short gestation. They then support growth through lactation. Some marsupials do develop placentas, although they are not relied on as the sole nutrient resource for the foetus (Figure 2). Here embryonic and extraembryonic lineages arise from a single cell type (Selwood & Johnson, 2006). These form a yolk sac type placenta (Freyer et al., 2003). Some marsupial species produce a chorioallantoic type placenta which is secondary to the yolk sac type. Marsupial placentas are often categorised as "non-invasive" which do not embed extensively into the uterine wall, but instead form a superficial association with the uterine epithelium, although some develop contact with maternal blood vessels. This is thought to be secondarily derived as marsupial ancestors have an invasive placenta (Laird et al., 2018). Some marsupial placentas have also been shown to produce hormones (Renfree, 2010).

The rise of the eutherian placenta occurred over 100 million years ago (Kim et al., 2017; Murphy & Eizirik, 2009). These mammals are referred to as true placental mammals. These are categorised by having a longer gestation time, relative to investment, followed by a shorter lactation time (Figure 2). Both humans and mice are eutherian mammals. Through the progression of evolution, the degree in which the placenta penetrates the epithelium generally increases. The least invasive is the epitheliochorial placenta, which doesn't produce any invasion of the uterine epithelium. Then there are the endotheliochorial placentas, in which the trophoblast

cells do invade the maternal endometrium but just reach the maternal capillaries without invading them. The most invasive placentas are haemochorial placentas, where the trophoblast is in direct contact with maternal blood (Carter & Enders, 2004). Both mice and human have haemochorial type placentas (Soares et al., 2018).

1.3 Imprinted genes: Evolutionary perspectives and theories of coadaptation and parental conflict

As the interaction between foetus and mother intensifies, the communication between the two has become more intricate, which allows the resources to be refined and tailored to the foetus's needs as development progresses. Alongside the rise of extraembryonic requirements, a battle for resources between the foetus and mother begins. Although the mother does benefit from a successful pregnancy, it cannot be at the cost of potential future offspring. Thus, the maternal investment is limited to that which also keeps the mother healthy. The foetus however, acting in its own and the paternal interest, desires maximum investment. This concept is the parental-offspring conflict hypothesis, theorised by Dr Trivers in 1974 (Trivers, 1974).

As predicted by Professor David Haig in 1989, this conflict is fought through genomes (Haig & Westoby, 1989). The trajectory of extraembryonic support and the emergence of the placenta tightly follows the rise of the unique model of inheritance known as "genomic imprinting". Imprinted genes abundance is correlated to the degree of placentation. While there is no evidence of genomic imprinting in all other vertebrates, (O'Neill et al., 2000; Yokomine et al., 2005) and in monotremes (Killian et al., 2001), marsupials do have some genomic imprinting, with an estimated 60 imprinted genes (Cao et al., 2023), which is limited in comparison to the degree of imprinting seen in mammals (Ager et al., 2008; Cao et al., 2023; Edwards et al., 2008; John & Surani, 2000; Killian et al., 2000; Killian et al., 2001; Renfree et al., 2008; Renfree et al., 2013; Suzuki et al., 2005; Toder et al., 1996; Weidman et al., 2006). Around 1% of mammalian genes are imprinted (Babak et al., 2008; Hubert & Demars, 2022; Morison et al., 2005) which consists of over 200 imprinted protein coding and non-coding RNAs (Ferguson-Smith, 2011; Tucci et al., 2019). Evolutionarily, this pattern produces a picture where the development of imprinting co-evolved alongside extra embryonic investment (Reik & Lewis, 2005). This evolutionary evidence leads to the concept that the two mechanisms, genomic imprinting, and extra embryonic investment, are inextricably

linked (Hanna, 2020). The higher the investment during gestation, the more imprinted genes are involved (John & Surani, 2000).

Process	Birds	Monotremes	Marsupials	Eutherians
<i>Dosage compensation</i>	Yes	Yes?	No	No
<i>X-chromosome inactivation</i>				
<i>Imprinted</i>	No	No?	Yes	Yes
<i>Random</i>	No	No?	No	Yes
<i>Imprinting</i>				
<i>Foetal growth</i>	No	No	Yes	Yes
<i>Postnatal metabolism</i>	No	Unknown	Unknown	Yes
<i>Behaviour</i>	Unknown	Unknown	Unknown	Yes

Table 1: Scale of extra embryonic investment and genomic imprinting.

"?" indicates the predicted status of X chromosomes in monotremes. Based on table from Reik and Lewis (2005).

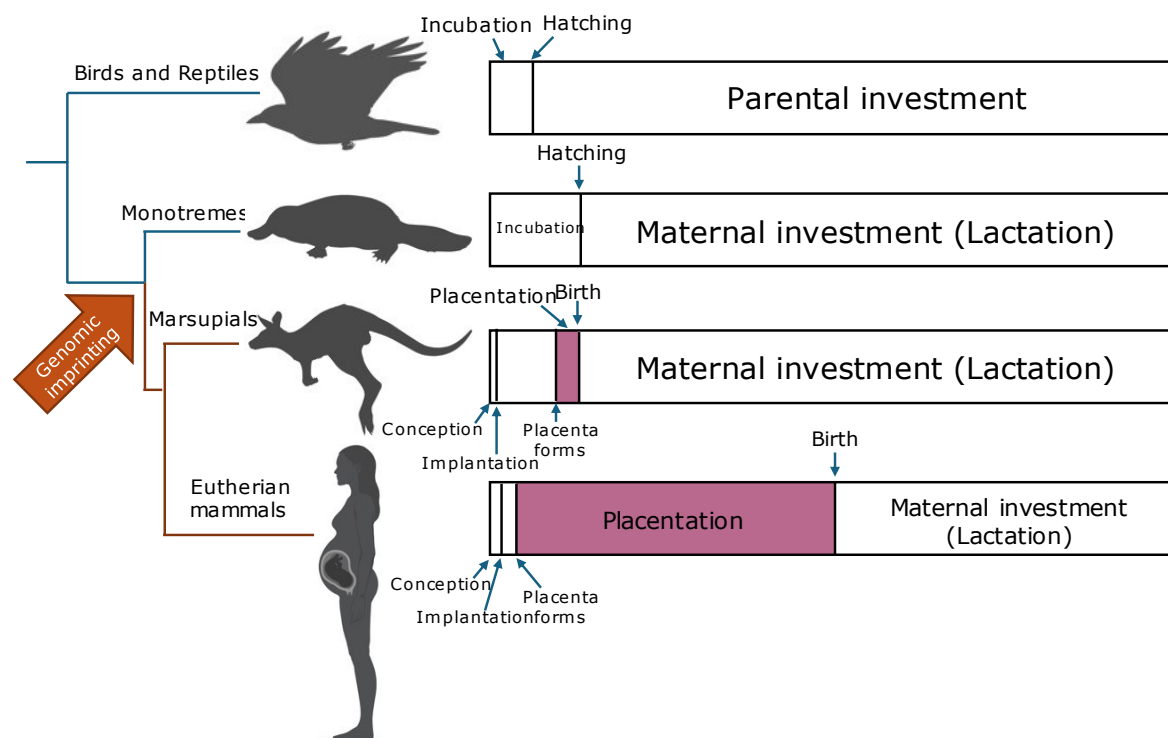


Figure 2: The evolution of the placenta and genomic imprinting, and the relationship between parental investment.

Adapted from Renfree et al. (2013) and Abbot and Capra (2017).

Evidence to support the parental conflict hypothesis is well demonstrated by the interaction between *Igf2* (insulin-like growth factor 2) and *Igf2r* (insulin-like growth factor 2 receptor). *Igf2*, which is expressed in the placenta, is paternally expressed and maternally silenced (DeChiara et al., 1990). Functionally, *Igf2* has been associated with foetal growth based on studies demonstrating foetal growth retardation by inactivation of its paternal copy (DeChiara et al., 1990). The growth promotion from *Igf2* is enacted through the Insulin-like growth factor 1 (*Igf1*) receptor which binds *Igf1*, *Igf2* and insulin (Sara & Hall, 1990). However, the maternally expressed *Igf2r* (Barlow et al., 1991) has a greater affinity for *Igf2* in effect blocking *Igf2*'s ability to promote growth. *Igf2r* also functions as a protein known as cation-independent mannose 6-phosphate receptor (CI-MPR) which operates to degrade *Igf2*, again reducing its impact on growth (Kornfeld & Mellman, 1989). This led to the proposal by Moore and Haig in 1991 that the higher affinity of *Igf2* to *Igf2r* and *Igf2r*'s ability to degrade *Igf2*, is a maternal response that evolved to limit the effects of the paternal production of *Igf2* (Moore & Haig, 1991), limiting growth in the fetus and underscoring the parental conflict hypothesis.

Besides the parental conflict hypothesis, there are many other proposed hypotheses which are used to understand the function of imprinted genes. One theory suggested is that imprinting could have evolved to prevent parthenogenesis, as the requirement for both genomes would prevent a successful parthenogenetic offspring. This would result in greater genetic diversity for the species, although there is no mechanism suggested for how this would have evolved (Moore & Haig, 1991; Solter, 1988) (Haig & Westoby, 1989; Li et al., 2025; Spencer & Clark, 2014). In opposition to this theory is the concept that the prevention of parthenogenetic offspring could be established by as little as one single imprinted loci and in turn the occurrence of multiple imprinted loci across the genome suggests a more complex function (Haig & Trivers, 1995). It is instead hypothesised that the prevention of pathogenesis is a positive by-product of the mechanism rather than the primary function (Moore & Haig, 1991) and the theory has largely fallen out of favour (Spencer & Clark, 2014). It has also been proposed that flexible gene expression is allowed through imprinting mechanisms for a fine-tuned control of development (Haig & Trivers, 1995; Moore & Haig, 1991). Although this has been criticized as genetic regulation has been achieved in other species by much simpler and means that are sufficiently functional (Varmuza & Mann, 1994). Both of these hypotheses are only partially supported by the evidence as they fail to explain the association between imprinted genes and growth nor can they account for the high frequency of imprinted genes in mammals specifically.

The alternative model that has the most support is the co-adaptive model. This hypothesis suggests that imprinted genes evolved through mutual adaptations of offspring and maternal traits to optimise developmental outcomes. This balancing act enhances compatibility between foetus and mother in resource allocation which promotes survival and reproductive success (Haig, 2014). Evidence to support this hypothesis is well demonstrated by paternally expressed gene 3 (*Peg3*) mutant (*Peg3^{KO}*) mothers (Curley et al., 2004). *Peg3^{KO}* mutant mothers present a harmonious phenotype to their *Peg3^{KO}* mutant pups. For example, while the *Peg3^{KO}* mutant mother presented a reduction in milk let-down, the *Peg3^{KO}* mutant pups had altered suckling behaviour (Curley et al., 2004) and while mutant mothers fail to increase their nutrient intake during pregnancy, the placental nutrient transfer was altered in mutant placentas (Curley et al., 2004). However, this evidence has been refuted by further studies on *Peg3^{KO}* mutant dams which demonstrated no maternal physiological or behavioural phenotype (Denizot et al., 2016).

Another example of the co-adaptive model is demonstrated by *Grb10* (Cowley et al., 2014). *Grb10* is imprinted in the placenta and the mammary tissue. In the placenta, *Grb10* fits the conflict hypothesis where it regulates foetal and placental growth. However, in the mammary gland as the tissue is not shared between mother and father and is only influenced by maternal genes, there is no direct genomic conflict within the tissue. Despite this, *Grb10*s expression in the mammary tissue suggests a role in lactation and ultimately regulation maternal investment. This co-ordinated response between mother and offspring supports the co-adaptation theory. Although it is possible that imprinting in the mammary tissue in this context could be the result of early life pressures, the presence of imprinting in mammary tissue does suggest an alternative or more complex theory than the parental conflict hypothesis (Cowley et al., 2014). These models highlight discrepancies in the parental conflict hypothesis; however, these theories are not mutually exclusive and together offer a broader understanding of the evolution of genomic imprinting.

1.4 Placental development, structure and function: Human versus mouse

The placenta is a structure which is unique to mammalian gestation and originates from the foetus. It is a temporary organ which only exists during the gestation of the foetus and is afterwards discarded (Burton & Fowden, 2015; Herrick EJ, 2023). It supports the growth and development of the foetus internally. It functions as an interface between

the circulatory systems of the mother and foetus allowing the exchange of nutrients and gases such as fatty acids, amino acids, and glucose. It acts as a waste removal system for the foetus by removing urea and carbon dioxide from the foetal blood and excreting it through the maternal systems (Burton & Fowden, 2015; Burton & Jauniaux, 2015; Herrick EJ, 2023). The placenta acts as the immune system for the foetus as the foetal immune system develops (Balasundaram P, 2023; Burton & Jauniaux, 2015). The foetal immune system takes on maternal antibodies from the maternal blood which builds foetal immunity. It also has a large endocrine function in the production of an intricate orchestra of hormones which facilitates defined stages in the development and growth of both mother and baby (Costa, 2016).

In mouse, although the first cell fate decision and differentiation to occur after fertilisation is the distinction between the inner cell mass (ICM) (later embryo) and the trophoblast (later placenta) at E3.5 (Rossant & Tam, 2009), placental development doesn't begin in earnest until around E4.5 when the blastocyst attaches to the uterine wall (Hemberger & Dean, 2014). This is when the extraembryonic ectoderm (ExE) begins to proliferate. At E5.5-E7.5 the ectoplacental cone (Epc) is established and trophoblast stem cells begin to differentiate into the placental lineages as marked by the expression of Achaete-scute complex homolog 2 (*Ascl2*), (spongiotrophoblast marker), trophoblast specific protein alpha (*Tpbpa*) (spongiotrophoblast marker) and Placental lactogen I (*Pl3d1*) (P-TG cell marker) along with the first expression of TS cell marker Glial cell missing 1 (*Gcm1*) (Simmons, 2014). Between E7.5 and E10.5 is where the distinct layers of the spongiotrophoblast and labyrinth are formed (Simmons, 2014) and the chorion has an increase expression of *Gcm1*, *Syna* (Syncytin-A) and heart and neural crest derivatives expressed transcript 1 (*Hand1*) (Simmons, 2014). The clear layering of the placenta is developed by E9.5 and all placental cell subtypes are present by E12.5 (Simmons, 2014). The labyrinth continues to expand until E18.5 (Simmons, 2014).

Both *Ascl2* and *Hand1* encode basic helix-loop-helix (bHLH) transcription factors which are functionally opposing during the differentiation of trophoblast giant cells (Hemberger & Cross, 2001; Scott et al., 2000). *Hand1* is crucial for the differentiation of polyploid trophoblast giant cells (TGC)s and regulates TGC invasion (Riley et al., 1998), whereas *Ascl2* functions to maintain diploid trophoblast cells by inhibiting differentiation or encouraging cell proliferation (Guillemot et al., 1994) and maintains giant cell precursors (Scott et al., 2000). Their expression is co-localised in the Epc and spongiotrophoblast suggesting their antagonistic functions may be co-ordinated (Scott et al., 2000). Both KOs are fatal with *Hand1*^{KO} fetuses arresting at E7.5 (Riley et al., 1998) and *Ascl2*^{KO} fetuses

arresting at E10 (Guillemot et al., 1994). In *Ascl2^{KO}* placentas the spongiotrophoblast is absent (Guillemot et al., 1994). *Hand1^{KO}* placentas had a reduced implantation site, a reduced trophoblast cell number in the Epc and defects in their trophoblast giant cells with a reduction in TGC density (Riley et al., 1998).

Gcm1 and *Tpbpa* also play a crucial role in placental development. *Tpbpa* regulates cell lineage specification (Hu & Cross, 2011). *Tpbpa* is first expressed between E7.5 and E8.5 in the ectoplacental cone. It is then expressed in the progenitors of trophoblast subtypes such as glycogen cells and some TGCs. Ablation of *Tpbpa^{KO}* is fatal by E11.5 and placentas had altered maternal vasculature as a result of reductions in canal-associated (C-)TG, spiral artery-associated (SpA-)TG cells and glycogen trophoblasts (Hu & Cross, 2011). *Gcm1* is crucial in the establishment of the labyrinth (Anson-Cartwright et al., 2000). *Gcm1*, marks sites along the chorionic plate which then begin the process of folding and invagination. *Gcm1* is expressed at the tips of the branching structures (Anson-Cartwright et al., 2000) as long as they are still expanding (Basyuk et al., 1999). This forms the two layers of the labyrinth Syncytiotrophoblast layer 1 (SynT-I) and Syncytiotrophoblast layer 2 (SynT-II). SynT-I is the layer which has direct contact with the maternal blood and facilitates the exchange of nutrients and gases, SynT-II is the supporting layer for SynT-I and aids in transporting and processing the molecules to encourage an efficient exchange system (Simmons, 2014). *Gcm1^{KO}* result in embryonic mortality by E10 and placentas where branching is prevented and the labyrinth fails to form (Anson-Cartwright et al., 2000).

Functionally the placenta is the same across mammals, but structurally there are distinct differences which are customised to each species pregnancy characteristics (Boyd et al., 2018; Imakawa & Nakagawa, 2017). A key difference between the human and the mouse is their litter sizes. Mice have a bicornuate uterus with two uterine horns (Boyd et al., 2018), which allows the mouse to support multiple offspring with the mouse average litter ranging between six to twelve pups (Boyd et al., 2018; McVey, 2014). Humans have a centrally located uterus which typically can facilitate a single embryo, resulting usually in singleton pregnancies (Boyd et al., 2018). The mouse being a small prey animal must be able to produce quickly; their gestation is 21 days long which is the shortest amongst mammals (Boyd et al., 2018). In contrast, human gestation is from 38-42 weeks which is an extended time scale to accommodate the growth of a larger brain compared to similarly sized animals (Boyd et al., 2018). These differences in the requirements for each placenta result in structural differences in the placenta between species.

The mature mouse placenta is discoid, with a diameter at term measuring between 1.5-2 cm and weighing between 100-200 mg (Boyd et al., 2018). There are three key regions of the mouse placenta, the decidua, the labyrinth and the junctional zone (Simmons & Cross, 2005)(Figure 3). The decidua which imbeds into the mother is derived from the maternal endometrium. Secretions from the decidua regulate trophoblast invasion and allow access to the maternal resources (Boyd et al., 2018). These secreted factors also allow immune tolerance at the interface which prevents the maternal system rejecting the foreign tissue. The junctional zone is the endocrine lineage of the mouse placenta. It consists of spongiotrophoblast cells, glycogen cells (GlyT) and TGC (Boyd et al., 2018; Coan et al., 2005). These cells produce placental lactogens and prolactin (Prl) hormones. TGCs invade the maternal tissues and generate structures in which the maternal blood flow can filter through the placenta. This zone is at the interface between the maternal and foetal tissues which allows delivery of hormones to both mother and foetus. The labyrinth is the key foetal structure consisting of intricate foetal blood vessel structures which surround various voids filled with maternal blood. This system filters the nutrients and hormones down to the umbilical cord and into the foetus (Coan et al., 2005).

In the mouse the seven key placental lineages that produce hormones are the spongiotrophoblast cells, glycogen cells and five TGCs (Figure 4). Spongiotrophoblast cells are the most abundant cell type within the junctional zone and functions as the most significant placental endocrine lineage (Coan et al., 2006). Spongiotrophoblast cells are heavily influenced by genes such as *Ascl2* and *Cdkn1c*. *Ascl2*, has demonstrated a restrictive function over spongiotrophoblast expansion (Tunster, McNamara, et al., 2016) along with Cyclin-dependent kinase inhibitor 1C (*Cdkn1c*) which has demonstrated reduced spongiotrophoblast lineage in *Cdkn1c^{KO}* models. The other main cell type of the junctional zone are the glycogen cells which function as an energy supply for the placenta as they store glycogen throughout gestation (Coan et al., 2006). *Cdkn1c* has significant influence over glycogen cells by supporting their differentiation (Tunster et al., 2011). Glycogen cells also produce some prolactin (*Prl*) family members which are crucial placental hormones (section 1.5)(Simmons, Rawn, et al., 2008).

Within the mouse placenta there are five distinct TGC lineages (Figure 4). TGCs are the first cell subtype to form that is terminally differentiated. These cells express key *Prls* and are defined by their large nuclei (Simmons et al., 2007). The secondary parietal (P-)TG cells form the interface between the junctional zone and maternal decidua, along with surrounding the implantation site (Simmons et al., 2007) their number has been shown to be regulated by *Ascl2* (Tunster, McNamara, et al.,

2016). SpA-TG cells are located in the maternal decidua and line the maternal blood system (Simmons et al., 2007). Maternal blood C-TG cells line the canals containing maternal blood that enter the junctional zone and pass through the labyrinth (Simmons et al., 2007). Sinusoidal (S-)TG cells are located within sinusoidal spaces in the labyrinth zone of the placenta and are in direct contact with maternal blood (Simmons et al., 2007). S-TG cells have been found to require *Cdkn1c* for their development with *Cdkn1c*^{KO} models presenting substantial areas of pooled maternal blood and extensive collagen deposits adjacent to these areas suggesting S-TG cell dysfunction (Tunster et al., 2011). Pockets located underneath the decidua which are where the maternal blood leaves the placenta are lined with channel (Ch-)TG cells (Gasperowicz et al., 2013; Rai & Cross, 2014).

The endocrine population of the mouse placenta is concentrated in the junctional zone. The junctional zone includes glycogen cells, spongiotrophoblast cells and multiple TGC types. The progenitors of these cells originate from trophoblast stem cells within the Epc. These differentiate into the various placental lineages through genetic regulators such as *Ascl2* and *Cdkn1c* (Table 2). Single cell RNA sequencing data from Jiang et al. (2023), showed a variety of expression profiles for populations of cells expressing *Peg3* or *Phlda2*. *Phlda2* was expressed in two sub-populations of cells. These were both labyrinth trophoblast progenitor cells between E11.5 and E14.5, one group which was marked with *Epcam* and *Met* expression and the other marked with *Epcam* and *Egfr*. *Peg3* expression was identified in four subpopulations. These were TS cells and ExE cells between E7.5 and E10.5 which were marked by *Lin28a* and *Eomes* expression. *Peg3* was also identified in S-TGC precursors from E9.5-E14.5, and S-TG cells from E11.5-E14.5 which had the marker *Ctsq*. *Peg3* was also expressed in the labyrinth trophoblast progenitor cells between E11.5 and E14.5, which was marked with *Epcam* and *Met* expression, a population that was also identified to have *Phlda2* expression. In an investigation into cell populations pre-chorioallantoic fusion (E8.5), cells co-expressing both *Peg3* and *Phlda2* were identified in labyrinth trophoblast progenitor cells and both sub populations of syncytiotrophoblast cells (SynT-I and SynT-II) (Jiang et al., 2023). Jiang et al 2023, demonstrate that only Placental lactogen II (*Pl3b1*) and *Peg3* overlapped in expression in a population of cells specific to TS cells and the ExE identified by *Lin28a* and *Eomes* expression and again the co-expression of *Peg3* and *Phlda2* in the labyrinth (Jiang et al., 2023).

The regulation of the IC2 domain genes by the antisense RNA transcript *Kcnq1ot1* has been well documented (Fitzpatrick et al., 2002). Like *Phlda2*, the imprinted genes *Cdkn1c* and *Ascl2* are maternally expressed. *Ascl2* plays a significant role in the development of the spongiotrophoblast

(Bogutz et al., 2018) and that *Cdkn1c* functions to develop and maintain the labyrinth and TGCs more specifically (Simmers et al., 2023). *Ascl2* is involved in the differentiation of trophoblast progenitors and is essential for establishing the spongiotrophoblast (Guillemot et al., 1994), where *Phlda2* suppresses cell proliferation of trophoblast cells (Tunster, Creeth, et al., 2016). *Ascl2* action is therefore earlier in development than *Phlda2*. In Jiang et al 2023, investigations into populations of Epc cells revealed three distinct populations, progenitors of SpT cells (E1) expressing *Tpbpa*, *Cdx2* and *Ascl2* were distinct from a population of bipotential progenitors (P1) which expressed *Phlda2* and could differentiate into SpT progenitors (E1) at E7.5-E8.5 (Jiang et al., 2023). In addition, *Ascl2* and *Cdkn1c* were identified in SpT cells from E9.5-E14.5 and *Ascl2* was also seen in cells expressing *Pcdh12* between E9.5-E14.5 (Jiang et al., 2023). Cell type and cellular process markers are represented in Table 2 (Marsh & Belloch, 2020; Simmons, 2014).

Cell Type	Expression marker	Spatiotemporal location	Reference
C-TG cell	<i>Prl2c</i> , <i>Prl3b1</i>	E12.5-E18.5	(Simmons et al., 2007).
CH-TG cell	<i>Ctsq</i>	E10.5-E18.5	(Gasperowicz et al., 2013)
Decidua	<i>Prl8a2</i>	E8.5-E18.5	(Simmons, Natale, et al., 2008).
ExE/ Chorion/ TS cells	<i>Cdx2</i> , <i>Eomes</i> , <i>Esrrb</i>	E5.5-E8.5	(Chawengsaksohak et al., 1997; Luo et al., 1997; Russ et al., 2000)
Glycogen cells	<i>Pcdh12</i> , <i>Prl7b1</i> , <i>Cdkn1c</i>	E7.5-E18.5: <i>Pcdh12</i> is GlyT specific. <i>Prl7b1</i> also expressed in C-TG cell and SpA-TG cell. <i>Cdkn1c</i> supports differentiation of GlyT cells.	(Bouillot et al., 2006; Coan et al., 2006; Simmers et al., 2023; Simmons, Natale, et al., 2008)
Glycogen cells and spongiotrophoblast	<i>Tpbpa</i>	E8.5: Expressed by SpT and GlyT in the Epc. E10.5-E18.5: Expressed in the junctional zone.	(Lescisin et al., 1988)
P-TG cells (all)	<i>Prl3d1</i> , <i>Prl3b1</i>	Until E10.5: <i>Prl3d1</i> exclusive to primary and secondary P-TG cells; expression reduced at E10.5. E10.5-E18.5:	(Carney et al., 1993; Simmons et al., 2007; Simmons, Natale, et al., 2008)

		<i>Prl3b1</i> at E10.5 expression rises and remains high until E18.5. <i>Prl3b1</i> is also expressed in SpT and S-TG cells.	
SpA-TG cell	<i>Prl2c</i> , <i>Prl7b1</i>	E8.5–E18.5: Marker of SpA-TG cells however not exclusively expressed.	(Mould et al., 2012; Simmons et al., 2007; Simmons, Natale, et al., 2008)
S-TG cell	<i>Ctsq</i> , <i>Prl3b1</i>	E12.5–E18.5: Sub population of P-TG cells also express <i>Ctsq</i> ; <i>Prl3b1</i> is also expressed in SpT and P-TG cells.	(Ishida et al., 2004; Simmons et al., 2007)
Spongiotrophoblast	Prolactin family 8 subfamily A member 8 (<i>Prl8a8</i>), <i>Ascl2</i>	E12.5–E18.5: Exclusively expressed in SpT. <i>Ascl2</i> , maintains trophoblast progenitors.	(Bogutz et al., 2018; Simmons, Natale, et al., 2008)
Syncytiotrophoblast layer 1 (Labyrinth)	<i>Syna</i>	8.5-E14.5:	(Charron et al., 2012; Dupressoir et al., 2009; Nagai et al., 2010; Simmons, Natale, et al., 2008)
Syncytiotrophoblast layer II (Labyrinth)	<i>Gcm1</i> , <i>Synb</i> (Syncytin-B)	E8.5-E14.5:	(Charron et al., 2012; Dupressoir et al., 2011; Nagai et al., 2010; Simmons, Natale, et al., 2008)
Syncytiotrophoblast (general)	<i>Dlx3</i>	E7.5: Expressed in base of Epc. E10.5-E18.5: Expressed in syncytiotrophoblast.	(Berghorn et al., 2005; Morasso et al., 1999; Simmons, Natale, et al., 2008)

Table 2: Table of cell type makers and cellular process markers (Marsh & Blelloch, 2020; Simmons, 2014).

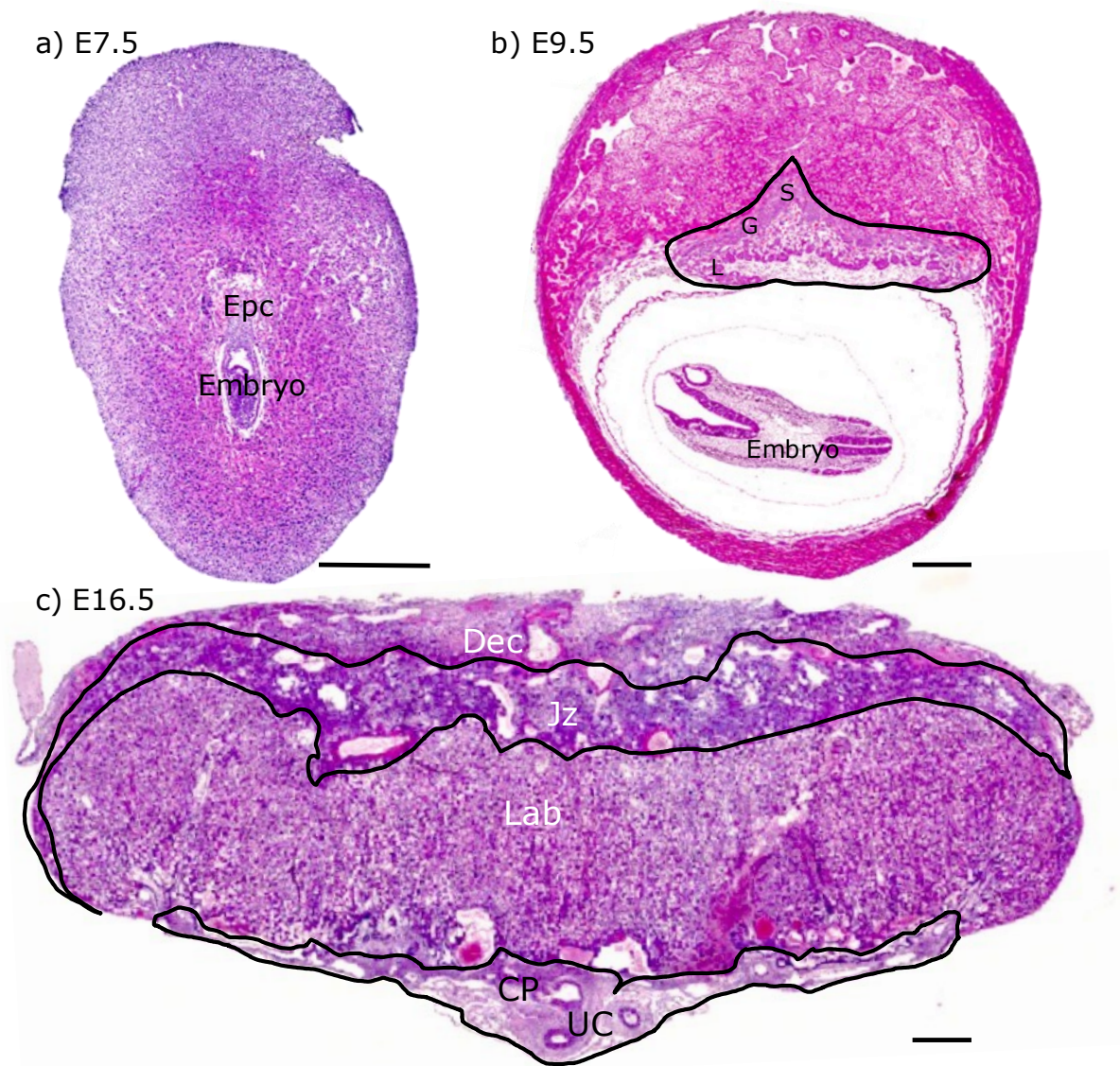


Figure 3: Mouse placental structures.

a) E7.5. ectoplacental cone (Epc). **b)** E9.5 developing spongiotrophoblast (S), trophoblast giant cell layer (G) and developing labyrinth (L). **c)** E16.5 placenta. Decidua (Dec), junctional zone (Jz), labyrinth (Lab), chorionic plate (CP) and umbilical cord (UC). Scale bar: 500 μ m.

The human placenta is attached to the uterine wall with the foetal membrane extending from its edges. Like the mouse placenta, it is also discoid. On average, it measures 22 cm in diameter and 500 grams in weight at full term (Boyd et al., 2018). The maternal section is at the origin point of implantation at the uterine wall and comprises the decidua basalis. This contains the maternal blood vessels and undergoes constant remodeling during the growth of the placenta to allow the foetal-maternal exchange. The foetal structure contains the chorionic villi, which protrude into the intervillous spaces which contain the maternal blood (Boyd et al.,

2018). Each finger-like villous contains a combination of arteries and veins originating from the foetus. A coating of syncytiotrophoblast (STB) cells covers each villous which facilitates the uptake of nutrients from the maternal blood in the intervillous space (Boyd et al., 2018). These cells also play a key role in hormone production (Imakawa & Nakagawa, 2017). This allows these hormones to influence both the mother and foetus as they are being produced at the crossroads of the nutrient exchange point. Hormones of note in the human system are progesterone, estrogen, human chorionic gonadotropin (hCG) and a variety of placental lactogens (Imakawa & Nakagawa, 2017). Other related structures are the foetal membranes, the amnion and chorion produce the amniotic sac which encases the foetus and is filled with amniotic fluid (Boyd et al., 2018). The chorion arises from the trophoblast of the blastocyst where the amnion originates in the inner cell mass.

The three broad trophoblast cell subtypes in the human placenta are the villous cytotrophoblast (VCT), STB and extravillous cytotrophoblast (EVT) (Figure 4), although single cell sequencing has revealed multiple subtypes for each population (Liu et al., 2018) their general roles are described here. The VCT form a layer on each placental villi and function as a stem cell population by constantly supporting the formation of the STB and allowing fusion of the STB layer (Kliman et al., 1986; Wang & Zhao, 2010). The VCT are able produce hCG before differentiation but otherwise do not have a significant endocrine function (Kao et al., 1988). The STB form the external layer of the villi and are in direct contact with the maternal blood which allows them to facilitate the exchange of oxygen, nutrients and waste between foetus and mother. These cells are unable to divide mitotically and are continuously replenished by the VCT (Wang & Zhao, 2010). The STB are the predominant endocrine lineage of the human placenta and are known to produce hCG (Cole, 1997), human placental lactogen (hPL) (Kliman et al., 1986), progesterone (Tuckey, 2005), estrogens (Levitz & Young, 1977), placental growth hormone (Alsat et al., 1998), placental growth hormone (Lacroix et al., 2002) and many other growth factors and cytokines (Costa, 2016). The temporal location and function of these hormones will be discussed further in Section 1.5. Their location allows these hormones to be directly released into the maternal blood (Wang & Zhao, 2010). The EVT, which also differentiate from VCT, invades the maternal wall by migrating from the placental villi into the maternal decidua. They then remodel the maternal spiral arteries to develop the structures required for the blood supply to and from the placenta and foetus (Wang & Zhao, 2010). The EVT cells do not primarily function in an endocrine capacity but do contribute to some local signaling (Lacroix et al., 2005).

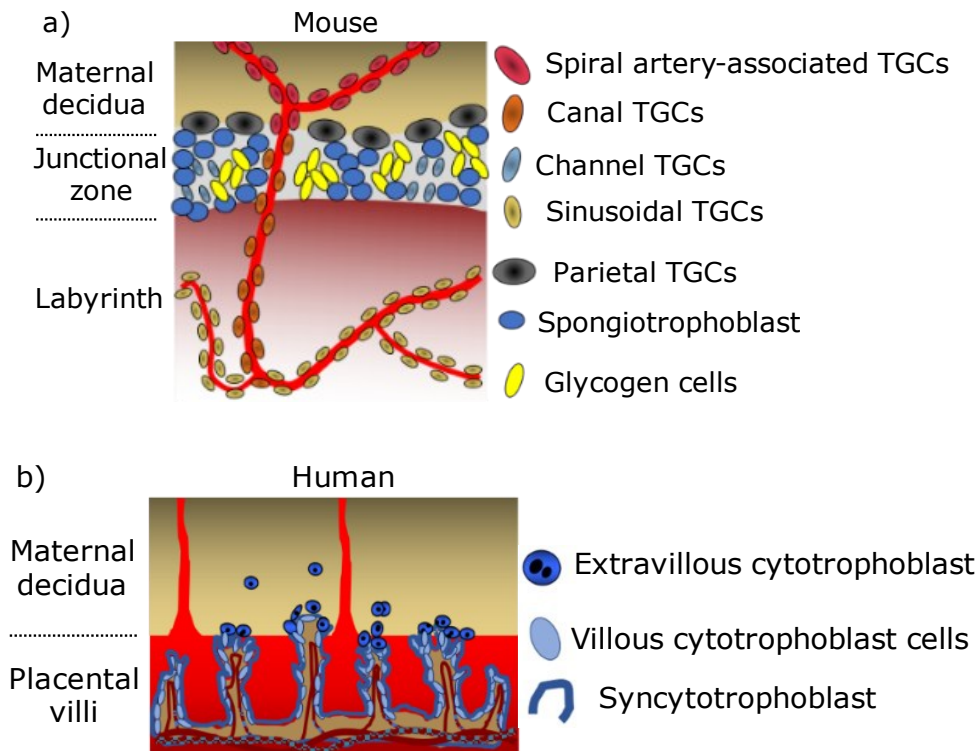


Figure 4: Placental lineages.

a) Mouse placental structure showing cell types and lineages. **b)** Human placental structure showing cell types and lineages. Adapted from Creeth and John (2020).

Despite the differences in gestational length, the viability of the new-born is somewhat similar between both species. Both mouse and human offspring come with significant requirements for maternal care post birth. As a result, the mouse model can play a crucial role in the investigation into the placental influence over maternal care investment (Coan et al., 2005). As proxies, the structures that have the same functionality can be used to compare roles. Mouse models offer practical advantages such as similar functions, short reproductive cycle and the capability for genetic manipulation however their key limiting feature is their reduced capacity for invasion into the uterine wall. This makes mice a poor model for invasion models such as preeclampsia. For this rat and non-human primate models can be used as they have a closer anatomical and physiological match to humans (Sones & Davisson, 2016). In addition, cell culture can be used as a good intermediary between species as comparative analysis equivalent cell types can be assessed under test conditions.

1.5 Placental hormones prime maternal resources

The behaviour of maternal care is defined by a pattern of behaviour exhibited by the mother that enhances the survival and reproductive success of her offspring (Bridges, 2015; Bridges & Nephew, 2009; John et al., 2023; Saltzman & Maestriperi, 2011; Sinha et al., 2022), which presents as changes in a new mothers behavioural and motivational repertoire directed towards her young (Creeth et al., 2019). In detail, it consists of actions that provide fundamental requirements for the young offspring, including, protection, shelter, warmth, nutrients, and education, (Bridges & Nephew, 2009; Sinha et al., 2022), all of which significantly increase infant mortality and poor outcomes when they are in short supply (Rutter, 1985; Zeanah et al., 2005). These actions require the investment of time and energy from the mother at the cost of investing in her own care, meaning that maternal care behaviour is a limited resource (Gross, 2005). Interestingly, the maternal bond itself is sought after resource as shown by preference trials between tactile comfort and food as demonstrated by Rhesus monkeys in the 1960s (Harlow et al., 1965) which demonstrate the roles of a mother's warmth, comfort and affection as a form of social and emotional education resource (Arling & Harlow, 1967; Baker & McGrath, 2011). The introduction of young to an adult of the same species does not immediately trigger maternal behaviours, as shown by male and virgin female rats who both do not present parental behaviours until several days after exposure to young (Brunton & Russell, 2008). However, maternal care has been rapidly induced using blood transfusions from late pregnant females to non-pregnant females (Terkel et al., 1972) suggesting that there are physiological preparations during pregnancy which induce these behaviours.

A crucial role played by the placenta is in its endocrine function (Petraglia et al., 1996). The production and regulation of various hormones over the gestational period orchestrate diverse developmental processes. Many of these processes prepare physiological resources, such as lactation, for the support of the developing foetus or young, which is one component of maternal investment. The other component is the induction of maternal care behaviour (Grattan, 2011; Saltzman & Maestriperi, 2011; Servin-Barthet et al., 2023; Smiley et al., 2019). The maternal brain's exposure to placental hormones re-organises neural circuitry surrounding maternal behaviours and the motivation to implement them (Brunton & Russell, 2010; Glynn et al., 2016; Hoekzema et al., 2017). The alterations in the maternal brain are the result of placental hormone action (Grattan, 2011; Grattan & Ladyman, 2020). The priming is actioned by progesterone, oestrogen, glucocorticoids and lactogens targeting a region within the hypothalamus called the medial preoptic area (Ammari et al., 2023;

Brunton & Russell, 2008; Grattan & Ladyman, 2020; Mann & Bridges, 2001; Smiley et al., 2019) which is responsible for regulating maternal behaviour (Jacobson et al., 1980; Numan, 1974; Numan et al., 1988; Numan et al., 1977). These neuronal changes are broad and range from changes in individual neuronal population patterns of activity to total remodelling of circuit characteristics (Grattan & Ladyman, 2020; Smiley et al., 2019).

A key hormone in the human system is hPL. This hormone is produced by the syncytiotrophoblast cells in the placenta (Petraglia et al., 1996). Production of hPL begins in the first trimester and increases over the duration of gestation, peaking and plateauing in the third trimester (Aaron Geno et al., 2021). Most of the hormone enters the maternal circulation, where foetal circulation of hPL is minimal (Palomba & Daolio, 2018). In relation to physical maternal resources, it is involved in developing the mammary glands in preparation for breast feeding (Cronin & Gemignani, 2018; Johnson, 2010) where it influences milk production and secretion (Johnson, 2010). Despite being in low concentrations in the foetal system, it regulates foetal development by prompting the production of foetal growth factors such as IGFs, insulin, adrenocortical hormones, and pulmonary surfactants (Handwerger & Freemerk, 2000), in effect acting as the foetal growth hormone (Palomba & Daolio, 2018). There are many changes to the endocrinology of a pregnant woman to accommodate the increased supply of metabolic fuel in the maternal blood. These include insulin resistance, more efficient plasma amino acid transport, increased plasma lipids and hyperinsulinemia (Berga et al., 2016). Despite its high association with insulin, hPLs relationship to gestational diabetes is unclear (Rassie et al., 2022).

The secretion of hPL is heavily influenced by maternal metabolic status, foetal demand, and placental size. Maternal circulation of hPL has been linked to placental and foetal weight (Palomba & Daolio, 2018). Moderate hPL expression has been associated with a health-conscious diet during pregnancy, where higher levels of hPL have been linked to increased custom birth weight centiles (CBWC) and a higher risk of large for gestational age (LGA) (Garay et al., 2022; Rassie et al., 2022) and low levels have been linked to postnatal anxiety, depression, and low birth weight (Sumption et al., 2020). This correlative data suggests that hPL levels may contribute to maternal mood disorders. Additional factors such as gestational age can have a negative effect hPL, because of a decrease in functional syncytiotrophoblast mass (Ghoshal et al., 2019), again, resulting in complications such as low birth weight (Sumption et al., 2020). In both forms of maternal resources, nutrient supply (during gestation and lactation) and maternal care, hPL is a crucial regulator.

Another series of important placental hormones are the placental growth hormone (GH) gene family (Lacroix et al., 2002). These genes are located on the long arm of chromosome 17 in a 47 kb cluster (Barsh et al., 1983; Chen et al., 1989; Hirt et al., 1987). Across the five family members there is a high degree of conservation between the structures, suggesting they evolved by gene duplication (Chen et al., 1989; Miller & Eberhardt, 1983). Four of the family members are expressed in the placenta, (Barrera-Saldaña et al., 1983), with the one remaining family member being expressed in the pituitary (Martial et al., 1979; Nachtigal et al., 1993). Placental GH functions by regulating IGF1. IGF1 through gluconeogenesis, lipolysis and anabolisms increases glucose, fatty acids, glycerol and essential amino acids in maternal blood (Lacroix et al., 2002).

Both primate and rodent placentas produce a series of pregnancy-specific glycoproteins (PSGs) from syncytiotrophoblast cells in human and spongiotrophoblast cells in mouse. There are 17 known PSGs in the mouse genome and 10 in human (McLellan et al., 2005) of which their orthologs are unclear. In the mouse, these function to remodel the placenta and maternal vasculature and are required for successful pregnancy (Moore & Dveksler, 2014). Although clearly functionally related to pregnancy, largely their specific roles remain undefined (Roberts et al., 2016).

Prolactin (PRL) is another key hormone in mammalian pregnancy and again focuses on regulating maternal resources. In humans it is heavily involved in lactation (Bole-Feysot et al., 1998; Johnson, 2010). Like hPL, prolactin levels increase gradually throughout pregnancy. Foeto-placental steroids block prolactin at the mammary gland until parturition when the sudden reduction in foeto-placental steroids induces milk secretion (McNeilly, 1975). Prolactin stimulates hyperphagia which leads to an increase in food supply for the foetus during gestation and via lactation after gestation (Gerardo-Gettens et al., 1989; Ladyman et al., 2010; Marshall et al., 2024; Sauv e & Woodside, 1996). Leptin usually inhibits food intake, however during pregnancy high prolactin levels produce central leptin resistance, allowing fat stores to accumulate (Augustine & Grattan, 2008; Naef & Woodside, 2007). During gestation, prolactin levels importantly increase around the maternal pituitary gland and act on the hypothalamus, amygdala and brainstem which all express prolactin receptors (Brown et al., 2010; Grattan & Ladyman, 2020; Kokay et al., 2018; Pi & Grattan, 1998a, 1998b). hPL also binds the prolactin receptor at equal affinity to prolactin and both hormones induce high levels of prolactin receptor activation in the brain throughout gestation (Grattan & Ladyman, 2020).

Human and mouse prolactin is derived from a common ancestral gene (Simmons, Rawn, et al., 2008). Human prolactin is synthesised in the anterior pituitary gland and uterine decidua (Handwerker & Brar, 2001) from a single PRL family gene (Cooke & Liebhaber, 1995; Riddle et al., 1933; Soares, 2004), where mouse prolactin-like hormones, of which there are twenty-two family members (Soares, 2004; Soares et al., 2007; Soares & Linzer, 2001), contain one-megabase segment (Wiemers et al., 2003) and are produced in the placenta (Astwood & Greep, 1938; Creeth & John, 2020; Georgescu et al., 2021; Rawn et al., 2015). Prolactin is involved in parental behaviour for a broad range of animals from fish to birds to mammals (Bole-Feysot et al., 1998). Its involvement in maternal behaviour has been heavily investigated in the rodent model (Bridges et al., 1985; Bridges et al., 1990; Bridges et al., 1997). In the mouse model, prolactin related hormones and steroids have been implicated in the role of programming maternal care (Creeth & John, 2020). Despite the wide range of prolactin-like hormones in the mouse model, it is hard to identify distinct roles for specific family members, as it seems there is inbuilt functional redundancy in the system (Ain et al., 2004; Green, 2004). That being said, Prl3d1 and Prl3b1 have been identified as highly expressed, functional members of the family (Rawn et al., 2015), with Prl3d1-3 spiking at mid-gestation and Prl3b1 becomes dominant in the second half of pregnancy (Soares, 2004). Due to their similarity in roles and their origins of secretion for the purposes of this study the Human hormone of interest will be hPL and the mouse model counterpart will be the family of prolactin-like hormones.

1.6 The importance of studying placental lineages: The placental programming hypothesis and placental endocrine insufficiency

The placenta is a temporary organ which develops for the purpose of inducing and maintaining a pregnancy and is then discarded. The predominantly understood function of the placenta is to provide nutrients for the foetus throughout the pregnancy, tailored to the different phases of foetal development (Benirschke, 2004; Burton & Fowden, 2015; Costa, 2016; Gude et al., 2004). Placental research is heavily weighted towards the foetus (Grattan & Ladyman, 2020), however, largely overlooked is the presence of a second organism within this system, the mother (D'Alton et al., 2019; Guttmacher et al., 2014; Smith, 2023). The mother is also present during the different phases of foetal development and is exposed to the hormone fluctuations produced by the placenta. This is not an unintentional relationship as placental hormones have a targeted and

purposeful role in preparing the mother for motherhood through the release of these hormones (Creeth & John, 2020).

An early concept regarding pregnancy's capacity to impact adult health is known as "foetal programming" (Barker, 1995). Barker's hypothesis links the conditions during foetal development to long-term health risks, initially linking low birth weight to cardiovascular disease (Barker, 1995; Barker & Osmond, 1986; Faa et al., 2024). The hypothesis had its critics in the lack of causation between the statistical evidence and poor health outcomes (Lancet, 2001; Paneth & Susser, 1995). To void the gap between correlation and causation the "placental programming hypothesis" was devised and develops the hypothesis one step further in establishing the link. The placental programming hypothesis concerns the association between placental abnormalities and adverse outcomes for both the mother and foetus (Barker et al., 1990; Creeth & John, 2020; Dicke & Henderson, 1988; Hales & Barker, 2013). Importantly, evidence points to the placenta's ability to adapt to environmental cues and maternal signals (Creeth & John, 2020) both of which shape the structure and ultimately the function of the placenta, putting the placenta in the position of the conductor to this finely tuned system.

In extreme circumstances, placental malformations are correlated with death for both mother and foetus (Wada et al., 2023), but in less severe cases a variety of maladies can develop that may not be immediately attributed to the placenta. For the foetus, the immediate risks of placental disfunction are complications such as intrauterine growth restriction (IUGR) (Sharma et al., 2016) or small for gestational age (SGA) (Dicke & Henderson, 1988; Sharma et al., 2016), and LGA (Hong & Lee, 2021). The long-term health consequences for the resulting offspring are disorders such as cardiovascular disease (Aye et al., 2017; Barker, 1991; Barker, 1995; Barker & Osmond, 1986), neurodevelopmental disorders (Sharma et al., 2016), diabetes (Hales et al., 1991; Hales & Barker, 2013), obesity (Hong 2021), and hypertension (Aye et al., 2017; Barker et al., 1990).

For the mother, placental malformations during pregnancy are linked to diseases such ischemic placental disease (IPD), which includes pre-eclampsia, SGA and placental abruption (Ananth et al., 2010; Parker et al., 2015), hypertension (Aye et al., 2017), and gestational diabetes mellitus (GDM) (McIntyre et al., 2019). The mother's enduring risks are cardiovascular disease (Aye et al., 2017), type two diabetes (Diaz-Santana et al., 2022) and mental health issues (depression and anxiety) (Creeth & John, 2020). These mental health issues in turn project poor maternal care for the resulting offspring and poor child to mother interactions (Creeth & John, 2020). The mother's poor maternal care behaviour also produces long-term consequences for the offspring (Alves

et al., 2022), such as attention deficit/hyperactivity disorder (ADHD), phobias, panic disorders, substance abuse, alcohol dependence, autism, schizophrenia, anxiety, and depression (Bernard-Bonnin et al., 2004; Creeth & John, 2020; Lahti et al., 2015; Levine et al., 2015; Serati et al., 2017; Wiles et al., 2006).

Placenta development studies have identified a key role for imprinted genes (discussed in section 1.8) in the regulation of placental lineages (Creeth & John, 2020; Fowden et al., 2006; Hanna, 2020). These alter the structure of the placenta and in turn influence the functionality of the placenta (Creeth & John, 2020). The concept that imprinted genes could regulate placental development came at the convergence of two key models. Firstly, evolutionary biologists proposed the “parent-offspring conflict” theory which detailed the misalignment between the genetic interests of the mother and the father/offspring (Trivers, 1974). Soon after, genetic experiments revealed that the maternal and paternal genome was not equal (McGrath & Solter, 1984; Surani & Barton, 1983; Surani et al., 1987) resulting in the development of the imprinted gene model (section 1.1) (Reik, 1989; Solter, 1988; Surani et al., 1988). These two ideas allowed evolutionary biologist Professor Haig, to suggest that the parent offspring conflict could play out in paternally and maternally inherited alleles (Haig & Graham, 1991; Haig & Westoby, 1989) which was quickly supported in studies of the genomic imprinting of *Igf2* in mice (Barlow et al., 1991; Haig & Graham, 1991).

Imprinting centres generate imprinted domains (Fitzpatrick et al., 2002; Lin et al., 2003; Shiura et al., 2009; Thorvaldsen et al., 1998) and regulate cell growth of the various placental cell types (Creeth & John, 2020). The endocrine lineage is a region of the placenta that adjusts in size with variations in these genes (Creeth & John, 2020), ultimately becoming a proxy regulator of placental hormone levels. In addition, expression of these genes has been linked to depression and anxiety (Janssen, Capron, et al., 2016), indicating their role in the placental programming hypothesis system and their link to maternal mental health outcomes.

Environmental factors impact the formation of the placenta. Factors such as diet, stress, obesity, and smoking can cause mis-formation of the placenta, again contributing to its functionality. It is hypothesised that the response to the environment is enacted by these imprinted genes (Creeth & John, 2020). Stress may influence the expression of these imprinted genes, resulting in a structural and functional response in the placenta and ultimately maternal mental health consequences (Creeth & John, 2020).

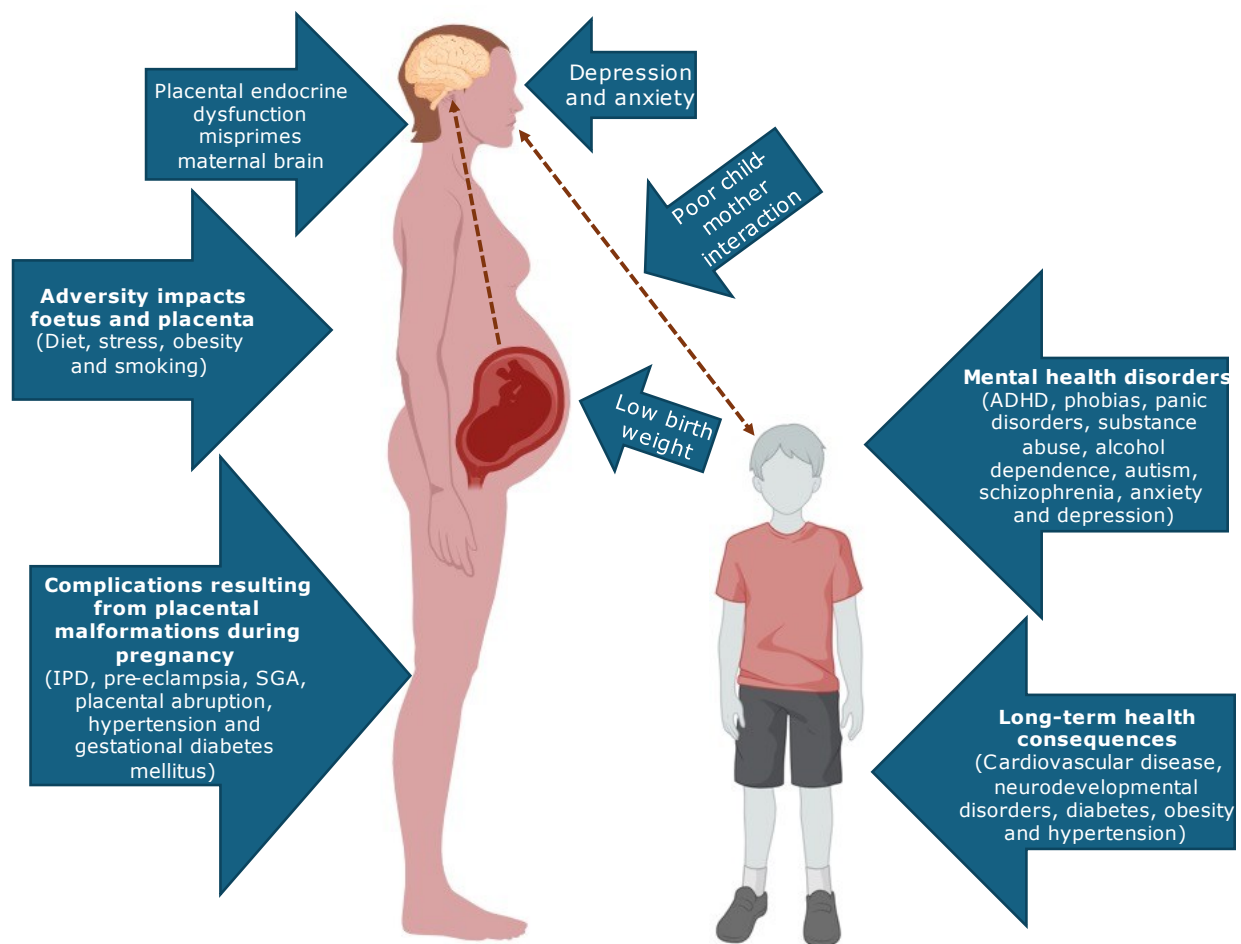


Figure 5: Placental programming hypothesis and placental endocrine insufficiency.

Adversities during pregnancy impact both the mother and the foetus. Adversities cause dysfunction of the placental structure. Malformation of the placenta impacts the nutrient supply to the foetus resulting in low birth weight. Malformations to the endocrine lineage of the placenta disrupt appropriate hormone exposure to the maternal brain, causing a lack of preparation for maternal care and resulting in depression and anxiety. Mother and child relationships burdened by maternal mood disorders cause further poor outcomes for offspring. Adapted from: Creeth and John (2020).

Combining the environmental and genetic components into one picture we have the "placental endocrine insufficiency hypothesis" (Creeth & John, 2020). It is theorised that placental hormones are the acting agent in the system of the placental programming hypothesis (Creeth & John, 2020). This research project will focus on genetic regulation of the endocrine lineage of the placenta and the impact that has on hormone production.

1.7 The real-world impact: Maternal anxiety and depression

A previously overlooked symptom of pregnancy is the impact pregnancy has on maternal mental health. Throughout history, female descriptions of depression (along with other female maladies) were deemed to be hysterical (Jackson, 2019; Ussher, 2011; Young et al., 2018) and were not considered as a serious medical issue by the medical community until the feminist movement of the 1960s increased recognition of health issues faced exclusively by women (Health, 2021; Jackson, 2019). Mental health issues such as anxiety and depression are now being recognised as one of the most common co-morbidities of pregnancy (Chauhan & Potdar, 2022). Depression and anxiety affect 12% and 15% of pregnant women respectively, often presenting simultaneously (NICE, 2020).

Confounding the diagnosis of maternal mental health complications, perinatal mental health disorders are not as commonly identified as postpartum disorders (Chauhan & Potdar, 2022). The Diagnostic and Statistical Manual of Mental Disorders (DSM) did not recognise the perinatal onset of depression until DSM 5 in 2013 (Munk-Olsen et al., 2016), previously using "postpartum onset" as a classifying descriptor. With clinical studies being hesitant to include pregnant people (Fox, 2023; Zhao et al., 2021), identifying symptoms, diagnosis and treatment of perinatal depression is impaired, resulting in a culture of insufficient identification and inadequate treatment (Cox et al., 2016; Munk-Olsen et al., 2016; Shorey et al., 2018). In a study on self-reported anxiety, the prevalence in the first trimester was 18%, 19% in the second trimester and 25% in the third trimester, where the postpartum rate was 15% (Dennis et al., 2017). The postpartum rate was comparable to incidents of clinical diagnosis for all time onsets which was also 15% (Dennis et al., 2017). The rates reported during gestation suggest an increase in risk during pregnancy, with a comparable to normal occurrence postpartum, supporting the notion of an under diagnosed pregnant populace, resulting in an under treated population for perinatal mental health issues (Cox et al., 2016; Dagher et al., 2021).

Another reason why symptoms can be hard to identify in this population is because a change in the physiology of a pregnant person is expected during pregnancy. These "expected/normal" changes can be similar to those seen in people entering depressive states, for example normal changes during pregnancy affect sleep patterns and eating behaviours. This makes an "abnormal" change more difficult to recognise. Perinatal depression symptoms range from changes in sleep patterns and appetite to difficulty concentrating, persistent feelings of sadness or excessive worry and fear, reduction in energy, lack of interest in daily activities, feelings of guilt, hopelessness, worthlessness, and suicidal thoughts

(Association, 2013; Cox et al., 2016; Dagher et al., 2021). The symptoms of perinatal mental health illnesses present at various intensities and various times during gestation. They have a variety of subcategories which highlights the requirement for tailored care. For perinatal depression, the distinct categories present as anhedonia, anxious anhedonia, severe and moderate anxious depression and resolved depression (Putnam et al., 2017). Appropriate screening tools are required to identify changes that should be considered as a concern (Cox et al., 2016; Dagher et al., 2021).

Current treatments involve therapy, social support, and medication (Cox et al., 2016). However, the use of antidepressants during pregnancy is a complicated issue (Isoherranen & Thummel, 2013; Lupattelli et al., 2014). Again, pregnant people being excluded from clinical trials means that antidepressants are not commonly approved to be used while pregnant and most data around use comes from post-market surveillance rather than pre-clinical trials (Besag & Vasey, 2023; Cooper et al., 2007; Coverdale, 2008; Rahimi et al., 2006; Smolina et al., 2015; Stock & Norman, 2019; Tanguay et al., 2023; Udechuku et al., 2010). Hesitation from pregnant women to enter clinical trials exacerbates this issue (Zhao et al., 2021), despite many pregnant women identifying the lack of available treatments (Zhao et al., 2021). All of these issues create a difficult environment to get a clear picture of the true risks to the foetus from exposure to antidepressants (Besag & Vasey, 2023; Cooper et al., 2007; Coverdale, 2008; Rahimi et al., 2006; Smolina et al., 2015; Stock & Norman, 2019; Tanguay et al., 2023; Udechuku et al., 2010). Although advice suggests making decisions on an individual basis, when balancing the risk of exposing the foetus to antidepressants against the risk of an unmedicated depressed pregnant woman, the literature favours the use of antidepressants (Molenaar et al., 2018; Muzik & Hamilton, 2016). Although the effect of antidepressants on the foetus is poorly understood and not without risk (Besag & Vasey, 2023; Cooper et al., 2007; Coverdale, 2008; Rahimi et al., 2006; Tanguay et al., 2023; Udechuku et al., 2010), the complications resulting from the unmedicated depressed pregnant woman are known and potentially severe, including the resulting consequences to the foetus (Muzik & Hamilton, 2016).

To detail these complications, depression during pregnancy has been associated with increased rates of premature birth (Girchenko et al., 2022; Mochache et al., 2018), spontaneous preterm labour (Dayan et al., 2002), a higher rate of low birthweight (Diego et al., 2006; Girchenko et al., 2022), increased rates of placental abnormalities (Lahti-Pulkkinen et al., 2018; Saeed et al., 2024), and preeclampsia (Girchenko et al., 2022). An important distinction that has recently been highlighted is the correlation between the use of antidepressants and the risk of

miscarriage/spontaneous abortion. It was previously believed that antidepressants could cause spontaneous abortion, however this was in comparison to the rates of spontaneous abortion in the “non-depressed” public. When comparing to the rates of spontaneous abortion for “medicated depressed mothers” versus “non-medicated depressed mothers”, the medicated population has a reduced rate of spontaneous abortion (Kjaersgaard et al., 2013) indicating that the spontaneous abortion symptom is attributed to the depression itself (Magnus et al., 2021; Wang et al., 2021) rather than the antidepressants.

The foetus also suffers long-term physiological consequences from a pregnancy complicated by depression, such as growth restriction (Girchenko et al., 2022). In addition, the mental health impacts on the mother cause a significant decline in her capacity to provide maternal care (Bernard-Bonnin et al., 2004; Stolzenberg & Champagne, 2016), compounding the consequences for mother and child. The mother is more at risk of postnatal depression (Blom et al., 2010; O'Hara, 2009), which can lead to bonding issues with the child (Lutkiewicz et al., 2020). Although it has been determined that the lack of bonding itself does not cause further problems with the offspring (Fransson et al., 2020), poor bonding can result in difficulties surrounding caregiving (Kerstis et al., 2016; Lyons-Ruth et al., 1990; Martins & Gaffan, 2000; Moehler et al., 2006; Murray, 1992). The children of depressed mothers are at higher risk of cognitive impairment (Rogers et al., 2020; Santos et al., 2024), behavioural issues (Beardslee et al., 1983; Cummings & Davies, 1994; Hayes et al., 2013; Keller et al., 1986; Rogers et al., 2020; Rosenthal et al., 2018), and their own mental health risks (Girchenko et al., 2022; Rosenthal et al., 2018). These complications are seen into adolescence and can affect the following generation (Rogers et al., 2020; Rosenthal et al., 2018).

Although not largely recognised, the scale of this issue is far reaching and has significant implications on current health systems and future generations. A 2017 study estimated that the cost of these conditions in the United Kingdom (UK) was around £6.6 billion per year (Bauer et al., 2016). A former UK Prime Minister promised £290 million investment over 2016-2021 into specialist perinatal mental health care for mothers before and after childbirth (Cameron & Hunt, 2016) and further funding contributing to women’s health hubs has been promised (Barclay, 2023) as some recognition around medical misogyny has been identified by the UK government (Women and equalities committee, 2024).

It has been proposed that the hormones produced by the placenta play a role in maternal mental health. It is theorised that placental lactogens target the maternal brain and alter its structure (Grattan & Ladyman, 2020), allowing for the mother to prepare for motherhood (Stolzenberg &

Champagne, 2016). Any form of disruption to this process, mis-primes the maternal brain and results in mental health complications. This is where this thesis's research ties in. The genes investigated in this project have an impact on the endocrine lineage of the placenta, regulating the maternal brain's hormone exposure and influencing the maternal mental health.

1.8 Imprinted genes regulation of the placenta

1.8.1 IC1/IC2 Domain and KvDMR1: Imprinting control regions

The rates of meiotic recombination in certain regions of DNA demonstrate a sex bias depending on the gamete. This pattern suggests that there are extended regions of open chromatin specific to either the sperm or the egg. These open chromatin regions are accessible to epigenetic machinery which determine the expression of the genes within the region, which allows the formation of large sections of imprinted genes also known as ICs (Thomas & Rothstein, 1991). Mouse and human have highly conserved regions of ICs (Carrion et al., 2023; Engemann et al., 2000; Taniguchi et al., 1997). For humans, an IC functionally related to the placenta is located on chromosome 11p15.5 (Taniguchi 1997) whereas in mice this clusters homologous region is on mouse distal chromosome 7 (Ferguson-Smith et al., 1991; Searle & Beechey, 1990). These clusters are known as IC1 and IC2. IC1 contains maternally expressed non-coding RNA *H19* and paternally expressed protein coding *Ins2* (Deltour et al., 1995) and *Igf2* (DeChiara et al., 1991; Ferguson-Smith et al., 1991) within a 100 kilobase region. The 800 kb domain that is IC2, contains maternally expressed protein coding genes such as *Ascl2/Mash2*, (Guillemot et al., 1995) *Cdkn1c* (Hatada & Mukai, 1995) and *Phlda2* (Qian et al., 1997). An interesting DMR within the IC2 domain is KvDMR1(KCNQ1OT1 transcript Voluntary differentially methylated region 1) (Bielinska et al., 2000). This region was identified during research surrounding Beckwith-Wiedemann syndrome, which revealed the methylation status of KvDMR1 to be the cause of the disease (Choufani et al., 2010; Gomes et al., 2009; Reik & Maher, 1997). KvDMR1 is maternally methylated (Figure 6). The region contains an antisense RNA transcript *Kcnq1ot1*, which is located within intron 1 of *Kcn1q*. This antisense RNA regulates at least six neighbouring genes (Fitzpatrick et al., 2002). Biallelic expression of *Kcnq1ot1* results in biallelic expression of genes upstream and downstream of KvDMR1 that are usually maternally expressed (Bourc'his et al., 2001; Hata et al., 2002; Kaneda et al., 2004). The genes affected are *Ascl2*, *Cdkn1c*, *Slc22a1* (*Impt1/Orct12/Tssc5*), *Tssc4*, *Kcnq1* (contains the KvDMR1 element within

intron 1) and *Phlda2* (a.k.a. *Ipl/Tssc3*) (Fitzpatrick et al., 2002; Salas et al., 2004).

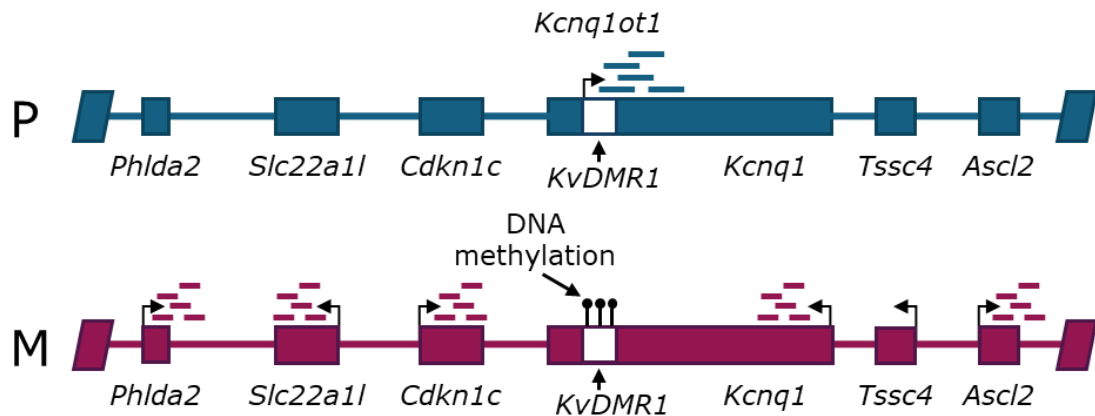


Figure 6: Schematic of KvDMR1 imprinting control region.

Paternal chromosome (P) expresses the *Kcnq1ot1* antisense RNA transcript which depresses six surrounding genes *Phlda2*, *Slc22a1*, *Cdkn1c*, *Kcnq1*, *Tssc4* and *Ascl2*. *Kcnq1* on the maternal chromosome (M) is methylated and does not express *Kcnq1ot1* resulting in the neighbouring genes expression. Adapted from Fitzpatrick et al. (2002); Salas et al. (2004).

The deletion of the KvDMR1 region on the paternal allele resulted in lighter placenta and lighter embryos, 50-20% smaller than their littermates (Fitzpatrick et al., 2002). Considering that the *Kcn1q* antisense has multiple upstream and downstream targets, further studies were undertaken to determine which related element was responsible for this consequence. Many of the targets have been thoroughly investigated and have been revealed to be involved in placental development. For example, *Cdkn1c* plays a role in suppressing proliferation whilst promoting differentiation in a variety of tissues. Overexpression of *Cdkn1c* in mice results in growth restricted embryo phenotypes (Andrews et al., 2007). A knockout model for *Cdkn1c* shows placentomegaly, where the endocrine lineage is expanded. This model also has an increase in premature birth and preeclampsia (Kanayama et al., 2002; Takahashi et al., 2000). *Cdkn1c* fits the functional imprinting pattern described in

Figure 1, as it is maternally expressed, paternally silenced and functions to restrain placenta development and foetal growth. *Ascl2* plays a similar role, despite only being imprinted in the placenta and not being imprinted in the foetus. Overexpression of *Ascl2* produces foetal growth restrictions alongside a reduction in the development of multiple endocrine lineages of the placenta (Tunster, Creeth, et al., 2016). A complete knockout of *Ascl2* is fatal for the embryo resulting in development only up until E9.5 (Guillemot et al., 1995), where a partially rescued expression knockout

model produces foetal growth restrictions and placental defects (Bogutz et al., 2018). This demonstrates the *Asc/2* is sensitive to dosage where only a single copy produces a functional placenta. One of the remaining targets of KvDMR1 is a gene of interest in this thesis's research project and will be discussed in detail in the following section.

1.8.2 Pleckstrin homology like domain family A member 2 (*Phlda2*)

Novel imprinted genes were sought after on chromosome 11p15.5 where a known IC had been identified (Qian et al., 1997). At the time this was defined as "consistent allelic bias" in RNA expression. In human, exon trapping identified a 200 bp putative exon sequence which matched a partial cDNA sequence or expressed sequence tag (EST) in an EST database. Using Northern blotting a 0.8 kilobase (kb) RNA sequence was identified in the human placenta. Placental cDNA library screening recovered a 770 bp cDNA sequence which contained a 152 amino acid open reading frame. Upstream of the cDNA sequence contained a C/G rich sequence with a TATA motif, indicating a promoter region for the gene. This cDNA sequence was then used to map the protein and a basic local alignment search tool (protein) (BLAST(P)) identified highly similar mouse and human proteins. This was the first identification of human *PHLDA2*, which was initially referred to as *IPL* (Imprinted in Placenta and Liver) (Qian et al., 1997). The mouse homolog was searched for by screening the EST databases to identify cDNA sequences similar to the human *IPL* (Qian et al., 1997). This identified a 749 bp cDNA sequence with an open reading frame of 144 amino acids, in which a TATA box was identified 12 bp upstream, indicating the genes promoter. This gene was localised to the distal region of chromosome seven which is homologous to the human chromosome 11 region, both of which contain homologs of other imprinted genes such as H19, further suggesting this was human *IPL*'s murine homolog. This mouse transcript was found to be expressed in the placenta, foetal liver and adult kidney of the mouse, demonstrating that the mouse *IPL* is more prominently expressed in tissues outside of the placenta than the human *IPL*, whilst both mouse and human homologs are strongly present in placental tissues of each species (Qian et al., 1997).

To ascertain if this newly identified gene was imprinted, maternal and paternal alleles were distinguished using sequence polymorphisms. For human, at position 93 of the cDNA an Alu I restriction site was created by a T to C polymorphism which did not alter the protein sequence. In testing placenta, foetal and adult tissue samples, expression was consistently biased towards the maternally allele, confirming Human *PHLDA2*'s imprinting status and identifying which allele was imprinted (Qian et al., 1997). For mouse, a neutral A to C polymorphism was used

at position 218. The allele expression pattern again revealed a maternal expression bias (Qian et al., 1997). Notably the murine *Ipl* demonstrated tissue and temporal specific “leakiness” of the imprinted gene (Qian et al., 1997). The imprinting mechanism was found to be regulated through KvDMR1 as described in section 1.8.1 (Fitzpatrick et al., 2002; Salas et al., 2004). To summarise this finding, *IPL* or *PHLDA2* as it will be referred to here, is expressed in the placenta of both human and mice (Qian et al., 1997) and is a maternally expressed and paternally silenced gene in both species (Qian et al., 1997).

The PHLDA2 protein contains a single pleckstrin homology (PH) domain with short N and C terminal extensions (Saxena et al., 2002). The N and C terminal extensions do not have identified functional motifs (Saxena et al., 2002). The PH domain is a molecule containing around 100 amino acids which forms a protein structure described as a β -sandwich of 3 + 4 stranded β sheets and contains variable intervening loops and one amphipathic α helix. This structure functionally creates a binding pocket on the surface of the protein which allows the protein to interact with other molecules (Lemmon & Ferguson, 1998). The molecules that the PH domain commonly binds to are phosphatidylinositol phosphate lipids (PIPs), and PHLDA2’s PH domain specifically has a poor selectivity and moderate affinity to phosphatidylinositol 4,5-bisphosphate (PIP2) and phosphatidylinositol 3,4,5-triphosphate (PIP3) (Frank et al., 2002; Saxena et al., 2002). An image of PHLDA2 protein structure can be seen in Figure 7.

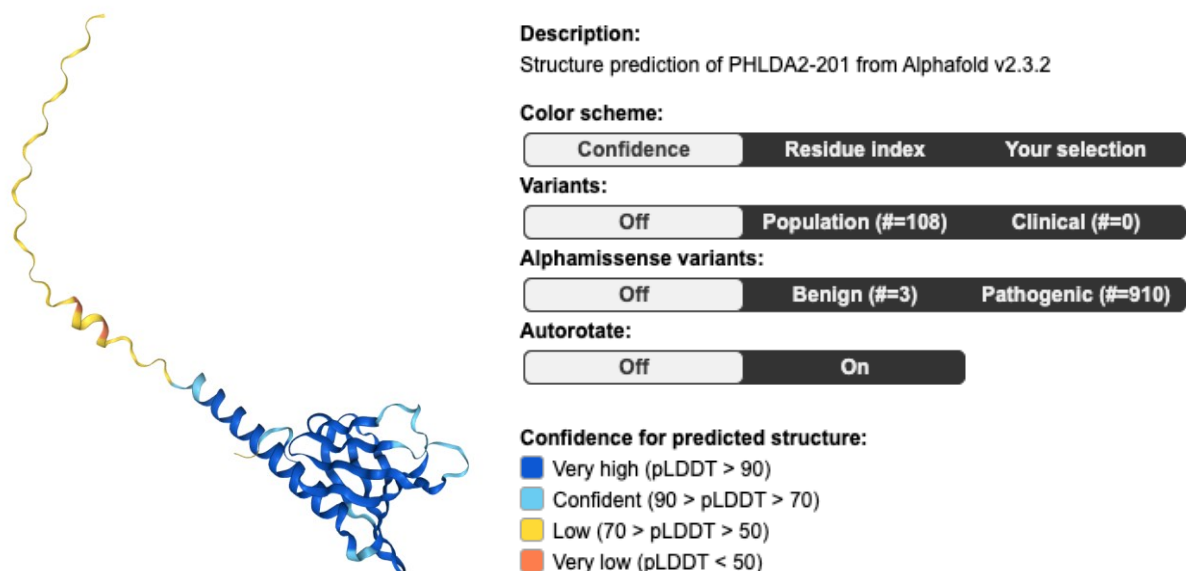


Figure 7: PHLDA2 protein structure.

Image from The Human Protein Atlas: PHLDA2 (2025).

In relation to cellular function, PHLDA2 appears in cancer research due to its role in regulating cell proliferation and apoptosis (Lee & Feinberg,

1998; Müller et al., 2000; Xiao et al., 2021; Yang & Gu, 2024; Zhao et al., 2018). In fact, PHLDA2 goes by another name, tumour suppressor STF cDNA3 (TSSC3) (Lee & Feinberg, 1998). PHLDA2 is primarily localised to the cell cytoplasm (The UniProt, 2025) and is regulated by epidermal growth factor receptor (*EGFR*)/erythroblastosis oncogene B (*ERBB2*) signaling, which functions to inhibit cell proliferation when PHLDA2's PH domain competes with the PH domain of protein kinase B (AKT) for binding to membrane lipids (Wang et al., 2018). When PHLDA2 concentrations are high, PHLDA2 blocks AKT from attaching to the cell membrane and activating the phosphatidylinositol 3-kinase (PI3K)/AKT pathway, which reduces cell growth (Wang et al., 2018). When PHLDA2 concentrations are low, AKT increases its activity which results in faster cell proliferation (Wang et al., 2018). PHLDA2's cell proliferation role is also governed by its regulation over the cell cycle. Overexpression of *PHLDA2* causes cells to arrest at quiescent cell cycle phase, with an increase in cells in the Gap (G)0/G1 phase (Jin et al., 2015). *PHLDA2* overexpression also causes a decrease in the ratio of cells in synthesis (S) phase, meaning less cells are preparing to divide (Jin et al., 2015). Cyclin E and Cyclin D1 proteins which regulate the progression from G1 to S phase were significantly decreased in the *PHLDA2* overexpressing cells suggesting that PHLDA2 inhibits them. A knockdown model was also used to determine how PHLDA2 regulates cell cycling. The *PHLDA2* knockdown increased the ratio of cells in S phase whilst decreasing the cells in G0/G1 phase (Jin et al., 2015). These results suggest that high expression of *PHLDA2* halts the cell cycle to inhibit trophoblast cell proliferation (Jin et al., 2015) while low *PHLDA2* encourages cell cycling and cell proliferation. In cell migrations assays *PHLDA2* overexpressing cells demonstrated a reduced capacity for cellular migration (Jin et al., 2015) and *PHLDA2* knockdown cells demonstrated an increased capacity for cell migration and invasion. This suggests that trophoblast cell invasion capacity is regulated by *PHLDA2* which is important for the invasion of the trophoblasts into the maternal uterine wall.

In the gastrulating mouse embryo, *Phlda2* expression is restricted to the most posterior extent of the primitive streak and the lateral mesoderm. These cells derive the lateral and extra-embryonic mesoderm (Dunwoodie & Beddington, 2002). *Phlda2* is also expressed prior to gastrulation in extra-embryonic tissues and after gastrulation in the extra-embryonic mesoderm, ectoderm and endoderm (Dunwoodie & Beddington, 2002). Later in development, *Phlda2* is expressed in the yolk sacs visceral endoderm and in type II trophoblast in the labyrinthine layer of the mouse placenta (Saxena et al., 2003). In humans, PHLDA2 is expressed strongly in VCT cells and is not expressed in the syncytiotrophoblast (Saxena et al., 2003). Weak PHLDA2 expression was identified in cells of the villous mesenchyme (Saxena et al., 2003). The extravillous

trophoblast tissues such as the intervillous trophoblast islands and the cytotrophoblast columns in the basal plate also had weak PHLDA2 expression (Saxena et al., 2003). The expression patterns between mouse and human, suggest that mouse type II labyrinthine trophoblast and human VCT could be homologous structures (Saxena et al., 2003). In the mouse, after E14.5, labyrinth *Phlda2* expression declines as placental growth ceases (Saxena et al., 2003), whereas PHLDA2 was found throughout gestation in human placentas, as the human placenta has a continuous growth throughout gestation and mouse placenta halts around E14.5, this data further underscores *Phlda2/PHLDA2*'s role in cell growth (Saxena et al., 2003).

As per our described model, *Phlda2*'s pattern of imprinting would assume that it will function to constrict foetal growth and maternal investment. In mice, *Phlda2* was originally identified as regulating glycogen cells which impacted the junctional zone (Frank et al., 2002; Salas et al., 2004). This theory was further developed when it was found that *Phlda2* negatively regulates expansion of the spongiotrophoblast lineage which is a key component of the junctional zone (Tunster et al., 2010). Increased expression of *Phlda2* in the mouse model causes a reduction in the size of the spongiotrophoblast lineage, a reduction in glycogen at E14.5, E16.5 and E18.5 and a foetal growth restriction (Tunster et al., 2014). This aligns with the human system where elevated levels of PHLDA2 have been linked to foetal growth restriction (Apostolidou et al., 2007; Ishida et al., 2012; McMinn et al., 2006). Through studies on *Phlda2* dosage, it was found that *Phlda2* produces the maximum alteration in the placenta with one extra dose. The two-fold *Phlda2* (*2xPhlda2*) phenotype mis-localises the glycogen cells into the labyrinth which occurs later in gestation (E16.5). Normal *Phlda2* levels prevent this mis-localisation which suggests that *Phlda2* provides a mechanism to direct nutrient supply to the foetus when it requires its highest resources, this maximises the maternal resources and enhances growth (Tunster et al., 2010). *Phlda2* knockout (*Phlda2^{KO}*) models show a threefold increase in placental glycogen (Tunster, Creeth, et al., 2016). Although, *Phlda2^{KO}* increases the size of the placenta via expansion of the spongiotrophoblast lineage, foetal weight is still reduced compared to a fully WT litters with both mutant and non-transgenic fetuses lighter (Tunster, Creeth, et al., 2016) likely due to the role *Phlda2* plays in the location of glycogen cells. It was found that of the components regulated by KvDMR1, 50% of the growth retardation can be attributed to *Phlda2* (Frank et al., 2002; Salas et al., 2004).

It has been experimentally demonstrated that the regulation of the spongiotrophoblast is a proxy for regulating hormone production, with larger spongiotrophoblast producing an increase in the level of hormones

and smaller spongiotrophoblast cells producing a lower level (John, 2022; John et al., 2022). This can be seen in studies surrounding *Phlda2* dosage. *Phlda2*^{KO} placentas show an increase in expression of multiple Prl family members including *Prl3b1*, Prolactin family 8 subfamily A member 8 (*Prl8a8*) and *Prl2c* (Tunster, Creeth, et al., 2016), whereas *2xPhlda2* placenta have a reduction in *Prl3c1*, *Prl7a2*, *Prl8a1*, *Prl8a9*, *Psg17*, *Pgs18*, *Psg19* and *Psg21* (Tunster, Creeth, et al., 2016). In human studies, high *PHLDA2* expression is negatively associated with hPL levels in the maternal serum (Janssen, Tunster, et al., 2016), meaning that high *PHLDA2* expression is present in mothers with lower levels of hPL and low *PHLDA2* expression is found in mothers with higher levels of hPL. This data fits with the mouse model in suggesting that *PHLDA2* is regulating the hormone producing region of the placenta and in turn regulating hormone levels. There have been studies which have linked an increase in placental size to an increase in hPL, however the *PHLDA2* expression for these placentas was not tested and neither was the exact cell type which caused the increase in placental size (Lopez-Espinoza et al., 1986; Ramos-Román, 2011; Rassie et al., 2022; Ursell et al., 1973) This fits into the placental endocrine insufficiency model discussed in section 1.6, as hormone concentration is suggested to be the active agent in regulating parental investment.

During pregnancy, changes to the maternal brain are seen as a normal part of preparation for maternal behaviors in humans (Section 1.5) (Brunton & Russell, 2010; Hoekzema et al., 2017). It has been demonstrated experimentally that these brain alterations are a result of the action of placental hormone exposure (Section 1.5) (Grattan, 2011; Grattan & Ladyman, 2020). In mouse studies, changes in the hippocampus and hypothalamus were altered by varying doses of *Phlda2* (Creeth et al., 2018). These changes were identified in wild type mothers carrying fetuses of either *2XPhlda2* or *Phlda2*^{KO} genotypes compared to WT control litters. Once these pups were born, WT mothers carrying *Phlda2*^{KO} fetuses exhibited increased maternal caregiving. This presented as decreased nest building, increased self-directed behaviour and increased pup nurturing. The reverse held true, with a reduced maternal behavior exhibited with wild type mothers carrying *2xPhlda2* fetuses. This was described as reduced nursing and grooming, whilst showing an increased investment in nest building (Creeth et al., 2018). These results demonstrate the theory that the foeto-placental unit can influence the maternal behaviour, as *Phlda2* dosage impacts placental hormone levels, this reinforces the theory that placental hormones program the maternal brain (John, 2022). In humans, it is hypothesised that hPL is transported to the brain during pregnancy and acts on receptors in a variety of different brain regions including the hypothalamus (Grattan & Ladyman, 2020) and with humans having an inverse relationship between hPL and

PHLDA2 levels (Janssen, Capron, et al., 2016), it can also be suggested that *PHLDA2* may regulate placental hormones and by proxy human maternal behaviours. High *PHLDA2* expression has also been associated with reduced foetal movement (RFM) pregnancies (Janssen, Tunster, et al., 2016). Placental complications such as pre-eclampsia are defined by trophoblast cell invasion depth (Kadyrov et al., 2003) and *PHLDA2* regulates cell invasion and migration capacity (Jin et al., 2015), suggesting *PHLDA2*'s role in pre-eclampsia. This theory is further underscored by the correlation between low hPL in humans and postnatal depression and anxiety symptoms, again reinforcing the idea that hPL contributes to maternal mood symptoms (Sumption et al., 2020).

Expression of <i>Phlda2</i>	Species	Placental Structure	Hormone concentration	Foetal Growth Restriction	Maternal behaviour
Increased <i>Phlda2</i>	Mouse	Reduction in endocrine layer	Decreased	Yes	Decreased maternal care behaviours
	Human	Unknown	Decreased hPL	Yes	Maternal depression and anxiety linked to low hPL, RFM
Decreased <i>Phlda2</i>	Mouse	Expansion of endocrine layer	Increase in expression of family of <i>Prls</i> RNA	Yes	Increased maternal care behaviours
	Human	Increased placental weight related to higher hPL, linked to <i>PHLDA2</i> undetermined	Increased hPL	Increased CBWCs linked to increased hPL	Unknown

Table 3: Relationships between *Phlda2* expression levels, placenta structure, hormone concentrations, foetal weight, and maternal behaviour for both human and mouse models.

References are in the surrounding text.

A further consequence is the effect on the adult offspring. For both WT and *2XPhlda2* offspring experiencing the altered maternal behavior, anxiety-like symptoms, atypical social behavior, mild depression and reduced cognitive abilities were all exhibited (Harrison et al., 2021). As previously stated, in humans, children from foetal growth restricted

pregnancies exhibit a greater risk of neurological disorders such as ADHD, depression, anxiety and schizophrenia (Bernard-Bonnin et al., 2004; Creeth & John, 2020; Lahti et al., 2015; Levine et al., 2015; Serati et al., 2017; Wiles et al., 2006). These human outcomes mimic the outcomes from the *Phlda2* mouse models and demonstrate a consistent function across the two species, although the specific link between *PHLDA2* levels and offspring consequences in human has not been determined.

This research project paired the paternally silenced, maternally expressed *PHLDA2* against the maternally silenced, paternally expressed gene, *PEG3*, which will be discussed in detail in the following section.

1.8.3 Paternally expressed gene 3 (*Peg3*)

Peg3 was first identified alongside *Peg1* whilst screening cDNA libraries of parthenogenetic embryos compared to control embryos of an equivalent developmental stage to specifically identify paternally expressed genes (Kaneko-Ishino et al., 1995). Both *Peg3* and *Peg1* were not expressed in parthenogenones suggesting their maternal allele was silenced (Kaneko-Ishino et al., 1995). This was confirmed using restriction fragment length polymorphism (RFLP) analysis of C57BL/6J female and *Mus spretus* male crosses resulting in a C57BL/6J x *Mus spretus* filial (F)₁ embryo. This analysis demonstrated that only the *Mus spretus* paternal *Peg3* copy was expressed, confirming that *Peg3* is paternally expressed and maternally silenced (Kuroiwa et al., 1996). This expression pattern was confirmed for E13.5 embryos, neonates and neonate kidneys, liver, lungs and anterior and posterior brain regions, six-month-old adults and their kidneys, liver, lungs, brain and cerebellum (Kuroiwa et al., 1996). In situ hybridisation of E9.5-E12.5 embryos also revealed that *Peg3* is expressed in the hypothalamus, branchial arches, early somites and other mesodermal mouse tissues (Kuroiwa et al., 1996).

Fluorescent in situ hybridisation (FISH) was used to establish *Peg3*'s chromosomal location. Despite not being adjacent to the IC1 and IC2 domains discussed in section 1.8.1, *Peg3* is also located on mouse chromosome seven (Kuroiwa et al., 1996). However, *Peg3* was the first imprinted gene to be localised to the A2-B1 band in the proximal region of chromosome seven (Kuroiwa et al., 1996) as opposed to the region of chromosome seven which houses *Phlda2*, in bands 7F4/F5 at the distal end (Ensembl, 2017; Qian et al., 1997; Searle & Beechey, 1990). As discussed in section 1.8.2, the human homolog for the *Phlda2* region is chromosome 11p15.5 (Qian et al., 1997). Although both *Phlda2* and *Peg3* are located on chromosome seven in the mouse genome, they are not located on the same chromosome in humans. In the human genome, the region identified to contain *Peg3* was chromosome 19 (Ashworth et al.,

1995; Brown et al., 1993; Jansen et al., 1993; Saunders & Seldin, 1990; Stubbs et al., 1996). In order to locate human *PEG3*, researchers used probes for mouse *Peg3* to target human chromosome 19 specific cosmids, which resulted in a region of overlapping cosmids at the proximal end of chromosome 19 with *PEG3*'s location being revealed as 19q13.4 (Kim et al., 1997) which is now listed as 19q13.1-13.3 (The UniProt, 2025). Using an EST database several human cDNA sequences were identified as having significant matches to mouse *Peg3*. Northern blots using a probe derived from the human *PEG3* clone were screened on a variety of human RNA tissue samples, revealing high *PEG3* expression in placenta, testes and ovaries, modest expression in the brain and low expression in the prostate, heart, pancreas, and intestine (Kim et al., 1997). This expression pattern differed most significantly in the brain where it was highly expressed in mouse and moderately expressed in human and the ovary where the mouse had low *Peg3* expression, and the human had high *PEG3* expression (Kim et al., 1997).

To confirm the imprinting status of *PEG3* in human, polymorphisms were searched for across the gene. This revealed one polymorphism, 41 bp from the end of *PEG3*'s open reading frame at codon 1452, which was a guanine (G) to adenine (A) change resulting in an amino acid shift from arginine (AR) to histidine (H). Across 32 placental samples only six individuals were heterozygous for this polymorphism and all of which expressed the paternal allele (Hiby et al., 2001). This pattern was also found to be true in the maternal decidua (Hiby et al., 2001). Human *PEG3* was found to be imprinted when the presence of a differentially methylated CpG-rich region was found to encompass *PEG3*'s promoter (Murphy et al., 2001) suggesting that its allelic expression is regulated by DNA methylation on its promoter (Kim et al., 2012).

Northern blot analysis of the adult mouse brain identified a 9 kb mRNA transcript. The predicted amino acid sequence, which was 1572 amino acids long, contained twelve Cysteine²-Histidine² Krüppel-type zinc finger motifs which were widely spaced (Kuroiwa et al., 1996). Unusually for zinc finger proteins, these were spaced around 30-40 amino acids apart unlike the more common six amino acid spacing (Kuroiwa et al., 1996). Comparing mouse and human sequences revealed that the zinc finger regions are highly conserved between mouse and human at the nucleotide and amino acid level whereas the interfinger spacer regions are not conserved across species (Kim et al., 1997). An image of the *PEG3* protein can be seen in Figure 8. Functionally, individual zinc fingers rest their helical region into the major groove of DNA and amino acid side chains from the helix contact specific bases in the DNA structure at three to four base pairs per zinc finger motif. Multiple zinc fingers in a row allow for recognition of longer or more specific sequences (Iuchi, 2001;

Pavletich & Pabo, 1991). Zinc finger structures are a common structure found on transcription factors as their ability to bind to the major groove of DNA allows them to regulate transcription (El-Baradi & Pieler, 1991; Pieler & Bellefroid, 1994), hence *Peg3/PEG3* has been identified as bona fide transcription factor (Kuroiwa et al., 1996; Relaix et al., 1996). *Peg3* is present in the nucleus at higher levels than it is in the cytoplasm (Deng & Wu, 2000) where it can perform its transcription factor function.

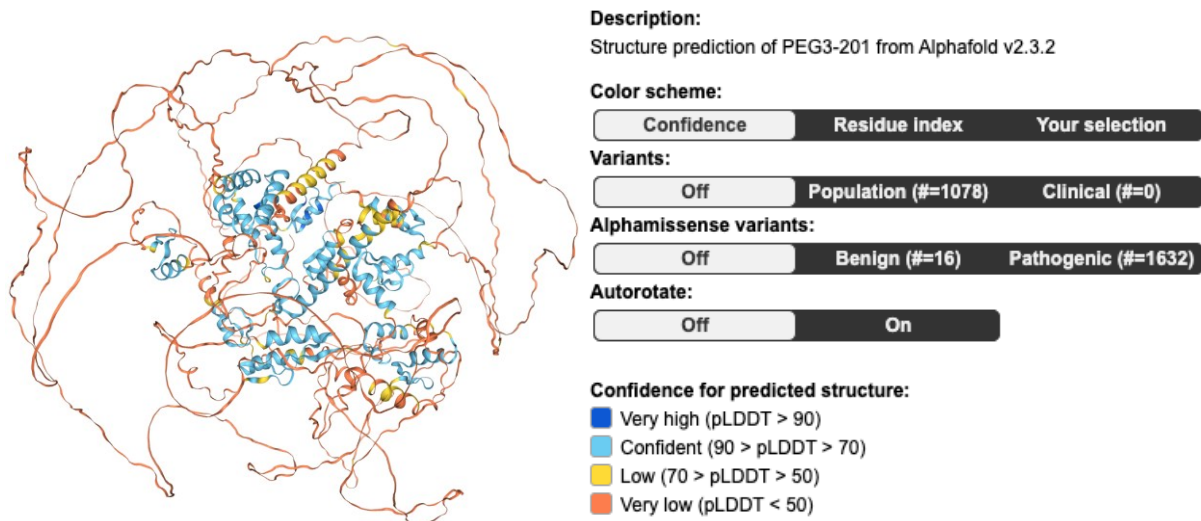


Figure 8: PEG3 protein structure.

Image from The Human Protein Atlas: PEG3 (2025).

A transcription factor's function is to bind to DNA and regulate transcription, which results in an incredibly complex network of follow up interactions and downstream functions. The complete binding domain of *Peg3* was identified as AGTnnCnnnTGGCT (Thiaville et al., 2013). However, *Peg3* was also able to bind TGGCT with its core nucleotide bases (Thiaville et al., 2013). This suggests *Peg3* is able to regulate a wide range of genes and pathways suggesting it's function to be diverse. As the mouse and human sequences are highly conserved across species, they have both been functionally implicated in many of the same pathways, for example, human and mouse *Peg3* have been shown to be involved in the p53 pathway which mediates neuronal death pathway (Deng & Wu, 2000; Relaix et al., 2000; Yamaguchi et al., 2002) by working in co-operation with *Siah1a/SIAH1A* in inducing apoptosis (Relaix et al., 2000). *Peg3* has demonstrated its ability to promote β -catenin degradation, inhibiting the wingless/integrated (Wnt) signalling pathway (Jiang et al., 2010). Thiaville et al. (2013), also demonstrated multiple gene targets of *Peg3* relating to control of mitochondria functions or tissue development (Thiaville et al., 2013). *Peg3* also suppresses the transcription of multiple genes involved in cellular metabolism (Lee et al., 2015; Thiaville et al., 2013). Specific genes which *Peg3* binds to their

promoters or enhancers are *ufm*, *Mrpl45*, *Cry2*, *Per1*, *Slc25a29*, *Slc38a2*, *Slc38a2* and *Slc38a4* of which the latter two are functionally involved in neutral amino acid transport (Lee et al., 2015).

As *Peg3* is a paternally expressed, maternally silenced gene, this expression pattern in relation to the maternal resource conflict hypothesis assumes that this gene promotes placental/ foetal growth and maternal investment. In the mouse placenta, the expression of *Peg3* is from all trophoblast cell types (Hiby et al., 2001). Here, the number of cells of the endocrine lineages are positively regulated by *Peg3*. It is theorised that it functions upstream of *Phlda2* as it influences more cell types, as expansion of both spongiotrophoblast and glycogen cell lineages require *Peg3*. When knocking out *Peg3*, *Peg3^{KO}* placenta possess 50% and 37% fewer spongiotrophoblast cells and 40% and 29% fewer glycogen cells for male and female placenta respectively (Tunster et al., 2018). In humans, *PEG3* expression is localised to the VCT cells from six to twelve weeks gestation making the expression pattern not comparable to the mouse model (Hiby et al., 2001). Placental weight has not been analysed in its relation to *PEG3* expression in human.

Peg3 has been linked to maternal investment. Postnatally, mutant *Peg3^{KO}* dams of wild type litters neglect their pups. Mutant mothers performed worse at the pup retrieval task, had poor nest building skills, demonstrated protective crouching behaviour more slowly and had reduced milk let-down (Li et al., 1999). The maternal behaviour deficit in these mutant dams is so significant that it has an impact on pup survival rates (Curley et al., 2005; Li et al., 1999). The numbers vary between studies but has been shown to have as high of a mortality rate as 92% for mutant dam and mutant litter combinations (Curley et al., 2005). Although this has been argued by further studies that have demonstrated no affection maternal behaviour (Denizot et al., 2016). Atypical maternal behaviour has also exhibited by wild type dams carrying *Peg3^{KO}* mutant pups (McNamara et al., 2018) which demonstrates the role the placenta plays in its action on the mother. For the mouse brain, *Peg3* is expressed in the hypothalamus (Kuroiwa et al., 1996) and hippocampus (Moreno et al., 2022) which are regions that are involved in maternal behaviour (Bicks et al., 2015; Curley et al., 2005). *Peg3^{KO}* mouse brains have reduced oxytocin neurons in the hypothalamus (Li et al., 1999). Many aspects of maternal care have been shown to be regulated by oxytocin and it is theorised that the *Peg3^{KO}* mouse's reduction in oxytocin may cause the maternal care deficits (Bridges, 2015). Some impacted pre-natal behaviours include a reduced maternal food intake during pregnancy (Curley et al., 2005). In humans *PEG3* is also expressed in the hypothalamus (Karlsson et al., 2021) which could indicate that the brain expression pattern is conserved across species.

In mouse, the *Peg3^{KO}* placenta has a reduced spongiotrophoblast lineage (Tunster et al., 2018). The reduced size of the spongiotrophoblast section results in a reduction in the expression of placental hormones from the *Prl* family (Tunster et al., 2018). Microarray studies have shown that *Peg3^{KO}* influences the expression of multiple *Prls* (Broad & Keverne, 2011; Lee et al., 2015; Thiaville et al., 2013). The transcription factor targets of *Peg3* are other imprinted genes such as *Grb10* which plays a role in regulating embryo growth and in the postnatal period mediates nutrient supply and demand (Cowley et al., 2014). *Grb10* is promoted by *Peg3* (Thiaville et al., 2013). A variety of placental hormone genes have reduced expression in *Peg3^{KO}* male placentas such as *Tpbpa*, *Prl8a8*, and *Prl6a1* as well as *Prl8a1* which is reduced in both male and female *Peg3^{KO}* placentas. All of which are reduced by 40-60% compared to control (Tunster et al., 2018). There are some *Prls* which were upregulated in the absence of *Peg3* in female placentas, such as *Psg17* and *Psg19* (Tunster et al., 2018). This is the result of *Peg3s* transcriptional factor status, which demonstrates the complexity of its interaction. Broadly, *Peg3* is thought to have two opposing roles, it functions as a transcriptional repressor (Thiaville et al., 2013) whose targets may include placental hormones, as well as functioning as a positive regulator of endocrine cells (Tunster et al., 2018).

This is all indirect evidence, as the actual levels of placental hormones in the mouse mother has not been determined. In addition, the relationship between *PEG3* and *hPL* in humans has not been directly linked. Diagnosed depression has been associated with a 41% reduction in *PEG3* in humans in which depression scores had an inverse relationship to *PEG3* expression levels in the placenta (Janssen, Capron, et al., 2016). Clinically diagnosed depression was also correlated with 44% reduced expression of *hPL* (Janssen, Capron, et al., 2016). Indirectly, this links low *PEG3* to low *hPL*, low *hPL* to depression and low *PEG3* to depression but does not provide causative evidence (Janssen, Capron, et al., 2016). In relation to the maternal programming/placental endocrine insufficiency hypothesis, this suggests that the low expression in *PEG3* could cause lower hormone production, resulting in lower hormone exposure for the mother which mis-primes the maternal brain and results in maternal depression. That being said, there are many missing pieces to this story, and it is challenging to identify cause or consequence between gene expression and depression in humans (McNamara et al., 2018). In mice, *Peg3^{KO}* has a low-birth-weight phenotype (Li et al., 1999). Indirectly, this provides evidence that the human and mouse are comparable models as the instances of low birth weights in depressed pregnant mothers is significantly higher (Sumption et al., 2020), indirectly linking low *PEG3* expression to low birthweight.

Expression of <i>Peg3</i>	Species	Placental Structure	Hormone concentration	Foetal Growth Restriction	Maternal behaviour
Increased <i>Peg3</i>	Mouse	Unknown	Unknown	Unknown	Unknown
	Human	Unknown	Unknown	Unknown	Unknown
Decreased <i>Peg3</i>	Mouse	Reduced endocrine compartment	Reduced expression of <i>Prl</i> family RNAs, actual concentration unknown	Growth retardation	Impairment of maternal behaviour
	Human	Unknown	Low hPL	Small for gestational age offspring from depressed mothers	Maternal depression

Table 4: Relationships between *Peg3* expression levels, placenta structure, hormone concentrations, foetal weight, and maternal behaviour for both human and mouse models.

References are in the surrounding text.

Peg3^{KO} offspring also had reduced instances of ultrasonic vocalisations (McNamara et al., 2018) which indicates to some degree that the maternal behaviour may be altered by the pups' altered behaviour. Although they are growth restricted at birth, they also engage in less suckling behaviour which at least partially contributes to a growth restriction that persists until adulthood (Curley et al., 2005). As described previously in the *Phlda2* model, the *Peg3* model has long-term impacts on the health of the offspring which again produces similar long-term consequences in humans.

1.9 Antagonistic function: *Peg3* versus *Phlda2*

Upon reflection of the actions of *Peg3* and *Phlda2*, their equal and opposite functions on the placenta, maternal brain and maternal behaviour indicate that they play a reciprocal role to one another. This being heavily underpinned by their opposite expression patterns, with *Phlda2* being maternally expressed and paternally silenced and *Peg3* being paternally expressed and maternally silenced. Their impacts can be visualised as a dial between "maternalisation" and "paternalisation" of the

placenta, the maternal brain, ultimately adjusting the maternal investment into the foetus (Figure 9).

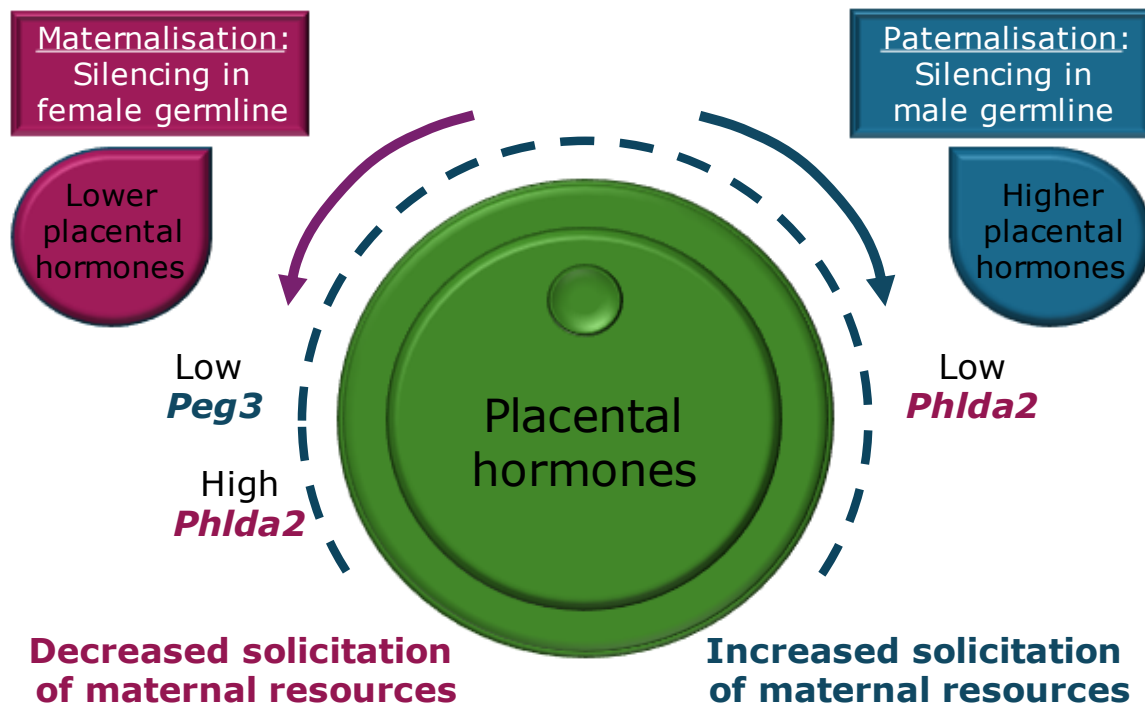


Figure 9: Genomic imprinting adjusts maternalisation or paternalisation

in their antagonistic function to regulate placental hormones which modulate the allocation of maternal resources. Adapted from Creeth et al. (2019).

An opportunity to be able to directly test the relationship between paternally expressed *Peg3* and maternally expressed *Phlda2* is possible with the generation of a knockout model of both genes. This double knockout model will establish if there is a possibility for a “rescue effect” of each knockout by the competing knockout, as they generally affect the placenta in opposing ways. Understanding if the presence of both genes produces a phenotypically similar placenta as the absence of both genes will identify their specific roles within placental development more distinctly. Because *Peg3* influences more cell types than *Phlda2* (Hiby et al., 2001; Tunster et al., 2010)(Figure 10) it is hypothesised that *Peg3* operates upstream of *Phlda2* and earlier in the differentiation of these cell types. This means its function will be performed in the ectoplacental cone and influences spongiotrophoblast, glycogen cells and TGCs, where *Phlda2* acts during the formation of the spongiotrophoblast and later in development of that lineage (Figure 10). The slight discrepancies between the two known roles would suggest that the double knockout model would not produce a complete “recovery” but in which regions and to what extent is unclear.

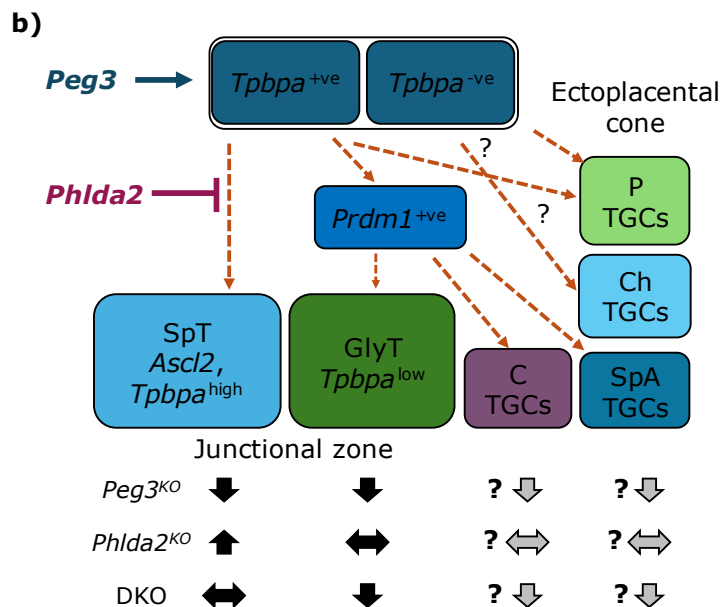
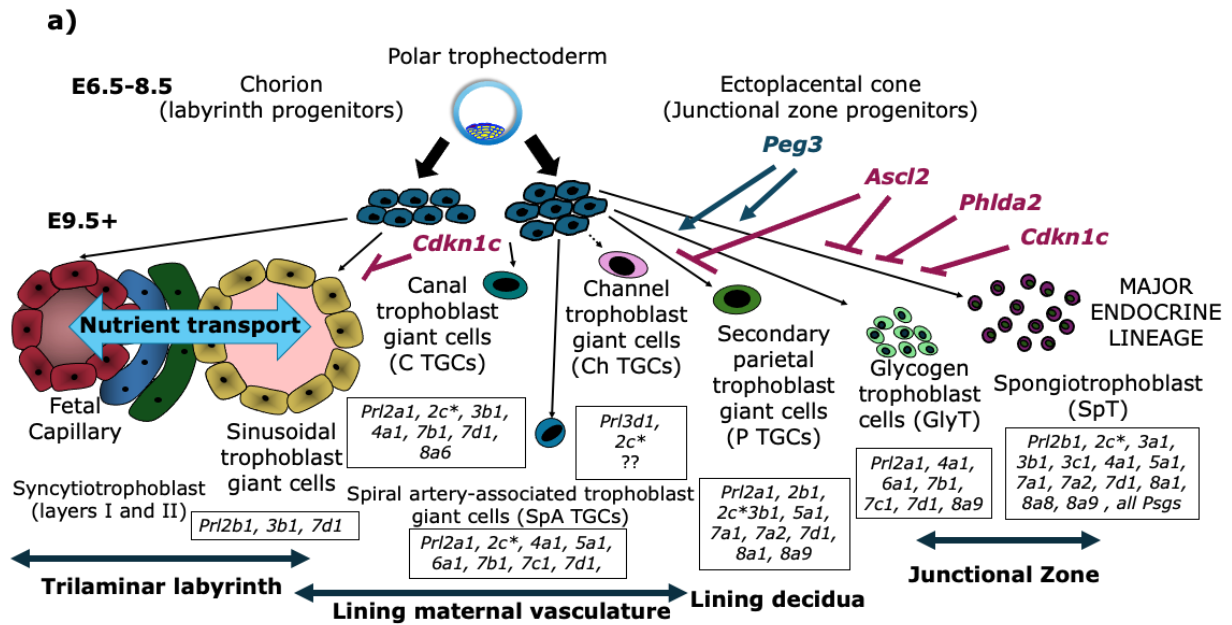


Figure 10: Imprinted genes regulation of placental endocrine lineages.

a) Originating from the ectoplacental cone are nine placental lineages. Each lineages hormone production is detailed in boxes below lineage. Paternally expressed/maternally silenced genes (blue text) expand endocrine lineages. Maternally expressed/paternally silenced genes (red text) restrict endocrine lineages. **b)** The function of *Peg3* occurs upstream of *Phlda2* in spongiotrophoblast and glycogen cell progenitors. Known and theorised impacts of knockout models on lineages depicted with arrows.

Importantly, the similarities and differences of within both models is important to parse. Although many aspects of both *Peg3* and *Phlda2* are conserved across mouse and humans, mouse *Peg3* has shown some

distinct differences from human *PEG3* (Hiby et al., 2001) and significant structural differences between the species can impede research. A summary of research findings for both genes in relation to placental endocrine insufficiency in both mouse and human is detailed in Figure 11.

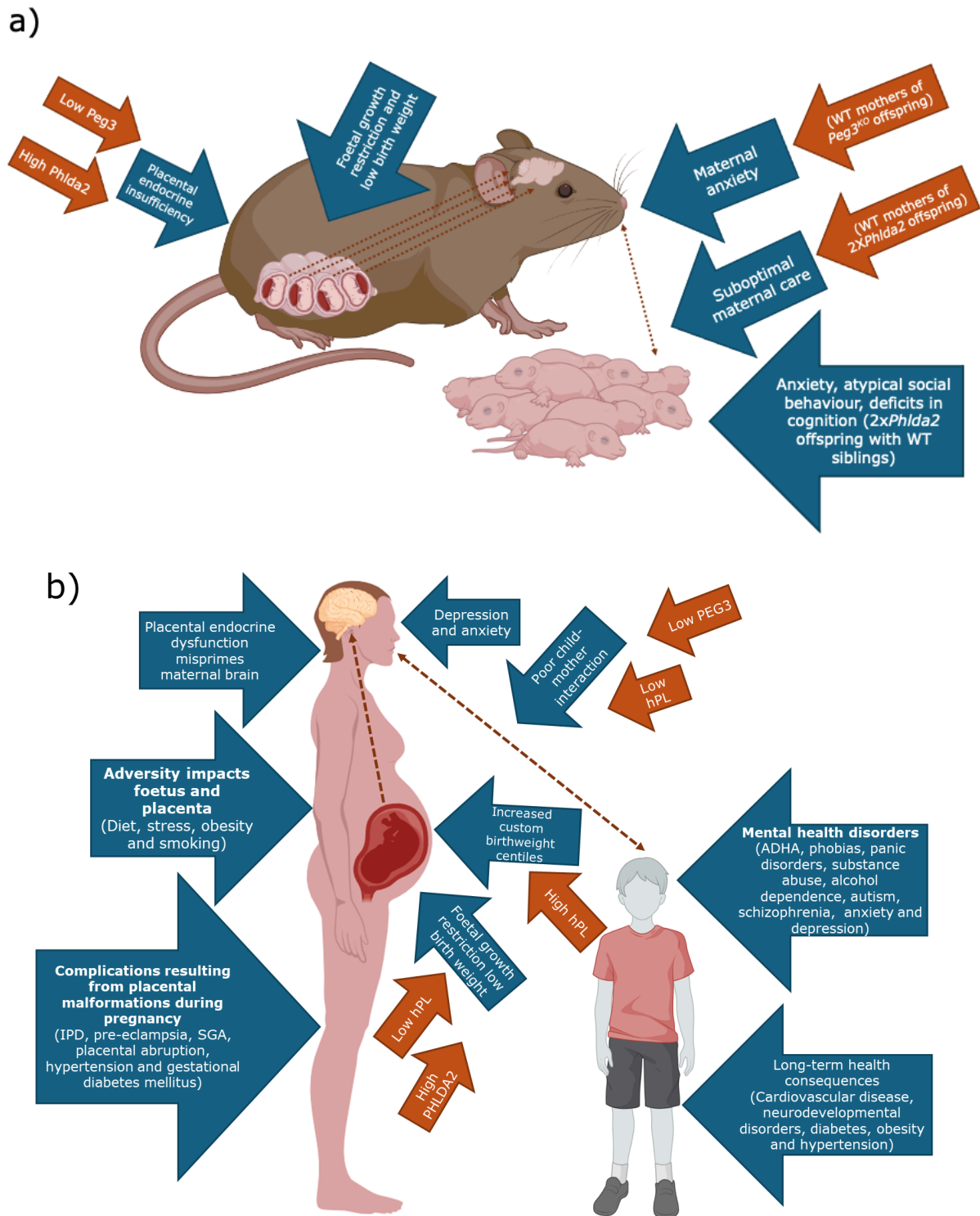


Figure 11: Functional roles of *Peg3* and *Phlda2* in the placental programming hypothesis.

a) Mouse model findings relating to *Peg3* and *Phlda2*'s roles in the regulation of the placental endocrine and the resulting impacts on mouse maternal behaviour. **b)** Human studies indirect evidence surrounding *PEG3* and *PHLDA2* association with *hPL* levels and the impacts on maternal mental health and poor outcomes for offspring. Adapted from John (2022) (summary of work presented at the Physiology Online 2021 symposium).

1.10 Trophoblast stem cells

A key bridging model between species is the trophoblast stem cell. Early embryonic development is conserved across species. A common stage of development found in placental animals is the blastocyst (Frankenberg et al., 2016). The blastocyst is a key stage in development in which the first lineage commitments are made by the different structures within it. The two structural differences in the blastocyst are the inner cell mass and the trophectoderm. At this stage the inner cell mass contains embryonic stem (ES) cells which give rise to all adult lineages and the embryo proper. The outer lining of cells known as the trophectoderm contain trophoblast stem cells which give rise to the placenta and all placental lineages (Adjaye et al., 2005; Johnson, 1979)(Figure 12). At this point in both species, trophoblast stem cells derive all placental endocrine lineages. As both genes of interest are being investigated on their potential to derive the endocrine lineage, this thesis is able to put both species models to the test in a comparable format using analysis of knockout models in trophoblast stem cells.

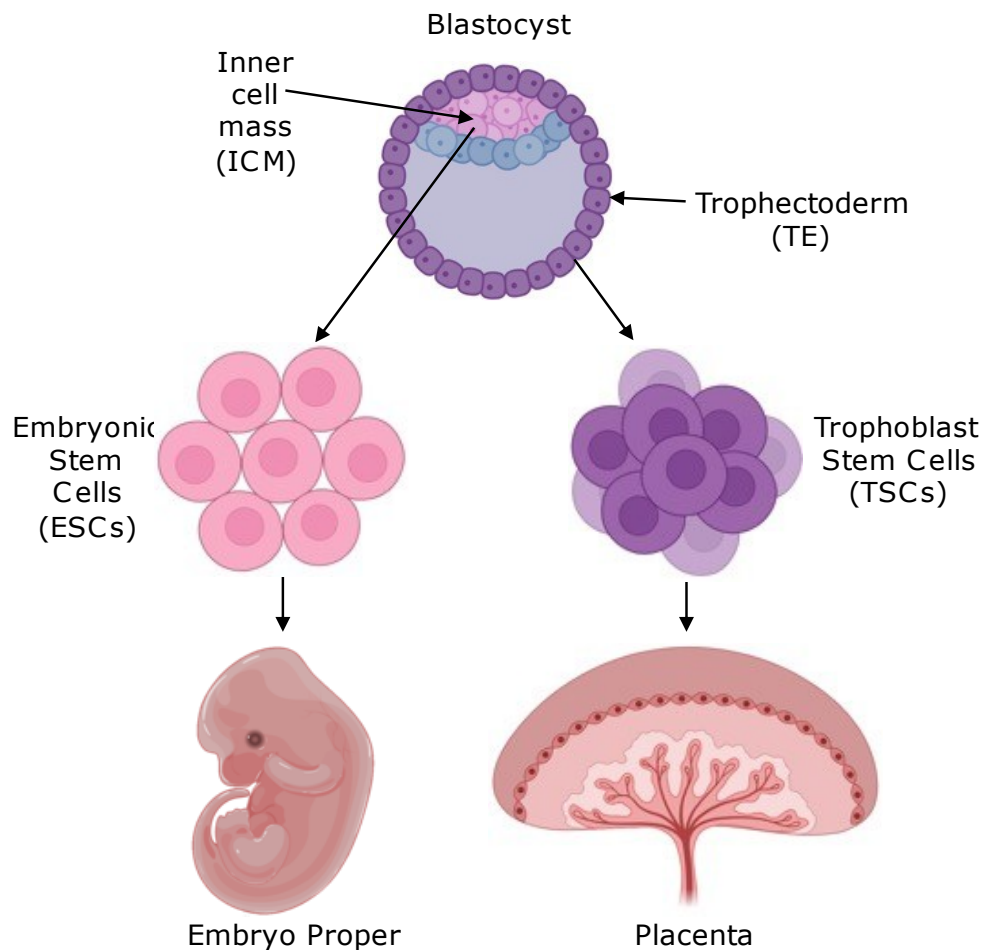


Figure 12: Location and isolation of trophoblast stem cells.

Mouse trophoblast stem cells were derived by Dr Satoshi Tanaka in 1998 (Tanaka et al., 1998), not long after being initially derived in the rat in 1991 (Faria & Soares, 1991). Ever since, there have been efforts to derive these cells in human. The first successful derivations were performed by Dr Hiroaki Okae in 2018 (Okoe et al., 2018). In studies of the gene expression pattern of human placenta, it was determined that activation of epidermal growth factor (EGF) and Wnt coupled with inhibition of transforming growth factor β 1 (TGF- β), Rho-associated protein kinase (ROCK) and histone deacetylase (HDAC) maintained the environment required for long term human trophoblast stem (hTS) cell culture (Okoe et al., 2018). The cells that were established under these conditions were human VCT cells. Experiments confirmed that these cells could give rise to the three main lineages of the human placenta (Okoe et al., 2018). Cell lines could not be derived from full term pregnancies as it is possible that the pluripotency of the developing organ is lost near full term. It is possible that there could be certain locations within the placenta where these cells are maintained until full term however this will need to be identified via further attempts (Okoe et al., 2018).

These successful cell lines were established via two methods. One was from the first trimester placenta, the other was from the E7 human blastocyst (Okae et al., 2018). When these cells were injected into SCID mice they produced some EVT-like cells and some cells resembling STB cells that form during implantation were also identified. Finally, the hosts serum contained hCG. Together this data demonstrated that these cells possessed key characteristics of invading hTS cells during implantation (Okae et al., 2018). The chimeric capabilities of these cells could not be determined as it was not possible to test if these could contribute to the human placenta due to ethical reasons (Okae et al., 2018).

The molecular environment between mouse and human are distinct. Mouse trophoblast stem (TS) cells require activation of fibroblast growth factor-4 (FGF4) and TGF- β and inhibition of the Wnt signalling pathway and ROCK whereas the human TS cells require Wnt and EGF activation along with HDAC, TGF- β and ROCK. One key difference is the opposing requirements of Wnt and TGF- β . An absent element required for the human TS cells is the role of FGF, whose activation is a key component of the mouse TS cell environment (Tanaka et al., 1998), which is likely because the human TS cells don't express FGF (Okae et al., 2018).

The pattern of growth of the placenta differs between mouse and human (Rossant, 2015). Placental development in mice starts with implantation, then the polar trophoderm forms Epc and ExE. The epiblast secretes FGF ligands which support the maintenance of multipotent trophoblast cells. In contrast, primitive cytotrophoblast (CT) cells and STB cells form from the human trophoderm. These cells form primary villi when the primitive STB cells invade the maternal endometrium and the primitive CT cells penetrate the primitive STB cells. The Epc and ExE do not appear in human blastocysts, and their embryos only have transient interaction between epiblast and trophoblast cells (Okae et al., 2018).

Trophoblast stem cells allow the use of genetic modification in placenta research. One method is to derive trophoblast stem cells from mouse strains which already contain the genetic modification of interest. The other is to introduce the transgene modification to wild type trophoblast stem cells, which is the only available method for human cells. *PHLDA2* has been over expressed in hTS stem cells. This showed suppressed cell migration and invasion (Jin et al., 2016). However, these cells were an early trophoblast stem cell model for humans which was not sufficiently validated. In a study with the Okae cells both *PHLDA2* and *PEG3* were targeted in a mass screening knock out experiment (Shimizu et al., 2023). Cells were transfected with CRISPR targets for 850 genes and were then screened for differences in growth rates, EVT differentiation or STB differentiation. In this study, *PEG3* was not identified as having a significant impact on the phenotype of the cells. Despite *PHLDA2* also not

presenting a significant phenotype, *PHLDA2* was a notable gene of interest within the study so underwent further assessment. Here, *PHLDA2* did not show any growth promoting or growth restricting phenotype. For both knockouts, they did not show any initial significance during the wider screening and therefore were selected to be investigated further. Most notably they were not analysed for their hormone production potential. Therefore, this leaves the research question of this thesis open for further investigation.

1.11 Sexual dimorphism

The research community is experiencing a global reckoning around sex-specific outcomes. Previous exclusion of females in clinical trials has led to symptoms, drug dosages and diagnosis parameters being mapped on male bodies and applied to female bodies. The research community is just now realising the extent to which this method is problematic (Buvinić et al., 2006; Holdcroft, 2007; Östberg Lloyd & Sand Horup, 2023; Patwardhan et al., 2024; Thomson, 2023; Whiting, 2024; Winchester, 2021). Some notable examples where male data has significantly differed from females are heart attack symptoms, ADHD and autism diagnosis, stroke symptoms, and autoimmune disorders (Whiting, 2023). All of these causing generations of poorly diagnosed and inadequately treated female populations. After a Change.org petition (Change.org, 2021) in 2023, even crash test dummies have recently added a female adult for the first time in the history of automobile safety, despite females being 73% more likely to be injured in a crash than men (Epker, 2023). This cultural shift has had a ripple effect throughout biological research where data is now expected to be split by sex and statistically analysed as such.

This too applies to placenta. Despite the placenta being an organ so heavily tied to female health, as they are the ones who harbour it during pregnancy, it is in fact a foetal tissue. This means that it is gendered in addition to the foetus being gendered. So, as well as having different outcomes for male and female foetuses, the impacts of male and female placenta must be investigated. Upon macro-analysis of sex specific differences, the male placenta is heavier at term than female placentas for both human and mouse (Christians, 2022). In addition, sexually dimorphic effects have been identified in maternal brain priming, for example, low levels of hPL were associated with negative scores for Edinburgh postnatal depression scale (EPDS) and State-trait anxiety inventory (STAI), ten weeks postnatal for mothers who had female offspring and placenta but not for male offspring (Sumption et al., 2020).

The *Peg3* knockout model has already demonstrated a great degree of sexual dimorphism with a reduction in size of the spongiotrophoblast and glycogen cell lineages which is more significant in male placentas than in female (Tunster et al., 2018). This data suggests that the female placenta is more able to compensate for the loss of *Peg3* expression than male placenta. It is theorised that the males lack of adaptability is a consequence of the increased resources required for the male foetus (Aiken & Ozanne, 2013; DiPietro & Voegtline, 2017; Sutherland & Brunwasser, 2018). The male foetus requires more investment from the placenta, therefore is more significantly impacted than the female foetus when the placenta is compromised (Eriksson et al., 2010; Salazar-Petres et al., 2022), with female placentas having a greater reserve of resources, and male placentas having to function at their upper limits (Eriksson et al., 2010). This is further demonstrated in diet studies of pregnant mice, where placental gene expression patterns showed a significantly different response to an altered diet depending on the fetuses' sex (Mao et al., 2010). The previous investigations into this thesis's *Phlda2* models did not address the question of sexual dimorphism, therefore its sexually dimorphic impact is still yet to be dissected. In relation to this research, previous model's findings will now be re-evaluated based on sex and their sexual dimorphic consequences will be evaluated.

1.12 Summary

This thesis addressed the gap in knowledge regarding the imprinted genes *Peg3* and *Phlda2s* regulation of placental hormones and their antagonistic interaction between one another. It is hypothesised that where *Peg3* functions to expand placental endocrine lineages, its KO will restrict them. Conversely, where *Phlda2* functions to restrict placental endocrine lineages, its overexpression will restrict them and its KO will expand them. When the two KOs are combined, a correction back to WT phenotype placenta is hypothesised with a comparable to WT endocrine compartment.

This hypothesis extends to mouse and human trophoblast stem cells models, where all KOs in both mouse and human TS cells lines will be assessed for their endocrine potential. In both species, it's anticipated that *Peg3*^{KO} TS lines will have a reduction in placental hormones, *Phlda2*^{KO} TS cell lines will have an increase in placental hormones and the DKO TS cell lines will have a comparable to WT hormone production capacity.

Additionally, this thesis also addresses the gap in knowledge between quantifying placental hormone production with functional output by

developing a quantitative regional RNA expression assay for placental hormones.

Finally, it is also hypothesised that these models will have varying degrees of sexual dimorphism, potentially impacting the male placentas more significantly than the females.

1.12.1 Aims and objectives

Each chapter's aims and objective are as follows:

Chapter 3:

Aims: This chapter aims to understand the sexual dimorphic characteristics of a loss of imprinting model of *Phlda2*. It also aims to establish a quantitative regional RNA expression assay.

Objectives: Based on previous research by Tunster, Creeth, et al. (2016); Tunster et al. (2014) examining the consequences of a *Phlda2* loss of imprinting model on placental endocrine lineages, this chapter investigated the sexually dimorphic impacts of the *Phlda2* loss of imprinting model on the placenta by measuring the endocrine lineage of WT and mutant placentas and their capacity for hormone production whilst assessing sexually dimorphic elements.

Chapter 4:

Aims: This chapter aims to further characterise *Peg3^{KO}* and *Phlda2^{KO}* models whilst conducting the first investigation into the DKO model at E16.5 and all models sexually dimorphic characteristics.

Objectives: Combining previous research on *Phlda2* and *Peg3*, where using a knockout model of *Phlda2* produces an enlarged endocrine lineage (Tunster, Creeth, et al., 2016) and a knockout model of *Peg3* produces a restricted endocrine lineage (Tunster et al., 2018), this chapter investigated the antagonistic interaction between a maternally expressed imprinted gene, *Phlda2*, and a paternally expressed imprinted gene, *Peg3*, by producing a double knockout. In addition, analysis of the sexually dimorphic elements of the *Peg3* and *Phlda2* knockouts were conducted. This chapter detailed the restorative impact of the double knockout and the degree in which these two genes behave antagonistically to each other, all whilst determining their endocrine potential in the mouse system.

Chapter 5:

Aims: This chapter aims to derive mouse and human trophoblast stem cell lines for each of the KO models. It aims to test the effects of the KOs on the cell lines endocrine potential.

Objectives: This final chapter attempted to map the findings from the mature mouse placenta KO models (Chapter 4) onto the human system. Using trophoblast stem cells of both human and mouse, *PEG3*^{KO}, *PHLDA2*^{KO} and DKO cell lines were derived. Mouse TS cell knockouts were derived from blastocysts where human TS cell knockouts were derived using CRISPR technology. Both human and mouse models were tested for their ability to derive the different lineages of the placenta and their capacity for endocrine production.

Chapter 2: Methods

2.1 Mouse model and husbandry

Three mouse model strains were used for the experiments in this thesis. These were *Phlda2*^{+/+BACx1}, *Peg3*^{KO} and *Phlda2*^{KO}. The process of each of their generation is detailed below.

2.1.1 *Phlda2*^{+/+BACx1(BL6)}: A *Phlda2* loss of imprinting mouse model

The *Phlda2*^{+/+BACx1(BL6)} model is a loss of imprinting model, or more simply a double expression model of *Phlda2*. This model was generated in Professor Ros John's laboratory, the process of which is detailed in Tunsters 2010 paper (Tunster et al., 2010). The method used in the 2010 paper is further detailed in the generation of an earlier line known as 10-15, which can be found in John (2001). A 129/Sv gridded pBeloBAC library (Genome Systems, St Louis) was combined with a *Cdkn1c* probe. This was used to define a clone fragment which extends 65 kb upstream and 20 kb downstream of *Cdkn1c*. This region includes *Slc22a18* and *Phlda2*. The resulting BAC DNA was used for pronuclear injection to generate the transgenic founders. Southern blots were used to characterise transgenic embryos. A PhosphoImager was used to determine the copy number of BAC inserts by comparing the intensity of hybridisation of this fragment with the endogenous locus.

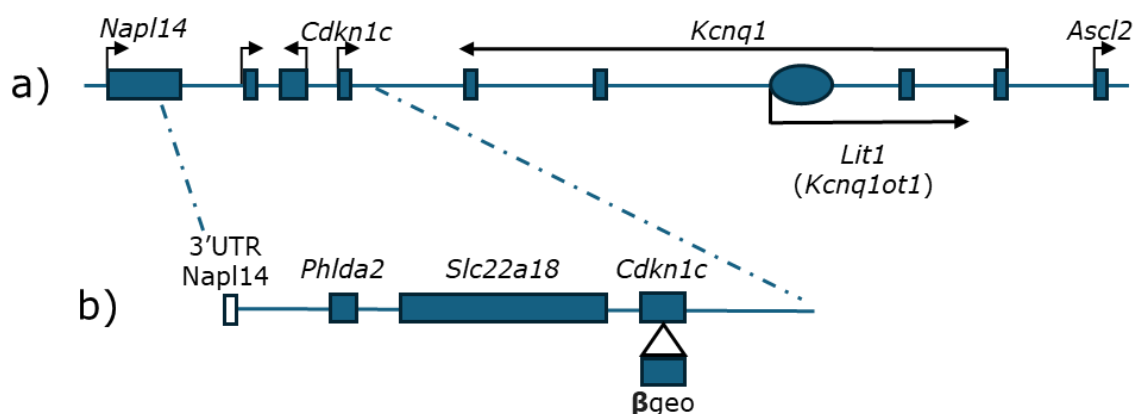


Figure 13: Genomic map of the IC2 region distal mouse chromosome 7.

a) The oval marks KvDMR1, which is in an intron of *Kcnq1* and is methylated on the maternal allele. Direction of transcription is indicated by arrows. **b)** Map of the 85-kb transgene (BAC144D14). Positions of the intact *Phlda2*, *Slc22a18*, and *Cdkn1c* are represented by filled boxes. The transgene includes the 3' untranslated region (UTR) of *Napl14* (white box) but not the 5' untranslated region. The modified BAC used to generate

the *Phlda2*^{+/+BACx1(BL6)} line has a β -galactosidase-neomycin (*β geo*) fusion gene inserted into *Cdkn1c*, indicated by the arrow and filled box. Image adapted from Tunster 2010.

This line was bred in C57BL/6 for >20 generations. For the purposes of the experiments conducted in Chapter 3, *Phlda2*^{+/+BACx1(BL6)} males were mated with *Phlda2*^{+/+} wild type to generate the experimental tissues (Figure 16) for E9.5, E16.5 placental samples, see protocol 2.3.1 and to generate blastocysts for trophoblast stem cell derivation, see protocol 2.8.1. Animal husbandry details are described in section 2.1.4.

2.1.2 *Phlda2*^{KO} mouse model

The *Phlda2*^{KO} mouse model was generated by the institute for Cancer Genetics and Department of Pathology and Anatomy and Cell Biology at Columbia University in New York and the Barbraham Institute in Cambridge (Salas et al., 2004). Two different approaches were used in the initial targeting. The initial *Phlda2*^{neo} targeting vector ligated a 5-kb region upstream using a 5' genomic *Not1* restriction site and a 6-kb *EcoRI/XbaI* restriction site downstream flanking *Phlda2*. The next approach, *Phlda2*^{loxP}, took the P_{gk}-Neo cassette in pPNT-Delta*Phlda2* and replaced it with pLNL. Homologous recombination was verified using PCR. The deletions removed both of *Phlda2*'s exons and deleted half of its upstream CpG island. Both vectors were transfected into ES cells and the resulting cells were used for germline chimera generation. These were bred onto C57BL6;129Sv background (Salas et al., 2004). This strain was then provided to Professor Ros John by Professor Benjamin Tycko where it was bred onto a pure 129Sv background.

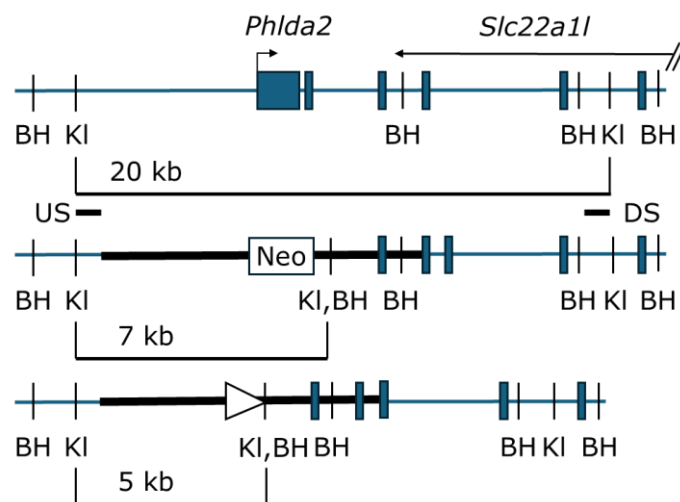


Figure 14: Schematic of *Phlda2*^{KO} generation.

Phlda2 was replaced by phosphoglycerine Kinase (P_{gk})-Neomycin (Neo). Exons are represented by boxes. The triangle represents the recombined

loxP sites. Upstream probe (US), Downstream probe (DS). Restriction enzyme sites kpnI (KI) and BamHI (BH). Adapted from Frank 2002.

For the purposes of the experiments conducted in Chapters 4 and 5, a female heterozygous for the *Phlda2*^{KO} allele was used to generate the experimental tissues (Figure 17) for E9.5, E16.5 placental samples, see protocol 2.3.1 and to generate blastocysts for trophoblast stem cell derivation, see protocol 2.8.1. Animal husbandry details are described in section 2.1.4.

2.1.3 *Peg3*^{KO} mouse model

The *Peg3*^{KO} model was generated at the Wellcome CRC Institute of Cancer and Developmental Biology, and the Physiology Laboratory at the University of Cambridge (Li et al., 1999). R1 ES cells were transfected with a 4.8-kb IRES- β geo-SV40 polyadenylation selection cassette which inserted into the 5' coding exon of *Peg3*, rendering the gene functionally silent. The resulting cells were selected against G418. The surviving colonies were screened with southern DNA blot hybridisation. Confirmed KO cells were used to generate germline chimera males which were mated with WT 129Sv and MF1 females resulting in a *Peg3*^{KO} mouse line. The *Peg3*^{KO} transgenic mouse model was generously donated to Professor Ros John's laboratory by Professor Azim Surani. The strain was maintained by maternal transmission. *Peg3* deficient fetuses were generated by crossing *Peg3*^{+/-} males with wild type 129 females. A population of these mice were subsequently maintained in house at Cardiff University.

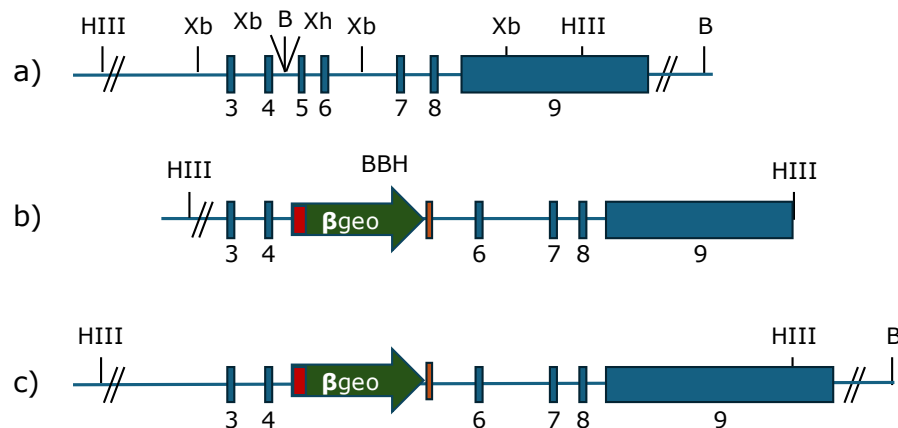


Figure 15: Schematic of *Peg3*^{KO} generation.

a) Mouse *Peg3* genomic locus which contains exons three to nine (blue boxes) and restriction enzyme sites Hind III (HIII), Bgl II (B), Xba I (Xb) and Xho (Xh). **b)** Target construct inserted into exon five containing β geo selection cassette with internal ribosome entry site (red box), *lacZ-neo*

fusion gene (green arrow) and SV40 polyadenylation (orange box). c) Mutant locus. Adapted from Li et al. (1999).

For the purposes of the experiments conducted in Chapters 4 and 5, a male heterozygous for the *Peg3*^{KO} allele was used to generate the experimental tissues (Figure 17) for E9.5, E16.5 placental samples, see protocol 2.3.1 and to generate blastocysts for trophoblast stem cell derivation, see protocol 2.8.1. Animal husbandry details are described in section 2.1.4.

2.1.4 Animal husbandry

The University of Cardiff ethical committee approved all animal breeding. All work was conducted with the UK Home Office project license PPI1320481. The mouse house was under standard control settings with temperature at 21 °C ± 2 and humidity at 50% ± 10%. A 12-hour light-dark cycle was maintained with light hours beginning at 06:00 h. The cage size was 45 x 12 x 12 cm and included environmental enrichment elements such as chew-stick, cardboard tube and nestlet bedding. On an *ad libitum* basis tap water and standard chow (Formulab Diet 5008, TestDiet, UK) were available. Maintenance of the mouse house was performed by technical staff which included weekly cage cleaning, which was performed on a schedule which minimised disruption to breeding.

2.1.5 Breeding schemes and generation of experimental tissues

The *Phlda2*^{+/+BACx1(BL6)} mouse model was maintained on a BL6 background where *Peg3*^{KO} and *Phlda2*^{KO} models were maintained on a *Mus musculus* 129S2/SvHsD (129) (Harlan Laboratories UK Limited (Ltd), 129) background. Natural matings were used to generate E7.5, E9.5, E14.5 and E16.5 placental tissues. Superovulation was used for E3.5 blastocyst generation required for TS cell derivation for which details can be found in the methods section 2.8.1. Mouse genotyping was performed by taking ear clippings before weaning then assessing them via the genotyping method detailed in 2.2.

To generate tissues for Chapter 3, matings were performed by crossing virgin C57BL/6 females with *Phlda2*^{+/+BACx1(BL6)} males, resulting in *Phlda2*^{+/+BACx1(BL6)} transgenic (Tg) and *Phlda2*^{+/+} wild type (WT) offspring (Figure 16).

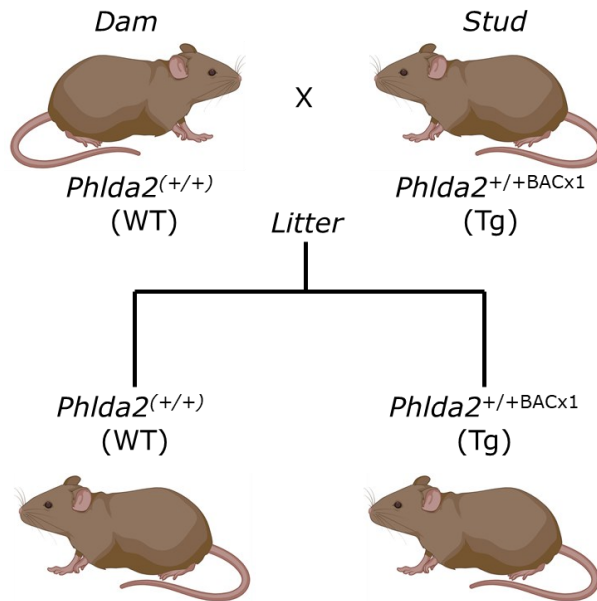
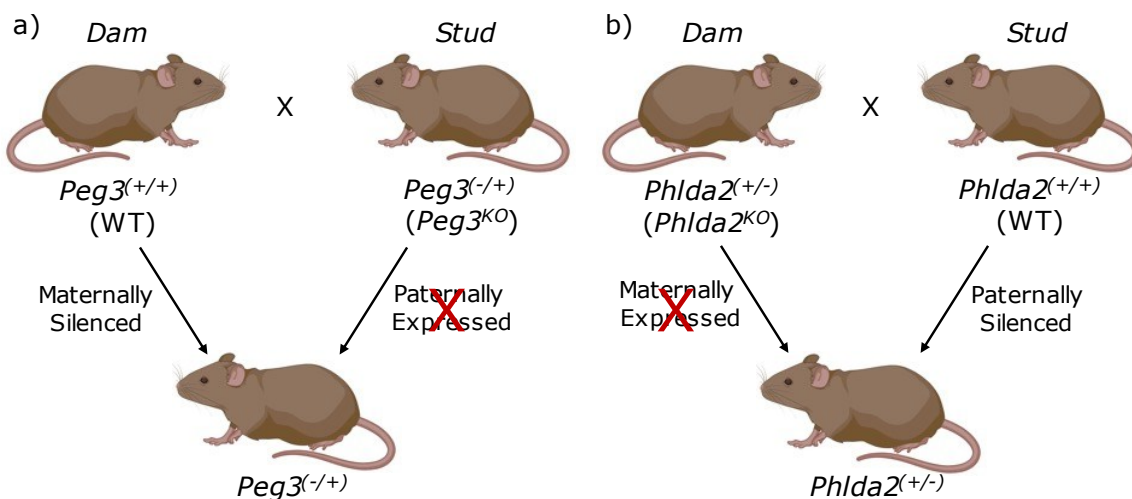


Figure 16: Breeding scheme to generate experimental materials for *Phlda2*^(+/+) WT and *Phlda2*^{+/+BACx1}(BL6) transgenic (Tg) tissues.

For the investigation into the interactions between *Phlda2* and *Peg3*, a double KO (DKO) was of interest. Due to the nature of these KO models, a mating cross was available which gave rise to the four genotypes of interest. Crosses of *Phlda2*^(+/-) females with *Peg3*^(-/+) males, resulted in wild-type *Phlda2*^(+/+); *Peg3*^(+/+) (WT), *Peg3*^(-/+); *Phlda2*^(+/+) (*Peg3*^{KO}), *Phlda2*^(+/-); *Peg3*^(+/+) (*Phlda2*^{KO}) and *Phlda2*^(+/-); *Peg3*^(-/+) (DKO) offspring (Figure 17). This allowed for experimental samples to be controlled more efficiently against litter size and weight. This mating cross was used for Chapter 4 and 5.



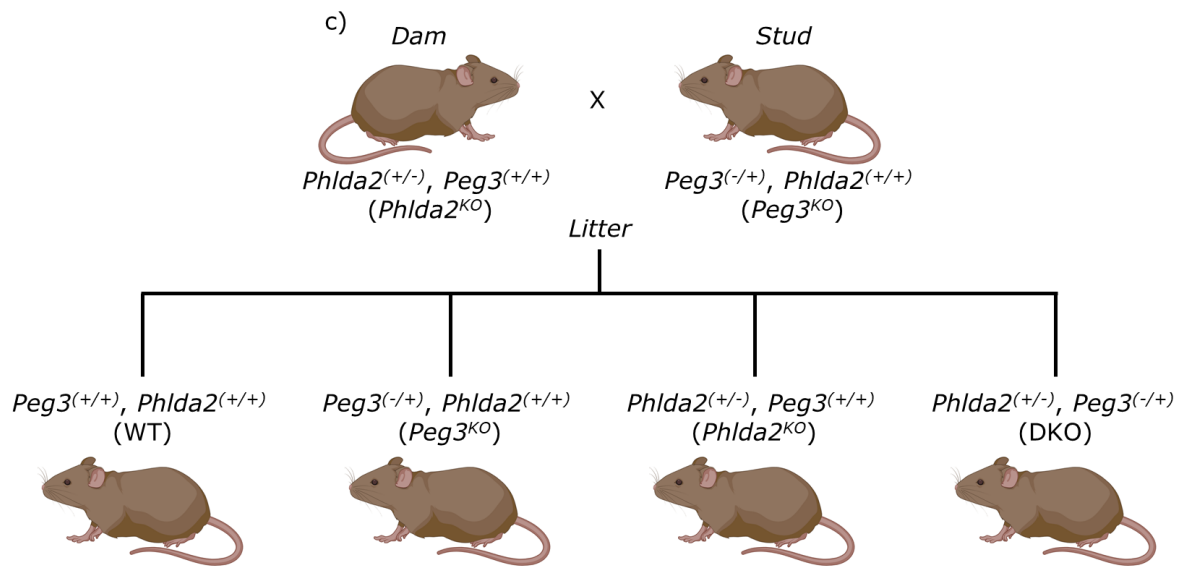


Figure 17: Breeding scheme to generate experimental materials for WT, $Peg3^{KO}$, $Phlda2^{KO}$ and DKO tissues.

a) Pattern of inheritance for $Peg3^{KO}$ (Paternally expressed/Maternally silenced). A male containing a heterogeneous KO of $Peg3$ was mated with a $Peg3^{+/+}$ (WT) female to produce $Peg3^{KO}$ offspring. **b)** Pattern of inheritance for $Phlda2^{KO}$ (Maternally expressed/paternally silenced). A female containing a heterogeneous KO of $Phlda2$ was mated with a $Phlda2^{+/+}$ (WT) male to produce $Phlda2^{KO}$ offspring. **c)** Mating cross used to generate experimental tissues with predicted ratios of offspring genotypes.

Natural matings were achieved by using female dams between 5-14 weeks old and housing them with previously validated studs. This was usually with one male and one female, but occasionally two females could be paired with one male. A mating was recorded when a vaginal plug was identified between 08:00–10:30 h the following morning. This was determined to be day E0.5. The female was then removed from the mating cage. Her weight was recorded, and she was placed into a cage with other females at two-five females per cage.

Superovulation procedure is detailed in methods section 2.8.1.

2.1.6 Dissection

On the desired E day of the placenta, the female was weighed to determine if the pregnancy was still present. The weight margins were more difficult to distinguish in the earlier E days. If the pregnancy was determined to be present, schedule one would be used to cull the female. Dissection would recover all placenta, which were then prepared according to requirements for following experimental techniques.

Details of E3.5 or E12.5 dissections for derivation of trophoblast stem cells or mouse embryonic fibroblast (MEF) cells are in protocols 2.8.1 and 2.7.3.1 respectively.

At E7.5 and E9.5 the placenta and embryo are contained with the decidua (maternal component) which can be referred to as a “pod”. This pod was dissected free from the uterine wall whole and either placed into 4 °C phosphate-buffered saline (PBS) and then fixed in 4% paraformaldehyde (PFA) to prepare the tissue for sectioning and staining (protocols 2.3.2).

At E14.5 and E16.5 the uterus was removed. The foetus and placental units were dissected one at a time into 4 °C PBS. Both foetus and placenta were weighed separately. The foetuses were culled via schedule one decapitation. The placenta was bisected with a razor blade and one half was fixed in 4% PFA to prepare the tissue for sectioning and staining (see methods 2.3.2). The other half was snap frozen on dry ice and stored at -80 °C in preparation for the RNA to qRT-PCR pipeline or RNA to RNAseq pipeline (2.10.1). The yolk sac from each foetus/placenta combination was collected to be used for genotyping (see methods 2.2).

2.2 Genotyping

2.2.1 DNA extraction

Ear clippings, yolk sacs or cell samples were collected as per their individual methods. The samples were digested by incubating them overnight at 55 °C in lysis buffer (1 M Tris 8.0 pH 8.0 (Sigma, Cat No. T6664), 0.5 M Ethylenediaminetetraacetic acid (EDTA) pH 8.0 (Sigma, Cat No. M5755), 10% Sodium dodecyl sulphate (SDS) (Sigma, Cat No. 11667289001), 5 M Sodium chloride (NaCl) in distilled water (dH₂O)) containing Proteinase K (20 mg/mL (PK), Promega, Cat No. V3021). A 1 in 10 dilution of the sample was prepared in 10 mM Tris (pH 8.0). The dilution was inactivated by incubating it at 95 °C for 20 minutes.

2.2.2 Polymerase chain reaction (PCR)

Mice, placenta, and cell lines were genotyped via PCR. Samples were prepared as outlined in protocols 2.2.4.1 and 2.8.2, and DNA was extracted in protocol 2.2.1. The details of the primers are found in Table 7, which includes the master mix requirements and PCR program for each one. A master-mix was prepared using the reaction mixes in Table 5 and Table 6. The master-mix was aliquoted into PCR tubes at 14 µL per tube followed by 1 µL of the lysed sample. The samples were then run on the primer specific PCR program as outlines in Table 8, Table 9 and Table 10.

For primers with high GC content betain was used to reduce amplification of secondary structures and improve the amplification efficiency, the use of betain is noted for each primer in Table 5.

Master Mix without Betain	1x reaction (µL)
Water, Molecular Biology Reagent (Sigma, Cat No. W4502)	11.5
DreamTaq Green Buffer (10X) (Thermo Fisher Scientific (Life Technologies, Cat No. B71))	1.5
dNTPs (10 mM, Thermo Fisher Scientific (Life Technologies), Cat No. R0192)	0.3
Primers (0.025 µmole, Sigma)	0.6
DreamTaq Hot Start DNA Polymerase, 500 U (Thermo Fisher Scientific (Life Technologies), Cat No. EP1702)	0.1
Volume	14

Table 5: Reaction mix for PCR.

Master Mix with Betain	1x reaction (µL)
Water, Molecular Biology Reagent	8.5
DreamTaq Green Buffer (10X)	1.5
dNTPs	0.3
Primers	0.6
5M Betaine (Cat No. B0300, Sigma)	3.0
DreamTaq Hot Start DNA Polymerase	0.1
Volume	14

Table 6: Reaction mix for PCR with betain.

Primer	Betain	PCR Program	Sequence	Product	Reference
<i>Phlda2</i> ^{+/+BACx1(BL6)} F	No	DTAQ	CACATACGTTCCGCCATTCC	BAC - 484 bp	(Tunster, McNamara, et al., 2016)
<i>Phlda2</i> ^{+/+BACx1(BL6)} R	No	DTAQ	CCACTTCAACGTAACACCCGC	BAC - 484 bp	
<i>Phlda2</i> F	No	Phlda2	GCTTCAAGCAATGGGTAAGG	187 bp WT band 1731 bp KO band	Unpublished, designed in house.
<i>Phlda2</i> R	No	Phlda2	TCCAGTGATGGAGGTTGTCA	187 bp WT band 1731 bp KO band	
<i>Peg3</i> WT F	Yes	Peg3 64	CAAAGCACATCTGACCACTCA	Forward primer for <i>Peg3</i> genotyping 170bp from WT and HET >5kb in HOM	Unpublished, designed in house.
<i>Peg3</i> TG F	Yes	Peg3 64	CGTTGGCTACCCGTGATATT	Forward primer for <i>Peg3</i> genotyping <695bp in KO	
<i>Peg3</i> Common R	Yes	Peg3 64	TATGCACACAGCCTCTGCTC	Common reverse primer for <i>Peg3</i> WT F and <i>Peg3</i> TG F	
<i>Oma1</i> F	No	DTAQ	TTACGTCCATCGTGGACAGCAT	246 X-chromosome band	(Wolstenholme et al., 2013)
<i>Oma1</i> R	No	DTAQ	TGGGCTGGGTGTTAGCCTTAT	246 X-chromosome band	
<i>Ssty</i> F	No	DTAQ	CTGGAGCTCTACAGTGATGA	342 Y-chromosome band	
<i>Ssty</i> R	No	DTAQ	CAGTTACCAATCAACACATCAC	342 Y-chromosome band	

Table 7: Primer details. Forward primer (F), Reverse primer (R).

2.2.2.1 PCR programs

Step	Temperature	Time	Cycles
Initial denaturation	95 °C	3 minutes	1
Denaturation	95 °C	30 seconds	35
Annealing	60 °C	30 seconds	
Extension	72 °C	2 minutes	
Final Extension	72 °C	7 minutes	1
Hold	4 °C	Indefinite	1

Table 8: Standard PCR program.

Step	Temperature	Time	Cycles
Initial denaturation	95 °C	3 minutes	1
Denaturation	95 °C	30 seconds	35
Annealing	64 °C	30 seconds	
Extension	72 °C	1 minute	
Final Extension	72 °C	10 minutes	1
Hold	4 °C	Indefinite	1

Table 9: *Peg3* 64 PCR program.

Step	Temperature	Time	Cycles
Initial denaturation	95 °C	3 minutes	1
Denaturation	95 °C	30 seconds	34
Annealing	60 °C	30 seconds	
Extension	72 °C	30 seconds	
Final Extension	72 °C	3 minutes	1
Hold	4 °C	Indefinite	1

Table 10: DTAQ PCR program.

2.2.3 Gel electrophoresis

The resulting PCR product was run on a 1.5 % agarose gel in Tris-acetate-EDTA (TAE) buffer (Table 11) for 20-25 minutes from 80-150 V.

TAE Buffer Recipe	50 X
Tris free base (TRIZMA(R) BASE, PRIMARY STANDARD, Cat No. T1503, Sigma)	242 g
Disodium EDTA	18.61 g
Glacial Acetic Acid (ACETIC ACIDGLACIAL, REAGENTPLUS , =99% Cat No. A6283, Sigma)	57.1 mL
DDI H2O to 1 L	x
Total volume	1 L

Table 11: TAE buffer mix.

The gel was imaged using the Gel Doc EZ image (Bio-Rad).

2.2.4 Weight data

2.2.4.1 Tissue generation (E14.5 and E16.5)

Timed matings were set up between parents of desired genotypes as described in section 2.1.5. On E14.5 or E16.5 schedule 1 was performed on pregnant dams. Each foetus and placenta pair were dissected separately and allocated an embryo number.

2.2.4.2 Sample weighing

The placenta and embryo were weighed separately on a laboratory balance. Their weights were recorded in micrograms. Placenta was then bisected. Half was frozen at -80 °C in preparation for RNA extraction. The other was then fixed in 4% PFA for staining.

2.3 RNAscope

2.3.1 Tissue generation for sections

Timed matings were set up between parents of desired genotypes as described in section 2.1.5. On E7.5, E9.5, E14.5 or E16.5 schedule one

was performed on pregnant dams. For E7.5 and E9.5 pregnancies the placenta and embryo are housed within a “pod”. Each pod was dissected in full and fixed in 4% PFA. For E14.5 and E16.5 each foetus and placenta pair were dissected separately and allocated an embryo number. The placenta was bisected and fixed in 4% PFA in preparation for staining.

2.3.2 Tissue mounting and sectioning (E7.5, E9.5, E14.5 and E16.5)

For E7.5 and E9.5 samples the entire pod was placed into cold diethylpyrocarbonate (DEPC) treated PBS and fixed in 4% PFA. Between three and eight fixed pods were mounted in paraffin wax per wax block and were orientated down the midplane. Sections were taken at 18 x 8 µm per sample at two sections per slide.

The E14.5 and E16.5 placentae were removed from the extraembryonic membranes and their yolk sac. The yolk sac was processed for genotyping (section 2.2). The placenta was bisected down the midplane. Half of the placenta was placed in cold DEPC treated PBS and was fixed in 4% PFA. The placentae were mounted in paraffin wax with the midsection mounted on the top. Sections were taken from the midplane at 18 x 8 µm and were mounted two sections per slide. The first and last slide had a haematoxylin and eosin (H & E) staining performed by the in-house service at Cardiff University (Cardiff University Bioimaging Hub Core Facility, RRID:SCR_022556).

2.3.3 RNAscope staining protocol

Placental tissues at E7.5, E9.5, E14.5 and E16.5 were collected via the process outlined in protocol 2.3.2. The RNAscope® Multiplex Fluorescent kit (ACDBio, Cat No. 323110) was used for fluorescent staining of RNA in situ. Each experimental set included a control slide containing positive control (ACDBio, Cat No. 320881) and negative control (ACDBio, Cat No. 320871) probes. For each experimental slide, one section had probes applied and the other would be used as a “no probes” control to correct for autofluorescence.

Slides were baked in HybEZ II oven (ACDBio) for one hour at 60 °C. At room temperature (RT (20-25 °C)) the slides were deparaffinised in a fume hood with two five-minute incubations with agitation in fresh xylene (Fisher scientific, Cat No. 10335942) and two, two-minute incubations with agitation in fresh 100% EtOH. The slides were airdried for five minutes. A pap pen (Merck, Cat No. Z672548) was used to produce a hydrophobic barrier around each tissue section on the slide, which allowed the two sections on the slide to have different combinations of probes or fluorophores. Hydrogen peroxide (H₂O₂) (ACDBio, Cat No. 322381) was

applied at room temperature (RT) (20-25 °C) for 10 minutes. The slides were then washed twice in dH₂O for five minutes per wash.

The 70 mL target retrieval (ACDBio, Cat No. 322000) was diluted into 630 mL of dH₂O and was heated to 98-104 °C. The slides were placed in the target retrieval for 15 minutes. Slides were washed twice in dH₂O for five minutes per wash. The slides were then air dried. Protease plus (ACDBio, Cat No. 322380) was applied to the tissue and the slides were incubated in the humidified HybEZ oven for 15 minutes at 40 °C. The slides were washed twice in dH₂O for one minute per wash. The probes (Table 12) were applied to the tissue and were incubated in the humidified HybEZ oven for two hours at 40 °C. The slides were washed in wash buffer (ACDBio, 310091) twice for two minutes per wash, then transferred into a coplin jar containing 5X saline sodium citrate (SCC) (Diluted from SSC buffer 20X in dH₂O, Sigma, Cat No. S6639) and stored overnight at RT.

The slides were then washed in wash buffer twice for two minutes per incubation. RNAscope Multiplex FL V2 Amp1 (ACDBio, Cat No. 323110) was applied to the tissue and was incubated in the humidified HybEZ oven for 30 minutes at 40 °C. Slides were then washed three times in wash buffer for five minutes per wash. RNAscope Multiplex FL V2 Amp2 (ACDBio, Cat No. 323110) was applied to the tissue and was incubated in the humidified HybEZ oven for 30 minutes at 40 °C. Slides were then washed three times in wash buffer for five minutes per wash. RNAscope Multiplex FL V2 Amp3 (ACDBio, Cat No. 323110) was applied to the tissue and was incubated in the humidified HybEZ oven for 15 minutes at 40 °C. Slides were then washed three times in wash buffer for five minutes per wash.

The C1 signal was developed by applying HRP C1 (ACDBio, Cat No. 323110) and incubating the slides in the humidified HybEZ oven for 15 minutes at 40 °C. The slides were washed in wash buffer twice for five minutes per wash. The C1 fluorophore was applied at the optimised dilution for 30 minutes at 40 °C in the humidified HybEZ oven. The fluorophores used were TSA® Plus fluorescein, TSA® Plus Cyanine 3, and TSA® Plus Cyanine 5 (Akoya Biosciences, Cat No. NEL741001KT). Stocks were prepared following Perkin Elmer's TSA® Plus System instructions. The slides were washed twice for two minutes per wash. RNAscope Multiplex FL v2 HRP blocker (ACDBio, Cat No. 323110) was applied and incubated at 40 °C in the humidified HybEZ oven for 15 minutes.

The signals for C2 and C3 were amplified, and the fluorophores were tagged by repeating the same steps as described for C1. The DNA stain DAPI was applied to each slide for 30 seconds and was washed off with dH₂O. The slides were mounted in Prolong gold antifade (Thermofisher scientific, Cat No P36930) and were stored at 4 °C.

Channel	Probe	Product Code	Expression levels RNAseq NCBI database	E7.5		E9.5		E14.5		E16.5	
				Fluorophore	Dilution	Fluorophore	Dilution	Fluorophore	Dilution	Fluorophore	Dilution
C1	<i>Pcdh12</i>	489891	-	Fluorescein	1/500	Fluorescein	1/500				
C1	<i>Pri3b1</i>	423671	3734.45	Cy5	1/1000	Cy5	1/1000	Cy5	1/5000	Cy5	1/5000
C1	<i>Cdkn1c</i>	458331	219.142	Fluorescein	1/1000	Fluorescein	1/1000				
C1	<i>Tpbpa</i>	405511	-	Cy5	1/500	Cy5	1/500				
C2	<i>Cdkn1c</i>	458331	219.142	Cy3	1/1000	Cy3	1/1000				
C2	<i>Ascl2</i>	412211	4.725	Cy5 /Cy3	1/1000	Cy5 /Cy3	1/1000				
C2	<i>Tpbpa</i>	405551	-	Cy5	1/500	Cy5	1/500				
C2	<i>Phlda2</i>	528461	4.372	Cy3	1/1000	Cy3	1/1000				
C3	<i>Phlda2</i>	528461	163.773	Cy3	1/1000	Cy3	1/1000				
C3	<i>Peg3</i>	528201	77.837	Fluorescein	1/500	Fluorescein	1/500				
C3	<i>Pcdh12</i>	489891	-	Fluorescein	1/500	Fluorescein	1/500				

Table 12: Details of probes used for RNAscope. Expression levels from RNAseq act as a guide for initial fluorophore dilutions. Including channels and product codes.

2.4 Slide scanner and confocal imaging

The tissue section was imaged using the Zeiss Axio scan Z1 and Zen 3.6 software. A program was designed to image the tissues in bright field and fluorescence.

2.4.1 Program details

2.4.1.1 Bright field imaging

Tissue detection was used on the H & E-stained slides. The program automatically identified the tissue and outlined it as the area to image. A 20X lens captured the tissue in multiple frames then laced them together to produce a full image of the sample.

2.4.1.2 Fluorescence imaging

2.4.1.2.1 Tissue detection

The tissue was outlined manually using the polygon function in the tissue detection feature. The microscope then used a coarse focus to identify the focus point of the tissue using a 10X lens. This mapped six locations across the tissue to coarse focus on and then pinpoint fine focus with a 20X lens on locations related to the coarse focus. This allowed the machine to focus across a large piece of tissue, adapting to variations in depth and thickness and still producing one image.

2.4.3.1.2.2 Binning mode

The light channels, intensity and exposure were set to fit the sample being imaged. The light intensity parameters were standardised across tissue types and dyes following the parameters in Table 13 and Table 14.

	DAPI	Cy5	Cy3	Fluoresceine
Beam splitter	395	660	570	495
Filter Ex. Wavelength	335-383	625-655	538-562	450-490
Filter Em. Wavelength	420-470	665-715	570-640	500-550
Excitation wavelength	353	650	458	493
Emission wavelength	465	673	561	513

Table 13: Light intensity parameters.

Tissue Type	DAPI		Cy3		Cy5		Fluoresceine	
	Light Intensity	Exposure Time						
E7.5	50%	45 ms	100%	30 ms	100%	7 ms	50%	90 ms
E9.5	50%	45 ms	100%	30 ms	100%	7 ms	50%	90 ms
E14.5	50%	200ms	-	-	100%	170 ms	-	-
E16.5	50%	200ms	-	-	100%	170 ms	-	-

Table 14: Light intensity and exposure times.

2.5 E9.5 Parietal trophoblast giant cell counting

Paraffin embedded, H & E stained, E9.5 samples were imaged on the slide scanner using protocol 2.4.1.1. The images were graded on their proximity to the midplane and the quality of the mounting and staining. The images were then counted on Zen blue software. Samples were counted blind by two independent counters. The counting area was defined by placing a parallel line across the pod at the chorionic plate and only the cells above this plate were counted. The P-TG cells were characterised by their large size and location along the interface of the developing junctional zone and decidua. The P-TG cells were marked using the "event" function of Zen blue. Four sections per sample were counted and were averaged. An example of a counted images can be seen in Figure 18.



Figure 18: E9.5 pod with P-TG cells counted. (red X).

2.6 Cell Counting with Zen program

A cell count was conducted on placental cells producing *Prl3b1*. *Prl3b1* RNA was stained using the RNAscope protocol using *Prl3b1* probe 423671 with Cy5 dye in a 1/5000 dilution. To count a large volume of slides in a consistent way the Zen 3.6 software was used to process the images to prepare them for cell counting and implemented a standardised counting method across all images. Counting was performed blind.

2.6.1 Image processing

2.6.1.1 Background subtraction

The background of the image was removed by a process called background subtraction. This program used the "rolling ball" algorithm (Sternberg 1983) which takes a grey scale image and estimates the background signal intensity in case of uneven exposure. This corrected for uneven illumination across an image and removed smooth background. The program was set to a radius of 50 pixels which included the largest cells. This generated an image that had been corrected.

2.6.1.2 Gaussian smoothing

The image resulting from the background subtraction was then taken and processed via Gaussian smoothing. Due to the nature of the imaging technique, it is common that the microscope will have errors in its fluorescent detection. These errors present as single highly fluorescent pixels. The algorithm will not be able to distinguish between these pixels from true signal, as they will still be above the noise of the background subtraction. To remove these a Gaussian smoothing program was applied to each slide. This averages each pixel with its neighbouring pixels which in the case of an error will be pixels with low to no signal, effectively muting these errors. A two-dimensional Gauss bell curve was used to weight the neighbouring pixel. The parameters set were adjusted per channel. For DAPI Sigma X and Sigma Y were 2.00 pixels and for Cy5 1.00 pixel was used. This program then produced a new image that has been background subtracted and gaussian smoothed.

2.6.1.3 Background subtraction for signal detection and *Pr13b1* signal definition

The slide scanner works by detecting photons released by fluorophores when they emit light. Because the photons are released in 360 degrees, the photon detector detects signal in a bell curve around the fluorophore despite it being emitted by one true fluorophore (Figure 19). This produced a spread of positive pixels for each true signal, although representative of only one RNA molecule, ultimately resulting in a set of signals in the positive slide that are "false signals" even though they are not present in the no probes control as the signal itself produces its own background signal.

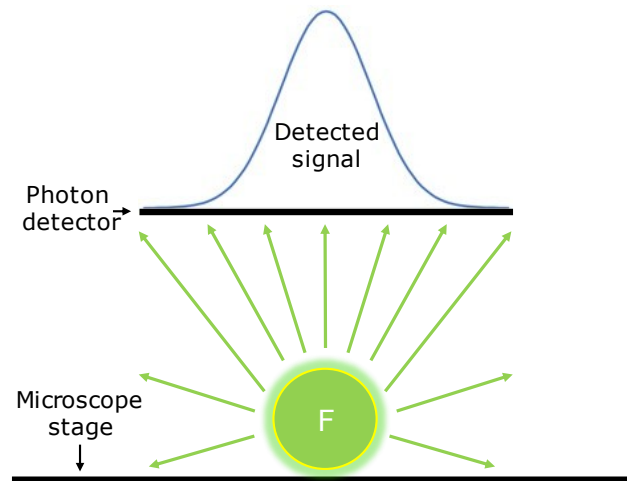


Figure 19: Diagram of photon release and detection. Fluorophore (F).

All slides had two adjacent sections of placenta mounted; one was stained with probes and the other was used as a no probes control. The no probes control was used to produce parameters for a background subtraction program. There were distinctive problems that arose due to the nature of the *Pr13b1* stain, which had an abundant and intense signal. The signal was so strong that the light exposure for the no probes control was exceptionally brief, meaning the autofluorescence produced in this slide was unusually low. This program used the DAPI signal with a diameter threshold of 280 pixels and circularity of 0.500 to identify cells and measured the highest Cy5 signal within a ring width of 10 pixels around the nuclei. The average maximum intensity of each cell was calculated, the median signal intensity is more commonly used but is less stringent. Then three standard deviations were added to the average maximum, which allows for a more precise correction due to the nature of the background signal being so low. This value was used as a lower threshold on the signal, which everything below this calculated pixel intensity was deemed as background and was excluded.

2.6.2 Cell Counting

2.6.2.1 Defining regions

It was important to gather data that was defined by its region. It was possible to perform the counts on both regions with the same parameters, however data defined by the junctional zone and labyrinth separately was desired. All slides had adjacent sections that were stained with H & E. This staining was performed by the Cardiff University Bioimaging Hub Core Facility (RRID:SCR_022556) which was imaged on the slide scanner (protocol 2.4.1.1) and were used as an additional guide to help with the

morphology of each individual section. The junction zone was defined and counted using the protocols described in 2.6.2.2 to 2.6.2.3. Then the labyrinth was counted in a separately defined zone. A “full” count was also performed which included junctional zone, labyrinth and decidua to gain total values. Once each region was analysed the counting program produced an area measurement which was recorded as the area of the counted region.

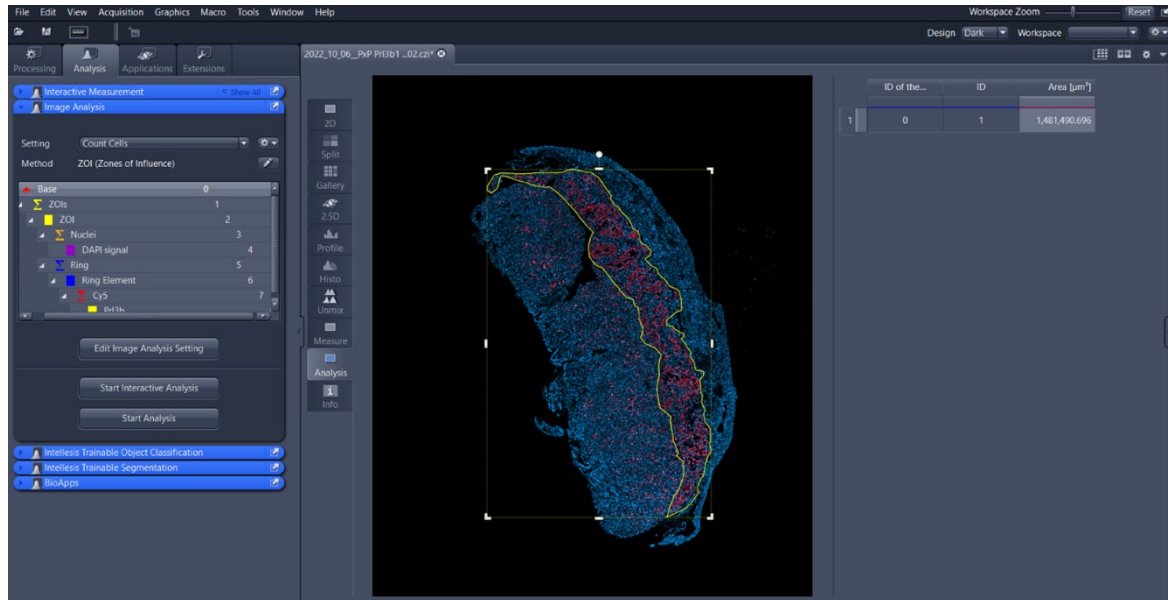


Figure 20: Defined region for counting with area value presented.

2.6.2.2 Cell identification

The DAPI signal was used to identify cells using a lower threshold value of 280 pixels and circularity of 0.500. This produced a total number of cells per region of interest (highlighted in purple Figure 21).

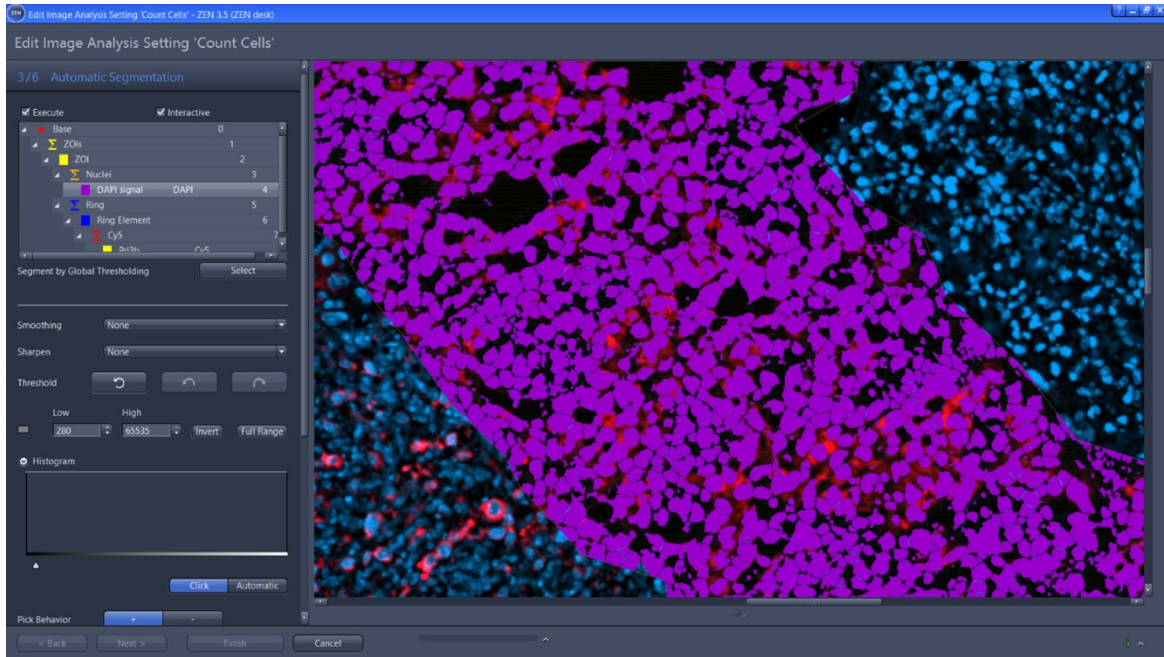


Figure 21: Zen program using counting program showing signal deemed to be nuclei in purple.

2.6.2.3 Ring element

The ring element was set to a diameter of 10 pixels around the nucleus of the defined cell. This reported *Pr13b1* signal within a 10-pixel diameter of the nucleus of anything that had been identified as a cell.

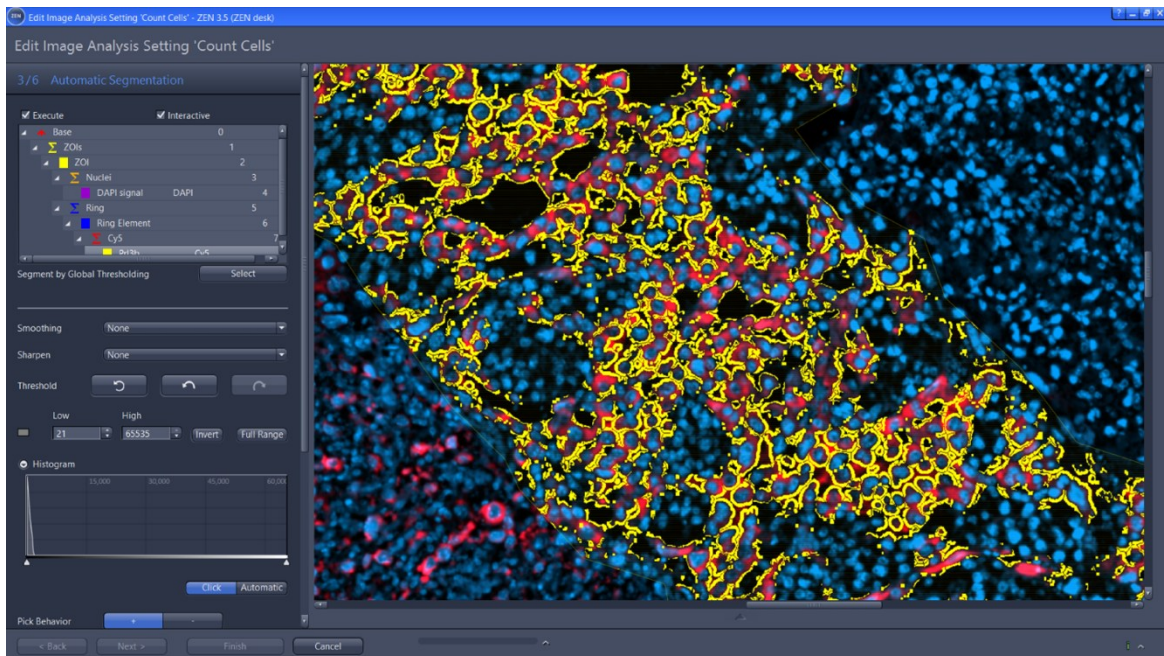


Figure 22: Image showing Cy5 signal in the perimeter of a cell in yellow within the junctional zone.

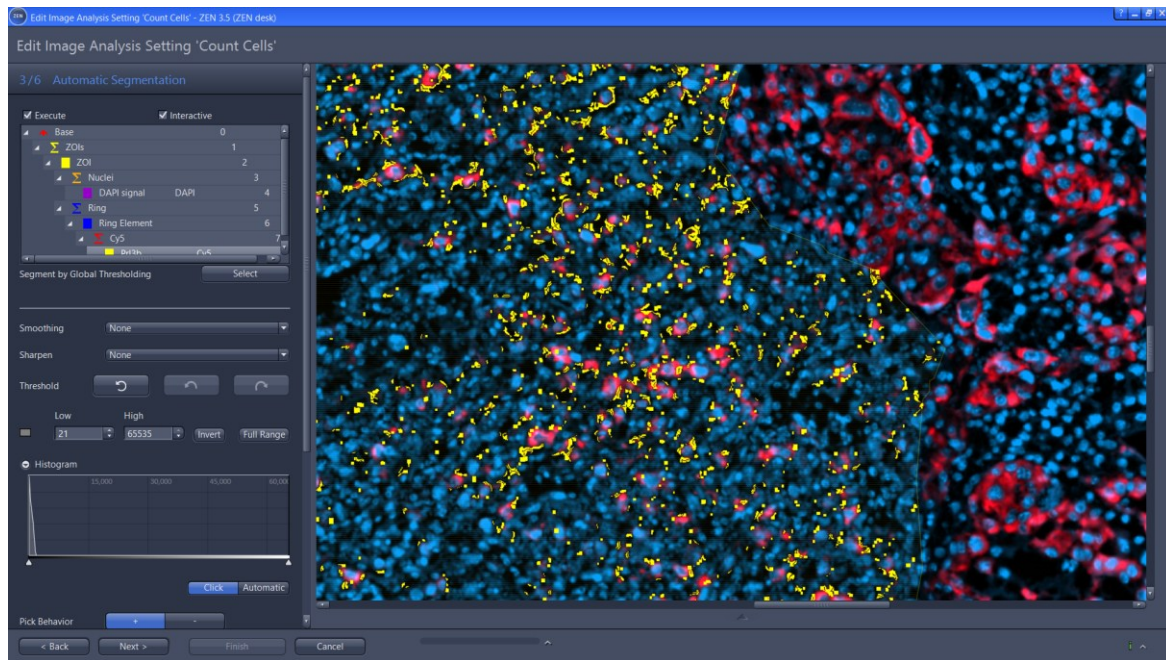


Figure 23: Image showing Cy5 signal in the perimeter of a cell in yellow within the labyrinth.

The ring element produced a total number of cells within the region of interest that contain Cy5 signal above background levels within a 10-pixel radius of that identified cell. These results were then exported into an excel spreadsheet for processing.

2.6.3 Data processing

The data that was generated from the ring element analysis was exported into an excel spreadsheet which contained every Cy5 signal linked to its parent of origin cell. A formula on Excel consolidated the parent of origin number and categorised the cells into positive and negative for Cy5 signal.

The formula to identify the number of cells within a region of interest was:

$$=COUNT(UNIQUE(\$A:\$A))$$

Equation 1: Excel formula to consolidate parent of origin cell number.

This formula counts all the unique parent IDs within the output data. The formula to identify which of those cells contains Cy5 signal within their perimeter was:

=COUNT(UNIQUE(FILTER(\$A:\$A,\$F:\$F>0,"")))

Equation 2: Excel formula to identify Cy5 signal within each cell.

This formula consolidates the unique parent ID numbers and filters out those that do not contain a signal within their perimeter.

2.6.4 Parietal trophoblast giant cell identification and quantification

The zen software was used to identify P-TG cells within the junctional zone. P-TG cells are located at the interface between the maternal decidua and the junctional zone. All cells identified by the program were measured by the program and their area was reported in the excel spreadsheet. A lower size limit was defined as 250 μm^2 . Cells above this size were deemed to be P-TG cells.

2.6.5 Decidua area measurement

The decidua was measured by the region contour polygon function which allowed manual definition of a region and produced an area measurement.

2.7 General tissue culture methods

2.7.1 Mycoplasma testing

Mycoplasma testing was conducted once per month on cells growing in the cell culture laboratory. The testing was performed using a PCR with primers able to detect 16s rRNA for all the most common types of mycoplasma contamination.

Oligo name	Sequence (5'-3')	GC (%)	Tm (°C)
Myco-5-1 F	CGCCTGAGTAGTACGTTTCGC	60	59
Myco-5-2 F	CGCCTGAGTAGTACGTACGC	60	59
Myco-5-3 F	TGCCTGAGTAGTACATTCGC	50	57.42
Myco-5-4 F	TGCCTGGGTAGTACATTCGC	55	59.82
Myco-5-5 F	CGCCTGGGTAGTACATTCGC	60	60.87
Myco-5-6 F	CGCCTGAGTAGTATGCTCGC	60	59

Myco-3-1 R	GCGGTGTGTACAAGACCCGA	60	60
Myco-3-2 R	GCGGTGTGTACAAAACCCGA	55	61.16
Myco-3-3 R	GCGGTGTGTACAAACCCGA	60	60

Table 15: Mycoplasma testing primer set sequences, GC percentages and melting temperatures.

Primers target Mycoplasma sequences from *M. Laidlawii*, *M. Fermentans*, *M. Hominis*, *M. Arginine* and, *M. Orale*, and include a further eight species (Uphoff and Drexler, 2002).

Desalted and dry primers were ordered from Sigma at 0.025 μ mole. They were suspended in 10 mM Tris as per the details provided by Sigma. A forward primer set was prepared by adding 10 μ L of each forward primer and diluting it in 40 μ L of 10 mM Tris. A reverse primer set was prepared by adding 10 μ L of each reverse primer and diluting it in 70 μ L of 10 mM Tris. A 100 μ L sample of cell culture supernatant was collected from an 80-100% confluent well after the cells and media had been incubated for 72 hours, making sure to test a variety of cell types and cell culture medias. The 100 μ L sample was collected into a 1.5 mL centrifuge tube. The sample was denatured at 95 °C for five minutes. The tubes were then spun at maximum speed for two minutes. A PCR reaction was set up using the mycoplasma primer mix (Table 15) and run on the PCR program detailed in Table 16.

Step	Temperature	Time	Cycles
Initial denaturation	95 °C	2 minutes	1
Denaturation	94 °C	30 seconds	
Annealing	50 °C	30 seconds	5
Extension	72 °C	35 seconds	
Denaturation	94 °C	15 seconds	
Annealing	56 °C	15 seconds	30
Extension	72 °C	30 seconds	
Hold	4 °C	Indefinite	1

Table 16: Mycoplasma PCR program.

The PCR products were run on a 1.5 % agarose gel with 5 μ L per 10 mL of safeview dye for 25 minutes at 80 V. The gels were visualised under UV light and imaged on a geldoc imager.

2.7.2 Foetal bovine serum inactivation

50 mL aliquots of foetal bovine serum (FBS) were thawed in a water bath at 37° C. Once thawed it was placed in the fridge whilst water bath was warmed to 56 °C (Pr-2). The FBS was then incubated at 56 °C for 30 minutes, occasionally mixed by inverting. The FBS was then cooled in the fridge and added to the media.

2.7.3 Mouse embryonic feeders (MEF)

2.7.3.1 MEF generation

Timed matings were set up for CD1 mice. On E12.5 (Day one) the uterus was dissected into cold PBS (pH 7.2 Thermo Fisher Scientific (Life Technologies) Cat no. 20012027). The uterus was transferred into a 10 cm petri dish containing cold PBS (-) (Without Calcium, Magnesium or phenol red, Gibco, Cat No. 20012027) and Penicillin-Streptomycin (10000 U/mL) (Thermo Fisher Scientific (Life Technologies), Cat no. 15140122). A 6 well tissue culture plate (Nunc 6 Well Multidish Nunclon Delta SI, Nunc, Cat No. 140685) was set up with 4 mL of "MEF media" (Base media Gibco DMEM, High Glucose, GlutaMAX Supplement, HEPES, Cat no, 15235697, with 50 ug/mL Penicillin-Streptomycin (10000 U/mL), 10 % FBS (inactivated) (ES-cell FBS qualified US origin, Thermo Fisher Scientific (Life Technologies), Cat No. 16141079) and *B*-mercaptoethanol (*B*-ME) (Thermo Fisher Scientific (Life Technologies), Cat No. M3148) in each well. Each embryo pod was dissected from the uterus and moved into a new dish of cold PBS (-). The yolk sac was removed from each embryo and the embryo was moved into a new plate of cold PBS (-). Using sharp sterilised tweezers, the innards of the embryo were removed, and the remaining tissue was moved into a new plate of cold PBS (-). Using a 2 mL syringe each embryo was collected individually with the smallest volume of PBS (-). A 19 G needle was attached to the end of the syringe and the embryo was expelled through the needle into the pre-prepared 6 well plate containing MEF media. The cells were dissociated further by collecting the contents of the well and flushing it through the needle a further three times. These were then incubated at 37 °C and 5% CO₂. This was referred to as passage zero (P0). After 24 hours (day two) the media was aspirated and replaced with MEF media. After a further 24 hours (day three) each 6 well containing P0 MEFs was passaged onto two 10 cm plates. The media was aspirated off each well and the well was

washed with PBS (-). The PBS (-) was aspirated and 1 mL of Trypsin (Gibco Trypsin-EDTA (0.05%) Fisher Scientific, Cat No. 11580626) was added. The cells were incubated in the trypsin for five minutes at 37 °C. Trypsinisation was stopped by adding 1 mL of MEF media to the well. The cells were then manually suspended by vigorous hand pipetting with a P1000. 500 µL of the cell suspension was then pipetted into a 10 cm dish containing 10 mL of prewarmed MEF media. These cells were then referred to as P1 and were placed back into the incubator.

2.7.3.2 Freezing MEFs

To create a stock of early passage MEFs, these confluent 10 cm plates were frozen. Each plate was washed with PBS (-) and the cells were trypsinised as previously detailed. During trypsinisation a 2X freezing media was prepared, concentration of 50% FBS, 20% DMSO (Sigma, Cat No. D8418) and 30% MEF media. Once the cells were trypsinised, they were suspended in MEF media. The freezing media was added slowly, and the solution was aliquoted into cryovials (1.0 mL Cryotube, Nunc, Cat No. 377224K). The cryotubes were then loaded into a Mr Frosty (Nalgene, Cat No. 5100-0001) which was placed into a -80 °C for four hours. The tubes were then put into long-term storage at -150 °C.

2.7.3.3 MEF inactivation

MEF cells support the growth of TS cells by producing metabolites and other factors that the TS cells require. However, MEF cells could outcompete TS cells so must be inactivated before being placed in the same plate with them. Inactivation allows the cells to live and continue to metabolise, but prevents them from dividing, ultimately stopping their growth. Mitomycin C (MMC) (From *Streptomyces caespit*, Merck Life Science Limited Cat no: M0503-2 Milligrams) was suspended in 10 mL of PBS (-) and aliquot into 500 µL and 250 µL aliquots and stored in a -20 °C freezer. MEFs were grown to 80-90% confluence in 10 cm plate. MMC was added to the media to a final volume of 10 mg/mL. Cells were incubated for three to four hours in the incubator. Cells were washed twice in PBS (-) and either frozen as an inactive MEF stock, or immediately used for co-culture or used to generate conditioned media.

2.7.4 Conditioned media

Conditioned media was prepared by culturing MMC-treated (inactivated) MEF cells in TS media for 72 hours. Appropriate cell densities can be found in Table 17.

Diameter of dish	100 mm	150 mm
Conditioned Media plated cell number	2.4x10 ⁶	6 x 10 ⁶

Table 17: Cell densities for producing conditioned media.

The inactive MEFs live for 10 days producing metabolites and other factors that support TS cell growth. These cells can provide three batches of conditioned media over the 10-day period. Once the media was collected it was centrifuged at 2300 g for 20 minutes at 4° C. The media was filtered using a 0.45 µM filter. It was then stored at -80° C.

2.8 Mouse trophoblast stem (mTS) cells

2.8.1 Generation of mTS cells

The protocol published by S. Tanaka 2006 (Pages 34-55), was followed. Female mice were superovulated via two timed injections of PG600 (Merck, Cat No. 161386 R2) on day one and three. Timed matings were set up on day three and the female mice were plug checked on the morning of day four. On day six inactive MEFs were plated onto 4-well plates at 1 x 10⁵.

Diameter of plate	4 well plate	35 mm	60 mm	100 mm	150 mm
Co-culture density	4 x 10 ⁴ /well	2 x 10 ⁵	4 x 10 ⁵	1.2 x 10 ⁶	3 x 10 ⁶

Table 18: Inactive MEFs co-culture plating densities.

On day seven the embryos were at E3.5. The 4-well feeder plates media was replaced with fresh media (TS + 1.5X F4H (Table 20)) before dissections began. The oviducts were removed from the female and flushed with M2 (Sigma Aldrich. Cat No. M7167). The embryos recovered were washed three times in M2 and transferred into the 4-well plates containing feeders, one embryo per well. From this point the stage of the embryo was monitored daily as the stage of the embryo indicated when the next step should be executed, and the transgenes could affect the progression of the embryo. From now on the protocol will refer to the predicted stage of development. The E3.5 (day seven) embryo had blastulated. On day eight the embryo had hatched and was beginning to plate down. On day nine the cells formed an outgrowth of TS cells and the

media was refreshed carefully so as to avoid disturbing the embryo. On day 10 the outgrowth of TS cells was a suitable size to be disaggregated.

TS cell media	(mL)
<i>B</i> -ME	3.5 μ L
ES Cell FBS (20%) (Gibco, Cat No. 16141-079)	100 mL
1 mM Sodium Pyruvate (Gibco, Cat No. 11360-070)	6 mL
50 μ g/mL Penicillin/ Streptomycin	6 mL
100X Glutamax (Gibco, Cat No. 35050-061)	6 mL
RPM1 1640 (Gibco, Cat No. 11504566)	382 mL
Total volume	500 mL

Table 19: TS media additives and concentrations.

TS + 1.5X F4H medium	Volumes
TS cell media (Table 19)	10 mL
Basic FGF4 (25 ng/mL) (Peprotech, Cat No. 100-31)	15 μ L
Heparin stock solution (1 μ g/mL) (Sigma, Cat No. H6279)	15 μ L
Total volume	10 mL

Table 20: TS+1.5X F4H media recipe.

The media was aspirated from the well and the cells were washed twice in PBS (-). The well was trypsinised with 100 μ L 0.1% trypsin (0.4 mM EDTA) and incubated for five minutes at 37° C, 5% CO₂/95% air. The cells were disaggregated using a hand pipette, focusing on the location of the plated down embryo. The trypsinisation was then stopped by adding 400 μ L of TS + 1.5X F4H. After eight hours the well was aspirated, and the media was replaced with 500 μ L of TS + 1.5X F4H conditioned. The media was refreshed every 48 hours while the cells were monitored. Between days 13 and 18 TS colonies started developing. These appeared as flat, jelly-like epithelial sheets, with a border of TG cells.

Other cell types occasionally developed in each well. It was possible for these cells to outcompete the TS cells. Under these circumstances the TS cells were removed from the well using the following steps. Feeder plates were prepared as previously described. A 96-well plate had 50 μ L of trypsin added to each well (one well per line). The media was removed from the TS cell plates containing the colonies. Each well was washed

twice in 500 μ L PBS (-), the second lot of PBS (-) was left in the well. Using a dissection microscope in the tissue culture hood the TS cell colonies were picked up with a P10 and added to the 96 well plate. The clumps of cells were manually disaggregated by pipette mixing using a hand pipette containing 150 μ L of TS +1.5XF4H. The disaggregated cells were then added to the fresh feeder plates. The media was replaced in these cells after eight hours. Colonies reformed three to four days after picking the colonies and the wells were fed every 48 hours. If only a few patches of TS cells formed the entire well was disaggregated again using the method applied on day 10.

Once the well was 50% confluent the line was passaged onto a 6 well plate. Once the 6 well plate reached 80-90% confluency the cells were passaged into a 10 cm plate with inactivated MEFs. The line was then large enough to be genotyped (protocol 2.2). These cells were grown until they were large enough to be frozen and stored.

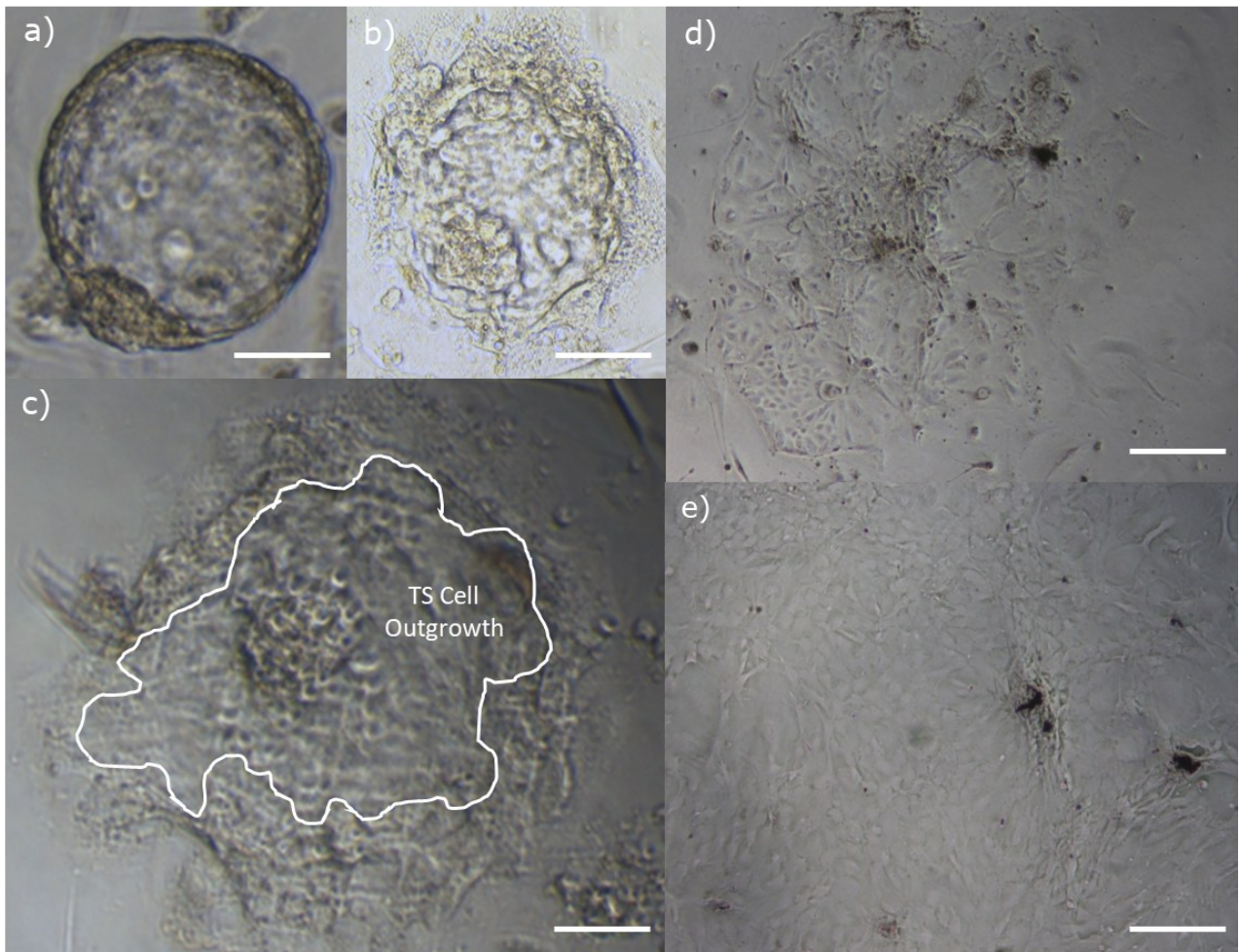


Figure 24: Phases of mouse trophoblast stem cell derivation.
a) Day seven blastulated embryo. **b)** Hatched embryo plating down. **c)** Day 10 embryo with large TS cell outgrowth. **d)** TS cell colony after

embryo disaggregation. **e)** TS cell line growth. Scale bars represent 50 μm .

2.8.2 mTS cell genotyping

During the freezing or passaging process a sample of the cell line was taken for genotyping. TS cells were separated from MEFs via their plating speeds. Once the cells had been plated onto the 10 cm plate, any MEFs that were still with the TS cells were given one hour to plate down as they have a faster rate of plating down than TS cells. This purified the TS cell collection. One hour after plating, 1 mL of media from the 10 cm plate was collected into a 1.5 mL autoclave microcentrifuge tube. The tube was spun at 380 g for five minutes. The supernatant was removed, and the cell pellet was suspended in lysis buffer (1 M Tris 8.0 pH 8.0 (Sigma), 0.5 M EDTA pH 8.0 (Sigma), 10% SDS (Sigma), 5 M NaCl in water) containing Proteinase K (20 mg/mL PK, Sigma UK). This was digested at 55 °C for one hour followed by a 20-minute incubation at 85 °C to inactivate the PK. This sample was then processed via genotyping (protocol 2.2).

2.8.3 mTS Cell differentiation assay

TS cells were induced to differentiate by withdrawal of FGF4 and Heparin. Their differentiation proceeds along the trophoblast cell lineage and results in formation of all trophoblast subtypes, predominantly giant cells. A 6 well plate containing 40,000 cells per well was set up with conditioned TS + 1.5F4H. 24 hours after plating (D0), media was aspirated, and wells were washed twice in PBS. Conditioned TS medium without FGF4 and Heparin was added. The media was changed every 2 days until 10 days differentiation. At each two-day timepoint cells were collected and counted for a proliferation assay.

2.8.4 TS cell counting proliferation analysis

Cells were resuspended in 1 mL media. 10 μL of cell suspension was pipetted onto a haemocytometer. Cells were counted in four large (red in Figure 25) squares, including those over or touching the lines on top and on the left, but not cells over or touching the right or bottom lines. The concentration in cells per mL was calculated using the Equation 3.

$$\frac{\text{Cell count}}{4} \times 10,000$$

Equation 3: Cell number calculation.

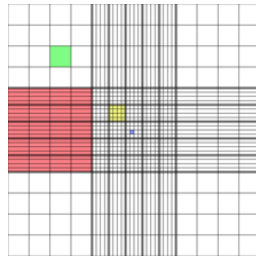


Figure 25: Haemocytometer used for counting cells.

2.9 Human trophoblast stem cells

2.9.1 Training in Japan and acquiring human trophoblast stem cells

Human trophoblast stem cells were gifted to Professor Ros Johns laboratory by Professor Okae from the University of Kumamoto. Training for working with hTS was provided by Dr Sekiya.

2.9.2 Maintenance of human trophoblast stem cells

Human trophoblast stem cells were cultured in hTS cell media with 0.5 μ L per mL of iMatrix511 (ReproCELL, Cat No. NP892-011), incubated at 37 $^{\circ}$ C for 10 minutes prior to adding cells.

hTS basal media	500 (mL)
DMEM/F12 (with L-glutamine) (Corning, Cat No. 10-090 CV)	485
30% BSA (Sigma-Aldrich, Cat No. A9205)	2.5
50 μ g/mL Penicillin/ Streptomycin	2.5
Insulin-Transferrin-Selenium-Ethanolamine (ITS -X) (100X) (Thermo Fisher Scientific, Cat No. 51500056)	5
KnockOut Serum Replacement (KSR) (Gibco, Cat No.11520366)	5
Total volume	500 mL

Table 21: hTS basal media recipe.

hTS medium	40 mL
hTS basal media (Table 21)	40 mL
10 mM ROCK Inhibitor Y27632 (MedChemExpress, Cat No. HY-10071)	10 μ L
100 μ g/mL EGF (Corning, Cat No.354052)	10 μ L
100 μ g/mL Recombinant Human Bone Morphogenic Protein-4 (BMP) (R&D Systems, Cat No. 314-BP-050)	4 μ L
Valproic Acid (VPA) (Apexbio, Cat No. B1251-APE)	5 μ L
10 mM A83-01 (TargetMol, Cat No. ABIN4879842)	20 μ L
4 mM CHIR99021 (Sigma-Aldrich, Cat No. SML1046)	20 μ L
200 mM L-Ascorbic acid (Cayman Chemical, Cat No.16457)	40 μ L
Total volume	40 mL

Table 22: hTS media recipe.

Frozen vials were thawed in a water bath at 37 °C. They were then transferred into a 15 mL centrifuge tube with 1 mL of pre-warmed TS basal medium. Cells were centrifuged at 380 g for three minutes. The supernatant was aspirated, and the cell pellets were gently suspended in 1 mL of pre-warmed TS medium. The cells were transferred into pre-prepared plates. Cells were passaged every 48 hours at ratios of 1:2, 1:4 or 1:8 depending on density.

2.9.3 Passaging of hTS cells

Plates were pre prepared with iMatrix511 and incubated for 10 minutes at 37 °C. The TS medium was aspirated from each well. A 1:1 mixture of TrypLE (TrypLE™ Express Enzyme (1X), no phenol red, Gibco, Cat No. 12604021) and PBS (-) was added to each well and the plates were incubated for 15 minutes at 37 °C. The cells were suspended in Basal TS medium and transferred into a 15 mL tube. The cells were centrifuged at 380 g for three minutes. The supernatant was aspirated, and the cells were gently suspended in pre-warmed TS medium. The cells were then transferred into prepared plates.

2.9.4 Freezing human trophoblast stem cells

Prepare fresh freezing media.

hTS Cell Freezing media	(%)
FBS	50
TS basal medium	30
DMSO	20

Table 23: Freezing media for hTS cells.

The TS media was aspirated from each well. A 1:1 mix of TrypLE-PBS was added to each well and incubated for 15 minutes at 37 °C. The cells were suspended in Basal TS medium and transferred into a 15 mL tube. The cells were centrifuged at 380 g for three minutes. The cells were gently suspended in pre-warmed TS media in a 15 mL tube. The freezing media was added to the 15 mL tube at a 1:1 ratio of cell suspension to cell freezing media. The cell/freezing media mixture was then transferred into cryovials. The cryovials were placed into a Mr Frosty which was stored in a -80°C freezer overnight. Once frozen, the cells were stored in a -150°C freezer.

2.9.5 Preparing human trophoblast stem cell KO lines

Guide RNA sequences were designed using CRISPOR and snappene programs (Table 24).

CRISPR	Sequence	PAM	Design credit
<i>PHLDA2</i> CRISPR sequence, 5'-sgRNA-1	CAGCTATAAAGGCCGCGCCG	GGG	Dr Asato Sekiya
<i>PHLDA2</i> CRISPR sequence, 5'-sgRNA-2	GGCAGCTATAAAGGCCGCGC	CGG	Dr Asato Sekiya
<i>PHLDA2</i> CRISPR sequence, 3'-sgRNA-1	GTCCCGGCTGTTAGGGCGCA	TGG	Dr Asato Sekiya
<i>PHLDA2</i> CRISPR sequence, 3'-sgRNA-2	GTCGGACCGAGGCTAGGACG	GGG	Dr Asato Sekiya
<i>PEG3</i> CRISPR sequence, 5' gRNA 1	GCGACGACGACATGACCCGG	CGC	Professor Nicholas Allen
<i>PEG3</i> CRISPR sequence, 5' gRNA 2	GATGACCCGCCATCCCCGAG	CTC	Professor Nicholas Allen

Table 24: CRISPR sequences.

The sequences were ordered at 2 nmol with standard desalting (IDT, Alt-RTM CRISPR-Cas9 crRNA). Guides were suspended in 10 µl of IDTE buffer (pH 8.0 Cat No.11-05-01-13) to a concentration of 200 µM. The guides

were then combined with a tracr (20 nmol of tracrRNA in 100 μ l of IDTE) which hybridises to crRNA to activate the Cas9 enzyme.

Ribonucleoprotein (RNP) Complex	(μl)
Guide RNA	1.7
tracrRNA	1.7
IDT duplex buffer	1.7
Total volume	5.1

Table 25: RNP complex recipe.

The complex was heated to 20 °C for two minutes and then cooled slowly to RT. The cas9 mix was then prepared by adding 1.25 μ l of Cas9 with 0.76 μ l of Cas9 Storage Buffer in a 0.2 mL tube. The cas9 mixture was then added to each of the guide RNAs at a 1:1 ratio of RNP complex to cas9. These were then incubated at 95 °C for two minutes then at RT for 20 minutes.

Reagents were prepared for nucleofection. The Lonza P3 Primary Cell Solution Box kit (Cat. No. PBP3-00675) was used along with the Lonza Amaxa P3 Primary Cell kit (Cat. No. V4XP-3032) cuvettes.

Nucleofection Solution	(μl)
Lonza P3 buffer	15.6
Lonza Supplement 1	4.4
Guide mix 1	1
Guide mix 2	1
Total volume	22

Table 26: Nucleofection solution recipe.

Media was aspirated from wells and 1:1 TrypLE-PBS (-) was added, then plates were incubated for 15 minutes at 37 °C. Once detached, cells were transferred into a 15 mL tube containing pre-warmed TS basal media. Cells were then centrifuged at 380 g for three minutes. The supernatant was then aspirated, and the cells were suspended in pre-warmed TS media. Cells were counted and a population of 200,000 cells were transferred into a 1.5 mL tube which was centrifuged at 380 g for three minutes. The supernatant was aspirated, and the cells were resuspended in 22 μ l of the Lonza kit nucleofection solution. The suspended cells were

then pipetted into a cuvette. The cuvette was placed into the 4D-Nucleofector (Lonza Bioscience) and had program CA137 (Electrical potential: 1200 V, pulse width: 30 milliseconds, pulse number: 1) applied. The cells were then slowly diluted with 200 μ L of pre-warmed TS media.

2.9.6 Single cell cloning

2.9.6.1 Single cell cloning by dilution

From this point cells were directed to form single cell colonies. There were three different methods used to produce single cell colonies. The dilution method was one of these. After the cells had settled post nucleofection, the cells were counted and 200 hTS cells were diluted into 13 mL of pre-warmed TS media. From this 100 μ L was aliquoted into preprepared 48 well plates. This produced an average of one cell per well. After three days the media was changed. Between days six and eight the colonies were visible and were selected based on morphology to be passaged. Only those colonies that were singular in each well were selected. Cells were grown up until they were large enough to be frozen and genotyped (method 2.2) using KO confirmation primers detailed in Table 27.

Primer	TM	Annealing	Sequence	Expected band size
<i>PHLDA2</i> F	60	59.91	GCGGGGAGGGGCAGCTATAAAG	WT allele: 1048 bp KO allele: 471 or 244 bp
<i>PHDLA2</i> R	60	59.87	GCGGGGAGGGGCAGCTATAAAG	
<i>PEG3</i> F (1)	60	59.97	GCTCCTGCCTTTTTGGTGTG	WT allele: 627 bp KO allele: 462 bp
<i>PEG3</i> R (1)	60	59.68	AGCAGCCTGTTGCAAATTCC	
<i>PEG3</i> F (2)	60	59.86	GCGACCGGTGTCCTCTTAG	WT allele: 728 bp KO allele: 561 bp
<i>PEG3</i> F (2)	60	60.11	CAGGTTCCCAGGCTCATCTG	

Table 27: Primer sequences for hTS knockout confirmation.

2.9.6.2 Single cell cloning by fluorescence-activated cell (FAC) sorting

To allow FAC sorting, cells had to be combined with a fluorescent tracrRNA (5'ATTO550, Integrated DNA technology, Cat No. 1075928) to identify cells that had taken up the transgene. The BD FACs Aria machine was used and operated by Mr Mark Bishop as an in-house service. Around 24 hours after nucleofection cells were trypsinised and moved into a 15

mL falcon tube in TS media and placed on ice. Multiple 96-well plates were also prepared with iMatrix511 and TS media and placed on ice. Using a control line, the cell size was determined by the machine. The transfected cells were then processed, collecting the top 10% of cells in relation to their intensity of the fluorescent signal. A single cell was placed into each well. Plates were monitored over the growth of the colonies and colonies were passaged when they reached an appropriate size and morphology. Cells were grown up until they could be frozen and genotyped (method 2.2) using KO confirmation primers detailed in Table 27.

2.9.6.3 Single cell cloning by colony picking

Before nucleofection 10 cm plates were prepared with iMatrix511. After the nucleofection step cells were split across two 10 cm plates, one containing 10% of the cells and one containing the remaining 90% of the cells. These plates were fed every 48 hours until colonies were an appropriate size for picking, which was after four to five days. The colonies were then picked from the 10% plate. Half of the media on the plate was removed and 7-10 mL of dissociation buffer (Gibco, Cat No. 13151014) was added. The plate was then incubated for five-ten minutes. Using a P20 set at 5 mL, individual clones were picked under a microscope and transferred into a preprepared 96 well plate. The 10 cm plate was then re-fed and was used for further colony picking. The 10% and 90% plates were frozen to bank the bulk transfected cells. Picked colonies were then grown up until they were able to be frozen and genotyped (method 2.2) using KO confirmation primers detailed in Table 27.

2.9.7 Differentiation assay

Wells of 6 well plates were coated in 5 mg/mL Col IV (Collagen IV, Corning, Cat No. CF718) in PBS (-) and incubated for 1.5 hours at 37 °C. This media was then replaced with TS media. Cells were suspended in TS media and counted. Per well, 100,000 cells were plated down. After 48 hours or once wells had reached 50% confluency, cells were entered into the differentiation trial. For each line "Day 0" plates were grown alongside the differentiation plate as an undifferentiated control. The cells to undergo differentiation were moved into ST(2D) medium.

ST(2D) Media	Volumes
Basal medium	10 mL
10 mM Y27632	2.5 μ L
KSR	400 μ L
5 mM Forskolin (Santa Cruz Biotechnology, Cat No. sc-3562A)	4 μ L
Total volume	10 mL

Table 28: Differentiation media recipe.

On day five, the serum was collected from each well into 2 mL tubes and stored at -80 °C. The rest of the media was removed from the well and the plates were snap frozen on dry ice then transferred to a -80 °C freezer. Cells were then harvested for RNA, DNA or protein following protocols 2.10.1, 2.2.1 or 2.11.

2.10 Quantitative reverse transcription polymerase chain reaction (qRT-PCR)

2.10.1 RNA extraction

For extracting RNA from E14.5 or E16.5 placenta the GenElute (TM) Mammalian Total RNA Miniprep Kit (Sigma-Aldrich, Cat No. RTN350) was used. Placenta samples bisected in protocol 2.2.4.1 and stored at -80 °C were bisected again, giving a quarter of a placenta. This was lysed in 500 μ L of lysis buffer (Sigma-Aldrich, Cat No. RTN350) containing 5 μ L *B*-ME. Samples were then homogenised using a motorised sterile pestle. The lysate was pipetted into the GenElute Filtration Column and centrifuged at 9069 g for two minutes. 500 μ L of 70% EtOH was mixed with the filtered lysate. The mixture was then loaded into the GenElute Binding Column and centrifuged at 9069 g for 30 seconds. The column was then washed with 250 μ L of wash solution 1 (Sigma-Aldrich, Cat No. RTN350) and centrifuged at 9069 g for 30 seconds. A DNase I solution was prepared for each sample with 10 μ L of DNase I with 70 μ L of DNase Digest Buffer (Sigma-Aldrich, Cat No. RTN350), which was then pipetted onto the membrane and incubated at RT for 15 minutes. The column was then washed with 250 μ L of wash solution 1 (Sigma-Aldrich, Cat No. RTN350) and centrifuged at 9069 g for 30 seconds. The column was then washed with 500 μ L of wash solution 2 (Sigma-Aldrich, Cat No. RTN350) and

centrifuged at 9069 g for 30 seconds. A second wash with 500 μ l of wash solution 2 was done with a centrifuge at 9069 g for two minutes. The binding column was transferred into a collection tube where the RNA was eluted in 15 μ l of either RNase free H₂O or elution solution (Sigma-Aldrich, Cat No. RTN350) and centrifuged at 9069 g for one minute.

For extracting RNA from cell samples RNeasy Micro kit (Qiagen, Cat No. 74004) was used. Cells were lysed in their plate in 350 μ L Buffer RLT plus B-ME (Qiagen, Cat No. 74004) and collected into a 1.5 mL tube. The samples were then vortexed for one minute to homogenise cells. Samples were pipette mixed with a 1:1 ratio of cell lysate and 70% EtOH. This mixture was then transferred to a RNeasy MinElute spin column in a 2 mL collection tube and centrifuged for 15 seconds at \geq 8000 g. To each spin column, 350 μ L of Buffer RW1 (Qiagen, Cat No. 74004) was added and the samples were centrifuged for 15 seconds at \geq 8000 g. A DNase treatment was applied to each sample using 10 μ L of DNase I stock solution to 70 μ L Buffer RDD (Qiagen, Cat No. 74004), which was then incubated for 15 minutes at RT. Samples were washed with 350 μ L Buffer RW1 and centrifuged for 15 seconds at \geq 8000 g. 500 μ L of Buffer RPE (Qiagen, Cat No. 74004) was then added to the spin column which was centrifuged for 15 seconds at \geq 8000 g. 500 μ L of 80% EtOH was added to the samples which were then centrifuged for two minutes at \geq 8000 g. The membrane was dried by centrifuging it at full speed for five minutes with their caps off. The column was then placed into a collection tube and 14 μ L RNase-free water was pipetted directly onto the membrane. This was centrifuged at full speed for one minute. Once RNA samples were prepared their concentration and purity was determined with a Nanodrop (Thermo Scientific™ NanoDrop™ One/OneC Microvolume UV-Vis Spectrophotometer). RNA integrity was measured using the 4200 TapeStation system (G2991BA, Agilent).

2.10.2 DNase treatment

RNA samples were treated with DNase. Using the RNA concentrations determined by the Nanodrop, a standard quantity of RNA was diluted into a set volume of RNase free water. The DNase mix was then set up.

Reagent	Volumes for Placenta Samples	Volumes for Cell Samples
RNA in RNase free water	7 μ L of RNA (2 μ g)*	8.5 μ l of RNA (0.5 μ g)*
RNase free DNase 10X Reaction Buffer (Promega, Cat No. M6101)	1 μ L	1 μ L

RQ1 RNase-Free DNase (Promega, Cat No. M6101)	2 μ L	0.5 μ L
Total volume	10 μL	10 μL

Table 29: DNase treatment reagent recipe.

Samples were then incubated at 37 °C for 30 minutes. 1 μ L of DNase Stop Solution (Promega, Cat No. M6101) was added to each tube to terminate the reaction. The tubes were then incubated at 65 °C for 10 minutes to inactivate the DNase.

2.10.3 cDNA synthesis and sample validation

Each sample was set up with a reverse transcriptase negative (RT-) control. With the reverse transcriptase positive (RT+) tube containing 9 μ L DNase1 treated RNA, plus 2 μ L RNase free H₂O (total volume 11 μ L) and the RT- tube containing 1 μ L DNase1 treated RNA, plus 10 μ L RNase free H₂O (total volume 11 μ L). 1 μ L 500 mg/mL Random hexamers (Promega, Cat No. C1181) was added to each tube. The tubes were then incubated at 70 °C for five minutes. These were then spun down for 30 seconds and placed on ice. A cDNA master-mix was prepared following the Table 30.

cDNA master-mix	1X (μL)
5X First-Strand Buffer (Thermo Fisher Scientific (Life Technologies), Cat No. 10777019)	4
10 mM dNTPs	1
0.1 M DTT (Thermo Fisher Scientific (Life Technologies), Cat No. 10777019)	1
RNaseOUT Recombinant RNase Inhibitor (Thermo Fisher Scientific (Life Technologies), Cat No. 10777019)	1
Total volume	7

Table 30: cDNA mastermix.

Samples were then incubated at 37 °C for one minute. 1 μ L of SuperScript™ III RT (200 units/ μ L) (Thermo Fisher Scientific (Life Technologies), Cat No. 18080044) was added to each RT+ tube and 1 μ L RNase free H₂O to each RT- tube. Samples were incubated at 50 °C for one hour for 2.0 μ g samples and for 2 hours for 0.5 μ g samples. The reaction was stopped by heating the samples to 70 °C for 15 minutes then placing them on ice. A PCR was then run on the samples following protocol 2.2.2, with *B-actin* primers (Table 7).

2.10.4 qRT-PCR

Targeted qRT-PCR primers were ordered from sigma at 0.025 μ mole and were suspended as instructed by the supplier. A working stock of the primer was diluted following the instructions in Table 31.

Primer Mix Working Stock	(μ L)
100 mM stock of Forward Primer	25
100 mM stock of Reverse Primer	25
10 mM Tris (made from Sigma 1M stock)	50
Total volume	100

Table 31: Primer working mix.

2.10.5 Primer design

Primers were designed using Primer3. qRT-PCR primers were designed to amplify a sequence shorter than 250 bp and spanned an intron. The gene target sequences were found on NCBI, where the mRNA sequence was listed. This sequence was copied and pasted into Primer3. The introns were identified and flagged using the symbols || to annotate them. The product ranges and target locations were then specified. The “pick primers” function was then selected. The primer sequences were then evaluated based on their binding efficiencies and target specificity. Once ordered, they were validated on cDNA and gDNA samples to confirm the band sizes of their products.

2.10.6 Plate preparation

Each 384-well plate was laid out with 6 target primers which investigated a specific subset of targets (Table 32). Each set was also run with two reference genes. The qRT-PCR plates were prepared in duplicate.

Primer	Sequence	Species	Part of project	Marker	Details	References
<i>B-actin</i> F	CCTGTATGC CTCTGGTC GTA	Mouse	<i>Phlda2</i> ^{+/+BACx1(B^{L6})} and mTS	Reference gene	cDNA: 260 bp, gDNA: 260 bp	(Saruta et al., 2010) Tunster 2009 PhD
<i>B-actin</i> R	CCATCTCCT GCTCGAAG TCT					
<i>Blimp1</i> F	GGGTACTTC TGTTCAAGC CG	Mouse	mTS	S-TG cells, spiral artery (SpA-) TGCs and C-TG cells	cDNA: 182 bp, gDNA: 6568 bp	Unpublished, designed in house.
<i>Blimp1</i> R	TCCTGTTGG CATTCTTGG GA					
<i>Cdx2</i> F	AAGACAAAT ACCGGGTG GTG	Mouse	mTS	TS cell marker	169 bp	Feodor duPasquier

<i>Cdx2</i> R	CTGCGGTT CTGAAACCA AAT					Price PhD, 2012
<i>CGA</i> F	ATGTTCTCC ATTCCGCTC CT	Human	hTS	hCG	Spans intron 2, cDNA: 189 bp, gDNA: approx 390 bp	Unpublished, designed in house.
<i>CGA</i> R	AAGTGGAC TCTGAGGT GACG					
<i>CGB</i> F	CAGCATCCT ATCACCTCC TGGT	Human	hTS	hCG	cDNA: 102 bp	(Okae et al., 2018)
<i>CGB</i> R	CTGGAACAT CTCCATCCT TGGT					
<i>Ctsq</i> F	TGGAAACG TGCACTTGG TAG	Mouse	<i>Phlda2</i> ^{+/+} BACx1(B L6)	Spongiotrop hoblast giant cell	cDNA: 196 bp, gDNA: 1059 bp.	Matthew Lee Bosworth PhD from Cardiff Published 2019
<i>Ctsq</i> R	GTGGGATC AGTTTGCCT GTT					
<i>Dlx3</i> F	CGTTTCCAG AAAGCCCA GTA	Mouse	<i>Phlda2</i> ^{+/+} BACx1(B L6)	Labyrinth	cDNA: 169 bp, gDNA: 1678 bp	Matthew Lee Bosworth PhD from Cardiff Published 2019
<i>Dlx3</i> R	ACTGTTGTT GGGGCTGT GTT					
<i>Eomes</i> F	GGCAAAGC GGACAATA ACAT	Mouse	mTS	TS cell marker	2 transcripts, Spans 2 introns, cDNA: 192 bp	(Astwood & Greep, 1938)
<i>Eomes</i> R	AGCCTCGG TTGGTATTT GTG					
<i>Essrb</i> F	AACAGCCC CTACCTGAA CCT	Mouse	mTS	TS cell marker	Includes all 5 t/c; cDNA: 249 bp	(Astwood & Greep, 1938)
<i>Essrb</i> R	CTCATCTGG TCCCCAAGT GT					
<i>Flk1</i> F	GGCGGTGG TGACAGTAT CTT	Mouse	<i>Phlda2</i> ^{+/+} BACx1(B L6)	Endothelium	cDNA: 163 bp	Matthew Lee Bosworth PhD from Cardiff Published 2019
<i>Flk1</i> R	GTCACTGAC AGAGCGCA TGA					
<i>Gapdh</i> F	CACAGTCAA GGCCGAGA ATG	Mouse	<i>Phlda2</i> ^{+/+} BACx1(B L6) and mTS	Reference gene	cDNA: 242 bp, gDNA: 242 bp	Tunster PhD, 2009
<i>Gapdh</i> R	TCTCGTGGT TCACACCCA TC					
<i>Gcm1</i> F	AGCCTGTGT TGAGCAGA CCT	Mouse	<i>Phlda2</i> ^{+/+} BACx1(B L6)	Labyrinth	Between exon 1 and exon 2. cDNA: 173 bp, gDNA: 1945 bp.	Tunster 2009 PhD Matthew Lee Bosworth PhD from Cardiff Published 2019
<i>Gcm1</i> R	TGTCGTCC GAGCTGTA GATG					
<i>Hand1</i> F	CGCCTGGC TACCAGTTA CAT	Mouse	mTS	P-TGC	Between exon 1 and exon 2. cDNA: 200 bp, gDNA: 1740 bp.	Tunster 2009 PhD (Arima et al., 2006)
<i>Hand1</i> R	GCGCCCTTT AATCCTCTT CT					
<i>hPL</i> (<i>CSH1/2</i>) F	CATGACTCC CAGACCTCC TTC	Human	hTS	hPL	cDNA: 97 bp	(Dutton et al., 2012)

<i>hPL</i> (<i>CSH1/2</i>) R	TGCGGAGC AGCTCTAGA TTG					
<i>Pcsk6</i> F	GATATGAC GCCAGCAA CGAG	Mouse	mTS	S-TG cell, SpA-TG cell and C-TG cell	cDNA: 210 bp, gDNA: 23855 bp	Unpublished, designed in house.
<i>Pcsk6</i> R	CCAACTGG CGCTGTAAA TGT					
<i>Pcdh12</i> F	AAGCAGAA CCTGACCTG GAA	Mouse	<i>Phlda2</i> ^{+/+BACx1(B L6)} and mTS	Glycogen cell	cDNA: 173 bp, gDNA: 6276 bp	Unpublished, designed in house.
<i>Pcdh12</i> R	GTGAGGGG CAATGACAA TCT					
<i>Peg3</i> F	AAACTCAC ACTCCGTTG G	Mouse	mTS	Imprinted gene	cDNA: 190 bp, gDNA: approx 1300 bp	Designed by S Tunster
<i>Peg3</i> R	GTCTCGAG GCTCCACAT CTC					
<i>PEG3</i> F	CTCACAACA CAATCCAG GAC	Human	hTS	Imprinted gene	Ref: Feng et al. 2008, cDNA: 149 bp	Anna Janssen 2015 PhD
<i>PEG3</i> R	TAGACCTCG ACTGGTGCT TG					
<i>Phlda2</i> F	CAGCAAGC ACGGGAAT ATCT	Mouse	mTS	Imprinted gene	Spans exon 1 - exon 2. cDNA: 188 bp	Designed by S Tunster
<i>Phlda2</i> R	TCAGCGCTC TGAGTCTGA AA					
<i>PHLDA2</i> F	GAGAGCTG CTGGAACG CG	Human	hTS	Imprinted gene	cDNA: 68 bp	(Apostolidou et al., 2007)
<i>PHLDA2</i> R	CGCACGGG AAGTTCTTC TG					
<i>Prl2c</i> F	TCCAGAAAA CAAGGAAC AAGC	Mouse	<i>Phlda2</i> ^{+/+BACx1(B L6)} and mTS	SpA-TG cell, P-TG cell, GlyT	Amplifies from Prl2c2, Prl2c3, Prl2c4, Prl2c5 (proliferin genes). cDNA: 161 bp, gDNA products vary.1274 (c2), 1274 (c3), 1271 bp (c5)	Matthew Lee Bosworth PhD from Cardiff Published 2019
<i>Prl2c</i> R	TGTCTGTG GCTTTGGA GATG					
<i>Prl3b1</i> F	AGCAGCCTT CTGGTGTT GTC	Mouse	<i>Phlda2</i> ^{+/+BACx1(B L6)} and mTS	P-TGC	cDNA: 197 bp, gDNA: 1417 bp	(Kaiser et al., 2015)
<i>Prl3b1</i> R	TGTGACACC ACAATCACA CG					
<i>Prl3d1-3</i> F	TTGGCCGC AGATGTGTA TAG	Mouse	mTS	P-TGC	Amplifies from Prl3d1, Prl3d2 and Prl3d3, cDNA: 233 bp, gDNA: 3490	Unpublished, designed in house.
<i>Prl3d1-3</i> R	AGTCCTG GAAGAGCA GTCA					
<i>Prl7b1</i> F	CAGCACATC AATAGCCTT GC	Mouse	<i>Phlda2</i> ^{+/+BACx1(B L6)} and mTS	Glycogen cell, S-TG cell, SpA-TG cell and C- TG cell	cDNA: 162 bp, gDNA: 2390 bp	Matthew Lee Bosworth PhD from Cardiff Published 2019
<i>Prl7b1</i> R	TTGGTGATT TGAGTGGC AAA					

<i>Prl8a8</i> F	TCAGAGCT GCATCTCAC TGC	Mouse	<i>Phlda2</i> ^{+/+BACx1(B L6)}	Spongiotrop hoblast specific	cDNA: 173 bp, gDNA: 1206 bp	(Napso et al., 2021)
<i>Prl8a8</i> R	GGGACATC TTTCATGGC ACT					
<i>PSG1</i> F	GAGGAGAA CACACAAG CAGC	Human	hTS	Syncytiotrop hoblast	Spans intron 1, cDNA: 183, gDNA: approx 1422 bp	Unpublished, designed in house.
<i>PSG1</i> R	AAGAACATC CTTCCCCTC GG					
<i>Psg17</i> F	CCCTTCGAA CCGTAAGTC AA	Mouse	<i>Phlda2</i> ^{+/+BACx1(B L6)}	Spongiotrop hoblast specific	cDNA: 222, gDNA: 1196 bp	Unpublished, designed in house.
<i>Psg17</i> R	CACAAGTGC TCCTTTGTA CCAG					
<i>Rgs5</i> F	TGAGAAGC CAGAGAAG CCTG	Mouse	mTS	S-TG cell, SpA-TG cell and C-TG cell	qRT-PCR: 218 bp; 13632 bp from gDNA	Unpublished, designed in house.
<i>Rgs5</i> R	GCCTTCTCC GCCATTTTG AT					
<i>SDHA</i> F	GAACATCG GAAGTGGC ACTC	Human	hTS	Reference gene	cDNA: 231 bp	Unpublished, designed in house.
<i>SDHA</i> R	CCTCTGCTC CGTAGATG GTC					
<i>Syna</i> F	CAGGGACA CAAAGACC CCTA	Mouse	<i>Phlda2</i> ^{+/+BACx1(B L6)}	Syncytiotrop hoblast layer I (SynT-I)	cDNA: 180 bp	Matthew Lee Bosworth PhD from Cardiff Published 2019
<i>Syna</i> R	ACCAGAGG AGTTGAGG CAGA					
<i>Synb</i> F	CTGGCACTT CATTCCCAT TT	Mouse	<i>Phlda2</i> ^{+/+BACx1(B L6)}	Syncytiotrop hoblast layer I (SynT-I)	cDNA - 163bp	Matthew Lee Bosworth PhD from Cardiff Published 2019
<i>Synb</i> R	TGGCTGTA GGCTCTCA GGTT					
<i>Tpbpa</i> F	TGAAGAGC TGAACCACT GGA	Mouse	mTS	Spongiotrop hoblast specific	Between exon 1 and exon 2. cDNA: 150 bp, gDNA: 1350 bp.	Tunsters 2009 PhD (Napso et al., 2021)
<i>Tpbpa</i> R	CTTGCAGTT CAGCATCCA AC					
<i>YWHAZ</i> F	TTCTTGATC CCCAATGCT TC	Human	hTS	Reference gene	cDNA: 211bp, gDNA: 828bp	Designed by A Janssen, Published 2015.
<i>YWHAZ</i> R	AGTTAAGG GCCAGACC CAGT					

Table 32: List of qRT-PCR primers.

A master-mix for both plates was prepared following Table 33.

Reagent	X1 (μL)	One 384 well plate (Pipette error x 440)
Water, Molecular Biology Reagent	2.6	1040 μL (1144 μL)
qPCRBIO SyGreen Blue Mix Lo-ROX (Cat No. PB20.15-20, PCR Biosystems Ltd)	5	2000 μL (2200 μL)
Forward and reverse primer mix (10 μM)	0.4	-
Template (1:100 dilution)	2	-
Total	10	-

Table 33: Master-mix for qRT-PCR plates.

The master-mix was split into eight separate mixes and the primers were added to each. The master-mix was aliquoted into each well at 8 μL per well. The 1:100 dilution of the cDNA sample was added to each well at 2 μL per well. Reactions were performed in replicates of three. The plates were then loaded into the QuantStudio™ 5 Real-Time PCR System, 384 well (Applied Biosystems). The temperature program was run as shown in Figure 26.

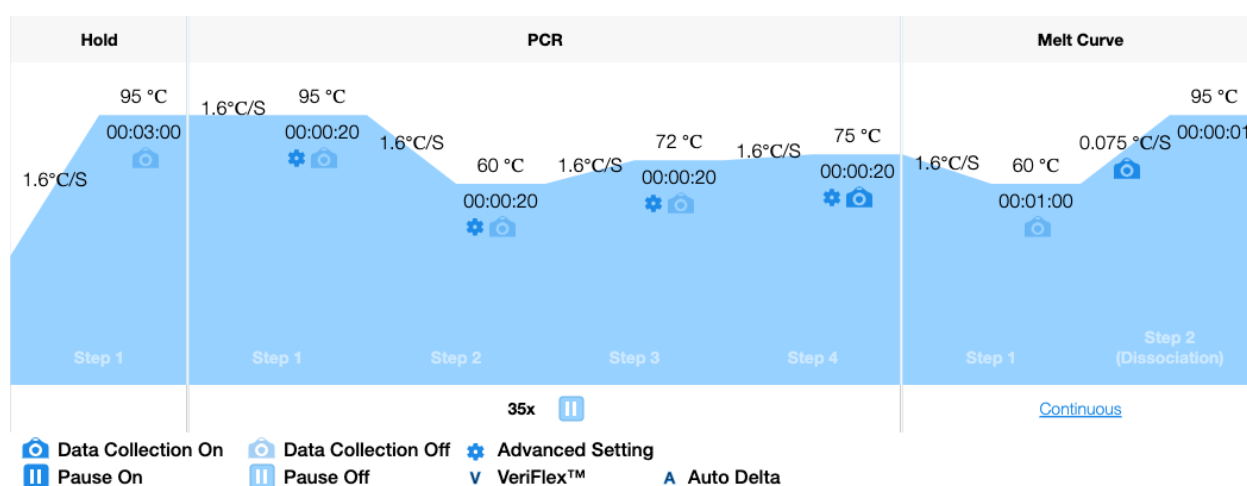


Figure 26: qRT-PCR temperature amplification program.

The crossover point (CP) results were exported to excel and were analysed. Relative expression of each gene was calculated according to the $2^{-\Delta\Delta\text{Ct}}$ method and fold change was calculated around WT controls.

2.11 Protein Analysis

2.12 Enzyme-linked immunosorbent assay

The Mouse Prl3b1 (Prolactin-3B1) (FineTest, Cat No. EM1597) and Mouse Prl3d1 (Prolactin-3D1) (FineTest, Cat No. EM1598) enzyme-linked immunosorbent assay (ELISA) kits were used to measure protein concentrations of samples. Tissue and cell samples were collected following the protocols described in 2.2.4.1 and 2.8.1. Tissue samples were placed on ice and washed with PBS to remove residual blood. The samples were then homogenised in lysate. The cells were suspended in lysate. The homogenised lysates were then centrifuged for five minutes at 4 °C. The supernatant was then collected. The plate was washed twice in wash buffer (FineTest, Cat No. EM1597/8) before adding the standards, samples and the blank. Immediately after, 50 µL of Biotin-labelled Antibody (FineTest, Cat No. EM1597/8) was added to each well. The wells were mixed for one minute manually by tapping the plate. The plate was then incubated for 45 minutes at 37 °C. The plate was then washed three times in wash buffer with a one-minute incubation per wash. To each well 100 µL of HRP-Streptavidin Conjugate (FineTest, Cat No. EM1597/8) was added. The plate was sealed and incubated at 37 °C for 30 minutes. The plate was then washed five times in wash buffer with a one-minute incubation per wash. 90 µL TMB substrate (FineTest, Cat No. EM1597/8) solution was then added to each well. The plate was incubated for 10-20 minutes at 37 °C. 50 µL of stop solution was then added and the optical density (OD) absorbance was read on a microplate reader at 450 nm. The sample concentration was then calculated using the standard curve generated by the standards.

2.13 Western blotting

Cell samples were lysed in Laemmli buffer in their plates using a scrapper to manually rupture the cells. The samples were then incubated at 95 °C for five minutes. Samples were loaded into an SDS-PAGE gel (sodium dodecyl sulphate-polyacrylamide gel) which was prepared using Table 34.

For 1 gel	Resolving (Bottom)				For 1 gel	Stacking (Top)
	10%	12%	6%	16%		6%
dH ₂ O	1.5 mL	1.25 mL	1 mL	0.75 mL	dH ₂ O	825 µL
30% acrylamide	1.25 mL	1.5 mL	1.75 mL	2 mL	30% acrylamide	250 µL
1.25M Tris pH8.8	0.95 mL	0.95 mL	0.95 mL	0.95 mL	1.25M Tris pH6.8	155 µL
10% SDS	38 µL	38 µL	38 µL	38 µL	10% SDS	12.5 µL
10% Am persulfate	38 µL	38 µL	38 µL	38 µL	10% Am persulfate	12.5 µL
TEMED	3.8 µL	3.8 µL	3.8 µL	3.8 µL	TEMED	1.25 µL

Table 34: Recipe for western blotting gel.

Samples were then run at 200 V for 45-60 minutes. A semi-dry transfer was used to transfer the proteins to the membrane. The gel was then incubated in transfer buffer (TB1x) on a shaker for 10 minutes. The polyvinylidene fluoride (PVDF) membrane was activated in Methanol (MetOH) for three to five minutes and two pieces of 3MM Whatmann paper was soaked in TB1x. The transfer was then set up with 1 x Whatmann on the bottom, followed by the activated membrane, the gel, then another Whatmann. The lid was then screwed tightly onto the transfer apparatus. The transfer was then performed at 50 mA for smaller gels and 100 mA for larger gels, for 1 hour and 30 minutes. Once complete the gel was stained with GelCode for 10-15 minutes and then incubated in dH₂O overnight. The membrane was incubated in TBST for 10 minutes before being blocked in 4% non-fat milk (Marvel) in TBST (Tris buffered saline with Tween-20; 100 mM Tris, HCl, 1.5 M NaCl, 0.5% Tween-20, pH 7.5) for 1-1.5 hours at RT. The primary antibody was diluted in 4% milk-TBST following details in Table 35.

Antibody	Concentration	Secondary	Observed Molecular weight
Beta-actin Monoclonal antibody, Mouse, (Proteintech, Cat No. 60008-1-Ig)	1:3000	1:4000 HRP NA931VS Goat anti-mouse	42 kDa
PHLDA2 Polyclonal antibody, Rabbit, (Proteintech, Cat No. 14661-1-AP)	1:600	1:3000 HRP Goat anti-Rabbit	17 kDa
PEG3 Polyclonal antibody, Rabbit, (Proteintech, Cat No. 23569-1-AP)	1:600	1:3000 HRP Goat anti-Rabbit	200-220 kDa
Placental lactogen Polyclonal antibody (hPL), Rabbit, (Proteintech, Cat No. 16326-1-AP)	1:2500	1:3000 HRP Goat anti-Rabbit	25 kDa

Table 35: Primary and secondary information for westerns.

Membranes were incubated overnight at 4 °C then washed in TBST three times for 10 minutes each on a shaker. The secondary antibody was also diluted in 4% milk-TBST and was selected based on the information in Table 35. Membranes were incubated in their secondary antibody for 1.5-2 hours at RT then were washed in TBST three times for 10 minutes per time on shaker. Membranes were then stained with ECL (equal parts reagent A and B) (Immobilon Western Chemiluminescent HRP substrate, Merck, Cat No. WBKLS0050) for 30 seconds to 1 minute, then were transferred into the camera. X-ray images were then taken of the membrane in a dark room.

2.14 Statistical analysis

The sample size for each group was calculated using Equation 4 and are presented in the relevant methods section.

$$d = \frac{M_2 - M_1}{\sqrt{\frac{SD_1^2 + SD_2^2}{2}}}$$

Equation 4: Effect size calculation (Cohens d).

Data was analysed using IBM SPSS software (Version 29.0.2.0(20)). Graphical representations were presented as mean and standard error of the mean (SEM) and were prepared using GraphPad Prism software (Version 10.4.0 (527)). Specifics for each statistical analysis, including sample size are detailed in the corresponding figure caption. Where relevant, litter size was included as a covariate in an ANCOVA.

2.15 Figures

All figures in chapters 1 and 2 were designed in BioRender with permissions. All graphs were generated using Graphpad prism (Version 10.4.0 (527)).

Chapter 3: Characterising the sexually dimorphic effect of two-fold *Phlda2* modelling loss of imprinting on the developing mouse placenta

3.1 Overview

This chapter investigates the overexpression of *Phlda2* on the developing mouse placenta. The experiments detailed in this chapter are using the *Phlda2*^{+/+BACx1(BL6)} mouse strain as described in Tunster et al. (2010) and section 2.1.1 and aim to further characterise the model's effect on the placenta.

A summary of previous research around *Phlda2*'s regulation of the placenta can be found in section 1.8.2. Tunster's model has previously demonstrated that two-fold *Phlda2* resulted in reduced spongiotrophoblast cells in the junctional zone layer for E14.5, but this phenotype was recovered by E16.5 (Tunster et al., 2010). This loss of imprinting of *Phlda2* had a small effect on foetal growth with a 13% reduction in weight by E18.5, but no significant long-term effect on postnatal growth, suggesting that a different element within the KvDMR1 domain influences foetal size. The *Phlda2* loss of imprinting model, however, does mis-localise glycogen cells into the labyrinth. This happens later in gestation (E16.5). It was theorised that *Phlda2* facilitates nutrient supply to the foetus when it has the greatest demand for resources. As the standard amount of *Phlda2* prevents the mis-localisation of glycogen cells, the WT placentas maximise their maternal resources and enhance growth (Tunster, Creeth, et al., 2016). As the foetal weight was not altered in earlier stages of development but was significantly reduced by E18.5, this reinforces the hypothesis that the late mis-localisation of glycogen cells restricts growth of the foetus in later developmental stages (Tunster, Creeth, et al., 2016). It was determined that the *Phlda2*^{+/+BACx1} model expressed 2.8 times the amount of *Phlda2* compared to WT control, as well as 1.8 times the WT level of *Slc22a18*. There was no effect on the expression of *Cdkn1c* (Tunster et al., 2010). Investigation into the morphological effects of the model revealed that *Phlda2* produced the maximum alteration to the placenta with just one extra dose, as higher doses did not cause a more significant phenotype (Tunster et al., 2010). This 2010 study also suggested that *Phlda2* may play a more specific role in the regulation of the endocrine lineage. The ratio of junctional zone to labyrinth area was reduced by 2.3 fold compared to WT at both E14.5 and E16.5. This had an impact on the overall weight of the placenta, reducing it significantly to WT (Tunster, Creeth, et al., 2016; Tunster et al., 2010).

These initial investigations were conducted using a mixed genetic background (Tunster et al., 2010) and a pure 129 background (Tunster, Creeth, et al., 2016). *Phlda2*^{+/+BACx1} was later bred onto a BL6 background. This move to the BL6 strain was conducted because of interest in placental metabolism, as BL6 placentas were determined to accumulate twice as much stored glycogen as 129 (Tunster et al., 2012). This transition recorded notable differences in the placental phenotype of the strains. BL6 had a heavier placenta than 129 (Tunster et al., 2012). The BL6 WT junctional zone was significantly larger than the 129 WT junctional zone, so much so, that when *Phlda2*^{+/+BACx1} was introduced onto the BL6 strain, the *Phlda2*^{+/+BACx1(BL6)} junctional zone was still larger than the 129 WT junctional zone. The *Phlda2*^{+/+BACx1} transgene produced a replicable reduction in the endocrine compartment across strains, in that both backgrounds had a 50% reduction from WT in endocrine compartment size (Tunster et al., 2012). However, the foetal growth restriction which was seen at 13% when *Phlda2*^{+/+BACx1} was introduced to the 129 background, was no longer present when it was introduced onto the BL6 background. In addition, the WT foetal weight from both strains was the same, given that the placental weight was higher in the BL6 strain, it meant that the foetal to placental weight ratio was 30% higher in the 129 strain (Tunster et al., 2012). This suggested that the 129 placenta was more efficient at supporting growth than BL6, meaning there would be a wider potential for response to genetic manipulation in BL6 placenta than in 129 placenta. Finally, the expression of *Cdkn1c* (Takahashi et al., 2000), *Igf2* (DeChiara et al., 1991; Lopez et al., 1996) and *Phlda2* (Frank 2002) were demonstrated to be lower on the BL6 background than 129 suggesting the BL6 background would be affected to a greater degree than 129 (Tunster et al., 2012). The BL6 background is the background used in the current study.

The hypothesis of this chapter is that the *Phlda2*^{+/+BACx1(BL6)} strain will have an impact on placental hormone production by restricting the expansion of placental endocrine lineages. Previous characterisation of this line did not explore potentially sexually dimorphic effects. It is hypothesised that analysing the data with a focus on sex specific outcomes, some previously masked findings will be uncovered.

3.2 Aims

The *Phlda2* loss of imprinting model's effects on placental and foetal weight have previously been analysed and published in Fitzpatrick et al. (2002), Salas et al. (2004), Tunster et al. (2010) and (Tunster, Creeth, et al., 2016). However, the sex specific effects have not been characterised. It has previously been demonstrated that the mouse placenta has

sexually dimorphic characteristics (Eriksson et al., 2010; Mao et al., 2010; Salazar-Petres et al., 2022; Sumption et al., 2020; Tunster et al., 2018). This study aimed to explore sexual dimorphic effects of altered *Phlda2* expression. To achieve this aim, the placental phenotypes were measured and analysed to identify which regions were more heavily impacted for each sex.

Functionally, the junctional zone is identified as the endocrine compartment of the placenta. A reduction or increase in the size of this section could be assumed to increase or decrease the amount of hormone that the placenta produces. It is possible however, that other compensatory mechanisms could arise to correct hormone output or hormone exposure to either mother or foetus, whilst leaving the phenotypically altered size of the junctional zone in place. With the aim of more cohesively connecting the size of the junctional zone to the hormonal output of the placenta, E14.5 placentae were stained for *Pr13b1* and an automated cell counting program was designed to count cells expressing *Pr13b1*, giving a regionally specific quantitative measure of hormone production. The resulting data was assessed to determine the differences in functional output between wildtype and *Phlda2*^{+/+}BACx1(BL6) placenta and was also used to investigate the differing impacts for male and female placenta. See Appendix 1 for chapter specific methods.

3.3 Results

3.3.1 Placental weight reduced in *Phlda2*^{+/+}BACx1(BL6)

Placental and foetal weights were taken upon dissection of E14.5 mixed wild type (WT) and *Phlda2*^{+/+}BACx1(BL6) (Tg) litters.

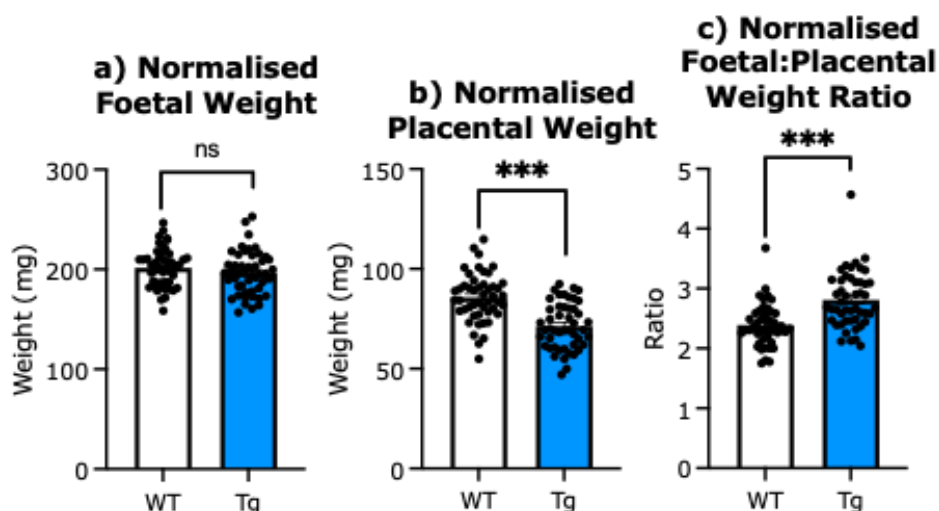


Figure 27: Foetal and placental weight data for WT and Tg.

a) Wet weights of WT and Tg foetuses at E14.5 show no significant difference. **b)** Tg placenta weighed 17% less than WT placenta. **c)** Tg F:P ratio was 18% higher than WT. WT ($n = 48$), Tg ($n = 48$). Data from 12 litters, litter size between 7-10 (average 8 ± 0.91). Weights normalised against WT weight across litters. Error bars represent standard error of the mean \pm (SEM). Statistical significance calculated using two-way ANCOVA with Šidák correction and litter size as covariate. $^{NS}P > .05$, $*P < .05$, and $**P < .01$ $***P < .001$ $****P < .0001$ (Appendix 2).

Further analysis was conducted to investigate if there was a sexually dimorphic response to the transgenic modification.

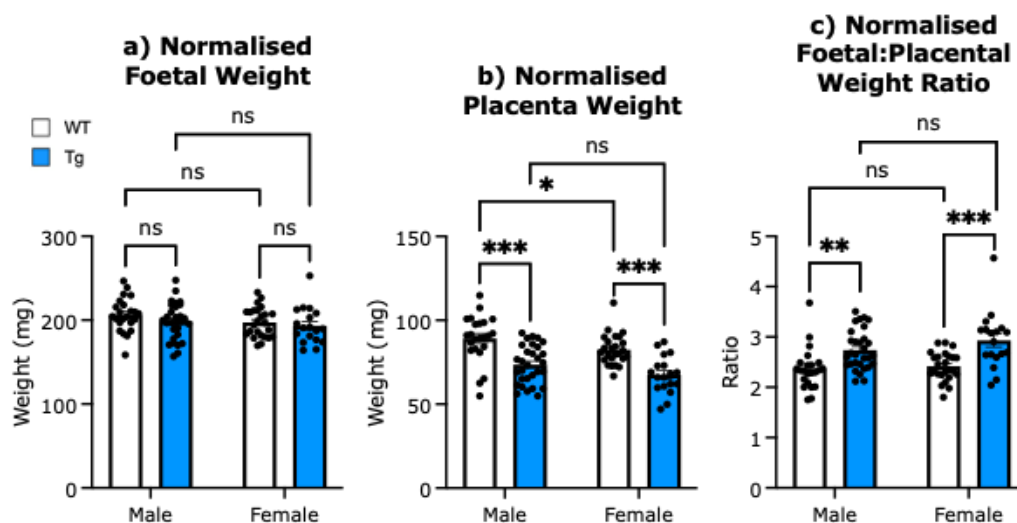


Figure 28: Foetal and placental weight data for WT and Tg.

a) Wet weights of WT and Tg foetuses at E14.5 show no significant difference. **b)** WT female placenta weighed 8% less than WT male placenta. Tg placenta weighed 18% less than WT placenta for both males and females. **c)** Tg Foetal: placental weight ratios were 16% ($P < .001$) and 22% ($P < .001$) more than WT for males and females respectively. WT male ($n = 23$), Tg male ($n = 30$), WT female ($n = 25$) and Tg female ($n = 18$). Data from 12 litters, litter size between 7-10 (average 8 ± 0.91). Normalised against WT weight across litters. Error bars represent \pm SEM. Statistical significance calculated using two-way ANCOVA with Šidák correction. $^{NS}P > .05$, $*P < .05$, and $**P < .01$ $***P < .001$ $****P < .0001$ (Appendix 3).

The significance of some of the comparisons was altered by the ANCOVA analysis approach. Foetal weight was adjusted marginally, but not to the degree where it reaches significance. Placental weight did not change in both female and male for any comparison except M-Tg vs F-Tg which was altered non-significantly. Foetal placental weight ratios also had altered P values (Males WT vs Tg ANOVA $P < .0001$, ANCOVA $P = .001$), (Females WT vs Tg ANOVA $P < .0001$, ANCOVA $P < .001$).

3.3.2 *Phlda2*^{+/+}BACx1(BL6) impacts female placentas more significantly than males

A total of 33 mixed wild type (WT) and *Phlda2*^{+/+}BACx1(BL6) (Tg) E14.5 placentas were stained for *Pr13b1* using the RNAscope method detailed in section 2.3.3. These were then processed using Zen software to define area measurements and the automatic counting method as described in methods section 2.6

3.3.2.1 The reduction in junctional zone and labyrinth area is more pronounced in female *Phlda2*^{+/+}BACx1(BL6) placentas

Using Zen 3.8 the area of each region was measured. The impact on litter size of the data was also investigated using an ANCOVA statistical analysis with litter size as a covariate.

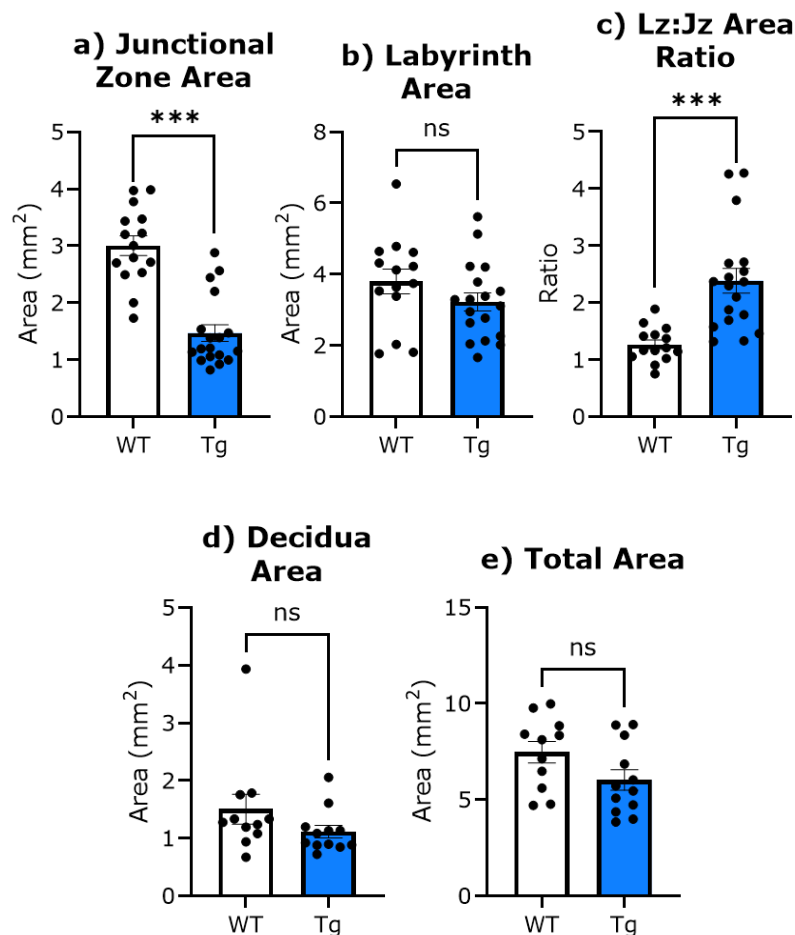


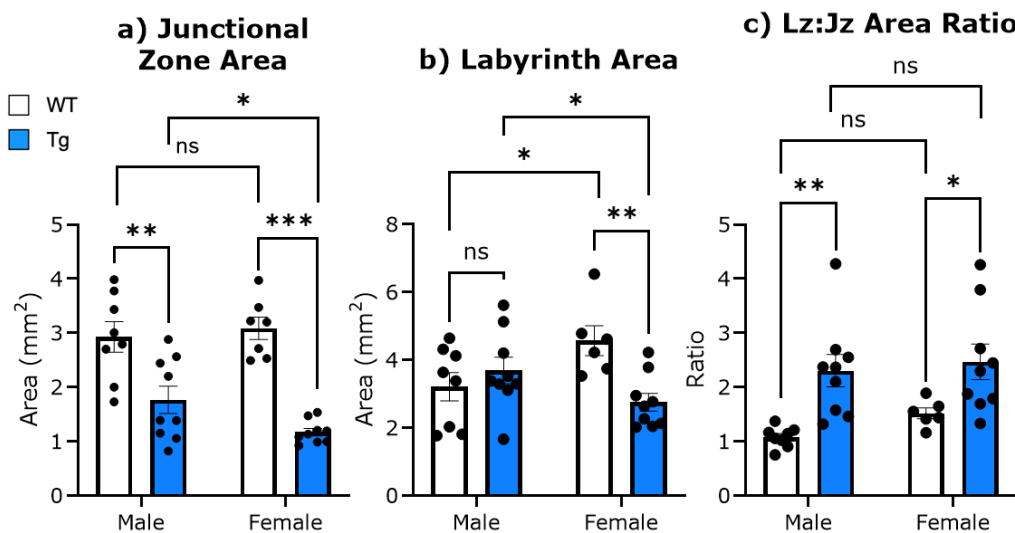
Figure 29: Area of placental subsections for WT and Tg.

a) Tg junctional zones were 51% smaller than WT. **b)** Tg labyrinth was not significantly smaller than WT. **c)** Labyrinth to junctional zone area ratio was higher in Tg compared to WT with an 88% increase. **d)** Decidua area measurements show no significant difference between WT and Tg.

e) No significant difference between WT and Tg in total area measurements. WT ($n = 15$), and Tg ($n = 18$). Data from 12 litters, litter size between 6-10 (average 8 ± 0.20). Error bars represent \pm SEM. Statistical significance calculated using a two-way ANCOVA with litter size as a covariate using a Šidák correction. $^{NS}P > .05$, $^*P < .05$, $^{**}P < .01$, $^{***}P < .001$, $^{****}P < .0001$ (Appendix 4).

A reduction in the junctional zone size was seen between WT and Tg placentas ($P < .001$). This affected the junctional zone to labyrinth zone size ratio ($P < .001$) as the labyrinth was not significantly altered by the transgene, although the statistics suggest a sexually dimorphic response (GENOTYPE*SEX: $F_{1,27} = 9.76$, $P = .004$). The total area was not significantly reduced by the transgene ($P = .073$), but again a sexually dimorphic result is suggested by the initial statistical information (GENOTYPE*SEX: $F_{1,18} = 6.43$, $P = .021$).

Initial comparisons between ANOVA and ANCOVA analysis show marginal changes to significance. For junctional zone size and junctional zone to labyrinth zone ratios both ANOVA and ANCOVA showed P -values of $< .001$. Comparisons for labyrinth size remained non-significant although moved from a P value of $.089$ for ANOVA to a P value of $.138$ for ANCOVA. Along with decidua size comparisons which had an ANOVA P value of $.438$ and ANCOVA P value of $.273$. Finally, total area moved from a significant P value of $.038$ for ANOVA to a non-significant P value of 0.073 for ANCOVA. When this data was split by sex the impact of the litter size and sexual dimorphism became apparent.



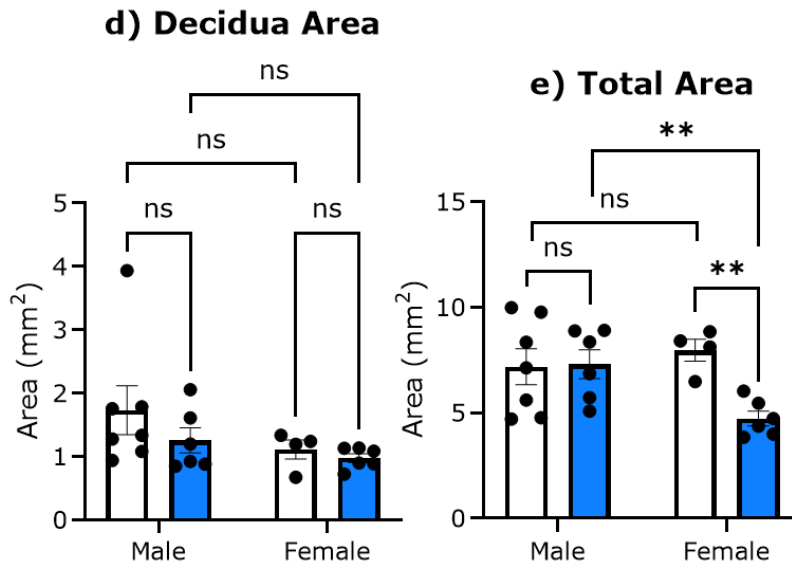


Figure 30: Area of placental sub-sections split by sex for WT and Tg.

a) Junctional zone area measurements WT and Tg placenta at E14.5. Tg junctional zones were 40% smaller than WT in males and 62% smaller than WT in females. Female Tg junctional zone area was significantly smaller than Male Tg junctional zone area by 34%. **b)** Labyrinth area measurements of WT and Tg placenta at E14.5. Tg labyrinth was not significantly different in males than WT. Female WT labyrinth was 42% larger than Male WT labyrinth. Female Tg labyrinth was 40% smaller than Female WT labyrinth. Female Tg labyrinth was also 25% smaller than Male Tg labyrinth. **c)** Labyrinth to junctional zone area ratio (Lz:Jz) was higher in Tg compared to WT. Males have a 114% increase and females with a 63% increase. **d)** Decidua area measurements of WT and Tg show no significant difference between any groups. **e)** Total area measurements of WT and Tg placenta at E14.5. Total area was not significantly different for males, whereas female Tg measured 41% smaller than WT. Female Tg placentas were also 35% smaller than M Tg placentas in total size. WT male ($n = 8$), and Tg male ($n = 9$), WT female ($n = 7$), Tg female ($n = 9$). Data from 12 litters, litter size between 6-10 (average 8 ± 0.20). Error bars represent \pm SEM. Statistical significance calculated using a two-way ANCOVA with litter size as a covariate using a Šidák correction. ^{NS} $P > .05$, * $P < .05$, ** $P < .01$, *** $P < .001$, **** $P < .0001$ (Appendix 5).

Using litter size as a covariate exposes the sexual dimorphism of this transgenic modification. The analysis of the junctional zone size reveals that the impact of the transgenic modification on the female junctional zone is significantly higher than the impact on the male Tg junctional zone. Similarly, this is seen in the analysis of the labyrinth size, where female WT labyrinths are 42% larger than male WT labyrinths. In Tg

placentas, the labyrinth responds differently by sex, males slightly increasing in size by 15%, whereas females had a reduction in size by 40% compared to their WT counterparts. To emphasise this further, female Tg labyrinths were 25% smaller than male Tg labyrinths. Total area also revealed a more nuanced story when factoring in litter size, with male total area not being impacted by the transgene while females showed a 41% reduction than WT in Tgs, and again female Tgs were 35% smaller than male Tgs in total size.

3.3.2.2 Comparison of manual and automated counting program

The results of the automatic counting program were compared to a manual counting performed by Amelia Stodart (Table 36).

	Counting Method	WT	Tg	P
Total junctional zone cells	Manual	10956.7±640.5	6173.0±586.6	<.0001
	Automatic	10011.9±418.2	4753.5±465.1	<.001
Junctional zone <i>Pr13b1</i> positive cells	Manual	5761.8±336.3	3364.0±368.8	.0001
	Automatic	8287.2±292.7	4198.7±412.5	<.001

Table 36: Comparison between manual and automatic counting (±SEM).

The automatic counting program had a reduced SEM to the manual counting method. The automatic counting was deemed to be a reliable alternative to manual counting.

3.3.2.3 Cell counting using RNAscope automated counting program confirms significant reductions in *Pr13b1* expressing cells in *Phlda2*^{+/+}BACx1(BL6) placentas

3.3.2.3.1 Both male and female *Phlda2*^{+/+}BACx1(BL6) junctional zones cell numbers are reduced to WT, while females are more significantly impacted

The automatic counting program detailed in the methods section 2.6 was used to count a variety of parameters including the number of cells within each region which were producing *Pr13b1* RNA at the time of dissection/fixation. *Pr13b1* is specifically expressed by the spongiotrophoblast cells and not by glycogen cells in the junctional zone (Simmons 2007). It is also expressed by the TG cells subpopulations, C-TG cells, S-TG cells and P-TG cells but not in SpA-TG cells (Simmons

2007). The TG cells counted by the automatic counting program identifies the P-TG cell populations that form the interface between the junctional zone and maternal decidua.

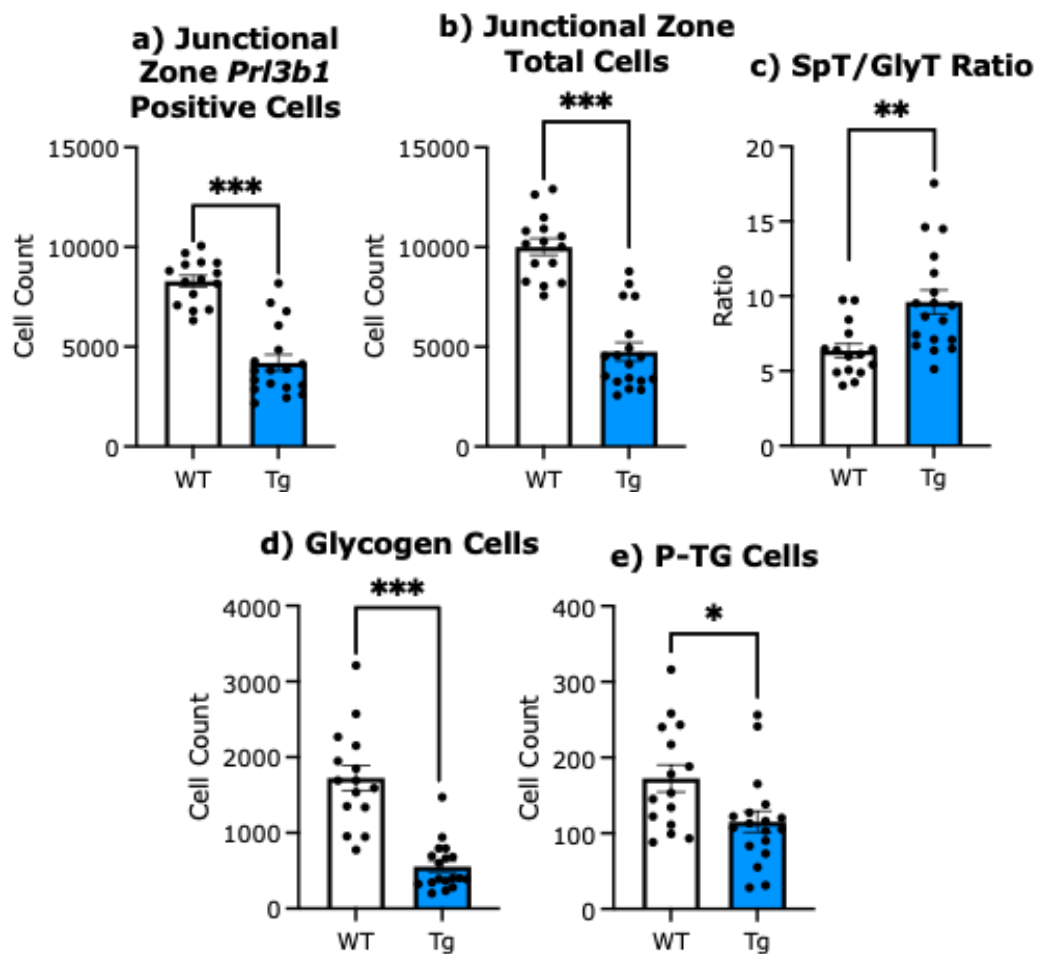


Figure 31: Cell counts for WT and Tg junctional zone.

a) Tg junctional zones had 49% (GENOTYPE: $F_{1,28} = 63.52$, $P < .001$) fewer *Prl3b1* positive cells than WT. **b)** Tg junctional zone contained 53% fewer total cells than WT. **c)** Spongiotrophoblast cell to glycogen cell (SpT/GlyT) ratios are increased in Tg by 51%. **d)** Tg placentas had a 68% decrease in glycogen cell number. **e)** P-TG cell counts for WT and Tg E14.5 placentas. Tg placentas had 33% fewer TG cells than WT. WT male ($n = 8$), and Tg male ($n = 9$), WT female ($n = 7$), Tg female ($n = 9$). Data from 12 litters, litter size between 6-10 (average 8 ± 0.20). Error bars represent \pm SEM. Statistical significance calculated using a two-way ANCOVA with litter size as a covariate using a Šidák correction. $^{NS}P > .05$, $*P < .05$, $**P < .01$, $***P < .001$, $****P < .0001$ (Appendix 6).

The number of cells expressing *Prl3b1* in the junctional zone was reduced by 49% in Tg placentas compared to WT. The total number of cells within the junctional zone was also reduced by 53%. The spongiotrophoblast cell to glycogen cell ratio was increased in Tgs compared to WT by 51%. Glycogen cells were reduced in Tg placentas by 68%, as well as P-TG cells

which were reduced by 33%. With the ANCOVA performed on this pooled data, there was no change in significance for junctional zone *Pr13b1* positive cell number, total junctional zone cells and glycogen cell number. P-TG cell *P* values moved from $P=.0163$ for ANOVA analysis to $P=.014$ for ANCOVA and the spongiotrophoblast to glycogen cell ratio moved from $P=.003$ in the ANOVA to $P=.004$ in the ANCOVA. This data was further analysed for its sexually dimorphic impacts.

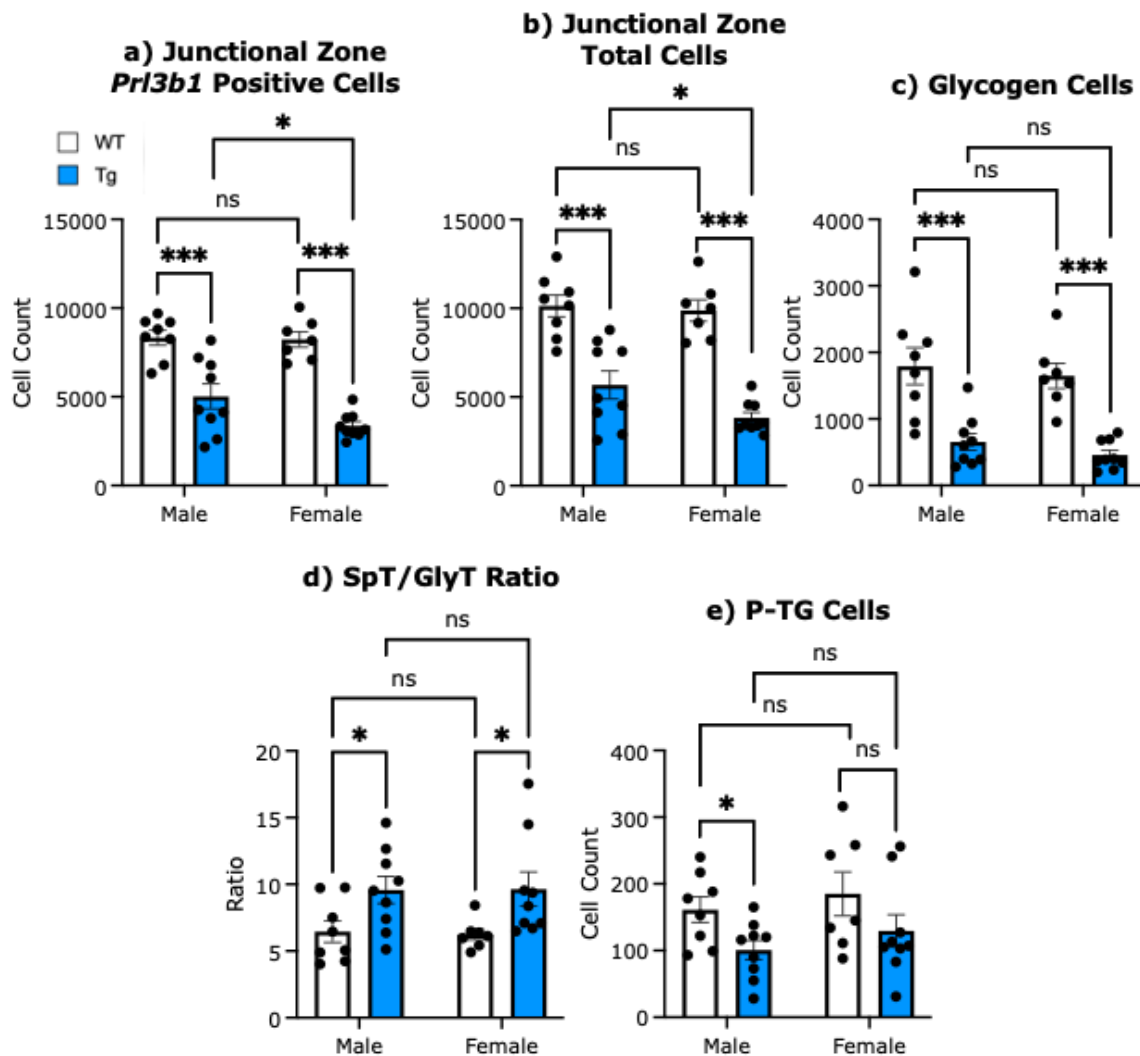


Figure 32: Cell counts for sex split WT and Tg junctional zone.
a) Tg junctional zones contained 40% fewer *Pr13b1* positive cells than WT in males and 59% fewer than WT in females. Female Tg junctional zones contained 33% fewer *Pr13b1* positive cells than males Tg junctional zones.
b) Tg junctional zones contained 44% fewer cells in males than WT and 61% fewer cells than WT in females. Female Tg junctional zones contain 33% fewer total cells than M Tg junctional zones.
c) Glycogen cells were reduced in number between in Tg compared to WT. Males had a 64% decrease in glycogen cell number and females had a 72% decrease.
d) Spongiotrophoblast cells to glycogen cell ratios (SpT/GlyT) are increased in Tg compared to WT. Male ratios are increased by 48% and female

ratio are increased by 54%. **e)** Male Tg placentas had 38% fewer TG cells than WT. WT male ($n = 8$), and Tg male ($n = 9$), WT female ($n = 7$), Tg female ($n = 9$). Data from 12 litters, litter size between 6-10 (average 8 ± 0.20). Error bars represent \pm SEM. Statistical significance calculated using a two-way ANCOVA with litter size as a covariate using a Šidák correction. $^{NS}P > .05$, $^{*}P < .05$, $^{**}P < .01$, $^{***}P < .001$, $^{****}P < .0001$ (Appendix 7).

Both male and female junctional zones had fewer total cells, fewer *Pr13b1* positive cells and fewer glycogen cells than their WT counterparts. No significant difference between females and males in WT or Tg groups indicates that there isn't a sexually dimorphic difference between WT groups. The ratio of spongiotrophoblast cells to glycogen cells increased in both females and males. P-TG cell comparisons lost the significant difference seen in the pooled sexes and only males retain their significance.

Using litter size as a covariate has further revealed the sexually dimorphic impact being more severe in female placentas. For the analysis of *Pr13b1* positive cells in the junctional zone, while comparisons between male and female WT remained not significant with a cell count reduction of just 1% in male WT compared to female WT, the difference between Tg placentas showed a 33% reduction in *Pr13b1* positive cells in female Tg compared male Tg junctional zones. This pattern was also observed in total junctional zone cell number, with WT females having a reduction of 2% compared to WT males and Tg females having a 33% reduction in junctional zone cells compared to Tg males.

3.3.2.3.2 Pooled automated cell count analysis masks significant impact on *Phlda2*^{+/+BACx1(BL6)} female labyrinths

A more detailed analysis on the impacts of *Phlda2*^{+/+BACx1(BL6)} on the labyrinth was also conducted by looking at cell counts and *Pr13b1* positive cell numbers within the labyrinth.

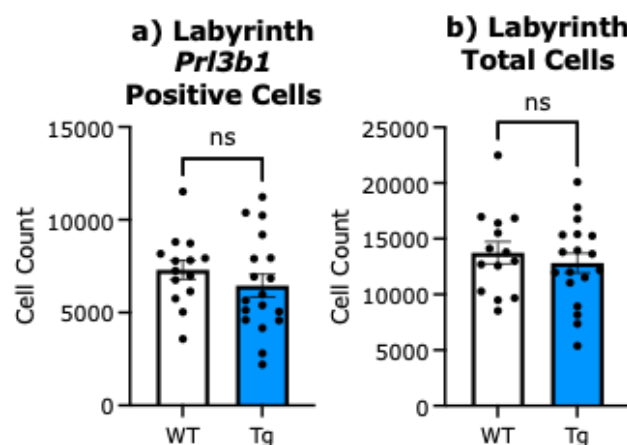


Figure 33: Labyrinth zone cell counts for WT and Tg placenta.

a) There was no difference in labyrinth *Pr13b1* positive cell number between WT and Tg. **b)** There was no difference in labyrinth total cell number between WT and Tgs. WT ($n = 15$), and Tg ($n = 18$). Data from 12 litters, litter size between 6-10 (average 8 ± 0.20). Error bars represent \pm SEM. Statistical significance calculated using a two-way ANCOVA with litter size as a covariate using a Šidák correction. ^{NS} $P > 0.05$, $*P < .05$, $**P < .01$, $***P < .001$, $****P < .0001$ (Appendix 8).

No significant difference was seen between WT and Tg for labyrinth *Pr13b1* positive cells or total cells when the data was pooled, although statistical analysis indicates a sexually dimorphic characteristic which was investigated further.

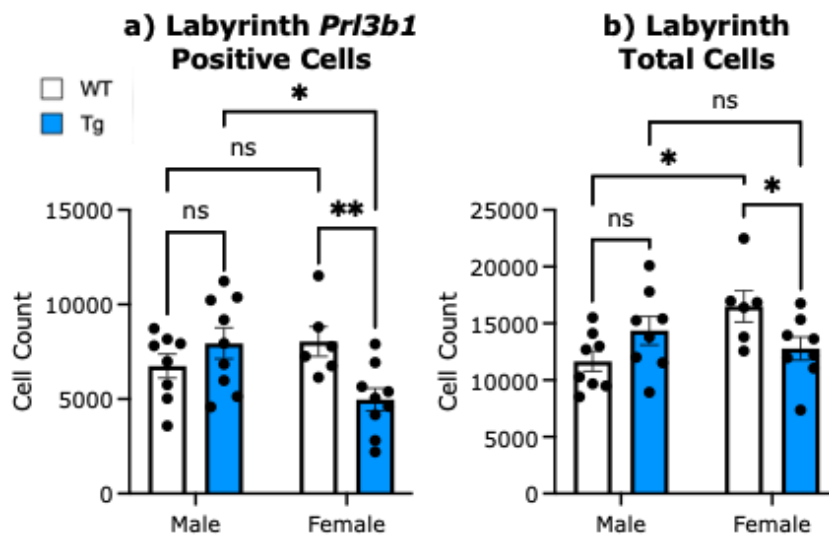


Figure 34: Labyrinth cell counts for sex split WT and Tg placenta.

a) Female Tg labyrinths contained 38% (GENOTYPE: $F_{1,27} = 7.88$, $P = .009$) fewer *Pr13b1* positive cells than female WT labyrinths. Female Tg labyrinths also contained 37% fewer *Pr13b1* positive cells than male Tg labyrinths. **b)** Total labyrinth cell numbers were 42% higher in female WT labyrinths compared to male WT labyrinths. Female Tg labyrinths contained 28% fewer cells than WT females. WT male ($n = 8$), and Tg male ($n = 9$), WT female ($n = 7$), Tg female ($n = 9$). Data from 12 litters, litter size between 6-10 (average 8 ± 0.20). Error bars represent \pm SEM. Statistical significance calculated using a two-way ANCOVA with litter size as a covariate using a Šidák correction. ^{NS} $P > .05$, $*P < .05$, $**P < .01$, $***P < .001$, $****P < .0001$ (Appendix 9).

After splitting the data by sex, the impact of the reduction in cell numbers in the labyrinth for female placentas was revealed. This data reflects the results seen in the area measurements of the labyrinth. It is apparent that the male labyrinth responds in the opposite manner, by increasing in number of *Pr13b1* positive cells in the Tg group compared to WT. Although this increase is non-significant, this nullifies the reduction seen in the

female samples when the sexes are pooled. In analysis of the *Pr13b1* positive cells within the labyrinth area *P* values comparing female Tgs to female WT move from $P=.0447$ in ANOVA to $P=.009$ in the ANCOVA. Similarly comparing female Tgs to male Tgs, $P=.025$ in ANOVA and $P=.013$ in ANCOVA. A similar pattern is seen in the analysis of the total cells of the labyrinth, although the comparison between male and female WT samples also shows a significant difference with the WT female labyrinth having significantly more total cells than the WT males. For the total cell values, a difference between female WT and Tg becomes apparent with a 28% reduction in total cells for females only.

3.3.2.3.3 Full placenta cell counts reinforce female placentas as most impacted by *Phlda2*^{+/+BACx1(BL6)}

Finally, analysis of the placenta as a whole was conducted.

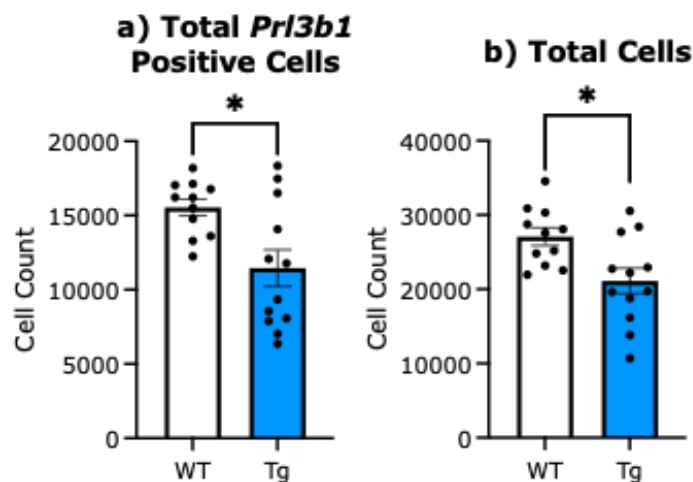


Figure 35: Total placental cell counts for WT and Tg placenta.

a) Total *Pr13b1* positive cell numbers were reduced by 26% compared to WT. **b)** Total cell counts were 22% less than WT in Tg placentas. WT ($n = 16$), and Tg ($n = 18$). Data from 12 litters, litter size between 6-10 (average 8 ± 0.20). Error bars represent \pm SEM. Statistical significance calculated using a two-way ANCOVA with litter size as a covariate using a Šidák correction. ^{NS} $P > .05$, $*P < .05$, $**P < .01$, $***P < .001$, $****P < .0001$ (Appendix 10).

Comparing the total cell numbers and total *Pr13b1* positive cells between WT and Tg, Tg has a significant reduction in both. For this analysis ANOVA produced *P* values of $P=.0300$ for WT to Tg comparisons for total *Pr13b1* cell numbers and $P=.0382$ for total cell numbers. The ANCOVA produced $P=.013$ and $P=.024$ respectively. A further analysis of the sexual dimorphism was also conducted.

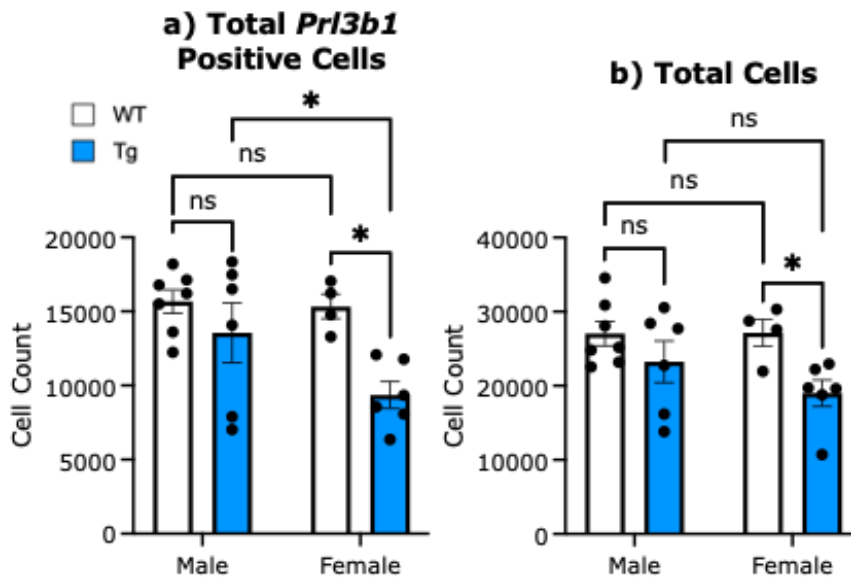


Figure 36: Total cell counts for sex split WT and Tg placenta.

a) Total *Prl3b1* positive cells were 39% reduced in Female Tg placentas compared to Female WT placentas. Female Tg placentas also had 31% fewer *Prl3b1* positive cells than Male Tg placentas. **b)** Female Tg placentas had 30% fewer total cells than female WT placentas. WT male ($n = 8$), and Tg male ($n = 9$), WT female ($n = 7$), Tg female ($n = 9$). Data from 12 litters, litter size between 6-10 (average 8 ± 0.20). Error bars represent \pm SEM. Statistical significance calculated using a two-way ANCOVA with litter size as a covariate using a Šidák correction. $^{NS}P > .05$, $^{*}P < .05$, $^{**}P < .01$, $^{***}P < .001$, $^{****}P < .0001$ (Appendix 11).

When split by sex, the impact on the female placenta is more significant. Total *Prl3b1* positive cells are only significantly reduced for female placentas and not for males. No significance is seen in any comparison for total cell counts. As per other parameters measured, the ANCOVA has further revealed sexual dimorphism between females and males in their impacts from the transgene. In the ANOVA analysis the impact on total *Prl3b1* positive cells was demonstrated with 39% reduction in female Tg placentas compared to female WT placentas ($P = .0437$), the ANCOVA shifted this P value to $P = .01$. More importantly the reduction in total cells for female Tg placentas was 31% reduced from WT (ANCOVA, $P = .017$) where the ANOVA produced a value of $P = .1649$. The male reduction is a non-significant (14%, $P = .287$).

Representative images of the impact of the transgenic modification on male and female placentas were collated into a representative figure which can be seen in Figure 37.

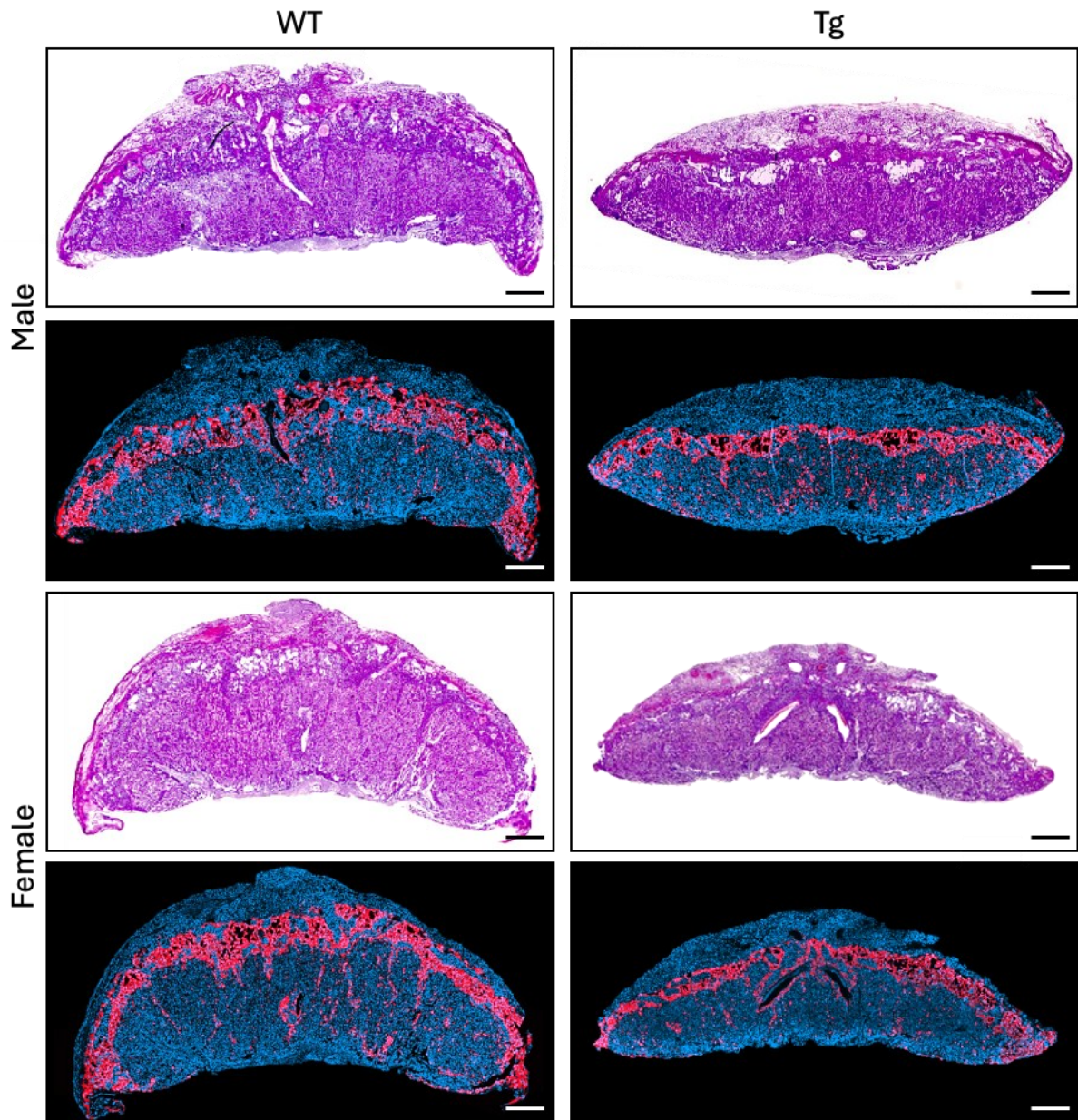


Figure 37: Representative RNAscope images of WT and Tg.

Male and female placenta from Tg matings were stained with H & E to use as a structural guide for each placenta. Using RNAscope multiplexing they were stained with *Prl3b1* probe C2 42361 which was dyed with Cy5. The nucleus was stained with DAPI. Tg junctional zones were 40% ($P=.003$) smaller than WT in males and 62% ($P<.001$) smaller than WT in females. Female Tg junctional zone area was significantly smaller than Male Tg junctional zone area by 34% ($P=.03$). Total area was not significantly different for males, where female Tg measured 41% ($P=.009$) smaller than WT. Female Tg placentas were also 35% ($P=.007$) smaller than M Tg placentas in total size. Tg junctional zones contained 40% ($P <.001$) fewer *Prl3b1* positive cells than WT in males and 59% ($P<.001$) fewer than WT in females. Female Tg junctional zones contained 33% ($P=.019$) fewer *Prl3b1* positive cells than males Tg junctional zones. Female Tg labyrinths contained 38% ($P=.009$) fewer *Prl3b1* positive cells than

female WT. Female Tg labyrinths also contained 38% ($P=.013$) fewer *Prl3b1* positive cells than male Tgs. Total *Prl3b1* positive cells were reduced by 39% ($P=.01$) in Female Tg placentas compared to Female WT placentas. Female Tg placentas also had 31% ($P=.017$) fewer *Prl3b1* positive cells than Male Tg placentas. Scale bar 500 μm .

3.3.3 Pooled sex qRT-PCR analysis masks impact on female placentas placental hormone and lineage marker RNA expression

To understand the impact on placental lineages and production of a wider variety of placental hormones qRT-PCR was used to investigate the gene expression profile of *Phlda2*^{+/+BACx1(BL6)} placentas. Placentas were collected by dissection of E14.5 mixed WT and Tg pregnancies as described in methods sections 2.1.5 and 2.1.6. RNA was extracted from the samples and converted into cDNA as per protocols 2.10.1 and 2.10.3. Data was generated from 4 litters, using a litter size range between 7-10 (average 8 ± 0.33) pups per litter. Male WT ($n = 4$), Male Tg ($n = 4$), Female WT ($n = 4$) and Female Tg ($n = 4$). Initial investigations pooled WT and Tg samples to look at RNA targets in the Prl family.

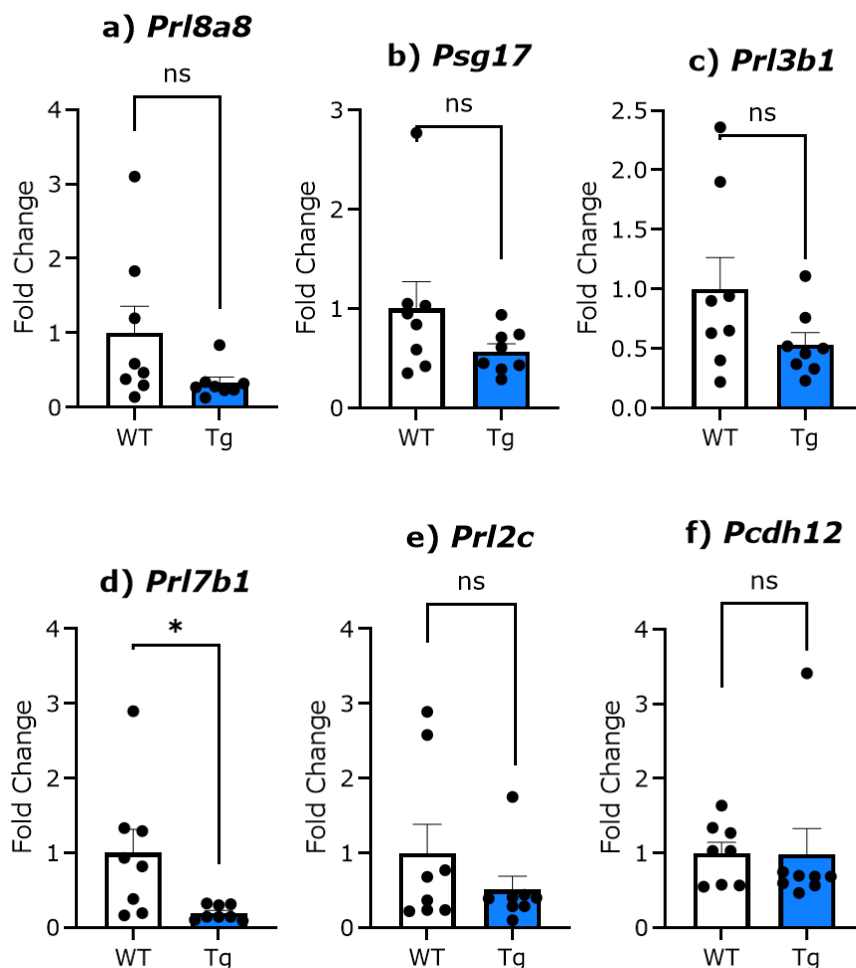
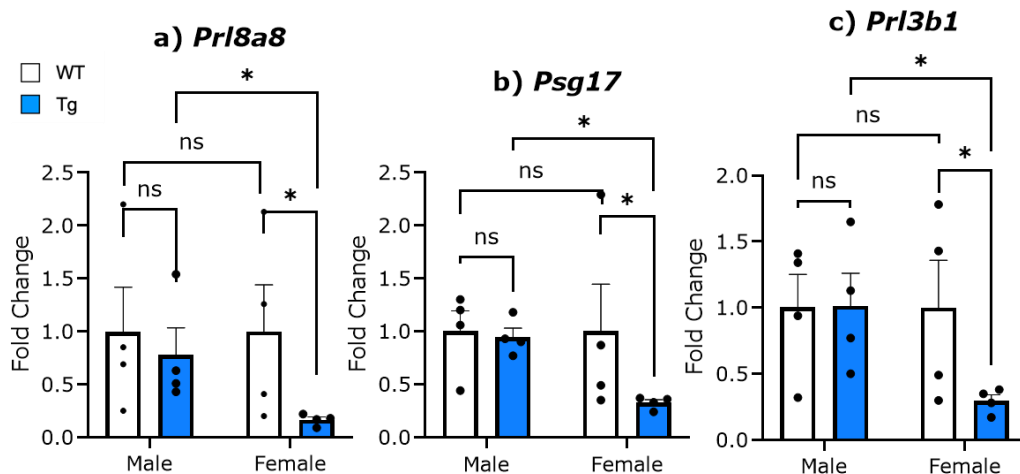


Figure 38: qRT-PCR analysis of Prl family members for WT and Tg.

a) qRT-PCR for WT and Tg placenta at E14.5. *Prl8a8* expression was not significantly different between WT and Tg. **b)** Expression of *Psg17* was not significantly different between WT and Tg. **c)** Expression of *Prl3b1* was not significantly different between WT and Tg. **d)** Expression of *Prl7b1* was reduced by 78% in Tg compared to WT. **e)** Expression of *Prl2c* was not significantly different between WT and Tg. **f)** Expression of *Pcdh12* was not significantly different between WT and Tg. Data from 4 litters, litter size between 7-10 (average 8 ± 0.33). WT ($n = 8$), Tg ($n = 8$). Error bars represent \pm SEM. Statistical significance calculated using a two-way ANCOVA with litter size as a covariate using a Šidák correction. ^{NS} $P > .05$, * $P < .05$, ** $P < .01$, *** $P < .001$, **** $P < .0001$ (Appendix 12).

Although all genes investigated, with the exception of *Pcdh12* (0.88%, $P = .188$), show a reduction in expression from WT to Tg ranging from 20-50% (*Prl8a8* 53%, $P = .076$, *Psg17* 37%, $P = .066$, *Prl3b1* 34%, $P = .131$, *Prl2c* 20%, $P = .274$), only *Prl7b1* actually reaches significance with a reduction in expression of 78% ($P = .01$). This could be due to conflicting responses to the transgenic modification across sexes which was further investigated.



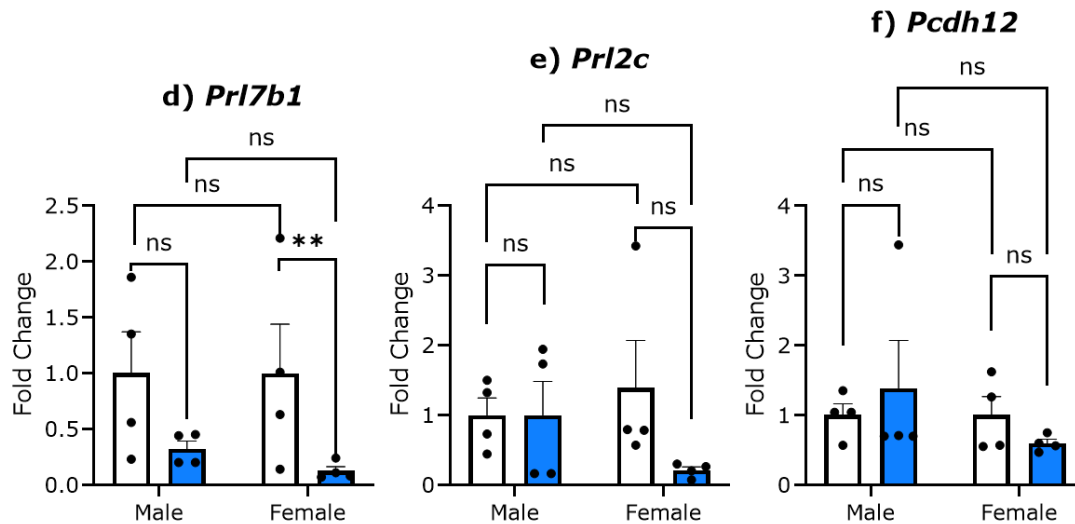


Figure 39: qRT-PCR analysis of Prl family members for WT and Tg split by sex.

a) *Prl8a8* expression was reduced by 84% in Tg females compared to WT females. Female Tg *Prl8a8* expression was also reduced by 61% compared to Male Tgs. **b)** Expression of *Psg17* was reduced by 68% in Tg females compared to WT females. Females Tgs *Psg17* expression was also reduced by 62% compared to Male Tgs. **c)** Expression of *Prl3b1* was reduced by 71% in Tg females compared to WT females. Females Tgs *Prl3b1* expression was also reduced by 72% compared to Male Tgs. **d)** Expression of *Prl7b1* was reduced by 88% in Tg females compared to WT females. Male *Prl7b1* expression was reduced by 68% however this was not significant. There was no significant difference seen between female and male Tgs for *Prl7b1* expression. **e)** There was no significant difference seen in expression between groups for *Prl2c*. **f)** There was no significant difference seen in expression between groups for *Pcdh12*. Data from 4 litters, litter size between 7-10 (average 8 ± 0.33). Male WT ($n = 4$), Male Tg ($n = 4$), Female WT ($n = 4$) and Female Tg ($n = 4$). Error bars represent \pm SEM. Statistical significance calculated using a two-way ANCOVA with litter size as a covariate using a Šidák correction. ^{NS} $P > .05$, $*P < .05$, $**P < .01$, $***P < .001$, $****P < .0001$ (Appendix 13).

Once the data had been split by sex, it was demonstrated that the impact on gene expression affected the female placenta more significantly than the male. *Prl8a8* had a non-significant 22% ($P = .866$) reduction in expression in male placentas, where female placentas experienced an 84% ($P = .026$) reduction in expression. Furthermore, comparisons between male Tg *Prl8a8* expression and female Tg *Prl8a8* expression showed a 61% ($P = .03$) reduction in expression in female Tgs compared to Tgs. This pattern was also seen in *Psg17* and *Prl3b1* with female Tgs showing a 62% ($P = .019$) and 72% ($P = .028$) reduction in expression compared to male Tgs respectively. Although reduction in *Prl7b1* doesn't reach significance in male Tgs compared to WT (68%, $P = .235$), females

have a similar yet more significant response with an 88% ($P=.01$) in Tgs compared to WT females, because of this, this is the only gene investigated where the reduction holds significance when the sexes are pooled. *Pcdh12* shows opposite responses from female and male placentas, however nothing reaches significance. Investigation into labyrinth markers was then conducted.

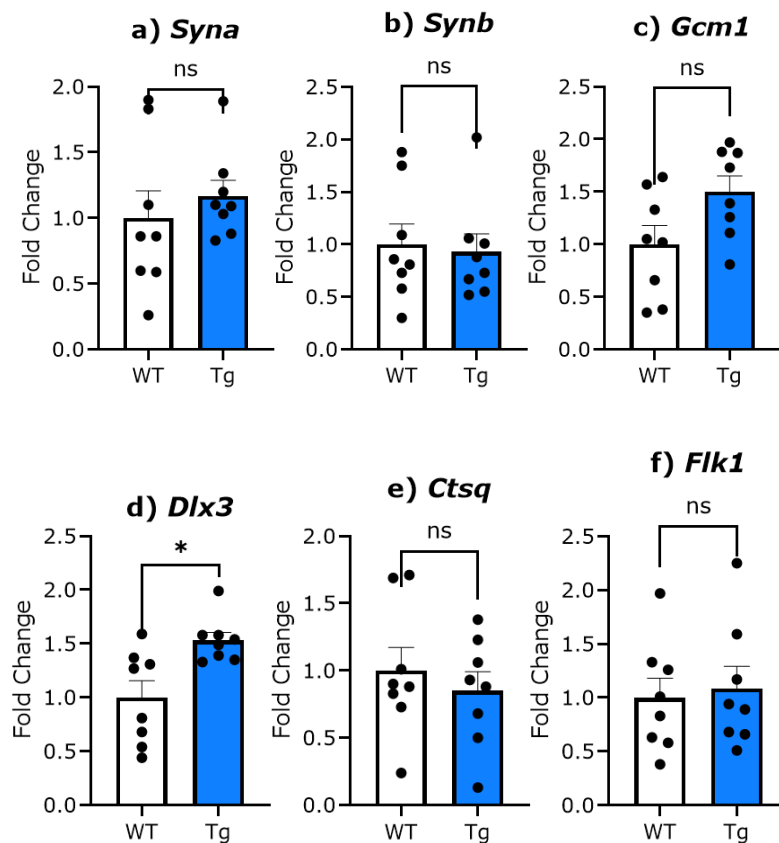


Figure 40: qRT-PCR analysis of labyrinth related genes WT and Tg. **a)** *Syna* expression was not significantly different between WT and Tg. **b)** Expression of *Synb* was not significantly different between WT and Tg. **c)** Expression of *Gcm1* was not significantly different between WT and Tg. **d)** Expression of *Dlx3* was significantly increased by 53 % in Tgs compared to WT. **e)** Expression of *Ctsq* was not significantly different between WT and Tg. **f)** Expression of *Flk1* was not significantly different between WT and Tg. Data from 4 litters, litter size between 7-10 (average 8 ± 0.33). WT ($n = 8$), Tg ($n = 8$). Error bars represent \pm SEM. Statistical significance calculated using a two-way ANCOVA with litter size as a covariate using a Šidák correction. $^{NS}P > .05$, $^{*}P < .05$, $^{**}P < .01$, $^{***}P < .001$, $^{****}P < .0001$ (Appendix 14).

In analysis of gene expression relating to the labyrinth, all genes except *Dlx3* showed no significant difference between WT and Tg pooled groups, with *Dlx3* having a 53% ($P=.04$) increase in expression in Tg placentas.

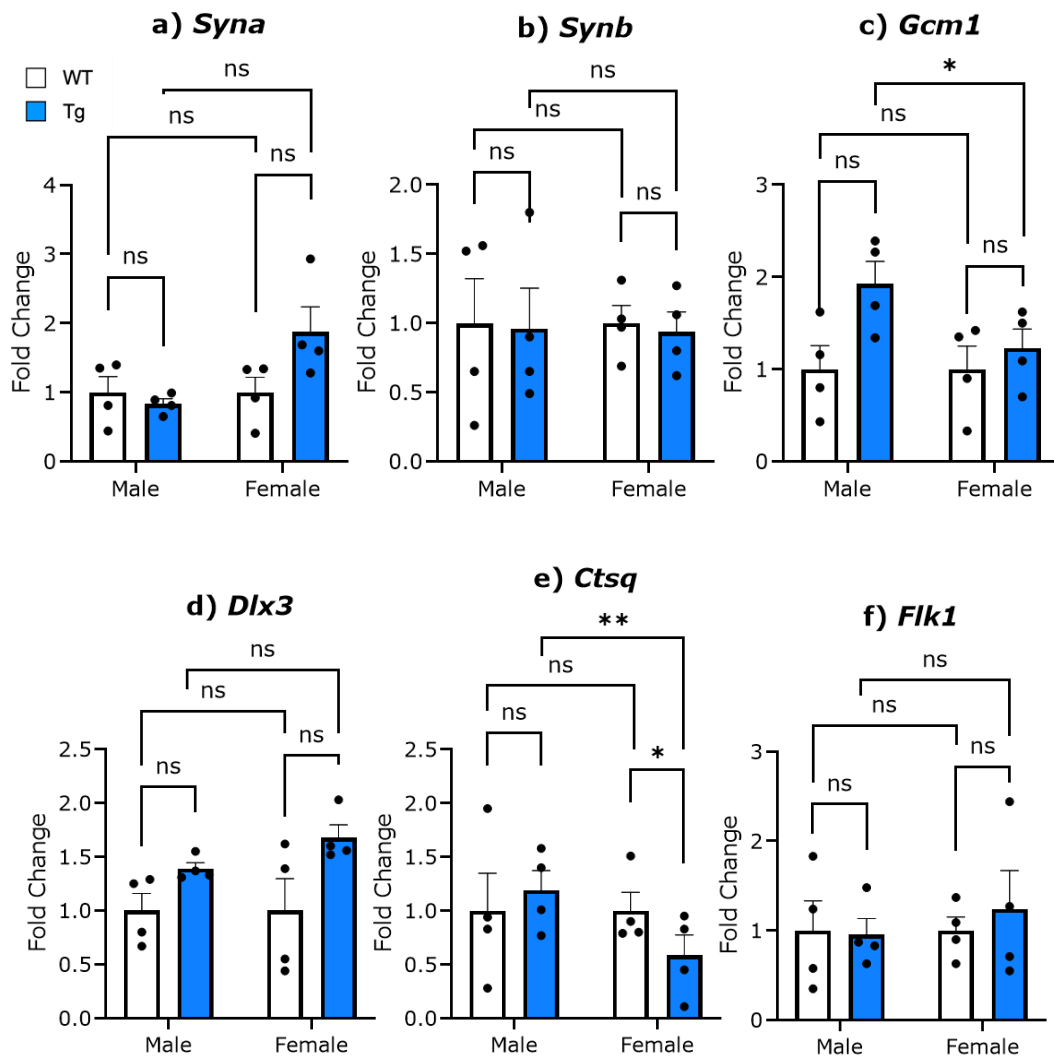


Figure 41: qRT-PCR analysis of labyrinth related genes for WT and Tg split by sex.

a) *Syna* expression showed no significant difference between groups. **b)** Expression of *Synb* showed no significant difference between groups. **c)** Expression of *Gcm1* is reduced by 70% in Female Tgs compared to male Tgs. **d)** Expression of *Dlx3* showed no significant difference between groups. **e)** Expression of *Ctsq* was reduced by 42% female Tgs compared to female WTs. Female Tgs also have a 61% reduction in expression of *Ctsq* compared to Male Tgs. **f)** There was no significant difference seen in expression between groups for *Flk1*. Data from 4 litters, litter size between 7-10 (average 8 ± 0.33). Male WT ($n = 4$), Male Tg ($n = 4$), Female WT ($n = 4$) and Female Tg ($n = 4$). Error bars represent \pm SEM. Statistical significance calculated using a two-way ANCOVA with litter size as a covariate using a Šidák correction. NSP > .05, *P < .05, **P < .01, ***P < .001, ****P < .0001 (Appendix 15).

Splitting this data by sex lost significance for *Dlx3*, although both sexes have a similar increase in expression neither reach significance on their own. *Gcm1* expression is increased in the male to a greater degree than in the female, resulting in a significant reduction in expression in female Tg compared to male Tg (70%, $P=.04$). A sexual dimorphic expression pattern was revealed in the expression pattern of *Ctsq*. Male placentas have a slight increase in expression of *Ctsq* (19%, $P=.684$) which nullified the reduction of expression seen in female placentas when the sexes were pooled. Not only do female Tg placentas show a 42% ($P=.022$) in *Ctsq* expression compared to female WT, but they also have a 61% ($P=.01$) reduction compared to male Tgs.

3.4 Discussion

This chapter investigated the impact of a two-fold expression of *Phlda2*, modelling loss of imprinting on mouse placental development in males and females. Overall, the placenta showed significant alteration in weight, structure, and gene expression. Specifically affecting the endocrine lineage, the junctional zone and ultimately its expression of hormone related RNA transcripts. These were comparable to previous findings by Tunster et al. (2010) and Tunster, Creeth, et al. (2016) using a similar model. This analysis incorporated new elements, such as factoring in litter size as a covariate and a sexually dimorphic assessment. It was also the first project to use quantitative *Prl3b1* staining as a proxy for the hormone production capacity of the placenta.

3.4.1 Analysis of foetal and placental weights demonstrate sexual dimorphism in *Phlda2*^{+/+BACx1(BL6)} placenta

Replicating the analysis of foetal and placental weights for WT and Tg produced the same results as demonstrated in Tunster et al. (2010) and Tunster, Creeth, et al. (2016), with no difference between groups at E14.5. A similar reduction was seen in placental weights with Tunster et al. (2010) and Tunster, Creeth, et al. (2016), which demonstrated a 21% ($P= <.0001$ ($P = 3.12 \times 10^{-10}$)) reduction in placental weight on a mixed background (129/Sv:C57BL/6) and the *Phlda2*^{+/+BACx1(BL6)} model in this thesis showing a reduction in weight of 17% ($P<.001$). Tunster, Creeth, et al. (2016) foetal to placental weight ratios also matched the *Phlda2*^{+/+BACx1(BL6)} model analysis, with the 2016 data showing an 18.3% ($P= <.0001$) increase in the ratio for Tg placentas and this project having a 17.7% ($P<.001$) increase. This showed that broadly the move onto the BL6 mouse strain did not alter the effect of the transgene.

When factoring in sex whilst investigating foetal weight, again no difference was seen between WT and Tg groups of both sexes, as well as WT and Tg groups not being significantly different from one another across sexes. Again, demonstrating no effect on the foetal weight that previously may have been masked by pooling the sexes. This implies that the in whatever way the placenta is impacted it is functional in supporting foetal growth. Placental weight showed initial differences between WT males and WT females with a reduction in females placentas. When comparing Tg and WT within the sexes, females showed a marginally increased reduction compared to males. Female Tg placenta weighed 9% (ANOVA $P=.0478$) less than Male Tg placenta. This reduction matched the reduction seen in comparing WT male and WT female placentas, ultimately suggesting that placental weight does not show a sexually dimorphic response by significantly impacting one sex more than the other.

As the foetal weight is not impacted, this suggests that even though the Tg placenta is reduced in size, on a macro level the *Phlda2*^{+/+BACx1(BL6)} placenta is able to function efficiently enough to support 'normal' growth of the foetus. To further understand the dynamics of this result, area measurements of each structure within the placenta and hormone production values will be assessed to determine which components are impacted most and how that affects placental efficiency or its ability to support foetal growth. As foetal weight is an all-encompassing data point, a more detailed analysis of the foetus would aid in understanding if the structurally disrupted placenta has an impact on different elements of the foetus. No significant difference was seen when comparing the sexes, although the female ratio was increased more than males. The full weight of the placenta encompasses many functionally diverse regions, it is possible that significant alterations within the placenta could still be sexually dimorphic and could be compensated for elsewhere, however the overall weight is comparable. These findings meet the hypothesis around *Phlda2*^{+/+BACx1(BL6)} impacting the placenta. The lack of sexual dimorphism is likely due to the macro assessment of the placenta.

3.4.2 Automated RNAscope program demonstrates reductions in functional endocrine output of *Phlda2*^{+/+BACx1(BL6)} placentas

3.4.2.1 Sexual dimorphism in placental structure: Junctional zone and labyrinth area impacts in *Phlda2*^{+/+BACx1(BL6)} placentas

In the area measurements conducted in Tunster, Creeth, et al. (2016), using 129 strain mice, the junctional zone area demonstrated a reduction in size by 57% ($P<.0001(P= 2.10 \times 10^{-5})$) with no significant effect on the labyrinth and a 21% ($P<.0001(P= 3.30 \times 10^{-3})$) reduction in total size for

Tg placentas (Tunster, Creeth, et al., 2016). In replicating these investigations for this thesis, the *Phlda2*^{+/+BACx1(BL6)} model demonstrated a 51% ($P < .001$) smaller junctional zone than WT with no significant difference in labyrinth size and a total size reduction of 19% ($P = .038$). To probe further into this model the statistics were run compensating for litter size and the data was split by sex to determine any sexually dimorphic impacts.

When the analysis was split by sex, female results differed in the intensity of the reduction in size of the junctional zone, showed a significant reduction in labyrinth area where males showed a slight increase and showed a significant reduction in total area where males did not. Statistical relevance was only revealed once the data was also processed with an ANCOVA using litter size as a covariate. The labyrinth showed a strong genotype*sex interaction, with the two sexes responding in the opposite direction. Male labyrinths slightly increased in size where females labyrinths reduced in size significantly, resulting in female Tg labyrinths being 25% smaller than male Tg labyrinths. The more radical decrease in junctional zone size, coupled with the reduction in the labyrinth for female placentas culminates in the total placenta area being significantly reduced in female Tg (-41%, $P = .009$) where it was not in male Tg (+2%, $P = .668$). This data does not totally align with the weight data, however, weight data encompasses the entire placenta, where the structural measurements tell a more nuanced story and the slight increase in labyrinth size for the males may be reducing the overall impact on total size. Although endocrine compartment impacts were hypothesised for this analysis, impacts on the labyrinth were unexpected. The function of the labyrinth is to provide nutrients to the foetus, perhaps the increase in size of the male labyrinth is to attempt to direct more nutrients towards the more demanding male foetus whilst it is in this compromised state, whereas the female placenta is not making that adjustment. Overall, these area measurements have demonstrated a more radical impact on the female placenta than its male counterpart as a result of *Phlda2* loss of imprinting.

3.4.2.2 Manual counting validates effectiveness of newly established RNAscope counting methodology

Previous papers have used different methods to determine alterations to cell type compositions within the placenta for this genetic model. Most of these methods involved manual counting on H & E stained sections. This required an experienced eye and assumed the expression status of each cell. During this project a new automated counting program was developed for more accurate identification of cell types. Using *Pr13b1* as a

target, this also gave a more quantitative measure of *Prl3b1* expression and potential placental endocrine production.

This data was compared to a manual count in a pilot trial of the program. Manual counting was performed by Amelia Stodart. The automated counting method was determined to match the manual counting and allowed for a greater throughput of samples giving a higher statistical power. Any errors introduced by the automated counting were applied consistently across samples, where human errors could be applied in a randomly distributed fashion. Automated counting generally had reduced standard errors than manual counting within groups, demonstrating a more accurate measurement. This achieves one of the key aims of this chapter in establishing a regionally specific automated cell counting program.

3.4.2.3 Analysis of junctional zone *Prl3b1* expressing cells and glycogen cell distribution in *Phlda2*^{+/+BACx1(BL6)}: Quantitative insights and sexual dimorphism

Tunster et al. (2010) did not investigate the expression of *Prl3b1* in its *Phlda2* loss of imprinting model. Tunster, Creeth, et al. (2016) used *in situ* hybridisation of *Prl3b1* probes which suggested a reduction in expression between the control and their *Phlda2* loss of imprinting model, but this was not done quantitatively. To elaborate on this work, the automated counting program which was designed for the purposes of quantifying the *Prl3b1* output of each placenta was used. Between WT and Tg junctional zones, all metrics investigated were altered by *Phlda2*^{+/+BACx1(BL6)}. This was seen as a reduction in the number of junctional zone cells expressing *Prl3b1* as well as a reduction in total cells within the junctional zone. Both of these metrics were more significantly reduced in female junctional zones. This result is in direct contradiction to the hypothesis, as it was believed that male placentas would be more vulnerable and therefore more likely to be significantly impacted.

Glycogen cell analysis was previously quantified with glycogen values being determined via biochemical concentration. In Tunster et al. (2010), the comparison between WT and a *Phlda2* loss of imprinting model showed a 25% loss in placental glycogen. In this thesis, glycogen cells were accurately identified as being within the junctional zone and being *Prl3b1* negative. This approach determined that Tg placentas have a reduction of glycogen cells of 68% ($P < .001$) which causes the ratio of glycogen cells within the junctional zone to be increased in the Tg group compared to WT by 51% ($P = .004$). Glycogen cells build a store of glycogen within their cytoplasm from E12.5 (Bouillot et al., 2006; Coan et al., 2006), which is believed to be used by the foetus in late gestation, a

common function across mammalian placenta (Christie, 1967). This lower amount of glycogen in the Tg group suggests reduced resources for the foetus.

3.4.2.4 Sexual dimorphism in labyrinth structure and function: Impact of *Phlda2*^{+/+BACx1(BL6)} on hormonal expression and cell distribution

Previous analysis by Tunster et al. (2010) showed a non-significant reduction in labyrinth area in Tg compared to WT which was repeated in the area calculations in this project (3.3.2.1). Although *Prl3b1* staining was performed on E14.5 placentas in Tunster, Creeth, et al. (2016), the expression within the labyrinth was not investigated in detail. In this thesis, initial investigation into labyrinth cell counting again suggested no impact on the labyrinth by genotype when the sexes were pooled, replicating previous area measurement analysis by Tunster, Creeth, et al. (2016). When the data was split by sex, the female labyrinth was specifically impacted and the male labyrinth was not. This was not anticipated by the hypothesis, as the labyrinth is not primarily tasked with hormone production. In relation to imprinted genes and their regulation of maternal investment, reductions in the cell number of the labyrinth would adjust nutrient delivery to the foetus and would regulate investment through that means. That being said, one of the cell types being reduced in the labyrinth is the S-TG cells which are located within the sinusoidal spaces within the labyrinth region and produce *Prl3b1* (Simmons et al., 2007). These cells are in direct contact with maternal blood which would indicate a significant functional impact on hormone exposure to the maternal system (Simmons et al., 2007). This suggests that there is an additional reduction in endocrine function of the female placenta resulting from modifications to the labyrinth, as well as the adjustments to the junctional zone. This aligns with sex split labyrinth area measurement data from section 3.3.2.1, whilst adding a functional and hormonal output element.

3.4.2.5 Sex-specific reductions in cell count and *Prl3b1* expression in *Phlda2*^{+/+BACx1(BL6)} placenta

The data from the full placental counts reflect a combination of the previous data. Again, a more significant impact is demonstrated in the female placenta. The total cell numbers are significantly reduced in female Tg samples only compared to female WT. For the hormone production of *Prl3b1*, females are significantly reduced compared to their WT counterparts. In addition, despite female WT placentas having no significant difference in *Prl3b1* RNA expression from male WT placentas, female Tg placentas showed a significant reduction from male Tg placentas, suggesting that the overall output of the female placentas

Prl3b1 is significantly impacted, where the males are not. This again defies the hypothesis with the female placentas being hypothesised to be able to withstand more disruption than males. This data has achieved the aim of applying the new method of quantitative regional staining whilst demonstrating the functional conclusions that can be drawn from the data it produces.

3.4.3 Sexually dimorphic gene expression alterations reflect impacts on junctional zone and labyrinth structures of *Phlda2*^{+/+BACx1(BL6)} placenta

In previous studies, a reduction in *Hand1*, *Ascl2*, *Prl8a8*, *Tpbpa*, gap junction protein beta 3 (*Gjb3*), 1,4- α -glucan branching enzyme (*Gbe1*), and FMS-like tyrosine kinase 1 (*Flt1*) and an increase in *Gcm1*, glycogenin (*Gyg*) and kinase insert domain protein receptor (*Flk1*) was seen in previous qRT-PCR assessments of the *Phlda2*^{+/+BACx1} model compared to WT (Tunster et al., 2010), which was assessed before the strain was bred onto the BL6 background. This data suggested that although there was only a small reduction in glycogen cell markers (*Gjb3*), there was a significant change in the microenvironment provided by the spongiotrophoblast seen in the change in expression of enzymes critical for glycogen metabolism (*Gyg* and *Gbe1*). The reduction in *Tpbpa* and *Ascl2* suggested a reduction in the junctional zone and the reduction in *Prl8a8* suggests a reduction in spongiotrophoblast cells was the greatest contributor to that decrease. The increase in expression of the marker for the branching labyrinth (*Gcm1*) and decrease in expression of *Flt1* reflected the change in ratio between the junctional zone and labyrinth. The increase in *Flk1* expression suggested an increase in foetal vasculature (Shalaby et al., 1995). The reduction in *Hand1* expression, which is essential for TGC differentiation (Riley et al., 1998), suggested reductions in TGCs, although this was not reflected by *in situ* data (Tunster et al., 2010). These results ultimately showed a significant alteration in the ratio between glycogen cells and spongiotrophoblasts in the junctional zone and a change in the ratio between the labyrinth and junctional zone (Tunster et al., 2010).

In this thesis, the reduction in *Prl8a8* is still present, however is not significant. Similar reductions were also seen in other Prl family members *Prl3b1*, *Prl2c* and *Psg17*, with only *Prl7b1*, a glycogen cell marker, reaching significance. This correlates to the glycogen cell counting data from section 3.3.2.3.1 and previous glycogen cell reductions seen in (Tunster et al., 2010). When the data was split by sex it was clear why each pooled reduction did not reach significance. There was no significant alteration to the expression of any genes of interest in male placentas, however four genes of interest decreased in expression in female

Phlda2^{+/+BACx1(BL6)} compared to female WT (*Pr18a8*, *Psg17*, *Pr13b1* and *Ctsq*). *Pr17b1*, was reduced in both sexes but was only significant in females which is why it presented as significant when the samples were pooled. The reduction of *Pr18a8*, *Psg17*, *Pr13b1* and *Pr17b1* demonstrates a significant reduction in the size of the junctional zone and endocrine capacity for female *Phlda2*^{+/+BACx1(BL6)} placentas. Reductions in *Pr18a8*, *Psg17* and *Pr13b1* indicating specific reductions in the spongiotrophoblast lineage. This result correlates to the more significant reduction in junctional size and *Pr13b1* positive cells seen in female placentas in section 3.3.2.1 and 3.3.2.3.1. Female placental *Pr17b1* expression reduction also correlates to the size reduction in the area measurements of the junctional zone 3.3.2.1 and to glycogen cell counting data in section 3.3.2.3.1. *Ctsq* is a marker of S-TG cells (Ishida et al., 2004; Outhwaite et al., 2015) which gives further evidence to suggest the reduction in S-TG cells in the labyrinth for *Phlda2*^{+/+BACx1(BL6)} females as suggested in 3.3.2.3.2. As S-TG cells are in direct contact with maternal blood (Simmons et al., 2007), the reduction of these cells could result in a significant reduction in exposure of placental hormones to the maternal system. *Gcm1* was also reduced in female *Phlda2*^{+/+BACx1(BL6)} placentas compared to male *Phlda2*^{+/+BACx1(BL6)} placentas. *Gcm1* is crucial for labyrinth development (Anson-Cartwright et al., 2000; Simmons, Natale, et al., 2008) its reduction ties to the data for female labyrinth area measurement reductions and reductions in cells in the female labyrinth (section 3.3.2.3.2 and 3.3.2.1). This further reinforces a sexually dimorphic response within the labyrinth and in *Phlda2*^{+/+BACx1(BL6)} placentas overall. This sex specific impact on the labyrinth has been previously reported in IGR studies (Jeong et al., 2023), where the labyrinth of the female was impacted and not the male, again potentially due to the male's higher foetal demands on the placenta.

In conclusion the transition from 129 to BL6 showed similar reductions in the junctional zone for both spongiotrophoblast and glycogen cell lineages. However, only the glycogen cell reductions remained for both sexes, and only female placentas still had significant reductions in spongiotrophoblast markers. Significant structural changes to the labyrinth were again only seen in female placentas with *Gcm1* and *Ctsq* results. Although previous analysis of prior *Phlda2*^{+/+BACx1} models did not assess for sexual dimorphic effects, the pooled data did demonstrate more of an impact than the current model. This could be the result of two possibilities, either the female placentas in the previous assessments were so heavily impacted that statistically their impact was still revealed when the data was pooled or previous *Phlda2*^{+/+BACx1(BL6)} strains impacted males more significantly than this strain. Both reductions in labyrinth gene expression markers and female specific reductions in gene expression were not previously hypothesised. Regardless, this model has

demonstrated significantly different gene expression profiles for female placentas.

3.5 Limitations

As mouse pregnancies harbour multiple pups with multiple placentae, it can be assumed that there are mechanisms within the mouse pregnancy that regulate the hormone exposure to the mother as increases in placenta number naturally result in an increase in total placental hormone levels. In the mouse model, there is a relationship between the size of the placenta and the number of pups present in the pregnancy, higher pup numbers within a pregnancy have smaller placentas per pup (Coan et al., 2008). This does not directly lead to smaller pups, as the placentas demonstrate a more efficient pup size to placenta size ratio in slightly larger litters, although, at the higher end of litter numbers, pup size is restricted (Coan et al., 2008). A smaller placenta per pup could reduce the overall amount of placental hormone that the mother is exposed to. However, research to further understand the relationship between placenta number and placental hormone regulation in mouse is largely unexplored. In humans, there is no indication of a hormone regulatory mechanism, as blood concentrations of both hCG and hPL are 2.5 and 1.5 times higher throughout pregnancy for twins compared to singleton pregnancies respectively (Spellacy et al., 1978; Thiery et al., 1977) and were reported to be even higher in triplet pregnancies. This lack of regulation is possibly due to multiparous pregnancies being rare in human pregnancies, in direct contrast to mice where multiparous pregnancies are standard. As there is no sign of post regulation in humans, it could be suggested that RNA data collected from human pregnancies could be a more reliable measurement of maternal hormone exposure. Most of the data used in these human studies used hormone levels in maternal blood, however, there is also the potential for the maternal brain to vary in its sensitivity to placental hormones which would be another avenue for research in this field (Pope et al., 2017). As the regulation of hormones produced by multiple placentas in the mouse is not a direct question of this thesis project, the idea to incorporate litter size into the statistical analysis allows potential mechanisms to be corrected for. In the analysis conducted throughout the remainder of this thesis, the ANCOVA with litter size as a covariate will be used as the standard analysis.

The issue around regulation of placental hormones confounds the ability to determine hormone exposure to the maternal brain, specifically in the mouse model. While methods such as qRT-PCR can be used to determine the increase or decrease in placental hormone transcripts, it cannot determine protein concentration or hormone exposure to the brain. The

development of the automated counting of *Prl3b1* positive cells used in section 3.3.2.3 of this thesis is quantitative to RNA production. Although, post transcriptional regulation and proximity to maternal blood adjusts the concentration of hormone in the maternal blood and hormone exposure to the brain, this quantitative RNA data is an important piece of the larger puzzle. Although, it does not directly equate to the concentration of hormones to the maternal brain it does demonstrate an alteration to the regulation of the production of the hormone. This data coupled with protein analysis and hormone concentration in the blood gives the full picture of the effect of the transgenic modification. As the junctional zone is the endocrine compartment and is adjacent to the maternal tissues, alterations in junctional zones specific endocrine function would likely have a more significant functional impact resulting in a more severe impact on the maternal systems hormone levels than alterations to the labyrinth. Although, modifications to S-TG cells specifically, within the labyrinth and their proximity to maternal blood could also be crucial to functional impacts. This new methodology provides that additional piece of data, as it is regionally specific and cell type specific to the different structures within the placenta, and therefore holds a more functional significance in its results. One potential improvement to this technique would be to add stereology to the method. This would give a 3D reading of the placental structures for the entire tissue and would provide a more detailed insight into tissue wide hormone production.

3.6 Summary

The key findings from this chapter are presented in Table 37.

Analysis	Key findings
Placental and foetal weight data	<ul style="list-style-type: none"> • While foetal weights were unaffected in Tg, Tg placentas were reduced in both males and females.
Placental region area measurements	<ul style="list-style-type: none"> • While Tg junctional zones were impacted in both sexes, female junctional zones were more significantly reduced in size. • Male Tg labyrinths were not affected where female Tgs were reduced in size. • This resulted in a significantly reduced total area for female Tg placenta but not for males.
RNAscope <i>Prl3b1</i> counting	<ul style="list-style-type: none"> • While the junctional zones of both sexes were reduced in all metrics compared to WT, female junctional zones were more significantly impacted than male junctional zones.

	<ul style="list-style-type: none"> • Pooled analysis of of labyrinth function masked significant impacts on <i>Pr13b1</i> and total cell number reductions in female labyrinths only. • Full placenta <i>Pr13b1</i> positive cells and total cells were only significantly reduced in female samples and not in males when assessed by sex.
qRT-PCR data	<ul style="list-style-type: none"> • Reductions in expression of <i>Pr18a8</i>, <i>Psg17</i>, <i>Pr13b1</i>, <i>Pr12c</i> and <i>Ctsq</i> were masked during pooled analysis of sexes. • <i>Pr18a8</i>, <i>Psg17</i>, <i>Pr13b1</i>, <i>Pr17b1</i> and <i>Ctsq</i> expression is significantly reduced in females and not in males.

Table 37: Key findings of Chapter 3.

A summary of key sexually dimorphic characteristics is presented in Table 38.

Metric	M-WT vs M-Tg	F-WT vs F-TG	M-Tg vs F-Tg
Foetal weight	-	-	-
Placental weight	↓	↓	-
Junctional zone area	↓	↓	↓
Junctional zone <i>Pr13b1</i> positive cells	↓	↓	↓
Labyrinth area	-	↓	↓
Labyrinth <i>Pr13b1</i> positive cells	-	↓	↓
RNA expression: <i>Pr18a8</i> , <i>Psg17</i> , <i>Pr13b1</i> , <i>Pr17b1</i> , <i>Ctsq</i>	-	↓	↓

Table 38: Key sexually dimorphic impacts of *Phlda2*^{+/+BACx1(BL6)}.

This chapter provides further evidence that the loss of imprinting of *Phlda2* does not have a detectable impact on foetal weight at E14.5. In addition, *Phlda2* loss of imprinting model has demonstrated a sexually dimorphic impact, with the stronger effect on female placentas than male placentas. Although both sexes junctional zones are reduced in size, cell number and *Pr13b1* expressing cell number compared to WT, the impacts on the female placenta are more severe and there is a female only impact

on the labyrinth and on RNA expression of lineage markers and other placental hormones (Table 38). It could be hypothesised that mothers of predominantly female litters could have a greater impact on maternal behaviours in this model than predominantly male litters. An interesting follow up experiment could be to implement these genetic alterations on male only and female only litters to more cleanly demonstrate the impact of sex in this context. This could be possible using sex sorted semen (Bai et al., 2025).

In Human, male placentas have been identified as being more vulnerable to impairment due to the maximum output required to support the developing male foetus (Aiken & Ozanne, 2013; DiPietro & Voegtline, 2017; Sutherland & Brunwasser, 2018). This means that the male foetus has less of a buffer to environmental changes in the uterus and are for that reason more likely to be susceptible to intrauterine complications such as disabilities or foetal death. Female placentas, for this same reason, demonstrate a higher capability at weathering and surviving suboptimal intrauterine conditions (Bale, 2011). The female's adaptation does come at a cost as females in suboptimal conditions are more vulnerable to less severe health complications such as anxiety and depression (Sandman et al., 2013; Sutherland & Brunwasser, 2018). In summary, males prioritise maximising growth in suboptimal environments resulting in more significant physiological complications where females reduce growth to be able to withstand suboptimal conditions (Clifton, 2010). This hypothesis matches the outcome of this model, as the *Phlda2*^{+/+BACx1(BL6)} model does not impact foetal weight for either sex, the males are therefore not being asked to compromise their foetal growth requirements. Able to weather milder conditions, male placentas are less impacted, resulting in fewer adjustments in their placental morphology. In contrast, the suboptimal conditions are causing the females to demonstrate a more significant impact than the males in terms of impacts on the labyrinth as well as junctional zones, *Prl3b1* positive cell numbers in RNAscope and *Prl* expression levels in qRT-PCR.

Chapter 4: Characterisation of *Peg3* and *Phlda2* antagonism in the developing mouse placenta

4.1 Overview

The two modes of genetic imprinting discussed in section 1.1, are paternally silenced genes which restrain growth and maternally silenced genes which promote growth or paternally expressed genes which promote growth and maternally expressed genes which restrict growth (Haig & Graham, 1991; John, 2013). Although both modes of expression have an opposite impact on the placenta, an interesting experiment to understand if the two behave antagonistically to each other is to remove one of each mode at the same time.

This chapter investigates the interaction between *Peg3* and *Phlda2* within the developing mouse placenta. It will do this by working with *Peg3*^{KO} and *Phlda2*^{KO} mouse strains, alongside a double knockout (DKO) model which contains functional knockouts of both *Peg3* and *Phlda2*. The DKO model will aid in highlighting how each gene of interest functions. If the removal of both genes produces the same phenotype as when both genes are present, this would indicate reciprocal roles of each gene. If the resulting phenotype does not resemble the WT phenotype, this would indicate that there is some unequal role or interaction between the two genes that is no longer functional when they are both absent. The opposing imprinting patterns and conflicting roles of *Peg3* and *Phlda2* on placental development suggest an antagonistic function or complex mechanism of interaction, justifying investigation into their regulatory roles and functions.

Both *Peg3*^{KO} and *Phlda2*^{KO} models have been independently investigated in their effects on the developing mouse placenta. Investigation of the *Peg3*^{KO} mouse strains placenta revealed a reduction in spongiotrophoblast and glycogen cells, both of which impacted male placentas to a greater degree than female placentas (Tunster et al., 2018). A more complicated picture of effects of loss of function of *Peg3* on hormone expression was also reported. Tunster et al. (2018) demonstrated a down regulation in three members of the *Prl* family and two spongiotrophoblast markers whilst also seeing an increase in two *Psgs* (Tunster et al., 2018). This analysis was done by qRT-PCR and did not ask the question of if sex had an impact on the response to the transgenic modification. The *Phlda2*^{KO} mouse strains placenta has an increased placental size, resulting from an expansion in the junctional zone (Salas et al., 2004; Tunster, Creeth, et al., 2016). The increased junctional zone has been linked to an increased

expression of *Prl3b1* (Tunster, Creeth, et al., 2016). Neither of these aspects of the *Phlda2*^{KO} model have been investigated for their sexually dimorphic impact.

It is hypothesised that the DKO placenta will develop a similar to WT phenotype, structurally and in relation to its functional hormone output. It is also hypothesised that the transgenic placentas will demonstrate some sexually dimorphic characteristics which will be more pronounced in male placentas.

4.2 Aims

These models have never been crossed to understand if there are equal roles between the two. To understand if these genes behave antagonistically, the interaction between them at early stages in development were investigated. RNAscope was used to identify cells which co-localise *Peg3* and *Phlda2* expression in the Epc and lineage progenitors at E7.5 and in the early stages of the placental lineages at E9.5, along with a series of associated genes of interest. This was paired with cell counting analysis of the four genotypes at E9.5 and RNAscope analysis of each genotype stained for the knockout genes and a spongiotrophoblast cell marker which revealed the dynamic of how each of the knockouts impacted expression.

For the later stages of development, this chapter investigated both *Peg3*^{KO} and *Phlda2*^{KO} placental and foetal weight data at E16.5 to determine the sex specific impacts of each of the genotypes. Weight data was analysed with the DKO group to understand if a correction to WT was demonstrated. Analysing each genotypes hormone output via quantitative *Prl3b1* staining added valuable information to each models' endocrine capacity, which again included the DKO placenta and gave an insight into which specific regions were corrected to WT. This assessment also investigated sexual dimorphism for each model. See Appendix 16 for chapter specific methods.

4.3 Results

4.3.1 Confirming co-expression: RNAscope multiplexing at E7.5 and E9.5 for *Peg3*, *Phlda2* and key lineage markers

A variety of combinations of multiplex RNAscope were performed on WT E7.5 and E9.5 embryo/placental pod units (pods). These were to identify co-expression of genes of interest along with which cell types were

expressing these genes. E7.5 was chosen as it is when the ectoplacental cone has established and is the beginning of the differentiation of the placental lineages as demonstrated by the expression of the lineage markers, *Ascl2*, *Tpbpa* and *Pr13d1* (Simmons 2014). By E9.5 the layers of the placenta are defined with the developing labyrinth and spongiotrophoblast clearly distinct (Simmons 2014). Mapping expression profiles of *Peg3* and *Phlda2* across these timeframes and with crucial lineage, structural and temporal markers will give insight into how these two genes of interest interact during these stages in regards to lineage expansion or restriction and will contribute to knowledge around their antagonistic interactions.

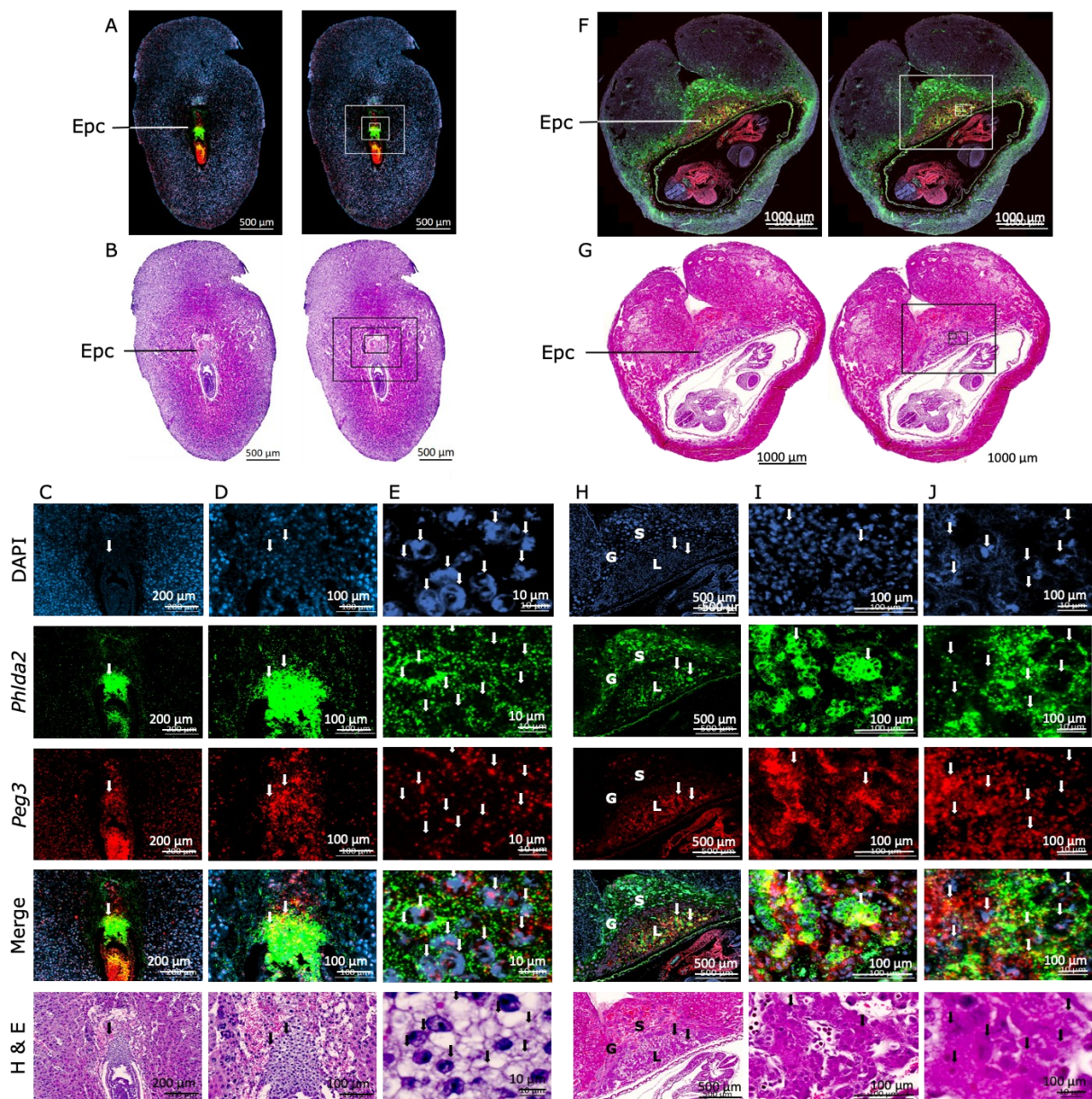


Figure 42: Duo-plex detection identifies co-localisation of *Peg3* and *Phlda2* expression.

A) Whole E7.5 WT mouse embryo/placental pod after *in situ* amplification of *Phlda2* (Green) and *Peg3* (Red). Co-localisation (Yellow). Nuclei labelled with DAPI (Blue). Ectoplacental cone (Epc) (20X). **B)** H & E stained (pink and purple bright field) section of whole E7.5 mouse embryo/placental pod (20X). **C)** Region of interest of E7.5 ectoplacental cone with co-localisation indicated with white arrow. (20X). **D)** Higher resolution of E7.5 ectoplacental cone with co-localisation indicated with white arrows. (40X) **E)** Higher resolution of E7.5 ectoplacental cone with co-localisation indicated with white arrows. (63X). **F)** Whole E9.5 WT mouse embryo/placental pod after *in situ* amplification of *Phlda2* (Green) and *Peg3* (Red). Co-localisation (Yellow). Nuclei labelled with DAPI (Blue) (20X). **G)** H & E stained section of whole E9.5 mouse embryo/placental pod (20X). **H)** Region of interest of E9.5 ectoplacental cone with co-localisation indicated with white arrows. L=Developing labyrinth, S= Developing spongiotrophoblast, G= Giant cell layer. (20X). **I)** Higher resolution of E7.5 ectoplacental cone with co-localisation indicated with white arrows. (40X) **J)** Higher resolution of E9.5 ectoplacental cone with co-localisation indicated with white arrows. (63X).

Co-expression of *Phlda2* and *Peg3* was seen at E7.5 in the Epc (Figure 42, C and D) with some cells showing greater expression of *Peg3* while *Phlda2* expression is lower in each cell (Figure 42, E). Co-expression of *Phlda2* and *Peg3* was seen at E9.5 in the developing labyrinth with larger clusters of co-expression (Figure 42, H and I). The surrounding populations of cells had different clusters of cells expressing just *Peg3* or *Phlda2* individually (Figure 42, J).

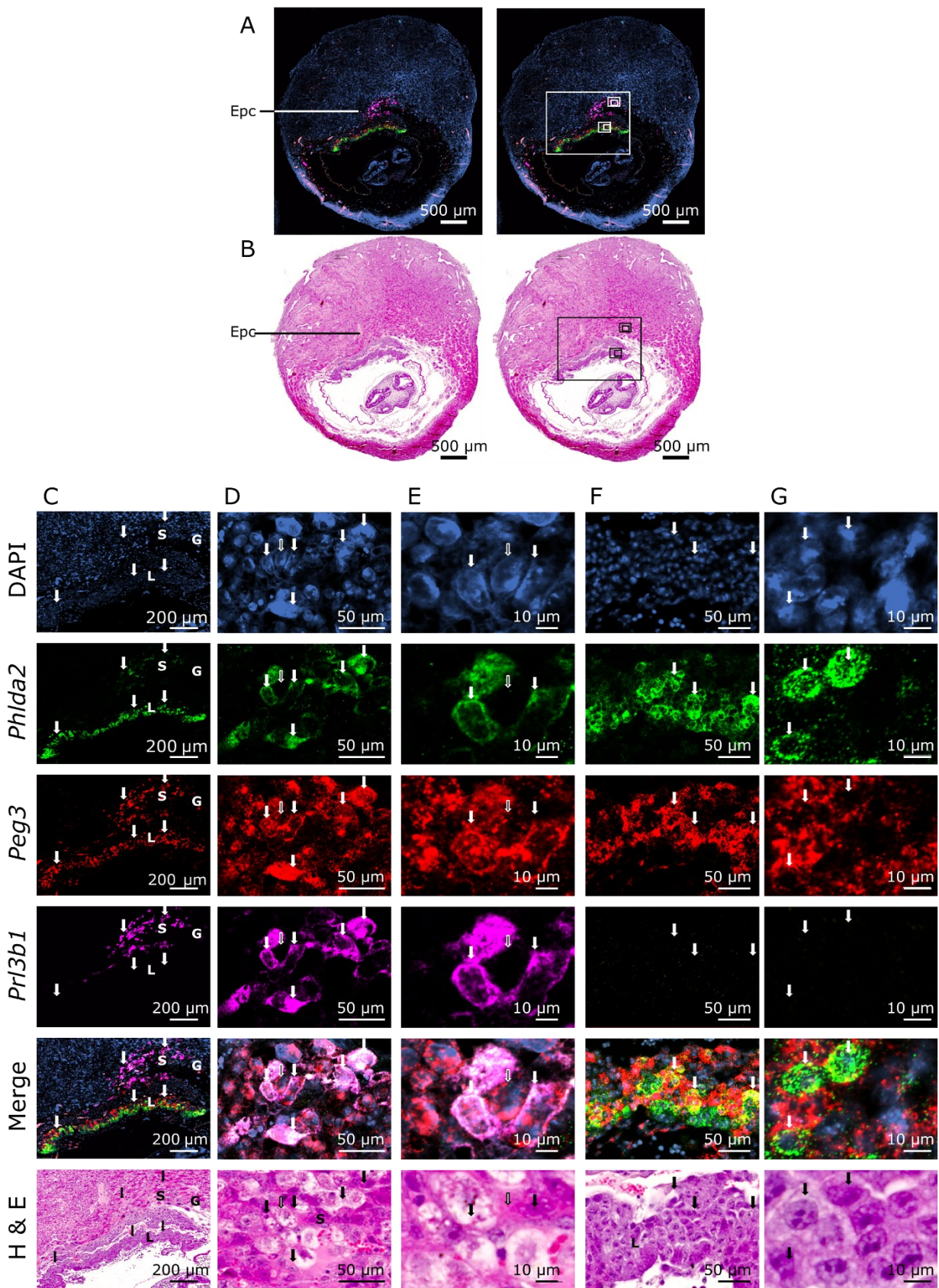


Figure 43: Multi-plex detection identifies co-localisation of *Peg3*, *Phlda2* and *Prl3b1* expression.

A) Whole E9.5 WT mouse embryo/placental pod after *in situ* amplification of *Peg3* (Red), *Phlda2* (Green) and *Pr13b1* (Pink). Co-localisation of all three (White). *Peg3* and *Phlda2* Co-localisation (Yellow). Nuclei labelled with DAPI (Blue). Ectoplacental cone (Epc). (20X). **B)** H & E stained (pink and purple bright field) section of whole E9.5 mouse embryo/placental pod (20X). **C)** Region of interest of E9.5 ectoplacental cone with co-localisation indicated with white arrows. (20X). L=Developing labyrinth, S= Developing spongiotrophoblast, G= Giant cell layer. **D)** Higher resolution of spongiotrophoblast with co-localisation indicated with white arrows. Single expression indicated with filled arrows (40X). **E)** Higher resolution of spongiotrophoblast with co-localisation indicated with white arrows. Single expression indicated with filled arrows (63X). **F)** Higher resolution of labyrinth with co-localisation indicated with white arrows (40X). **G)** Higher resolution of labyrinth with co-localisation indicated with white arrows (63X).

Co-expression of *Phlda2* and *Peg3* was seen at E9.5 in the developing spongiotrophoblast and developing labyrinth (Figure 43, C). The developing labyrinth did not express *Pr13b1* but did have large clusters of *Peg3* and *Phlda2* co-expression with surrounding cell populations of cells expressing just *Peg3* or *Phlda2* individually (Figure 43, F and G). The developing spongiotrophoblast contained small cell populations which co-expressed all three targets *Peg3*, *Phlda2* and *Pr13b1* (Figure 43, E and D). Here some surrounding cells express only *Peg3* (Figure 43, E and D).

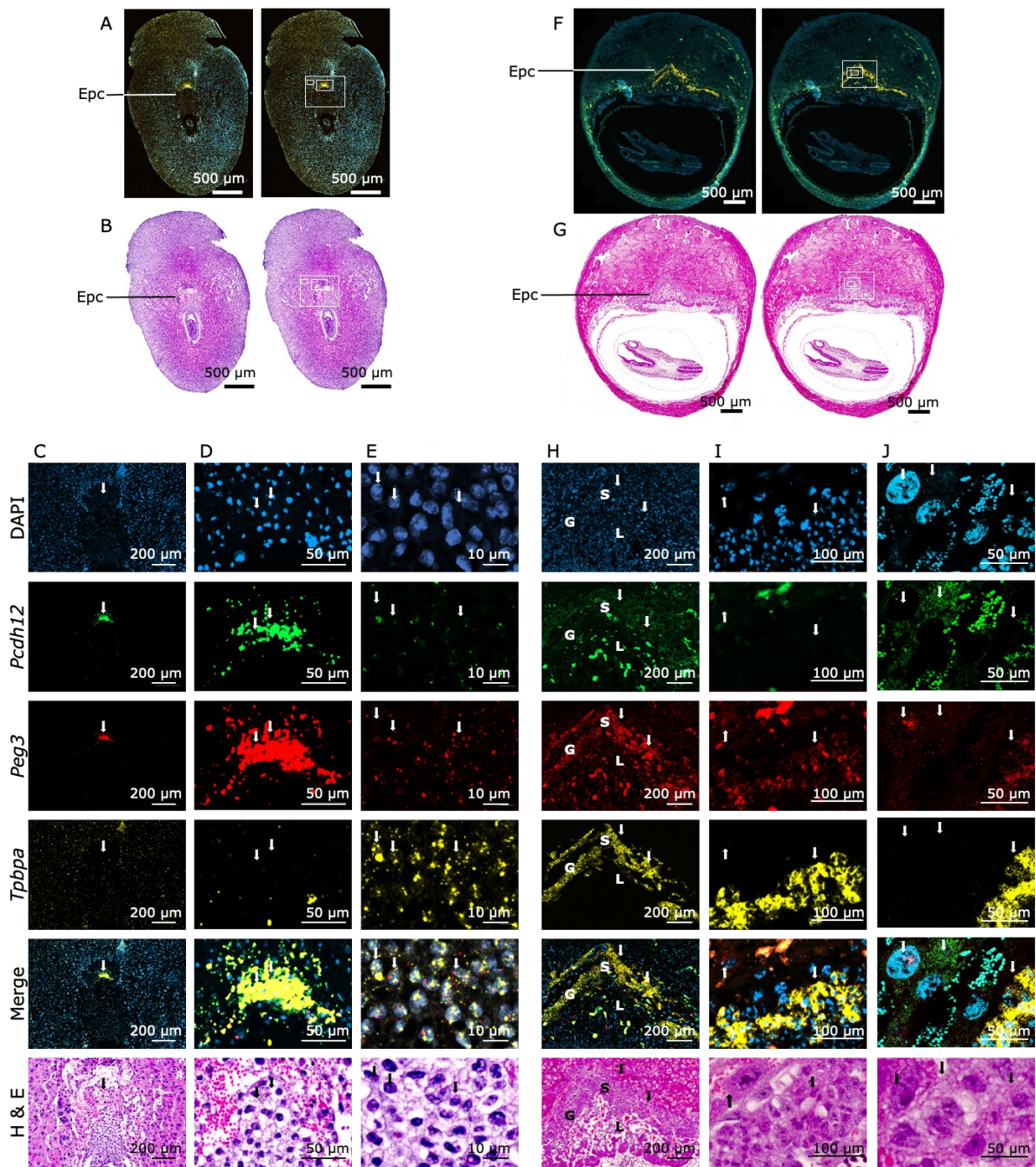


Figure 44: Multi-plex detection identifies co-localisation of *Peg3*, *Tpbpa* and *Pcdh12* expression.

A) Whole E7.5 WT mouse embryo/placental pod after *in situ* amplification of *Peg3* (Red), *Tpbpa* (Yellow) and *Pcdh12* (Green). Co-localisation (White). Nuclei labelled with DAPI (Blue). Ectoplacental cone (Epc). (20X). B) H & E stained (pink and purple bright field) section of whole E7.5 mouse embryo/placental pod (20X). C) Region of interest of E7.5 ectoplacental cone with co-localisation indicated with white arrows. (20X). D) Higher resolution of E7.5 ectoplacental cone with co-localisation indicated with white arrows. (40X). E) Higher resolution of E7.5 ectoplacental cone with co-localisation indicated with white arrows. (63X). F) Whole E9.5 WT mouse embryo/placental pod after *in situ* amplification

of *Peg3* (Red), *Tpbpa* (Yellow) and *Pcdh12* (Green). Co-localisation (White). Nuclei labelled with DAPI (Blue) (20X). G) H & E stained section of whole E9.5 mouse embryo/placental pod (20X). **H)** Region of interest of E9.5 ectoplacental cone with co-localisation indicated with white arrows. (20X). **I)** Higher resolution of E9.5 ectoplacental cone with co-localisation indicated with white arrows. (40X). **J)** Higher resolution of E9.5 ectoplacental cone with co-localisation indicated with white arrows. (63X).

At E7.5, *Peg3* was highly co-localised with the glycogen cell marker *Pcdh12* (Figure 44, D and E). The *Tpbpa* staining of the developing spongiotrophoblast doesn't define a key structure (Figure 44, D and E). At E9.5, two distinct populations are present, these are *Tpbpa* and *Peg3* co-expressing cells and *Pcdh12* and *Peg3* co-expressing cells (Figure 44, H-J), suggesting that at E9.5, *Peg3* is expressed in both the glycogen cells and spongiotrophoblast.

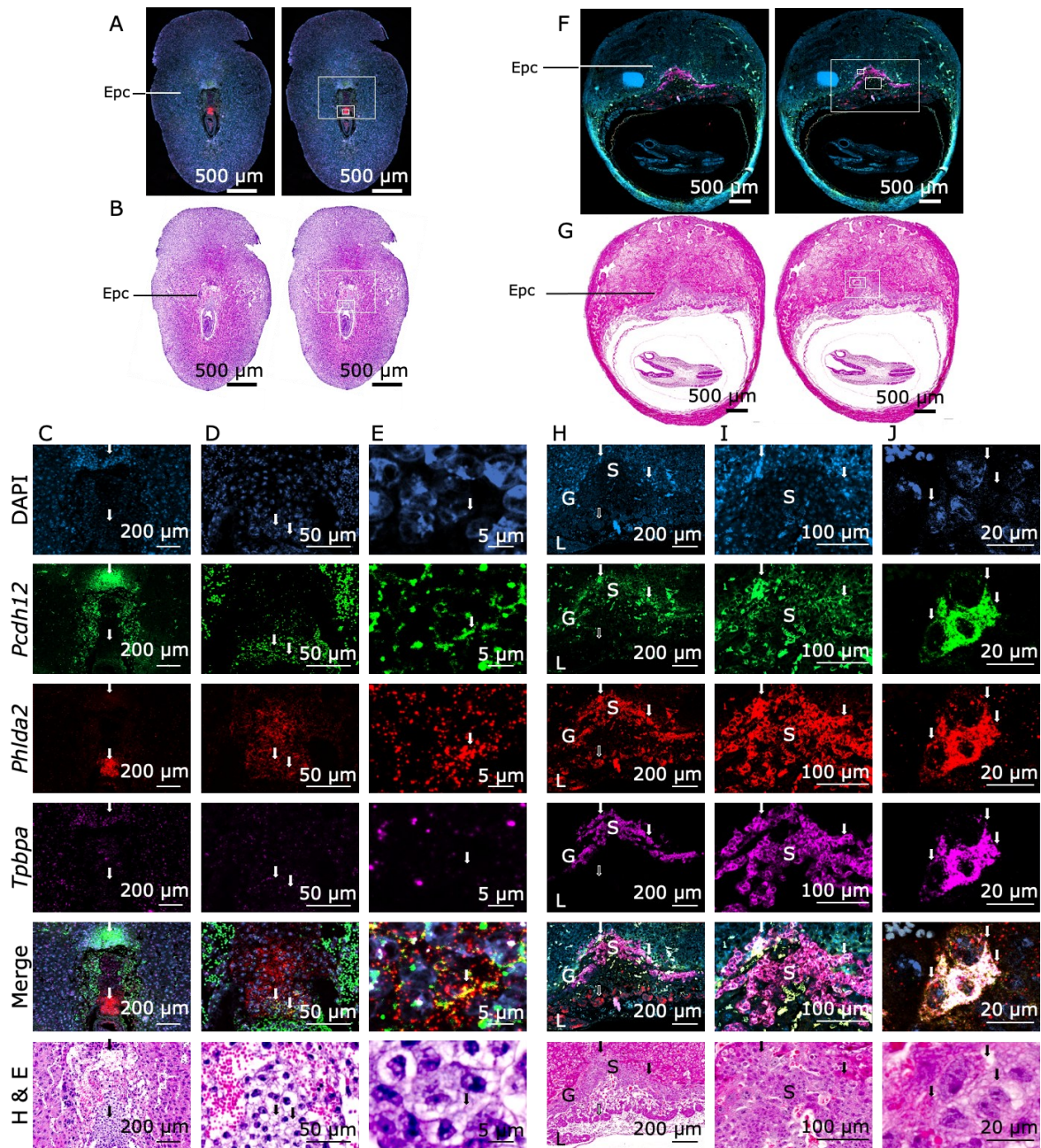


Figure 45: Multi-plex detection identifies co-localisation of *Pcdh12*, *Phlda2* and *Tpbpa* expression.

A) Whole E7.5 WT mouse embryo/placental pod after *in situ* amplification of *Pcdh12* (Green), *Phlda2* (Red) and *Tpbpa* (Pink). Co-localisation of all three (White). *Pcdh12* and *Phlda2* co-localisation (Yellow). Nuclei labelled with DAPI (Blue). Ectoplacental cone (Epc). (20X). **B)** H & E stained (pink and purple bright field) section of whole E7.5 mouse embryo/placental pod (20X). **C)** Region of interest of E7.5 ectoplacental cone with co-localisation indicated with white arrows. (20X). **D)** Higher resolution of region of interest of E7.5 ectoplacental cone with co-localisation indicated with white arrows. (40X). **E)** Higher resolution of region of interest of E7.5 ectoplacental cone with co-localisation indicated with white arrows (63X). **F)** Whole E9.5 WT mouse embryo/placental pod after *in situ*

amplification of *Pcdh12* (Green), *Phlda2* (Red) and *Tpbpa* (Pink). Co-localisation of all three (White). *Pcdh12* and *Phlda2* co-localisation (Yellow). Nuclei labelled with DAPI (Blue) (20X). **G**) H & E stained section of whole E9.5 mouse embryo/placental pod (20X). **H**) Region of interest of E9.5 ectoplacental cone with co-localisation indicated with white arrows. L=Developing labyrinth, S= Developing spongiotrophoblast, G= Giant cell layer (20X). **I**) Higher resolution of region of interest of E9.5 ectoplacental cone with co-localisation indicated with white arrows. (40X). **J**) Higher resolution of region of interest of E9.5 ectoplacental cone with co-localisation indicated with white arrows (63X).

At E7.5, *Phlda2* was co-localised with the glycogen cell marker *Pcdh12* along with populations of cells that were just expressing *Phlda2* (Figure 45, D and E). The *Tpbpa* staining of the developing spongiotrophoblast doesn't define a key structure (Figure 45, D and E). At E9.5, *Phlda2* was expressed in populations on its own in the developing labyrinth. There was a large co-expressing population of *Phlda2* and *Tpbpa* in the spongiotrophoblast cells along with some cells which expressed all three markers (Figure 45, H-J).

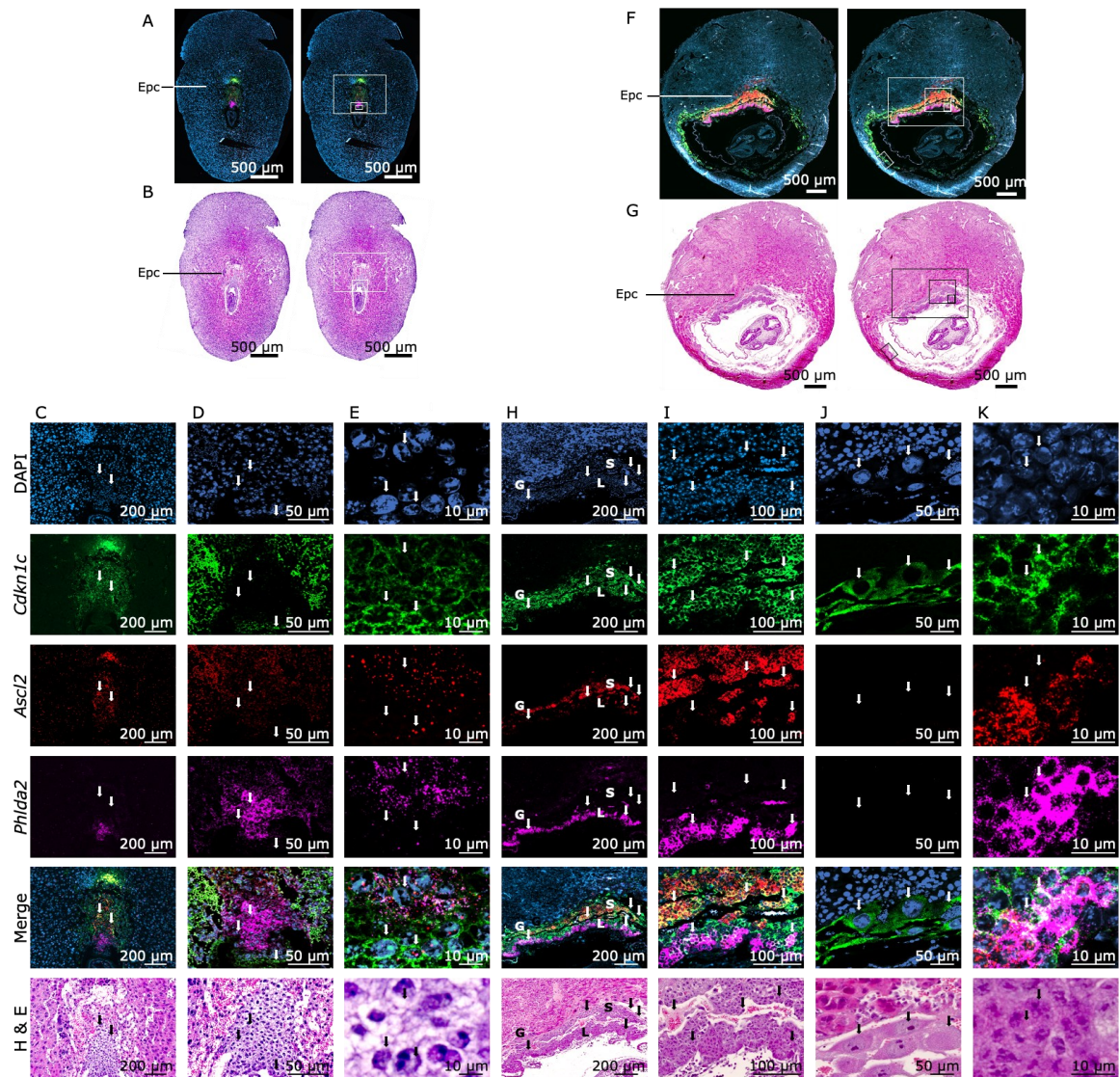


Figure 46: Multi-plex detection identifies co-localisation of *Ascl2*, *Phlda2* and *Cdkn1c* expression.

A) Whole E7.5 WT mouse embryo/placental pod after *in situ* amplification of *Phlda2* (Pink), *Cdkn1c* (Green) and *Ascl2* (Red). Co-localisation of all three (White). *Cdkn1c* and *Ascl2* co-localisation (Yellow). Nuclei labelled with DAPI (Blue). Ectoplacental cone (Epc). (20X). **B)** H & E stained (pink and purple bright field) section of whole E7.5 mouse embryo/placental pod (20X). **C)** Region of interest of E7.5 ectoplacental cone with co-localisation indicated with white arrows. (20X). **D)** Higher resolution of region of interest with co-localisation indicated with white arrows (40X). **E)** Higher resolution of ectoplacental cone with co-localisation indicated with white arrows (63X). **F)** Whole E9.5 WT mouse embryo/placental pod after *in situ* amplification of *Phlda2* (Pink), *Cdkn1c* (Green) and *Ascl2* (Red). Co-localisation (White). *Cdkn1c* and *Ascl2* co-localisation (Yellow). Nuclei labelled with DAPI (Blue) (20X). **G)** H & E stained section of whole E9.5 mouse embryo/placental pod (20X). **H)** Region of interest of E9.5 ectoplacental cone with co-localisation indicated with white arrows. (20X). L=Developing labyrinth, S= Developing spongiotrophoblast, G= Giant cell

layer. **I)** Higher resolution of spongiotrophoblast with co-localisation indicated with white arrows (40X). **J)** Trophoblast giant cell layer with *Cdkn1c* expression indicated with white arrows (63X). **K)** Higher resolution of spongiotrophoblast with co-localisation indicated with white arrows (63X).

At E7.5, *Phlda2* and *Cdkn1c* are expressed in distinct cell populations in the Epc. *Ascl2* expression was low throughout the Epc and was co-localised with *Cdkn1c* and *Phlda2* in separate populations (Figure 46, C-E). At E9.5, *Cdkn1c* is expressed solely in the P-TG cells forming the interface between the junctional zone and maternal decidua (Figure 46, J). *Cdkn1c* and *Ascl2* are co-expressed in the developing spongiotrophoblast where *Phlda2* is expressed more predominantly in the developing labyrinth. *Ascl2* is more closely co-expressed with *Phlda2*, although there are some populations of *Ascl2* and *Cdkn1c* co-expression (Figure 46, I). Finally, there is a small population of cells which express all three in the developing labyrinth (Figure 46, K).

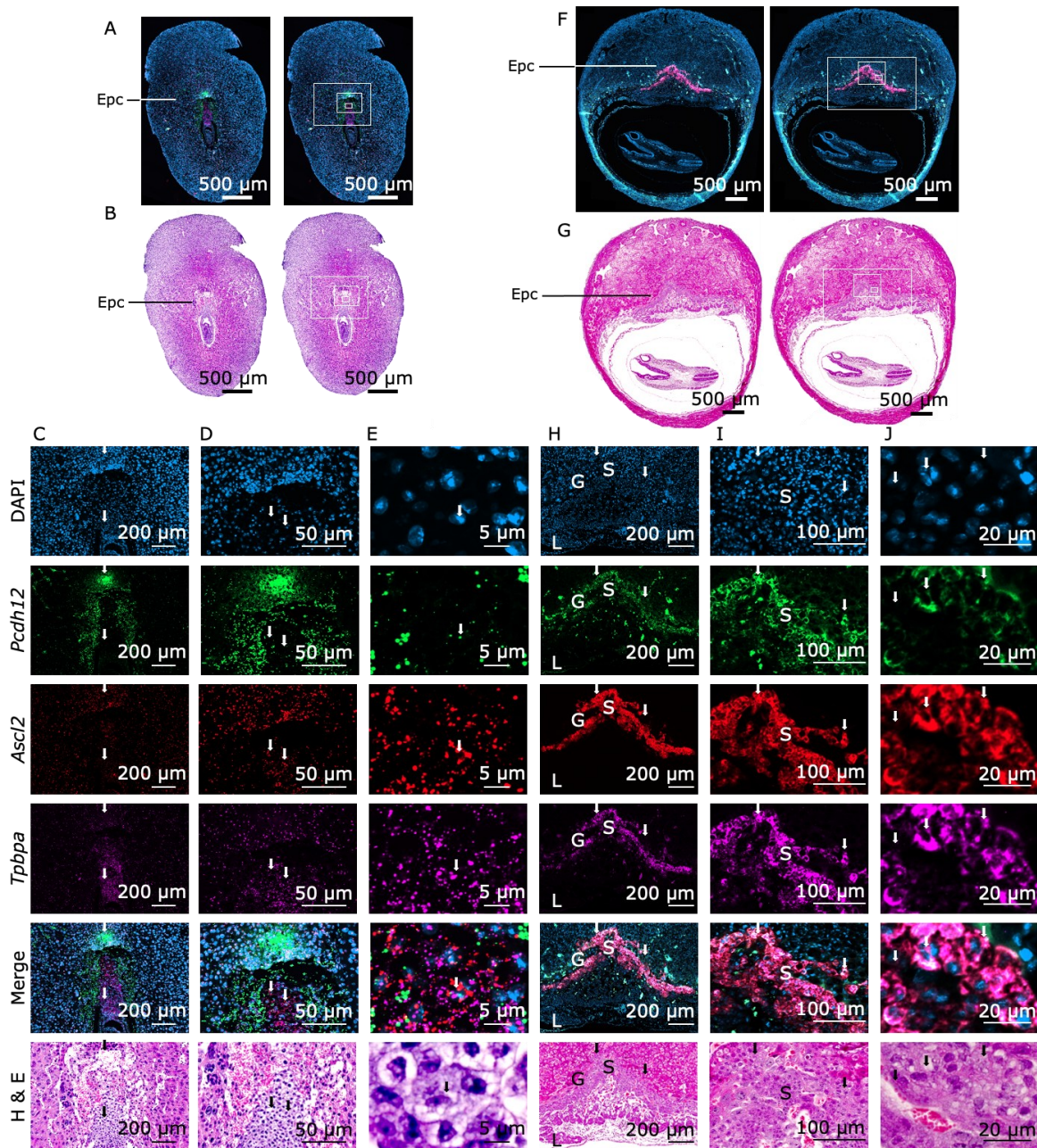


Figure 47: Multi-plex detection identifies co-localisation of *Pcdh12*, *Ascl2*, and *Tpbpa* expression.

A) Whole E7.5 WT mouse embryo/placental pod after *in situ* amplification of *Tpbpa* (Pink), *Pcdh12* (Green) and *Ascl2* (Red). Co-localisation of all three (White). Nuclei labelled with DAPI (Blue). Ectoplacental cone (Epc). (20X). **B)** H & E stained (pink and purple bright field) section of whole E7.5 mouse embryo/placental pod (20X). **C)** Region of interest of E7.5 ectoplacental cone with co-localisation indicated with white arrows. (20X). **D)** Higher resolution of region of interest with co-localisation indicated with white arrows (40X). **E)** Higher resolution of ectoplacental cone with co-localisation indicated with white arrows (63X). **F)** Whole E9.5 WT mouse embryo/placental pod after *in situ* amplification of *Tpbpa* (Pink), *Pcdh12* (Green) and *Ascl2* (Red). Co-localisation (White).

Nuclei labelled with DAPI (Blue) (20X). **G**) H & E stained section of whole E9.5 mouse embryo/placental pod (20X). **H**) Region of interest of E9.5 ectoplacental cone with co-localisation indicated with white arrows. (20X). L=Developing labyrinth, S= Developing spongiotrophoblast, G= Giant cell layer. **I**) Higher resolution of spongiotrophoblast with co-localisation indicated with white arrows (40X). **J**) Higher resolution of spongiotrophoblast with co-localisation indicated with white arrows (63X).

At E7.5, *Ascl2* expression was low and co-expressed with *Tpbpa* than with *Pcdh12* which also had low expression (Figure 47, D and E). At E9.5, *Tpbpa* and *Ascl2* show a high degree of co-expression throughout the developing spongiotrophoblast. *Ascl2* is also co-expressed with *Pcdh12* but to a lesser extent (Figure 47, H and I). There are also small populations of cells which express all three markers (Figure 47, H-J).

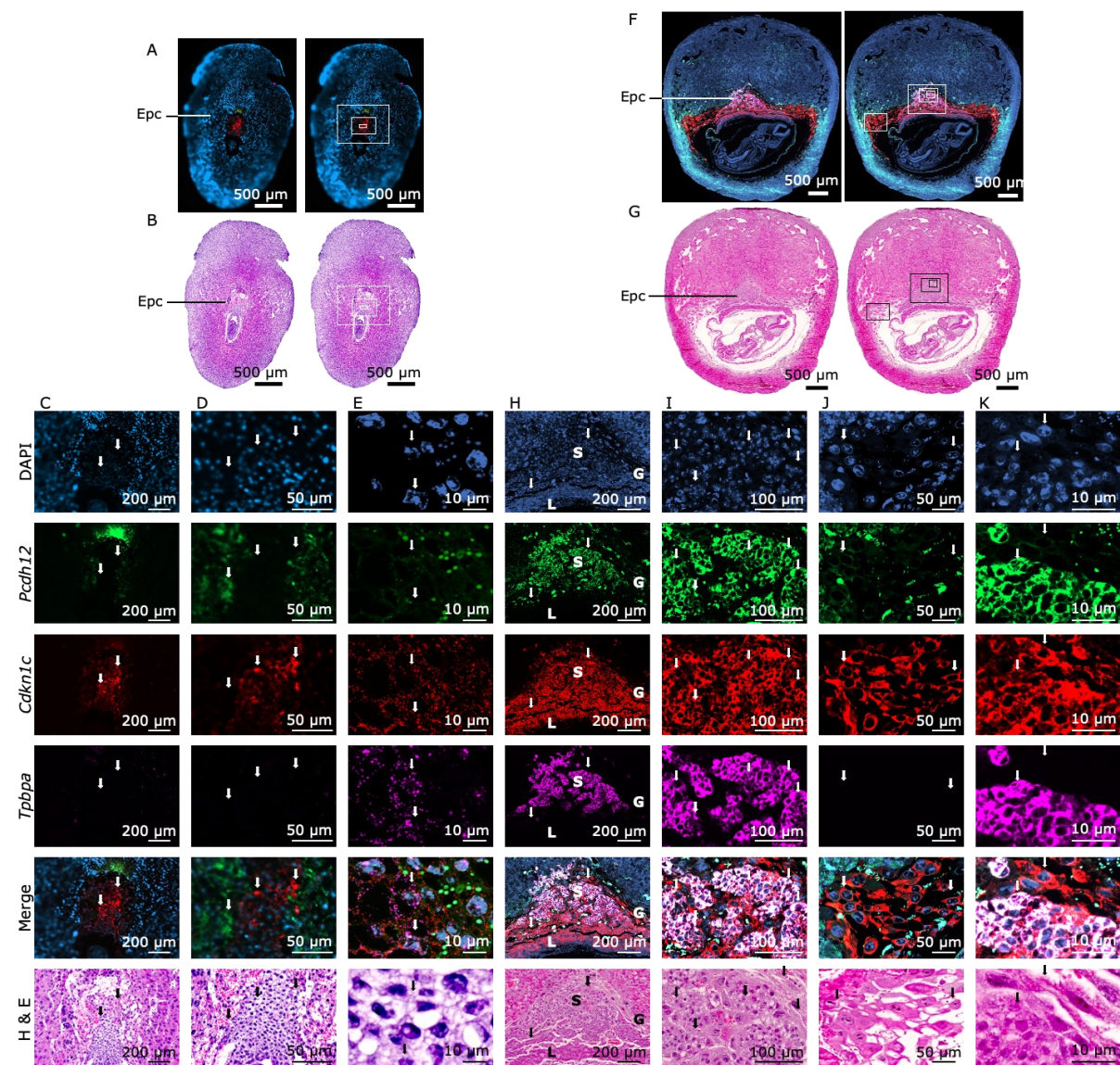


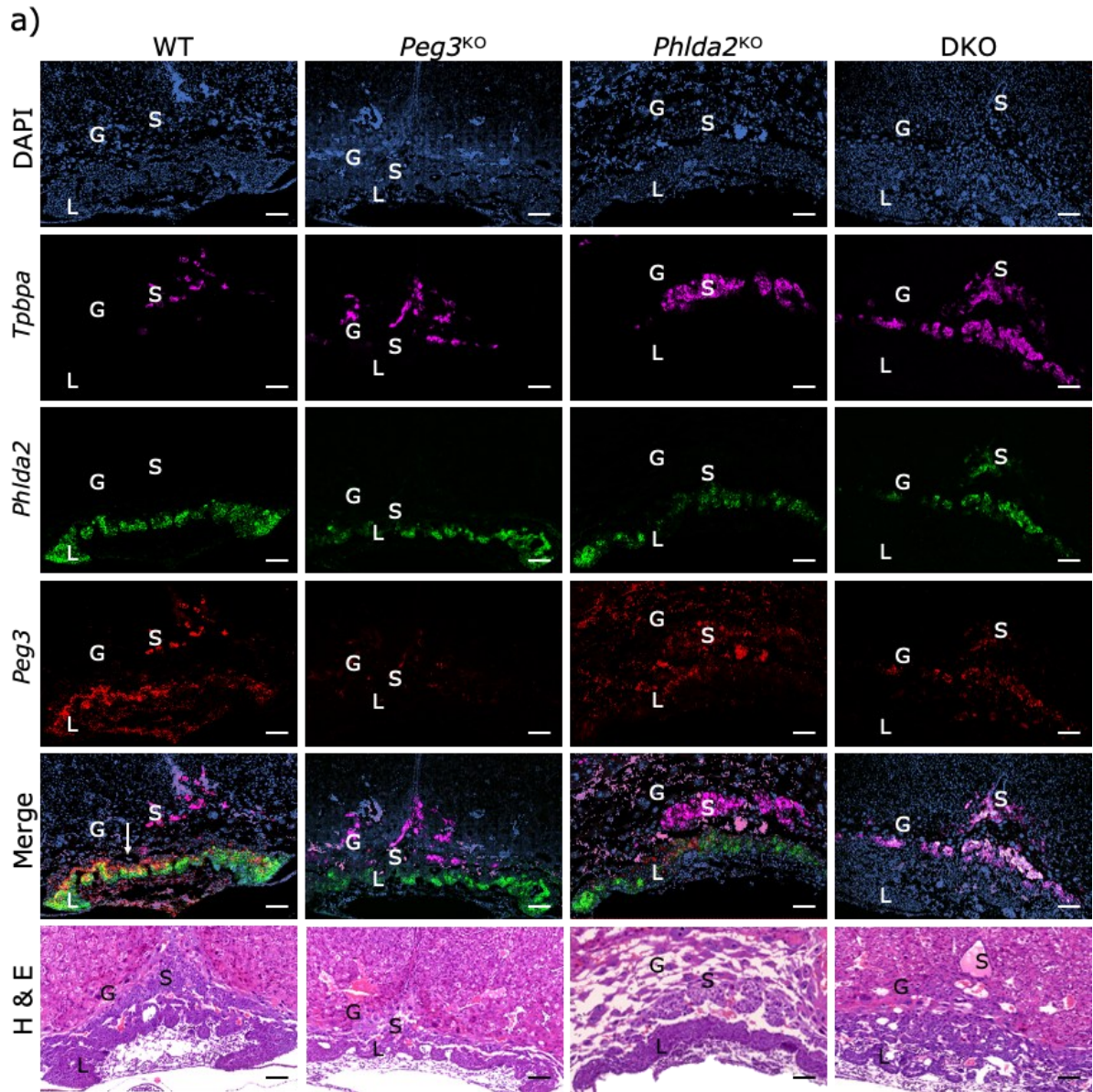
Figure 48: Multi-plex detection identifies co-localisation of *Tpbpa*, *Cdkn1c* and *Pcdh12* expression.

A) Whole E7.5 WT mouse embryo/placental pod after *in situ* amplification of *Tpbpa* (Pink), *Pcdh12* (Green) and *Cdkn1c* (Red). Co-localisation of all three (White). Nuclei labelled with DAPI (Blue). Ectoplacental cone (Epc). (20X). **B)** H & E stained (pink and purple bright field) section of whole E7.5 mouse embryo/placental pod (20X). **C)** Region of interest of E7.5 ectoplacental cone with co-localisation indicated with white arrows. (20X). **D)** Higher resolution of region of interest with co-localisation indicated with white arrows (40X). **E)** Higher resolution of ectoplacental cone with co-localisation indicated with white arrows (63X). **F)** Whole E9.5 WT mouse embryo after *in situ* amplification of *Tpbpa* (Pink), *Pcdh12* (Green) and *Cdkn1c* (Red). Co-localisation (White). Nuclei labelled with DAPI (Blue) (20X). **G)** H & E stained section of whole E9.5 mouse embryo/placental pod (20X). **H)** Region of interest of E9.5 ectoplacental cone with co-localisation indicated with white arrows. (20X). L=Developing labyrinth, S= Developing spongiotrophoblast, G= Giant cell layer. **I)** Higher resolution of spongiotrophoblast with co-localisation indicated with white arrows (40X). **J)** Trophoblast giant cell layer with *Cdkn1c* expression indicated with white arrows (63X). **K)** Higher resolution of spongiotrophoblast with co-localisation indicated with white arrows (63X).

At E7.5, *Cdkn1c* was expressed in the Epc and was co-localised with *Tpbpa* which also had low expression (Figure 48, C-E). At E9.5, *Cdkn1c* was expressed across the developing spongiotrophoblast and developing labyrinth (Figure 48, C-I). *Cdkn1c* was also solely expressed in the P-TG cells (Figure 48, J). There was a large population of cells which expressed all three targets in the developing spongiotrophoblast along with populations of cells just expressing *Cdkn1c* (Figure 48, K).

4.3.2 RNAscope on E9.5 samples of each genotype do demonstrate expression of knockout targets

Two litters per genotype were stained using RNAscope for *Peg3*, *Phlda2* and *Tpbpa* using the protocol 2.3 and were imaged by confocal to determine the expression of the knockout targets. Representative images of each genotype are presented in Figure 49.



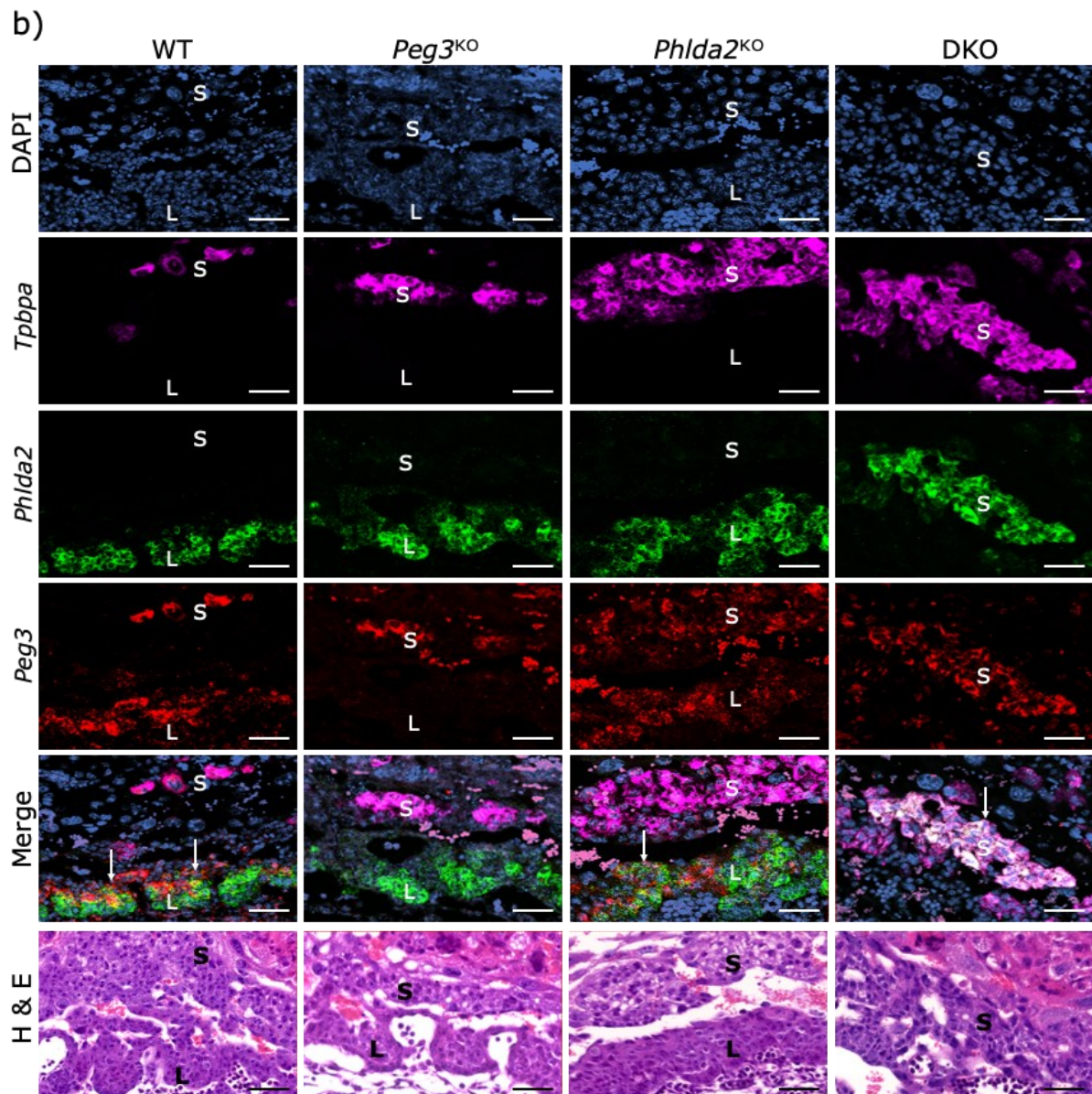


Figure 49: Representative images of multi-plex detection identifying co-localisation of RNA expression of *Peg3*, *Phlda2* and *Tpbpa*.

Peg3 (Red), *Phlda2* (Green) and *Tpbpa* (Pink). Co-localisation (White). Co-localisation indicated with white arrows. Nuclei labelled with DAPI (Blue). H & E stained (pink and purple bright field). L=Developing labyrinth, S= Developing spongiotrophoblast, G= Giant cell layer. All images taken using tile function of confocal microscope under oil immersion (63X). **a)** Scale bar 100µm. **b)** Scale bar 50µm.

All genotypes expressed their knockout targets to some degree (Figure 49). The *Peg3*^{KO} placenta expressed *Peg3* in the developing spongiotrophoblast and was co-localised with *Tpbpa*, but not in the labyrinth where the WT placenta expressed *Peg3* in both regions. The *Peg3*^{KO} placenta expressed *Phlda2* in a similar amount and pattern as the

WT placenta. The *Phlda2*^{KO} placenta expressed *Phlda2* in a similar degree and pattern to WT. The *Phlda2*^{KO} placenta expressed *Peg3* in a more diffuse pattern than WT, some of which was co-localised with *Tpbpa*. The DKO placenta expressed both *Peg3* and *Phlda2* to similar degrees to WT and was co-localised with *Tpbpa*.

4.3.3 P-TG cell counting of E9.5 samples to assess phenotype establishment timeline

Of the 153 embryo placental pods sectioned and stained 94 were deemed appropriate to count. The counting protocol 2.5 was used.

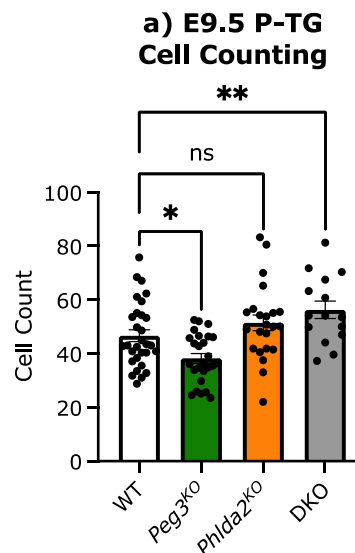


Figure 50: E9.5 P-TG cell counts for WT, *Peg3*^{KO}, *Phlda2*^{KO} and DKO.

a) P-TG cell numbers were decreased by 18% ($P=.039$) in *Peg3*^{KO} samples compared to WT and increased in DKO by 21% ($P=.007$) compared to WT. WT ($n = 30$), *Peg3*^{KO} ($n = 26$), *Phlda2*^{KO} ($n = 23$) and DKO ($n = 15$). Data from 19 litters, litter size between 5-11 (average $9 \pm .14$). Error bars represent standard error of the mean (SEM). Statistical significance calculated using a two-way ANCOVA with Šidák correction and litter size as covariate. ^{ns} $P > .05$, $*P < .05$, and $**P < .01$ $***P < .001$ $****P < .0001$ (Appendix 17).

A significant decrease in P-TG cells was seen in *Peg3*^{KO} samples. A non-significant increase in P-TG cells was seen in *Phlda2*^{KO} and a significant increase was seen in DKO samples. DKO did not correct to WT numbers. Statistics suggest that litter size has a significant influence over this assay.

4.3.4 E16.5 Placental and foetal impacts from KO models

Placental and foetal weights were taken upon dissection of E16.5 mixed WT, *Peg3*^{KO}, *Phlda2*^{KO} and DKO litters.

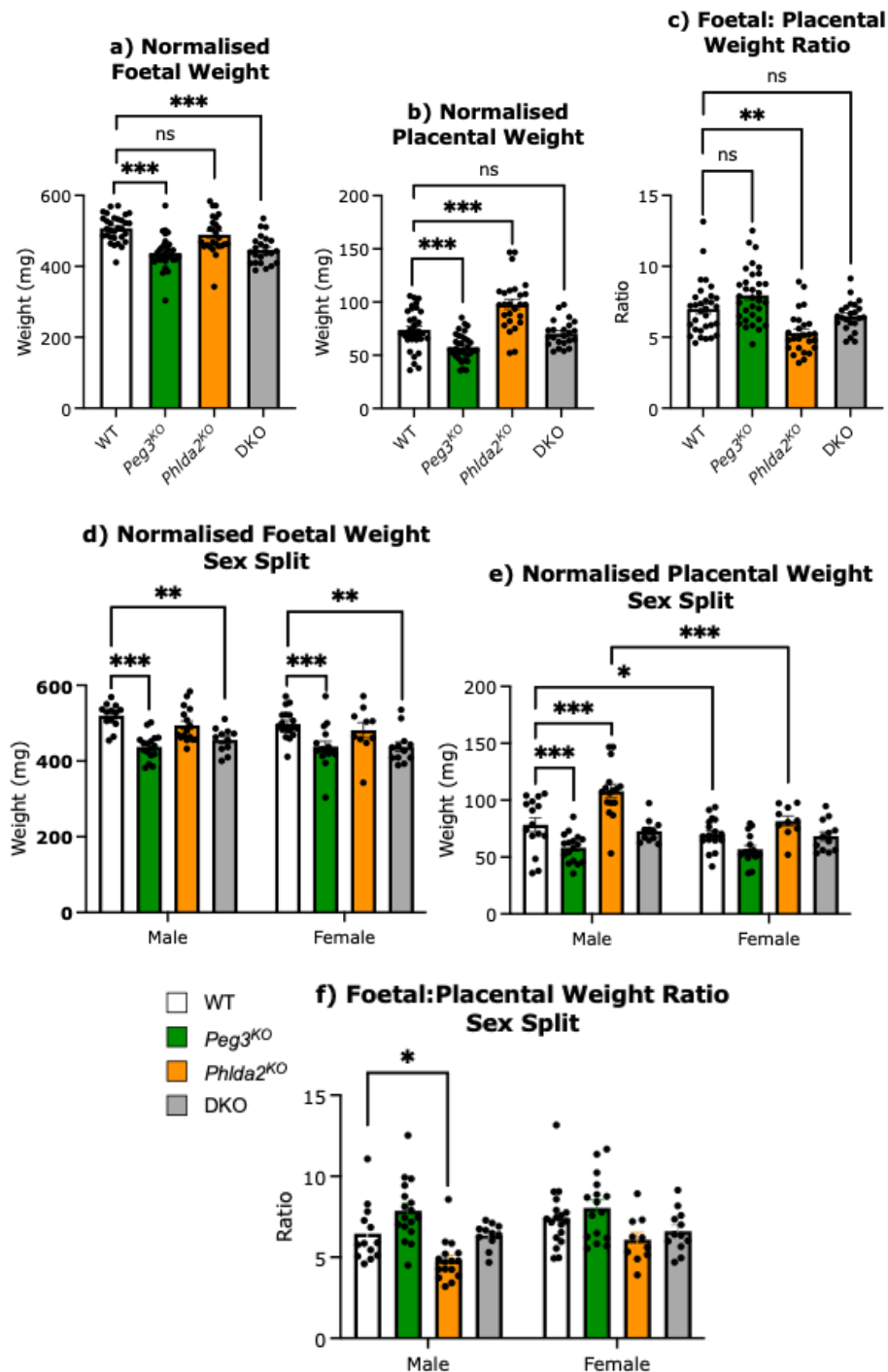


Figure 51: Foetal and placental weight data for WT, *Peg3*^{KO}, *Phlda2*^{KO} and DKO at E16.5.

a) *Peg3*^{KO} and DKO foetal weight was reduced by 14% ($P < .001$) and 12% ($P < .001$) respectively compared to WT. **b)** *Peg3*^{KO} placental weight was reduced by 22% compared to WT ($P < .001$). *Phlda2*^{KO} was increased by 32% compared to WT ($P < .001$). **c)** *Phlda2*^{KO} ratio was reduced by 24%

compared to WT ($P=.006$). **d)** *Peg3^{KO}* fetuses were 16% ($P<.001$) and 12% ($P<.001$) lighter than WT fetuses in male and females. DKO fetuses were 12% lighter than WT in both males ($P=.008$) and females ($P=.003$). **e)** Male *Peg3^{KO}* placenta weighed 26% less than male WT placenta ($P<.001$). Male *Phlda2^{KO}* placenta weighed 38% more than male WT placenta ($P<.001$). WT female placentas were 11% lighter than WT male placentas. *Phlda2^{KO}* female placentas are 24% lighter than *Phlda2^{KO}* males. **f)** The *Phlda2^{KO}* ratio decreased by 25% ($P=.028$) for males compared to WT. WT ($n = 30$), *Peg3^{KO}* ($n = 33$), *Phlda2^{KO}* ($n = 27$), DKO ($n = 23$). WT male ($n = 13$), *Peg3^{KO}* male ($n = 17$), *Phlda2^{KO}* male ($n = 16$), DKO male ($n = 11$), WT female ($n = 18$), *Peg3^{KO}* female ($n = 16$), *Phlda2^{KO}* ($n = 10$), DKO ($n = 12$). Data from 16 litters, litter size between 5-10 (Average $7\pm.13$). Error bars represent \pm SEM. Statistical significance calculated using a two-way ANCOVA with Šidák correction and litter size as covariate. ^{NS} $P>.05$, * $P<.05$, and ** $P<.01$ *** $P<.001$ **** $P<.0001$ (Appendix 18).

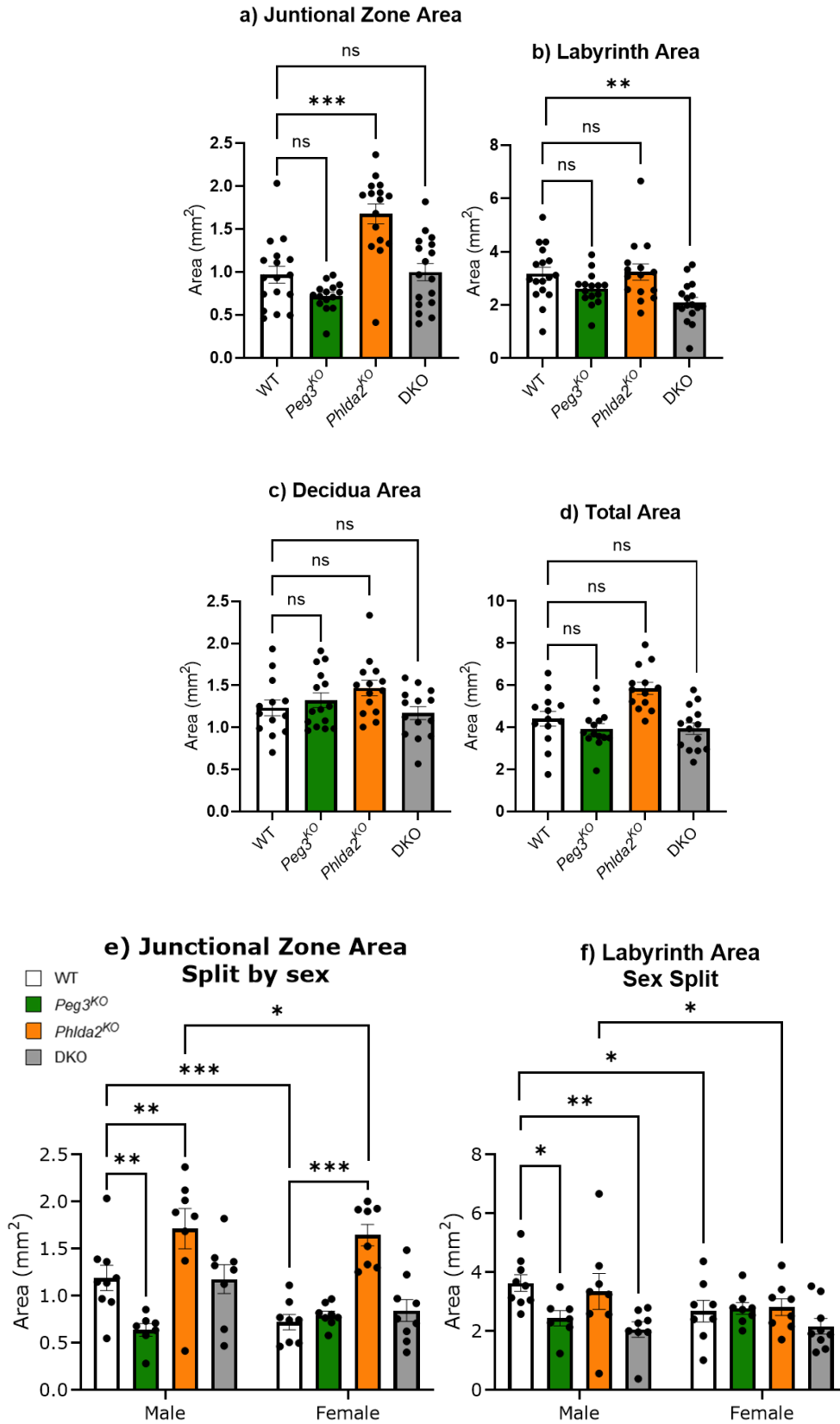
Placental and foetal weight were reduced in all *Peg3^{KO}* pooled and sex split groups, with only the female *Peg3^{KO}* placentas not reaching significance. This increased the ratio of foetal to placental weight compared to WT for all pooled and sex split groups but not significantly. The foetal weight of *Phlda2^{KO}* groups were not affected by the knockout, where the placental weight was increased compared to WT in all groups except females. This also reduced the placental to foetal weight ratio in those groups. The DKO group showed a significant reduction to WT in foetal weight in all groups but no change in placental weight. This did not significantly alter the placental to foetal weight ratio for this group. Sex differences were seen for *Peg3^{KO}* and *Phlda2^{KO}* groups for placental weight compared to WT with both only affecting the male placental weight.

4.3.5 RNAscope automated counting program demonstrates more significant impact on male KO placentas

A total of 65 E16.5 placentas samples from mixed WT, *Peg3^{KO}*, *Phlda2^{KO}* and DKO litters were stained for *Pr13b1* using the RNAscope method detailed in section 2.3.3. These were then processed using Zen software using area measurements and the automatic counting method as described in methods section 2.6.

4.3.5.1 Area measurements: Greater structural alterations in male placentas in KO models compared to females

Using Zen software the areas of each placental region were measured. The impact on litter size of the data was also investigated using an ANCOVA statistical analysis with litter size as a covariate.



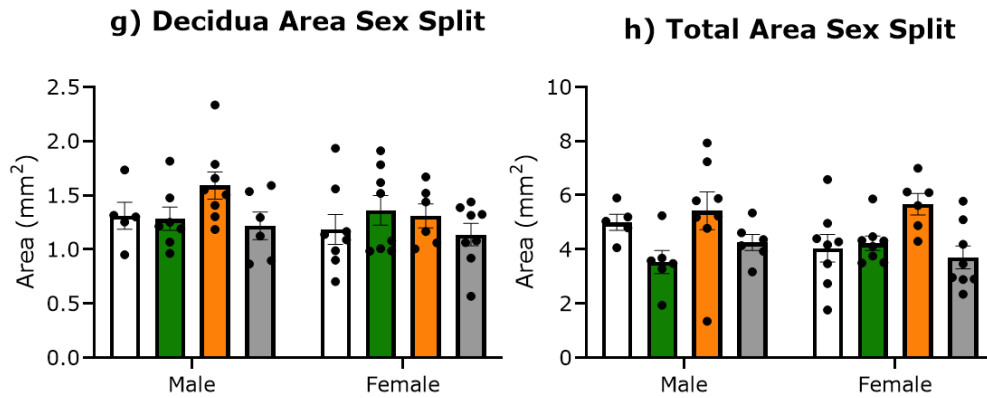


Figure 52: Area of placental subsections for WT, *Peg3*^{KO}, *Phlda2*^{KO} and DKO.

a) Junctional zone area was increased by 73% in *Phlda2*^{KO} samples compare to WT ($P < .001$). **b)** Labyrinth area was decreased by 35% in DKO samples compared to WT. **c)** There was no significant difference seen between any groups in decidua area. **d)** There was no significant difference seen between any groups in total area. **e)** *Peg3*^{KO} junctional zones were 46% ($P = .002$) smaller than WT in males and 10% ($P = .947$) larger than WT in females. *Phlda2*^{KO} junctional zones were 44% ($P = .002$) and 129% ($P < .001$) larger than WT in males and females respectively. Female WT junctional zones were 40% smaller than male WT junctional zones ($P < .001$). Female *Phlda2*^{KO} junctional zones were 4% smaller than male *Phlda2*^{KO} junctional zones ($P = .015$). **f)** *Peg3*^{KO} labyrinth area was 33% ($P = .031$) smaller in males than WT. DKO labyrinth measured 44% ($P = .004$) smaller than WT in males. Female WT labyrinth area was 26% smaller than male WT labyrinth area ($P = .015$) and female *Phlda2*^{KO} labyrinth area were 16% smaller than *Phlda2*^{KO} males ($P = .028$). **g)** There was no significant difference seen between any groups in decidua area. **h)** There was no significant difference seen between any groups in total area. WT ($n = 17$), *Peg3*^{KO} ($n = 15$), *Phlda2*^{KO} ($n = 16$) and DKO ($n = 17$). WT male ($n = 9$), *Peg3*^{KO} male ($n = 7$), *Phlda2*^{KO} male ($n = 8$), DKO male ($n = 8$), WT female ($n = 8$), *Peg3*^{KO} female ($n = 8$), *Phlda2*^{KO} female ($n = 8$), DKO ($n = 9$). Data from 16 litters, litter size between 5-10 (average $8 \pm .18$). Error bars represent \pm SEM. Statistical significance calculated using a two-way ANCOVA with Šidák correction and litter size as covariate. ^{ns} $P > .05$, * $P < .05$, and ** $P < .01$ *** $P < .001$ **** $P < .0001$ (Appendix 19).

When the sexes were pooled the junctional zone area was increased by 73% in *Phlda2*^{KO} samples compare to WT ($P < .001$) but was not changed in any other genotype. When the data was split by sex, *Peg3*^{KO} junctional zones were 46% ($P = .002$) smaller than WT in males and slightly larger (10%, ns) than WT in females. *Phlda2*^{KO} junctional zones were 44% ($P = .002$) and 129% ($P < .001$) larger than WT in males and females respectively. Female WT junctional zones were 40% smaller than male

WT junctional zones ($P < .001$) and female *Phlda2^{KO}* junctional zones were 4% smaller than male *Phlda2^{KO}* junctional zones ($P = .015$).

Labyrinth area was decreased by 35% in DKO samples compared to WT when the sexes were pooled. When the data was split by sex, *Peg3^{KO}* labyrinth area and DKO labyrinth area were 33% ($P = .031$) and 44% ($P = .004$) smaller in males than male WT. Genotype did not alter female labyrinth area when comparing to other female genotypes. When comparing across the sexes, female WT labyrinth area was 26% smaller than male WT labyrinth area ($P = .015$) and female *Phlda2^{KO}* labyrinth area were 16% smaller than *Phlda2^{KO}* males. There was no significant difference seen between any groups in decidua area or total area.

The ratios between junctional zone area and labyrinth area were compared.

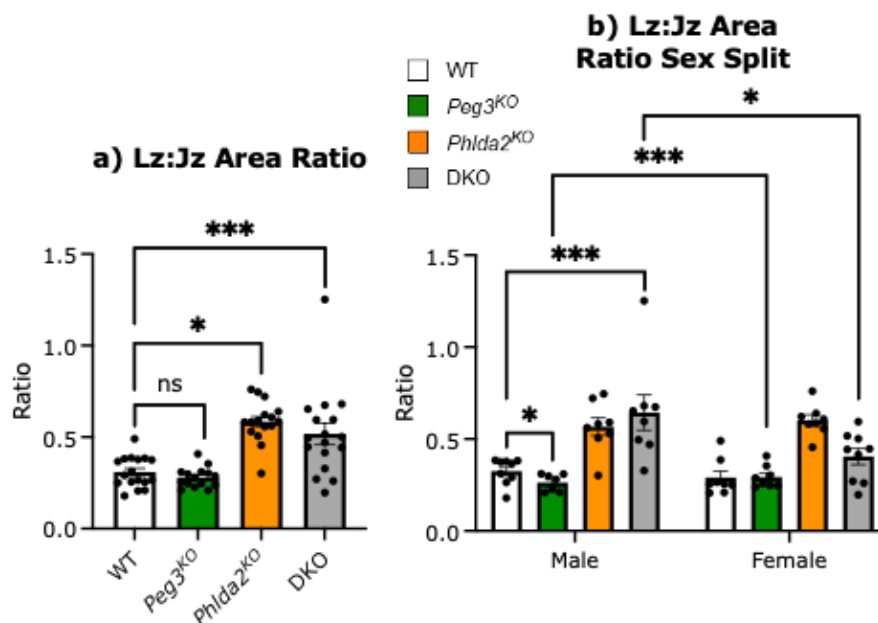


Figure 53: Region ratios for WT, *Peg3^{KO}*, *Phlda2^{KO}* and DKO placentas.

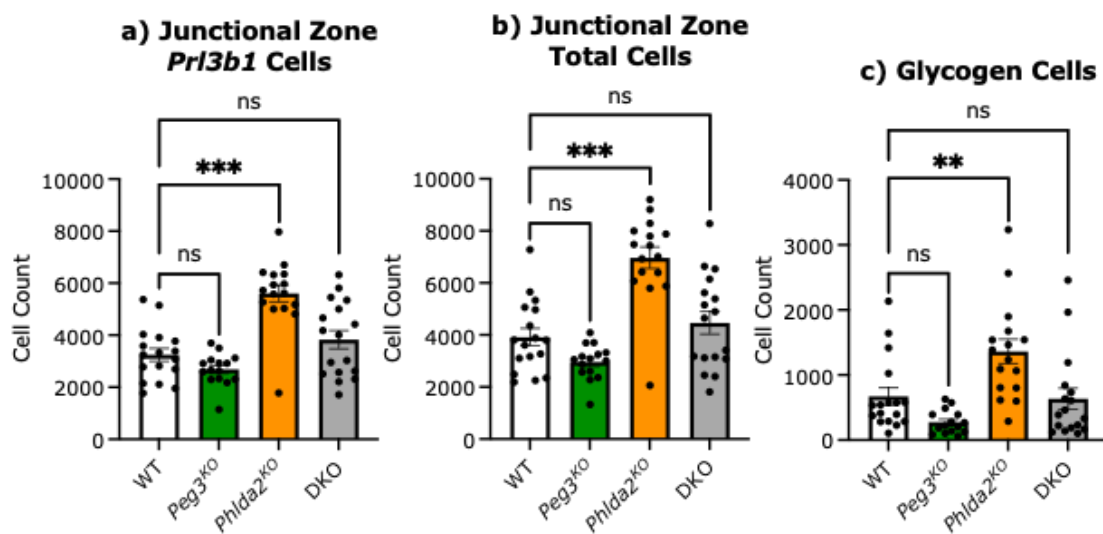
a) The ratio between junctional zone area and labyrinth area (Lz:Jz) increased in *Phlda2^{KO}* and DKO samples by 89% ($P = .017$) and 68% ($P < .001$) respectively. **b)** The Lz:Jz ratio decreased in *Peg3^{KO}* male samples by 19% ($P = .011$) and increased in DKO male samples by 14% ($P < .001$). *Peg3^{KO}* female samples had an 11% ($P < .001$) increased Lz:Jz ratio compared to *Peg3^{KO}* male samples. DKO females had a 37% ($P = .018$) decrease in their ratio compared to DKO male samples. WT ($n = 17$), *Peg3^{KO}* ($n = 15$), *Phlda2^{KO}* ($n = 16$) and DKO ($n = 17$). WT male ($n = 9$), *Peg3^{KO}* male ($n = 7$), *Phlda2^{KO}* male ($n = 8$), DKO male ($n = 8$), WT female ($n = 8$), *Peg3^{KO}* female ($n = 8$), *Phlda2^{KO}* female ($n = 8$), DKO ($n = 9$). Data from 16 litters, litter size between 5-10 (average $8 \pm .18$). Error

bars represent \pm SEM. Statistical significance calculated using a two-way ANCOVA with Šidák correction and litter size as covariate. $^{ns}P > .05$, $^{*}P < .05$, and $^{**}P < .01$ $^{***}P < .001$ $^{****}P < .0001$ (Appendix 20).

When the sexes were pooled, the ratio between junctional zone area and labyrinth area (Lz:Jz) increased in *Phlda2*^{KO} and DKO samples by 89% ($P = .017$) and 68% ($P < .001$) respectively. When split by sex, the Lz:Jz ratio decreased in *Peg3*^{KO} male samples by 19% ($P = .011$) and increased in DKO male samples by 14% ($P < .001$) but was not changed across female genotypes. Comparing across the sex showed, *Peg3*^{KO} female samples had an 11% ($P < .001$) increased Lz:Jz ratio compared to *Peg3*^{KO} male samples and that DKO females had a 37% ($P = .018$) decrease in their ratio compared to DKO male samples.

4.3.5.2 Impacts of KOs on glycogen and *Pr13b1* expressing cells in the junctional zone

The automatic counting program detailed in the methods section 2.6 was used to count a variety of parameters including the number of cells within each region which were producing *Pr13b1* RNA at the time of dissection/fixation.



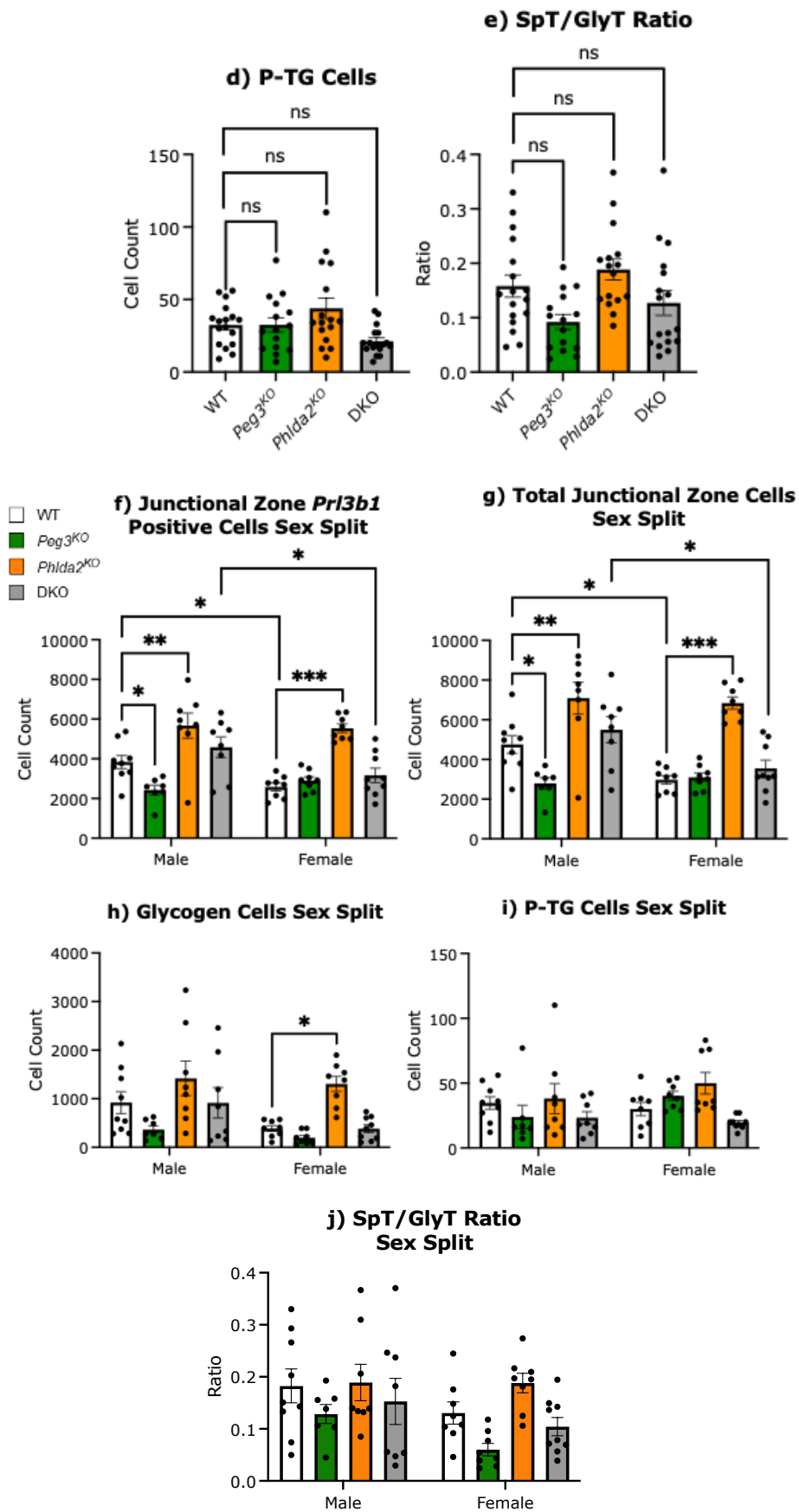


Figure 54: Junctional zone cell counting parameters for WT, *Peg3*^{KO}, *Phlda2*^{KO} and DKO.

a) *Phlda2*^{KO} junctional zones contained 73% ($P < .001$) more *Prl3b1* positive cells than WT. **b)** Total cells in the junctional zone were increased in the *Phlda2*^{KO} group by 78% ($P < .001$) compared to WT. **c)** Glycogen cells were increased by 103% ($P = .004$) in *Phlda2*^{KO} placentas compared to WT. **d)** There was no significant difference seen between any groups in numbers of P-TG cells. **e)** There was no significant difference between any groups in the ratio between glycogen and spongiotrophoblast cells (SpT/GlyT). **f)** *Peg3*^{KO} junctional zones contained 37% ($P = .011$) fewer positive cells than WT in males. *Phlda2*^{KO} junctional zones contained 48% ($P = .004$) and 115% ($P < .001$) more *Prl3b1* positive cells than WT in males and females respectively. WT female junctional zones had 38% ($P = .020$) fewer *Prl3b1* positive cells than WT males. DKO females had 31% ($P = .015$) fewer *Prl3b1* positive cells than DKO males. **g)** *Peg3*^{KO} junctional zones contained 41% ($P = .038$) fewer total cells than WT males. *Phlda2*^{KO} junctional zones contained 49% ($P = .004$) and 130% ($P < .001$) more total cells than WT in males and females respectively. Female WT junctional zones had 38% ($P = .009$) fewer total cells than male WTs. DKO females had 31% ($P = .006$) fewer total cells than DKO males. **h)** *Phlda2*^{KO} females had a 236% ($P = .011$) increase in glycogen cells compared to WT females. **i)** There were no significant differences seen between any groups in number of P-TG cells. **j)** There was no significant difference between any groups in the ratio between glycogen and spongiotrophoblast cells. WT ($n = 17$), *Peg3*^{KO} ($n = 15$), *Phlda2*^{KO} ($n = 16$) and DKO ($n = 17$). WT male ($n = 9$), *Peg3*^{KO} male ($n = 7$), *Phlda2*^{KO} male ($n = 8$), DKO male ($n = 8$), WT female ($n = 8$), *Peg3*^{KO} female ($n = 8$), *Phlda2*^{KO} female ($n = 8$), DKO ($n = 9$). Data from 16 litters, litter size between 5-10 (average $8 \pm .18$). Error bars represent \pm SEM. Statistical significance calculated using a two-way ANCOVA with Šidák correction and litter size as covariate. ^{ns} $P > .05$, * $P < .05$, and ** $P < .01$ *** $P < .001$ **** $P < .0001$ (Appendix 21).

Phlda2^{KO} junctional zones contained 73% ($P < .001$) more *Prl3b1* positive cells than WT. When split by sex, *Peg3*^{KO} junctional zones contained 37% ($P = .011$) fewer positive cells than WT in males. *Phlda2*^{KO} junctional zones contained 48% ($P = .004$) and 115% ($P < .001$) more *Prl3b1* positive cells than WT in males and females respectively. WT female junctional zones had 38% ($P = .020$) fewer *Prl3b1* positive cells than WT males and DKO females had 31% ($P = .015$) fewer *Prl3b1* positive cells than DKO males.

Total cells in the junctional zone were increased in the *Phlda2*^{KO} group by 78% ($P < .001$) compared to WT but were not significantly different in *Phlda2*^{KO} or DKO groups. When split by sex, *Peg3*^{KO} junctional zones contained 41% ($P = .038$) fewer total cells than WT males and *Phlda2*^{KO} junctional zones contained 49% ($P = .004$) and 130% ($P < .001$) more total cells than WT in males and females respectively, where DKO junctional zones were not significantly different from their WT

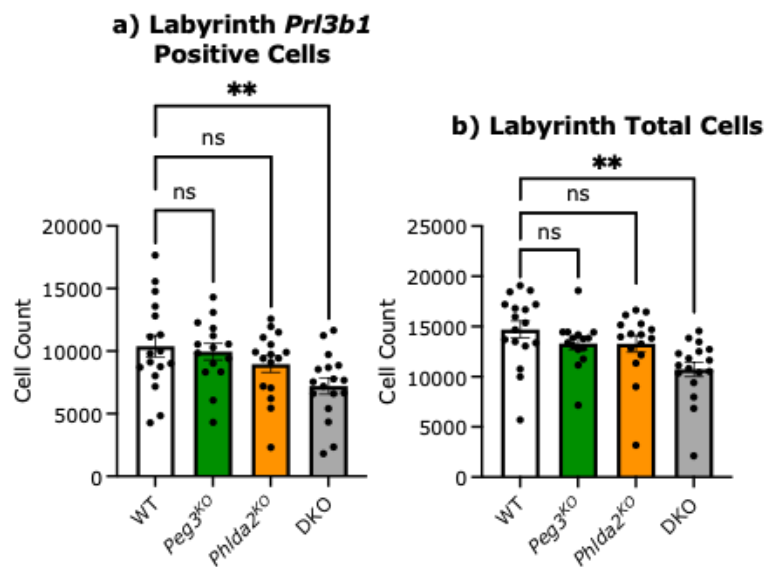
counterparts. When comparing across sexes, female WT junctional zones had 38% ($P=.009$) fewer total cells than male WTs and DKO females had 31% ($P=.006$) fewer total cells than DKO males.

Glycogen cells were increased by 103% ($P=.004$) in *Phlda2*^{KO} placentas compared to WT but were not altered in any other pooled sex group. When split by sex, *Phlda2*^{KO} females had a 236% ($P=.011$) increase in glycogen cells compared to WT females. Males also showed an increase but not significantly. No other group comparison had a significant difference.

There was no significant difference seen between any groups in numbers of P-TG cells and there was no significant difference between any groups in the ratio between glycogen and spongiotrophoblast cells (SpT/GlyT).

4.3.5.3 Labyrinth automated cell counting: Impacts on *Pr13b1* expressing cells

Cell counts were also performed on the labyrinth region.



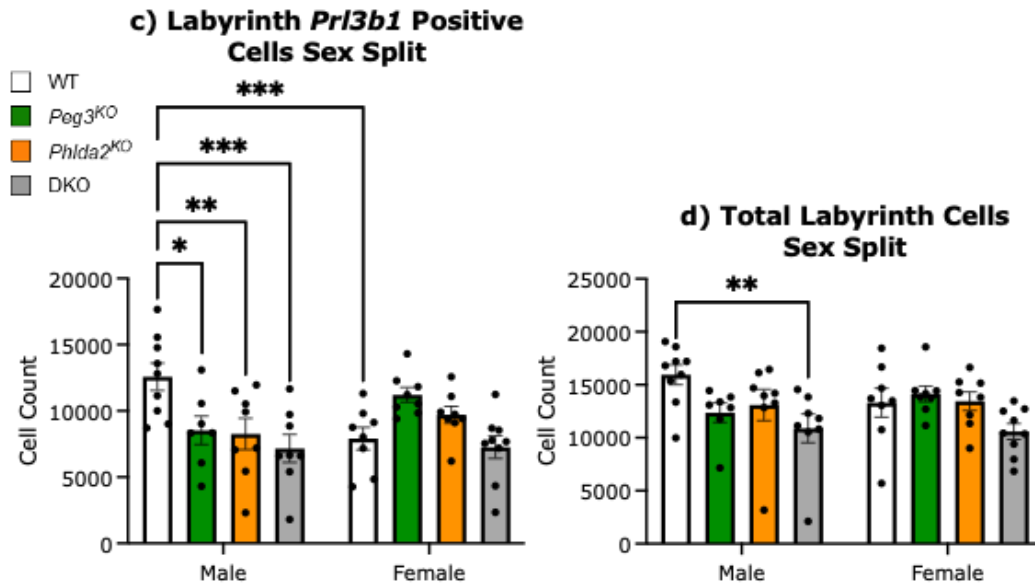


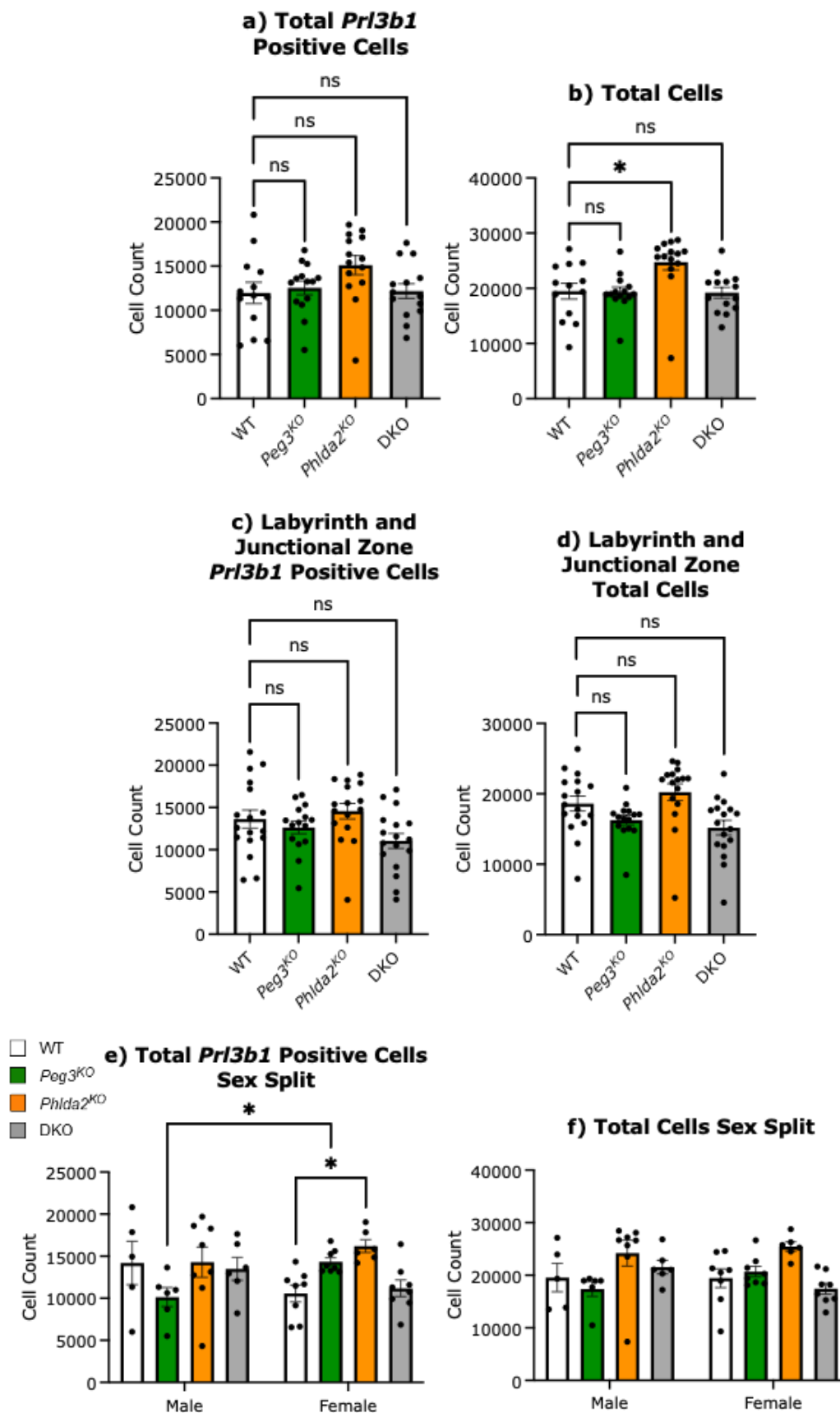
Figure 55: Cell counts within E16.5 labyrinth region for WT, *Peg3^{KO}*, *Phlda2^{KO}* and DKO.

a) DKO labyrinths contain 31% ($P=.006$) fewer *Prl3b1* positive cells than WT. **b)** DKO labyrinths contain 27% ($P=.005$) fewer total cells than WT. **c)** *Peg3^{KO}* labyrinths contained 32% ($P=.028$) fewer *Prl3b1* positive cells than WT in males. *Phlda2^{KO}* labyrinths contained 35% ($P=.007$) fewer *Prl3b1* positive cells than WT in males. DKO labyrinths had 43% ($P<.001$) fewer *Prl3b1* positive cells than WT in males. Female WT contained 37% ($P<.001$) fewer *Prl3b1* positive cells than male WT labyrinths. **d)** DKO labyrinth contained 32% ($P=.012$) fewer total cells than WT in males. WT ($n = 17$), *Peg3^{KO}* ($n = 15$), *Phlda2^{KO}* ($n = 16$) and DKO ($n = 17$). WT male ($n = 9$), *Peg3^{KO}* male ($n = 7$), *Phlda2^{KO}* male ($n = 8$), DKO male ($n = 8$), WT female ($n = 8$), *Peg3^{KO}* female ($n = 8$), *Phlda2^{KO}* female ($n = 8$), DKO ($n = 9$). Data from 16 litters, litter size between 5-10 (average $8 \pm .18$). Error bars represent \pm SEM. Statistical significance calculated using a two-way ANCOVA with Šidák correction and litter size as covariate. ^{ns} $P>.05$, $*P<.05$, and $**P<.01$ $***P<.001$ $****P<.0001$ (Appendix 22).

DKO labyrinths contain 31% ($P=.006$) fewer *Prl3b1* positive cells and 27% ($P=.005$) fewer total cells than WT when the data is pooled. When the data is split by sex, *Peg3^{KO}*, *Phlda2^{KO}* and DKO, labyrinths contained 32% ($P=.028$), 35% ($P=.007$) and 43% ($P<.001$) fewer *Prl3b1* positive cells than WT in males, respectively. Male DKO labyrinths contained 32% ($P=.012$) fewer total cells than WT in males. This data indicates that the labyrinth is not corrected within the DKO genotype. When comparing across the sexes, female WT contained 37% ($P<.001$) fewer *Prl3b1* positive cells than male WT labyrinths.

4.3.5.4 Quantification of *Pr13b1* expressing cells across the placenta

Cell counts of the entire placenta were also analysed.



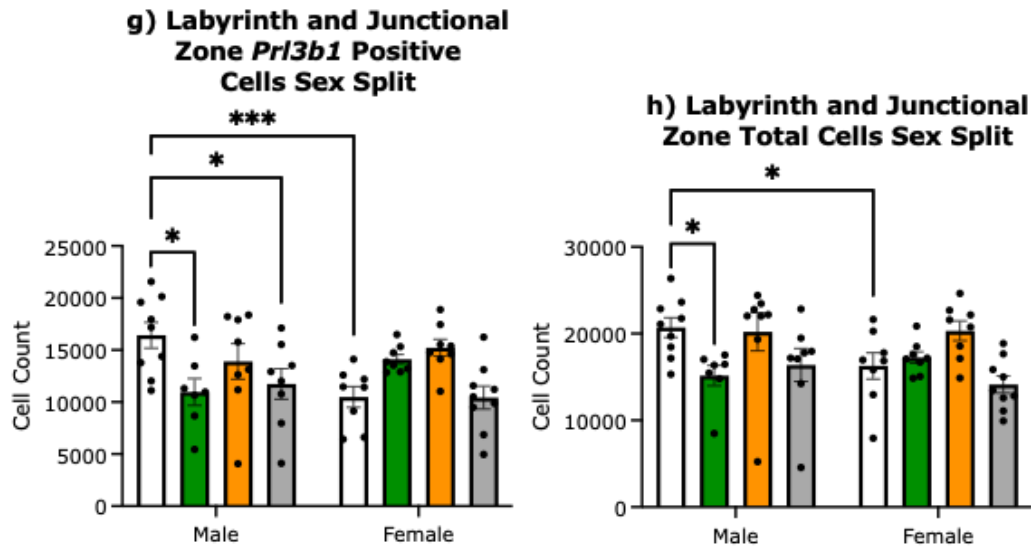


Figure 56: Total cell counts of E16.5 placenta for WT, *Peg3*^{KO}, *Phlda2*^{KO} and DKO.

a) There was no significant difference in total *Prl3b1* positive cells between any groups. **b)** *Phlda2*^{KO} placentas contained 27% ($P=.025$) more total cells than WT placentas. **c)** There was no significant difference in the labyrinth and junctional zone positive cells between any groups. **d)** There was no significant difference in the labyrinth and junctional total cell numbers between any groups. **e)** Female *Phlda2*^{KO} placenta had 26% ($P=.042$) more total *Prl3b1* positive cells than female WT placenta. *Peg3*^{KO} females had 41% ($P=.023$) more total *Prl3b1* positive cells than *Peg3*^{KO} males. **f)** There were no significant differences seen between any groups for total cell numbers. **g)** Labyrinth and junctional zone *Prl3b1* positive cells were reduced in male *Peg3*^{KO} and DKO placentas by 33% ($P=.019$) and 28% ($P=.023$) compared to WT males. Female WT placentas had 36% fewer *Prl3b1* positive cells than male WT. **h)** Total cells from labyrinth and junctional zones were reduced in *Peg3*^{KO} male samples by 27% ($P=.051$). Female WT samples had 21% ($P<.001$) fewer cells in their labyrinth and junctional zones than male WT. WT ($n = 17$), *Peg3*^{KO} ($n = 15$), *Phlda2*^{KO} ($n = 16$) and DKO ($n = 17$). WT male ($n = 9$), *Peg3*^{KO} male ($n = 7$), *Phlda2*^{KO} male ($n = 8$), DKO male ($n = 8$), WT female ($n = 8$), *Peg3*^{KO} female ($n = 8$), *Phlda2*^{KO} female ($n = 8$), DKO ($n = 9$). Data from 16 litters, litter size between 5-10 (average $8 \pm .18$). Error bars represent \pm SEM. Statistical significance calculated using a two-way ANCOVA with Šidák correction and litter size as covariate. ^{NS} $P > .05$, $*P < .05$, $**P < .01$ $***P < .001$ $****P < .0001$ (Appendix 23).

There was no significant difference in total *Prl3b1* positive cells between any groups when the data was pooled. When the data was split by sex, female *Phlda2*^{KO} placenta had 26% ($P=.042$) more total *Prl3b1* positive cells than female WT placenta and *Peg3*^{KO} females had 41% ($P=.023$) more total *Prl3b1* positive cells than *Peg3*^{KO} males. When assessing total cell number, *Phlda2*^{KO} placentas contained 27% ($P=.025$) more total cells

than WT placentas when the data was pooled but there no significant differences seen between any groups for total cell numbers.

When the data was corrected to exclude decidua measurements in total cell counts, there was no significant difference in the labyrinth and junctional zone *Pr13b1* positive cells or total cell numbers between any groups. When this data was split by sex, labyrinth and junctional zone *Pr13b1* positive cells were reduced in male *Peg3^{KO}* and DKO placentas by 33% ($P=.019$) and 28% ($P=.023$) compared to WT males. Female WT placentas had 36% fewer *Pr13b1* positive cells than male WT. Total cells from labyrinth and junctional zones were reduced in *Peg3^{KO}* male samples by 27% ($P=.051$) and female WT samples had 21% ($P<.001$) fewer cells in their labyrinth and junctional zones than male WT.

Representative images of the impact of each of the genotypes on male and female placentas were collated into Figure 57.

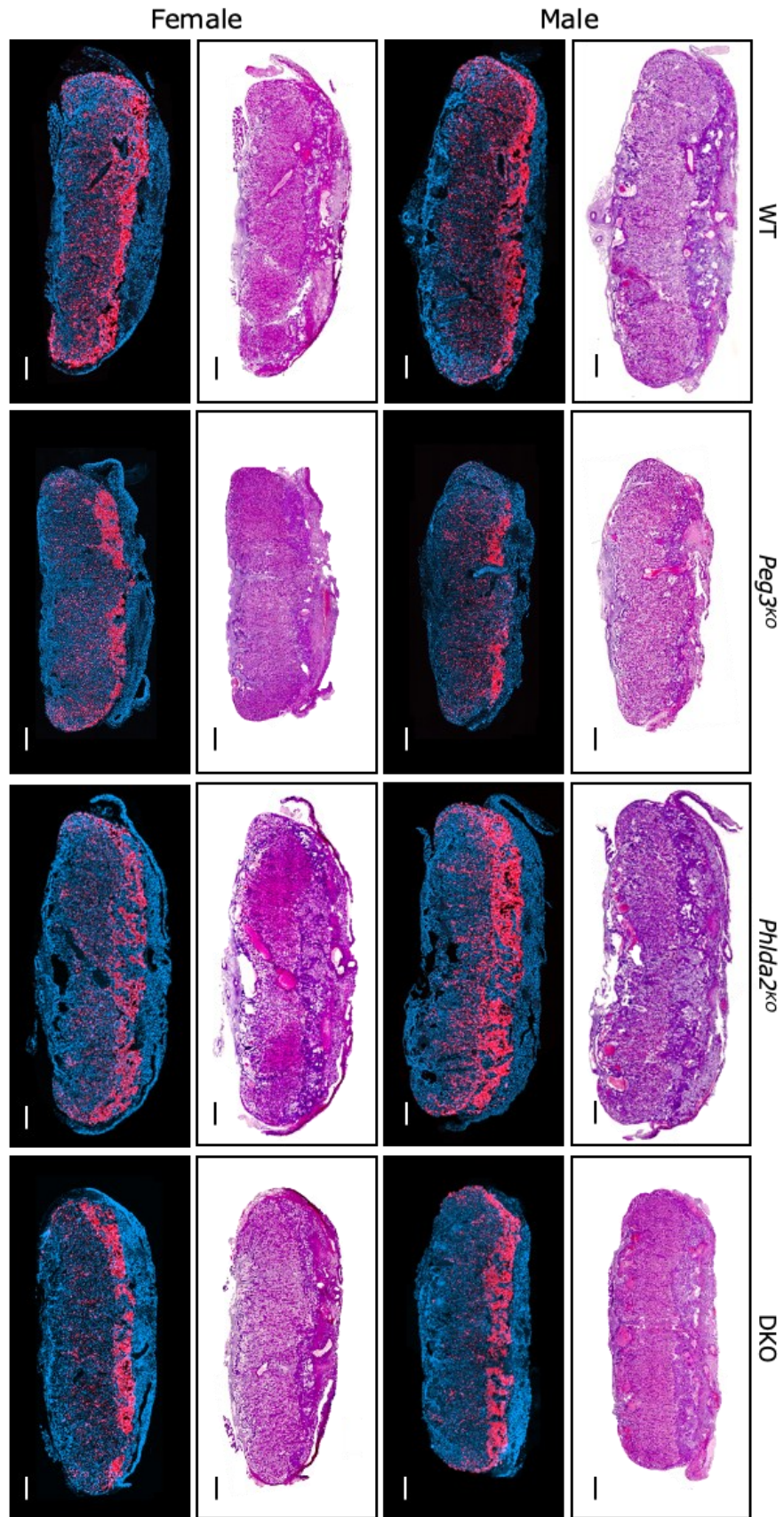


Figure 57: Representative images of E16.5 placenta for male and female, WT, *Peg3*^{KO}, *Phlda2*^{KO} and DKO placentas.
Scale bar 500 μ m.

4.4 Discussion

4.4.1 *Peg3* and *Phlda2* co-expression with key endocrine regulators in placental lineage progenitors

The multiplexing of *Peg3* and *Phlda2* showed co-expression in the Epc of E7.5 placentas (Figure 42, C-E). At E9.5, there were small populations of co-expressing cells in the developing junctional zone and larger clustered populations of co-expressing cells in the developing labyrinth (Figure 42, H-J). To identify which cell types more specifically were expressing each gene of interest, multiplexing with the spongiotrophoblast and TGC marker, *Tpbpa* and the glycogen cell marker *Pcdh12* were performed with each gene. *Peg3* was co-expressed with *Pcdh12* in the E7.5 samples in glycogen cells. At E9.5, *Peg3* was co-expressed with *Tpbpa* in the developing spongiotrophoblast as well as being expressed on its own in the developing labyrinth (Figure 44). *Phlda2* was co-expressed with *Pcdh12* in E7.5 samples. At E9.5, although there was a population of *Phlda2* expressing cells in the labyrinth that had no co-expressing with *Tpbpa* or *Pcdh12*, there was a population of cells expressing all three markers in the developing spongiotrophoblast, which is an expression pattern exhibited by glycogen cells (Figure 45).

These results provide evidence towards the understanding of the interaction between *Peg3* and *Phlda2*. It could indicate that both genes play a role in the development of both the spongiotrophoblast and the labyrinth. The multiplexing assay used identifies RNA molecules, neither *Phlda2* nor *Peg3* are non-coding RNAs, so this does not directly indicate their function within the same region of a cell. However, the presence of both RNAs in the same cell could be indirect evidence to indicate that the genes are regulated by the same elements and could have a coordinated response to the same developmental signals or other stimuli and potentially co-ordinated function. *Peg3* is a transcription factor which primarily functions within the nucleus, with the binding motif 5'-GTGGCAGT-3' (Lee et al., 2015). In a search conducted on TFLink, *Peg3* is not a listed transcription factor of *Phlda2* nor is *Phlda2* listed as one of *Peg3*'s target (Liska O, 2022). It is likely that *Peg3* could influence pathways that indirectly modulate *Phlda2*. *Phlda2* protein functions in the cytoplasm, not the nucleus, which again suggests a different method of functionality. Their temporal synchronicity demonstrates that their action takes place at the same timepoint in development. This data does not make conclusions as to whether the function of one suppresses or counteracts the activity of the other, however it does not exclude this hypothesis as their spatial and temporal expression patterns have now been demonstrated to be linked.

Single cell RNA sequencing data from Jiang et al. (2023), showed a variety of expression profiles for populations of cells expressing *Peg3* or *Phlda2* that supports this result as discussed in section 1.4. These RNA-sequencing co-expression results align with multiple RNAscope figures (Figure 42, Figure 43, Figure 44 and Figure 45) where co-expressing populations of both genes of interest at E9.5 were higher in the labyrinth than in the spongiotrophoblast (Jiang et al., 2023).

When this combination of *Peg3* and *Phlda2* was paired with *Pr13b1*, there was some cross over of all three (Figure 43). The majority of the *Phlda2* expression was in the developing labyrinth, which was highly co-localised with a large proportion of the *Peg3* expressing cells. In the developing junctional zone, there was a population of *Peg3* positive cells which are highly co-localised with *Pr13b1* cells. Within this population is a sub population of cells that were also expressing *Phlda2*. As *Pr13b1* is expressed at a higher rate in the junctional zone than in the labyrinth, it makes sense that there is more co-localisation with *Peg3* than *Phlda2* as *Peg3* also has a larger population of *Peg3* expressing cells in the junctional zone than *Phlda2*. This result could suggest that *Peg3* has a more direct role on the regulation of the junctional zone than *Phlda2* and in turn a more direct role in the regulation of *Pr13b1* expression. This result is again re-enforced by single cell RNA sequencing data from Jiang et al 2023, where only *Pr13b1* and *Peg3* overlapped in expression in a population of cells specific to TSCs and the Exe identified by *Lin28a* and *Eomes* expression and again the co-expression of *Peg3* and *Phlda2* in the labyrinth (Jiang et al., 2023).

Other genes regulated by KvDMR1 were also stained by multiplex to understand their co-localisations and interactions. These genes are involved in crucial lineage development and their co-expression with *Peg3* or *Phlda2* links the genes of interest to that function. A combination of *Ascl2*, *Phlda2* and *Cdkn1c* revealed that at E7.5 there was some co-localisation of all three in the developing junctional zone, suggesting that *Phlda2* plays a role in the progenitors of both the spongiotrophoblast cells and glycogen cells.

At E9.5, a large population of *Cdkn1c* expressing TGCs surrounds the yolk sac, which were negative for both *Ascl2* and *Phlda2*. In the developing labyrinth there was little co-localisation between *Phlda2* and *Ascl2*, where *Cdkn1c* co-localised with both *Phlda2* and *Ascl2* in separate cell populations. The co-localisation between *Phlda2* and *Ascl2* was present but much lower than any other combination. *Ascl2* inhibits differentiation of trophoblast cells and encourages cell proliferation (Guillemot et al., 1994) by maintaining giant cell precursors (Scott et al., 2000). As *Ascl2* was not highly co-localised with *Phlda2* this suggests that *Phlda2* has less involvement with TGC lineage restriction.

When *Cdkn1c* was paired with *Tpbpa* and *Pcdh12*, *Cdkn1c* showed some co-localisation with *Tpbpa* in E7.5 placenta. At E9.5 there was a population of TGCs that were *Cdkn1c* positive and negative for *Pcdh12* and *Tpbpa*. There was a separate population of cells that was positive for all three. At E7.5, glycogen cells have not yet formed (Bouillot 2006) however the *Pcdh12* does have expression at the top of the ectoplacental cone in all multiplex staining performed here. Glycogen cells progenitors are located in the central part of the ectoplacental cone at E7.5 but don't start to accumulate glycogen until around E10.5, in which they should appear as being *Pcdh12* positive. *Pcdh12* is widely used as a marker of glycogen cells (Bouillot et al., 2006; Rampon et al., 2005; Tunster et al., 2020) however this result suggests this may be a poor choice of marker. As *Cdkn1c* (another glycogen cell marker) is not co-localised with *Pcdh12* at E9.5, this would further underscore the questionability of using *Pcdh12* as a glycogen cell marker although these *Cdkn1c*+ve and *Pcdh12*-ve cells could be TGCs. *Cdkn1c* is crucial for glycogen cell differentiation and is required for the development of S-TG cells (Tunster et al., 2011). *Cdkn1c* co-localisation with *Phlda2* could support the idea that *Phlda2* plays a role in S-TG cell development which is supported by the evidence that the S-TG cells are reduced in *Phlda2*^{KO} and DKO placenta and in the *Phlda2*^{+/+BACx1(BL6)} strain from Chapter 3.

The regulation of the IC2 domain genes by the antisense RNA transcript *Kcnq1ot1* has been well documented (Fitzpatrick et al., 2002). Like *Phlda2*, the imprinted genes *Cdkn1c* and *Ascl2* are also regulated by *Kcnq1ot1* and are maternally expressed. This RNAscope data supports the claim that *Ascl2* plays a significant role in the development of the spongiotrophoblast (Bogutz et al., 2018) and that *Cdkn1c* functions to develop and maintain the labyrinth and S-TG cells more specifically (Simmers et al., 2023). The reduced overlap between *Ascl2* and *Phlda2* suggests differing roles despite both being regulated by the same mechanism. *Ascl2* is involved in the differentiation of trophoblast progenitors and is essential for establishing the spongiotrophoblast (Guillemot et al., 1994), where *Phlda2* suppresses cell proliferation of trophoblast cells (Tunster, Creeth, et al., 2016). *Ascl2* action is therefore earlier in development than *Phlda2*, although they are both present at each of these stages (Figure 46). This RNAscope data is corroborated by single cell RNA sequencing data from Jiang et al 2023, where investigation into populations of Epc cells revealed three distinct populations, progenitors of SpT cells (E1) expressing *Tpbpa*, *Cdx2* and *Ascl2* were distinct from a population of bipotential progenitors (P1) which expressed *Phlda2* and could differentiate into SpT progenitors (E1) at E7.5-E8.5 (Figure 46) (Jiang et al., 2023). In addition, *Ascl2* and *Cdkn1c* were identified in SpT cells from E9.5-E14.5 and *Ascl2* was also seen in cells expressing *Pcdh12* between E9.5-E14.5 both of which are

corroborated by the RNAscope results seen in Figure 46 (Jiang et al., 2023).

4.4.2 Evaluation of the effectiveness of *Peg3* and *Phlda2* knockouts on E9.5 placentas: Insights from RNAscope multiplexing

RNAscope-multiplexing was performed on E9.5 samples of the four genotypes of interest WT, *Peg3*^{KO}, *Phlda2*^{KO} and DKO (Figure 49). The experiment was done to determine how effective the knockout performed in the developing placenta and if there was any co-localisation or impact on the spongiotrophoblast marker *Tpbpa*. The *Peg3*^{KO} samples had a reduced *Peg3* signal, and *Phlda2* and *Tpbpa* expression patterns similar to WT. The *Phlda2*^{KO} samples had a similar *Phlda2* expression pattern to WT, a disrupted pattern of *Peg3* expression and a larger population of *Tpbpa* positive cells. The DKO samples had relocated expression of *Phlda2* from the developing labyrinth into the developing spongiotrophoblast. DKO samples also had a *Peg3* expression pattern different to the WT samples, with a shift from expression in the developing labyrinth to the developing spongiotrophoblast. There was also a larger population of *Tpbpa* positive cells in the DKO samples compared to WT. Most notably, all knockouts present some expression of the knocked-out target.

There are several potential causes for this result. A limitation to this assay is the inability to genotype these samples via PCR. Although thoroughly and meticulously checked in their production, the sample production method did not allow genotype sampling, meaning, there is a chance that the placental embryo pod being stained is not the genotype it is categorised as. Considering that all embryo pods stained and imaged are expressing some RNA from both targets, it is unlikely that all samples are WT, therefore it is reasonable to assume that the knockout samples are expressing the target sequences.

The way in which these knockouts are designed relies on the imprinted allele to be efficient at silencing the expression of the target from the imprinted allele. Unlike other knockouts which are bi-allelic, this knockout only removes the target from the expressed allele, *Peg3* from the paternal allele for example. However, the maternal alleles' *Peg3* is still present in the DNA and is silenced by the imprinting mechanism. There is a possibility that the absence of the expressed *Peg3* from that paternal allele may cause an alteration to the maternally silenced allele, resulting in some leaky maternal expression. The concept that an imprinted gene on an imprinted allele can change its expression pattern has been previously demonstrated. Growth-factor receptor bound protein 10 (Grb10), has tissue specific imprinting, in which it is paternally imprinted throughout the adult mouse except in a subset of neurons which it is

maternally imprinted (Plasschaert & Bartolomei, 2015). In another example, both *H19* and *Igf2* have demonstrated bi-allelic expression in a variety of tumours despite both having imprinted expression during embryo development (Kim & Lee, 1997; Van Gurp et al., 1994). When establishing *Phlda2*'s imprinting profile, leaky expression was identified. The imprinting of *Phlda2* was most functional in the extraembryonic membranes, placenta, foetal lung and liver and adult spleen, however the brain demonstrated a weak allelic expression bias, although overall had low expression levels, suggesting that *Phlda2* imprinting is temporally and tissue specific (Qian et al., 1997). As *Phlda2* is silenced through the *KvMR1* mechanism rather than direct methylation of the gene itself, as *Peg3* is, it is understandable that there would be a higher base expression from the paternal allele.

Some leaky expression was identified from both male and female placentas of the *Peg3*^{KO} strain at E14.5 (Tunster et al., 2018) at less than 1% of the WT level, with female placentas demonstrating a higher amount of leaky expression. This higher level of leaky expression demonstrated by the female placenta could be what allows the female placenta to avoid such a significant impact from the *Peg3* knockout compared to its male counterpart. This 2018 E14.5 result does not exclude the potential that at earlier developmental stages, expression from the imprinted allele could be even more significant. Despite this, the leaky expression would likely be too low to rescue the impact on *Peg3*^{KO} placenta even partially. This expression assessment has not been performed on the *Phlda2*^{KO} at E14.5. It is reasonable to assume a similar expression pattern to *Peg3*^{KO}, as results demonstrated in Figure 49 suggest a more significant expression of *Phlda2* from the *Phlda2*^{KO} strain than *Peg3* from the *Peg3*^{KO} strain. Although this imprinted gene knockout approach was deliberately chosen and has its' merits (John, 2010) more thorough temporal investigation into the effectiveness of both knockouts needs to be conducted.

Other than leaky expression, the proprietary nature of the RNAscope probes may be causing this result as it is possible that they may be binding to sections of the RNA that are still being transcribed. For example, the *Peg3*^{KO} targeting removed exon five which rendered the gene functionally silent but left the remaining exons intact. This could result in truncated *Peg3* RNA fragments being produced which would be detected by the RNAscope probes if they target those regions. Refining these probes to target sections within exon five would resolve this technical complication and determine if this expression profile seen in these RNAscope results is accurate.

The *Tpbpa* results demonstrate an alteration to the spongiotrophoblast lineage at this time point. With both *Phlda2*^{KO} and DKO placentas

presenting with larger populations of *Tpbpa* positive cells compared to WT, this suggests that *Phlda2* may act to restrict spongiotrophoblast lineage expansion at this timepoint. At this timepoint *Peg3* is still presenting a comparable to WT *Tpbpa* population. Considering the demonstration that the DKO placenta has a comparable to WT spongiotrophoblast at E16.5, this could indicate the *Peg3* functions later in the developmental timeframe. The absence of both resulting in *Phlda2*^{KO} allowing an expansion of the spongiotrophoblast lineage by E9.5 and *Peg3*^{KO} restricting that back to WT before E16.5. This correlates with data from Jiang et al. (2023) which identified a population of bipotential progenitors that expressed *Phlda2* which differentiated into spongiotrophoblast progenitors by E7.5-E8.5. Following this, *Peg3* was then expressed by TS cells and Exe cells between E7.5 and E10.5 (Jiang et al., 2023).

4.4.3 Assessing early phenotype development: P-TG cell variations in *Peg3*^{KO}, *Phlda2*^{KO} and DKO placentas

To identify if a phenotype was present at E9.5, manual counting of P-TG cells was conducted. A mild phenotype was identified for *Peg3*^{KO} and DKO samples with *Peg3*^{KO} placentas having 18% fewer P-TG cells than WT and DKO having 21% more than WT. *Phlda2*^{KO} was increased to WT but not significantly. In a previous study conducted on the *Peg3*^{KO} strain, no significant difference was seen in pan-TGC marker expression at E14.5, suggesting no TG cell phenotype at that timepoint (Tunster et al., 2018). The *Phlda2*^{KO} strain has demonstrated a varied impact on the different TG cell lineages. Expression of TG cell markers *Tle3* and *Ctsq* were not altered in *Phlda2*^{KO} placentas where *Prl2c* and *Prl3b1*, markers of both TG cell and spongiotrophoblast were (Tunster, Creeth, et al., 2016). Using more specific lineage markers with *in situ* hybridisation suggested that *Phlda2* does not impact TG cell numbers at E14.5 (Tunster, Creeth, et al., 2016). The DKO placenta has not previously been investigated in its TG cell phenotype. DKO having more TG cells than WT and *Phlda2*^{KO} at E9.5 suggests a complicated mechanism in which both knockouts in partnership increase the number of TG cells more than either knockout individually. There is the potential for the phenotype to be present at E9.5 and diminish in the later stages. This result would suggest the phenotype has established at this time point.

4.4.4 Sexual dimorphism in foetal and placental weights of E16.5 KO placentas

The analysis of the E16.5 foetal weights of the genotypes WT, *Peg3*^{KO}, *Phlda2*^{KO} and DKO was conducted. Here the *Phlda2*^{KO} model replicated the absence of foetal weight restrictions demonstrated in Tunster, Creeth, et

al. (2016). However, *Peg3^{KO}* had a significantly decreased foetal weight compared to WT for both male and female fetuses, which was not significant in Tunster et al. (2018). It is possible that either the larger data set used for this analysis or the use of litter size as a covariate in the statistical analysis or a combination of the two helped to reveal this phenotype. This result supports the evidence in Human that low *PEG3* expression is correlated with low birth weights (Sumption et al., 2020). Interestingly, the DKO group also shows a significant decrease in foetal weight compared to WT. The reduction in foetal weight for DKO placentas does track the reductions seen in the *Peg3^{KO}* group for females but reduces in the severity of the reduction in males. Females of *Peg3^{KO}* and DKO genotypes have a placental weight reduction of 12% compared to WT, but *Peg3^{KO}* males have 16% reduction in placental weight where DKO males only demonstrate a 12% decrease. This suggests that in males there is a recovery effect with the removal of both *Peg3* and *Phlda2* which is not demonstrated in females. This could be a reflection of the male fetuses increased demand on the placenta. The DKO placenta has been altered by the knockouts in a way in which the male foetus is able to recover slightly where the female is not.

In further analysis of sexual dimorphism of the E16.5 placental weight, although both sexes are impacted in the same way for each of the genotypes, the male placenta is impacted to a much greater degree. Male *Peg3^{KO}* are significantly lighter and male *Phlda2^{KO}* are significantly heavier, neither of which reach significance in females. There was also a significant difference in weight within the genotypes across sexes. The female WT and *Phlda2^{KO}* placenta were lighter than their male counterparts. Neither of these findings have been previously reported. Prior analysis of the *Phlda2^{KO}* strain was not analysed by sex. The pooled sex assessment in Figure 51,b, replicates the assessment conducted in Tunster et al 2018. The sex split analysis (Figure 51,e) demonstrates that the impact is more severe on males and does not hold statistical significance for females. For the *Peg3^{KO}* analysis, Tunster et al. (2018) reported a significant reduction in placental size for both sexes, where this analysis only reports a significant reduction in placental weight for males and not for females. Again, this could reflect the increased data set or the inclusion of litter size as a covariate in the statistical analysis but most likely is due to the assessments being performed at different time points, Tunster's at E14.5 and here at E16.5. To give reason to this result, it is theorised that the male placenta operates at a maximum requirement of resources throughout gestation, to be able to support a larger foetus. Because of its high demand, it is believed that the male placenta is more vulnerable to disruption. In general, male fetuses have been identified as being more vulnerable to adversities than female fetuses (DiPietro & Voegtline, 2017) and the fragility of the male placenta has been proposed

as the potential cause of that foetal vulnerability. This placental weight data corroborates this theory with the more significant impacts from the transgenic modifications in the male placentas and not female placentas (Figure 51,e).

For the DKO genotype, the placental weight is recovered to WT which suggests that the absence of both genetic targets produces a broadly similar placental phenotype to the presence of both. This does support the concept of antagonistic interaction between *Peg3* and *Phlda2* within the placenta. As this was not seen in the foetal weight data, it suggests that although the weight of the placenta is corrected, it does not regain its complete functionality, further suggesting that the correction occurs unevenly across the two knockouts and implies an unequal action of the two genes. The finer details of the DKO placental correction to WT are further investigated in the assessments of placental regions and cell types (section 4.3.5).

The lack of change in foetal weight coupled with the placental weight increase does mean that the foetal to placental weight ratio is significantly reduced in the *Phlda2^{KO}* group compared to WT. This again replicates the findings of Tunster, Creeth, et al. (2016). In the previously un-investigated sex split analysis, this reduction in the ratio holds true only for males. The larger placenta size compared to the not altered foetus size could indicate two potential processes, either the larger placenta is less efficient at providing nutrients to the foetus, suggesting a functional impairment alongside the increase in placental size, or there is a regulatory process outside of the placenta which removes the ability for the larger placenta to produce a larger foetus. In humans, while high *PHLDA2* has not been directly linked to increased CBWCs, it has been linked to high hPL levels which has been linked to increased foetal weight (Garay et al., 2022; Rassie et al., 2022). In the mouse, it has been suggested that *Phlda2*'s mechanistic output is more complex and may involve other elements in regulating foetal size (Tunster, Creeth, et al., 2016) which could be why no foetal size adjustment is identified here.

4.4.5 E16.5 placental region and cell type alterations: Genotypic and sexually dimorphic effects on junctional zone and labyrinth structures

The regional area measurements of E16.5 placentas revealed which sections of the placenta were impacted in response to each genotype. For junctional zone measurements, while the *Peg3^{KO}* samples did not show a significant decrease compared to WT, when the samples were split by sex, it was clear that the male samples did have a significant reduction in junctional zone area. This result was nullified in the pooled assessment by

the female samples having a slightly larger (ns) junctional zone area, demonstrating a sexually dimorphic response to a *Peg3*^{KO}. This sex difference was not identified in Tunster et al. (2018). In Tunster et al. (2018) analysis both sexes showed a reduction in junctional zone size, although the impact was more severe in the male placentas, the female's milder reduction in junctional zone size did reach significance and presented the opposite response to what was found in this thesis's analysis. *Phlda2*^{KO} samples had a significantly increased junctional zone area which was present in both male and female samples, something not previously investigated by Tunster et al. (2018). The junctional zone size was not significant from WT in either sex in the DKO genotype, suggesting that the interplay between the removal of both *Peg3* and *Phlda2* is balanced within the junctional zone. The female WT and *Phlda2*^{KO} junctional zones were smaller than their male counterparts which reflects the placental weight data.

When pooled, *Peg3*^{KO} and *Phlda2*^{KO} labyrinth sizes follow the size adjustment pattern demonstrated in the junctional zones although not statistically significant. When split by sex, the male labyrinth bears the brunt of the genetic impacts where the female labyrinth remains unaltered, with a significant reduction in size for *Peg3*^{KO} and DKO labyrinths compared to WT in males only. This *Peg3*^{KO} result was not reported in Tunster et al. (2018) analysis of the *Peg3*^{KO} strain. Tunster et al. (2018) data showed a reduction from WT in labyrinth size for *Peg3*^{KO} males only, however this was not significant. This difference is likely caused by a larger data set and more refined statistical analysis. Unlike the impact on the junctional zone, the DKO phenotype has a significantly smaller labyrinth than WT which remained significant in the male labyrinths when split by sex. This suggests that the correction mechanism of having both genetic targets absent does not function in the same way within the labyrinth as it does in the junctional zone. This further suggests that the genetic targets have an unequal action in developing the labyrinth lineage. *Phlda2*^{KO} labyrinths are not significantly different to WT in size, suggesting no action by *Phlda2* on this lineage, although it is expressed in the labyrinth (Figure 45)(Tunster et al., 2018), its action does not seem to encourage labyrinth lineage expansion. As the male *Peg3*^{KO} labyrinth is reduced in size, if *Phlda2* does not play a role in this lineage, its absence will not recover the reduction produced by the removal of *Peg3*. This effectively reinforces the sexually dimorphic impact of *Peg3*. *Peg3* is believed to act earlier in development resulting in an impact on a broader range of placental lineages including labyrinth lineages where *Phlda2* only regulates spongiotrophoblast lineages (Tunster, Creeth, et al., 2016). This result corroborates that hypothesis.

With the function of the junctional zone being hormone production and the function of the labyrinth being nutrient and gas exchange between foetus and mother, it is interesting to investigate the altered dynamics between the two in each of the genotypes of interest. Overall, both *Phlda2*^{KO} and DKO samples have an increased junctional zone area to labyrinth area ratio. When split by sex, the *Phlda2*^{KO} groups lose their significance, where a sex specific response is demonstrated in the *Peg3*^{KO} and DKO genotypes. Male *Peg3*^{KO} placentas have a lower ratio than male WT placentas where females are not significantly affected. Male DKO placentas have significantly increased ratio where females are not significantly affected. In addition, female *Peg3*^{KO} and DKO groups also have a significantly lower ratio than their male counterparts. A decrease in junctional zone area to labyrinth area ratio as seen in *Peg3*^{KO} male placentas could cause an impairment in nutrient and gas exchange, reducing the uptake of oxygen and nutrients to the foetus which would result in a reduction in foetal size as demonstrated in section 1.1 (Figure 51). This illuminates a potential mechanism behind the low birth weight in humans which has been linked to low *PEG3* expression (Sumption et al., 2020). An increase of the junctional zone area to labyrinth area ratio, as seen in the DKO male placentas, although it has the potential to improve nutrient and gas exchange, is still limited by the relatively smaller junctional zone causing a relative reduction on hormonal support, again causing the potential to limit foetal growth, which was also demonstrated in the foetal weight assessment of the DKO as seen in section 4.3.4 (Figure 51).

In the cell counting analysis of the junctional zone, *Pr13b1* positive cells were increased in the *Phlda2*^{KO} phenotype. When split by sex, again the male placenta was affected by the *Peg3*^{KO} where the female was not, nullifying its affect in the pooled analysis. Both male and female *Phlda2*^{KO} samples demonstrate a significant increase in *Pr13b1* within the junctional zone. Female WT and DKO samples all have significantly less *Pr13b1* positive cells than their male counterparts. This pattern is replicated exactly in the analysis of total cells in the junctional zone. *Pr13b1* being a key placental hormone represents the placentas endocrine capacity and its functional capacity. Although measured in previous studies of each genotype, the *Phlda2*^{KO} analysis was done with a non-quantifiable *in situ* hybridisation method and a non-region-specific qRT-PCR which was not analysed for sexual dimorphism (Tunster, Creeth, et al., 2016). *Pr13b1* RNAscope was performed on *Peg3*^{KO} placenta but without the automated counting method which allows a quantitative analysis (Tunster et al., 2018). In this thesis, the RNAscope analysis of *Pr13b1* positive cells provides insight into the functional output of the junctional zone and demonstrates that it has been altered, reduced in *Peg3*^{KO} males,

increased in *Phlda2*^{KO} males and females, and recovered in the DKO model.

It is hypothesised that glycogen cells play an energy storage role in the placenta (Coan et al., 2006; Tunster et al., 2020). Glycogen cell counts showed a higher number in *Phlda2*^{KO} samples which was upheld by females when the samples were split by sex. The spongiotrophoblast cell to glycogen cell ratios were not affected by any of the genotypes, because although the only the *Phlda2*^{KO} group had a significantly higher glycogen cell count than WT, the placentas held a consistent ratio between the cell types. Previously glycogen levels were analysed using a measurement of extracted glycogen from each placenta. Using this method glycogen showed an increase in *Phlda2*^{KO} placentas (Tunster, Creeth, et al., 2016) and a decrease in male and female *Peg3*^{KO} placentas, in males even accounting for an increase in placental size (Tunster et al., 2018). The discrepancy in these results is likely due to the variation between methodologies. In both studies glycogen cell markers were analysed via qRT-PCR and gave no response to either transgenic modification (Tunster et al., 2018; Tunster, Creeth, et al., 2016). This result is supported by this cell counting data. The lack of effect on the number of glycogen cells suggests that the impacts on the foetus are more likely to be due to placental functional impairments caused by altered placental structure demonstrated in sections 4.3.5.

The labyrinth cell counting showed a highly sexually dimorphic response. When pooled, both *Pr13b1* and total cell counts were significantly lower in DKO than in WT, with *Peg3*^{KO} and *Phlda2*^{KO} groups presenting similarly to WT. When split by sex the picture is quite complex. For *Pr13b1* positive cells in males, all genotypes showed a significant reduction in the number of positive cells in the labyrinth compared to WT, with the most significantly reduced number being the DKO labyrinths. For females, the WT group has a significantly reduced labyrinth compared to males. But within the female genotypes there are no significant differences between groups. There is also a different pattern compared to the males. Both *Peg3*^{KO} and *Phlda2*^{KO} females have higher numbers of *Pr13b1* positive cells than female WTs, where the male counterparts both significantly reduced compared to WT. This same pattern was seen in the analysis of total cells within the labyrinth although with a reduced degree of significance, as only male DKO samples had a significant reduction in total cells compared to WT. This result reflects the analysis of the labyrinth size analysis and further supports the suggestion that the reduction in labyrinth total cell and *Pr13b1* positive cell count impairs the functionality of the placenta.

For the counting analysis of the total placenta, no significant difference was seen for any group in the total number of *Pr13b1* positive cells. When split by sex, a significant difference was revealed, where *Peg3*^{KO} females

had significantly more total *Prl3b1* positive cells than male *Peg3^{KO}* placentas. This data was compromised by the quality of decidua for these samples. There were some samples that had torn decidua, removing them from the total placenta count, where their labyrinth and junctional zones were intact. To rectify this, an analysis was conducted on the combination of the junctional zone and labyrinth total cells and *Prl3b1* positive cells. This combined data provides insight into the idea that the alterations made on the junctional zones are compensated for in the labyrinth.

For the *Peg3^{KO}* samples, the reduction in *Prl3b1* positive cells and total cells in the junctional zone and labyrinth are reduced for males which results in the total reduction in *Prl3b1* positive cells and total cells for male *Peg3^{KO}* placentas. For females, slight increases in *Prl3b1* and total cells in the junctional zone paired with increases in both total and *Prl3b1* positive cells in the labyrinth result in a non-significant difference compared to female WT. For both sexes, both the junctional zone and the labyrinth were impacted in the same way. For the *Phlda2^{KO}* samples, the increased junctional zone total cell number and *Prl3b1* positive cell number was seen across both sexes. The labyrinth did not respond in the same way for male samples, as male *Phlda2^{KO}* labyrinths had less *Prl3b1* positive and total cells than WT males (ns). This result is reflected in the overall analysis of the placenta, as there is not an overall increase in total cell number or *Prl3b1* positive cell number for males. For females *Phlda2^{KO}* placentas, although the labyrinth also increases in cell count and *Prl3b1* positive cells, along with the junctional zone, this does not result in a total increase over all in either metric. The DKO samples, show no alteration in junctional zone cells within their sex compared to WT for either *Prl3b1* positive cells or total cells for males and females. In males however, the reduction in the labyrinth total cells and *Prl3b1* cells compared to WT is significant enough that it effects the total number of *Prl3b1* positive cells over all for this group. The female samples are not significantly altered in either metric. In summary, no compensatory cell number alteration was seen by the labyrinth to accommodate the junctional zone alteration.

The increase or decrease in the size and total cell number of the junctional zone does not affect the ratio of *Prl3b1* positive cells to *Prl3b1* negative cells. This is demonstrated by the increase in total cells and *Prl3b1* positive cells following the same trend per assessed region. This data suggests that there is no mechanism to regulate the number of positive cells over all in the placenta. To elaborate, with the reduced size of the junctional zone in the *Peg3^{KO}* samples, to combat a reduction in hormone production, a potential solution would be to have more *Prl3b1* producing cells. The same hypothesis could have also been applied to the *Phlda2^{KO}* placenta, with fewer *Prl3b1* positive cells proportionally.

However, neither of these features were identified, as the total number of cells in the junctional zone was increased or decreased the number of *Prl3b1* positive cells followed accordingly.

The location of the increased or decreased expression has a functional impact. The junctional zone alterations seen in this chapter or the S-TG cell alterations seen in Chapter 3 have the potential for a larger impact on the amount of hormone exposure to the mother, as these have greater access to the maternal system. For this reason, total placental *Prl3b1* may not be as relevant to the theory for this thesis. Instead, the focus should be on the functional impacts of the alterations. Although there may be some post translational modifications that could alter the amount of hormone produced by any of the transgenic placentas, at least at the RNA level, *Peg3^{KO}* placentas have a reduced *Prl3b1* expression in the junctional zone of male samples, *Phlda2^{KO}* placentas have an increase *Prl3b1* expression in both male and female junctional zones and DKO has no significant difference to WT.

4.5 Limitations

The RNAscope results conducted on the four genotypes (section 4.3.2) raises questions about the effectiveness of relying on the imprinting mechanism in the knockout models. Using the automatic counting method used for *Prl3b1* positive cell counting on E16.5 placentas in chapters three and four (method 2.6) on the level of expression of *Peg3* and *Phlda2* of each genotype could help to quantitatively assess the degree in which the targeted genes were reduced. This should be conducted at multiple developmental time points to assess if there is an adjustment in the degree in which the imprinted gene is expressed throughout development. qRT-PCR was performed on both E9.5 and E16.5 samples by another team member working on this project, which gave unclear results around *Peg3* and *Phlda2* expression from each of the genotypes. RNAscope would give a clearer picture of the targets expression and the quantifiable aspect should give a more conclusive result. If it is confirmed that the reliance on the strains imprinted form of the gene is complicating the effectiveness of the knockout itself, creating bi-allelic knockouts or siRNA knockdowns of these models would give a clearer picture of each genes' role.

The automated cell counting of *Prl3b1* positive cells, can be analysed as a proxy to actual hormone concentrations or a snapshot of the actual endocrine capacity of that genetic modification, however it does not account for any post transcriptional modifications to the *Prl3b1* RNA which could affect functional hormone concentration. Although post

transcriptional modifications for *Pr13b1* have not yet been identified or characterised this is likely due to a gap in knowledge rather than an actual absence. hPRL, for example has multiple post transcriptional modifications resulting in at least 6 protein variants (Qian et al., 2018). The RNA expression of *Pr13b1* using qRT-PCR has given unclear results in the analysis of the four genotypes at E9.5 and E16.5, as discussed previously. It is possible that the whole placenta analysis conducted by the qRT-PCR may dilute the *Pr13b1* expression in the junctional zone to the point where the genotypes are not demonstrating significant differences, similar to the whole placenta RNAscope analysis seen in section 4.3.5.4. RNAscope gives a region-specific analysis which is missing from qRT-PCR data, considering the location of expression does have a functional impact, the altered expressions within the regions are experimentally relevant. A more reliable piece of data would be the hormone level circulating in the blood of the pregnant mouse with a litter of just one genotype. This data has been elusive to this laboratory, with complications in producing the ideal litters, difficulty sampling the appropriate blood/serum and issues with protein analysis of Pr13b1 and Pr13d1. Although blood/serum protein testing would be an important addition to this research to attain in the future, the automated cell counting method coupled with a highly specific, regional and sensitive RNAscope method does provide a clean picture of each genotype's endocrine capacity.

4.6 Summary

The key findings from this chapter are presented in Table 39.

Analysis	Key findings
RNAscope multiplexing	<ul style="list-style-type: none"> • <i>Peg3</i> and <i>Phlda2</i> are co-expressed at E7.5 and E9.5 suggested antagonistic or coordinated roles. • <i>Peg3</i> and <i>Phlda2</i> was co-localised with <i>Pr13b1</i> at E9.5 indicating regulation of endocrine lineages. • <i>Phlda2</i> was expressed more heavily than <i>Peg3</i> in the developing labyrinth at E9.5 suggesting an unbalanced role in the labyrinth.
RNAscope on transgenic samples	<ul style="list-style-type: none"> • Some leaky expression of all knockout targets was identified in each genotype suggesting issues with RNAscope probes or residual expression caused by KO technique. • Increased <i>Tpbpa</i> populations in <i>Phlda2^{KO}</i> and DKO suggest endocrine lineage restriction performed by <i>Phlda2</i> before E9.5.

	<ul style="list-style-type: none"> • Comparable to WT <i>Tpbpa</i> population of <i>Peg3^{KO}</i> suggest later action of lineage expansion.
E9.5 TGC counting	<ul style="list-style-type: none"> • A phenotype could be detected at E9.5. • <i>Peg3^{KO}</i> samples had significantly fewer TG cells than WT at E9.5. • DKO samples had significantly more TG cells than WT at E9.5.
Placental and foetal weight data	<ul style="list-style-type: none"> • Foetal weight was significantly reduced in <i>Peg3^{KO}</i> and DKO pregnancies for both male and female offspring. • <i>Peg3^{KO}</i> placenta had a weight reduction in males only. • <i>Phlda2^{KO}</i> placenta weight increased in males only.
Placental region area measurements	<ul style="list-style-type: none"> • Both the junctional zone and labyrinth had a sexually dimorphic response to genotype. • <i>Peg3^{KO}</i> males have a significantly reduced junctional zone size. • Both <i>Phlda2^{KO}</i> males and females have significantly increased junctional zone areas. • DKO placentas had a significantly reduced labyrinth compared to WT.
RNAscope <i>Pr13b1</i> counting	<ul style="list-style-type: none"> • Both male and female <i>Phlda2^{KO}</i> junctional zones had higher total cell numbers and <i>Pr13b1</i> positive cell numbers. • DKO labyrinths did not have a recovery phenotype and were significantly reduced in both total cell count and <i>Pr13b1</i> positive cell counts to WT. • The <i>Pr13b1</i> positive cell number in the labyrinth had a sexually dimorphic response. • All transgenic labyrinths had a reduction in <i>Pr13b1</i> positive cells in males but not females. • Total <i>Pr13b1</i> positive cells was reduced in <i>Peg3^{KO}</i> and DKO male placentas.

Table 39: Summary of key findings for Chapter 4.

A summary of key sexually dimorphic findings from this chapter are presented in Table 40.

Metric	Group	WT vs <i>Peg3</i> ^{KO}	WT vs <i>Phlda2</i> ^{KO}	WT vs DKO
Foetal weight	Male	↓	-	↓
	Female	↓	-	↓
Placental weight	Male	↓	↑	-
	Female	-	-	-
Junctional zone area	Male	↓	↑	-
	Female	-	↑	-
Junctional zone <i>Pr13b1</i> positive cells	Male	↓	↑	-
	Female	-	↑	-
Labyrinth area	Male	↓	-	↓
	Female	-	-	-
Labyrinth <i>Pr13b1</i> positive cells	Male	↓	↓	↓
	Female	-	-	-

Table 40: Sexually dimorphic findings from Chapter 4.

This chapter successfully contributed to knowledge around the antagonistic function of *Peg3* and *Phlda2* in mouse placenta. It gained information about co-localisation of both genes and related genes at E7.5 and E9.5, detailing their specific tissue location and timeframe, with key documentation of *Peg3* and *Phlda2* co-localisation in key lineage progenitors at E7.5 and early lineage development at E9.5. TG cell counting at E9.5 revealed that a phenotype was developing at that timepoint and RNAscope of each of the genotypes revealed some unexpected expression of KO targets for each.

The analysis of E16.5 samples revealed an impact on foetal weight for both *Peg3*^{KO} and DKO foetuses. There was a sexually dimorphic response for placental weight with significant impacts on male placentas of *Peg3*^{KO} and *Phlda2*^{KO} but not in females (Table 40). The correction of DKO placental weight back to a WT phenotype was also observed. The sexually dimorphic theme carried over to analysis of the area measurements of placental regions, with both junctional zone and labyrinth zones having a sexually dimorphic response to genotypes, again with males being affected by *Peg3*^{KO} and not females (Table 40). The labyrinth DKO

samples were also significantly reduced in size in males suggesting the recovery mechanism back to WT is only balanced within the junctional zone region. The reduced size of the labyrinth in *Peg3^{KO}* and DKO also correlated with foetal size reductions for males (Table 40) suggesting a reduction in placental function.

Cell counting analysis revealed the impact on total cell number and the number of cells producing *Pr13b1* for each genotype. *Peg3^{KO}* junctional zones had reduced total cell counts and *Pr13b1* positive cell counts in males and not females, while *Phlda2^{KO}* junctional zones had increased total junctional zone cell counts and *Pr13b1* positive cell counts for both sexes (Table 40). DKO junctional zones did correct to WT levels for both metrics. The labyrinth again showed a sexually dimorphic response, with all male transgenic placentas having a reduced total cell and *Pr13b1* positive cell count compared to male WT and females having no significant difference (Table 40). Again, for DKO labyrinths, both total labyrinth cell counts and *Pr13b1* positive cell counts did not correct to WT for either metric concluding only a partial recovery back to WT for the DKO genotype in the junctional zone only. This is underscored by the unbalanced expression of *Peg3* and *Phlda2* in the labyrinth at E9.5. This data demonstrated the altered endocrine capacity of each genotype along with the sexually dimorphic impacts of each genotype.

Chapter 5: *Peg3* and *Phlda2* knockout in human and mouse trophoblast stem cells

5.1 Overview

This project aims to replicate mouse model experiments in the human model and to produce more causative results around the regulation of placental hormones by imprinted genes in human. The expression of this thesis's genes of interest and their correlation with pregnancy phenotypes in humans has been discussed in Chapter 1:section 1.8.2 and 1.8.3. In short, low *PEG3* expression has been linked to maternal depression (McNamara et al., 2018). Maternal depression has been indirectly linked with low *hPL* and SGA offspring in Humans (Sumption et al., 2020). Human *PHLDA2* expression is negatively associated with *hPL* levels (Janssen, Tunster, et al., 2016) and those mothers with decreased *hPL* are correlated with higher instances maternal depression and anxiety (Sumption et al., 2020). These interactions can only be described as a correlation and not causation.

The trophoblast stem cell model provides a bridge between the two species. The ability to perform the same knockout on the same cell format allows questions that can be asked of the mouse model to be asked of the human model in the same context. The experiments conducted in this thesis initially ask the question of how the knockout models behave in each species. It will give insight into the genes of interest's regulation of the endocrine lineages at early developmental stages in each model and will demonstrate the endocrine potential of each genotype. On a larger scale, it answers the question of whether these knockout models are functionally conserved across species, which could suggest that results that are found in the mouse model can be more directly applied to human.

It is hypothesised that both mouse and human *Peg3^{KO}* trophoblast stem cells will show a reduction in their potentiation to produce placental hormones. Conversely, it is expected that *Phlda2^{KO}* trophoblast stem cells of both species will have an increased capacity to produce placental hormones. Additionally, the DKO trophoblast stem cells are expected to demonstrate a correction back to WT levels of placental hormone production.

5.2 Aims

This chapter attempted to derive knockouts of *Peg3* and *Phlda2* in both mTS and hTS cell models, along with a double knock out. It then attempted to quantify each models' capacity to derive the endocrine lineage and ultimately its ability to produce key placental hormones.

Initially, this experiment aimed to derive mouse trophoblast stem cells with WT, *Peg3*^{KO} and *Phlda2*^{KO} and DKO transgenes. It then used a differentiation assay to determine each model's proliferation capacity, potential to develop key lineages and their capacity for hormone production. In collaboration with Professor Okae's laboratory at the University of Kumamoto in Japan, this project then attempted to replicate these knockout models and experimental assays in hTS cells. For chapter specific methods see Appendix 24.

5.3 Results

5.3.1 Mouse trophoblast stem cells

5.3.1.1 Mouse trophoblast stem cell derivation statistics

The details of the attempts at mouse trophoblast stem cell derivation are detailed in Table 41.

	Female Mice	Plugs	Number of mice that produced 0 blastocysts	Viable embryos	Cell line established	Cell lines banked
Total	154	58	132	174	61	33
Per mouse	-	0.38	-	1.15	0.35	0.21

Table 41: Summary of mouse trophoblast stem cell derivations.

The results of genotyping of the banked mTS cells.

	WT	<i>Peg3</i> ^{KO}	<i>Phlda2</i> ^{KO}	DKO
Male	5	5	5	8
Female	6	2	1	1

Table 42: Summary of the number of successfully banked cell lines of each genotype.

5.3.1.2 Mouse trophoblast stem cell validation

The trophoblast stem cell status of these lines was then validated. This was first done by preparing cDNA libraries (protocol 2.10.3) from the cell samples and identifying their expression of key trophoblast stem cell markers *Eomes* and *Cdx2* (protocol 2.2.2.1). Additionally, cells were differentiated for 10 days (protocol 2.8.3) and cDNA libraries were prepared from the differentiated cells (protocol 2.10.3). These were then analysed for their expression of *Pr13b1* and *Pr13d1*.

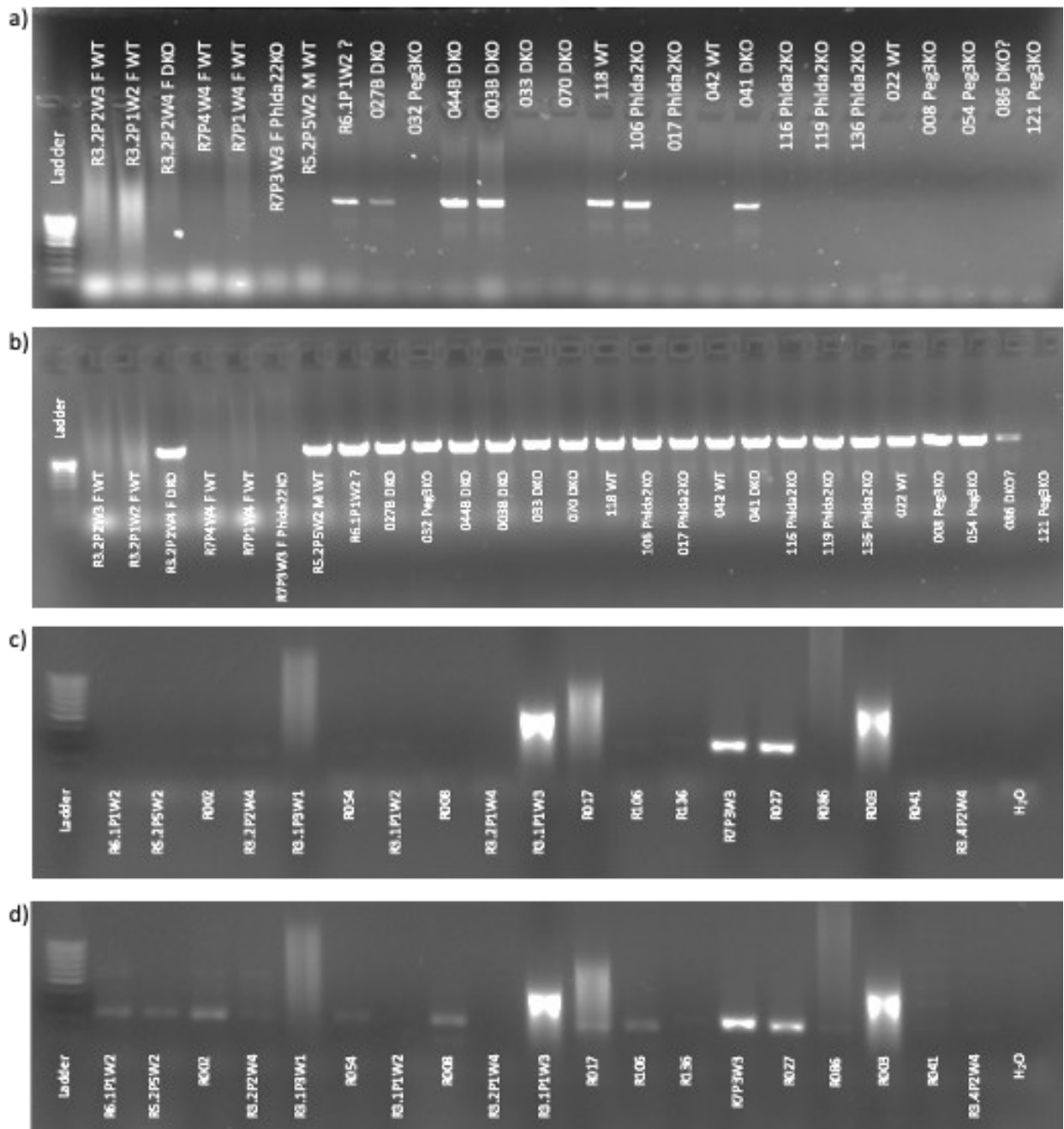


Figure 58: Example of validation techniques for mouse trophoblast stem cells.

a) *Eomes* expression of undifferentiated TS cell lines. **b)** *Cdx2* expression of undifferentiated TS cell lines. **c)** *Prl3b1* expression of 10 day differentiated TS cells. **d)** *Prl3d1* expression of 10 day differentiated TS cells.

5.3.1.3 Prl3b1 and Prl3d1 ELISA on differentiated mouse trophoblast stem cells

To determine whether the cell lines were viable for hormone production, ELISA was performed on differentiated TS cells. E9.5 and E14.5 placenta samples were used as controls. Both Prl3b1 and Prl3d1 were analysed.

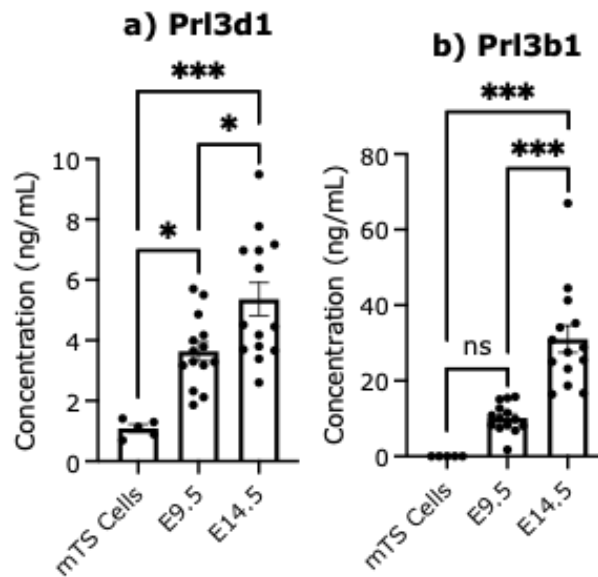


Figure 59: ELISA for Prl3d1 and Prl3b1 on 10-day differentiated mTS cells compared to E9.5 and E14.5 mouse placenta.

a) Prl3d1 was significantly higher than mTS in both E9.5 and E14.5 by 234% ($P=.011$) and 392% ($P<.001$) respectively. Prl3d1 was increased by 47% ($P=.019$) in E14.5 compared to E9.5. **b)** Prl3b1 protein concentration was significantly lower in mTS cells than E14.5 mouse placenta ($P<.001$). Prl3b1 protein concentration was 206% higher ($<.001$) in E14.5 compared to E9.5. All samples were WT. mTS ($n = 5$), E9.5 ($n = 14$) and E14.5 ($n = 14$). Error bars represent \pm SEM. Statistical significance calculated using a two-way ANOVA with Šidák correction. $^{ns}P>.05$, $^*P<.05$, and $^{**}P<.01$ $^{***}P<.001$ $^{****}P<.0001$ (Appendix 25).

All samples used were WT. Prl3d1 was significantly higher than mTS in both E9.5 and E14.5 by 234% ($P=.011$) and 392% ($P<.001$) respectively and Prl3d1 was increased by 47% ($P=.019$) in E14.5 compared to E9.5. Prl3b1 protein concentration was significantly lower in mTS cells than E14.5 mouse placenta ($P<.001$). Prl3b1 protein concentration was 206% higher ($<.001$) in E14.5 compared to E9.5. The overall concentrations of

Pr13b1 protein were much higher than Pr13d1. Pr13b1 protein was detected in 10 day differentiated mTS cells.

5.3.1.4 Mouse trophoblast stem cell differentiation

After analysis of genotype and trophoblast stem cell validity, at least four mTS lines per genotype were selected to be assessed via the differentiation protocol in section 2.8.3. These were run in duplicate. At two-day intervals these were imaged on a bright field microscope to monitor their proliferation and differentiation status.

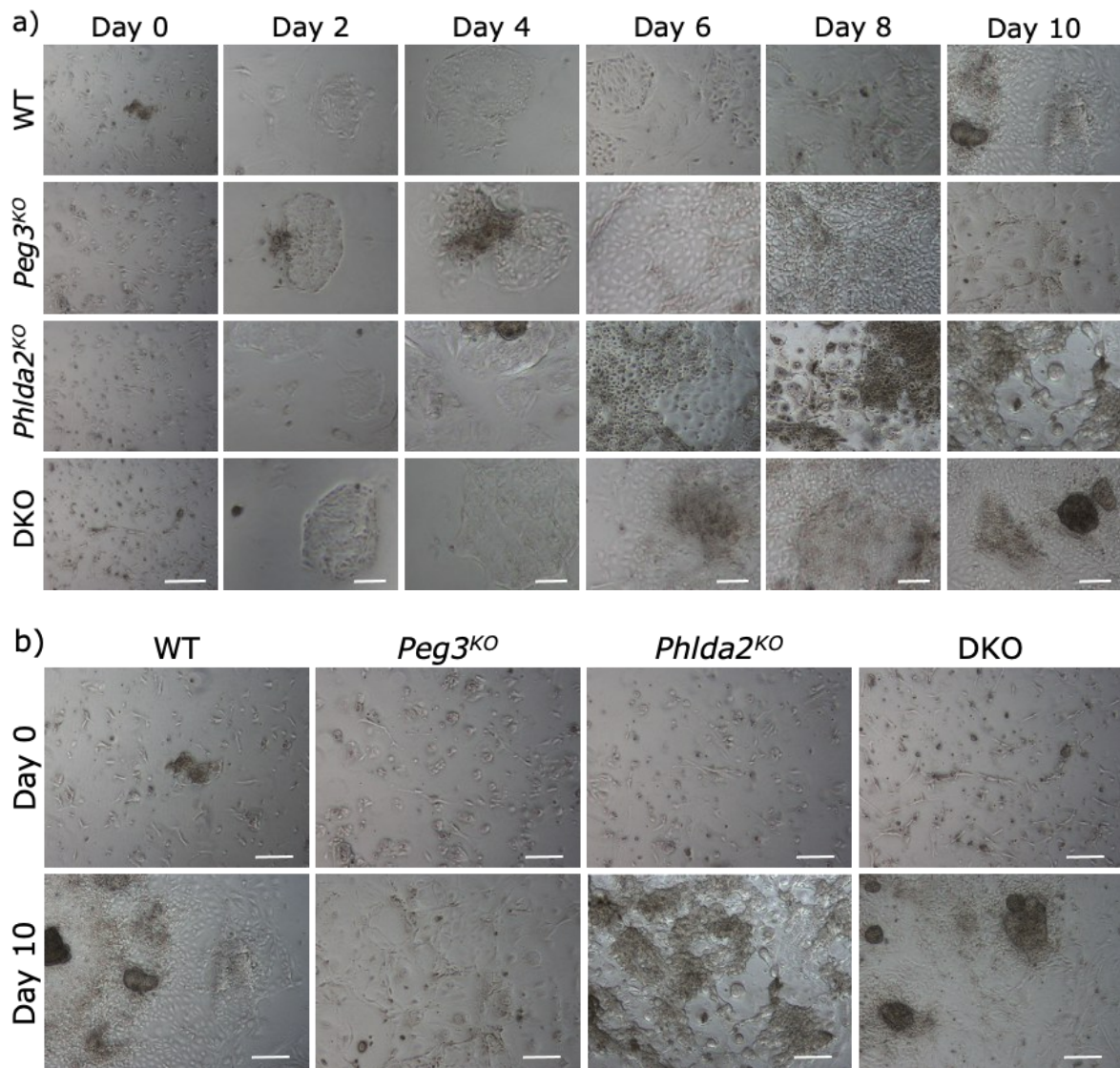


Figure 60: Representative images of differentiation trial for WT, Peg3^{KO}, Phlda2^{KO} and DKO mouse trophoblast stem cells.

Images taken at two-day intervals of a 10-day differentiation trial. **a)** Day 0 scale bar = 1000 μ m, Day 2-10 scale bar 100 μ m. **b)** Day 0 and day 10 wide shot images. Scale bar = 500 μ m.

Cells grew from colonies into confluent plates with varying phenotypes. There was no distinct phenotype per genotype. The phenotype was representative of the health of the line more than the genotype. The health of the line was determined by a variety of cell culture characteristics such as growth patterns, morphological changes, percentage of live cells, unexpected differentiations and high cell death. The presence of 'healthy' and 'unhealthy' cell lines was distributed evenly across the genotypes.

5.3.1.5 Mouse trophoblast stem cell proliferation

Over a 10-day differentiation trial cells were counted every two days to determine if their genotype had an impact on their ability to proliferate.

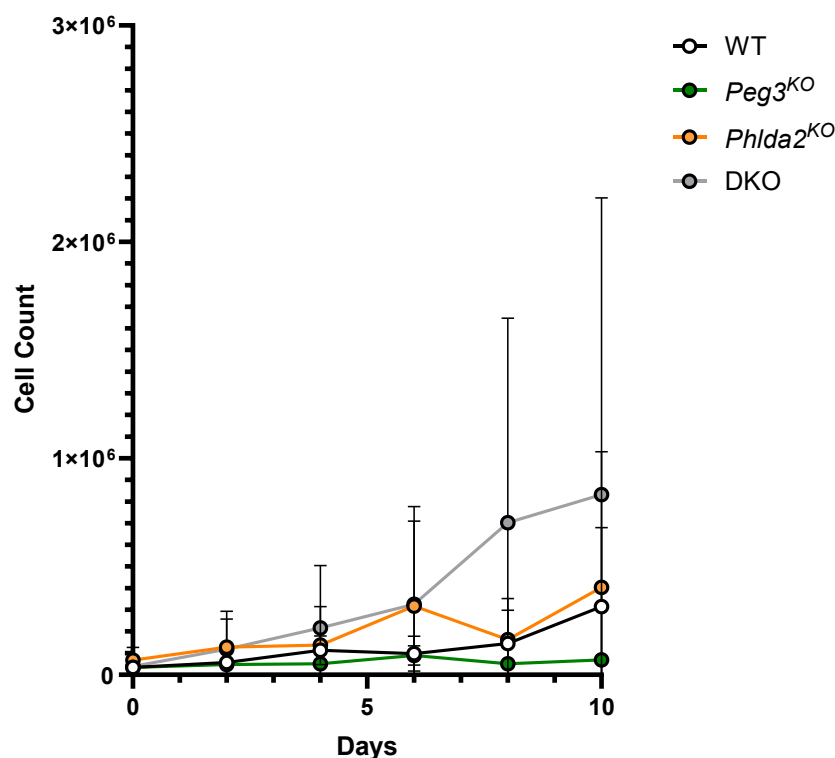


Figure 61: Proliferation assay of WT, *Peg3*^{KO}, *Phlda2*^{KO} and DKO mouse trophoblast stem cells.

No significant difference between genotypes for cell counts on days 0-10. Error bars represent standard error of the mean (SEM). WT ($n = 10$), *Peg3*^{KO} ($n = 10$), *Phlda2*^{KO} ($n = 8$), DKO ($n = 10$). Statistical significance calculated using a two-way ANOVA with Šidák correction. ^{NS} $P > .05$, $*P < .05$, and $**P < .01$ $***P < .001$ $****P < .0001$ (Appendix 26).

There was no significant impact on proliferation for any of the genotypes.

5.3.1.6 Mouse trophoblast stem cell qRT-PCR

Two independent mouse TS cell lines of each of the genotypes were differentiated for 10 days in duplicate (protocol 2.8.3). The differentiated cells were converted into cDNA libraries (protocol 2.10.1 to 2.10.3) and analysed via qRT-PCR (protocol 2.10.4) for the knockout targets, mouse trophoblast lineage markers, imprinted genes and Prl family members.

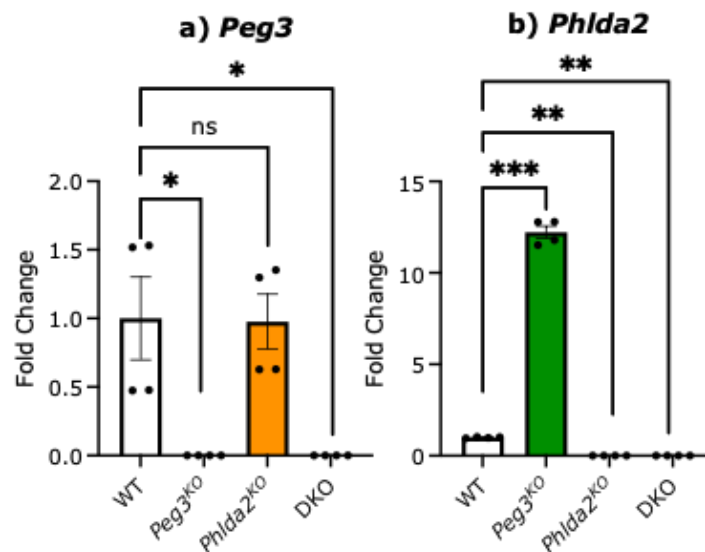


Figure 62: Knockout targets *Peg3* and *Phlda2* RNA expression in WT, *Peg3*^{KO}, *Phlda2*^{KO} and DKO in 10-day differentiated mTS cells. a) *Peg3* expression was successfully knocked out in both *Peg3*^{KO} ($P=.013$) and DKO ($P=.013$). b) *Phlda2* expression was successfully knocked out in both *Phlda2*^{KO} ($P=.007$) and DKO ($P=.007$). *Phlda2* expression was increased by 1122% in *Peg3*^{KO} ($P<.001$). Error bars represent \pm SEM. WT ($n = 4$), *Peg3*^{KO} ($n = 4$), *Phlda2*^{KO} ($n = 4$), DKO ($n = 4$). Statistical significance calculated using a two-way ANOVA with Šidák correction. ^{ns} $P>.05$, * $P<.05$, and ** $P<.01$ * $P<.001$ **** $P<.0001$ (Appendix 27).**

The expression of *Peg3* was successfully knocked out in both *Peg3*^{KO} ($P=.013$) and DKO ($P=.013$) 10-day differentiated mTS cells. The expression of *Peg3* was not significantly different from WT in *Phlda2*^{KO} differentiated mTS cells. *Phlda2* expression was successfully knocked out in both *Phlda2*^{KO} ($P=.007$) and DKO ($P=.007$) differentiated mTS cells. The expression of *Phlda2* was increased by 1122% ($P<.001$) in *Peg3*^{KO} differentiated mTS cells.

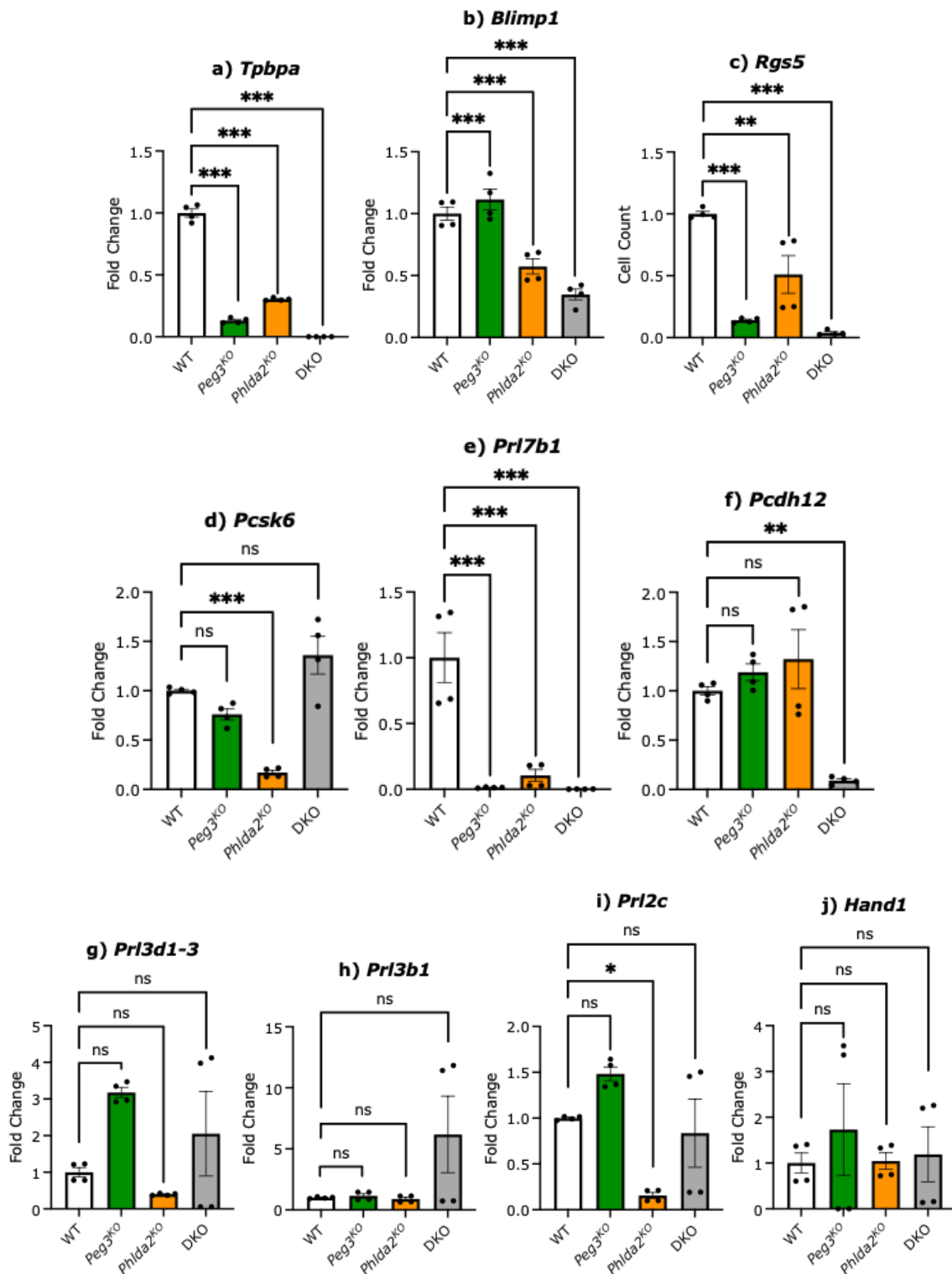


Figure 63: qRT-PCR of 10-day differentiated WT, *Peg3*^{KO}, *Phlda2*^{KO} and DKO mouse trophoblast stem cells.

a) *Tpbpa* expression was reduced in *Peg3*^{KO} by 87% ($P < .001$), *Phlda2*^{KO} by 70% ($P < .001$) and DKO by 99% ($P < .001$). **b)** *Blimp1* expression was increased in *Peg3*^{KO} by 11% ($P < .001$) and decreased in *Phlda2*^{KO} by 43% ($P < .001$) and DKO by 65% ($P < .001$). **c)** *Rgs5* expression was reduced in *Peg3*^{KO} by 86% ($P < .001$), in *Phlda2*^{KO} by 49% ($P = .004$) and in DKO by 96% ($P < .001$). **d)** *Pcsk6* expression was reduced by 83% in *Phlda2*^{KO}. **e)**

Prl7b1 expression was reduced by 99% in *Peg3^{KO}* ($P < .001$), 89% in *Phlda2^{KO}* ($P < .001$), and 99% in DKO ($P < .001$). **f)** *Pcdh12* expression is reduced by 91% in DKO. **g)** There was no significant difference for any transgenic group in *Prl3d1-3* expression. **h)** There was no significant difference for any transgenic group in *Prl3b1* expression. **i)** *Prl2c* expression is reduced by 84% in *Phlda2^{KO}*. **j)** There was no significant difference for any transgenic group in *Hand1* expression. Error bars represent \pm SEM. WT ($n = 4$), *Peg3^{KO}* ($n = 4$), *Phlda2^{KO}* ($n = 4$), DKO ($n = 4$). Statistical significance calculated using a two-way ANOVA with Šidák correction. ^{ns} $P > .05$, $*P < .05$, and $**P < .01$ $***P < .001$ $****P < .0001$ (Appendix 28).

In 10-day differentiated mTS cells, *Tpbpa* expression was reduced in *Peg3^{KO}* by 87% ($P < .001$), *Phlda2^{KO}* by 70% ($P < .001$) and DKO by 99% ($P < .001$). *Blimp1* expression was increased in *Peg3^{KO}* by 11% ($P < .001$) and decreased in *Phlda2^{KO}* and DKO by 43% ($P < .001$) and 65% ($P < .001$) respectively. *Rgs5* expression was reduced in *Peg3^{KO}* by 86% ($P < .001$), in *Phlda2^{KO}* by 49% ($P = .004$) and in DKO by 96% ($P < .001$). *Pcks6* expression was reduced by 83% in *Phlda2^{KO}*. *Prl7b1* expression was reduced by 99% in *Peg3^{KO}* ($P < .001$), 89% in *Phlda2^{KO}* ($P < .001$), and 99% in DKO ($P < .001$). *Pcdh12* expression is reduced by 91% in DKO and *Prl2c* expression is reduced by 84% in *Phlda2^{KO}* ($P < .001$). There was no significant difference for any transgenic group in *Prl3d1-3*, *Prl3b1* or *Hand1* expression.

5.3.2 Human trophoblast stem cells

Human trophoblast stem cell skills were learnt through a collaboration with Professor Hiroaki Okae at Kumamoto University in Japan. After gaining a place in a research internship program at the Institute of Molecular Embryology and Genetics, I underwent a training program which covered all fundamental protocols for hTS cell culture including CRISPR design, transfection and establishing single cell lines (protocol section 2.9).

5.3.2.1 Human CRISPR designs

The hTS cells used in this experiment were derived from CT cells as detailed in Professor Okae's 2018 paper, "Derivation of human trophoblast stem cells" (Okae, 2018). These lines were referred to as CT lines. All cell lines were female, as this was the standard methodology of the laboratory. Although once I had established a working protocol at the laboratory in Cardiff, WT male CT-hTS cells were sent with the intention to be transfected.

The base cell line was constructed with the lentivirus vector (CS-CA-MS) presented in Figure 64, a. The vector contained Cas9 and a Puro-

resistance gene which was inserted into the multiple cloning site (MCS). This generated pCS-CAG-Puro-Cas9. This resulted in Cas9 expressing hTS cells (CT27-Cas9). A hU6-sgRNA_scaffold-SV40-Neo was used to replace the CAG promoter. This generated pHU6-Neo-v2 which resulted in sgRNA expressing vectors (Figure 64, b).

The *PHLDA2*^{KO} CRISPRs were designed by Dr Asato Sekiya. Two 5' and two 3' CRISPR guide RNAs were mapped around exon one of *PHLDA2* using the web-based software tool CRISPOR.

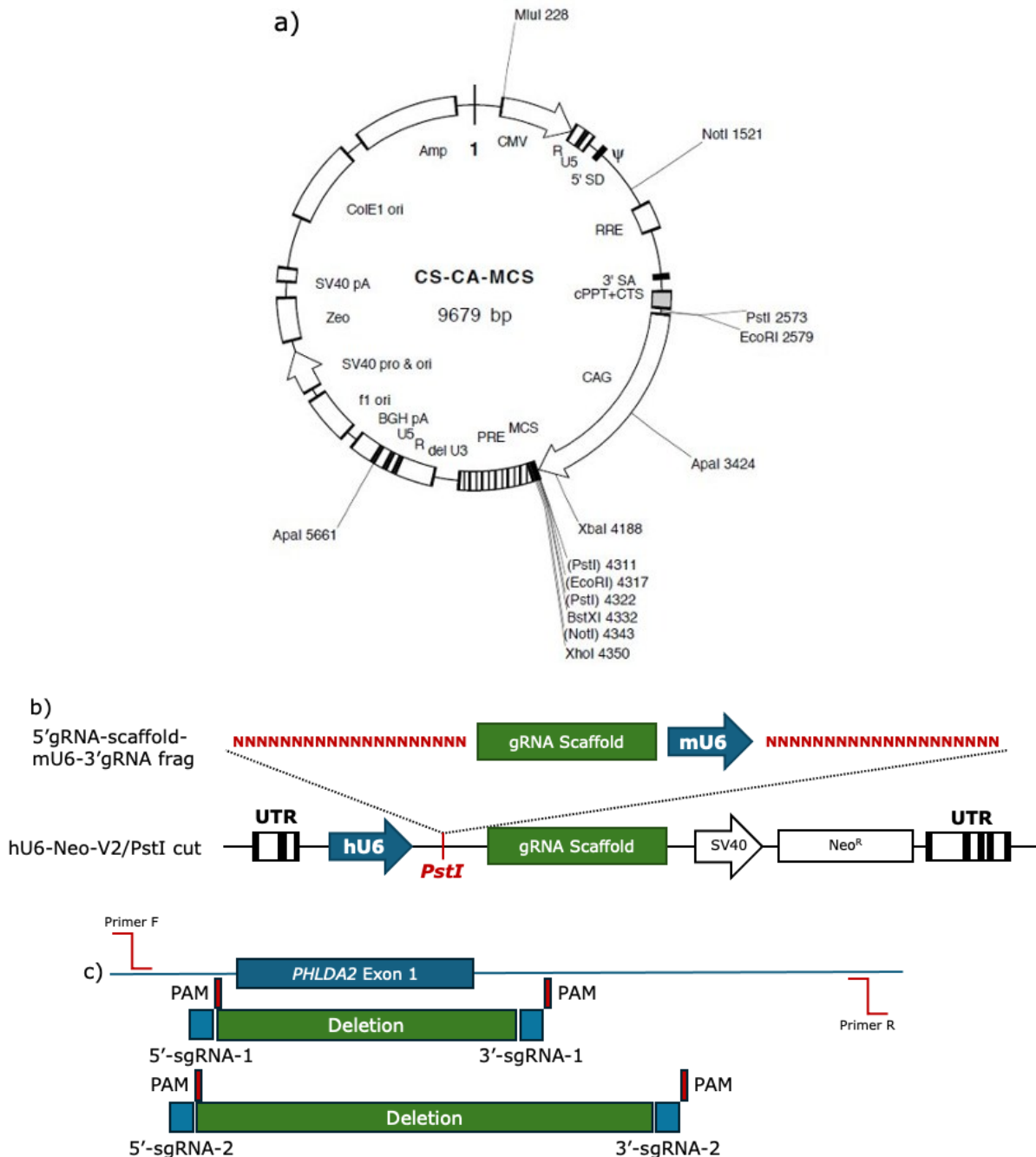


Figure 64: *PHLDA2* CRISPR design and trophoblast stem cell line knockouts.

a) Lentivirus vector (CS-CA-MSC). **b)** Lentivirus modification using hU6-sgRNA_scaffold-SV40-Neo-v2. **c)** PHLDA2 NM_00311.4 sequence with 5' (1 and 2) and 3' (1 and 2) guide RNAs targeting exon one of PHLDA2. Knockout confirmation primer locations identified with Primer F and Primer R.

The *PEG3*^{KO} CRISPR sgRNAs were designed under the guidance of Professor Nicholas Allen. These were designed to target Exon 5 of *PEG3*.

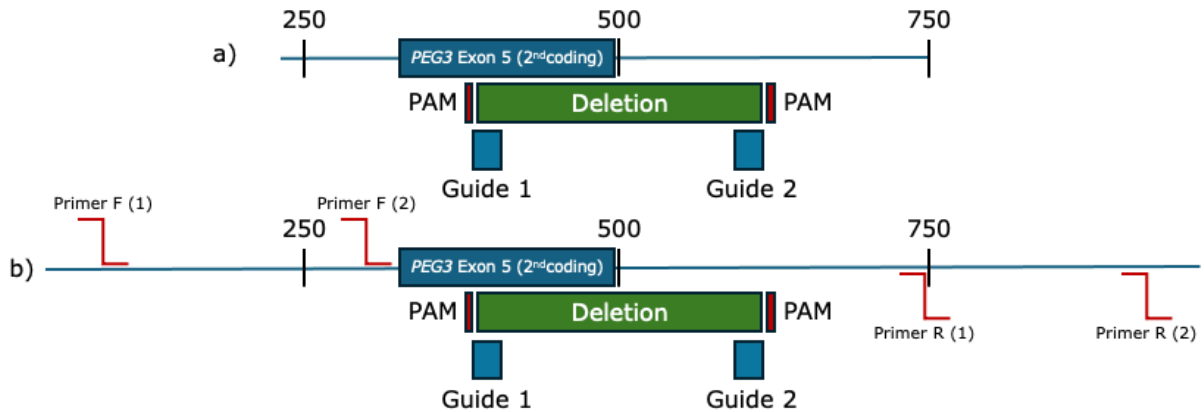


Figure 65: *PEG3* CRISPR design.

a) *PEG3* NM_006210.3 sequence with sgRNA target locations (Guide 1 and Guide 2 (and protospacer adjacent motifs (PAM)) functionally disabling *PEG3* by cutting exon five. **b)** Knockout confirmation primer locations identified with Primer F (1), Primer R (1), Primer F (2) and Primer R (2).

5.3.2.2 Human trophoblast stem cell knockout attempts

5.3.2.2.1 Human trophoblast stem knockout: *PHLDA2*^{KO}

All combination of *PHLDA2*^{KO} CRISPR guide RNA sequences were used to transfect four hTS cell populations. The knockout was validated using the knockout confirmation primers detailed in Table 27 and the genotyping method described in 2.2. All four sgRNA combinations successfully produced the *PHLDA2* knockout (Figure 66).

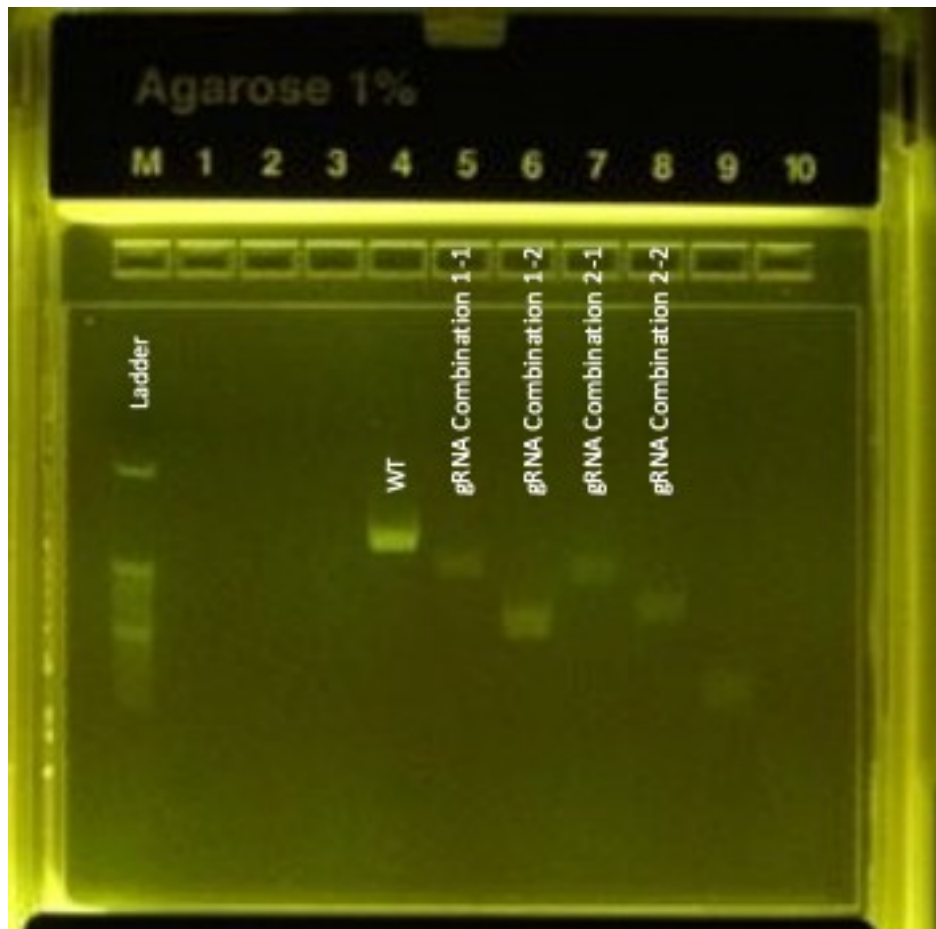


Figure 66: Gel confirmation of *PHLDA2*^{KO} results for four combinations of gRNAs.

All lines were frozen in bulk to be used for single cell cloning. The sgRNA combination 1-1 was selected for single cell cloning (protocol 2.9.6). Once clones had formed healthy populations they were genotyped (protocol 2.2) (Figure 67).

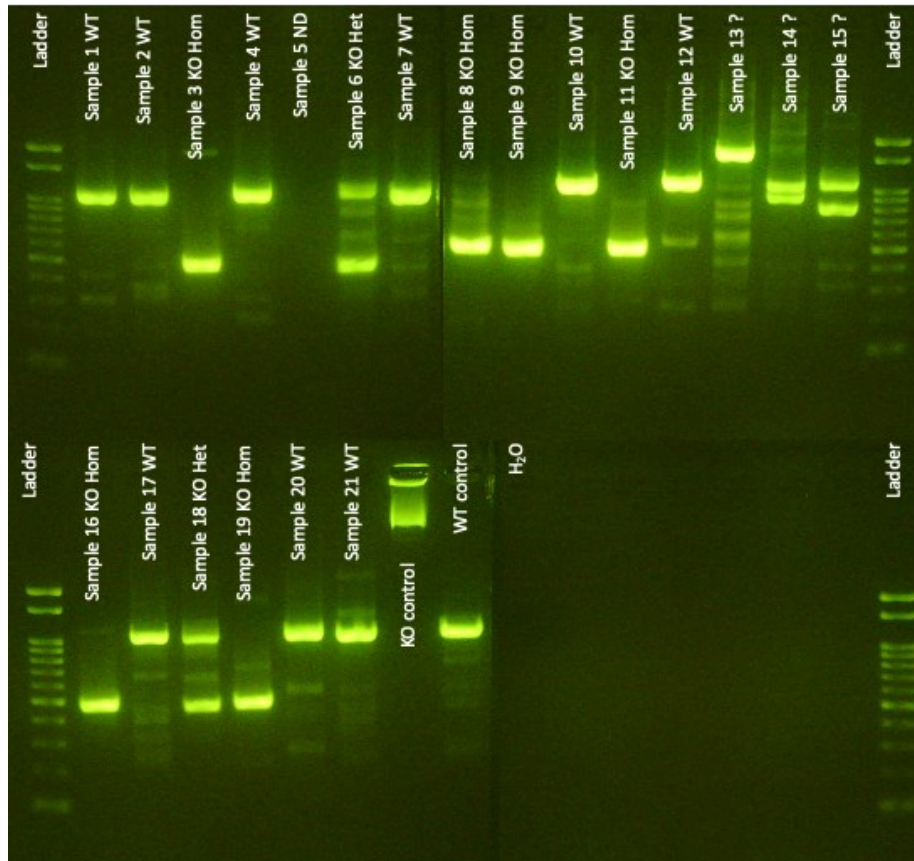


Figure 67: Genotype results of single cell colonies after *PHLDA2*^{KO} sgRNA combination 1-1.

The cell lines CT27_PHLDA2KO_3 (Homozygous), CT27_PHLDA2KO_8 (Homozygous), CT27_PHLDA2KO_9 (Homozygous), CT27_PHLDA2KO_16 (Homozygous) and CT27_PHLDA2KO_6 (Heterozygous) were selected to be grown up and banked. These were then sent to Cardiff University for follow up experiments. The bulk stocks of the other sgRNA combinations were also sent, along with five different strains of “empty”/WT lines, which contained no sgRNA sequences.

PHLDA2^{KO} was also performed on male hTS cells but was unsuccessful at establishing the knockout.

5.3.2.2.2 Human trophoblast stem knockout: *PEG3*^{KO}

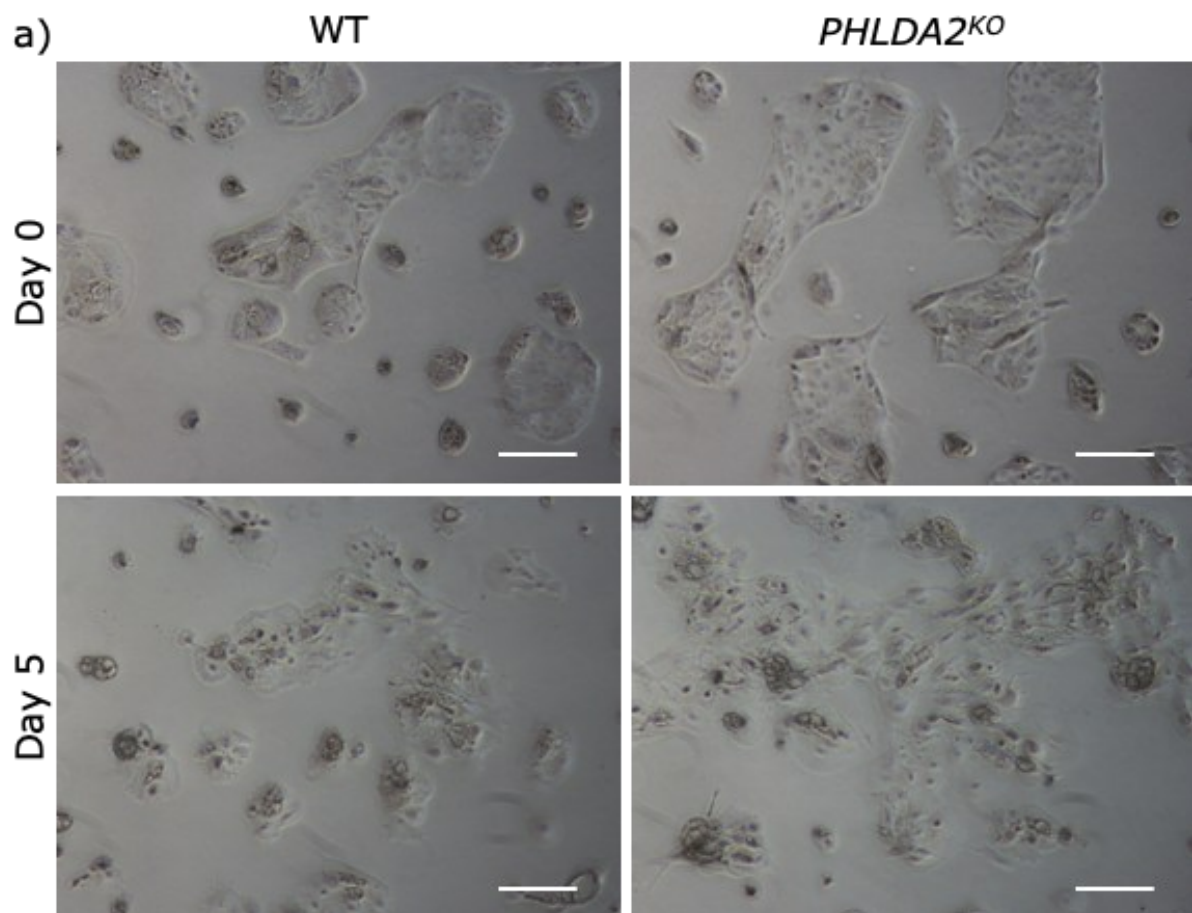
Despite multiple attempts using FACs sorting, single cell cloning by dilution and colony picking, only one line was produced that contained the *PEG3*^{KO} and this was only a heterozygous knockout. In multiple follow up attempts which included male hTS cells, several independent *PEG3*^{KO} lines were generated and were all heterozygous (Unpublished data, John 2025). To date no homozygous *PEG3*^{KO}s have been generated in hTS cells in either sex.

5.3.2.2.3 Human trophoblast stem cell: Double knockout

Attempts were also made to produce a double knockout by transfecting already existing *PHLDA2*^{KO} lines with *PEG3*^{KO} CRISPR sgRNAs. Despite multiple attempts no double knockout was established.

5.3.2.3 Human trophoblast stem differentiation

Human trophoblast stem cells were differentiated using the protocol described in 2.9.7. A representative image for WT and *PHLDA2*^{KO} lines is presented in Figure 68.



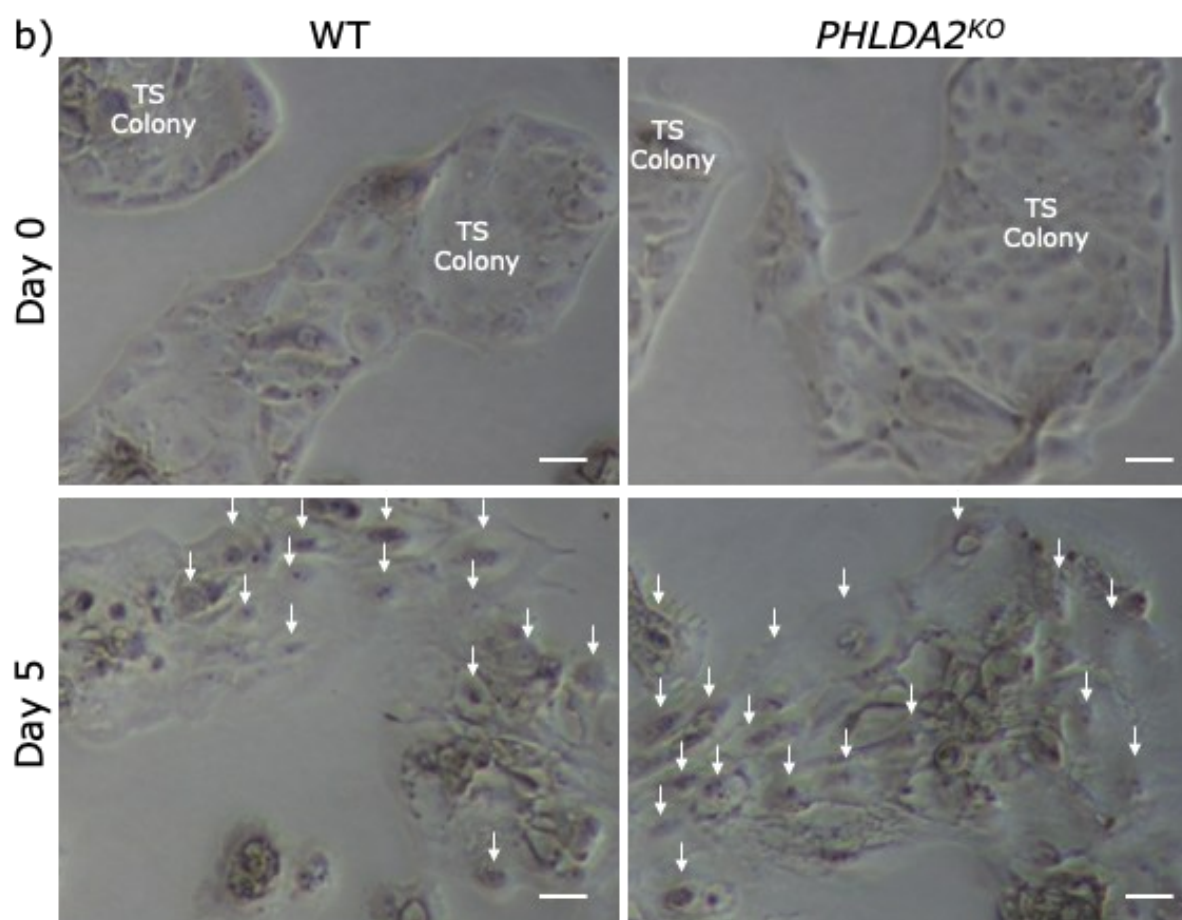


Figure 68: Representative images of differentiation trial of WT and *PHLDA2^{KO}* hTS cells.

a) Images taken at day 0 and day 5 of a differentiation trial. Scale bar = 1000 μm . **b)** Area of interest of day 0 and day 5 differentiation trial images. White arrows indicate syncytiotrophoblast cells. Trophoblast stem cell colonies are labelled. Scale bar = 200 μm .

The health of the established hTS cell lines was high and replicable. Both WT and *PHLDA2^{KO}* genotypes grew from TS colonies and differentiated into syncytiotrophoblast cells.

5.3.2.4 Human trophoblast stem Western blot analysis

Protein was extracted from two WT and two independently derived *PHLDA2^{KO}* hTS cell lines using the protocol described in 2.11. The protein samples were then run through the western blotting protocol described in 2.13 and stained with the antibodies detailed in Table 35.

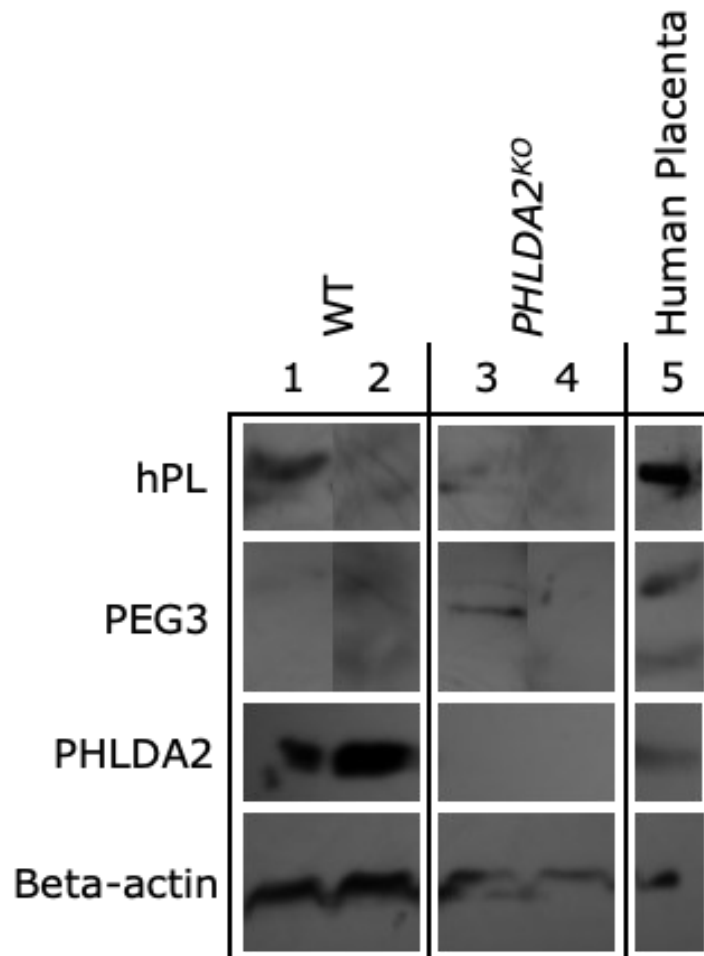


Figure 69: Western blot analysis of differentiated WT and *PHLDA2*^{KO} hTS cells.

Protein expression of Beta-actin, PHLDA2, PEG3 and hPL for WT and PHLDA2KO lines using a Human placental sample as a control.

With comparable concentrations of Beta-actin, the PHLDA2 protein was cleanly knocked out of the *PHLDA2*^{KO} hTS cells compared to WT in which the expression was strong compared to the human placenta control. Isolation of PEG3 using western was difficult due to its nuclear location but was identified in human placenta controls and *PHLDA2*^{KO} hTS cells. The presence of hPL in five day differentiated hTS cells was thought to be unlikely. With strong expression in human placenta, one differentiated WT hTS sample did produce a clear signal, validating the assay. However, this was not demonstrated by the other three tested hTS cells.

5.3.2.5 Human trophoblast stem cell qRT-PCR

Two independent strains of both WT and *PHLDA2*^{KO} hTS cells were differentiated for five days in duplicate following the protocol outlined in 2.9.7. RNA was extracted and converted into cDNA libraries (protocols

2.10.1 and 2.10.3). The cDNA libraries were then analysed via qRT-PCR (protocol 2.10.4).

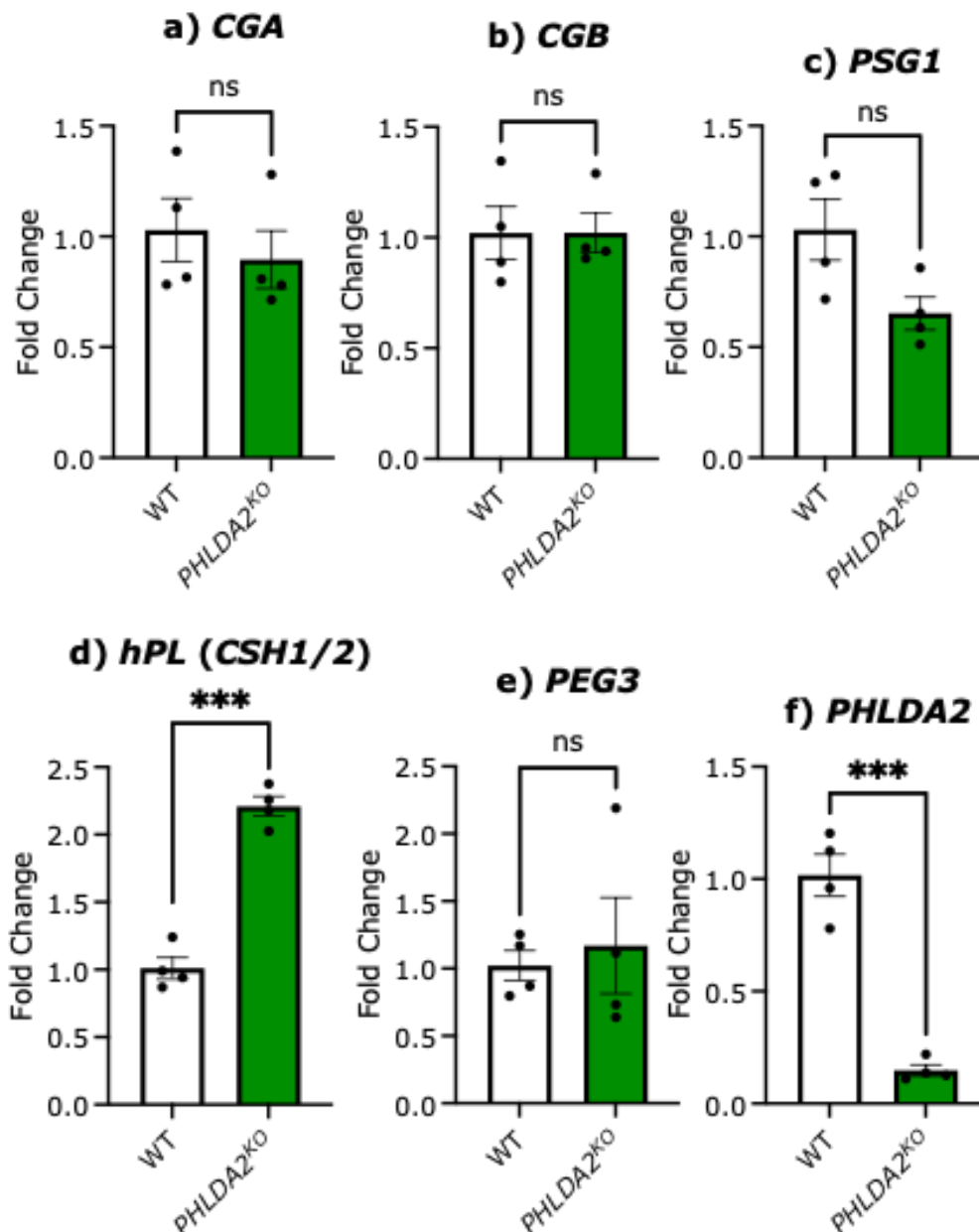


Figure 70: qRT-PCR of five day differentiated WT and *PHLDA2*^{KO} and hTS cells.

a) *CGA* expression was not significantly altered in *PHLDA2*^{KO}. **b)** *CGB* expression was not significantly altered in *PHLDA2*^{KO}. **c)** *PSG1* expression was not significantly altered in *PHLDA2*^{KO}. **d)** *hPL* expression was increased by 119% in *PHLDA2*^{KO}. **e)** *PEG3* expression was not significantly altered in *PHLDA2*^{KO}. **f)** *PHLDA2* expression was decreased by 85% in *PHLDA2*^{KO}. Error bars represent ±SEM. WT ($n = 4$), *PHLDA2*^{KO} ($n = 4$). Statistical significance calculated using a two-way ANOVA with Šidák correction. ^{ns} $P > .05$, * $P < .05$, and ** $P < .01$ *** $P < .001$ **** $P < .0001$ (Appendix 29).

The expression of *PHLDA2* was significantly decreased in *PHLDA2^{KO}* hTS cells compared to WT demonstrating the success of the *PHLDA2* targeting. The expression of *CGA*, *CGB*, *PSG1* and *PEG3* was not significantly altered in five day differentiated *PHLDA2^{KO}* hTS cells. However, hPL expression was significantly increased by 119% ($P < .001$) in five day differentiated *PHLDA2^{KO}* hTS cells.

5.4 Discussion

5.4.1 Mouse TS cells

5.4.1.1 Challenges in *Peg3^{KO}* mouse strain fertility and mouse trophoblast stem cells derivation: Impacts on experimental design

There were significant hurdles in producing the number of cell lines needed for a complete set of the genotypes required to perform the desired experiments. The 129-mouse strain used does demonstrate issues with fertility already, with significantly increased unfertilised eggs and reduced litter sizes compared to BL6 strain mice (Hino et al., 2009). In addition, although not previously documented in mice, abnormal DNA methylation of human *PEG3* has been associated with low sperm motility and severely impaired sperm DNA integrity in males suffering from fertility issues (Song et al., 2022). Furthermore, in mice, *Peg3^{KO}* males have demonstrated a disrupted olfactory system which prevents them from developing a preference for oestrous odours, resulting in a decrease in male mating behaviour (Swaney et al., 2008).

Although not the focus of this study and without statistically powered evidence, the *Peg3^{KO}* mouse strain used in this thesis indicated impairment of both mating behaviour and fertility. The *Peg3^{KO}* males only plugged 38% of females which is reduced when comparing that to a 100% plugging rate in trials conducted on the 129 WT strain (Hino et al., 2009) suggesting their mating behaviour was impacted by the knockout. The *Peg3^{KO}* strain also had a 62% false positive rate for pregnant females, whereas WT 129s have a 50% false positive rate (Hino et al., 2009) and WT C57BL/6J mice have a 37% false-positive rate (Heyne et al., 2015). This false positive pregnancy data suggests that the impact on fertility for the *Peg3^{KO}* line is 12% for the genotype alone in addition to the already impaired 129 background. The idea was posed to attempt the experiment with a maternally derived *Peg3^{KO}* stud but anecdotally this did not resolve the issue.

Of the 154 females super-ovulated in this thesis, 132 of them did not produce any blastocysts, leaving just 22 females (14%) to produce all of

the material required to begin deriving the lines. Although this study was not designed to determine the fertility of this strain and therefore does not have statistical evidence to conclusively prove that theory, it would be reasonable to suggest that, as this is a genetic mutation that impacts placental development, it could influence fertility generally, impacting blastocyst generation, resulting in low blastocyst numbers.

Beginning the derivation process with very little material (low blastocyst numbers) immediately hindered the capability to produce all the required genotypes of both sexes. Papers using the mTS cell derivation method used in this thesis, or similar methods, do not often provide derivation statistics, making it difficult to know if the conversion yields were lower than expected. In a paper investigating additive compositions, from the additives used in Santoshi's protocol, the TS cell line conversion rates were 100%, 42% and 56% for 129xBL6, CD1xCD1, and CD1xBL6 matings respectively (Ohinata & Tsukiyama, 2014), whereas the experiments conducted in this thesis had a conversion rate of 19%.

The successful mouse trophoblast stem cell lines had a bias towards males with 70% of them being male. This could imply that there is an inherent stability in male trophoblast stem cells which allowed them to more easily be derived. This does not appear in the literature although sex of cell lines, like sex specific phenotypes of other structures has only recently been discussed and has not been explored for trophoblast stem cells specifically. Sex specific analysis of WT trophoblast stem cells would be an interesting avenue for future research.

Although it is possible that the potential fertility issues impacting these mouse strains could be influencing the viability of the blastocysts themselves, further impacting the derivation process, it is likely there was also an issue with the protocol. For example, mTS derivation has poorly defined cell culture conditions due to the necessity of FBS use, although a high quality FBS product was used, there is the potential that this could have produced suboptimal culture conditions. In addition, the protocol used was from 2006. There was hesitation to move away from this method as it was previously used in this laboratory and was successful in an attempt in 2010. This limited the modifications to the methodology to alterations in additive concentrations, additive storage conditions and additive preparation protocols, more stringent care around MEFs and production of conditioned media. During the project, a laboratory became available that was otherwise unoccupied, as the shared laboratory was a potential threat to the consistency of the protocol conditions, the experiments were moved to the newly available laboratory. The move into the new laboratory did allow for some success in derivation. In March of 2024 a well-defined protocol for the generation of knockout mouse models using CRISPR cas9 technology of an already established mTS line

was published (Doria-Borrell et al., 2024). This method would help resolve some of the issues around fertility and mTS cell derivation seen in this thesis. Regardless, after two intensive years of derivation attempts and the successful derivation of only 33 mTS lines, it was decided to attempt the analysis of the cells without the desired four genotypes, in duplicate, in each sex.

5.4.1.2 Mouse trophoblast stem cell validation: Implications on experimental outcomes

There was an inconsistent expression of mouse trophoblast stem cell markers over the cell lines produced, although they were consistent in their morphology and growth patterns. From the successfully derived lines, 74% expressed *Cdx2*, 53% expressed *Esrrb* and only 37% expressed *Eomes*, with 26% of all lines expressing all three. *Cdx2* is a transcriptional regulator that is essential in the early stages of the trophoblast lineage (Tolkunova et al., 2006) and is routinely used as a trophoblast stem cell marker (Gao et al., 2024). *Esrrb* is a transcription factor that maintains the pluripotency of trophoblast stem cells. It targets *Sox2*, *Fgfr2*, *Bmp4*, *Eomes* and *Cdx2* (Gao et al., 2019). The reduction of *Esrrb* expression is a marker of differentiation in TS cells, however, doesn't necessarily invalidate the cell lines for experimental use. *Eomes* also operates as an indicator of pluripotency (Latos & Hemberger, 2016). *Cdx2* expression was used to validate each mTS cell line, and the *Esrrb* and *Eomes* expression ranked each cell line on their degree of pluripotency, the most pluripotent being the fittest for analysis.

In the RNA analysis of the differentiated mTS cells, 31% expressed *Prl3b1* and 74% expressed *Prl3d1*. There were no lines which expressed only *Prl3b1* whereas 43% of mTS cell lines only expressed *Prl3d1*. Finally, 32% of cells expressed both *Prl3b1* and *Prl3d1*. None of these expression patterns were correlated with any of the mTS cell markers. The expression of *Prl3b1* was low and the *Prl3d1* expression was higher. In the context of the experiments conducted for this thesis, *Prl3b1* and *Prl3d1* were not good markers for mTS cells as the genotypes studied have the potential to alter each cell lines capacity to express them. However, they could be used to map the differentiation status of the cell lines to the developmental timeframe *in vivo*.

There is an unknown discrepancy between *in vivo* and *in vitro* developmental time frames. Most differentiation assays state that mTS cells are completely differentiated between day four and day six (Gao et al., 2024; Ullah et al., 2020). However, the genotypes within this project could alter the timeframes of differentiation *in vitro*, therefore a 10-day differentiation protocol was used. The surrounding tissue *in vivo*

influences the differentiation of the trophoblast stem cells, something that *in vitro* trials cannot replicate. Organoid culture attempts to answer some of these questions but raises other questions in its place, as the mTS cells organoid culture protocol is still being developed, and is reportedly still unreliable, it was not used for these experiments. As described in Chapter 1 (1.5), *Pr13d1* spikes during mid-gestation whereas *Pr13b1* is expressed in the second half of mouse pregnancy. In the ELISA analysis of differentiated mTS cells, the *Pr13b1* protein levels were lower than the detectable level, whereas *Pr13d1* was most similar to the E9.5 sample. The RNA expression data (Figure 49) coupled with the protein analysis done by ELISA (Figure 59) suggests that the 10-day differentiated mTS cells are most similar to a mid-gestation time point.

5.4.1.3 Consistent morphology and proliferation across mouse trophoblast stem cell proliferation assay

The mTS differentiation trials demonstrated the morphology and proliferation was consistent within each cell line and not distinct to a certain genotype. Each cell line was run through the trial in duplicate at least one time but most lines were run in duplicate multiple times. Each individual line was highly replicable in its morphology and growth rate. The genotype had no impact on the cell lines proliferation potential, this result is replicated in a knockdown model of *Phlda2* which showed no impact on cell proliferation (Takao et al., 2012).

5.4.1.4 Complex response to transgenic modifications in mouse trophoblast stem cells: Evaluating cell type and lineage marker expression

The qRT-PCR results for the day-10 differentiated mTS cells present a complex response to the transgenic modifications. To detail these, the presence of any knockout significantly reduced the spongiotrophoblast marker *Tpbpa* and there was no detection of *Tpbpa* in DKO mTS cells. For the SpA-TG cell and decidua marker, *Blimp1*, *Peg3^{KO}* was significantly elevated to WT where both *Phlda2^{KO}* and DKO were significantly reduced. For the SpA-TG cell and decidua marker, *Rgs5*, all knockouts were significantly reduced, with a greater impact on *Peg3^{KO}* and DKO. For the SpA-TG cell and decidua marker, *Pcsk6*, only *Phlda2^{KO}* was significantly reduced. The TS cell marker *Pr17b1* was significantly reduced in all knockouts. The glycogen cell marker *Pcdh12* was reduced in only the DKO samples. The expression of *Pr13d1* was present in all samples, with only a significant difference seen between *Peg3^{KO}* and *Phlda2^{KO}*. The expression of *Pr13b1* was consistent for WT, *Peg3^{KO}* and *Phlda2^{KO}*. However, the expression of *Pr13b1* in DKO was varied between the two cell lines tested, suggesting a varied response to the transgenic modification for each line.

For the Ch-TG cell and P-TG cell marker *Prl2c*, the only significance seen was between *Peg3^{KO}* and *Phlda2^{KO}*. The TG cell marker *Hand1* was not affected by transgene. This result correlates with the E16.5 counting data in Chapter 4: section 4.3.4 which suggests that TG cell number is not affected by these transgenic modifications.

Among the varied alterations in different TG cell types, the most interesting results are the *Tpbpa*, *Prl3b1* and *Prl3d1* results. The reduction in the spongiotrophoblast marker *Tpbpa* suggests that any knockout combination impairs the cell line's ability to produce the spongiotrophoblast lineage. It was hypothesised that the *Peg3^{KO}* cell line may have such a phenotype, as seen in Tunster et al. (2018) qRT-PCR analysis of E16.5 *Peg3^{KO}* placentas which demonstrated a reduction in *Tpbpa* expression. However, it was not expected from the *Phlda2^{KO}* cell line as an increase in *Tpbpa* was found in *Phlda2^{KO}* E16.5 placentas (Tunster, Creeth, et al., 2016). The detection of *Tpbpa* was within an optimal range for qRT-PCR amplification, meaning the analysis is robust. A difference between placenta samples and mTS cells could be a factor in this discrepancy. However, in a previous study on a mTS cell lines with decreased *Phlda2* expression, an increase in *Tpbpa* expression was demonstrated (Takao et al., 2012). The cell lines used in the Takao et al. 2012 study differed from the cell lines in this thesis in notable ways. The 2012 cell lines were knockdown cell lines which were derived by a small interfering RNA (siRNA) transfected into an already established mTS line supplied by Professor Satoshi Tanaka. A siRNA knockdown may have better efficacy in an imprinted gene transgenic model as it does not rely on the effectiveness of the imprinting mechanism and simply reduces the RNA levels of the target, producing a clearer reduction in the target. The 2012 paper reports a 70% decrease in *Phlda2* expression which will function independently of any other regulation of the imprinting mechanism, giving a consistent reduction over all developmental timeframes. The mTS lines supplied by Professor Satoshi Tanaka were thoroughly validated and robust, which avoids complications in their stability of pluripotency and basic cell culture maintenance. The 2012 paper also performed an eight-day differentiation and found the highest expression of *Phlda2* between days two and four, which would not have been identified in the analysis of the day-10 differentiated cells in this thesis.

The *Prl3b1* and *Prl3d1* expression patterns tell an interesting story around the cell lines response to the transgenic modifications. For both targets, there is an opposite effect from the two DKO cell lines analysed, one cell line having an increased expression compared to WT and the other having a similar or even reduced expression to WT. This data suggests that the response to the DKO is not consistent in this context. The reduced *Phlda2*

model in the Takao et al. 2012 paper has an increase in *placental lactogen-1 (Pl1)* that is synchronised with its reported increase in *Tpbpa* (Takao et al., 2012). This correlation is again not observed in the mTS models presented here.

Analysis of the knockout targets themselves demonstrate that the knockout of *Peg3* was successful in both *Peg3^{KO}* and DKO lines at this differentiation timepoint. It also suggests the removal of *Phlda2* does not influence *Peg3* expression as WT and *Phlda2^{KO}* cell lines had a similar expression level of *Peg3* at this time point. *Phlda2* expression shows the opposite story. Both *Phlda2^{KO}* and DKO cell lines have a successful knockout of *Phlda2*. The *Peg3^{KO}* sample had a significant increase in *Phlda2* expression compared to WT, suggesting that *Peg3* may have a role in regulating *Phlda2*. Although *Peg3* is a transcription factor, it does not have any direct binding sites to *Phlda2* as detailed in Chapter 4 section 4.4.1, this suggests that there is some intermediary regulator between the two. *Peg3* regulates genes involved in placental growth and maternal-foetal resource allocation, whereas *Phlda2* suppresses trophoblast proliferation. While in opposition to each other, this result further suggests a shared pathway in placental development, again pointing to an antagonistic interaction between the two genes of interest with the additional element of *Peg3* influencing pathways that modulate *Phlda2*. If *Peg3* does regulate *Phlda2* however, it will limit the capacity for the DKO sample to correct back to a WT phenotype as the loss of that interaction will cause a more complex result than just the absence of the two genes. This result could be the cause of the DKO's inability to correct to the WT phenotype in the labyrinth for example.

As these qRT-PCR results were unexpected, discussion around their validity arose. A series of qRT-PCR assays were also performed on E9.5 and E16.5 placenta samples of the same four genotypes, with similarly complicated results. Although these assays validate the mTS qRT-PCR results seen here, these were performed by other team members and will not be presented.

An interesting data comparison is the one between RNAscope (Figure 49) and qRT-PCR (Figure 62). RNAscope is a highly sensitive and highly precise method capable of detecting single RNA molecules. Other methods such as RNA sequencing or qRT-PCR lose some of their sensitivity due to RNA loss during RNA extraction or cDNA library preparation, which would suggest that RNAscope would have a higher sensitivity to low expressing genes, potentially causing discrepancies between methodologies. However, in an assessment of the RNAscope technique itself, it was found to have a concordance with qRT-PCR of 82-100% (Atout et al., 2022). To complicate the comparison, is the proprietary nature of the RNAscope probes. Each probe's exact 20 bp target sequence is not disclosed making

it challenging to synchronise qRT-PCR or PCR primer sequences to RNAscope probes. It is possible that there are some unidentifiable discrepancies between RNAscope and qRT-PCR in this study.

A blast analysis of all qRT-PCR primers was conducted to confirm targets (Appendix 30). Although most off target reads had low expression in the placenta, avoiding off target amplification in mTS and placenta samples, there were some off target matches that may cause complicated results. Some notable off target binding was found for the *B-actin* primer, which has two off target binding sites, expressed in the placenta with nearly identical amplicon lengths. As *B-actin* is used as a reference gene this could complicate all genes of interest results as they are presented as a ratio over the reference gene. A reference gene should be designed to avoid this. Many primers were also found to bind to genes that are associated with the gene of interest, *Prlc2c* and *Prl8a8* were found to bind to other family members which ultimately does not complicate the picture in this context. However, examples of primers with off target matches of unrelated genes that are expressed at a similar level in the placenta are *Flk1*, *Gcm1*, *Pcdh12* and *Syna*. The *Prl3d1-3* primer binds to *Ap2m1* and *Sqstm1* which both have higher expression in the placenta than *Prl3d1-3* according to reads per kilobase per million reads placed (RPKM) values from NCBI (National Center for Biotechnology Information (NCBI)). Using lineage markers to identify if a lineage is expanding or contracting can be compromised by the transgene modification itself. Genetic modifications can alter expression patterns of lineage markers without altering the lineage, as the expression from the cell may be altered without altering the cell number.

In summary, there are three key hurdles to understanding these results. Firstly, the lack of data surrounding the effectiveness of the silencing of each gene of interest from its imprinted allele throughout each sample's development and in this sample's specific context, as discussed in Chapter 4: section 4.4.2 and earlier in this chapter when discussing the Takoa et al. 2012 *Phlda2* knockdown model. Further details about the expression profiles of the targets during earlier phases of mTS differentiation and placental development will help understand the profile of the imprinted alleles "leakiness". Secondly, it is possible that this picture is further complicated by whatever caused the difficulty deriving the cell lines and the validity and health of the cell lines themselves, a more suitable line supplied by Dr Satoshi Tanaka and transfected to produce each knockout would resolve this issue. Finally, the potential for RNAscope and qRT-PCR target discrepancies resulting in different expression patterns for each target in each technique. More data comparing RNAscope and qRT-PCR during the different placental development stages and mTS differentiation stages will help understanding around how these two protocols align.

5.4.2 Human TS cells

5.4.2.1 Human trophoblast stem cell knockout development: strategies for *PHLDA2* and *PEG3* CRISPR targeting

The knockout of *PHLDA2* was designed without an attempt to mimic the *Phlda2* mouse knockout model. The mouse strain model used a knockout that removed both of *Phlda2*'s exons and deleted half of its upstream CpG island. The human CRISPR removes only exon one. This was a decision made to increase the efficiency of the CRISPR primers. The mouse model was made using homologous recombination which can remove a larger section of DNA more efficiently than the CRISPR technique. Although, the CRISPR technique could achieve a large deletion, it would compromise efficiency making it more challenging to produce the cell line. The removal of the first exon does successfully impair *PHLDA2* and therefore achieves the desired goal.

The *PEG3* target was designed to most similarly replicate the knockout performed in the mouse *Peg3*^{KO} line. One issue with the *Peg3*^{KO} targeting is that *Peg3* has a closely related genomic architecture to *Zim2*. In mouse, *Zim2* and *Peg3* do not have common exons. In human, *PEG3* and *ZIM2* are both paternally expressed and maternally silenced, share exons and have the same promoter. Both *PEG3* and *ZIM2* have 15 exons (National Center for Biotechnology Information (NCBI)), there are 4 exons which are unique to *ZIM2* and 2 exons which are unique to *PEG3*, which are connected by alternative splicing events of their shared 5' exon (Alliance of Genome Resources, 2024). The shared exons include the one that was targeted by Professor Azim Suranis' team in the mouse model used in this thesis, exon 5 (Li et al., 1999). This exon was targeted as it is the functional element of *PEG3* and no other exon targets would successfully impair *PEG3* function. Due to this similar architecture, there is the possibility that all previous studies performed on *Peg3*^{KO} in mice may be caused by a *Zim2* knockout. To avoid any complications with this issue, the CRISPR primers designed for the *PEG3*^{KO} of hTS cells also targeted exon 5, although this does leave the potential for *ZIM2* to also be targeted in this project. This problem also confounds the *PEG3* qRT-PCR results as reported in Table 94, meaning that any amplification from the primer may also be amplifying *ZIM2*.

5.4.2.2 Establishing *PHLDA2* and *PEG3* knockouts in human trophoblast stem cells: Protocol adjustments and experimental impacts

The *PHLDA2* knockout process ran incredibly smoothly under the guidance of Dr Asato Sekiya. This produced multiple healthy *PHLDA2*^{KO} lines that

were quickly re-established in the Cardiff University cell laboratory. Unfortunately, the same did not hold true for the attempts to knockout *PEG3* or to generate a double knockout. An attempt to strike a balance between protocols run in the Japan laboratory and protocols run in the Cardiff laboratory impacted a variety of aspects of the experiment. Previous experience in the Cardiff University laboratory came from CRISPR transfections of ES cells and did not always suit the hTS cells as well. The hTS cells did not take to FACs and were unable to develop colonies after sorting. Modifications made to the dilution protocol performed in Japan also prevented the cells from being able to proliferate after single cell isolation. Colony picking became the preferred method, however due to an error with the tracr attached to the sgRNAs, a successful round of picking and cell line derivation was performed on hTS cells which had a 0% transfection rate.

With the continuation of the inability to derive a homozygous *PEG3^{KO}* remaining, it could be suggested that the *PEG3^{KO}* may inhibit the proliferation of hTS cells and therefore prevent the development of a successful *PEG3^{KO}* hTS cell line. In the mass KO screening project using CRISPR, conducted by Shimizu et al. (2023), the *PEG3^{KO}* was not identified as having a significant impact on the cell lines phenotype. This was concluded from the evidence that no cell line that had significant impacts on hTS phenotype tested positive for the *PEG3^{KO}*. This is a reasonable conclusion from that evidence. However, it is possible that, although *PEG3* was a target of the mass screening, the *PEG3^{KO}* was actually never established in that screening and was not identified as having a significant impact on hTS cell line phenotype as it in fact didn't exist. If this is the case, this would re-enforce this unpublished evidence from Ros John's laboratory in which the *PEG3^{KO}* in hTS cells remains elusive (Unpublished data, 2025).

These various issues also impacted all attempts at targeting male hTS lines. Due to resource limitations, it was decided to focus research on the successfully established WT and *PHLDA2^{KO}* hTS lines.

5.4.2.3 *PHLDA2^{KO}* in human trophoblast stem cells increases *hPL* production

The differentiation procedure that the Japanese laboratory used to derive STB cells was used. Morphologically both lines looked the same and differentiated in the same way with syncytiotrophoblast cells developing around day three and full differentiation by day five. Protein analysis showed a clean knockout of PHLDA2 protein in the *PHLDA2^{KO}* samples and that the WT samples were producing high levels of PHLDA2. PEG3 protein levels were harder to assess. Although some specific bands were seen in

the human placenta control sample, inconsistent bands were present in all hTS cells. A similar story was found in the expression of hPL. Although at least one of the WT samples demonstrated that a five-day differentiated hTS cell could produce hPL protein, this was not consistent over the genotypes or samples.

The qRT-PCR performed on the same cells gave a clearer answer. The expression of *PSG1* and the hCG precursors *CGA* and *CGB* were not significantly affected by the *PHLDA2* targeting. These are all markers of the syncytiotrophoblast layer. This result does correlate to the analysis of growth promotion, and EVT and STB expansion analysed in Shimizu et al. (2023) as these were also not affected in their *PHLDA2^{KO}* cell line. The expression of *PEG3* was not altered in the *PHLDA2^{KO}* lines, which correlates to *PHLDA2*'s lack of targeting of *PEG3* (Liska O, 2022) and the mouse studies described in section 1.1. The expression of *PHLDA2* was successfully reduced in the *PHLDA2^{KO}* lines. The expression of *hPL* was significantly increased in the *PHLDA2^{KO}* lines which suggests a direct action between *PHLDA2* and *hPL* hormone levels. This was not investigated in Shimizu et al. (2023). This result is a key link in the theory between the regulation of imprinted genes and hormone expression. This is the first piece of direct evidence that the low expression of *PHLDA2* in mothers with high *hPL* is causative. Although the full desired set of hTS genotypes was not generated, results from the *PHLDA2^{KO}* lines are encouraging.

5.5 Limitations

The limitations to this chapter were in the multiple hurdles faced during the derivation of the mTS cell lines. This prevented the ability to assess any sexually dimorphic characteristics of the mTS cell line knockout models. The mTS cells questionable credibility as a model and the unexpected qRT-PCR results created a challenging set of circumstances to produce a clear picture of the impact of the genetic modifications on the mTS cell models. The time invested into the mTS analysis also impacted the ability to develop the full set of hTS cells. In addition, at the beginning of the project a set of the four genotypes was planned for female cells only. Once the promising result was found from the female *PHLDA2^{KO}* samples, the idea to also apply the knockouts to male lines was added to the project and further stretched the capacity of the project. In transgenic ES cell line experiments, the most stringent experimental approach is currently to produce three independent ES lines, in each sex, with three independent knockout targets. This is to avoid bias in a duplication of the same introduction of the transgene, to avoid the effects of using one individual to create the knockout and to clarify the response across both

sexes. That scope was too large to include in this project. The basis required to execute this work has been established and will hopefully be completed over the next few years.

5.6 Summary

The key findings from this chapter are presented in Table 43.

Analysis	Key findings
Mouse trophoblast stem cell derivation	<ul style="list-style-type: none"> 33 mTS lines were successfully derived and banked covering all four genotypes of interest and both sexes.
Mouse trophoblast stem cell validation	<ul style="list-style-type: none"> 10-day differentiated mTS cells were matched to a E9.5 developmental timeframe using protein expression profiles of Prl3b1 and Prl3d1 via ELISA.
Mouse trophoblast stem cell qRT-PCR	<ul style="list-style-type: none"> <i>Peg3^{KO}</i> mTS lines had reduced expression of <i>Tpbpa</i>, <i>Rgs5</i>, <i>Prl7b1</i> and <i>Peg3</i>. <i>Peg3^{KO}</i> mTS lines had an increase in <i>Blimp1</i> and <i>Phlda2</i> expression. <i>Phlda2^{KO}</i> mTS lines had reduced <i>Tpbpa</i>, <i>Blimp1</i>, <i>Rgs5</i>, <i>Prl7b1</i> and <i>Prl2c</i> expression compared to WT. DKO mTS lines had a reduced expression in <i>Tpbpa</i>, <i>Blimp1</i>, <i>Rgs5</i>, <i>Prl7b1</i>, <i>Pcdh12</i>, <i>Peg3</i> and <i>Phlda2</i>.
Human trophoblast stem cell CRISPR design and knockout attempts	<ul style="list-style-type: none"> CRISPR targets were designed and successfully knocked out both <i>PEG3</i> and <i>PHLDA2</i>. <i>PHLDA2^{KO}</i> cell lines were successfully derived and banked.
Human trophoblast stem cell differentiation assay	<ul style="list-style-type: none"> Differentiated <i>PHLDA2^{KO}</i> hTS cells demonstrate significant increase in <i>hPL</i> RNA expression via qRT-PCR.

Table 43: Key findings from Chapter 5.

This chapter successfully established the derivation of mTS lines of all the genotypes of interest. It confirmed that no knockout had an impact on mTS cell proliferation. qRT-PCR on mTS cell lines showed a complex response to each of the transgenic modifications. Interestingly, *Peg3*^{KO} lines showed a significant increase in *Phlda2* expression, indicating that *Peg3* has some indirect yet close regulation of *Phlda2*. This finding contributes to the picture surrounding the question of *Peg3* and *Phlda2* antagonistic interaction. If *Peg3* modulates *Phlda2* in some way, the absence of both *Peg3* and *Phlda2* could not mimic the presence of both, which will compromise the ability of the DKO genotype to correct to WT completely. This correlates with results from Chapter 4 where the DKO placenta's labyrinth did not correct to WT. This chapter also successfully designed CRISPRs for both *PEG3* and *PHLDA2*, resulting in the successful derivation of *PHLDA2*^{KO} hTS cell lines. Although no knockout could be linked to any effects on hormone output in mTS cells, the *PHLDA2*^{KO} significantly increased the expression of *hPL* in hTS cells providing the long missing causative evidence that imprinted genes generally and *PHLDA2* specifically regulate placental hormone expression in humans.

Chapter 6: General discussion

6.1 Overview

6.1.1 Main findings

Each chapter discusses the findings of that chapter. This chapter will cover the overall findings of the project along with a discussion around their implications and limitations. Suggestions regarding future directions of work will also be discussed.

Chapter	Key findings
<p><i>Chapter 3: Characterising the effect of loss of imprinting of Phlda2 on the developing mouse placenta.</i></p>	<ul style="list-style-type: none"> • <i>Phlda2</i>^{+/+BACx1(BL6)} reduced placental weight, junctional zone area and junctional zone <i>Pr13b1</i> positive cell number. • <i>Phlda2</i>^{+/+BACx1(BL6)} reduced labyrinth size and number of <i>Pr13b1</i> positive cells in female placentas only. • Four <i>Pr1</i> family members, along with labyrinth S-TG cell marker <i>Ctsq</i> were significantly reduced in female placentas and not male placentas.
<p><i>Chapter 4: Placental characterisation of Peg3 and Phlda2 antagonism in the developing mouse placenta.</i></p>	<ul style="list-style-type: none"> • <i>Peg3</i> and <i>Phlda2</i> are co-localised at E7.5 and E9.5 of mouse placental development. • <i>Peg3</i>^{KO} reduced foetal weight, placental weight, junctional zone size, <i>Pr13b1</i> positive cells and glycogen cells in the junctional zone in males. • <i>Phlda2</i>^{KO} increased placental weight, junctional zone size and <i>Pr13b1</i> positive cells in both sexes. • DKO placentas correct to WT in placental weight, junctional zone size and junctional zone <i>Pr13b1</i> positive cell number. • DKO labyrinths did not correct to WT in any assessed metric which correlates with foetal weight reductions in this group.
<p><i>Chapter 5: Peg3 and Phlda2 knockout in human and mouse trophoblast stem cells.</i></p>	<ul style="list-style-type: none"> • <i>Peg3</i>^{KO} mTS cell had increased <i>Phlda2</i> expression compared to WT. • <i>Peg3</i> indirectly suppresses <i>Phlda2</i> expression in mTS cells.

-
- *PHLDA2*^{KO} in hTS cells increase *hPL* expression.
-

Table 44: Summary of key findings.

A figure demonstrating this thesis's contributions to the placental programming hypothesis can be seen in Figure 71.

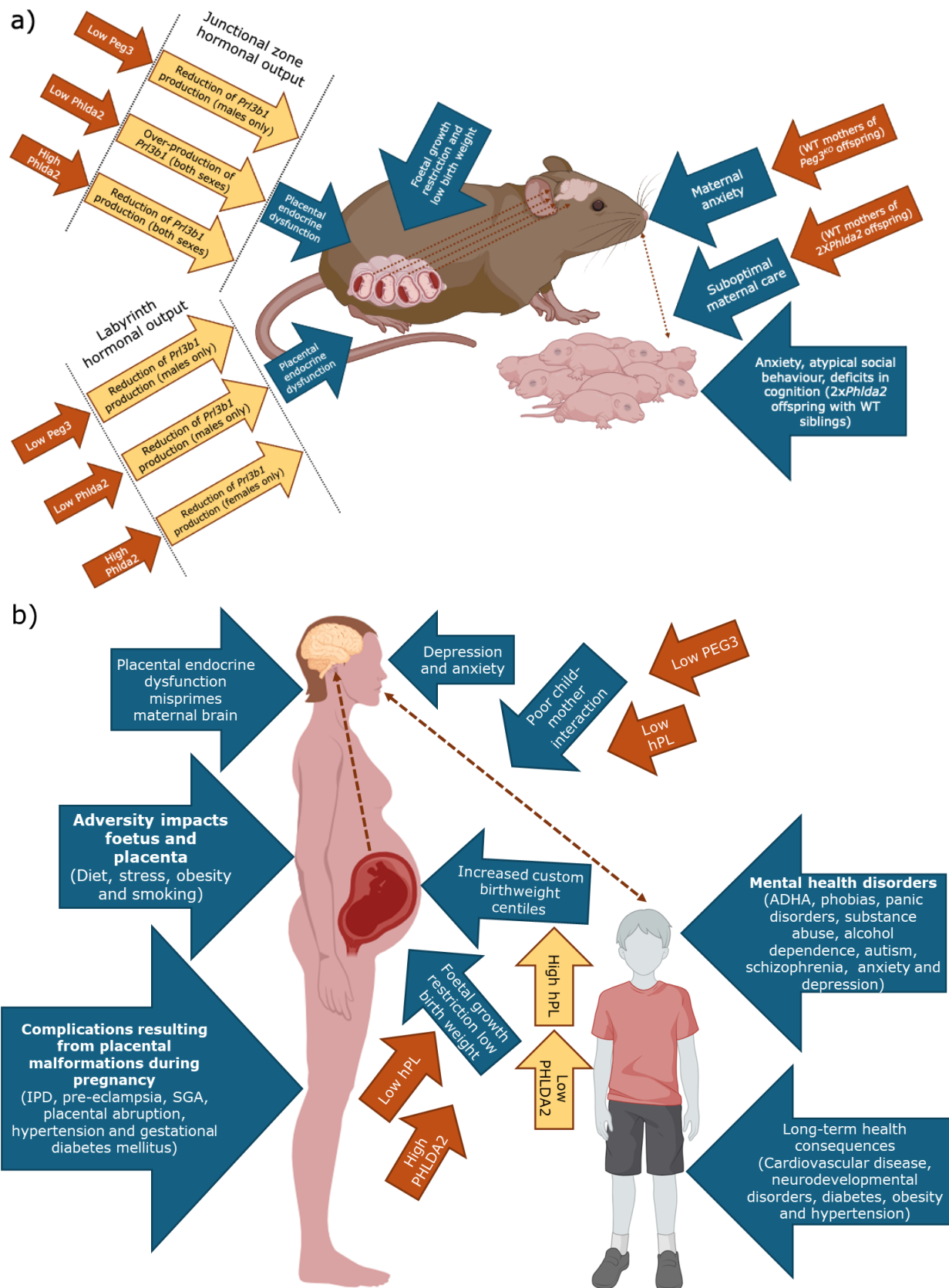


Figure 71: Updated figure of placental programming hypothesis this thesis's contributions (yellow arrows) around the imprinted genes *Peg3* and *Phlda2*'s placental hormone regulation in both human and mouse models. a) This thesis determined the hormonal

output for the junctional zone and labyrinth regions of each placental model, with *Peg3^{KO}* having a reduction in the production of *Prl3b1* in the junctional zone and labyrinth for males only, *Phlda2^{KO}* showing an increased production of *Prl3b1* in the junctional zone for both sexes and a decrease in *Prl3b1* production in the labyrinth for males only and for the *Phlda2^{+/+BACx1(BL6)}* model with a reduction of *Prl3b1* production in the junctional zone for both sexes and a reduction in the labyrinth for females only. **b)** This thesis contributed the finding that *PHLDA2* directly regulates *hPL* in humans with the *PHLDA2^{KO}* demonstrating increased *hPL* expression.

6.1.2 Sex specific sensitivities in imprinting: Exploring offspring sensitivities to imprinted genes from parent of the same sex

As previously identified, the placenta has a sexually dimorphic response to the environment in both human and mice (Aiken & Ozanne, 2013; DiPietro & Voegtline, 2017; Sutherland & Brunwasser, 2018). The sexually dimorphic characteristics of placenta were present in all the models investigated in this thesis. Most interestingly, the *Phlda2* loss of imprinting model showed a more significant impact on female placentas than male and whereas the *Peg3^{KO}* model showed a more significant impact on the male placenta. The *Phlda2^{KO}* model was sexually dimorphic in some metrics but had a balanced response in the junctional zone across males and females. An interesting aspect to these results is their modes of imprinting in relation to the sex of their more impacted offspring. *Phlda2* is maternally expressed and paternally silenced and its loss of imprinting impacts females to a greater degree. *Peg3* is paternally expressed and maternally silenced and its alteration has a greater impact on males. This pattern could suggest that there is an inherent sensitivity to the dosage of an imprinted gene for the offspring of the same sex as the parent which the imprinted allele is expressed, simply, male offspring are more sensitive to paternally expressed genes and female offspring are more sensitive to maternally expressed genes (Figure 72). To extend this concept it could also suggest that offspring of the opposite sex are prepared to withstand some attempted alteration from the parent of the opposing sex and inherently have more resilience to it. Although no previous analysis of imprinted models has shown a more significant impact on females, this direct comparison between the two modes of imprinting has not been made in one study before. This concept could be an interesting addition to the genetic conflict hypothesis.

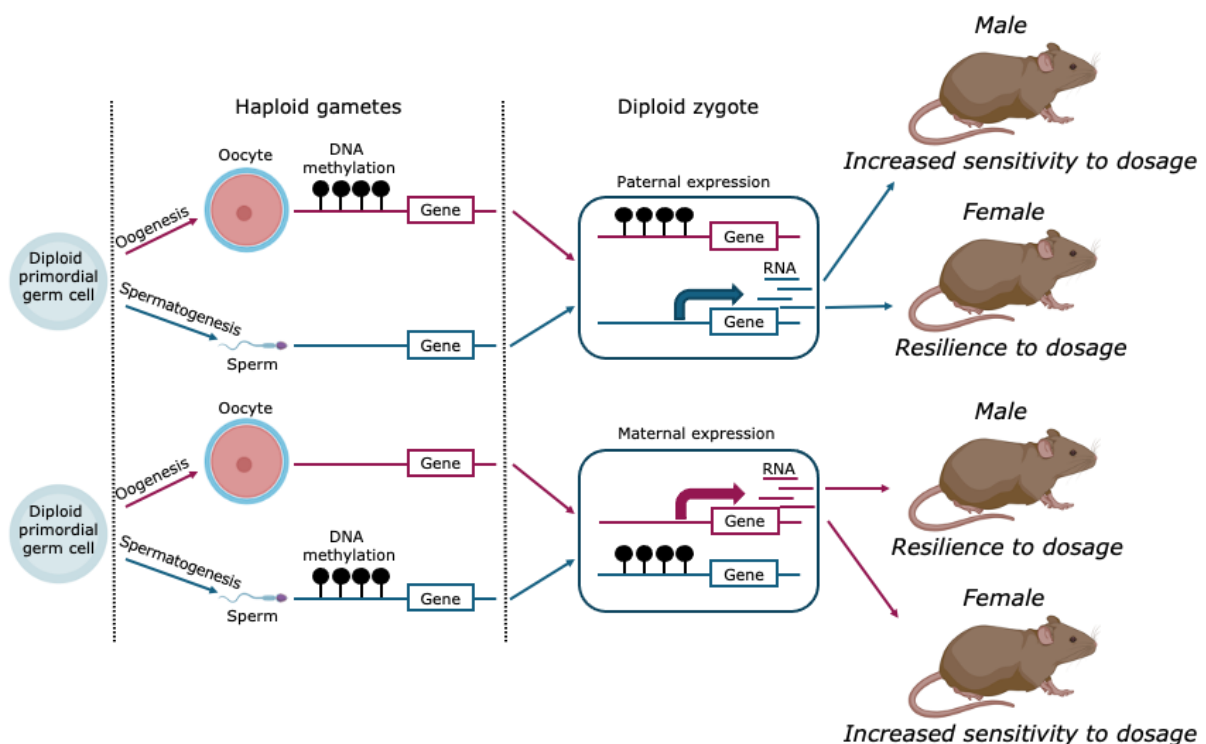


Figure 72: Hypothetical gendered offspring sensitivity to imprinted gene dosage.

Paternally expressed genes having a greater impact on male offspring and female offspring showing resilience to the dosage of paternally expressed genes as demonstrated by the *Peg3^{KO}* mouse model. Maternally expressed genes having a greater impact on the female offspring with male offspring showing greater resilience to maternally expressed gene dosage as demonstrated by the *Phlda2^{+/+}BACx1(BL6)* mouse model.

6.1.3 Differential roles of *Peg3* and *Phlda2*: Antagonistic interactions in the junctional zone versus unbalances roles in the labyrinth

The DKO model aided in highlighting how each gene of interest produces their phenotype. If the removal of both genes produces the same phenotype as when both genes are present, then that would indicate reciprocal roles of both. If the resulting phenotype is not the same this would indicate that there is some interaction between the two when they are both present that is removed when they are both absent. An equal and opposite regulation of the junctional zone by *Peg3* and *Phlda2* was demonstrated, however this was not demonstrated in the labyrinth. The junctional zone the *Peg3^{KO}* model had a reduction in multiple metrics. *Peg3^{KO}* junctional zones were 46% ($P=.002$) smaller than WT in males, *Peg3^{KO}* junctional zones contained 37% ($P=.011$) fewer positive cells that WT in males and *Peg3^{KO}* junctional zones contained 41% ($P=.038$) fewer total cells that WT males. *Phlda2^{KO}* junctional zones contained 48% ($P=.004$) more *Pr13b1* positive cells than WT in males. *Phlda2^{KO}* junctional

zones contained 49% ($P=.004$) and 130% ($P<.001$) more total cells than WT in males and females respectively. *Phlda2*^{KO} junctional zones also contained 48% ($P=.004$) and 115% ($P<.001$) more *Pr13b1* positive cells than WT in males and females respectively. *Phlda2*^{KO} junctional zones were also 44% ($P=.002$) and 129% ($P<.001$) larger than WT in males and females respectively. The DKO junctional zones corrected to WT in all of these metrics.

In the labyrinth however, this response did not hold true. As both *Peg3*^{KO} and *Phlda2*^{KO} models had reductions in total cell number and *Pr13b1* positive cell number in the labyrinth compared to WT, the resulting DKO labyrinth was the most significantly impacted of all the genotypes rather than demonstrating a recovery back to WT metrics. This result suggests an opposite function of *Phlda2* in developing the labyrinth lineage compared to the junctional zone. *Phlda2* functions to restrict the spongiotrophoblast lineage and its absence results in an expansion of the junctional zone, however the absence of *Phlda2* in the labyrinth produces a restricted labyrinth, suggesting *Phlda2* functions to expand the labyrinth while restricting the junctional zone. In Chapter 4, RNAscope multiplexing of *Peg3* and *Phlda2* showed that *Phlda2* was expressed more highly in the labyrinth than *Peg3* which could weigh the action of each of the targets unequally in the labyrinth, ultimately inhibiting the ability for the DKO labyrinth to correct back to WT when both *Peg3* and *Phlda2* are absent. In addition, in Chapter 5, the *Peg3*^{KO} mTS cell lines were shown to have increased expression of *Phlda2*, suggesting that *Peg3* may indirectly regulate *Phlda2*. This is another important complication which could prevent antagonistic behaviour between the two. If one regulates the other, the absence of both also removes that interaction, preventing the absence of both *Peg3* and *Phlda2* to be able to function the same as when both are present.

Regarding the total *Pr13b1* output of the placenta, neither genotype was impacted. The uneven response of the DKO labyrinth did not have a great enough impact to affect the DKO placentas *Pr13b1* production overall. Functionally however, the junctional zones role as the endocrine system means that the decreases in capacity seen in the *Peg3*^{KO} junctional zones and the increases in capacity seen in the *Phlda2*^{KO} junctional zones may have a more functional impact than the labyrinth. However, the foetal weight of the DKO sample's is not recovered to WT which is likely a result of the impaired labyrinth.

In summary, some important distinctions were identified between the function of *Peg3* and *Phlda2*, although they were found to not behave antagonistically in the labyrinth, they were found to behave antagonistically in the junctional zone.

6.2 Limitations and future directions of research

Limitations to this work have been independently highlighted in their relevant chapters, however, the projects limitations as a whole will be discussed here.

A single limitation that impacted the entire project's output was the difficulties establishing mouse trophoblast stem cells. The time and resources allocated to this aspect of the project reduced the ability to execute fully on other aspects of the project. With the full set of genotypes of both sexes not being derived in mTS cells, no investigation into sex specific outcomes could be conducted. Although the *Phlda2*^{KO} mouse placentas have a robust response across both sexes in the mice, the sexually dimorphic attributes of the *Peg3*^{KO} mouse model could be masking the true impact of the *Peg3*^{KO} on either sex. Further attempts to derive these lines would help fill some of the missing pieces in this part of the project. An emphasis on the methodology used would be recommended, with a suggestion towards CRISPR knockouts of already derived mTS lines of both sexes, making sure to not only modernise the approach but to also modernise the fundamental maintenance protocols surrounding these methods.

One of the most notable gaps in the project is the analysis of hTS cell lines knockout models other than the *PHLDA2*^{KO} in females. Although attempts were made to derive all eight combinations of the four genotypes across both sexes, only the initial female WT and *PHLDA2*^{KO} lines provided enough material for analysis. In replicating the mouse E16.5 placenta data, the female *PHLDA2*^{KO} hTS cells did show a significant increase in endocrine capacity, however it would have been valuable to demonstrate if that was replicable in males too. As for *PEG3*^{KO} attempts, despite the validation of the CRISPR designs and their ability to knockout *PEG3*, successful homozygous lines were not generated in time for analysis. Answering the question around whether *PEG3* directly impacts *hPL* levels would have helped with the larger picture of the two genes antagonistic interactions. The DKO hTS cell line would also have contributed to the knowledge around this system. Despite that, proving the direct causation between *PHLDA2* and *hPL* levels in the human model is still a notable finding of this work.

Now that the *PHLDA2*^{KO} hTS cell lines have been derived, further investigation into which cell types are affected by the knockout can be conducted. This could be done by an investigation into a wider range of RNA targets using RNA sequencing or RNAscope for cell-type markers. In addition, next generation sequencing of these cells could also provide a more thorough picture of the direct and follow-on effects of a *PHLDA*^{KO} in

hTS cells. Within hTS cell research there are teams that are developing an organoid culturing system for hTS cells. However, at the IFPA conference in September of 2023, it was made clear that the protocol was demonstrating some complications. The protocol itself was proving hard to standardise and is generating inconsistent data. Due to the problems already impacting the culture of mTS cells and hTS cells in this thesis, it was not feasible to undertake organoid culture until the protocol has stabilised.

As for other elements of the project that could be investigated further, the loss of imprinting of *Phlda2* mouse model investigated in Chapter 3, RNA sequencing was performed on the RNA that was used for qRT-PCR analysis. The bioinformatics on this data was performed by a bioinformatic specialist. This data supported the results found in the qRT-PCR data presented in this thesis with a sexually dimorphic impact on Prl family member expression in females. This data will be presented alongside the work presented in Chapter 3 in a publication.

For the characterisation of *Peg3*^{KO}, *Phlda2*^{KO} and DKO developing mouse placentas, a quantitative analysis of *Peg3* and *Phlda2* expression using the automated cell counting program used in Chapter 3 and Chapter 4 could give further evidence to the effectiveness of the knockout. This could be done at the E9.5 and E16.5 time points. Both of these time points were analysed via qRT-PCR and RNAseq for this grant project by another member of the team. Unfortunately, that data has produced a complex result similar to the qRT-PCR results seen in the mTS cell assessment in section 5.3.1.6. There has been a consistent issue pairing RNAscope and qRT-PCR data. One potential issue being that the RNAscope probe targets are proprietary, preventing the qRT-PCR primer from being able to be designed to amplify the same target. The inconsistencies could be introduced due to the nature of the two techniques. RNAscope captures all the RNA in place where through the preparation of cDNA libraries for qRT-PCR, RNA signal can be lost or not amplified. This loss can be uneven across genes as there are optimal RNA lengths, compositions, and locations for each step. The investigation into the expression of the imprinted genes for each of the genotypes plus further investigations into their expression of related genes could provide indirect evidence to indicate that the genes are regulated by the same elements and could have a coordinated response to the same stimuli.

Imprinted genes are an elaborate and complex mechanism of inheritance with subtle effects, making their study a murky field to explore. Fundamentally this project would have been significantly improved by a robust mTS cell model, allowing for a more thorough investigation into the knockout models in that system and freeing up more time for a more thorough investigation into other aspects of the project, namely hTS cell

models. The use of siRNA knockdowns could provide a more temporally consistent reduction in the target, demonstrating cleaner qRT-PCR and RNAscope results.

The most significant limitation to this work is the potential discrepancy between the amount of hormone produced by the placenta and their exposure to the maternal brain. The automated cell counting of *Prl3b1* positive cells, can be used as a proxy to actual hormone concentrations or a snapshot of the actual endocrine capacity of that genetic modification. However, it doesn't account for any post translational modifications to the *Prl3b1* RNA which could affect functional hormone concentration. Although post translational modifications for *Prl3b1* have not yet been identified or characterised this is likely due to a gap in knowledge rather than an actual absence. In human, hPRL for example has multiple post translational modifications resulting in at least 6 protein variants (Qian et al., 2018). The RNA expression of *Prl3b1* in qRT-PCR has given complicated results in the analysis of E9.5 and E16.5 samples as discussed previously. To address this, a more reliable piece of data would be the hormone level circulating in the blood of the pregnant mouse with a litter of just one genotype. This data has been elusive, with complications in producing the ideal litters, difficulty sampling the appropriate blood and issues with antibodies and protein analysis of *Prl3b1* and *Prl3d1*. As a result, this automated regional cell counting method coupled with a highly specific and sensitive RNAscope method does provide a cleaner picture of each genotypes functional endocrine capacity.

6.3 Concluding remarks

This thesis provided insights into multiple questions surrounding the functionality of imprinted genes in regulating placental hormones in both mouse and human. It provided further evidence to support the sexually dimorphic action of *Peg3* and *Phlda2*. An interesting aspect being a paternally expressed, maternally silenced imprinted gene having a more significant impact on male placentas and a maternally expressed, paternally silenced gene have a more significant effect on female placentas. This thesis linked these genetic responses to hormone output through a novel automated cell counting program which gave quantitative results for each genotypes functional endocrine capacity. This analysis demonstrated a significant reduction in *Prl3b1* for *Phlda2* loss of imprinting (*Phlda2*^{+/+BACx1(BL6)}) junctional zones, where a significant increase in *Prl3b1* was demonstrated by *Phlda2*^{KO} junctional zones. In addition, the male *Peg3*^{KO} junctional zones demonstrated a significant reduction in *Prl3b1*. In the analysis of the double knockout of *Phlda2* and *Peg3*, a

correction back to wild type expression of *Pr/3b1* was identified in the junctional zone but not the labyrinth. This data coupled with other assessments of the DKO placentas suggest some antagonistic interaction between *Peg3* and *Phlda2* during mouse placental development. A highly important and long elusive result produced by this thesis is the demonstration of conservation of function of imprinted genes between mouse to human. Correlative data has previously suggested a link between levels of imprinted gene expression and *hPL* however no causation was ever been demonstrated. This thesis has provided that causative data by demonstrating an increase in *hPL* in *PHLDA2^{KO}* hTS cells. This result provides further incentive to investigate imprinted genes in human pregnancy, as it suggests that they directly regulate placental hormones which have been linked to maternal depression and anxiety. This may be able to provide a screening assay for pregnant woman who might be prone to such complications and allow for preventative hormonal treatment.

References

- Aaron Geno, K., Cervinski, M. A., & Nerenz, R. D. (2021). Chapter 15 - Pregnancy and the fetus. In W. E. Winter, B. Holmquist, L. J. Sokoll, & R. L. Bertholf (Eds.), *Handbook of Diagnostic Endocrinology (Third Edition)* (pp. 543-579). Academic Press.
<https://doi.org/https://doi.org/10.1016/B978-0-12-818277-2.00015-7>
- Abbot, P., & Capra, J. A. (2017). What is a placental mammal anyway? *Elife*, 6, e30994. <https://doi.org/10.7554/eLife.30994>
- Adjaye, J., Huntriss, J., Herwig, R., BenKahla, A., Brink, T. C., Wierling, C., Hultschig, C., Groth, D., Yaspo, M. L., Picton, H. M., Gosden, R. G., & Lehrach, H. (2005). Primary differentiation in the human blastocyst: comparative molecular portraits of inner cell mass and trophectoderm cells. *Stem Cells*, 23(10), 1514-1525.
<https://doi.org/10.1634/stemcells.2005-0113>
- Ager, E. I., Pask, A. J., Gehring, H. M., Shaw, G., & Renfree, M. B. (2008). Evolution of the CDKN1C-KCNQ1 imprinted domain. *BMC Evol Biol*, 8, 163. <https://doi.org/10.1186/1471-2148-8-163>
- Aiken, C. E., & Ozanne, S. E. (2013). Sex differences in developmental programming models. *Reproduction*, 145(1), R1-13.
<https://doi.org/10.1530/rep-11-0489>
- Ain, R., Dai, G., Dunmore, J. H., Godwin, A. R., & Soares, M. J. (2004). A prolactin family paralog regulates reproductive adaptations to a physiological stressor. *Proceedings of the National Academy of Sciences*, 101(47), 16543-16548.
<https://doi.org/10.1073/pnas.0406185101>
- Alliance of Genome Resources. (2024). *Alliance of Genome Resources Consortium*. <https://www.alliancegenome.org>
- Alsat, E., Guibourdenche, J., Couturier, A., & Evain-Brion, D. (1998). Physiological role of human placental growth hormone. *Mol Cell Endocrinol*, 140(1-2), 121-127. [https://doi.org/10.1016/s0303-7207\(98\)00040-9](https://doi.org/10.1016/s0303-7207(98)00040-9)
- Alves, R. L., Portugal, C. C., Lopes, I. M., Oliveira, P., Alves, C. J., Barbosa, F., Summavielle, T., & Magalhães, A. (2022). Maternal stress and vulnerability to depression: coping and maternal care strategies and its consequences on adolescent offspring. *Translational Psychiatry*, 12(1), 463.
<https://doi.org/10.1038/s41398-022-02220-5>
- Ammari, R., Monaca, F., Cao, M., Nassar, E., Wai, P., Del Grosso, N. A., Lee, M., Borak, N., Schneider-Luftman, D., & Kohl, J. (2023). Hormone-mediated neural remodeling orchestrates parenting onset during pregnancy. *Science*, 382(6666), 76-81.
<https://doi.org/10.1126/science.adi0576>
- Ananth, C. V., Smulian, J. C., & Vintzileos, A. M. (2010). Ischemic placental disease: Maternal versus fetal clinical presentations by

- gestational age. *The Journal of Maternal-Fetal & Neonatal Medicine*, 23(8), 887-893. <https://doi.org/10.3109/14767050903334885>
- Andrews, S. C., Wood, M. D., Tunster, S. J., Barton, S. C., Surani, M. A., & John, R. M. (2007). Cdkn1c (p57Kip2) is the major regulator of embryonic growth within its imprinted domain on mouse distal chromosome 7. *BMC Dev Biol*, 7, 53. <https://doi.org/10.1186/1471-213x-7-53>
- Anson-Cartwright, L., Dawson, K., Holmyard, D., Fisher, S. J., Lazzarini, R. A., & Cross, J. C. (2000). The glial cells missing-1 protein is essential for branching morphogenesis in the chorioallantoic placenta. *Nat Genet*, 25(3), 311-314. <https://doi.org/10.1038/77076>
- Apostolidou, S., Abu-Amero, K., O'Donoghue, K., Frost, J., Olafsdottir, O., Chavele, K., Whittaker, J., Loughna, P., Stanier, P., & Moore, G. (2007). Elevated placental expression of the imprinted PHLDA2 gene is associated with low birth weight. *Journal of molecular medicine (Berlin, Germany)*, 85, 379-387. <https://doi.org/10.1007/s00109-006-0131-8>
- Arima, T., Hata, K., Tanaka, S., Kusumi, M., Li, E., Kato, K., Shiota, K., Sasaki, H., & Wake, N. (2006). Loss of the maternal imprint in Dnmt3Lmat^{-/-} mice leads to a differentiation defect in the extraembryonic tissue. *Developmental Biology*, 297(2), 361-373.
- Arling, G. L., & Harlow, H. F. (1967). Effects of social deprivation on maternal behavior of rhesus monkeys. *Journal of Comparative and Physiological Psychology*, 64(3), 371-377. <https://doi.org/10.1037/h0025221>
- Ashworth, L. K., Batzer, M. A., Brandriff, B., Branscomb, E., de Jong, P., Garcia, E., Garnes, J. A., Gordon, L. A., Lamerdin, J. E., Lennon, G., Mohrenweiser, H., Olsen, A. S., Slezak, T., & Carrano, A. V. (1995). An integrated metric physical map of human chromosome 19. *Nat Genet*, 11(4), 422-427. <https://doi.org/10.1038/ng1295-422>
- Association, A. P. (2013). Diagnostic and statistical manual of mental disorders. *Psychological association*. https://www.hakjisa.co.kr/common_file/bbs_DSM-5_Update_October2018_NewMaster.pdf
- Astwood, E. B., & Greep, R. O. (1938). A Corpus Luteum-Stimulating Substance in the Rat Placenta. *Proceedings of the Society for Experimental Biology and Medicine*, 38(5), 713-716. <https://doi.org/10.3181/00379727-38-9991>
- Atout, S., Shurrab, S., & Loveridge, C. (2022). Evaluation of the Suitability of RNAScope as a Technique to Measure Gene Expression in Clinical Diagnostics: A Systematic Review. *Mol Diagn Ther*, 26(1), 19-37. <https://doi.org/10.1007/s40291-021-00570-2>
- Augustine, R. A., & Grattan, D. R. (2008). Induction of central leptin resistance in hyperphagic pseudopregnant rats by chronic prolactin infusion. *Endocrinology*, 149(3), 1049-1055. <https://doi.org/10.1210/en.2007-1018>

- Aye, C. Y., Boardman, H., & Leeson, P. (2017). Cardiac Disease after Pregnancy: A Growing Problem. *Eur Cardiol*, 12(1), 20-23. <https://doi.org/10.15420/ecr.2017:4:1>
- Babak, T., DeVeale, B., Armour, C., Raymond, C., Cleary, M. A., van der Kooy, D., Johnson, J. M., & Lim, L. P. (2008). Global Survey of Genomic Imprinting by Transcriptome Sequencing. *Current Biology*, 18(22), 1735-1741. <https://doi.org/10.1016/j.cub.2008.09.044>
- Bai, L., Zhao, Y., Zhou, Y., Song, Y., Xiao, H., Zhao, G., Wang, Z., & Li, X. (2025). Advances in immunological sorting of X and Y chromosome-bearing sperm: from proteome to sex-specific proteins. *Front Vet Sci*, 12, 1523491. <https://doi.org/10.3389/fvets.2025.1523491>
- Baker, B., & McGrath, J. M. (2011). Maternal-infant synchrony: An integrated review of the literature [Journal Article]. *Neonatal, Paediatric & Child Health Nursing*, 14(3), 2-13. <https://search.informit.org/doi/10.3316/ielapa.638131608884585>
- Balasundaram P, F. A. (2023). Immunology at the Maternal-Fetal Interface. [Updated 2023 Aug 28]. In: StatPearls [Internet]. Treasure Island (FL): StatPearls Publishing; 2024 Jan-. Available from: <https://www.ncbi.nlm.nih.gov/books/NBK574542/>
- Bale, T. L. (2011). Sex differences in prenatal epigenetic programming of stress pathways. *Stress*, 14(4), 348-356. <https://doi.org/10.3109/10253890.2011.586447>
- Baran, Y., Subramaniam, M., Biton, A., Tukiainen, T., Tsang, E. K., Rivas, M. A., Pirinen, M., Gutierrez-Arcelus, M., Smith, K. S., Kukurba, K. R., Zhang, R., Eng, C., Torgerson, D. G., Urbanek, C., Li, J. B., Rodriguez-Santana, J. R., Burchard, E. G., Seibold, M. A., MacArthur, D. G., . . . Lappalainen, T. (2015). The landscape of genomic imprinting across diverse adult human tissues. *Genome Res*, 25(7), 927-936. <https://doi.org/10.1101/gr.192278.115>
- Barclay, S. M. (2023). £25 million for women's health hub expansion <https://www.gov.uk/government/news/25-million-for-womens-health-hub-expansion>
- Barker, D. J. (1991). The intrauterine origins of cardiovascular and obstructive lung disease in adult life. The Marc Daniels Lecture 1990. *J R Coll Physicians Lond*, 25(2), 129-133.
- Barker, D. J., Bull, A. R., Osmond, C., & Simmonds, S. J. (1990). Fetal and placental size and risk of hypertension in adult life. *British Medical Journal*, 301(6746), 259. <https://doi.org/10.1136/bmj.301.6746.259>
- Barker, D. J. P. (1995). Fetal origins of coronary heart disease. *BMJ*, 311(6998), 171. <https://doi.org/10.1136/bmj.311.6998.171>
- Barker, D. J. P., & Osmond, C. (1986). Infant mortality, childhood nutrition, and ischaemic heart disease in England and Wales. *The Lancet*, 327(8489), 1077-1081. [https://doi.org/https://doi.org/10.1016/S0140-6736\(86\)91340-1](https://doi.org/https://doi.org/10.1016/S0140-6736(86)91340-1)

- Barlow, D. P., & Bartolomei, M. S. (2014). Genomic imprinting in mammals. *Cold Spring Harb Perspect Biol*, 6(2). <https://doi.org/10.1101/cshperspect.a018382>
- Barlow, D. P., Stöger, R., Herrmann, B. G., Saito, K., & Schweifer, N. (1991). The mouse insulin-like growth factor type-2 receptor is imprinted and closely linked to the Tme locus. *Nature*, 349(6304), 84-87. <https://doi.org/10.1038/349084a0>
- Barrera-Saldaña, H. A., Seeburg, P. H., & Saunders, G. F. (1983). Two structurally different genes produce the same secreted human placental lactogen hormone. *J Biol Chem*, 258(6), 3787-3793.
- Barsh, G. S., Seeburg, P. H., & Gelinas, R. E. (1983). The human growth hormone gene family: structure and evolution of the chromosomal locus. *Nucleic Acids Research*, 11(12), 3939-3958.
- Basyuk, E., Cross, J. C., Corbin, J., Nakayama, H., Hunter, P., Nait-Oumesmar, B., & Lazzarini, R. A. (1999). Murine Gcm1 gene is expressed in a subset of placental trophoblast cells. *Dev Dyn*, 214(4), 303-311. [https://doi.org/10.1002/\(sici\)1097-0177\(199904\)214:4<303::Aid-aja3>3.0.Co;2-b](https://doi.org/10.1002/(sici)1097-0177(199904)214:4<303::Aid-aja3>3.0.Co;2-b)
- Bauer, A., Knapp, M., & Parsonage, M. (2016). Lifetime costs of perinatal anxiety and depression. *Journal of Affective Disorders*, 192, 83-90. <https://doi.org/10.1016/j.jad.2015.12.005>
- Beardslee, W. R., Bemporad, J., Keller, M. B., & Klerman, G. L. (1983). Children of parents with major affective disorder: a review. *Am J Psychiatry*, 140(7), 825-832. <https://doi.org/10.1176/ajp.140.7.825>
- Benirschke, K. (2004). The Placenta: Structure and Function. *NeoReviews*, 5(6), e252-e261. <https://doi.org/10.1542/neo.5-6-e252>
- Berga, S. L., Nitsche, J. F., & Braunstein, G. D. (2016). Chapter 21 - Endocrine Changes in Pregnancy. In S. Melmed, K. S. Polonsky, P. R. Larsen, & H. M. Kronenberg (Eds.), *Williams Textbook of Endocrinology (Thirteenth Edition)* (pp. 831-848). Elsevier. <https://doi.org/https://doi.org/10.1016/B978-0-323-29738-7.00021-6>
- Berghorn, K. A., Clark, P. A., Encarnacion, B., Deregis, C. J., Folger, J. K., Morasso, M. I., Soares, M. J., Wolfe, M. W., & Roberson, M. S. (2005). Developmental expression of the homeobox protein Distal-less 3 and its relationship to progesterone production in mouse placenta. *J Endocrinol*, 186(2), 315-323. <https://doi.org/10.1677/joe.1.06217>
- Bernard-Bonnin, A. C., Canadian Paediatric, S., Mental, H., & Developmental Disabilities, C. (2004). Maternal depression and child development. *Paediatrics & Child Health*, 9(8), 575-583. <https://doi.org/10.1093/pch/9.8.575>
- Besag, F. M. C., & Vasey, M. J. (2023). Should Antidepressants be Avoided in Pregnancy? *Drug Safety*, 46(1), 1-17. <https://doi.org/10.1007/s40264-022-01257-1>

- Bicks, L. K., Koike, H., Akbarian, S., & Morishita, H. (2015). Prefrontal Cortex and Social Cognition in Mouse and Man [Review]. *Frontiers in Psychology*, 6. <https://doi.org/10.3389/fpsyg.2015.01805>
- Bielinska, B., Blaydes, S. M., Buiting, K., Yang, T., Krajewska-Walasek, M., Horsthemke, B., & Brannan, C. I. (2000). De novo deletions of SNRPN exon 1 in early human and mouse embryos result in a paternal to maternal imprint switch. *Nature Genetics*, 25(1), 74-78. <https://doi.org/10.1038/75629>
- Blackburn, D. G. (2015). Evolution of vertebrate viviparity and specializations for fetal nutrition: A quantitative and qualitative analysis. *Journal of Morphology*, 276(8), 961-990. <https://doi.org/https://doi.org/10.1002/jmor.20272>
- Blom, E. A., Jansen, P. W., Verhulst, F. C., Hofman, A., Raat, H., Jaddoe, V. W. V., Coolman, M., Steegers, E. A. P., & Tiemeier, H. (2010). Perinatal complications increase the risk of postpartum depression. The Generation R Study. *BJOG: An International Journal of Obstetrics & Gynaecology*, 117(11), 1390-1398. <https://doi.org/https://doi.org/10.1111/j.1471-0528.2010.02660.x>
- Bogutz, A. B., Oh-McGinnis, R., Jacob, K. J., Ho-Lau, R., Gu, T., Gertsenstein, M., Nagy, A., & Lefebvre, L. (2018). Transcription factor ASCL2 is required for development of the glycogen trophoblast cell lineage. *PLoS Genet*, 14(8), e1007587. <https://doi.org/10.1371/journal.pgen.1007587>
- Bole-Feysot, C., Goffin, V., Edery, M., Binart, N., & Kelly, P. A. (1998). Prolactin (PRL) and Its Receptor: Actions, Signal Transduction Pathways and Phenotypes Observed in PRL Receptor Knockout Mice. *Endocrine Reviews*, 19(3), 225-268. <https://doi.org/10.1210/edrv.19.3.0334>
- Bouillot, S., Rampon, C., Tillet, E., & Huber, P. (2006). Tracing the Glycogen Cells with Protocadherin 12 During Mouse Placenta Development. *Placenta*, 27(8), 882-888. <https://doi.org/https://doi.org/10.1016/j.placenta.2005.09.009>
- Bourc'his, D., Xu, G.-L., Lin, C.-S., Bollman, B., & Bestor, T. H. (2001). Dnmt3L and the Establishment of Maternal Genomic Imprints. *Science*, 294(5551), 2536-2539. <https://doi.org/10.1126/science.1065848>
- Boyd, K. L., Muehlenbachs, A., Rendi, M. H., Garcia, R. L., & Gibson-Corley, K. N. (2018). 17 - Female Reproductive System. In P. M. Treuting, S. M. Dintzis, & K. S. Montine (Eds.), *Comparative Anatomy and Histology (Second Edition)* (pp. 303-334). Academic Press. <https://doi.org/https://doi.org/10.1016/B978-0-12-802900-8.00017-8>
- Bridges, R. S. (2015). Neuroendocrine regulation of maternal behavior. *Frontiers in Neuroendocrinology*, 36, 178-196. <https://doi.org/https://doi.org/10.1016/j.yfrne.2014.11.007>

- Bridges, R. S., DiBiase, R., Loundes, D. D., & Doherty, P. C. (1985). Prolactin Stimulation of Maternal Behavior in Female Rats. *Science*, 227(4688), 782-784. <https://doi.org/10.1126/science.3969568>
- Bridges, R. S., & Nephew, B. C. (2009). Neuroendocrine Control: Maternal Behavior. In L. R. Squire (Ed.), *Encyclopedia of Neuroscience* (pp. 333-342). Academic Press. <https://doi.org/https://doi.org/10.1016/B978-008045046-9.01182-7>
- Bridges, R. S., Numan, M., Ronsheim, P. M., Mann, P. E., & Lupini, C. E. (1990). Central prolactin infusions stimulate maternal behavior in steroid-treated, nulliparous female rats. *Proceedings of the National Academy of Sciences*, 87(20), 8003-8007. <https://doi.org/10.1073/pnas.87.20.8003>
- Bridges, R. S., Robertson, M. C., Shiu, R. P. C., Sturgis, J. D., Henriquez, B. M., & Mann, P. E. (1997). Central Lactogenic Regulation of Maternal Behavior in Rats: Steroid Dependence, Hormone Specificity, and Behavioral Potencies of Rat Prolactin and Rat Placental Lactogen I*. *Endocrinology*, 138(2), 756-763. <https://doi.org/10.1210/endo.138.2.4921>
- Broad, K. D., & Keverne, E. B. (2011). Placental protection of the fetal brain during short-term food deprivation. *Proc Natl Acad Sci U S A*, 108(37), 15237-15241. <https://doi.org/10.1073/pnas.1106022108>
- Brown, R. S. E., Kokay, I. C., Herbison, A. E., & Grattan, D. R. (2010). Distribution of prolactin-responsive neurons in the mouse forebrain. *Journal of Comparative Neurology*, 518(1), 92-102. <https://doi.org/https://doi.org/10.1002/cne.22208>
- Brown, S. D. M., Chartier, F., Johnson, K., & Cavanna, J. S. (1993). Mapping the Hrc Gene to Proximal Mouse Chromosome 7: Delineation of a Conserved Linkage Group with Human 19q. *Genomics*, 18(2), 459-461. <https://doi.org/https://doi.org/10.1006/geno.1993.1502>
- Brunton, P. J., & Russell, J. A. (2008). The expectant brain: adapting for motherhood. *Nature Reviews Neuroscience*, 9(1), 11-25. <https://doi.org/10.1038/nrn2280>
- Brunton, P. J., & Russell, J. A. (2010). Endocrine induced changes in brain function during pregnancy. *Brain Research*, 1364, 198-215. <https://doi.org/https://doi.org/10.1016/j.brainres.2010.09.062>
- Burton, G. J., & Fowden, A. L. (2015). The placenta: a multifaceted, transient organ. *Philos Trans R Soc Lond B Biol Sci*, 370(1663), 20140066. <https://doi.org/10.1098/rstb.2014.0066>
- Burton, G. J., & Jauniaux, E. (2015). What is the placenta? *Am J Obstet Gynecol*, 213(4 Suppl), S6.e1, S6-8. <https://doi.org/10.1016/j.ajog.2015.07.050>
- Buvinić, M., Medici, A., & Fernández E, e. a. (2006). Gender Differentials in Health. *Disease Control Priorities in Developing Countries*, 2nd edition. <https://www.ncbi.nlm.nih.gov/books/NBK11729/>

- Cameron, D. M., & Hunt, J. M. (2016). The Prime Minister will announce almost a billion pounds of investment to enhance mental health services across the country. <https://www.gov.uk/government/news/prime-minister-pledges-a-revolution-in-mental-health-treatment>
- Cao, W., Douglas, K. C., Samollow, P. B., VandeBerg, J. L., Wang, X., & Clark, A. G. (2023). Origin and Evolution of Marsupial-specific Imprinting Clusters Through Lineage-specific Gene Duplications and Acquisition of Promoter Differential Methylation. *Molecular Biology and Evolution*, 40(2), 22. <https://doi.org/10.1093/molbev/msad022>
- Carney, E. W., Prideaux, V., Lye, S. J., & Rossant, J. (1993). Progressive expression of trophoblast-specific genes during formation of mouse trophoblast giant cells in vitro. *Mol Reprod Dev*, 34(4), 357-368. <https://doi.org/10.1002/mrd.1080340403>
- Carrion, S. A., Michal, J. J., & Jiang, Z. (2023). Imprinted Genes: Genomic Conservation, Transcriptomic Dynamics and Phenomic Significance in Health and Diseases. *Int J Biol Sci*, 19(10), 3128-3142. <https://doi.org/10.7150/ijbs.83712>
- Carter, A. M., & Enders, A. C. (2004). Comparative aspects of trophoblast development and placentation. *Reproductive Biology and Endocrinology*, 2(1), 46. <https://doi.org/10.1186/1477-7827-2-46>
- Cassidy, F. C., & Charalambous, M. (2018). Genomic imprinting, growth and maternal-fetal interactions. *J Exp Biol*, 221(Pt Suppl 1). <https://doi.org/10.1242/jeb.164517>
- Cattanach, B. M., & Kirk, M. (1985). Differential activity of maternally and paternally derived chromosome regions in mice. *Nature*, 315(6019), 496-498. <https://doi.org/10.1038/315496a0>
- Change.org. (2021). Women are 73% more likely to be injured in a vehicle than men - Demand Equal Crash Testing. <https://www.change.org/p/women-are-73-more-likely-to-get-injured-in-a-car-crash-demand-equality-for-women>
- Charron, J., Bissonauth, V., & Nadeau, V. (2012). Implication of MEK1 and MEK2 in the establishment of the blood-placenta barrier during placentogenesis in mouse. *Reprod Biomed Online*, 25(1), 58-67. <https://doi.org/10.1016/j.rbmo.2012.02.012>
- Chauhan, A., & Potdar, J. (2022). Maternal Mental Health During Pregnancy: A Critical Review. *Cureus*, 14(10), e30656. <https://doi.org/10.7759/cureus.30656>
- Chawengsaksophak, K., James, R., Hammond, V. E., Köntgen, F., & Beck, F. (1997). Homeosis and intestinal tumours in Cdx2 mutant mice. *Nature*, 386(6620), 84-87. <https://doi.org/10.1038/386084a0>
- Chen, E. Y., Liao, Y.-C., Smith, D. H., Barrera-Saldaña, H. A., Gelinas, R. E., & Seeburg, P. H. (1989). The human growth hormone locus: nucleotide sequence, biology, and evolution. *Genomics*, 4(4), 479-497.

- Choufani, S., Shuman, C., & Weksberg, R. (2010). Beckwith-Wiedemann syndrome. *Am J Med Genet C Semin Med Genet*, 154c(3), 343-354. <https://doi.org/10.1002/ajmg.c.30267>
- Christians, J. K. (2022). The Placenta's Role in Sexually Dimorphic Fetal Growth Strategies. *Reproductive Sciences*, 29(6), 1895-1907. <https://doi.org/10.1007/s43032-021-00780-3>
- Christie, G. A. (1967). Comparative histochemical distribution of glycogen and alkaline phosphatases in the placenta. *Histochemie*, 9(2), 93-116. <https://doi.org/10.1007/BF00305853>
- Clifton, V. L. (2010). Review: Sex and the human placenta: mediating differential strategies of fetal growth and survival. *Placenta*, 31 Suppl, S33-39. <https://doi.org/10.1016/j.placenta.2009.11.010>
- Clutton-Brock, T. H., & Scott, D. (1991). *The Evolution of Parental Care* (Vol. 64). Princeton University Press. <https://doi.org/10.2307/j.ctvs32ssj>
- Coan, P. M., Angiolini, E., Sandovici, I., Burton, G. J., Constância, M., & Fowden, A. L. (2008). Adaptations in placental nutrient transfer capacity to meet fetal growth demands depend on placental size in mice. *J Physiol*, 586(18), 4567-4576. <https://doi.org/10.1113/jphysiol.2008.156133>
- Coan, P. M., Conroy, N., Burton, G. J., & Ferguson-Smith, A. C. (2006). Origin and characteristics of glycogen cells in the developing murine placenta. *Developmental Dynamics*, 235(12), 3280-3294. <https://doi.org/https://doi.org/10.1002/dvdy.20981>
- Coan, P. M., Ferguson-Smith, A. C., & Burton, G. J. (2005). Ultrastructural changes in the interhaemal membrane and junctional zone of the murine chorioallantoic placenta across gestation. *J Anat*, 207(6), 783-796. <https://doi.org/10.1111/j.1469-7580.2005.00488.x>
- Cole, L. A. (1997). Immunoassay of human chorionic gonadotropin, its free subunits, and metabolites. *Clin Chem*, 43(12), 2233-2243.
- Cooke, N. E., & Liebhaber, S. A. (1995). Molecular Biology of the Growth Hormone-Prolactin Gene System. In G. Litwack (Ed.), *Vitamins & Hormones* (Vol. 50, pp. 385-459). Academic Press. [https://doi.org/https://doi.org/10.1016/S0083-6729\(08\)60659-7](https://doi.org/https://doi.org/10.1016/S0083-6729(08)60659-7)
- Cooper, W. O., Willy, M. E., Pont, S. J., & Ray, W. A. (2007). Increasing use of antidepressants in pregnancy. *American Journal of Obstetrics and Gynecology*, 196(6), 544.e541-544.e545. <https://doi.org/https://doi.org/10.1016/j.ajog.2007.01.033>
- Costa, M. A. (2016). The endocrine function of human placenta: an overview. *Reproductive BioMedicine Online*, 32(1), 14-43. <https://doi.org/10.1016/j.rbmo.2015.10.005>
- Coverdale, J. H. M., MEd; McCullough, Laurence B. PhD; Chervenak, Frank A. MD. (2008). The Ethics of Randomized Placebo-Controlled Trials of Antidepressants With Pregnant Women: A Systematic Review. *Obstetrics & Gynecology*, 112(6), 1361-1368.

https://journals.lww.com/greenjournal/abstract/2008/12000/the_et_hics_of_randomized_placebo_controlled_trials.26.aspx#

- Cowley, M., Garfield, A. S., Madon-Simon, M., Charalambous, M., Clarkson, R. W., Smalley, M. J., Kendrick, H., Isles, A. R., Parry, A. J., Carney, S., Oakey, R. J., Heisler, L. K., Moorwood, K., Wolf, J. B., & Ward, A. (2014). Developmental programming mediated by complementary roles of imprinted Grb10 in mother and pup. *PLoS Biol*, *12*(2), e1001799. <https://doi.org/10.1371/journal.pbio.1001799>
- Cox, E., MD, Sowa, N. M., Meltzer-Brody, S. M., MPH, & Gaynes, B. M., MPH. (2016). The Perinatal Depression Treatment Cascade: Baby Steps Toward Improving Outcomes. *The journal of clinical psychiatry*. <https://www.psychiatrist.com/jcp/the-perinatal-depression-treatment-cascade/>
- Creeth, H. D. J., & John, R. M. (2020). The placental programming hypothesis: Placental endocrine insufficiency and the co-occurrence of low birth weight and maternal mood disorders. *Placenta*, *98*, 52-59. <https://doi.org/10.1016/j.placenta.2020.03.011>
- Creeth, H. D. J., McNamara, G. I., Isles, A. R., & John, R. M. (2019). Imprinted genes influencing the quality of maternal care. *Frontiers in Neuroendocrinology*, *53*, 100732. <https://doi.org/https://doi.org/10.1016/j.yfrne.2018.12.003>
- Creeth, H. D. J., McNamara, G. I., Tunster, S. J., Boque-Sastre, R., Allen, B., Sumption, L., Eddy, J. B., Isles, A. R., & John, R. M. (2018). Maternal care boosted by paternal imprinting in mammals. *PLOS Biology*, *16*(7), e2006599. <https://doi.org/10.1371/journal.pbio.2006599>
- Cronin, P. A., & Gemignani, M. L. (2018). 14 - Breast Diseases. In P. J. DiSaia, W. T. Creasman, R. S. Mannel, D. S. McMeekin, & D. G. Mutch (Eds.), *Clinical Gynecologic Oncology (Ninth Edition)* (pp. 320-352.e326). Elsevier. <https://doi.org/https://doi.org/10.1016/B978-0-323-40067-1.00014-0>
- Cummings, E. M., & Davies, P. T. (1994). Maternal Depression and Child Development. *Journal of Child Psychology and Psychiatry*, *35*(1), 73-122. <https://doi.org/https://doi.org/10.1111/j.1469-7610.1994.tb01133.x>
- Curley, J. P., Barton, S., Surani, A., & Keverne, E. B. (2004). Coadaptation in mother and infant regulated by a paternally expressed imprinted gene. *Proc Biol Sci*, *271*(1545), 1303-1309. <https://doi.org/10.1098/rspb.2004.2725>
- Curley, J. P., Pinnock, S. B., Dickson, S. L., Thresher, R., Miyoshi, N., Surani, M. A., & Keverne, E. B. (2005). Increased body fat in mice with a targeted mutation of the paternally expressed imprinted gene Peg3. *Faseb j*, *19*(10), 1302-1304. <https://doi.org/10.1096/fj.04-3216fje>

- D'Alton, M. E., Friedman, A. M., Bernstein, P. S., Brown, H. L., Callaghan, W. M., Clark, S. L., Grobman, W. A., Kilpatrick, S. J., O'Keeffe, D. F., Montgomery, D. M., Srinivas, S. K., Wendel, G. D., Wenstrom, K. D., & Foley, M. R. (2019). Putting the "M" back in maternal-fetal medicine: A 5-year report card on a collaborative effort to address maternal morbidity and mortality in the United States. *Am J Obstet Gynecol*, 221(4), 311-317.e311.
<https://doi.org/10.1016/j.ajog.2019.02.055>
- Dagher, R. K., Bruckheim, H. E., Colpe, L. J., Edwards, E., & White, D. B. (2021). Perinatal Depression: Challenges and Opportunities. *Journal of Women's Health*, 30(2), 154-159.
<https://doi.org/10.1089/jwh.2020.8862>
- Dayan, J., Creveuil, C., Herlicoviez, M., Herbel, C., Baranger, E., Savoye, C., & Thouin, A. (2002). Role of anxiety and depression in the onset of spontaneous preterm labor. *Am J Epidemiol*, 155(4), 293-301.
<https://doi.org/10.1093/aje/155.4.293>
- DeChiara, T. M., Efstratiadis, A., & Robertsen, E. J. (1990). A growth-deficiency phenotype in heterozygous mice carrying an insulin-like growth factor II gene disrupted by targeting. *Nature*, 345(6270), 78-80. <https://doi.org/10.1038/345078a0>
- DeChiara, T. M., Robertson, E. J., & Efstratiadis, A. (1991). Parental imprinting of the mouse insulin-like growth factor II gene. *Cell*, 64(4), 849-859. [https://doi.org/10.1016/0092-8674\(91\)90513-X](https://doi.org/10.1016/0092-8674(91)90513-X)
- Deltour, L., Montagutelli, X., Guenet, J.-L., Jami, J., & Páldi, A. (1995). Tissue- and Developmental Stage-Specific Imprinting of the Mouse Proinsulin Gene, Ins2. *Developmental Biology*, 168(2), 686-688.
<https://doi.org/https://doi.org/10.1006/dbio.1995.1114>
- Deng, Y., & Wu, X. (2000). Peg3/Pw1 promotes p53-mediated apoptosis by inducing Bax translocation from cytosol to mitochondria. *Proc Natl Acad Sci U S A*, 97(22), 12050-12055.
<https://doi.org/10.1073/pnas.97.22.12050>
- Denizot, A. L., Besson, V., Correra, R. M., Mazzola, A., Lopes, I., Courbard, J. R., Marazzi, G., & Sassoon, D. A. (2016). A Novel Mutant Allele of Pw1/Peg3 Does Not Affect Maternal Behavior or Nursing Behavior. *PLoS Genet*, 12(5), e1006053.
<https://doi.org/10.1371/journal.pgen.1006053>
- Dennis, C.-L., Falah-Hassani, K., & Shiri, R. (2017). Prevalence of antenatal and postnatal anxiety: Systematic review and meta-analysis. *British Journal of Psychiatry*, 210(5), 315-323.
<https://doi.org/10.1192/bjp.bp.116.187179>
- Diaz-Santana, M. V., O'Brien, K. M., Park, Y. M., Sandler, D. P., & Weinberg, C. R. (2022). Persistence of Risk for Type 2 Diabetes After Gestational Diabetes Mellitus. *Diabetes Care*, 45(4), 864-870.
<https://doi.org/10.2337/dc21-1430>
- Dicke, J. M., & Henderson, G. I. (1988). Placental Amino Acid Uptake in Normal and Complicated Pregnancies. *The American Journal of the Medical Sciences*, 295(3), 223-227.

<https://doi.org/https://doi.org/10.1097/00000441-198803000-00012>

- Diego, M. A., Jones, N. A., Field, T., Hernandez-Reif, M., Schanberg, S., Kuhn, C., & Gonzalez-Garcia, A. (2006). Maternal Psychological Distress, Prenatal Cortisol, and Fetal Weight. *Psychosomatic Medicine*, 68(5).
https://journals.lww.com/psychosomaticmedicine/fulltext/2006/09000/maternal_psychological_distress_prenatal.15.aspx
- DiPietro, J. A., & Voegtline, K. M. (2017). The gestational foundation of sex differences in development and vulnerability. *Neuroscience*, 342, 4-20. <https://doi.org/10.1016/j.neuroscience.2015.07.068>
- Doody, J. S., Burghardt, G. M., & Dinets, V. (2013). Breaking the Social-Non-social Dichotomy: A Role for Reptiles in Vertebrate Social Behavior Research? *Ethology*, 119(2), 95-103.
<https://doi.org/https://doi.org/10.1111/eth.12047>
- Doria-Borrell, P., Moya-Navamuel, M., Hemberger, M., & Pérez-García, V. (2024). Generation of Knockout Mouse Trophoblast Stem Cells by CRISPR/Cas9. In V. Zaga-Clavellina (Ed.), *Maternal Placental Interface: Methods and Protocols* (pp. 81-91). Springer US.
https://doi.org/10.1007/978-1-0716-3746-3_8
- Dunwoodie, S. L., & Beddington, R. S. (2002). The expression of the imprinted gene *Ipl* is restricted to extra-embryonic tissues and embryonic lateral mesoderm during early mouse development. *Int J Dev Biol*, 46(4), 459-466.
- Dupressoir, A., Vernochet, C., Bawa, O., Harper, F., Pierron, G., Opolon, P., & Heidmann, T. (2009). Syncytin-A knockout mice demonstrate the critical role in placentation of a fusogenic, endogenous retrovirus-derived, envelope gene. *Proc Natl Acad Sci U S A*, 106(29), 12127-12132. <https://doi.org/10.1073/pnas.0902925106>
- Dupressoir, A., Vernochet, C., Harper, F., Guégan, J., Dessen, P., Pierron, G., & Heidmann, T. (2011). A pair of co-opted retroviral envelope syncytin genes is required for formation of the two-layered murine placental syncytiotrophoblast. *Proc Natl Acad Sci U S A*, 108(46), E1164-1173. <https://doi.org/10.1073/pnas.1112304108>
- Dutton, P. J., Warrander, L. K., Roberts, S. A., Bernatavicius, G., Byrd, L. M., Gaze, D., Kroll, J., Jones, R. L., Sibley, C. P., Frøen, J. F., & Heazell, A. E. (2012). Predictors of poor perinatal outcome following maternal perception of reduced fetal movements--a prospective cohort study. *PLoS One*, 7(7), e39784.
<https://doi.org/10.1371/journal.pone.0039784>
- Edwards, C. A., Mungall, A. J., Matthews, L., Ryder, E., Gray, D. J., Pask, A. J., Shaw, G., Graves, J. A., Rogers, J., Dunham, I., Renfree, M. B., & Ferguson-Smith, A. C. (2008). The evolution of the DLK1-DIO3 imprinted domain in mammals. *PLoS Biol*, 6(6), e135.
<https://doi.org/10.1371/journal.pbio.0060135>
- El-Baradi, T., & Pieler, T. (1991). Zinc finger proteins: what we know and what we would like to know. *Mechanisms of Development*, 35(3),

- 155-169. [https://doi.org/https://doi.org/10.1016/0925-4773\(91\)90015-X](https://doi.org/https://doi.org/10.1016/0925-4773(91)90015-X)
- Engemann, S., Strödicke, M., Paulsen, M., Franck, O., Reinhardt, R., Lane, N., Reik, W., & Walter, J. (2000). Sequence and functional comparison in the Beckwith-Wiedemann region: implications for a novel imprinting centre and extended imprinting. *Hum Mol Genet*, 9(18), 2691-2706. <https://doi.org/10.1093/hmg/9.18.2691>
- Ensembl. (2017). GRCm38: Ensembl release 89. https://www.ensembl.org/Help/ArchiveRedirect?src=http%3A%2F%2Fmay2017.archive.ensembl.org%2FMus_musculus%2FGene%2FSummary%3Fdb%3Dcore%3Bg%3DENSMUSG00000010760
- Epker, E. (2023). Female Car Crash Test Dummy Represents Average Women For The First Time In 60+ Years. *Forbes*. <https://www.forbes.com/sites/evaepker/2023/09/12/fasten-your-seatbelts-a-female-car-crash-test-dummy-represents-average-women-for-the-first-time-in-60-years/>
- Eriksson, J. G., Kajantie, E., Osmond, C., Thornburg, K., & Barker, D. J. (2010). Boys live dangerously in the womb. *Am J Hum Biol*, 22(3), 330-335. <https://doi.org/10.1002/ajhb.20995>
- Faa, G., Fanos, V., Manchia, M., Van Eyken, P., Suri, J. S., & Saba, L. (2024). The fascinating theory of fetal programming of adult diseases: A review of the fundamentals of the Barker hypothesis. *Journal of Public Health Research*, 13(1), 22799036241226817. <https://doi.org/10.1177/22799036241226817>
- Faria, T. N., & Soares, M. J. (1991). Trophoblast Cell Differentiation: Establishment, Characterization, and Modulation of a Rat Trophoblast Cell Line Expressing Members of the Placental Prolactin Family*. *Endocrinology*, 129(6), 2895-2906. <https://doi.org/10.1210/endo-129-6-2895>
- Ferguson-Smith, A. C. (2011). Genomic imprinting: the emergence of an epigenetic paradigm. *Nature Reviews Genetics*, 12(8), 565-575. <https://doi.org/10.1038/nrg3032>
- Ferguson-Smith, A. C., & Bourc'his, D. (2018). The discovery and importance of genomic imprinting. *Elife*, 7. <https://doi.org/10.7554/eLife.42368>
- Ferguson-Smith, A. C., Cattanach, B. M., Barton, S. C., Beechey, C. V., & Surani, M. A. (1991). Embryological and molecular investigations of parental imprinting on mouse chromosome 7. *Nature*, 351(6328), 667-670. <https://doi.org/10.1038/351667a0>
- Ferguson-Smith, A. C., & Surani, M. A. (2001). Imprinting and the epigenetic asymmetry between parental genomes. *Science*, 293(5532), 1086-1089. <https://doi.org/10.1126/science.1064020>
- Fitzpatrick, G. V., Soloway, P. D., & Higgins, M. J. (2002). Regional loss of imprinting and growth deficiency in mice with a targeted deletion of KvDMR1. *Nature Genetics*, 32(3), 426-431. <https://doi.org/10.1038/ng988>

- Fowden, A. L., Sibley, C., Reik, W., & Constancia, M. (2006). Imprinted genes, placental development and fetal growth. *Horm Res, 65 Suppl 3*, 50-58. <https://doi.org/10.1159/000091506>
- Fox, M. (2023). Despite decades of promises, health research still overlooks women. *The Guardian*. <https://www.theguardian.com/science/2023/nov/20/women-health-research-jill-biden-white-house>
- Frank, D., Fortino, W., Clark, L., Musalo, R., Wang, W., Saxena, A., Li, C. M., Reik, W., Ludwig, T., & Tycko, B. (2002). Placental overgrowth in mice lacking the imprinted gene *Ipl* [Article]. *Proceedings of the National Academy of Sciences of the United States of America*, 99(11), 7490-7495. <https://doi.org/10.1073/pnas.122039999>
- Frankenberg, S. R., de Barros, F. R. O., Rossant, J., & Renfree, M. B. (2016). The mammalian blastocyst. *WIREs Developmental Biology*, 5(2), 210-232. <https://doi.org/https://doi.org/10.1002/wdev.220>
- Fransson, E., Sörensen, F., Kunovac Kallak, T., Ramklint, M., Eckerdal, P., Heimgärtner, M., Krägeloh-Mann, I., & Skalkidou, A. (2020). Maternal perinatal depressive symptoms trajectories and impact on toddler behavior – the importance of symptom duration and maternal bonding. *Journal of Affective Disorders*, 273, 542-551. <https://doi.org/https://doi.org/10.1016/j.jad.2020.04.003>
- Freyer, C., Zeller, U., & Renfree, M. B. (2003). The marsupial placenta: A phylogenetic analysis. *Journal of Experimental Zoology Part A: Comparative Experimental Biology*, 299A(1), 59-77. <https://doi.org/https://doi.org/10.1002/jez.a.10291>
- Frost, J. M., & Moore, G. E. (2010). The importance of imprinting in the human placenta. *PLoS Genet*, 6(7), e1001015. <https://doi.org/10.1371/journal.pgen.1001015>
- Gao, H., Gao, R., Zhang, L., Xiu, W., Zang, R., Wang, H., Zhang, Y., Chen, J., Gao, Y., & Gao, S. (2019). *Esrrb* plays important roles in maintaining self-renewal of trophoblast stem cells (TSCs) and reprogramming somatic cells to induced TSCs. *Journal of Molecular Cell Biology*, 11(6), 463-473. <https://doi.org/10.1093/jmcb/mjy054>
- Gao, Y., Han, W., Dong, R., Wei, S., Chen, L., Gu, Z., Liu, Y., Guo, W., & Yan, F. (2024). Efficient Reprogramming of Mouse Embryonic Stem Cells into Trophoblast Stem-like Cells via Lats Kinase Inhibition. *Biology*, 13(2).
- Garay, S. M., Sumption, L. A., & John, R. M. (2022). Prenatal health behaviours as predictors of human placental lactogen levels [Original Research]. *Frontiers in Endocrinology*, 13. <https://doi.org/10.3389/fendo.2022.946539>
- Gasperowicz, M., Surmann-Schmitt, C., Hamada, Y., Otto, F., & Cross, J. C. (2013). The transcriptional co-repressor TLE3 regulates development of trophoblast giant cells lining maternal blood spaces in the mouse placenta. *Dev Biol*, 382(1), 1-14. <https://doi.org/10.1016/j.ydbio.2013.08.005>

- Georgescu, T., Swart, J. M., Grattan, D. R., & Brown, R. S. E. (2021). The Prolactin Family of Hormones as Regulators of Maternal Mood and Behavior. *Front Glob Womens Health, 2*, 767467. <https://doi.org/10.3389/fgwh.2021.767467>
- Gerardo-Gettens, T., Moore, B. J., Stern, J. S., & Horwitz, B. A. (1989). Prolactin stimulates food intake in a dose-dependent manner. *Am J Physiol, 256*(1 Pt 2), R276-280. <https://doi.org/10.1152/ajpregu.1989.256.1.R276>
- Ghoshal, I., Bolar Suryakanth, V., Belle, V. S., & Prabhu, K. (2019). Role of Maternal Serum Human Placental Lactogen in First Trimester Screening. *Indian J Clin Biochem, 34*(3), 318-323. <https://doi.org/10.1007/s12291-018-0750-1>
- Girchenko, P., Robinson, R., Rantalainen, V. J., Lahti-Pulkkinen, M., Heinonen-Tuomaala, K., Lemola, S., Wolke, D., Schnitzlein, D., Hämäläinen, E., Laivuori, H., Villa, P. M., Kajantie, E., & Räikkönen, K. (2022). Maternal postpartum depressive symptoms partially mediate the association between preterm birth and mental and behavioral disorders in children. *Scientific Reports, 12*(1), 947. <https://doi.org/10.1038/s41598-022-04990-w>
- Glynn, L. M., Davis, E. P., Sandman, C. A., & Goldberg, W. A. (2016). Gestational hormone profiles predict human maternal behavior at 1-year postpartum. *Horm Behav, 85*, 19-25. <https://doi.org/10.1016/j.yhbeh.2016.07.002>
- Gomes, M. V., Huber, J., Ferriani, R. A., Amaral Neto, A. M., & Ramos, E. S. (2009). Abnormal methylation at the KvDMR1 imprinting control region in clinically normal children conceived by assisted reproductive technologies. *Molecular Human Reproduction, 15*(8), 471-477. <https://doi.org/10.1093/molehr/gap038>
- Grattan, D. (2011). A Mother's Brain Knows. *Journal of Neuroendocrinology, 23*(11), 1188-1189. <https://doi.org/https://doi.org/10.1111/j.1365-2826.2011.02175.x>
- Grattan, D. R., & Ladyman, S. R. (2020). Chapter 2 - Neurophysiological and cognitive changes in pregnancy. In E. A. P. Steegers, M. J. Cipolla, & E. C. Miller (Eds.), *Handbook of Clinical Neurology* (Vol. 171, pp. 25-55). Elsevier. <https://doi.org/https://doi.org/10.1016/B978-0-444-64239-4.00002-3>
- Green, J. A. (2004). Defining the function of a prolactin gene family member. *Proceedings of the National Academy of Sciences, 101*(47), 16397-16398. <https://doi.org/10.1073/pnas.0406934101>
- Gross, M. R. (2005). The evolution of parental care. *Q Rev Biol, 80*(1), 37-45. <https://doi.org/10.1086/431023>
- Gude, N. M., Roberts, C. T., Kalionis, B., & King, R. G. (2004). Growth and function of the normal human placenta. *Thromb Res, 114*(5-6), 397-407. <https://doi.org/10.1016/j.thromres.2004.06.038>
- Guillemot, F., Caspary, T., Tilghman, S. M., Copeland, N. G., Gilbert, D. J., Jenkins, N. A., Anderson, D. J., Joyner, A. L., Rossant, J., &

- Nagy, A. (1995). Genomic imprinting of Mash2, a mouse gene required for trophoblast development. *Nat Genet*, 9(3), 235-242. <https://doi.org/10.1038/ng0395-235>
- Guillemot, F., Nagy, A., Auerbach, A., Rossant, J., & Joyner, A. L. (1994). Essential role of Mash-2 in extraembryonic development. *Nature*, 371(6495), 333-336. <https://doi.org/10.1038/371333a0>
- Guttmacher, A. E., Maddox, Y. T., & Spong, C. Y. (2014). The Human Placenta Project: Placental structure, development, and function in real time. *Placenta*, 35(5), 303-304. <https://doi.org/https://doi.org/10.1016/j.placenta.2014.02.012>
- Haig, D. (2014). Coadaptation and conflict, misconception and muddle, in the evolution of genomic imprinting. *Heredity*, 113(2), 96-103. <https://doi.org/10.1038/hdy.2013.97>
- Haig, D., & Graham, C. (1991). Genomic imprinting and the strange case of the insulin-like growth factor II receptor. *Cell*, 64(6), 1045-1046. [https://doi.org/10.1016/0092-8674\(91\)90256-x](https://doi.org/10.1016/0092-8674(91)90256-x)
- Haig, D., & Trivers, R. (1995). The evolution of parental imprinting: a review of hypotheses. *Genomic imprinting: Causes and consequences*, 17-28.
- Haig, D., & Westoby, M. (1989). Parent-Specific Gene Expression and the Triploid Endosperm. *The American Naturalist*, 134(1), 147-155. <http://www.jstor.org.abc.cardiff.ac.uk/stable/2462281>
- Hales, C. N., Barker, D. J., Clark, P. M., Cox, L. J., Fall, C., Osmond, C., & Winter, P. D. (1991). Fetal and infant growth and impaired glucose tolerance at age 64. *British Medical Journal*, 303(6809), 1019. <https://doi.org/10.1136/bmj.303.6809.1019>
- Hales, C. N., & Barker, D. J. P. (2013). Type 2 (non-insulin-dependent) diabetes mellitus: the thrifty phenotype hypothesis*,†. *International Journal of Epidemiology*, 42(5), 1215-1222. <https://doi.org/10.1093/ije/dyt133>
- Handwerger, S., & Brar, A. (2001). Human Uteroplacental Lactogens: Physiology and Molecular Biology. In N. D. Horseman (Ed.), *Prolactin* (pp. 169-187). Springer US. https://doi.org/10.1007/978-1-4615-1683-5_9
- Handwerger, S., & Freemark, M. (2000). The Roles of Placental Growth Hormone and Placental Lactogen in the Regulation of Human Fetal Growth and Development. 13(4), 343-356. <https://doi.org/doi:10.1515/JPEM.2000.13.4.343> (Journal of Pediatric Endocrinology and Metabolism)
- Hanna, C. W. (2020). Placental imprinting: Emerging mechanisms and functions. *PLoS Genet*, 16(4), e1008709. <https://doi.org/10.1371/journal.pgen.1008709>
- Harlow, H. F., Dodsworth, R. O., & Harlow, M. K. (1965). Total social isolation in monkeys. *Proc Natl Acad Sci U S A*, 54(1), 90-97. <https://doi.org/10.1073/pnas.54.1.90>
- Harrison, D. J., Creeth, H. D. J., Tyson, H. R., Boque-Sastre, R., Hunter, S., Dwyer, D. M., Isles, A. R., & John, R. M. (2021). Placental

- endocrine insufficiency programs anxiety, deficits in cognition and atypical social behaviour in offspring. *Human Molecular Genetics*, 30(19), 1863-1880. <https://doi.org/10.1093/hmg/ddab154>
- Hata, K., Okano, M., Lei, H., & Li, E. (2002). Dnmt3L cooperates with the Dnmt3 family of de novo DNA methyltransferases to establish maternal imprints in mice. *Development*, 129(8), 1983-1993. <https://doi.org/10.1242/dev.129.8.1983>
- Hatada, I., & Mukai, T. (1995). Genomic imprinting of p57KIP2, a cyclin-dependent kinase inhibitor, in mouse. *Nat Genet*, 11(2), 204-206. <https://doi.org/10.1038/ng1095-204>
- Hayes, L. J., Goodman, S. H., & Carlson, E. (2013). Maternal antenatal depression and infant disorganized attachment at 12 months. *Attachment & Human Development*, 15(2), 133-153. <https://doi.org/10.1080/14616734.2013.743256>
- Health, N. I. o. (2021). Office of Research on Women's Health Historical Timeline. In.
- Hemberger, M., & Cross, J. C. (2001). Genes governing placental development. *Trends in Endocrinology & Metabolism*, 12(4), 162-168. [https://doi.org/10.1016/S1043-2760\(01\)00375-7](https://doi.org/10.1016/S1043-2760(01)00375-7)
- Hemberger, M., & Dean, W. (2014). First Cell Fate Decisions in Early Development: Towards Establishment of the Trophoblast Lineage. In B. A. Croy, A. T. Yamada, F. J. DeMayo, & S. L. Adamson (Eds.), *The Guide to Investigation of Mouse Pregnancy* (pp. 95-106). Academic Press. <https://doi.org/https://doi.org/10.1016/B978-0-12-394445-0.00008-4>
- Herrick EJ, B. B. (2023). Embryology, Placenta. *Embryology, Placenta*. [Updated 2023 May 1]. In: StatPearls [Internet]. Treasure Island (FL): StatPearls Publishing; 2024 Jan-. Available from: <https://www.ncbi.nlm.nih.gov/books/NBK551634/>
- Heyne, G. W., Plisch, E. H., Melberg, C. G., Sandgren, E. P., Peter, J. A., & Lipinski, R. J. (2015). A Simple and Reliable Method for Early Pregnancy Detection in Inbred Mice. *J Am Assoc Lab Anim Sci*, 54(4), 368-371.
- Hiby, S. E., Lough, M., Keverne, E. B., Surani, M. A., Loke, Y. W., & King, A. (2001). Paternal monoallelic expression of PEG3 in the human placenta. *Hum Mol Genet*, 10(10), 1093-1100. <https://doi.org/10.1093/hmg/10.10.1093>
- Hino, T., Oda, K., Nakamura, K., Toyoda, Y., & Yokoyama, M. (2009). Low fertility in vivo resulting from female factors causes small litter size in 129 inbred mice. *Reprod Med Biol*, 8(4), 157-161. <https://doi.org/10.1007/s12522-009-0024-y>
- Hirt, H., Kimelman, J., Birnbaum, M. J., Chen, E. Y., Seeburg, P. H., Eberhardt, N. L., & Barta, A. (1987). The Human Growth Hormone Gene Locus: Structure, Evolution, and Allelic Variations. *DNA*, 6(1), 59-70. <https://doi.org/10.1089/dna.1987.6.59>
- Hoekzema, E., Barba-Müller, E., Pozzobon, C., Picado, M., Lucco, F., García-García, D., Soliva, J. C., Tobeña, A., Desco, M., Crone, E. A.,

- Ballesteros, A., Carmona, S., & Vilarroya, O. (2017). Pregnancy leads to long-lasting changes in human brain structure. *Nature Neuroscience*, 20(2), 287-296. <https://doi.org/10.1038/nn.4458>
- Holdcroft, A. (2007). Gender bias in research: how does it affect evidence based medicine? *J R Soc Med*, 100(1), 2-3. <https://doi.org/10.1177/014107680710000102>
- Hong, Y. H., & Lee, J. E. (2021). Large for Gestational Age and Obesity-Related Comorbidities. *J Obes Metab Syndr*, 30(2), 124-131. <https://doi.org/10.7570/jomes20130>
- Hu, D., & Cross, J. C. (2011). Ablation of Tpbpa-positive trophoblast precursors leads to defects in maternal spiral artery remodeling in the mouse placenta. *Developmental Biology*, 358(1), 231-239. <https://doi.org/https://doi.org/10.1016/j.ydbio.2011.07.036>
- Hubert, J.-N., & Demars, J. (2022). Genomic Imprinting in the New Omics Era: A Model for Systems-Level Approaches [Mini Review]. *Frontiers in Genetics*, 13. <https://doi.org/10.3389/fgene.2022.838534>
- Imakawa, K., & Nakagawa, S. (2017). Chapter Four - The Phylogeny of Placental Evolution Through Dynamic Integrations of Retrotransposons. In W. R. Huckle (Ed.), *Progress in Molecular Biology and Translational Science* (Vol. 145, pp. 89-109). Academic Press. <https://doi.org/https://doi.org/10.1016/bs.pmbts.2016.12.004>
- Ishida, M., Monk, D., Duncan, A. J., Abu-Amero, S., Chong, J., Ring, S. M., Pembrey, M. E., Hindmarsh, P. C., Whittaker, J. C., Stanier, P., & Moore, G. E. (2012). Maternal inheritance of a promoter variant in the imprinted PHLDA2 gene significantly increases birth weight. *Am J Hum Genet*, 90(4), 715-719. <https://doi.org/10.1016/j.ajhg.2012.02.021>
- Ishida, M., Ono, K., Taguchi, S., Ohashi, S., Naito, J.-i., Horiguchi, K., & Harigaya, T. (2004). Cathepsin gene expression in mouse placenta during the latter half of pregnancy. *Journal of Reproduction and Development*, 50(5), 515-523.
- Isoherranen, N., & Thummel, K. E. (2013). Drug metabolism and transport during pregnancy: how does drug disposition change during pregnancy and what are the mechanisms that cause such changes? *Drug Metab Dispos*, 41(2), 256-262. <https://doi.org/10.1124/dmd.112.050245>
- Iuchi, S. (2001). Three classes of C2H2 zinc finger proteins. *Cellular and Molecular Life Sciences CMLS*, 58(4), 625-635. <https://doi.org/10.1007/PL00000885>
- Jackson, G. (2019). The female problem: how male bias in medical trials ruined women's health. *The Guardian*.
- Jacobson, C. D., Terkel, J., Gorski, R. A., & Sawyer, C. H. (1980). Effects of small medial preoptic area lesions on maternal behavior: Retrieving and nest building in the rat. *Brain Research*, 194(2), 471-478. [https://doi.org/https://doi.org/10.1016/0006-8993\(80\)91226-3](https://doi.org/https://doi.org/10.1016/0006-8993(80)91226-3)

- Jansen, G., Bartolomei, M., Kalscheuer, V., Merx, G., Wormskamp, N., Mariman, E., Smeets, D., Ropers, H. H., & Wieringa, B. (1993). No imprinting involved in the expression of DM-kinase mRNAs in mouse and human tissues. *Hum Mol Genet*, 2(8), 1221-1227. <https://doi.org/10.1093/hmg/2.8.1221>
- Janssen, A. B., Capron, L. E., O'Donnell, K., Tunster, S. J., Ramchandani, P. G., Heazell, A. E., Glover, V., & John, R. M. (2016). Maternal prenatal depression is associated with decreased placental expression of the imprinted gene PEG3. *Psychol Med*, 46(14), 2999-3011. <https://doi.org/10.1017/s0033291716001598>
- Janssen, A. B., Tunster, S. J., Heazell, A. E. P., & John, R. M. (2016). Placental PHLDA2 expression is increased in cases of fetal growth restriction following reduced fetal movements. *BMC Medical Genetics*, 17(1), 17. <https://doi.org/10.1186/s12881-016-0279-1>
- Jeong, D. S., Lee, J.-Y., Kim, M. H., & Oh, J. H. (2023). Regulation of sexually dimorphic placental adaptation in LPS exposure-induced intrauterine growth restriction. *Molecular Medicine*, 29(1), 114. <https://doi.org/10.1186/s10020-023-00688-5>
- Jiang, X., Wang, Y., Xiao, Z., Yan, L., Guo, S., Wang, Y., Wu, H., Zhao, X., Lu, X., & Wang, H. (2023). A differentiation roadmap of murine placentation at single-cell resolution. *Cell Discovery*, 9(1), 30. <https://doi.org/10.1038/s41421-022-00513-z>
- Jiang, X., Yu, Y., Yang, H. W., Agar, N. Y., Frado, L., & Johnson, M. D. (2010). The imprinted gene PEG3 inhibits Wnt signaling and regulates glioma growth. *J Biol Chem*, 285(11), 8472-8480. <https://doi.org/10.1074/jbc.M109.069450>
- Jin, F., Qiao, C., Luan, N., & Li, H. (2016). Lentivirus-mediated PHLDA2 overexpression inhibits trophoblast proliferation, migration and invasion, and induces apoptosis. *Int J Mol Med*, 37(4), 949-957. <https://doi.org/10.3892/ijmm.2016.2508>
- Jin, F., Qiao, C., Luan, N., & Shang, T. (2015). The expression of the imprinted gene pleckstrin homology-like domain family A member 2 in placental tissues of preeclampsia and its effects on the proliferation, migration and invasion of trophoblast cells JEG-3. *Clinical and Experimental Pharmacology and Physiology*, 42(11), 1142-1151. <https://doi.org/https://doi.org/10.1111/1440-1681.12468>
- John, R. M. (2001). Distant cis-elements regulate imprinted expression of the mouse p57 Kip2 (Cdkn1c) gene: implications for the human disorder, Beckwith-Wiedemann syndrome. *Human Molecular Genetics*, 10(15), 1601-1609. <https://doi.org/10.1093/hmg/10.15.1601>
- John, R. M. (2010). Engineering mouse models to investigate the function of imprinting. *Briefings in Functional Genomics*, 9(4), 294-303. <https://doi.org/10.1093/bfgp/elq010>
- John, Rosalind M. (2013). Epigenetic regulation of placental endocrine lineages and complications of pregnancy. *Biochemical Society*

- Transactions*, 41(3), 701-709.
<https://doi.org/10.1042/BST20130002>
- John, R. M. (2022). In support of the placental programming hypothesis: Placental endocrine insufficiency programs atypical behaviour in mothers and their offspring. *Exp Physiol*, 107(5), 398-404.
<https://doi.org/10.1113/ep089916>
- John, R. M., Higgs, M. J., & Isles, A. R. (2023). Imprinted genes and the manipulation of parenting in mammals. *Nature Reviews Genetics*, 24(11), 783-796. <https://doi.org/10.1038/s41576-023-00644-3>
- John, R. M., Lefebvre, L., & Surani, M. A. (2022). Genomic Imprinting: A Paradigm for Epigenetics of Human Diseases. In K. B. Michels (Ed.), *Epigenetic Epidemiology* (pp. 171-212). Springer International Publishing. https://doi.org/10.1007/978-3-030-94475-9_8
- John, R. M., & Surani, M. A. (2000). Genomic Imprinting, Mammalian Evolution, and the Mystery of Egg-Laying Mammals. *Cell*, 101(6), 585-588. [https://doi.org/10.1016/S0092-8674\(00\)80870-3](https://doi.org/10.1016/S0092-8674(00)80870-3)
- Johnson, M. (2010). Chapter Eleven - Endocrinology. In P. Bennett & C. Williamson (Eds.), *Basic Science in Obstetrics and Gynaecology (Fourth Edition)* (pp. 231-257). Churchill Livingstone.
<https://doi.org/https://doi.org/10.1016/B978-0-443-10281-3.00015-4>
- Johnson, M. H. (1979). Molecular differentiation of inside cells and inner cell masses isolated from the preimplantation mouse embryo. *Development*, 53(1), 335-344.
<https://doi.org/10.1242/dev.53.1.335>
- Kadyrov, M., Schmitz, C., Black, S., Kaufmann, P., & Huppertz, B. (2003). Pre-eclampsia and maternal anaemia display reduced apoptosis and opposite invasive phenotypes of extravillous trophoblast. *Placenta*, 24(5), 540-548. <https://doi.org/10.1053/plac.2002.0946>
- Kaiser, S., Koch, Y., Kühnel, E., Sharma, N., Gellhaus, A., Kuckenberger, P., Schorle, H., & Winterhager, E. (2015). Reduced Gene Dosage of Tfp2c Impairs Trophoblast Lineage Differentiation and Alters Maternal Blood Spaces in the Mouse Placenta1. *Biology of Reproduction*, 93(2), 31, 31-13.
<https://doi.org/10.1095/biolreprod.114.126474>
- Kalinka, A. T. (2015). How did viviparity originate and evolve? Of conflict, co-option, and cryptic choice. *BioEssays*, 37(7), 721-731.
<https://doi.org/https://doi.org/10.1002/bies.201400200>
- Kanayama, N., Takahashi, K., Matsuura, T., Sugimura, M., Kobayashi, T., Moniwa, N., Tomita, M., & Nakayama, K. (2002). Deficiency in p57Kip2 expression induces preeclampsia-like symptoms in mice. *Mol Hum Reprod*, 8(12), 1129-1135.
<https://doi.org/10.1093/molehr/8.12.1129>
- Kaneda, M., Okano, M., Hata, K., Sado, T., Tsujimoto, N., Li, E., & Sasaki, H. (2004). Essential role for de novo DNA methyltransferase Dnmt3a in paternal and maternal imprinting. *Nature*, 429(6994), 900-903. <https://doi.org/10.1038/nature02633>

- Kaneko-Ishino, T., Kuroiwa, Y., Miyoshi, N., Kohda, T., Suzuki, R., Yokoyama, M., Viville, S., Barton, S. C., Ishino, F., & Surani, M. A. (1995). Peg1/Mest imprinted gene on chromosome 6 identified by cDNA subtraction hybridization. *Nature Genetics*, *11*(1), 52-59. <https://doi.org/10.1038/ng0995-52>
- Kao, L. C., Caltabiano, S., Wu, S., Strauss, J. F., 3rd, & Kliman, H. J. (1988). The human villous cytotrophoblast: interactions with extracellular matrix proteins, endocrine function, and cytoplasmic differentiation in the absence of syncytium formation. *Dev Biol*, *130*(2), 693-702. [https://doi.org/10.1016/0012-1606\(88\)90361-2](https://doi.org/10.1016/0012-1606(88)90361-2)
- Karlsson, M., Zhang, C., Méar, L., Zhong, W., Digre, A., Katona, B., Sjöstedt, E., Butler, L., Odeberg, J., Dusart, P., Edfors, F., Oksvold, P., von Feilitzen, K., Zwahlen, M., Arif, M., Altay, O., Li, X., Ozcan, M., Mardinoglu, A., . . . Lindskog, C. (2021). A single-cell type transcriptomics map of human tissues. *Science Advances*, *7*(31), eabh2169. <https://doi.org/10.1126/sciadv.abh2169>
- Keller, M. B., Beardslee, W. R., Dorer, D. J., Lavori, P. W., Samuelson, H., & Klerman, G. R. (1986). Impact of severity and chronicity of parental affective illness on adaptive functioning and psychopathology in children. *Archives of General Psychiatry*, *43*(10), 930-937. <https://doi.org/10.1001/archpsyc.1986.01800100020004>
- Kerstis, B., Aarts, C., Tillman, C., Persson, H., Engström, G., Edlund, B., Öhrvik, J., Sylvén, S., & Skalkidou, A. (2016). Association between parental depressive symptoms and impaired bonding with the infant. *Archives of Women's Mental Health*, *19*(1), 87-94. <https://doi.org/10.1007/s00737-015-0522-3>
- Killian, J. K., Byrd, J. C., Jirtle, J. V., Munday, B. L., Stoskopf, M. K., MacDonald, R. G., & Jirtle, R. L. (2000). M6P/IGF2R imprinting evolution in mammals. *Mol Cell*, *5*(4), 707-716. [https://doi.org/10.1016/s1097-2765\(00\)80249-x](https://doi.org/10.1016/s1097-2765(00)80249-x)
- Killian, J. K., Nolan, C. M., Stewart, N., Munday, B. L., Andersen, N. A., Nicol, S., & Jirtle, R. L. (2001). Monotreme IGF2 expression and ancestral origin of genomic imprinting. *J Exp Zool*, *291*(2), 205-212. <https://doi.org/10.1002/jez.1070>
- Kim, J., Ashworth, L., Branscomb, E., & Stubbs, L. (1997). The human homolog of a mouse-imprinted gene, Peg3, maps to a zinc finger gene-rich region of human chromosome 19q13.4. *Genome Res*, *7*(5), 532-540. <https://doi.org/10.1101/gr.7.5.532>
- Kim, J., Ekram, M. B., Kim, H., Faisal, M., Frey, W. D., Huang, J. M., Tran, K., Kim, M. M., & Yu, S. (2012). Imprinting control region (ICR) of the Peg3 domain. *Human Molecular Genetics*, *21*(12), 2677-2687. <https://doi.org/10.1093/hmg/dds092>
- Kim, J., Farré, M., Auvil, L., Capitanu, B., Larkin, D. M., Ma, J., & Lewin, H. A. (2017). Reconstruction and evolutionary history of eutherian chromosomes. *Proceedings of the National Academy of Sciences*, *114*(27), E5379-E5388. <https://doi.org/10.1073/pnas.1702012114>

- Kim, K. S., & Lee, Y. I. (1997). Biallelic expression of the H19 and IGF2 genes in hepatocellular carcinoma. *Cancer Lett*, *119*(2), 143-148. [https://doi.org/10.1016/s0304-3835\(97\)00264-4](https://doi.org/10.1016/s0304-3835(97)00264-4)
- Kjaersgaard, M. I., Parner, E. T., Vestergaard, M., Sørensen, M. J., Olsen, J., Christensen, J., Bech, B. H., & Pedersen, L. H. (2013). Prenatal antidepressant exposure and risk of spontaneous abortion - a population-based study. *PLoS One*, *8*(8), e72095. <https://doi.org/10.1371/journal.pone.0072095>
- Kliman, H. J., Nestler, J. E., Sermasi, E., Sanger, J. M., & Strauss, J. F., 3rd. (1986). Purification, characterization, and in vitro differentiation of cytotrophoblasts from human term placentae. *Endocrinology*, *118*(4), 1567-1582. <https://doi.org/10.1210/endo-118-4-1567>
- Kokay, I. C., Wyatt, A., Phillipps, H. R., Aoki, M., Ectors, F., Boehm, U., & Grattan, D. R. (2018). Analysis of prolactin receptor expression in the murine brain using a novel prolactin receptor reporter mouse. *Journal of Neuroendocrinology*, *30*(9), e12634. <https://doi.org/https://doi.org/10.1111/jne.12634>
- Kornfeld, S., & Mellman, I. (1989). The biogenesis of lysosomes. *Annu Rev Cell Biol*, *5*, 483-525. <https://doi.org/10.1146/annurev.cb.05.110189.002411>
- Kuroiwa, Y., Kaneko-Ishino, T., Kagitani, F., Kohda, T., Li, L. L., Tada, M., Suzuki, R., Yokoyama, M., Shiroishi, T., Wakana, S., Barton, S. C., Ishino, F., & Surani, M. A. (1996). Peg3 imprinted gene on proximal chromosome 7 encodes for a zinc finger protein. *Nat Genet*, *12*(2), 186-190. <https://doi.org/10.1038/ng0296-186>
- Lacroix, M. C., Guibourdenche, J., Fournier, T., Laurendeau, I., Igout, A., Goffin, V., Pantel, J., Tsatsaris, V., & Evain-Brion, D. (2005). Stimulation of human trophoblast invasion by placental growth hormone. *Endocrinology*, *146*(5), 2434-2444. <https://doi.org/10.1210/en.2004-1550>
- Lacroix, M. C., Guibourdenche, J., Frenzo, J. L., Muller, F., & Evain-Brion, D. (2002). Human placental growth hormone--a review. *Placenta*, *23 Suppl A*, S87-94. <https://doi.org/10.1053/plac.2002.0811>
- Ladyman, S. R., Augustine, R. A., & Grattan, D. R. (2010). Hormone Interactions Regulating Energy Balance During Pregnancy. *Journal of Neuroendocrinology*, *22*(7), 805-817. <https://doi.org/https://doi.org/10.1111/j.1365-2826.2010.02017.x>
- Lahti, M., Eriksson, J. G., Heinonen, K., Kajantie, E., Lahti, J., Wahlbeck, K., Tuovinen, S., Pesonen, A. K., Mikkonen, M., Osmond, C., Barker, D. J. P., & Räikkönen, K. (2015). Late preterm birth, post-term birth, and abnormal fetal growth as risk factors for severe mental disorders from early to late adulthood. *Psychological Medicine*, *45*(5), 985-999. <https://doi.org/10.1017/S0033291714001998>
- Lahti-Pulkkinen, M., Cudmore, M. J., Haeussner, E., Schmitz, C., Pesonen, A.-K., Hämäläinen, E., Villa, P. M., Mehtälä, S., Kajantie, E.,

- Laivuori, H., Reynolds, R. M., Frank, H.-G., & Räikkönen, K. (2018). Placental Morphology Is Associated with Maternal Depressive Symptoms during Pregnancy and Toddler Psychiatric Problems. *Scientific Reports*, 8(1), 791. <https://doi.org/10.1038/s41598-017-19133-9>
- Laird, M. K., McShea, H., Murphy, C. R., McAllan, B. M., Shaw, G., Renfree, M. B., & Thompson, M. B. (2018). Non-invasive placentation in the marsupials *Macropus eugenii* (Macropodidae) and *Trichosurus vulpecula* (Phalangeridae) involves redistribution of uterine Desmoglein-2. *Molecular Reproduction and Development*, 85(1), 72-82. <https://doi.org/https://doi.org/10.1002/mrd.22940>
- Lancet, T. (2001). An overstretched hypothesis? *The Lancet*, 357(9254). <https://click.endnote.com/viewer?doi=10.1016%2Fs0140-6736%2800%2904027-7&token=WzM1ODg4MTAsIjEwLjEwMTYvczAxNDAtNjczNigwMCkwNDAYNy03Ii0.gi9dbIY7AEKUFjWfVjSHP9yrwuI>
- Latos, P. A., & Hemberger, M. (2016). From the stem of the placental tree: trophoblast stem cells and their progeny. *Development*, 143(20), 3650-3660. <https://doi.org/10.1242/dev.133462>
- Lee, M. P., & Feinberg, A. P. (1998). Genomic imprinting of a human apoptosis gene homologue, TSSC3. *Cancer Res*, 58(5), 1052-1056.
- Lee, S., Ye, A., & Kim, J. (2015). DNA-Binding Motif of the Imprinted Transcription Factor PEG3. *PLoS One*, 10(12), e0145531. <https://doi.org/10.1371/journal.pone.0145531>
- Lemmon, M. A., & Ferguson, K. M. (1998). Pleckstrin Homology Domains. In A. J. Pawson (Ed.), *Protein Modules in Signal Transduction* (pp. 39-74). Springer Berlin Heidelberg. https://doi.org/10.1007/978-3-642-80481-6_3
- Lescisin, K. R., Varmuza, S., & Rossant, J. (1988). Isolation and characterization of a novel trophoblast-specific cDNA in the mouse. *Genes Dev*, 2(12a), 1639-1646. <https://doi.org/10.1101/gad.2.12a.1639>
- Levine, T. A., Grunau, R. E., McAuliffe, F. M., Pinnamaneni, R., Foran, A., & Alderdice, F. A. (2015). Early Childhood Neurodevelopment After Intrauterine Growth Restriction: A Systematic Review. *Pediatrics*, 135(1), 126-141. <https://doi.org/10.1542/peds.2014-1143>
- Levitz, M., & Young, B. K. (1977). Estrogens in pregnancy. *Vitam Horm*, 35, 109-147. [https://doi.org/10.1016/s0083-6729\(08\)60522-1](https://doi.org/10.1016/s0083-6729(08)60522-1)
- Li, L. L., Keverne, E. B., Aparicio, S. A., Ishino, F., Barton, S. C., & Surani, M. A. (1999). Regulation of Maternal Behavior and Offspring Growth by Paternally Expressed Peg3. *Science*, 284(5412), 330-333. <http://www.jstor.org.abc.cardiff.ac.uk/stable/2898221>
- Li, Z.-k., Wang, L.-b., Wang, L.-y., Sun, X.-h., Ren, Z.-h., Ma, S.-n., Zhao, Y.-l., Liu, C., Feng, G.-h., Liu, T., Pan, T.-s., Shan, Q.-t., Xu, K., Luo, G.-z., Zhou, Q., & Li, W. (2025). Adult bi-paternal offspring generated through direct modification of imprinted genes in

- mammals. *Cell stem cell*, 32(3), 361-374.e366.
<https://doi.org/https://doi.org/10.1016/j.stem.2025.01.005>
- Lin, S. P., Youngson, N., Takada, S., Seitz, H., Reik, W., Paulsen, M., Cavaille, J., & Ferguson-Smith, A. C. (2003). Asymmetric regulation of imprinting on the maternal and paternal chromosomes at the Dlk1-Gtl2 imprinted cluster on mouse chromosome 12. *Nat Genet*, 35(1), 97-102. <https://doi.org/10.1038/ng1233>
- Liska O, B. B., Hidas A, Korcsmáros T, Papp B, Fazekas D, Ari E. (2022). *TF Link*. Database, baac083. Retrieved 26/11/2024 from <https://tflink.net/browse/>
- Liu, Y., Fan, X., Wang, R., Lu, X., Dang, Y. L., Wang, H., Lin, H. Y., Zhu, C., Ge, H., Cross, J. C., & Wang, H. (2018). Single-cell RNA-seq reveals the diversity of trophoblast subtypes and patterns of differentiation in the human placenta. *Cell Res*, 28(8), 819-832. <https://doi.org/10.1038/s41422-018-0066-y>
- Lopez, M. F., Dikkes, P., Zurakowski, D., & Villa-Komaroff, L. (1996). Insulin-like growth factor II affects the appearance and glycogen content of glycogen cells in the murine placenta. *Endocrinology*, 137(5), 2100-2108. <https://doi.org/10.1210/en.137.5.2100>
- Lopez-Espinoza, I., Smith, R. F., Gillmer, M., Schidlmeir, A., & Hockaday, T. D. (1986). High levels of growth hormone and human placental lactogen in pregnancy complicated by diabetes. *Diabetes research (Edinburgh, Scotland)*, 3(3), 119-125. <http://europepmc.org/abstract/MED/3519044>
- Luo, J., Sladek, R., Bader, J. A., Matthyssen, A., Rossant, J., & Giguère, V. (1997). Placental abnormalities in mouse embryos lacking the orphan nuclear receptor ERR-beta. *Nature*, 388(6644), 778-782. <https://doi.org/10.1038/42022>
- Lupattelli, A., Spigset, O., Twigg, M. J., Zagorodnikova, K., Mårdby, A. C., Moretti, M. E., Drozd, M., Panchaud, A., Hämeen-Anttila, K., Rieutord, A., Gjergja Juraski, R., Odalovic, M., Kennedy, D., Rudolf, G., Juch, H., Passier, A., Björnsdóttir, I., & Nordeng, H. (2014). Medication use in pregnancy: a cross-sectional, multinational web-based study. *BMJ Open*, 4(2), e004365. <https://doi.org/10.1136/bmjopen-2013-004365>
- Lutkiewicz, K., Bieleninik, Ł., Cieślak, M., & Bidzan, M. (2020). Maternal-Infant Bonding and Its Relationships with Maternal Depressive Symptoms, Stress and Anxiety in the Early Postpartum Period in a Polish Sample. *Int J Environ Res Public Health*, 17(15). <https://doi.org/10.3390/ijerph17155427>
- Lyons-Ruth, K., Connell, D. B., Grunebaum, H. U., & Botein, S. (1990). Infants at social risk: maternal depression and family support services as mediators of infant development and security of attachment. *Child Dev*, 61(1), 85-98. <https://doi.org/10.1111/j.1467-8624.1990.tb02762.x>
- MacArthur, R. H., & Wilson, E. O. (1967). *The theory of island biogeography*. Princetown University Press.

- Magnus, M. C., Havdahl, A., Morken, N. H., Wensaas, K. A., Wilcox, A. J., & Håberg, S. E. (2021). Risk of miscarriage in women with psychiatric disorders. *Br J Psychiatry*, *219*(3), 501-506. <https://doi.org/10.1192/bjp.2020.259>
- Mann, P. E., & Bridges, R. S. (2001). Chapter 18 Lactogenic hormone regulation of maternal behavior. In *Progress in Brain Research* (Vol. 133, pp. 251-262). Elsevier. [https://doi.org/https://doi.org/10.1016/S0079-6123\(01\)33019-4](https://doi.org/https://doi.org/10.1016/S0079-6123(01)33019-4)
- Mao, J., Zhang, X., Sieli, P. T., Falduto, M. T., Torres, K. E., & Rosenfeld, C. S. (2010). Contrasting effects of different maternal diets on sexually dimorphic gene expression in the murine placenta. *Proceedings of the National Academy of Sciences*, *107*(12), 5557-5562. <https://doi.org/10.1073/pnas.1000440107>
- Marsh, B., & Belloch, R. (2020). Single nuclei RNA-seq of mouse placental labyrinth development. *Elife*, *9*, e60266. <https://doi.org/10.7554/eLife.60266>
- Marshall, C. J., Blake, A., Stewart, C., Liddle, T. A., Denizli, I., Cuthill, F., Evans, N. P., & Stevenson, T. J. (2024). Prolactin Mediates Long-Term, Seasonal Rheostatic Regulation of Body Mass in Female Mammals. *Endocrinology*, *165*(4), bqae020. <https://doi.org/10.1210/endocr/bqae020>
- Martial, J. A., Hallewell, R. A., Baxter, J. D., & Goodman, H. M. (1979). Human Growth Hormone: Complementary DNA Cloning and Expression in Bacteria. *Science*, *205*(4406), 602-607. <https://doi.org/10.1126/science.377496>
- Martins, C., & Gaffan, E. A. (2000). Effects of early maternal depression on patterns of infant-mother attachment: a meta-analytic investigation. *J Child Psychol Psychiatry*, *41*(6), 737-746.
- McGrath, J., & Solter, D. (1984). Completion of mouse embryogenesis requires both the maternal and paternal genomes. *Cell*, *37*(1), 179-183. [https://doi.org/https://doi.org/10.1016/0092-8674\(84\)90313-1](https://doi.org/https://doi.org/10.1016/0092-8674(84)90313-1)
- McIntyre, H. D., Catalano, P., Zhang, C., Desoye, G., Mathiesen, E. R., & Damm, P. (2019). Gestational diabetes mellitus. *Nature Reviews Disease Primers*, *5*(1), 47. <https://doi.org/10.1038/s41572-019-0098-8>
- McLellan, A. S., Zimmermann, W., & Moore, T. (2005). Conservation of pregnancy-specific glycoprotein (PSG) N domains following independent expansions of the gene families in rodents and primates. *BMC Evol Biol*, *5*, 39. <https://doi.org/10.1186/1471-2148-5-39>
- McMinn, J., Wei, M., Schupf, N., Cusmai, J., Johnson, E. B., Smith, A. C., Weksberg, R., Thaker, H. M., & Tycko, B. (2006). Unbalanced Placental Expression of Imprinted Genes in Human Intrauterine Growth Restriction. *Placenta*, *27*(6), 540-549. <https://doi.org/https://doi.org/10.1016/j.placenta.2005.07.004>

- McNamara, G. I., Creeth, H. D. J., Harrison, D. J., Tansey, K. E., Andrews, R. M., Isles, A. R., & John, R. M. (2018). Loss of offspring Peg3 reduces neonatal ultrasonic vocalizations and increases maternal anxiety in wild-type mothers. *Hum Mol Genet*, 27(3), 440-450. <https://doi.org/10.1093/hmg/ddx412>
- McNeilly, A. S. (1975). Lactation and the physiology of prolactin secretion. *Postgrad Med J*, 51(594), 231-235. <https://doi.org/10.1136/pgmj.51.594.231>
- McVey, A. W. (2014). Appendix - Reproductive Parameters of Common, Commercially Available Mouse Strains. In B. A. Croy, A. T. Yamada, F. J. DeMayo, & S. L. Adamson (Eds.), *The Guide to Investigation of Mouse Pregnancy* (pp. 791-793). Academic Press. <https://doi.org/https://doi.org/10.1016/B978-0-12-394445-0.15001-5>
- Miller, W. L., & Eberhardt, N. L. (1983). Structure and evolution of the growth hormone gene family. *Endocr Rev*, 4(2), 97-130. <https://doi.org/10.1210/edrv-4-2-97>
- Mochache, K., Mathai, M., Gachuno, O., Vander Stoep, A., & Kumar, M. (2018). Depression during pregnancy and preterm delivery: a prospective cohort study among women attending antenatal clinic at Pumwani Maternity Hospital. *Ann Gen Psychiatry*, 17, 31. <https://doi.org/10.1186/s12991-018-0202-6>
- Moehler, E., Brunner, R., Wiebel, A., Reck, C., & Resch, F. (2006). Maternal depressive symptoms in the postnatal period are associated with long-term impairment of mother-child bonding. *Archives of Women's Mental Health*, 9(5), 273-278. <https://doi.org/10.1007/s00737-006-0149-5>
- Molenaar, N. M., Kamperman, A. M., Boyce, P., & Bergink, V. (2018). Guidelines on treatment of perinatal depression with antidepressants: An international review. *Australian & New Zealand Journal of Psychiatry*, 52(4), 320-327. <https://doi.org/10.1177/0004867418762057>
- Monk, D. (2015). Genomic imprinting in the human placenta. *Am J Obstet Gynecol*, 213(4 Suppl), S152-162. <https://doi.org/10.1016/j.ajog.2015.06.032>
- Moore, T., & Dveksler, G. (2014). Pregnancy-specific glycoproteins: complex gene families regulating maternal-fetal interactions. *The International Journal of Developmental Biology*, 58(2-3-4), 273-280. <https://doi.org/10.1387/ijdb.130329gd>
- Moore, T., & Haig, D. (1991). Genomic imprinting in mammalian development: a parental tug-of-war. *Trends in genetics*, 7(2), 45-49. [https://doi.org/https://doi.org/10.1016/0168-9525\(91\)90230-N](https://doi.org/https://doi.org/10.1016/0168-9525(91)90230-N)
- Morasso, M. I., Grinberg, A., Robinson, G., Sargent, T. D., & Mahon, K. A. (1999). Placental failure in mice lacking the homeobox gene Dlx3. *Proceedings of the National Academy of Sciences*, 96(1), 162-167. <https://doi.org/10.1073/pnas.96.1.162>

- Moreno, P., Fexova, S., George, N., Manning, J. R., Miao, Z., Mohammed, S., Muñoz-Pomer, A., Fullgrabe, A., Bi, Y., Bush, N., Iqbal, H., Kumbham, U., Solovyev, A., Zhao, L., Prakash, A., García-Seisdedos, D., Kundu, D. J., Wang, S., Walzer, M., . . . Papatheodorou, I. (2022). Expression Atlas update: gene and protein expression in multiple species. *Nucleic Acids Res*, *50*(D1), D129-d140. <https://doi.org/10.1093/nar/gkab1030>
- Morison, I. M., Ramsay, J. P., & Spencer, H. G. (2005). A census of mammalian imprinting. *Trends in genetics*, *21*(8), 457-465. <https://doi.org/10.1016/j.tig.2005.06.008>
- Mould, A., Morgan, M. A. J., Li, L., Bikoff, E. K., & Robertson, E. J. (2012). Blimp1/Prdm1 governs terminal differentiation of endovascular trophoblast giant cells and defines multipotent progenitors in the developing placenta. *Genes & Development*, *26*(18), 2063-2074. <https://doi.org/10.1101/gad.199828.112>
- Müller, S., van den Boom, D., Zirkel, D., Köster, H., Berthold, F., Schwab, M., Westphal, M., & Zumkeller, W. (2000). Retention of imprinting of the human apoptosis-related gene TSSC3 in human brain tumors. *Hum Mol Genet*, *9*(5), 757-763. <https://doi.org/10.1093/hmg/9.5.757>
- Munk-Olsen, T., Maegbaek, M. L., Johannsen, B. M., Liu, X., Howard, L. M., Di Florio, A., Bergink, V., & Meltzer-Brody, S. (2016). Perinatal psychiatric episodes: a population-based study on treatment incidence and prevalence. *Translational Psychiatry*, *6*(10), e919-e919. <https://doi.org/10.1038/tp.2016.190>
- Murphy, S. K., Wylie, A. A., & Jirtle, R. L. (2001). Imprinting of PEG3, the Human Homologue of a Mouse Gene Involved in Nurturing Behavior. *Genomics*, *71*(1), 110-117. <https://doi.org/https://doi.org/10.1006/geno.2000.6419>
- Murphy, W. J., & Eizirik, E. (2009). Placental mammals (Eutheria). *The timetree of life*, 471-474.
- Murray, L. (1992). Critical issues in residential care for young mothers and infants: An overview of model licensing rules. *Child Welfare: Journal of Policy, Practice, and Program*, *71*(2), 157-163.
- Muzik, M., & Hamilton, S. E. (2016). Use of Antidepressants During Pregnancy?: What to Consider when Weighing Treatment with Antidepressants Against Untreated Depression. *Maternal and Child Health Journal*, *20*(11), 2268-2279. <https://doi.org/10.1007/s10995-016-2038-5>
- Nachtigal, M. W., Nickel, B. E., & Cattini, P. A. (1993). Pituitary-specific repression of placental members of the human growth hormone gene family. A possible mechanism for locus regulation. *J Biol Chem*, *268*(12), 8473-8479.
- Naef, L., & Woodside, B. (2007). Prolactin/Leptin interactions in the control of food intake in rats. *Endocrinology*, *148*(12), 5977-5983. <https://doi.org/10.1210/en.2007-0442>

- Nagai, A., Takebe, K., Nio-Kobayashi, J., Takahashi-Iwanaga, H., & Iwanaga, T. (2010). Cellular expression of the monocarboxylate transporter (MCT) family in the placenta of mice. *Placenta*, 31(2), 126-133. <https://doi.org/10.1016/j.placenta.2009.11.013>
- Napso, T., Zhao, X., Lligoña, M. I., Sandovici, I., Kay, R. G., George, A. L., Gribble, F. M., Reimann, F., Meek, C. L., Hamilton, R. S., & Sferruzzi-Perri, A. N. (2021). Placental secretome characterization identifies candidates for pregnancy complications. *Commun Biol*, 4(1), 701. <https://doi.org/10.1038/s42003-021-02214-x>
- National Center for Biotechnology Information (NCBI). (2024). *Bethesda (MD): National Library of Medicine (US), National Center for Biotechnology Information*. <https://www.ncbi.nlm.nih.gov>
- NICE. (2020). Antenatal and postnatal mental health: clinical management and service guidance. *National institute for health and care excellence*. <https://www.nice.org.uk/guidance/cg192>
- Numan, M. (1974). Medial preoptic area and maternal behavior in the female rat. *Journal of Comparative and Physiological Psychology*, 87(4), 746-759. <https://doi.org/10.1037/h0036974>
- Numan, M., Corodimas, K. P., Numan, M. J., Factor, E. M., & Piers, W. D. (1988). Axon-sparing lesions of the preoptic region and substantia innominata disrupt maternal behavior in rats. *Behavioral Neuroscience*, 102(3), 381-396. <https://doi.org/10.1037/0735-7044.102.3.381>
- Numan, M., Rosenblatt, J. S., & Komisaruk, B. R. (1977). Medial preoptic area and onset of maternal behavior in the rat. *Journal of Comparative and Physiological Psychology*, 91(1), 146-164. <https://doi.org/10.1037/h0077304>
- O'Hara, M. W. (2009). Postpartum depression: what we know. *J Clin Psychol*, 65(12), 1258-1269. <https://doi.org/10.1002/jclp.20644>
- O'Neill, M. J., Ingram, R. S., Vrana, P. B., & Tilghman, S. M. (2000). Allelic expression of IGF2 in marsupials and birds. *Dev Genes Evol*, 210(1), 18-20. <https://doi.org/10.1007/pl00008182>
- Ohinata, Y., & Tsukiyama, T. (2014). Establishment of trophoblast stem cells under defined culture conditions in mice. *PLoS One*, 9(9), e107308. <https://doi.org/10.1371/journal.pone.0107308>
- Okae, H., Toh, H., Sato, T., Hiura, H., Takahashi, S., Shirane, K., Kabayama, Y., Suyama, M., Sasaki, H., & Arima, T. (2018). Derivation of human trophoblast stem cells. *Cell stem cell*, 22(1), 50-63. e56.
- Östberg Lloyd, C., & Sand Horup, C. (2023). Women's health: Is this the world's best – and most under-financed – investment? *World economic forum*. <https://www.weforum.org/agenda/2023/01/is-this-the-world-s-best-and-most-under-financed-investment-davos23/>
- Outhwaite, J. E., McGuire, V., & Simmons, D. G. (2015). Genetic ablation of placental sinusoidal trophoblast giant cells causes fetal growth

- restriction and embryonic lethality. *Placenta*, 36(8), 951-955.
<https://doi.org/https://doi.org/10.1016/j.placenta.2015.05.013>
- Palomba, S., & Daolio, J. (2018). Pregnancy Endocrinology☆. In I. Huhtaniemi & L. Martini (Eds.), *Encyclopedia of Endocrine Diseases (Second Edition)* (pp. 408-417). Academic Press.
<https://doi.org/https://doi.org/10.1016/B978-0-12-801238-3.03913-1>
- Paneth, N., & Susser, M. (1995). Early origin of coronary heart disease (the "Barker hypothesis"). *BMJ*, 310(6977), 411-412.
<https://doi.org/10.1136/bmj.310.6977.411>
- Parker, S. E., Werler, M. M., Gissler, M., Tikkanen, M., & Ananth, C. V. (2015). Placental abruption and subsequent risk of pre-eclampsia: a population-based case-control study. *Paediatr Perinat Epidemiol*, 29(3), 211-219. <https://doi.org/10.1111/ppe.12184>
- Patwardhan, V., Gil, G. F., Arrieta, A., Cagney, J., DeGraw, E., Herbert, M. E., Khalil, M., Mullany, E. C., O'Connell, E. M., Spencer, C. N., Stein, C., Valikhanova, A., Gakidou, E., & Flor, L. S. (2024). Differences across the lifespan between females and males in the top 20 causes of disease burden globally: a systematic analysis of the Global Burden of Disease Study 2021. *The Lancet Public Health*, 9(5), e282-e294. [https://doi.org/10.1016/S2468-2667\(24\)00053-7](https://doi.org/10.1016/S2468-2667(24)00053-7)
- Pavletich, N. P., & Pabo, C. O. (1991). Zinc Finger-DNA Recognition: Crystal Structure of a Zif268-DNA Complex at 2.1 Å. *Science*, 252(5007), 809-817. <https://doi.org/10.1126/science.2028256>
- Petraglia, F., Florio, P., Nappi, C., & Genazzani, A. R. (1996). Peptide Signaling in Human Placenta and Membranes: Autocrine, Paracrine, and Endocrine Mechanisms*. *Endocrine Reviews*, 17(2), 156-186.
<https://doi.org/10.1210/edrv-17-2-156>
- Pi, X.-J., & Grattan, D. R. (1998a). Differential expression of the two forms of prolactin receptor mRNA within microdissected hypothalamic nuclei of the rat. *Molecular Brain Research*, 59(1), 1-12. [https://doi.org/https://doi.org/10.1016/S0169-328X\(98\)00109-0](https://doi.org/https://doi.org/10.1016/S0169-328X(98)00109-0)
- Pi, X.-J., & Grattan, D. R. (1998b). Distribution of prolactin receptor immunoreactivity in the brain of estrogen-treated, ovariectomized rats. *Journal of Comparative Neurology*, 394(4), 462-474.
[https://doi.org/https://doi.org/10.1002/\(SICI\)1096-9861\(19980518\)394:4<462::AID-CNE5>3.0.CO;2-#](https://doi.org/https://doi.org/10.1002/(SICI)1096-9861(19980518)394:4<462::AID-CNE5>3.0.CO;2-#)
- Pieler, T., & Bellefroid, E. (1994). Perspectives on zinc finger protein function and evolution--an update. *Mol Biol Rep*, 20(1), 1-8.
<https://doi.org/10.1007/bf00999848>
- Plasschaert, R. N., & Bartolomei, M. S. (2015). Tissue-specific regulation and function of Grb10 during growth and neuronal commitment. *Proc Natl Acad Sci U S A*, 112(22), 6841-6847.
<https://doi.org/10.1073/pnas.1411254111>
- Pope, C. J., Oinonen, K., Mazmanian, D., & Stone, S. (2017). The hormonal sensitivity hypothesis: A review and new findings. *Med*

Hypotheses, 102, 69-77.

<https://doi.org/10.1016/j.mehy.2017.03.012>

- Putnam, K. T., Wilcox, M., Robertson-Blackmore, E., Sharkey, K., Bergink, V., Munk-Olsen, T., Deligiannidis, K. M., Payne, J., Altemus, M., Newport, J., Apter, G., Devouche, E., Viktorin, A., Magnusson, P., Penninx, B., Buist, A., Bilszta, J., O'Hara, M., Stuart, S., . . . Meltzer-Brody, S. (2017). Clinical phenotypes of perinatal depression and time of symptom onset: analysis of data from an international consortium. *The Lancet Psychiatry*, 4(6), 477-485. [https://doi.org/10.1016/s2215-0366\(17\)30136-0](https://doi.org/10.1016/s2215-0366(17)30136-0)
- Qian, N., Frank, D., O'Keefe, D., Dao, D., Zhao, L., Yuan, L., Wang, Q., Keating, M., Walsh, C., & Tycko, B. (1997). The IPL gene on chromosome 11p15.5 is imprinted in humans and mice and is similar to TDAG51, implicated in Fas expression and apoptosis. *Hum Mol Genet*, 6(12), 2021-2029. <https://doi.org/10.1093/hmg/6.12.2021>
- Qian, S., Yang, Y., Li, N., Cheng, T., Wang, X., Liu, J., Li, X., Desiderio, D. M., & Zhan, X. (2018). Prolactin Variants in Human Pituitaries and Pituitary Adenomas Identified With Two-Dimensional Gel Electrophoresis and Mass Spectrometry. *Front Endocrinol (Lausanne)*, 9, 468. <https://doi.org/10.3389/fendo.2018.00468>
- Rahimi, R., Nikfar, S., & Abdollahi, M. (2006). Pregnancy outcomes following exposure to serotonin reuptake inhibitors: a meta-analysis of clinical trials. *Reproductive Toxicology*, 22(4), 571-575. <https://doi.org/https://doi.org/10.1016/j.reprotox.2006.03.019>
- Rai, A., & Cross, J. C. (2014). Development of the hemochorial maternal vascular spaces in the placenta through endothelial and vasculogenic mimicry. *Dev Biol*, 387(2), 131-141. <https://doi.org/10.1016/j.ydbio.2014.01.015>
- Ramos-Román, M. A. (2011). Prolactin and Lactation as Modifiers of Diabetes Risk in Gestational Diabetes. *Horm Metab Res*, 43(09), 593-600. <https://doi.org/10.1055/s-0031-1284353>
- Rampon, C., Prandini, M. H., Bouillot, S., Pointu, H., Tillet, E., Frank, R., Vernet, M., & Huber, P. (2005). Protocadherin 12 (VE-cadherin 2) is expressed in endothelial, trophoblast, and mesangial cells. *Exp Cell Res*, 302(1), 48-60. <https://doi.org/10.1016/j.yexcr.2004.08.024>
- Rassie, K., Giri, R., Joham, A. E., Teede, H., & Mousa, A. (2022). Human Placental Lactogen in Relation to Maternal Metabolic Health and Fetal Outcomes: A Systematic Review and Meta-Analysis. *Int J Mol Sci*, 23(24). <https://doi.org/10.3390/ijms232415621>
- Rawn, S. M., Huang, C., Hughes, M., Shaykhutdinov, R., Vogel, H. J., & Cross, J. C. (2015). Pregnancy Hyperglycemia in Prolactin Receptor Mutant, but Not Prolactin Mutant, Mice and Feeding-Responsive Regulation of Placental Lactogen Genes Implies Placental Control of Maternal Glucose Homeostasis¹. *Biology of Reproduction*, 93(3), 75, 71-12. <https://doi.org/10.1095/biolreprod.115.132431>

- Reik, W. (1989). Genomic imprinting and genetic disorders in man. *Trends in genetics*, 5, 332-336.
[https://doi.org/https://doi.org/10.1016/0168-9525\(89\)90138-8](https://doi.org/https://doi.org/10.1016/0168-9525(89)90138-8)
- Reik, W., & Lewis, A. (2005). Co-evolution of X-chromosome inactivation and imprinting in mammals. *Nature Reviews Genetics*, 6(5), 403-410. <https://doi.org/10.1038/nrg1602>
- Reik, W., & Maher, E. R. (1997). Imprinting in clusters: lessons from Beckwith-Wiedemann syndrome. *Trends Genet*, 13(8), 330-334.
[https://doi.org/10.1016/s0168-9525\(97\)01200-6](https://doi.org/10.1016/s0168-9525(97)01200-6)
- Reik, W., & Walter, J. (2001). Genomic imprinting: parental influence on the genome. *Nature Reviews Genetics*, 2(1), 21-32.
<https://doi.org/10.1038/35047554>
- Relaix, F., Wei, X., Li, W., Pan, J., Lin, Y., Bowtell, D. D., Sassoon, D. A., & Wu, X. (2000). Pw1/Peg3 is a potential cell death mediator and cooperates with Siah1a in p53-mediated apoptosis. *Proc Natl Acad Sci U S A*, 97(5), 2105-2110.
<https://doi.org/10.1073/pnas.040378897>
- Relaix, F., Weng, X., Marazzi, G., Yang, E., Copeland, N., Jenkins, N., Spence, S. E., & Sassoon, D. (1996). Pw1, a Novel Zinc Finger Gene Implicated in the Myogenic and Neuronal Lineages. *Developmental Biology*, 177(2), 383-396.
<https://doi.org/https://doi.org/10.1006/dbio.1996.0172>
- Renfree, M. B. (2010). Review: Marsupials: Placental Mammals with a Difference. *Placenta*, 31, S21-S26.
<https://doi.org/https://doi.org/10.1016/j.placenta.2009.12.023>
- Renfree, M. B., Ager, E. I., Shaw, G., & Pask, A. J. (2008). Genomic imprinting in marsupial placentation. *Reproduction*, 136(5), 523-531. <https://doi.org/10.1530/rep-08-0264>
- Renfree, M. B., Suzuki, S., & Kaneko-Ishino, T. (2013). The origin and evolution of genomic imprinting and viviparity in mammals. *Philos Trans R Soc Lond B Biol Sci*, 368(1609), 20120151.
<https://doi.org/10.1098/rstb.2012.0151>
- Riddle, O., Bates, R. W., & Dykshorn, S. W. (1933). THE PREPARATION, IDENTIFICATION AND ASSAY OF PROLACTIN—A HORMONE OF THE ANTERIOR PITUITARY. *American Journal of Physiology-Legacy Content*, 105(1), 191-216.
<https://doi.org/10.1152/ajplegacy.1933.105.1.191>
- Riley, P., Anson-Cartwright, L., & Cross, J. C. (1998). The Hand1 bHLH transcription factor is essential for placentation and cardiac morphogenesis. *Nat Genet*, 18(3), 271-275.
<https://doi.org/10.1038/ng0398-271>
- Roberts, R. M., Green, J. A., & Schulz, L. C. (2016). The evolution of the placenta. *Reproduction*, 152(5), R179-189.
<https://doi.org/10.1530/rep-16-0325>
- Rogers, A., Obst, S., Teague, S. J., Rossen, L., Spry, E. A., Macdonald, J. A., Sunderland, M., Olsson, C. A., Youssef, G., & Hutchinson, D. (2020). Association Between Maternal Perinatal Depression and

- Anxiety and Child and Adolescent Development: A Meta-analysis. *JAMA Pediatrics*, 174(11), 1082-1092.
<https://doi.org/10.1001/jamapediatrics.2020.2910>
- Rosenthal, L., Earnshaw, V. A., Moore, J. M., Ferguson, D. N., Lewis, T. T., Reid, A. E., Lewis, J. B., Stasko, E. C., Tobin, J. N., & Ickovics, J. R. (2018). Intergenerational Consequences: Women's Experiences of Discrimination in Pregnancy Predict Infant Social-Emotional Development at 6 Months and 1 Year. *Journal of Developmental & Behavioral Pediatrics*, 39(3).
https://journals.lww.com/jrnldbpf/fulltext/2018/04000/intergenerational_consequences_women_s.6.aspx
- Rossant, J. (2015). Mouse and human blastocyst-derived stem cells: vive les differences. *Development*, 142(1), 9-12.
<https://doi.org/10.1242/dev.115451>
- Rossant, J., & Tam, P. P. L. (2009). Blastocyst lineage formation, early embryonic asymmetries and axis patterning in the mouse. *Development*, 136(5), 701-713.
<https://doi.org/10.1242/dev.017178>
- Russ, A. P., Wattler, S., Colledge, W. H., Aparicio, S. A. J. R., Carlton, M. B. L., Pearce, J. J., Barton, S. C., Surani, M. A., Ryan, K., Nehls, M. C., Wilson, V., & Evans, M. J. (2000). Eomesodermin is required for mouse trophoblast development and mesoderm formation. *Nature*, 404(6773), 95-99. <https://doi.org/10.1038/35003601>
- Rutter, M. (1985). Resilience in the Face of Adversity: Protective Factors and Resistance to Psychiatric Disorder. *British Journal of Psychiatry*, 147(6), 598-611. <https://doi.org/10.1192/bjp.147.6.598>
- Saeed, H., Wu, J., Tesfaye, M., Grantz, K. L., & Tekola-Ayele, F. (2024). Placental accelerated aging in antenatal depression. *American Journal of Obstetrics & Gynecology MFM*, 6(1).
<https://doi.org/10.1016/j.ajogmf.2023.101237>
- Salas, M., John, R., Saxena, A., Barton, S., Frank, D., Fitzpatrick, G., Higgins, M. J., & Tycko, B. (2004). Placental growth retardation due to loss of imprinting of Phlda2. *Mechanisms of Development*, 121(10), 1199-1210.
<https://doi.org/https://doi.org/10.1016/j.mod.2004.05.017>
- Salazar-Petres, E., Pereira-Carvalho, D., Lopez-Tello, J., & Sferruzzi-Perri, A. N. (2022). Placental structure, function, and mitochondrial phenotype relate to fetal size in each fetal sex in mice†. *Biology of Reproduction*, 106(6), 1292-1311.
<https://doi.org/10.1093/biolre/ioac056>
- Saltzman, W., & Maestriperi, D. (2011). The neuroendocrinology of primate maternal behavior. *Prog Neuropsychopharmacol Biol Psychiatry*, 35(5), 1192-1204.
<https://doi.org/10.1016/j.pnpbp.2010.09.017>
- Sandman, C. A., Glynn, L. M., & Davis, E. P. (2013). Is there a viability-vulnerability tradeoff? Sex differences in fetal programming. *J*

- Psychosom Res*, 75(4), 327-335.
<https://doi.org/10.1016/j.jpsychores.2013.07.009>
- SanMiguel, J. M., & Bartolomei, M. S. (2018). DNA methylation dynamics of genomic imprinting in mouse development. *Biol Reprod*, 99(1), 252-262. <https://doi.org/10.1093/biolre/i0y036>
- Santos, I. S., Blumenberg, C., Munhoz, T. N., Matijasevich, A., Salum, C., Santos Júnior, H. G., dos Santos, L. M., Correia, L. L., de Souza, M. R., Lira, P. I. C., Bortolotto, C. C., Barcelos, R., Altafim, E., Chicaro, M. F., Macana, E. C., & da Silva, R. S. (2024). Maternal depression and child development at 3 years of age: a longitudinal study in a Brazilian child development promotion program. *Pediatric Research*, 95(4), 1139-1146. <https://doi.org/10.1038/s41390-023-02876-9>
- Sara, V. R., & Hall, K. (1990). Insulin-like growth factors and their binding proteins. *Physiol Rev*, 70(3), 591-614.
<https://doi.org/10.1152/physrev.1990.70.3.591>
- Saruta, J., Lee, T., Shirasu, M., Takahashi, T., Sato, C., Sato, S., & Tsukinoki, K. (2010). Chronic stress affects the expression of brain-derived neurotrophic factor in rat salivary glands. *Stress*, 13(1), 53-60. <https://doi.org/10.3109/10253890902875167>
- Saunders, A. M., & Seldin, M. F. (1990). A molecular genetic linkage map of mouse chromosome 7. *Genomics*, 8(3), 525-535.
[https://doi.org/10.1016/0888-7543\(90\)90040-2](https://doi.org/10.1016/0888-7543(90)90040-2)
- Sauvé, D., & Woodside, B. (1996). The effect of central administration of prolactin on food intake in virgin female rats is dose-dependent, occurs in the absence of ovarian hormones and the latency to onset varies with feeding regimen. *Brain Res*, 729(1), 75-81.
- Saxena, A., Frank, D., Panichkul, P., Van den Veyver, I. B., Tycko, B., & Thaker, H. (2003). The Product of the Imprinted Gene IPL Marks Human Villous Cytotrophoblast and is Lost in Complete Hydatidiform Mole. *Placenta*, 24(8), 835-842.
[https://doi.org/https://doi.org/10.1016/S0143-4004\(03\)00130-9](https://doi.org/https://doi.org/10.1016/S0143-4004(03)00130-9)
- Saxena, A., Morozov, P., Frank, D., Musalo, R., Lemmon, M. A., Skolnik, E. Y., & Tycko, B. (2002). Phosphoinositide binding by the pleckstrin homology domains of Ipl and Tih1. *J Biol Chem*, 277(51), 49935-49944. <https://doi.org/10.1074/jbc.M206497200>
- Scott, I. C., Anson-Cartwright, L., Riley, P., Reda, D., & Cross, J. C. (2000). The HAND1 basic helix-loop-helix transcription factor regulates trophoblast differentiation via multiple mechanisms. *Mol Cell Biol*, 20(2), 530-541. <https://doi.org/10.1128/mcb.20.2.530-541.2000>
- Searle, A. G., & Beechey, C. V. (1990). Genome imprinting phenomena on mouse chromosome 7. *Genet Res*, 56(2-3), 237-244.
<https://doi.org/10.1017/s0016672300035333>
- Selwood, L., & Johnson, M. H. (2006). Trophoblast and hypoblast in the monotreme, marsupial and eutherian mammal: evolution and origins. *BioEssays*, 28(2), 128-145.
<https://doi.org/https://doi.org/10.1002/bies.20360>

- Serati, M., Barkin, J. L., Orsenigo, G., Altamura, A. C., & Buoli, M. (2017). Research Review: The role of obstetric and neonatal complications in childhood attention deficit and hyperactivity disorder – a systematic review. *Journal of Child Psychology and Psychiatry*, *58*(12), 1290-1300. <https://doi.org/https://doi.org/10.1111/jcpp.12779>
- Servin-Barthet, C., Martínez-García, M., Pretus, C., Paternina-Die, M., Soler, A., Khymenets, O., Pozo, Ó. J., Leuner, B., Vilarroya, O., & Carmona, S. (2023). The transition to motherhood: linking hormones, brain and behaviour. *Nature Reviews Neuroscience*, *24*(10), 605-619. <https://doi.org/10.1038/s41583-023-00733-6>
- Shalaby, F., Rossant, J., Yamaguchi, T. P., Gertsenstein, M., Wu, X. F., Breitman, M. L., & Schuh, A. C. (1995). Failure of blood-island formation and vasculogenesis in Flk-1-deficient mice. *Nature*, *376*(6535), 62-66. <https://doi.org/10.1038/376062a0>
- Sharma, D., Shastri, S., & Sharma, P. (2016). Intrauterine Growth Restriction: Antenatal and Postnatal Aspects. *Clin Med Insights Pediatr*, *10*, 67-83. <https://doi.org/10.4137/CMPed.S40070>
- Shimizu, T., Oike, A., Kobayashi, E. H., Sekiya, A., Kobayashi, N., Shibata, S., Hamada, H., Saito, M., Yaegashi, N., Suyama, M., Arima, T., & Okae, H. (2023). CRISPR screening in human trophoblast stem cells reveals both shared and distinct aspects of human and mouse placental development. *Proceedings of the National Academy of Sciences*, *120*(51), e2311372120. <https://doi.org/10.1073/pnas.2311372120>
- Shiura, H., Nakamura, K., Hikichi, T., Hino, T., Oda, K., Suzuki-Migishima, R., Kohda, T., Kaneko-Ishino, T., & Ishino, F. (2009). Paternal deletion of Meg1/Grb10 DMR causes maternalization of the Meg1/Grb10 cluster in mouse proximal Chromosome 11 leading to severe pre- and postnatal growth retardation. *Human Molecular Genetics*, *18*(8), 1424-1438. <https://doi.org/10.1093/hmg/ddp049>
- Shorey, S., Chee, C. Y. I., Ng, E. D., Chan, Y. H., Tam, W. W. S., & Chong, Y. S. (2018). Prevalence and incidence of postpartum depression among healthy mothers: A systematic review and meta-analysis. *J Psychiatr Res*, *104*, 235-248. <https://doi.org/10.1016/j.jpsychires.2018.08.001>
- Simmers, M. D., Hudson, K. M., Baptissart, M., & Cowley, M. (2023). Epigenetic control of the imprinted growth regulator Cdkn1c in cadmium-induced placental dysfunction. *Epigenetics*, *18*(1), 2088173. <https://doi.org/10.1080/15592294.2022.2088173>
- Simmons, D. G. (2014). Postimplantation Development of the Chorioallantoic Placenta. In B. A. Croy, A. T. Yamada, F. J. DeMayo, & S. L. Adamson (Eds.), *The Guide to Investigation of Mouse Pregnancy* (pp. 143-161). Academic Press. <https://doi.org/https://doi.org/10.1016/B978-0-12-394445-0.00012-6>

- Simmons, D. G., & Cross, J. C. (2005). Determinants of trophoblast lineage and cell subtype specification in the mouse placenta. *Developmental Biology*, 284(1), 12-24. <https://doi.org/https://doi.org/10.1016/j.ydbio.2005.05.010>
- Simmons, D. G., Fortier, A. L., & Cross, J. C. (2007). Diverse subtypes and developmental origins of trophoblast giant cells in the mouse placenta. *Dev Biol*, 304(2), 567-578. <https://doi.org/10.1016/j.ydbio.2007.01.009>
- Simmons, D. G., Natale, D. R., Begay, V., Hughes, M., Leutz, A., & Cross, J. C. (2008). Early patterning of the chorion leads to the trilaminar trophoblast cell structure in the placental labyrinth. *Development*, 135(12), 2083-2091. <https://doi.org/10.1242/dev.020099>
- Simmons, D. G., Rawn, S., Davies, A., Hughes, M., & Cross, J. C. (2008). Spatial and temporal expression of the 23 murine Prolactin/Placental Lactogen-related genes is not associated with their position in the locus. *BMC Genomics*, 9, 352. <https://doi.org/10.1186/1471-2164-9-352>
- Sinha, J. K., Aziz, A., Ghosh, S., & Raghunath, M. (2022). Maternal Behavior. In J. Vonk & T. K. Shackelford (Eds.), *Encyclopedia of Animal Cognition and Behavior* (pp. 4120-4125). Springer International Publishing. https://doi.org/10.1007/978-3-319-55065-7_1345
- Smiley, K. O., Ladyman, S. R., Gustafson, P., Grattan, D. R., & Brown, R. S. E. (2019). Neuroendocrinology and Adaptive Physiology of Maternal Care. In L. M. Coolen & D. R. Grattan (Eds.), *Neuroendocrine Regulation of Behavior* (pp. 161-210). Springer International Publishing. https://doi.org/10.1007/978-3-319-55065-7_1345
- Smith, K. (2023). *Women's health research lacks funding – these charts show how*. Nature. Retrieved 20th June from <https://www.nature.com/immersive/d41586-023-01475-2/index.html>
- Smolina, K., Hanley, G. E., Mintzes, B., Oberlander, T. F., & Morgan, S. (2015). Trends and Determinants of Prescription Drug Use during Pregnancy and Postpartum in British Columbia, 2002-2011: A Population-Based Cohort Study. *PLoS One*, 10(5), e0128312. <https://doi.org/10.1371/journal.pone.0128312>
- Soares, M. J. (2004). The prolactin and growth hormone families: Pregnancy-specific hormones/cytokines at the maternal-fetal interface. *Reproductive Biology and Endocrinology*, 2(1), 51. <https://doi.org/10.1186/1477-7827-2-51>
- Soares, M. J., Konno, T., & Alam, S. M. (2007). The prolactin family: effectors of pregnancy-dependent adaptations. *Trends Endocrinol Metab*, 18(3), 114-121. <https://doi.org/10.1016/j.tem.2007.02.005>
- Soares, M. J., & Linzer, D. I. H. (2001). Rodent Prolactin Family and Pregnancy. In N. D. Horseman (Ed.), *Prolactin* (pp. 139-167). Springer US. https://doi.org/10.1007/978-1-4615-1683-5_8

- Soares, M. J., Varberg, K. M., & Iqbal, K. (2018). Hemochorial placentation: development, function, and adaptations†. *Biology of Reproduction*, 99(1), 196-211.
<https://doi.org/10.1093/biolre/iroy049>
- Solter, D. (1988). DIFFERENTIAL IMPRINTING AND EXPRESSION OF MATERNAL AND PATERNAL GENOMES. *Annual Review of Genetics*, 22(Volume 22, 1988), 127-146.
<https://doi.org/https://doi.org/10.1146/annurev.ge.22.120188.001015>
- Sones, J. L., & Davisson, R. L. (2016). Preeclampsia, of mice and women. *Physiol Genomics*, 48(8), 565-572.
<https://doi.org/10.1152/physiolgenomics.00125.2015>
- Song, B., Chen, Y., Wang, C., Li, G., Wei, Z., He, X., & Cao, Y. (2022). Poor semen parameters are associated with abnormal methylation of imprinted genes in sperm DNA. *Reproductive Biology and Endocrinology*, 20(1), 155. <https://doi.org/10.1186/s12958-022-01028-8>
- Spellacy, W. N., Buhi, W. C., & Birk, S. A. (1978). Human placental lactogen levels in multiple pregnancies. *Obstet Gynecol*, 52(2), 210-212.
- Spencer, H. G., & Clark, A. G. (2014). Non-conflict theories for the evolution of genomic imprinting. *Heredity (Edinb)*, 113(2), 112-118.
<https://doi.org/10.1038/hdy.2013.129>
- Stock, S. J., & Norman, J. E. (2019). Medicines in pregnancy. *F1000Res*, 8. <https://doi.org/10.12688/f1000research.17535.1>
- Stolzenberg, D. S., & Champagne, F. A. (2016). Hormonal and non-hormonal bases of maternal behavior: The role of experience and epigenetic mechanisms. *Hormones and Behavior*, 77, 204-210.
<https://doi.org/https://doi.org/10.1016/j.yhbeh.2015.07.005>
- Stubbs, L., Carver, E. A., Shannon, M. E., Kim, J., Geisler, J., Generoso, E. E., Stanford, B. G., Dunn, W. C., Mohrenweiser, H., Zimmermann, W., Watt, S. M., & Ashworth, L. K. (1996). Detailed comparative map of human chromosome 19q and related regions of the mouse genome. *Genomics*, 35(3), 499-508.
<https://doi.org/10.1006/geno.1996.0390>
- Sumption, L. A., Garay, S. M., & John, R. M. (2020). Low serum placental lactogen at term is associated with postnatal symptoms of depression and anxiety in women delivering female infants. *Psychoneuroendocrinology*, 116, 104655.
<https://doi.org/https://doi.org/10.1016/j.psyneuen.2020.104655>
- Surani, M. A. (1998). Imprinting and the Initiation of Gene Silencing in the Germ Line. *Cell*, 93(3), 309-312.
[https://doi.org/10.1016/S0092-8674\(00\)81156-3](https://doi.org/10.1016/S0092-8674(00)81156-3)
- Surani, M. A., & Barton, S. C. (1983). Development of gynogenetic eggs in the mouse: implications for parthenogenetic embryos. *Science*, 222(4627), 1034-1036. <https://doi.org/10.1126/science.6648518>

- Surani, M. A. H., Barton, S. C., & Norris, M. L. (1984). Development of reconstituted mouse eggs suggests imprinting of the genome during gametogenesis. *Nature*, *308*(5959), 548-550. <https://doi.org/10.1038/308548a0>
- Surani, M. A. H., Barton, S. C., & Norris, M. L. (1987). Influence of parental chromosomes on spatial specificity in androgenetic ↔ parthenogenetic chimaeras in the mouse. *Nature*, *326*(6111), 395-397. <https://doi.org/10.1038/326395a0>
- Surani, M. A. H., Wolf, R., & Allen, N. (1988). Transgenes as molecular probes for genomic imprinting. *Trends in genetics*, *4*(3), 59-62. [https://doi.org/https://doi.org/10.1016/0168-9525\(88\)90040-6](https://doi.org/https://doi.org/10.1016/0168-9525(88)90040-6)
- Sutherland, S., & Brunwasser, S. M. (2018). Sex Differences in Vulnerability to Prenatal Stress: a Review of the Recent Literature. *Curr Psychiatry Rep*, *20*(11), 102. <https://doi.org/10.1007/s11920-018-0961-4>
- Suzuki, S., Renfree, M. B., Pask, A. J., Shaw, G., Kobayashi, S., Kohda, T., Kaneko-Ishino, T., & Ishino, F. (2005). Genomic imprinting of IGF2, p57(KIP2) and PEG1/MEST in a marsupial, the tammar wallaby. *Mech Dev*, *122*(2), 213-222. <https://doi.org/10.1016/j.mod.2004.10.003>
- Swaney, W. T., Curley, J. P., Champagne, F. A., & Keverne, E. B. (2008). The paternally expressed gene Peg3 regulates sexual experience-dependent preferences for estrous odors. *Behav Neurosci*, *122*(5), 963-973. <https://doi.org/10.1037/a0012706>
- Takahashi, K., Kobayashi, T., & Kanayama, N. (2000). p57Kip2 regulates the proper development of labyrinthine and spongiotrophoblasts. *Molecular Human Reproduction*, *6*(11), 1019-1025. <https://doi.org/10.1093/molehr/6.11.1019>
- Takao, T., Asanoma, K., Tsunematsu, R., Kato, K., & Wake, N. (2012). The maternally expressed gene Tssc3 regulates the expression of MASH2 transcription factor in mouse trophoblast stem cells through the AKT-Sp1 signaling pathway. *J Biol Chem*, *287*(51), 42685-42694. <https://doi.org/10.1074/jbc.M112.388777>
- Tanaka, S., Kunath, T., Hadjantonakis, A.-K., Nagy, A., & Rossant, J. (1998). Promotion of Trophoblast Stem Cell Proliferation by FGF4. *Science*, *282*(5396), 2072-2075. <https://doi.org/10.1126/science.282.5396.2072>
- Tanguay, N., Abdelouahab, N., Simard, M. N., Séguin, J. R., Marc, I., Herba, C. M., MacLeod, A. A. N., Courtemanche, Y., Fraser, W. D., & Muckle, G. (2023). Antidepressants use during pregnancy and child psychomotor, cognitive and language development at 2 years of age-Results from the 3D Cohort Study. *Front Pharmacol*, *14*, 1252251. <https://doi.org/10.3389/fphar.2023.1252251>
- Taniguchi, T., Okamoto, K., & Reeve, A. E. (1997). Human p57KIP2 defines a new imprinted domain on chromosome 11p but is not a tumour suppressor gene in Wilms tumour. *Oncogene*, *14*(10), 1201-1206. <https://doi.org/10.1038/sj.onc.1200934>

- Terkel, J., Blake, C. A., & Sawyer, C. H. (1972). Serum Prolactin Levels in Lactating Rats after Suckling or Exposure to Ether. *Endocrinology*, 91(1), 49-53. <https://doi.org/10.1210/endo-91-1-49>
- The Human Protein Atlas: PEG3. (2025). *PEG3_201 Protein Browser*. <https://www.proteinatlas.org/ENSG00000198300-PEG3/structure+interaction>
- The Human Protein Atlas: PHLDA2. (2025). *PHLDA2_201 Protein browser*. <https://www.proteinatlas.org/ENSG00000181649-PHLDA2/structure+interaction>
- The UniProt, C. (2025). UniProt: the Universal Protein Knowledgebase in 2025. *Nucleic Acids Research*, 53(D1), D609-D617. <https://doi.org/10.1093/nar/gkae1010>
- Thiaville, M. M., Huang, J. M., Kim, H., Ekram, M. B., Roh, T.-Y., & Kim, J. (2013). DNA-binding motif and target genes of the imprinted transcription factor PEG3. *Gene*, 512(2), 314-320. <https://doi.org/https://doi.org/10.1016/j.gene.2012.10.005>
- Thiery, M., Dhont, M., & Vandekerckhove, D. (1977). Serum HCG and HPL in twin pregnancies. *Acta Obstet Gynecol Scand*, 56(5), 495-497. <https://doi.org/10.3109/00016347709155019>
- Thomas, B. J., & Rothstein, R. (1991). Sex, maps, and imprinting. *Cell*, 64(1), 1-3. [https://doi.org/10.1016/0092-8674\(91\)90199-9](https://doi.org/10.1016/0092-8674(91)90199-9)
- Thomson, E. (2023). Over a million women around the world were asked 'What do you want most for your health and well-being?' Here's what they said *World economic forum*. <https://www.weforum.org/agenda/2023/11/women-health-wellbeing-white-ribbon-survey/>
- Thorvaldsen, J. L., Duran, K. L., & Bartolomei, M. S. (1998). Deletion of the H19 differentially methylated domain results in loss of imprinted expression of H19 and Igf2. *Genes Dev*, 12(23), 3693-3702. <https://doi.org/10.1101/gad.12.23.3693>
- Toder, R., Wilcox, S. A., Smithwick, M., & Graves, J. A. (1996). The human/mouse imprinted genes IGF2, H19, SNRPN and ZNF127 map to two conserved autosomal clusters in a marsupial. *Chromosome Res*, 4(4), 295-300. <https://doi.org/10.1007/bf02263680>
- Tolkunova, E., Cavaleri, F., Eckardt, S., Reinbold, R., Christenson, L. K., Schöler, H. R., & Tomilin, A. (2006). The Caudal-Related Protein Cdx2 Promotes Trophoblast Differentiation of Mouse Embryonic Stem Cells. *Stem Cells*, 24(1), 139-144. <https://doi.org/10.1634/stemcells.2005-0240>
- Trivers, R. L. (1974). Parent-Offspring Conflict. *American Zoologist*, 14(1), 249-264. <https://doi.org/10.1093/icb/14.1.249>
- Tucci, V., Isles, A. R., Kelsey, G., & Ferguson-Smith, A. C. (2019). Genomic Imprinting and Physiological Processes in Mammals. *Cell*, 176(5), 952-965. <https://doi.org/10.1016/j.cell.2019.01.043>
- Tuckey, R. C. (2005). Progesterone synthesis by the human placenta. *Placenta*, 26(4), 273-281. <https://doi.org/10.1016/j.placenta.2004.06.012>

- Tunster, S. J., Boqué-Sastre, R., McNamara, G. I., Hunter, S. M., Creeth, H. D. J., & John, R. M. (2018). Peg3 Deficiency Results in Sexually Dimorphic Losses and Gains in the Normal Repertoire of Placental Hormones [Original Research]. *Frontiers in Cell and Developmental Biology*, 6. <https://doi.org/10.3389/fcell.2018.00123>
- Tunster, S. J., Creeth, H. D. J., & John, R. M. (2016). The imprinted Phlda2 gene modulates a major endocrine compartment of the placenta to regulate placental demands for maternal resources. *Dev Biol*, 409(1), 251-260. <https://doi.org/10.1016/j.ydbio.2015.10.015>
- Tunster, S. J., McNamara, G. I., Creeth, H. D. J., & John, R. M. (2016). Increased dosage of the imprinted Ascl2 gene restrains two key endocrine lineages of the mouse Placenta. *Dev Biol*, 418(1), 55-65. <https://doi.org/10.1016/j.ydbio.2016.08.014>
- Tunster, S. J., Tycko, B., & John, R. M. (2010). The Imprinted *Phlda2* Gene Regulates Extraembryonic Energy Stores. *Molecular and Cellular Biology*, 30(1), 295-306. <https://doi.org/10.1128/mcb.00662-09>
- Tunster, S. J., Van de Pette, M., & John, R. M. (2011). Fetal overgrowth in the Cdkn1c mouse model of Beckwith-Wiedemann syndrome. *Dis Model Mech*, 4(6), 814-821. <https://doi.org/10.1242/dmm.007328>
- Tunster, S. J., Van de Pette, M., & John, R. M. (2012). Impact of genetic background on placental glycogen storage in mice. *Placenta*, 33(2), 124-127. <https://doi.org/https://doi.org/10.1016/j.placenta.2011.11.011>
- Tunster, S. J., Van De Pette, M., & John, R. M. (2014). Isolating the role of elevated Phlda2 in asymmetric late fetal growth restriction in mice. *Dis Model Mech*, 7(10), 1185-1191. <https://doi.org/10.1242/dmm.017079>
- Tunster, S. J., Watson, E. D., Fowden, A. L., & Burton, G. J. (2020). Placental glycogen stores and fetal growth: insights from genetic mouse models. *Reproduction*, 159(6), R213-r235. <https://doi.org/10.1530/rep-20-0007>
- Tyndale-Biscoe, H. (1979). Prototheria: The Biology of the Monotremes. Mervyn Griffiths. Academic Press, New York, 1978. x, 368 pp., illus. \$31. *Science*, 204(4399), 1300-1300. <https://doi.org/10.1126/science.204.4399.1300.a>
- Udechuku, A., Nguyen, T., Hill, R., & Szego, K. (2010). Antidepressants in Pregnancy: a Systematic Review. *Australian & New Zealand Journal of Psychiatry*, 44(11), 978-996. <https://doi.org/10.3109/00048674.2010.507543>
- Ullah, R., Naz, A., Akram, H. S., Ullah, Z., Tariq, M., Mithani, A., & Faisal, A. (2020). Transcriptomic analysis reveals differential gene expression, alternative splicing, and novel exons during mouse trophoblast stem cell differentiation. *Stem Cell Research & Therapy*, 11(1), 342. <https://doi.org/10.1186/s13287-020-01848-8>

- Ursell, W., Brudenell, M., & Chard, T. (1973). Placental Lactogen Levels in Diabetic Pregnancy. *British Medical Journal*, 2(5858), 80.
<https://doi.org/10.1136/bmj.2.5858.80>
- Ussher, J. M. (2011). *The madness of Women : Myth and Experience*. Taylor & Francis.
- Van Gurp, R. J., Oosterhuis, J. W., Kalscheuer, V., Mariman, E. C., & Looijenga, L. H. (1994). Biallelic expression of the H19 and IGF2 genes in human testicular germ cell tumors. *J Natl Cancer Inst*, 86(14), 1070-1075. <https://doi.org/10.1093/jnci/86.14.1070>
- Varmuza, S., & Mann, M. (1994). Genomic imprinting — defusing the ovarian time bomb. *Trends in genetics*, 10(4), 118-123.
[https://doi.org/https://doi.org/10.1016/0168-9525\(94\)90212-7](https://doi.org/https://doi.org/10.1016/0168-9525(94)90212-7)
- Wada, Y., Takahashi, H., Sasabuchi, Y., Usui, R., Ogoyama, M., Suzuki, H., Ohkuchi, A., & Fujiwara, H. (2023). Maternal outcomes of placental abruption with intrauterine fetal death and delivery routes: A nationwide observational study. *Acta Obstet Gynecol Scand*, 102(6), 708-715. <https://doi.org/10.1111/aogs.14569>
- Wang, X., Li, G., Koul, S., Ohki, R., Maurer, M., Borczuk, A., & Halmos, B. (2018). PHLDA2 is a key oncogene-induced negative feedback inhibitor of EGFR/ErbB2 signaling via interference with AKT signaling. *Oncotarget; Vol 9, No 38*.
<https://www.oncotarget.com/article/3674/>
- Wang, Y., Meng, Z., Pei, J., Qian, L., Mao, B., Li, Y., Li, J., Dai, Z., Cao, J., Zhang, C., Chen, L., Jin, Y., & Yi, B. (2021). Anxiety and depression are risk factors for recurrent pregnancy loss: a nested case-control study. *Health and Quality of Life Outcomes*, 19(1), 78.
<https://doi.org/10.1186/s12955-021-01703-1>
- Wang, Y., & Zhao, S. (2010). Integrated Systems Physiology: from Molecules to Function to Disease. In *Vascular Biology of the Placenta*. Morgan & Claypool Life Sciences Copyright © 2010 by Morgan & Claypool Life Sciences.
<https://doi.org/10.4199/c00016ed1v01y201008isp009>
- Weidman, J. R., Maloney, K. A., & Jirtle, R. L. (2006). Comparative phylogenetic analysis reveals multiple non-imprinted isoforms of opossum Dlk1. *Mamm Genome*, 17(2), 157-167.
<https://doi.org/10.1007/s00335-005-0116-x>
- Whiting, K. (2023). 6 conditions that highlight the women's health gap. *World economic forum*.
<https://www.weforum.org/agenda/2024/06/womens-health-gap-healthcare/>
- Whiting, K. (2024). Why the women's health gap exists – and how to close it – according to experts at Davos. *World economic forum*.
<https://www.weforum.org/agenda/2024/01/women-health-davos-2024/>
- Wiemers, D. O., Shao, L.-j., Ain, R., Dai, G., & Soares, M. J. (2003). The Mouse Prolactin Gene Family Locus. *Endocrinology*, 144(1), 313-325. <https://doi.org/10.1210/en.2002-220724>

- Wiles, N. J., Peters, T. J., Heron, J., Gunnell, D., Emond, A., Lewis, G., & for the, A. S. T. (2006). Fetal Growth and Childhood Behavioral Problems: Results from the ALSPAC Cohort. *American Journal of Epidemiology*, 163(9), 829-837.
<https://doi.org/10.1093/aje/kwj108>
- Winchester, N. (2021). Women's health outcomes: Is there a gender gap? *House of lords library*. <https://lordslibrary.parliament.uk/womens-health-outcomes-is-there-a-gender-gap/>
- Wolstenholme, J. T., Rissman, E. F., & Bekiranov, S. (2013). Sexual differentiation in the developing mouse brain: contributions of sex chromosome genes. *Genes Brain Behav*, 12(2), 166-180.
<https://doi.org/10.1111/gbb.12010>
- Women and equalities committee. (2024). Women's reproductive health conditions.
<https://publications.parliament.uk/pa/cm5901/cmselect/cmwomeq/337/report.html#footnote-251>
- Xiao, F., Liu, X., Chen, Y., & Dai, H. (2021). Tumor-Suppressing STF cDNA 3 Overexpression Suppresses Renal Fibrosis by Alleviating Anoikis Resistance and Inhibiting the PI3K/Akt Pathway. *Kidney Blood Press Res*, 46(5), 588-600.
<https://doi.org/10.1159/000517318>
- Yamaguchi, A., Taniguchi, M., Hori, O., Ogawa, S., Tojo, N., Matsuoka, N., Miyake, S., Kasai, K., Sugimoto, H., Tamatani, M., Yamashita, T., & Tohyama, M. (2002). Peg3/Pw1 is involved in p53-mediated cell death pathway in brain ischemia/hypoxia. *J Biol Chem*, 277(1), 623-629. <https://doi.org/10.1074/jbc.M107435200>
- Yang, X., & Gu, W. (2024). PHLDA2 is critical for p53-mediated ferroptosis and tumor suppression. *Journal of Molecular Cell Biology*, 16(7), mjae033. <https://doi.org/10.1093/jmcb/mjae033>
- Yokomine, T., Shirohzu, H., Purbowasito, W., Toyoda, A., Iwama, H., Ikeo, K., Hori, T., Mizuno, S., Tsudzuki, M., Matsuda, Y., Hattori, M., Sakaki, Y., & Sasaki, H. (2005). Structural and functional analysis of a 0.5-Mb chicken region orthologous to the imprinted mammalian Ascl2/Mash2-Igf2-H19 region. *Genome Res*, 15(1), 154-165.
<https://doi.org/10.1101/gr.2609605>
- Young, K., Fisher, J., & Kirkman, M. (2018). "Do mad people get endo or does endo make you mad?": Clinicians' discursive constructions of Medicine and women with endometriosis. *Feminism & Psychology*, 29(3), 337-356. <https://doi.org/10.1177/0959353518815704>
- Zeanah, C. H., Smyke, A. T., Koga, S. F., Carlson, E., & The Bucharest Early Intervention Project Core, G. (2005). Attachment in Institutionalized and Community Children in Romania. *Child Development*, 76(5), 1015-1028.
<https://doi.org/https://doi.org/10.1111/j.1467-8624.2005.00894.x>
- Zhao, G.-s., Gao, Z.-r., Zhang, Q., Tang, X.-f., Lv, Y.-f., Zhang, Z.-s., Zhang, Y., Tan, Q.-l., Peng, D.-b., Jiang, D.-m., & Guo, Q.-N. (2018). TSSC3 promotes autophagy via inactivating the Src-

mediated PI3K/Akt/mTOR pathway to suppress tumorigenesis and metastasis in osteosarcoma, and predicts a favorable prognosis. *Journal of Experimental & Clinical Cancer Research*, 37(1), 188. <https://doi.org/10.1186/s13046-018-0856-6>

Zhao, Y., Zhang, L., & Geng, Y. (2021). Clinical Drug Trial Participation: Perspectives of Pregnant Women and Their Spouses. *Patient Preference Adherence*, 15, 2343-2352. <https://doi.org/10.2147/ppa.S328969>

Appendix:

Appendix 1: Chapter 3: Methods

1.1 Chapter 3: Methods

1.1.1 Generation of tissues

Tissue was generated by crossing virgin C57BL/6 females with *Phlda2*^{+/+BACx1(BL6)} males, resulting in *Phlda2*^{+/+BACx1(BL6)} transgenic (Tg) and *Phlda2*^{+/+} wild type (WT) offspring. At E14.5 placenta was dissected as described in Chapter 2. Genotyping and sextyping was performed on the yolk sac of each foeto-placental unit as described in Chapter 2. Litters were excluded where litter size was under six or had an uneven distribution of genotypes or sex. 12 viable litters were collected for analysis. The placenta and foetus were weighed as described in protocol 2.1.6 before each foetus was killed by decapitation as stipulated in the project licence. The placenta was then bisected along the midline with half of the placenta fixed in 4% PFA and embedded in paraffin wax, and half frozen on dry ice and stored at -80 °C.

1.1.2 Weight data

Weight data was normalised against the population. The average weight of the WT foetuses in each litter was calculated, this was divided by the average weight of all WT foetuses within the population to generate a normalisation factor for each litter. The foetal and placental weights were then multiplied by the normalisation factor for its litter. Foetal: placental weight ratios were also generated by dividing the embryo weight by the placental weight.

	WT	Tg
Male	23	30
Female	25	18

Table 45: Group sizes for weight data analysis.

1.1.3 RNAscope and counting methods

Paraffin-embedded E14.5 midplane sections were stained for *Pr/3b1* using the RNAscope protocol described in Chapter 2. These were imaged as described in protocol 2.4. Area measurements of the junctional zone, labyrinth and full placenta were performed using Zen Blue software.

Placental cells were counted using the automatic counting protocol described in section 2.6.

	WT	Tg
Male	8	9
Female	7	9

Table 46: Group sizes for *Pr/3b1* stained cell counted placenta.

Samples were manually counted by Masters student, Amelia Stoddart to validate the automatic counting process as it was being established.

1.1.4 qRT-PCR methods

Half frozen placenta was cut again into two quarters. One quarter of the placenta was then processed through RNA extraction (protocol 2.10.1). A portion of the RNA was then converted into cDNA (protocol 2.10.3) which was then used for qRT-PCR analysis (protocol 2.10.4).

	WT	Tg
Male	4	4
Female	4	4

Table 47: Sample numbers used for qRT-PCR.

1.1.5 Statistics

Sample size was calculated using Equation 4 and data from (Tunster, Creeth, et al., 2016). The effect of genotype and sex were analysed using ANOVA with a Šidák correction. Evidence outside of this experiment began to suggest that litter size should be factored into this statistical analysis, as regardless of genotype, it is possible that any effect caused by an altered placenta could be nullified by other placentas present within each pregnancy. It is likely that a fully wild type pregnancy has some regulatory system to moderate placental hormones as foetal and placental numbers vary in pregnancy, as mice have pregnancies with multiple pups in one litter. Factoring in genotype further complicates this issue. Therefore, analysis was also conducted using an ANCOVA with a Šidák correction and using litter size as a covariate.

Appendix 2: Extended caption and result table for Figure 27.

Figure 27: Foetal and placental weight data for WT and Tg.

a) Wet weights of WT and Tg foetuses at E14.5 show no significant difference. **b)** Tg placenta weighed 17% less than WT placenta

(GENOTYPE: $F_{1,91} = 40.77, P < .001$). **c**) Tg F:P ratio was 18% higher than WT (GENOTYPE: $F_{1,91} = 27.29, P < .001$). WT ($n = 48$), Tg ($n = 48$). Data from 12 litters, litter size between 7-10 (average 8 ± 0.91). Weights normalised against WT weight across litters. Error bars represent standard error of the mean (SEM). Statistical significance calculated using two-way ANCOVA with Šidák correction and litter size as covariate. ^{NS} $P > .05$, * $P < .05$, and ** $P < .01$ *** $P < .001$ **** $P < .0001$.

Metric	Comparison	ANOVA <i>P</i> value	ANCOVA <i>P</i> value
Foetal weight	WT 202 ± 2.8 mg vs Tg 197 ± 3.1 mg	$P = .164$	$P = .160$
Placental weight	WT 85.8 ± 1.7 mg vs Tg 70.6 ± 1.7 mg	$P < .001$	$P < .001$
Foetal to placental weight ratio	WT $2.4 \pm .05$ vs Tg $2.8 \pm .07$	$P < .001$	$P < .001$

Table 48: Weight data for WT and Tg comparison results (\pm SEM) with *P* values for ANOVA and ANCOVA analysis. Significant *P* values in bold.

Appendix 3: Extended caption and result table for Figure 28.

Figure 28: Foetal and placental weight data for WT and Tg.

a) Wet weights of WT and Tg foetuses at E14.5 show no significant difference. **b**) WT female placenta weighed 8% less than WT male placenta (SEX: $F_{1,91} = 4.15, P = .045$). Tg placenta weighed 18% less than WT placenta for both males and females (GENOTYPE: $F_{1,91} = 17.43, P < .001$, GENOTYPE: $F_{1,91} = 23.99, P < .001$). **c**) Tg Foetal: placental weight ratios were 16% ($P < .001$) and 22% ($P < .001$) more than WT for males and females respectively. WT male ($n = 23$), Tg male ($n = 30$), WT female ($n = 25$) and Tg female ($n = 18$). Data from 12 litters, litter size between 7-10 (average 8 ± 0.91). Normalised against WT weight across litters. Error bars represent standard error of the mean (SEM). Statistical significance calculated using two-way ANCOVA with Šidák correction. ^{NS} $P > .05$, * $P < .05$, and ** $P < .01$ *** $P < .001$ **** $P < .0001$.

Metric	Comparison	ANOVA <i>P</i> value	ANCOVA <i>P</i> value
Foetal weight	M-WT 206 ± 4.2 mg vs M-Tg 199 ± 4.0 mg	.168	.161
	M-WT 206 ± 4.2 mg vs F-WT 197 ± 3.5 mg	.128	.127

	F-WT 197±3.5 mg vs F-Tg 193±5.2 mg	.524	.53
	M-Tg 199±4.0 mg vs F-Tg 193±5.2 mg	.394	.412
Placental Weight	M-WT 89.2±2.9 mg vs M-Tg 73.6±2.1 mg	<.001	<.001
	M-WT 89.2±2.9 mg vs F-WT 82.5±1.8 mg	.045	.045
	F-WT 82.5±1.8 mg vs F-Tg 67.5±2.6 mg	<.001	<.001
	M-Tg 73.6±2.1 mg vs F-Tg 67.5±2.6 mg	.079	.088
Foetal to placental weight ratio	M-WT 2.4±.08 vs M-Tg 2.7±.07	.001	.001
	M-WT 2.4±.08 vs F-WT 2.4±.05	.678	.674
	F-WT 2.4±.05 vs F-Tg 2.9±.13	<.001	<.001
	M-Tg 2.7±.07 vs F-Tg 2.9±.13	.121	.128

Table 49: Sex split weight data for WT and Tg comparison results (\pm SEM) with P values for ANOVA and ANCOVA analysis. Significant P values in bold.

Appendix 4: Extended caption and result table for Figure 29.

Figure 29: Area of placental subsections for WT and Tg.

a) Tg junctional zones were 51% ((GENOTYPE*SEX: $F_{1,28} = 3.97$, $P=.056$), (GENOTYPE: $F_{1,28} = 46.75$, $P<.001$)) smaller than WT. **b)** Tg labyrinth was not significantly smaller than WT (GENOTYPE*SEX: $F_{1,27} = 9.76$, $P=.004$). **c)** Labyrinth to junctional zone area ratio was higher in Tg compared to WT with an 88% increase (GENOTYPE: $F_{1,27} = 15.01$, $P<.001$). **d)** Decidua area measurements show no significant difference between WT and Tg. **e)** No significant difference between WT and Tg in total area measurements (GENOTYPE*SEX: $F_{1,18} = 6.43$, $P=.021$). WT ($n = 15$), and Tg ($n = 18$). Data from 12 litters, litter size between 6-10 (average 8 ± 0.20). Error bars represent \pm SEM. Statistical significance calculated using a two-way ANCOVA with litter size as a covariate using a Šidák correction. $^{NS}P>.05$, $^*P<.05$, $^{**}P<.01$, $^{***}P<.001$, $^{****}P<.0001$.

Metric	Comparison	ANOVA P value	ANCOVA P value
Junctional zone area	WT 3008580±173340 vs Tg 1468898±146241 μm^2	<.001	<.001
Labyrinth area	WT 3796207± 346474 mg vs Tg 3224453± 254392 μm^2	.089	.138

Lz:Jz Area Ratio	WT 1.298±.08 vs Tg 2.385±.21	<.001	<.001
Decidua Area	WT 1746657±339955 vs Tg 1062991±119559 μm^2	.438	.273
Total Area	WT 7573361±564508 vs Tg 6019347±531418 μm^2	.038	.073

Table 50: Placental area measurements for WT and Tg comparison (\pm SEM) with *P* values for ANOVA and ANCOVA analysis. Significant *P* values in bold.

Appendix 5: Extended caption and result table for Figure 30.

Figure 30: Area of placental sub-sections split by sex for WT and Tg. **a)** Junctional zone area measurements WT and Tg placenta at E14.5 (GENOTYPE*SEX: $F_{1,28} = 3.97$, $P = .056$). Tg junctional zones were 40% (GENOTYPE: $F_{1,28} = 10.61$, $P = .003$) smaller than WT in males and 62% (GENOTYPE: $F_{1,28} = 38.80$, $P < .001$) smaller than WT in females. Female Tg junctional zone area was significantly smaller than Male Tg junctional zone area by 34% (SEX: $F_{1,28} = 5.24$, $P = .03$). **b)** Labyrinth area measurements of WT and Tg placenta at E14.5 (GENOTYPE*SEX: $F_{1,27} = 9.792$, $P = .004$). Tg labyrinth was not significantly different in males than WT. Female WT labyrinth was 42% (SEX: $F_{1,27} = 5.73$, $P = .024$) larger than Male WT labyrinth. Female Tg labyrinth was 40% (GENOTYPE: $F_{1,27} = 10.74$, $P = .003$) smaller than Female WT labyrinth. Female Tg labyrinth was also 25% (SEX: $F_{1,27} = 4.20$, $P = .05$) smaller than Male Tg labyrinth. **c)** Labyrinth to junctional zone area ratio (Lz:Jz) was higher in Tg compared to WT. Males have a 114% increase (GENOTYPE: $F_{1,27} = 8.30$, $P = .008$) and females with a 63% increase (GENOTYPE: $F_{1,27} = 6.50$, $P = .017$). **d)** Decidua area measurements of WT and Tg show no significant difference between any groups. **e)** Total area measurements of WT and Tg placenta at E14.5 (GENOTYPE*SEX: $F_{1,18} = 6.43$, $P = .021$). Total area was not significantly different for males, whereas female Tg measured 41% (GENOTYPE: $F_{1,18} = 8.70$, $P = .009$) smaller than WT. Female Tg placentas were also 35% (SEX: $F_{1,18} = 9.36$, $P = .007$) smaller than M Tg placentas in total size. WT male ($n = 8$), and Tg male ($n = 9$), WT female ($n = 7$), Tg female ($n = 9$). Data from 12 litters, litter size between 6-10 (average 8 ± 0.20). Error bars represent \pm SEM. Statistical significance calculated using a two-way ANCOVA with litter size as a covariate using a Šidák correction. ^{NS} $P > .05$, $*P < .05$, $**P < .01$, $***P < .001$, $****P < .0001$.

Metric	Comparison	ANOVA <i>P</i> value	ANCOVA <i>P</i> value
Junctional zone area	M-WT 2929287± 282085 vs M-Tg 1766808± 252445 μm^2	.0035	.003
	M-WT 2929287± 282085 vs F-WT 3087874±204700 μm^2	.128	.548
	F-WT 3087874±204700 vs F-Tg 1170988±70542 μm^2	<.0001	<.001
	M-Tg 1766808± 252445 vs F-Tg 1170988±70542 μm^2	.269	.030
Labyrinth area	M-WT 3214646±416876 vs M-Tg 3691397±389678 μm^2	.933	.253
	M-WT 3214646±416876 vs F-WT 4571621±439800 μm^2	.1398	.024
	F-WT 4571621±439800 vs F-Tg 2757510±262074 μm^2	.0179	.003
	M-Tg 3691397±389678 vs F-Tg 2757510±262074 μm^2	.361	.05
Lz:Jz area ratio	M-WT 1.07±.07 vs M-Tg 2.3±.30	.0011	.008
	M-WT 1.07±.07 vs F-WT 1.52±.10	.853	.289
	F-WT 1.52±.10 vs F-Tg 2.47±.33	.0010	.017
	M-Tg 2.3±.30 vs F-Tg 2.47±.33	.856	.403
Decidua area	M-WT 2110041± 485644 vs M-Tg 1181942± 227421 μm^2	.185	.139
	M-WT 2110041± 485644 vs F-WT 1110736±148620 μm^2	.991	.872
	F-WT 1110736±148620 vs F-Tg 944040±74363 μm^2	.256	.43
	M-Tg 1181942± 227421 vs F-Tg 944040±74363 μm^2	.995	.669
Total area	M-WT 7184553±849702 vs M-Tg 7302182±679095 μm^2	>.9999	.668
	M-WT 7184553±849702 vs F-WT 7962169±515652 μm^2	.9748	.626
	F-WT 7962169±515652 vs F-Tg 4736513±350922 μm^2	.039	.009
	M-Tg 7302182±679095 vs F-Tg 4736513±350922 μm^2	.0803	.007

Table 51: Placental area measurements for WT and Tg split by sex comparison results (\pm SEM) with *P* values for ANOVA and ANCOVA analysis. Significant *P* values in bold.

Appendix 6: Extended caption and result table for Figure 31.

Figure 31: Cell counts for WT and Tg junctional zone.

a) Tg junctional zones had 49% (GENOTYPE: $F_{1,28} = 63.52$, $P < .001$) fewer *Pr13b1* positive cells than WT. **b)** Tg junctional zone contained 53% (GENOTYPE: $F_{1,28} = 69.84$, $P < .001$) fewer total cells than WT. **c)** Spongiotrophoblast cell to glycogen cell (SpT/GlyT) ratios are increased in Tg by 51% (GENOTYPE: $F_{1,28} = 10.04$, $P = .004$). **d)** Tg placentas had a 68% (GENOTYPE: $F_{1,28} = 40.52$, $P < .001$) decrease in glycogen cell number. **e)** P-TG cell counts for WT and Tg E14.5 placentas. Tg placentas had 33% (GENOTYPE: $F_{1,28} = 6.87$, $P = .014$) fewer TG cells than WT. WT male ($n = 8$), and Tg male ($n = 9$), WT female ($n = 7$), Tg female ($n = 9$). Data from 12 litters, litter size between 6-10 (average 8 ± 0.20). Error bars represent \pm SEM. Statistical significance calculated using a two-way ANCOVA with litter size as a covariate using a Šidák correction. $^{NS}P > .05$, $*P < .05$, $**P < .01$, $***P < .001$, $****P < .0001$.

Metric	Comparison	ANOVA P value	ANCOVA P value
Junctional zone <i>Pr13b1</i> positive cells	WT 8287 \pm 292 vs Tg 4198 \pm 412	<.001	<.001
Junctional zone total cells	WT 10012 \pm 418 vs Tg 4753 \pm 465	<.001	<.001
SpT:GlyT ratio	WT 6.3 \pm .5 vs Tg 9.6 \pm .8	.003	.004
Glycogen cells	WT 1724 \pm 168 vs Tg 554 \pm 74	<.001	<.001
P-TG Cells	WT 172 \pm 18 vs Tg 115 \pm 14	.0163	.014

Table 52: Cell counts of the junctional zone for WT and Tg comparison

results (\pm SEM) with P values for ANOVA and ANCOVA analysis. Significant P values in bold.

Appendix 7: Extended caption and result table for Figure 32.

Figure 32: Cell counts for sex split WT and Tg junctional zone.

a) Tg junctional zones contained 40% (GENOTYPE: $F_{1,28} = 18.35$, $P < .001$) fewer *Pr13b1* positive cells than WT in males and 59% (GENOTYPE: $F_{1,28} = 45.76$, $P < .001$) fewer than WT in females. Female Tg junctional zones contained 33% (SEX: $F_{1,28} = 6.16$, $P = .019$) fewer *Pr13b1* positive cells than males Tg junctional zones. **b)** Tg junctional zones contained 44% (GENOTYPE: $F_{1,28} = 22.08$, $P < .001$) fewer cells in males than WT and 61% (GENOTYPE: $F_{1,28} = 46.94$, $P < .001$) fewer cells than WT in females. Female Tg junctional zones contain 33% (SEX: $F_{1,28} = 5.21$, $P = .03$) fewer total cells than M Tg junctional zones. **c)** Glycogen cells were reduced in number between in Tg compared to WT. Males had a

64% (GENOTYPE: $F_{1,28} = 17.42$, $P < .001$) decrease in glycogen cell number and females had a 72% decrease (GENOTYPE: $F_{1,28} = 21.48$, $P < .001$). **d)** Spongiotrophoblast cells to glycogen cell ratios (SpT/GlyT) are increased in Tg compared to WT. Male ratios are increased by 48% (GENOTYPE: $F_{1,28} = 4.50$, $P = .043$) and female ratio are increased by 54% (GENOTYPE: $F_{1,28} = 5.12$, $P = .032$). **e)** Male Tg placentas had 38% (GENOTYPE: $F_{1,28} = 4.20$, $P = .05$) fewer TG cells than WT. WT male ($n = 8$), and Tg male ($n = 9$), WT female ($n = 7$), Tg female ($n = 9$). Data from 12 litters, litter size between 6-10 (average 8 ± 0.20). Error bars represent \pm SEM. Statistical significance calculated using a two-way ANCOVA with litter size as a covariate using a Šidák correction. ^{NS} $P > .05$, * $P < .05$, ** $P < .01$, *** $P < .001$, **** $P < .0001$.

Metric	Comparison	ANOVA P value	ANCOVA P value
Junctional zone <i>Pr/3b1</i> positive cells	M-WT 8335 \pm 424 vs M-Tg 5023 \pm 705	.0002	<.001
	M-WT 8335 \pm 424 vs F-WT 8231 \pm 423	>.999	.938
	F-WT 8231 \pm 423 vs F-Tg 3373 \pm 237	<.0001	<.001
	M-Tg 5023 \pm 705 vs F-Tg 3373 \pm 237	.1097	.019
Junctional zone total cells	M-WT 10128 \pm 615 vs M-Tg 5677 \pm 787	<.0001	<.001
	M-WT 10128 \pm 615 vs F-WT 9878 \pm 604	.999	.834
	F-WT 9878 \pm 604 vs F-Tg 3830 \pm 296	<.0001	<.001
	M-Tg 5677 \pm 787 vs F-Tg 3830 \pm 296	.176	.03
Glycogen cells	M-WT 1793 \pm 278 vs M-Tg 653 \pm 127	.0004	<.001
	M-WT 1793 \pm 278 vs F-WT 1647 \pm 188	.9944	.615
	F-WT 1647 \pm 188 vs F-Tg 456 \pm 71	.0004	<.001
	M-Tg 653 \pm 127 vs F-Tg 456 \pm 71	.9592	.375
SpT:GlyT Ratio	M-WT 6.46 \pm .08 vs M-Tg 9.6 \pm 1.0	.00154	.043
	M-WT 6.46 \pm .08 vs F-WT 6.25 \pm .42	.999	.905
	F-WT 6.25 \pm .42 vs F-Tg 9.64 \pm 1.2	.00143	.032

	M-Tg 9.6±1.0 vs F-Tg 9.64±1.2	.999	.982
P-TGCs	M-WT 161±19 vs M-Tg 101±14	.3342	.05
	M-WT 161±19 vs F-WT 185±33	.9816	.545
	F-WT 185±33 vs F-Tg 130±24	.4734	.128
	M-Tg 101±14 vs F-Tg 130±24	.9284	.26

Table 53: Cell counts of the junctional zone for sex split WT and Tg comparison results (\pm SEM) with P values for ANOVA and ANCOVA analysis. Significant P values in bold.

Appendix 8: Extended caption and result table for Figure 33.

Figure 33: Labyrinth zone cell counts for WT and Tg placenta.

a) There was no difference in labyrinth *Prl3b1* positive cell number between WT and Tg (GENOTYPE*SEX: $F_{1,27} = 6.90$, $P = .014$). **b)** There was no difference in labyrinth total cell number between WT and Tgs (GENOTYPE*SEX: $F_{1,27} = 5.19$, $P = .031$). WT ($n = 15$), and Tg ($n = 18$). Data from 12 litters, litter size between 6-10 (average 8 ± 0.20). Error bars represent \pm SEM. Statistical significance calculated using a two-way ANCOVA with litter size as a covariate using a Šidák correction. ^{NS} $P > 0.05$, * $P < .05$, ** $P < .01$, *** $P < .001$, **** $P < .0001$.

Metric	Comparison	ANOVA P value	ANCOVA P value
Labyrinth <i>Prl3b1</i> positive cells	WT 7305±508 vs Tg 6458±610	.207	.184
Labyrinth total cells	WT 13741±1004 vs Tg 12815±892	.312	.245

Table 54: Cell counts of the labyrinth for WT and Tg comparison (\pm SEM) with P values for ANOVA and ANCOVA analysis. Significant P values in bold.

Appendix 9: Extended caption and result table for Figure 34.

Figure 34: Labyrinth cell counts for sex split WT and Tg placenta.

a) Female Tg labyrinths contained 38% (GENOTYPE: $F_{1,27} = 7.88$, $P = .009$) fewer *Prl3b1* positive cells than female WT. Female Tg labyrinths also contained 37% (SEX: $F_{1,27} = 6.99$, $P = .013$) fewer *Prl3b1* positive cells than male Tg labyrinths. **b)** Total labyrinth cell numbers were 42% (SEX: $F_{1,27} = 6.52$, $P = .017$) higher in female WT labyrinths compared to male WT labyrinths. Female Tg labyrinths contained 28% (GENOTYPE: $F_{1,27} = 5.96$, $P = .022$) fewer cells than WT females. WT male ($n = 8$), and Tg male ($n = 9$), WT female ($n = 7$), Tg female ($n = 9$). Data from 12 litters, litter size between 6-10 (average 8 ± 0.20). Error

bars represent \pm SEM. Statistical significance calculated using a two-way ANCOVA with litter size as a covariate using a Šidák correction. ^{NS} $P > .05$, $*P < .05$, $**P < .01$, $***P < .001$, $****P < .0001$.

Metric	Comparison	ANOVA P value	ANCOVA P value
Labyrinth <i>Pr13b1</i> positive cells	M-WT 6749 \pm 634 vs M-Tg 7947 \pm 815	.7984	.362
	M-WT 6749 \pm 634 vs F-WT 8044 \pm 788	.8181	.263
	F-WT 8044 \pm 788 vs F-Tg 4968 \pm 603	.0447	.009
	M-Tg 7947 \pm 815 vs F-Tg 4968 \pm 603	.025	.013
Labyrinth total cells	M-WT 11664 \pm 887 vs M-Tg 13669 \pm 1311	.4501	.431
	M-WT 11664 \pm 887 vs F-WT 16509 \pm 1403	.0453	.017
	F-WT 16509 \pm 1403 vs F-Tg 11960 \pm 1215	.1931	.022
	M-Tg 13669 \pm 1311 vs F-Tg 11960 \pm 1215	.9012	.531

Table 55: Cell counts of labyrinth for sex split WT and Tg comparison

results (\pm SEM) with P values for ANOVA and ANCOVA analysis. Significant P values in bold.

Appendix 10: Extended caption and result table for Figure 35.

Figure 35: Total placental cell counts for WT and Tg placenta.

a) Total *Pr13b1* positive cell numbers were reduced by 26% (GENOTYPE: $F_{1,18} = 7.59$, $P = .013$) compared to WT. **b)** Total cell counts were 22% (GENOTYPE: $F_{1,18} = 6.09$, $P = .024$) less than WT in Tg placentas. WT ($n = 16$), and Tg ($n = 18$). Data from 12 litters, litter size between 6-10 (average 8 ± 0.20). Error bars represent \pm SEM. Statistical significance calculated using a two-way ANCOVA with litter size as a covariate using a Šidák correction. ^{NS} $P > .05$, $*P < .05$, $**P < .01$, $***P < .001$, $****P < .0001$.

Metric	Comparison	ANOVA P value	ANCOVA P value
Total <i>Pr13b1</i> positive cells	WT 15544 \pm 560 vs Tg 11460 \pm 1228	.03	.013

Total cells	WT 27077±1190 vs Tg 21121±1715	.0382	.024
-------------	---	--------------	-------------

Table 56: Cell counts of whole placenta for WT and Tg comparison (\pm SEM) with P values for ANOVA and ANCOVA analysis. Significant P values in bold.

Appendix 11: Extended caption and result table for Figure 36.

Figure 36: Total cell counts for sex split WT and Tg placenta.

a) Total *Prl3b1* positive cells were 39% (GENOTYPE: $F_{1,18} = 8.32, P = .01$) reduced in Female Tg placentas compared to Female WT placentas. Female Tg placentas also had 31% (SEX: $F_{1,18} = 6.98, P = .017$) fewer *Prl3b1* positive cells than Male Tg placentas. **b)** Female Tg placentas had 30% (GENOTYPE: $F_{1,18} = 5.57, P = .03$) fewer total cells than female WT placentas. WT male ($n = 8$), and Tg male ($n = 9$), WT female ($n = 7$), Tg female ($n = 9$). Data from 12 litters, litter size between 6-10 (average 8 ± 0.20). Error bars represent \pm SEM. Statistical significance calculated using a two-way ANCOVA with litter size as a covariate using a Šidák correction. ^{NS} $P > .05$, * $P < .05$, ** $P < .01$, *** $P < .001$, **** $P < .0001$.

Metric	Comparison	ANOVA <i>P</i> value	ANCOVA <i>P</i> value
Total <i>Prl3b1</i> positive cells	M-WT 15666±787 vs M-Tg 13554±2017	.7968	.359
	M-WT 15666±787 vs F-WT 15332±825	>.999	.688
	F-WT 15332±825 vs F-Tg 9366±903	.0437	.01
	M-Tg 13554±2017 vs F-Tg 9366±903	.1649	.017
Total cells	M-WT 27036±1661 vs M-Tg 23241±2823	>.999	.287
	M-WT 27036±1661 vs F-WT 27150±1819	>.999	.888
	F-WT 27150±1819 vs F-Tg 19002±1782	.1344	.03
	M-Tg 23241±2823 vs F-Tg 19002±1782	.9866	.116

Table 57: Cell counts of whole placenta for sex split WT and Tg comparison results (\pm SEM) with P values for ANOVA and ANCOVA analysis. Significant P values in bold.

Appendix 12: Extended caption and result table for Figure 38.

Figure 38: qRT-PCR analysis of Prl family members for WT and Tg.

a) qRT-PCR for WT and Tg placenta at E14.5. *Prl8a8* expression was not significantly different between WT and Tg. **b)** Expression of *Psg17* was not significantly different between WT and Tg. **c)** Expression of *Prl3b1* was not significantly different between WT and Tg. **d)** Expression of *Prl7b1* was reduced by 78% (GENOTYPE: $F_{1,11} = 9.71$, $P = .01$) in Tg compared to WT. **e)** Expression of *Prl2c* was not significantly different between WT and Tg. **f)** Expression of *Pcdh12* was not significantly different between WT and Tg. Data from 4 litters, litter size between 7-10 (average 8 ± 0.33). WT ($n = 8$), Tg ($n = 8$). Error bars represent \pm SEM. Statistical significance calculated using a two-way ANCOVA with litter size as a covariate using a Šidák correction. ^{NS} $P > .05$, * $P < .05$, ** $P < .01$, *** $P < .001$, **** $P < .0001$.

Gene	WT	Tg	P value
<i>Prl8a8</i>	1 \pm .28	.47 \pm .17	.076
<i>Psg17</i>	1 \pm .22	.63 \pm .12	.066
<i>Prl3b1</i>	1 \pm .20	.65 \pm .18	.131
<i>Prl7b1</i>	1 \pm .26	.22 \pm .05	.01
<i>Prl2c</i>	1 \pm .25	.80 \pm .39	.274
<i>Pcdh12</i>	1 \pm .14	.99 \pm .35	.188

Table 58: Prl family qRT-PCR values for WT and Tg

(\pm SEM) with P values for ANCOVA analysis. Significant P values in bold.

Appendix 13: Extended caption and result tables for Figure 39.

Figure 39: qRT-PCR analysis of Prl family members for WT and Tg split by sex.

a) *Prl8a8* expression was reduced by 84% in Tg females compared to WT females (GENOTYPE: $F_{1,11} = 6.60$, $P = .026$). Female Tg *Prl8a8* expression was also reduced by 61% compared to Male Tgs (SEX: $F_{1,11} = 6.21$, $P = .03$). **b)** Expression of *Psg17* was reduced by 68% in Tg females compared to WT females (GENOTYPE: $F_{1,11} = 7.93$, $P = .017$). Females Tgs *Psg17* expression was also reduced by 62% compared to Male Tgs (SEX: $F_{1,11} = 7.49$, $P = .019$). **c)** Expression of *Prl3b1* was reduced by 71% in Tg females compared to WT females (GENOTYPE: $F_{1,11} = 5.59$, $P = .037$). Females Tgs *Prl3b1* expression was also reduced by 72% compared to Male Tgs (SEX: $F_{1,11} = 6.42$, $P = .028$). **d)** Expression of *Prl7b1* was reduced by 88% in Tg females compared to WT females (GENOTYPE: $F_{1,11} = 9.79$, $P = .01$). Male *Prl7b1* expression was reduced by 68% however this was not significant. There was no significant difference seen between female and male Tgs for *Prl7b1* expression. **e)** There was no significant difference seen in expression between groups for *Prl2c*. **f)** There was no significant difference seen in expression between groups for *Pcdh12*. Data from 4 litters, litter size between 7-10 (average 8 ± 0.33). Male WT ($n =$

4), Male Tg ($n = 4$), Female WT ($n = 4$) and Female Tg ($n = 4$). Error bars represent \pm SEM. Statistical significance calculated using a two-way ANCOVA with litter size as a covariate using a Šidák correction. ^{NS} $P > .05$, $*P < .05$, $**P < .01$, $***P < .001$, $****P < .0001$.

Gene	M-WT	M-Tg	F-WT	F-Tg
<i>Prl8a8</i>	1 \pm .42	.77 \pm .26	1 \pm .44	.17 \pm .03
<i>Psg17</i>	1 \pm .19	.95 \pm .08	1 \pm .44	.33 \pm .03
<i>Prl3b1</i>	1 \pm .25	1.01 \pm .2	1 \pm .36	.30 \pm .05
<i>Prl7b1</i>	1 \pm .37	.32 \pm .07	1 \pm .44	.13 \pm .04
<i>Prl2c</i>	1 \pm .24	1.39 \pm .6	1 \pm .49	.21 \pm .05
<i>Pcdh12</i>	1 \pm .16	1.38 \pm .6	1 \pm .26	.60 \pm .06

Table 59: Prl family qRT-PCR values for sex split WT and Tg (\pm SEM).

Gene	M-WT vs M-Tg	M-WT vs F WT	F-WT vs F Tg	M-Tg vs F-Tg
<i>Prl8a8</i>	.866	.97	.026	.03
<i>Psg17</i>	.971	.919	.017	.019
<i>Prl3b1</i>	.937	.974	.037	.028
<i>Prl7b1</i>	.235	.969	.01	.084
<i>Prl2c</i>	.854	.962	.101	.063
<i>Pcdh12</i>	.898	.874	.06	.059

Table 60: Prl family comparison P values for qRT-PCR.

ANCOVA with litter size as a covariate. Significant P values in bold.

Appendix 14: Extended caption and result table for Figure 40.

Figure 40: qRT-PCR analysis of labyrinth related genes WT and Tg.

a) *Syna* expression was not significantly different between WT and Tg. **b)** Expression of *Synb* was not significantly different between WT and Tg. **c)** Expression of *Gcm1* was not significantly different between WT and Tg. **d)** Expression of *Dlx3* was significantly increased by 53 % in Tgs compared to WT (GENOTYPE: $F_{1:11} = 5.42$, $P = .04$). **e)** Expression of *Ctsq* was not significantly different between WT and Tg. **f)** Expression of *Flk1* was not significantly different between WT and Tg. Data from 4 litters, litter size between 7-10 (average 8 ± 0.33). WT ($n = 8$), Tg ($n = 8$). Error bars represent \pm SEM. Statistical significance calculated using a two-way ANCOVA with litter size as a covariate using a Šidák correction. ^{NS} $P > .05$, $*P < .05$, $**P < .01$, $***P < .001$, $****P < .0001$.

Gene	WT	Tg	P value
<i>Syna</i>	1±.15	1.36±.26	.975
<i>Synb</i>	1±.16	.95±.15	.636
<i>Gcm1</i>	1±.17	1.58 ±.20	.689
<i>Dlx3</i>	1±.16	1.53±.08	.04
<i>Ctsq</i>	1±.18	.88±.17	.136
<i>Flk1</i>	1±.17	1.09±.22	.635

Table 61: Labyrinth related qRT-PCR values for WT and Tg (±SEM) with *P* values for ANCOVA analysis. Significant *P* values in bold.

Appendix 15: Extended caption and result tables for Figure 41.

Figure 41: qRT-PCR analysis of labyrinth related genes for WT and Tg split by sex.

a) *Syna* expression showed no significant difference between groups. **b)** Expression of *Synb* showed no significant difference between groups. **c)** Expression of *Gcm1* is reduced by 70% in Female Tgs compared to male Tgs (GENOTYPE: $F_{1:11} = 5.40$, $P = .04$). **d)** Expression of *Dlx3* showed no significant difference between groups. **e)** Expression of *Ctsq* was reduced by 42% female Tgs compared to female WTs (GENOTYPE*SEX: $F_{1:11} = 4.80$, $P = .051$), (GENOTYPE: $F_{1:11} = 7.06$, $P = .022$). Female Tgs also have a 61% reduction in expression of *Ctsq* compared to Male Tgs (SEX: $F_{1:11} = 9.52$, $P = .01$). **f)** There was no significant difference seen in expression between groups for *Flk1*. Data from 4 litters, litter size between 7-10 (average 8 ± 0.33). Male WT ($n = 4$), Male Tg ($n = 4$), Female WT ($n = 4$) and Female Tg ($n = 4$). Error bars represent ±SEM. Statistical significance calculated using a two-way ANCOVA with litter size as a covariate using a Šidák correction. NS $P > .05$, * $P < .05$, ** $P < .01$, *** $P < .001$, **** $P < .0001$.

Gene	M-WT	M-Tg	F-WT	F-Tg
<i>Syna</i>	1±.23	.86±.07	1±.22	1.88±.36
<i>Synb</i>	1±.32	.96±.29	1±.13	.94±.14
<i>Gcm1</i>	1±.25	1.92±.25	1±.25	1.23±.21
<i>Dlx3</i>	1±.16	1.39±.05	1±.30	1.68±.12
<i>Ctsq</i>	1±.35	1.19±.18	1±.17	.59±.19
<i>Flk1</i>	1±.33	.95±.18	1±.16	1.24±.23

Table 62: Labyrinth related qRT-PCR values for sex split WT and Tg (±SEM).

Gene	M-WT vs M-Tg	M-WT vs F WT	F-WT vs F Tg	M-Tg vs F-Tg
<i>Syna</i>	.686	.978	.661	.384
<i>Synb</i>	.999	.871	.509	.404

<i>Gcm1</i>	.171	.984	.409	.04
<i>Dlx3</i>	.202	.893	.08	.642
<i>Ctsq</i>	.684	.963	.022	.01
<i>Flk1</i>	.932	.881	.459	.489

Table 63: Labyrinth related qRT-PCR comparison *P* values for qRT-PCR.

ANCOVA with litter size as a covariate. Significant *P* values in bold.

Appendix 16: Chapter 4: Methods

1.2 Chapter 4: Methods

1.2.1 Generation of tissues

Tissue was generated by crossing *Phlda2*^(+/-) females with *Peg3*^(-/+) males, resulted in wild-type *Phlda2*^{(+/+);Peg3}^(+/+) (WT), *Peg3*^{(-/+);Phlda2}^(+/+)(*Peg3*^{KO}), *Phlda2*^{(+/-);Peg3}^(+/+)(*Phlda2*^{KO}) and *Phlda2*^{(+/-);Peg3}^(-/+) (DKO) offspring. At E16.5 placenta was dissected as described in Chapter 2. Genotyping and sextyping was performed on the yolk sac of each foeto-placental unit as described in Chapter 2. Litters were excluded where litter size was under six or had an uneven distribution of genotypes or sex. 16 viable litters were collected for analysis. The placenta and foetus were weighed as described in protocol 2.2.4 before each foetus was killed by decapitation as stipulated in the project licence. The placenta was then bisected along the midline with half of the placenta was fixed in 4% PFA and embedded in paraffin wax, and half was frozen on dry ice and stored at -80 °C.

1.2.2 Weight data

Due to the number of genotypes, each litter had its average foetal weight calculated. The average foetal weight of each litter was divided by the average foetal weight of the whole population giving the normalisation factor for each litter. Foetal and placental weights were then multiplied by their normalisation factor. Foetal placental ratios were also generated by dividing the embryo weight by the placental weight.

	WT	<i>Peg3</i>^{KO}	<i>Phlda2</i>^{KO}	DKO
Male	13	17	16	11
Female	18	16	10	12

Table 64: Group sizes for morphological analyses.

1.2.3 RNAscope and cell counting

Paraffin-embedded WT E7.5 and E9.5 samples were stained in multiplex using probes listed in Table 12. These were imaged using slide scanner and confocal microscopes as described in section 2.4. Images are presented in a panel.

Paraffin-embedded E9.5 samples of each of the genotypes were stained by the in-house service at Cardiff University (Cardiff University Bioimaging Hub Core Facility, RRID:SCR_022556) with an H & E stain. P-TG cells were counted using protocol 2.5.

Paraffin-embedded E16.5 midplane sections were stained for *Prl3b1* using the RNAscope protocol described in 2.3.3. These were imaged as described in section 2.4. Area measurements of the junctional zone, labyrinth and placenta were performed using Zen Blue software. Placental cells were counted using the automatic counting protocol described in section 2.6.

	WT	<i>Peg3</i> ^{KO}	<i>Phlda2</i> ^{KO}	DKO
Male	6	7	6	6
Female	9	6	6	9

Table 65: Group sizes for *Prl3b1* counted placenta.

1.2.4 Statistics

Sample size was calculated using Equation 4 and data from (Janssen, Tunster, et al., 2016) and (Creeth et al., 2018). The effect of genotype and sex were analysed using ANCOVA with a Šidák correction and using litter size as a covariate.

Appendix 17: Extended caption for Figure 50.

Figure 50: E9.5 P-TG cell counts for WT, *Peg3*^{KO}, *Phlda2*^{KO} and DKO.

a) P-TG cell numbers were decreased by 18% ($P=.039$) in *Peg3*^{KO} samples compared to WT and increased in DKO by 21% ($P=.007$) compared to WT (GENOTYPE: $F_{1:3} = 10.87$, $P<.001$) (LITTERSIZE: $F_{1:1} = 7.54$, $P=.008$). WT ($n = 30$), *Peg3*^{KO} ($n = 26$), *Phlda2*^{KO} ($n = 23$) and DKO ($n = 15$). Data from 19 litters, litter size between 5-11 (average $9 \pm .14$). Error bars represent \pm SEM. Statistical significance calculated using a two-

way ANCOVA with Šidák correction and litter size as covariate. ^{NS} $P > .05$, $*P < .05$, and $**P < .01$ $***P < .001$ $****P < .0001$.

Appendix 18: Extended caption and results tables for Figure 51.

Figure 51: Foetal and placental weight data for WT, *Peg3*^{KO}, *Phlda2*^{KO} and DKO at E16.5.

a) *Peg3*^{KO} and DKO foetal weight was reduced by 14% ($P < .001$) and 12% ($P < .001$) respectively compared to WT (GENOTYPE: $F_{1:3} = 16.61$, $P < .001$). **b)** *Peg3*^{KO} placental weight was reduced by 22% compared to WT ($P < .001$). *Phlda2*^{KO} was increased by 32% compared to WT ($P < .001$) (GENOTYPE: $F_{1:3} = 26.01$, $P < .001$). **c)** *Phlda2*^{KO} ratio was reduced by 24% compared to WT ($P = .006$) (GENOTYPE: $F_{1:3} = 9.29$, $P < .001$). **d)** *Peg3*^{KO} foetuses were 16% ($P < .001$) and 12% ($P < .001$) lighter than WT foetuses in male and females. DKO foetuses were 12% lighter than WT in both males ($P = .008$) and females ($P = .003$) (GENOTYPE*SEX: $F_{1:3} = .265$, $P = .851$) (GENOTYPE: $F_{1:3} = 16.6$, $P < .001$) (SEX: $F_{1:3} = 2.9$, $P = .091$). **e)** Male *Peg3*^{KO} placenta weighed 26% less than male WT placenta ($P < .001$). Male *Phlda2*^{KO} placenta weighed 38% more than male WT placenta ($P < .001$). WT female placentas were 11% lighter than WT male placentas (SEX: $F_{1:1} = 4.6$ $P = .034$). *Phlda2*^{KO} female placentas are 24% lighter than *Phlda2*^{KO} males (SEX: $F_{1:1} = 18.6$, $P < .001$) (GENOTYPE*SEX: $F_{1:3} = 4.12$, $P = .008$) (GENOTYPE: $F_{1:3} = 26.01$, $P < .001$) (SEX: $F_{1:1} = 12.04$, $P < .001$). **f)** The *Phlda2*^{KO} ratio decreased by 25% ($P = .028$) for males compared to WT. (GENOTYPE*SEX: $F_{1:3} = 1.03$, $P = .384$) (GENOTYPE: $F_{1:3} = 9.29$, $P < .001$) (SEX: $F_{1:1} = 2.46$, $P = .120$). Error bars represent standard error of the mean (SEM). WT ($n = 30$), *Peg3*^{KO} ($n = 33$), *Phlda2*^{KO} ($n = 27$), DKO ($n = 23$). WT male ($n = 13$), *Peg3*^{KO} male ($n = 17$), *Phlda2*^{KO} male ($n = 16$), DKO male ($n = 11$), WT female ($n = 18$), *Peg3*^{KO} female ($n = 16$), *Phlda2*^{KO} ($n = 10$), DKO ($n = 12$). Data from 16 litters, litter size between 5-10 (Average $7 \pm .13$). Error bars represent \pm SEM. Statistical significance calculated using a two-way ANCOVA with Šidák correction and litter size as covariate. ^{NS} $P > .05$, $*P < .05$, and $**P < .01$ $***P < .001$ $****P < .0001$.

Metric	Group	WT	<i>Peg3</i> ^{KO}	<i>Phlda2</i> ^{KO}	DKO
Foetal weight	Total	507±6.7 mg	437±7.9 mg	489±10.2 mg	446±8.3 mg
	Male	519±9.1 mg	437±8.2 mg	494±11.4 mg	455±10.1 mg
	Female	497±9.0 mg	438±14.0 mg	481±19.9 mg	437±13.0 mg
Placental weight	Total	73.9±3.3 mg	57.6±2.2 mg	97.9±4.7 mg	70.5±2.5 mg

	Male	78.5±6.1 mg	58.3±3.1 mg	108.0±5.9 mg	72.8±3.1 mg
	Female	70.1±3.2 mg	56.9±3.2 mg	81.7±4.3 mg	68.3±4.0 mg
Foetal to placental weight ratio	Total	7.0±.3	8.0±.3	5.3±.3	6.5±.2
	Male	6.5±.5	7.9±.5	4.8±.3	6.3±.2
	Female	7.4±.4	8.0±.5	6.1±.5	6.6±.4

Table 66: Group averages and SEMs for placental and foetal weight.

Metric	Group	WT vs <i>Peg3</i> ^{KO}	WT vs <i>Phlda2</i> ^{KO}	WT vs DKO
Foetal weight	Total	P<.001	<i>P</i> =.546	P<.001
	Male	P<.001	<i>P</i> =.725	P=.008
	Female	P<.001	<i>P</i> =.938	P=.003
Placental Weight	Total	P<.001	P<.001	<i>P</i> =.556
	Male	P<.001	P<.001	<i>P</i> =.426
	Female	<i>P</i> =.182	<i>P</i> =.327	<i>P</i> =.999
Foetal to placental weight ratio	Total	<i>P</i> =.356	P=.006	<i>P</i> =.932
	Male	<i>P</i> =.321	P=.028	<i>P</i> =1.000
	Female	<i>P</i> =.991	<i>P</i> =.299	<i>P</i> =.794

Table 67: Genotype *P* values for placental and foetal weight.
Significant *P* values in bold.

Metric	WT Male vs WT Female	<i>Peg3</i> ^{KO} Male vs <i>Peg3</i> ^{KO} Female	<i>Phlda2</i> ^{KO} Male vs <i>Phlda2</i> ^{KO} Female	DKO Male vs DKO Female
Foetal weight	<i>P</i> =.200	<i>P</i> =.852	<i>P</i> =.389	<i>P</i> =.307
Placental Weight	P=.034	<i>P</i> =.880	P<.001	<i>P</i> =.586
Foetal to placental weight ratio	<i>P</i> =.232	<i>P</i> =.825	<i>P</i> =.053	<i>P</i> =.873

Table 68: Sex *P* values for placental and foetal weight data.
Significant *P* values in bold.

Appendix 19: Extended caption and results tables for Figure 52.

Figure 52: Area of placental subsections for WT, *Peg3*^{KO}, *Phlda2*^{KO} and DKO.

a) Junctional zone area was increased by 73% in *Phlda2*^{KO} samples compare to WT ($P < .001$) (GENOTYPE: $F_{1:3} = 25.39$, $P < .001$). **b)** Labyrinth area was decreased by 35% in DKO samples compared to WT (GENOTYPE: $F_{1:3} = 6.01$, $P = .002$). **c)** There was no significant difference seen between any groups in decidua area (GENOTYPE: $F_{1:3} = 1.18$, $P = .332$). **d)** There was no significant difference seen between any groups in total area (GENOTYPE: $F_{1:3} = 6.54$, $P = .001$). **e)** *Peg3*^{KO} junctional zones were 46% ($P = .002$) smaller than WT in males and 10% ($P = .947$) larger than WT in females. *Phlda2*^{KO} junctional zones were 44% ($P = .002$) and 129% ($P < .001$) larger than WT in males and females respectively. Female WT junctional zones were 40% smaller than male WT junctional zones ($P < .001$). Female *Phlda2*^{KO} junctional zones were 4% smaller than male *Phlda2*^{KO} junctional zones ($P = .015$) (GENOTYPE*SEX: $F_{1:3} = 4.24$, $P = .010$). (GENOTYPE: $F_{1:3} = 25.39$, $P < .001$) (SEX: $F_{1:1} = 11.69$, $P = .001$). **f)** *Peg3*^{KO} labyrinth area was 33% ($P = .031$) smaller in males than WT. DKO labyrinth measured 44% ($P = .004$) smaller than WT in males. Female WT labyrinth area was 26% smaller than male WT labyrinth area ($P = .015$) and female *Phlda2*^{KO} labyrinth area were 16% smaller than *Phlda2*^{KO} males ($P = .028$). (GENOTYPE*SEX: $F_{1:3} = 3.06$, $P = .037$). (GENOTYPE: $F_{1:3} = 6.01$, $P = .002$) (SEX: $F_{1:1} = 3.35$, $P = .074$). **g)** There was no significant difference seen between any groups in decidua area (GENOTYPE*SEX: $F_{1:3} = 1.46$, $P = .242$). (GENOTYPE: $F_{1:3} = 1.18$, $P = .332$) (SEX: $F_{1:1} = 2.10$, $P = .156$). **h)** There was no significant difference seen between any groups in total area (GENOTYPE*SEX: $F_{1:3} = 1.37$, $P = .268$) (GENOTYPE: $F_{1:3} = 6.54$, $P = .001$) (SEX: $F_{1:1} = 0.886$, $P = .353$). WT ($n = 17$), *Peg3*^{KO} ($n = 15$), *Phlda2*^{KO} ($n = 16$) and DKO ($n = 17$). WT male ($n = 9$), *Peg3*^{KO} male ($n = 7$), *Phlda2*^{KO} male ($n = 8$), DKO male ($n = 8$), WT female ($n = 8$), *Peg3*^{KO} female ($n = 8$), *Phlda2*^{KO} female ($n = 8$), DKO ($n = 9$). Data from 16 litters, litter size between 5-10 (average $8 \pm .18$). Error bars represent standard error of the mean (SEM). Statistical significance calculated using a two-way ANCOVA with Šidák correction and litter size as covariate. ^{NS} $P > .05$, * $P < .05$, and ** $P < .01$ *** $P < .001$ **** $P < .0001$.

Metric	Group	WT	<i>Peg3</i> ^{KO}	<i>Phlda2</i> ^{KO}	DKO
Junctional zone area	Total	966667 ±98003	718660 ±42738	1676427 ±116997	998392 ±100475
	Male	1187476 ±135063	636173 ±67634	1710742 ±212841	1174760 ±153471
	Female	718256 ±80901	790834 ±42708	1642111 ±114131	841619 ±115280
Labyrinth area	Total	3184295 ±279064	2616786 ±185627	3318949 ±380814	2079722 ±207010
	Male	3626307 ±280676	2430661 ±261616	3338530 ±609044	2046930 ±265147
	Female	2670519	2764568	2807799	2159277

		±363997	±198010	±285450	±266238
Decidua area	Total	1252833 ±110246	1369329 ±93447	1541271 ±116229	1198435 ±87847
	Male	1311063 ±124693	1282478 ±107306	1590645 ±125845	1217487 ±126750
	Female	1184887 ±137909	1361098 ±137373	1310116 ±110328	1137057 ±103613
Total Area	Total	4307542 ±390492	3953581 ±288979	5952580 ±360335	3891321 ±321710
	Male	4997225 ±296854	3533138 ±429912	5423563 ±694388	4260249 ±295768
	Female	4044781 ±511776	4230681 ±268600	5667901 ±393995	3704210 ±427291

Table 69: Group averages and SEMs for placental region area measurements (μm^2).

Metric	Group	WT vs <i>Peg3</i> ^{KO}	WT vs <i>Phlda2</i> ^{KO}	WT vs DKO
Junctional zone area	Total	<i>P</i> =.173	<i>P</i><.001	<i>P</i> =1.000
	Male	<i>P</i>=.002	<i>P</i>=.002	<i>P</i> =.949
	Female	<i>P</i> =.947	<i>P</i><.001	<i>P</i> =.907
Labyrinth area	Total	<i>P</i> =.296	<i>P</i> =1.000	<i>P</i>=.005
	Male	<i>P</i>=.031	<i>P</i> =1.000	<i>P</i>=.004
	Female	<i>P</i> =1.000	<i>P</i> =1.000	<i>P</i> =.797
Decidua area	Total	<i>P</i> =.998	<i>P</i> =.786	<i>P</i> =.996
	Male	<i>P</i> =.987	<i>P</i> =.877	<i>P</i> =.999
	Female	<i>P</i> =.987	<i>P</i> =.557	<i>P</i> =1.000
Total Area	Total	<i>P</i> =.850	<i>P</i> =.074	<i>P</i> =.889
	Male	<i>P</i> =.363	<i>P</i> =.607	<i>P</i> =.942
	Female	<i>P</i> =.993	<i>P</i> =.164	<i>P</i> =.996

Table 70: Genotype comparison *P* values for placental region area measurements. Significant *P* values in bold.

Metric	WT Male vs WT Female	<i>Peg3</i> ^{KO} Male vs <i>Peg3</i> ^{KO} Female	<i>Phlda2</i> ^{KO} Male vs <i>Phlda2</i> ^{KO} Female	DKO Male vs DKO Female
Junctional zone area	<i>P</i><.001	<i>P</i> =.239	<i>P</i>=.015	<i>P</i> =.066
Labyrinth area	<i>P</i>=.015	<i>P</i> =.421	<i>P</i>=.028	<i>P</i> =.710
Decidua area	<i>P</i> =.284	<i>P</i> =.324	<i>P</i> =.102	<i>P</i> =.384
Total area	<i>P</i> =.196	<i>P</i> =.217	<i>P</i> =.410	<i>P</i> =.444

Table 71: Sex comparison *P* values for placental region area measurements. Significant *P* values in bold.

Appendix 20: Extended caption and results tables for Figure 53.

Figure 53: Region ratios for WT, *Peg3*^{KO}, *Phlda2*^{KO} and DKO placentas.

a) The ratio between junctional zone area and labyrinth area (Lz:Jz) increased in *Phlda2*^{KO} and DKO samples by 89% ($P=.017$) and 68% ($P<.001$) respectively (GENOTYPE: $F_{1:3} = 7.74$, $P<.001$). **b)** The Lz:Jz ratio decreased in *Peg3*^{KO} male samples by 19% ($P=.011$) and increased in DKO male samples by 14% ($P<.001$). *Peg3*^{KO} female samples had an 11% ($P<.001$) increased Lz:Jz ratio compared to *Peg3*^{KO} male samples. DKO females had a 37% ($P=.018$) decrease in their ratio compared to DKO male samples (GENOTYPE*SEX: $F_{1:3} = 4.40$, $P=.008$) (GENOTYPE: $F_{1:3} = 7.74$, $P<.001$) (SEX: $F_{1:1} = 5.71$, $P=.021$). WT ($n = 17$), *Peg3*^{KO} ($n = 15$), *Phlda2*^{KO} ($n = 16$) and DKO ($n = 17$). WT male ($n = 9$), *Peg3*^{KO} male ($n = 7$), *Phlda2*^{KO} male ($n = 8$), DKO male ($n = 8$), WT female ($n = 8$), *Peg3*^{KO} female ($n = 8$), *Phlda2*^{KO} female ($n = 8$), DKO ($n = 9$). Data from 16 litters, litter size between 5-10 (average $8 \pm .18$). Error bars represent standard error of the mean (SEM). Statistical significance calculated using a two-way ANCOVA with Šidák correction and litter size as covariate. ^{NS} $P>.05$, * $P<.05$, and ** $P<.01$ *** $P<.001$ **** $P<.0001$.

Metric	Group	WT	<i>Peg3</i> ^{KO}	<i>Phlda2</i> ^{KO}	DKO
Lz:Jz area ratio	Total	.31±.02	.28±.01	.58±.03	.52±.06
	Male	.33±.02	.26±.02	.57±.05	.64±.10
	Female	.29 ±.03	.29±.02	.60±.03	.41±.04

Table 72: Group averages and SEMs for placental region area measurements (μm^2).

Metric	Group	WT vs <i>Peg3</i> ^{KO}	WT vs <i>Phlda2</i> ^{KO}	WT vs DKO
Lz:Jz area ratio	Total	$P=.288$	$P=.017$	$P<.001$
	Male	$P=.011$	$P=.261$	$P<.001$
	Female	$P=.985$	$P=.105$	$P=.256$

Table 73: Genotype comparison *P* values for placental region area measurements.

Significant *P* values in bold.

Metric	WT Male vs WT Female	<i>Peg3</i> ^{KO} Male vs <i>Peg3</i> ^{KO} Female	<i>Phlda2</i> ^{KO} Male vs <i>Phlda2</i> ^{KO} Female	DKO Male vs DKO Female
Lz:Jz area ratio	$P=.639$	$P<.001$	$P=.507$	$P=.018$

Table 74: Sex comparison *P* values for placental region area measurements.

Significant *P* values in bold.

Appendix 21: Extended caption and results tables for Figure 54.

Figure 54: Junctional zone cell counting parameters for WT, *Peg3*^{KO}, *Phlda2*^{KO} and DKO.

a) *Phlda2*^{KO} junctional zones contained 73% (*P*<.001) more *Prl3b1* positive cells than WT (GENOTYPE: $F_{1:3} = 21.62$, *P*<.001). **b)** Total cells in the junctional zone were increased in the *Phlda2*^{KO} group by 78% (*P*<.001) compared to WT (GENOTYPE: $F_{1:3} = 24.84$, *P*<.001). **c)** Glycogen cells were increased by 103% (*P*=.004) in *Phlda2*^{KO} placentas compared to WT (GENOTYPE: $F_{1:3} = 9.89$, *P*<.001). **d)** There was no significant difference seen between any groups in numbers of P-TG cells (GENOTYPE: $F_{1:3} = 3.92$, *P*=.013). **e)** There was no significant difference between any groups in the ratio between glycogen and spongiotrophoblast cells (SpT/GlyT) (GENOTYPE: $F_{1:3} = 4.41$, *P*=.007). **f)** *Peg3*^{KO} junctional zones contained 37% (*P*=.011) fewer positive cells than WT in males. *Phlda2*^{KO} junctional zones contained 48% (*P*=.004) and 115% (*P*<.001) more *Prl3b1* positive cells than WT in males and females respectively. WT female junctional zones had 38% (*P*=.020) fewer *Prl3b1* positive cells than WT males. DKO females had 31% (*P*=.015) fewer *Prl3b1* positive cells than DKO males. (GENOTYPE*SEX: $F_{1:3} = 2.59$, *P*=.078) (GENOTYPE: $F_{1:3} = 21.62$, *P*<.001) (SEX: $F_{1:1} = 4.76$, *P*=.033). **g)** *Peg3*^{KO} junctional zones contained 41% (*P*=.038) fewer total cells than WT males. *Phlda2*^{KO} junctional zones contained 49% (*P*=.004) and 130% (*P*<.001) more total cells than WT in males and females respectively. Female WT junctional zones had 38% (*P*=.009) fewer total cells than male WTs. DKO females had 31% (*P*=.006) fewer total cells than DKO males. (GENOTYPE*SEX: $F_{1:3} = 2.51$, *P*=.068) (GENOTYPE: $F_{1:3} = 24.36$, *P*<.001) (SEX: $F_{1:1} = 7.50$, *P*=.008). **h)** *Phlda2*^{KO} females had a 236% (*P*=.011) increase in glycogen cells compared to WT females. (GENOTYPE*SEX: $F_{1:3} = .723$, *P*=.543) (GENOTYPE: $F_{1:3} = 9.89$, *P*<.001) (SEX: $F_{1:1} = 5.67$, *P*=.021). **i)** There were no significant differences seen between any groups in number of P-TG cells. (GENOTYPE*SEX: $F_{1:3} = 1.11$, *P*=.354) (GENOTYPE: $F_{1:3} = 3.92$, *P*=.013) (SEX: $F_{1:1} = 1.17$, *P*=.284). **j)** There was no significant difference between any groups in the ratio between glycogen and spongiotrophoblast cells (GENOTYPE*SEX: $F_{1:3} = .617$, *P*=.607) (GENOTYPE: $F_{1:3} = 4.41$, *P*=.007) (SEX: $F_{1:1} = 5.04$, *P*=.029). WT (*n* = 17), *Peg3*^{KO} (*n* = 15), *Phlda2*^{KO} (*n* = 16) and DKO (*n* = 17). WT male (*n* = 9), *Peg3*^{KO} male (*n* = 7), *Phlda2*^{KO} male (*n* = 8), DKO male (*n* = 8), WT female (*n* = 8), *Peg3*^{KO} female (*n* = 8), *Phlda2*^{KO} female (*n* = 8), DKO (*n* = 9). Data from 16 litters, litter size between 5-10 (average 8±.18). Error bars represent standard error of the mean (SEM). Statistical significance calculated using a two-way ANCOVA with Šidák

correction and litter size as covariate. ^{ns} $P > .05$, $*P < .05$, and $**P < .01$
 $***P < .001$ $****P < .0001$.

Metric	Group	WT	<i>Peg3</i> ^{KO}	<i>Phlda2</i> ^{KO}	DKO
Junctional zone <i>Prl3b1</i> positive cells	Total	3244±247	2684±157	5604±323	3832±349
	Male	3835±327	2432±241	5671±631	4582±521
	Female	2580±200	2903±186	5535±217	3164±362
Total junctional zone cells	Total	3915±337	2959±174	6966±414	4466±440
	Male	4755±450	2797±284	7091±800	5498±662
	Female	2968±222	3099±218	6841±303	3548±411
Glycogen cells	Total	670±135	275±46	1363±188	634±162
	Male	920±224	364±74	1419±356	915±315
	Female	388±61	196±47	1306±156	384±79
P-TG Cells	Total	32.5±3.5	32.5±5.0	44.0±7.1	21.3±2.4
	Male	34.6±4.8	23.9±9.0	38.0±11.6	23.3±4.7
	Female	30.0±5.2	40.1±3.6	49.9±8.3	19.6±1.7
SpT/GlyT ratio	Total	.16±.02	.09±.01	.19±.02	.13±.02
	Male	.18±.03	.13±.02	.19±.03	.15±.04
	Female	.13 ±.02	.06±.01	.19±.02	.10±.02

Table 75: Group averages and SEMs for junctional zone cell counts.

Metric	Group	WT vs <i>Peg3</i> ^{KO}	WT vs <i>Phlda2</i> ^{KO}	WT vs DKO
Junctional zone <i>Prl3b1</i> positive cells	Total	$P = .691$	$P < .001$	$P = .461$
	Male	$P = .011$	$P = .004$	$P = .763$
	Female	$P = .991$	$P < .001$	$P = .844$
Total junctional zone cells	Total	$P = .335$	$P < .001$	$P = .704$
	Male	$P = .038$	$P = .004$	$P = .892$
	Female	$P = 1.000$	$P < .001$	$P = .944$
Glycogen cells	Total	$P = .338$	$P = .004$	$P = 1.000$
	Male	$P = .281$	$P = .384$	$P = 1.000$
	Female	$P = .986$	$P = .011$	$P = 1.000$
P-TG Cells	Total	$P = 1.000$	$P = .469$	$P = .407$
	Male	$P = .873$	$P = 1.000$	$P = .705$
	Female	$P = .870$	$P = .273$	$P = .830$
SpT/GlyT ratio	Total	$P = .137$	$P = .747$	$P = .928$
	Male	$P = .621$	$P = 1.000$	$P = .989$
	Female	$P = .372$	$P = .519$	$P = .984$

Table 76: Genotype *P* values for junctional zone cell counts.
Significant *P* values in bold.

Metric	WT Male	<i>Peg3</i> ^{KO} Male	<i>Phlda2</i> ^{KO} Male	DKO Male
--------	---------	--------------------------------	----------------------------------	----------

	vs WT Female	vs <i>Peg3</i> ^{KO} Female	vs <i>Phlda2</i> ^{KO} Female	vs DKO Female
Junctional zone <i>Pr13b1</i> positive cells	P=.020	P=.425	P=.722	P=.015
Total junctional zone cells	P=.009	P=.689	P=.669	P=.006
Glycogen cells	P=.058	P=.596	P=.732	P=.051
P-TG Cells	P=.635	P=.110	P=.238	P=.792
SpT/GlyT ratio	P=.161	P=.103	P=.962	P=.155

Table 77: Sex comparison P values for junctional zone cell counts. Significant P values in bold.

Appendix 22: Extended caption and results tables for Figure 55.

Figure 55: Cell counts within E16.5 labyrinth region for WT, *Peg3*^{KO}, *Phlda2*^{KO} and DKO.

a) DKO labyrinths contain 31% ($P=.006$) fewer *Pr13b1* positive cells than WT (GENOTYPE: $F_{1:3} = 4.74$, $P=.005$). **b)** DKO labyrinths contain 27% ($P=.005$) fewer total cells than WT. (GENOTYPE: $F_{1:3} = 4.41$, $P=.007$). **c)** *Peg3*^{KO} labyrinths contained 32% ($P=.028$) fewer *Pr13b1* positive cells than WT in males. *Phlda2*^{KO} labyrinths contained 35% ($P=.007$) fewer *Pr13b1* positive cells than WT in males. DKO labyrinths had 43% ($P<.001$) fewer *Pr13b1* positive cells than WT in males. Female WT contained 37% ($P<.001$) fewer *Pr13b1* positive cells than male WT labyrinths (GENOTYPE*SEX: $F_{1:3} = 5.84$, $P=.002$) (GENOTYPE: $F_{1:3} = 4.74$, $P=.005$) (SEX: $F_{1:1} = .015$, $P=.902$). **d)** DKO labyrinth contained 32% ($P=.012$) fewer total cells than WT in males (GENOTYPE*SEX: $F_{1:3} = 1.46$, $P=.235$) (GENOTYPE: $F_{1:3} = 4.41$, $P=.007$) (SEX: $F_{1:1} = .078$, $P=.781$). WT ($n = 17$), *Peg3*^{KO} ($n = 15$), *Phlda2*^{KO} ($n = 16$) and DKO ($n = 17$). WT male ($n = 9$), *Peg3*^{KO} male ($n = 7$), *Phlda2*^{KO} male ($n = 8$), DKO male ($n = 8$), WT female ($n = 8$), *Peg3*^{KO} female ($n = 8$), *Phlda2*^{KO} female ($n = 8$), DKO ($n = 9$). Data from 16 litters, litter size between 5-10 (average $8\pm.18$). Error bars represent standard error of the mean (SEM). Statistical significance calculated using a two-way ANCOVA with Šidák correction and litter size as covariate. ^{NS} $P>.05$, * $P<.05$, and ** $P<.01$ *** $P<.001$ **** $P<.0001$.

Metric	Group	WT	<i>Peg3</i> ^{KO}	<i>Phlda2</i> ^{KO}	DKO
	Total	10386 ±878	9962 ±667	8961±674	7216±650

Labyrinth <i>Pr13b1</i> positive cells	Male	12581±1034	8532±1082	8237±1180	7164±1055
	Female	7915±849	11212±560	9683±639	7261±855
Total labyrinth cells	Total	14708±851	13310±612	13276±834	10733±724
	Male	15949±936	12364±925	13093±1485	10891±1351
	Female	10577±1365	14136±744	13457±875	10592±744

Table 78: Group averages and SEMs for labyrinth cell counts.

Metric	Group	WT vs <i>Peg3^{KO}</i>	WT vs <i>Phlda2^{KO}</i>	WT vs DKO
Labyrinth <i>Pr13b1</i> positive cells	Total	<i>P</i> =1.000	<i>P</i> =.586	<i>P</i>=.006
	Male	<i>P</i>=.028	<i>P</i>=.007	<i>P</i><.001
	Female	<i>P</i> =.089	<i>P</i> =.810	<i>P</i> =.996
Total labyrinth cells	Total	<i>P</i> =.750	<i>P</i> =.804	<i>P</i>=.005
	Male	<i>P</i> =.134	<i>P</i> =.331	<i>P</i>=.012
	Female	<i>P</i> =.996	<i>P</i> =1.000	<i>P</i> =.387

Table 79: Genotype comparison *P* values for labyrinth cell counts.
Significant *P* values in bold.

Metric	WT Male vs WT Female	<i>Peg3^{KO}</i> Male vs <i>Peg3^{KO}</i> Female	<i>Phlda2^{KO}</i> Male vs <i>Phlda2^{KO}</i> Female	DKO Male vs DKO Female
Labyrinth <i>Pr13b1</i> positive cells	<i>P</i><.001	<i>P</i> =.062	<i>P</i> =.319	<i>P</i> =.790
Total labyrinth cells	<i>P</i> =.083	<i>P</i> =.266	<i>P</i> =.786	<i>P</i> =.780

Table 80: Sex comparison *P* values for labyrinth cell counts.
Significant *P* values in bold.

Appendix 23: Extended caption and results tables for Figure 56.

Figure 56: Total cell counts of E16.5 placenta for WT, *Peg3^{KO}*, *Phlda2^{KO}* and DKO.

a) There was no significant difference in total *Pr13b1* positive cells between any groups (GENOTYPE: $F_{1:3} = 2.26$, $P = .094$). **b)** *Phlda2^{KO}* placentas contained 27% ($P = .025$) more total cells than WT placentas (GENOTYPE: $F_{1:3} = 5.09$, $P = .004$). **c)** There was no significant difference in the labyrinth and junctional zone positive cells between any groups (GENOTYPE: $F_{1:3} = 3.20$, $P = .030$). **d)** There was no significant difference in the labyrinth and junctional total cell numbers between any groups

(GENOTYPE: $F_{1:3} = 5.02, P = .004$). **e)** Female *Phlda2*^{KO} placenta had 26% ($P = .042$) more total *Prl3b1* positive cells than female WT placenta. *Peg3*^{KO} females had 41% ($P = .023$) more total *Prl3b1* positive cells than *Peg3*^{KO} males. (GENOTYPE*SEX: $F_{1:3} = 3.53, P = .022$) (GENOTYPE: $F_{1:3} = 2.26, P = .094$) (SEX: $F_{1:1} = .015, P = .904$). **f)** There were no significant differences seen between any groups for total cell numbers (GENOTYPE*SEX: $F_{1:3} = 1.66, P = .190$) (GENOTYPE: $F_{1:3} = 5.09, P = .004$) (SEX: $F_{1:1} = .005, P = .944$). **g)** Labyrinth and junctional zone *Prl3b1* positive cells were reduced in male *Peg3*^{KO} and DKO placentas by 33% ($P = .019$) and 28% ($P = .023$) compared to WT males. Female WT placentas had 36% fewer *Prl3b1* positive cells than male WT. (GENOTYPE*SEX: $F_{1:3} = 5.18, P = .003$) (GENOTYPE: $F_{1:3} = 3.20, P = .030$) (SEX: $F_{1:1} = .604, P = .440$). **h)** Total cells from labyrinth and junctional zones were reduced in *Peg3*^{KO} male samples by 27% ($P = .051$). Female WT samples had 21% ($P < .001$) fewer cells in their labyrinth and junctional zones than male WT. (GENOTYPE*SEX: $F_{1:3} = 1.95, P = .132$) (GENOTYPE: $F_{1:3} = 5.02, P = .004$) (SEX: $F_{1:1} = 1.25, P = .268$). WT ($n = 17$), *Peg3*^{KO} ($n = 15$), *Phlda2*^{KO} ($n = 16$) and DKO ($n = 17$). WT male ($n = 9$), *Peg3*^{KO} male ($n = 7$), *Phlda2*^{KO} male ($n = 8$), DKO male ($n = 8$), WT female ($n = 8$), *Peg3*^{KO} female ($n = 8$), *Phlda2*^{KO} female ($n = 8$), DKO ($n = 9$). Data from 16 litters, litter size between 5-10 (average 8 ± 1.8). Error bars represent \pm SEM. Statistical significance calculated using a two-way ANCOVA with Šidák correction and litter size as covariate. ^{NS} $P > .05$, * $P < .05$, and ** $P < .01$ *** $P < .001$ **** $P < .0001$.

Metric	Group	WT	<i>Peg3</i> ^{KO}	<i>Phlda2</i> ^{KO}	DKO
Total <i>Prl3b1</i> positive cells	Total	11970 \pm 1214	12546 \pm 784	15114 \pm 1076	12176 \pm 842
	Male	14199 \pm 2578	10143 \pm 1130	14296 \pm 1796	13494 \pm 1366
	Female	10577 \pm 1005	14349 \pm 482	16204 \pm 760	11186 \pm 989
Total cells	Total	19484 \pm 1438	19282 \pm 920	24739 \pm 1424	19201 \pm 968
	Male	19555 \pm 2696	17393 \pm 1402	24200 \pm 2465	21553 \pm 1294
	Female	19439 \pm 1777	20697 \pm 1016	25456 \pm 881	17437 \pm 1054
Labyrinth and junctional zone <i>Prl3b1</i> positive cells	Total	13630 \pm 1078	12645 \pm 751	14564 \pm 932	11048 \pm 889
	Male	16416 \pm 1246	10965 \pm 1288	13909 \pm 1712	11747 \pm 1470
	Female	10495 \pm 997	14115 \pm 458	15219 \pm 821	10426 \pm 1096
	Total	18622 \pm 1060	16268 \pm 685	20242 \pm 1194	15199 \pm 1037

Labyrinth and junctional zone <i>Pr13b1</i> positive cells	Male	20705±1142	15162±1166	20185±2196	16389±1894
	Female	16279±1514	17236±675	20299±1133	14141±986

Table 81: Group averages and SEMs for total cell counts.

Metric	Group	WT vs <i>Peg3^{KO}</i>	WT vs <i>Phlda2^{KO}</i>	WT vs DKO
Total <i>Pr13b1</i> positive cells	Total	<i>P</i> =1.000	<i>P</i> =.284	<i>P</i> =1.000
	Male	<i>P</i> =.294	<i>P</i> =1.000	<i>P</i> =.997
	Female	<i>P</i> =.168	<i>P</i>=.042	<i>P</i> =1.000
Total cells	Total	<i>P</i> =1.000	<i>P</i>=.025	<i>P</i> =1.000
	Male	<i>P</i> =.965	<i>P</i> =.371	<i>P</i> =.978
	Female	<i>P</i> =.994	<i>P</i> =.103	<i>P</i> =.939
Labyrinth and junctional zone <i>Pr13b1</i> positive cells	Total	<i>P</i> =.984	<i>P</i> =.964	<i>P</i> =.185
	Male	<i>P</i>=.019	<i>P</i> =.558	<i>P</i>=.023
	Female	<i>P</i> =.198	<i>P</i> =.067	<i>P</i> =1.000
Labyrinth and junctional zone <i>Pr13b1</i> positive cells	Total	<i>P</i> =.519	<i>P</i> =.769	<i>P</i> =.145
	Male	<i>P</i>=.051	<i>P</i> =1.000	<i>P</i> =.196
	Female	<i>P</i> =.998	<i>P</i> =.272	<i>P</i> =.864

Table 82: Genotype comparison *P* values for total cell counts.

Significant *P* values in bold.

Metric	WT Male vs WT Female	<i>Peg3^{KO}</i> Male vs <i>Peg3^{KO}</i> Female	<i>Phlda2^{KO}</i> Male vs <i>Phlda2^{KO}</i> Female	DKO Male vs DKO Female
Total <i>Pr13b1</i> positive cells	<i>P</i> =.076	<i>P</i>=.023	<i>P</i> =.385	<i>P</i> =.297
Total cells	<i>P</i> =.996	<i>P</i> =.177	<i>P</i> =.612	<i>P</i> =.099
Labyrinth and junctional zone <i>Pr13b1</i> positive cells	<i>P</i><.001	<i>P</i> =.087	<i>P</i> =.503	<i>P</i> =.567

Labyrinth and junctional zone <i>Pr13b1</i> positive cells	P=.028	P=.324	P=.947	P=.254
--	---------------	--------	--------	--------

Table 83: Sex comparison P values for total cell counts.
Significant P values in bold.

Appendix 24: Chapter 5: Methods

1.3 Chapter 5: Methods

1.3.1 Mouse trophoblast stem cell derivation

7.3.1.1 Mouse trophoblast stem cell derivation

Mouse trophoblast stem cells lines were derived using the protocol described in 2.8.1. E3.5 blastocysts were generated by crossing *Phlda2*^(+/-) females with *Peg3*^(-/+) males, resulting in wild type (*Peg3*^(+/+), *Phlda2*^(+/+))(WT), *Peg3*^(-/+), *Phlda2*^(+/+) (*Peg3*^{KO}), *Phlda2*^(+/-), *Peg3*^(+/+) (*Phlda2*^{KO}) and *Phlda2*^(+/-), *Peg3*^(-/+) (DKO) blastocysts. Once a line was successfully derived it was genotyped using the protocol described in 2.8.2. The cell line was then banked by being frozen and stored at -150°C.

7.3.1.2 Mouse trophoblast validation assay

Mouse trophoblast stem cells were collected and had their RNA extracted using protocol 2.10.1. The RNA was then converted to cDNA using protocol 2.10.2. The cDNA libraries were analysed using primers designed for qRT-PCR to identify if they were expressing trophoblast stem cell markers. The cells were also differentiated using the differentiation protocol described in 2.8.3. The differentiated cells were then analysed for the expression of hormone RNAs such as *Pr13b1* and *Pr13d1-3* to determine if they were differentiating into the endocrine lineages, once encouraged to differentiate. A combination of these results would determine which lines were appropriate for further assessment.

7.3.1.3 Mouse trophoblast stem cell differentiation assay

At least four lines per genotype were differentiated using the protocol described in 2.8.3. The cell lines were imaged on a brightfield microscope at two-day intervals.

7.3.1.4 Mouse trophoblast stem cell proliferation assay

During the mouse trophoblast stem cell differentiation assay, cells were collected at two-day intervals. The cells were counted using the protocol described in 2.8.4.

7.3.1.5 Mouse trophoblast stem cell qRT-PCR

Two independent mTS cell lines of each of the genotypes were differentiated for 10 days in duplicate (protocol 2.8.3). The differentiated cells were converted into cDNA libraries (protocol 2.10.3) and analysed via qRT-PCR (protocol 2.10.4) for mouse trophoblast lineage markers and imprinted genes of interest (Table 32).

7.3.1.6 ELISA

An ELISA was performed on differentiated WT mouse TS cells using the protocol described in section 2.12. The ELISA was performed by Dr Ekaterina Lysikova. The differentiated mouse TS cell samples were compared to E9.5 and E14.5 mouse placenta protein samples.

1.3.2 Human CRISPR primer designs and knockout line derivations

Details of CRISPR designs and derivation attempts are detailed in the results sections 5.3.2.1 and 5.3.2.2.

7.3.2.1 Human trophoblast stem cell differentiation assay

Human trophoblast stem cells were differentiated using the protocol described in 2.9.7. Two independently derived wild type and two independently derived *PHLDA2*^{KO} hTS stem cell lines were run through the protocol in duplicate.

7.3.2.2 Human trophoblast stem cell Western assays

Protein was extracted from two independently derived wild type and two independently derived *PHLDA2*^{KO} hTS cell lines using the protocol described in 2.11. The protein samples were then run through the

western blotting protocol described in 2.13 and stained with the antibodies detailed in Table 35.

7.3.2.3 Human trophoblast stem cell qRT-PCR

Two independent strains of both WT and *PHLDA2^{KO}* hTS cells were differentiated for five days in duplicate following the protocol outlined in 2.9.7. RNA was extracted and converted into cDNA libraries (protocols 2.10.1 and 2.10.3). The cDNA libraries were then analysed via qRT-PCR (protocol 2.10.4) using qRT-PCR primers detailed in Table 32.

Appendix 25: Extended caption and results tables for Figure 59.

Figure 59: ELISA for Prl3d1 and Prl3b1 on 10-day differentiated mTS cells compared to E9.5 and E14.5 mouse placenta.

a) Prl3d1 was significantly higher than mTS in both E9.5 and E14.5 by 234% ($P=.011$) and 392% ($P<.001$) respectively. Prl3d1 was increased by 47% ($P=.019$) in E14.5 compared to E9.5 (SAMPLETYPE: $F_{1:2} = 14.46$, $P<.001$). **b)** Prl3b1 protein concentration was significantly lower in mTS cells than E14.5 mouse placenta ($P<.001$). Prl3b1 protein concentration was 206% higher ($<.001$) in E14.5 compared to E9.5 (SAMPLETYPE: $F_{1:2} = 29.00$, $P<.001$). All samples were WT. mTS ($n = 5$), E9.5 ($n = 14$) and E14.5 ($n = 14$). Statistical significance calculated using a two-way ANOVA with Šidák correction. ^{ns} $P>.05$, * $P<.05$, and ** $P<.01$ *** $P<.001$ **** $P<.0001$.

Protein	mTS	E9.5	E14.5
Prl3d1	1.089±0.131	3.637±0.310	5.36±0.549
Prl3b1	0.042±0.002	10.14±1.027	31.06±3.570

Table 84: Group averages and SEMs for ELISA results.

Protein	mTS vs E9.5	mTS vs E14.5	E9.5 vs E14.5
Prl3d1	$P=.011$	$P<.001$	$P=.019$
Prl3b1	$P=.122$	$P<.001$	$P<.001$

Table 85: Sample type comparison P values for ELISA results.

Appendix 26 Extended caption for Figure 61.

Figure 61: Proliferation assay of WT, *Peg3^{KO}*, *Phlda2^{KO}* and DKO mouse trophoblast stem cells.

No significant difference between genotypes for cell counts on Day 0 (GENOTYPE: $F_{1:3} = 1.29$, $P=.293$). No significant difference between genotypes for cell counts on Day 2 (GENOTYPE: $F_{1:3} = 0.79$, $P=.509$). No

significant difference between genotypes for cell counts on Day 4 (GENOTYPE: $F_{1:3} = 0.85$, $P = .481$). No significant difference between genotypes for cell counts on Day 6 (GENOTYPE: $F_{1:3} = 0.82$, $P = .492$). No significant difference between genotypes for cell counts on Day 8 (GENOTYPE: $F_{1:3} = 3.60$, $P = .023$). No significant difference between genotypes for cell counts on Day 10 (GENOTYPE: $F_{1:3} = 1.32$, $P = .285$). Error bars represent standard error of the mean (SEM). WT ($n = 10$), *Peg3*^{ko} ($n = 10$), *Phlda2*^{ko} ($n = 8$), DKO ($n = 10$). Statistical significance calculated using a two-way ANOVA with Šidák correction. ^{ns} $P > .05$, * $P < .05$, and ** $P < .01$ *** $P < .001$ **** $P < .0001$.

Day	WT	<i>Peg3</i> ^{ko}	<i>Phlda2</i> ^{ko}	DKO
0	34725±2720	50900±12395	67750±20986	39000±11189
2	56625±3128	152313±43125	128000±52773	118350±55486
4	113000±27185	291667±83702	137500±72624	216550±91196
6	136500±41375	216300±54486	317438±162740	326100±121459
8	145200±48310	104450±29945	162625±66925	731200±293167
10	314650±115498	167650±46533	403500±221519	832500±433427

Table 86: Genotype averages and SEMs for proliferation assay.

Day	WT vs <i>Peg3</i> ^{ko}	WT vs <i>Phlda2</i> ^{ko}	WT vs DKO
0	$P = .928$	$P = .392$	$P = 1.000$
2	$P = .620$	$P = .896$	$P = .902$
4	$P = .669$	$P = 1.000$	$P = .935$
6	$P = .993$	$P = .782$	$P = .692$
8	$P = 1.000$	$P = 1.000$	$P = .070$
10	$P = .999$	$P = 1.000$	$P = .624$

Table 87: Genotype comparison *P* values for proliferation assay.

Appendix 27: Extended caption and results tables for Figure 62.

Figure 62: Knockout targets *Peg3* and *Phlda2* RNA expression in WT, *Peg3*^{ko}, *Phlda2*^{ko} and DKO in 10-day differentiated mTS cells.

a) *Peg3* expression was successfully knocked out in both *Peg3*^{ko} ($P = .013$) and DKO ($P = .013$) (GENOTYPE: $F_{1:3} = 9.84$, $P < .001$). **b)** *Phlda2* expression was successfully knocked out in both *Phlda2*^{ko} ($P = .007$) and DKO ($P = .007$). *Phlda2* expression was increased by 1122% in *Peg3*^{ko} ($P < .001$) (GENOTYPE: $F_{1:3} = 1288.39$, $P < .001$). Error bars represent \pm SEM. WT ($n = 4$), *Peg3*^{ko} ($n = 4$), *Phlda2*^{ko} ($n = 4$), DKO ($n = 4$). Statistical significance calculated using a two-way ANOVA with Šidák correction. ^{ns} $P > .05$, * $P < .05$, and ** $P < .01$ *** $P < .001$ **** $P < .0001$.

Gene	WT	<i>Peg3</i> ^{ko}	<i>Phlda2</i> ^{ko}	DKO
------	----	---------------------------	-----------------------------	-----

<i>Peg3</i>	1±.303	0.0004±.00001	0.9767±.201	0.0006±.0001
<i>Phlda2</i>	1±.018	12.22±.331	0.005207±.002	0.005207±.002

Table 88: Group averages and SEMs qRT-PCR results of 10-day differentiation mTS cells.

Gene	WT vs <i>Peg3</i> ^{KO}	WT vs <i>Phlda2</i> ^{KO}	WT vs DKO
<i>Peg3</i>	P=.013	P=1.000	P=.013
<i>Phlda2</i>	P<.001	P=.007	P=.007

Table 89: Genotype comparison P values for RNA expression in 10-day differentiated mouse trophoblast stem cells.

Appendix 28: Extended caption and results tables for Figure 63.

Figure 63: qRT-PCR of 10-day differentiated WT, *Peg3*^{KO}, *Phlda2*^{KO} and DKO mouse trophoblast stem cells.

a) *Tpbpa* expression was reduced in *Peg3*^{KO} by 87% ($P<.001$), *Phlda2*^{KO} by 70% ($P<.001$) and DKO by 99% ($P<.001$) (GENOTYPE: $F_{1:3}= 626.26$, $P<.001$). **b)** *Blimp1* expression was increased in *Peg3*^{KO} by 11% ($P<.001$) and decreased in *Phlda2*^{KO} by 43% ($P<.001$) and DKO by 65% ($P<.001$) (GENOTYPE: $F_{1:3}= 33.56$, $P<.001$). **c)** *Rgs5* expression was reduced in *Peg3*^{KO} by 86% ($P<.001$), in *Phlda2*^{KO} by 49% ($P=.004$) and in DKO by 96% ($P<.001$) (GENOTYPE: $F_{1:3}= 31.80$, $P<.001$). **d)** *Pcks6* expression was reduced by 83% in *Phlda2*^{KO} (GENOTYPE: $F_{1:3}= 24.70$, $P<.001$). **e)** *Prl7b1* expression was reduced by 99% in *Peg3*^{KO} ($P<.001$), 89% in *Phlda2*^{KO} ($P<.001$), and 99% in DKO ($P<.001$) (GENOTYPE: $F_{1:3}= 24.30$, $P<.001$). **f)** *Pcdh12* expression is reduced by 91% in DKO (GENOTYPE: $F_{1:3}= 12.51$, $P<.001$). **g)** There was no significant difference for any transgenic group in *Prl3d1-3* expression (GENOTYPE: $F_{1:3}= 4.38$, $P=.027$). **h)** There was no significant difference for any transgenic group in *Prl3b1* expression (GENOTYPE: $F_{1:3}= 2.69$, $P=.093$). **i)** *Prl2c* expression is reduced by 84% in *Phlda2*^{KO} (GENOTYPE: $F_{1:3}= 12.51$, $P<.001$). **j)** There was no significant difference for any transgenic group in *Hand1* expression (GENOTYPE: $F_{1:3}= 0.31$, $P=.073$). Error bars represent ±SEM. WT ($n = 4$), *Peg3*^{KO} ($n = 4$), *Phlda2*^{KO} ($n = 4$), DKO ($n = 4$). Statistical significance calculated using a two-way ANOVA with Šidák correction. ^{NS} $P>.05$, * $P<.05$, and ** $P<.01$ *** $P<.001$ **** $P<.0001$.

Gene	WT	<i>Peg3</i> ^{KO}	<i>Phlda2</i> ^{KO}	DKO
<i>Tpbpa</i>	1±.033	0.1307±.010	0.3028±.005	0.0004±.0001
<i>Blimp1</i>	1±.053	1.114±.083	0.5737±.060	0.3472±.044
<i>Rgs5</i>	1±.040	0.1402±.009	0.5108±.152	0.03897±.009
<i>Pcks6</i>	1±.014	0.7606±.055	0.1703±.022	1.361±.191
<i>Prl7b1</i>	1±.191	0.01271±.001	0.1056±.044	0.001413±.000
<i>Pcdh12</i>	1±.041	1.189±.084	1.322±.299	.09077±.019

<i>Prl3d1-3</i>	1±.126	3.176±.136	0.3967±.014	2.053±1.154
<i>Prl3b1</i>	1±.034	1.159±.174	0.8964±.139	6.181±3.143
<i>Prl2c</i>	1±.010	1.483±.074	0.1555±.032	0.8353±.371
<i>Hand1</i>	1±.222	1.731±1	1.046±.180	1.188±.600

Table 90: Group averages and SEMs qRT-PCR results of 10-day differentiation mouse trophoblast stem cells.

Gene	WT vs <i>Peg3</i> ^{ko}	WT vs <i>Phlda2</i> ^{ko}	WT vs DKO
<i>Tpbpa</i>	P<.001	P<.001	P<.001
<i>Blimp1</i>	P<.001	P<.001	P<.001
<i>Rgs5</i>	P<.001	P=.004	P<.001
<i>Pcsk6</i>	P=.531	P<.001	P=.147
<i>Prl7b1</i>	P<.001	P<.001	P<.001
<i>Pcdh12</i>	P=.958	P=.680	P=.009
<i>Prl3d1-3</i>	P=.124	P=.980	P=.786
<i>Prl3b1</i>	P=1.000	P=1.000	P=.209
<i>Prl2c</i>	P=.461	P=.050	P=.992
<i>Hand1</i>	P=.956	P=1.000	P=1.000

Table 91: Genotype comparison P values for RNA expression in 10-day differentiated mouse trophoblast stem cells.

Appendix 29: Extended caption and results tables for Figure 70.

Figure 70: qRT-PCR of five day differentiated WT and *PHLDA2*^{ko} and hTS cells.

a) CGA expression was not significantly altered in *PHLDA2*^{ko} (GENOTYPE: F_{1:1}= 0.48, P=.515). **b)** CGB expression was not significantly altered in *PHLDA2*^{ko} (GENOTYPE: F_{1:1}= 0.56, P=.996). **c)** PSG1 expression was not significantly altered in *PHLDA2*^{ko} (GENOTYPE: F_{1:1}= 5.85, P=.052). **d)** hPL expression was increased by 119% in *PHLDA2*^{ko} (GENOTYPE: F_{1:1}= 121.61, P<.001). **e)** PEG3 expression was not significantly altered in *PHLDA2*^{ko} (GENOTYPE: F_{1:1}= .155, P=.707). **f)** *PHLDA2* expression was decreased by 85% in *PHLDA2*^{ko} (GENOTYPE: F_{1:1}= 80.44, P<.001). Error bars represent ±SEM. WT (n = 4), *PHLDA2*^{ko} (n = 4). Statistical significance calculated using a two-way ANOVA with Šidák correction. ^{ns}P>.05, *P<.05, and **P<.01 ***P<.001 ****P<.0001.

Gene	WT	<i>Phlda2</i> ^{ko}
CGA	1±.14	0.896±.12
CGB	1±.12	1.022±.08
PSG1	1±.13	0.653±.07
hPL (CSH1/2)	1±.08	2.209±.07

<i>PEG3</i>	1±.11	1.17±.71
<i>PHLDA2</i>	1±.09	0.148± .02

Table 92: Group averages and SEMs for expression in five day differentiated hTS stem cells.

Gene	WT vs <i>Phlda2</i>^{KO}
<i>CGA</i>	<i>P</i> =.515
<i>CGB</i>	<i>P</i> =.996
<i>PSG1</i>	<i>P</i> =.052
<i>hPL (CSH1/2)</i>	<i>P</i><.001
<i>PEG3</i>	<i>P</i> =.707
<i>PHLDA2</i>	<i>P</i><.001

Table 93: Genotype comparison *P* values for expression in five day differentiated hTS cells.

Appendix 30: qRT-PCR primer blast results.

Primer	Sequence	Species	Blast Results	Target	Target Amplified Variants	Target Sudonames	Target Location	RPM K	Off Target Name	Off Target Amplified Variants	Off Target Sudonames	Off Target Location	Off Target Expression in Placenta RPKM	Off Target Potential Complications	Part of project	Marker	Details
<i>B-actin</i> F	CCTGTATGCCTCTGGT CGTA	Mouse	Targets, Lrrc58, beta (Actb), Acta2	<i>B-actin</i>	Standard	Actb; beta-actin; E430023M04Rik	5 G2; 5 81.8 cM	1493	Leucine rich repeat containing 58 (Lrrc58)	Standard	1810012N18Rik; C330018J07Rik	16 B3; 16 26.49 cM	19	Yes	<i>Phlda2^{+/+}BACk1</i> (BL6) and <i>mTS</i>	Reference gene	cDNA: 260 bp, gDNA: 260 bp
<i>B-actin</i> R	CCATCTCCTGCTCGAA GTCT								Actin alpha 2, smooth muscle, aorta, (Acta2)	Standard and X1	Actvs; a-SMA; SMAalpha; SMAalphaA; alphaSMA; 0610041G09Rik	19 C1; 19 29.41 cM	168	Yes			
<i>Blimp1</i> F	GGGTACTTCTGTCAA GCCG	Mouse	Targets Prdm1 and Zch3h3	Prdm1 (Blimp1)	1, 2, 6, 7, 4, 5, 9, 8, X5, X3, 3,	Blimp1; Blimp-1; PRDI-BF1; ZNFPR1A1; b2b1765Clo	10 B2; 10 23.24 cM	2	-	-	-	-	-	-	<i>mTS</i>	Sinusoidal TGCs (S-TGCs), spiral artery (SpA-) TGCs and C-TGCs	cDNA: 182 bp, gDNA: 6568 bp
<i>Blimp1</i> R	TCCTGTTGGCATTCTTG GGA								-	-	-	-	-				
<i>Cdx2</i> F	AAGACAAATACGGGT GGTG	Mouse	Targets Cdx2	Caudal type homeobox 2 (Cdx2)	Standard	Cdx-2	5 G3; 5 86.86 cM	5	zinc finger CCCH type containing 3 (Zc3h3)	-	Smiel; Zc3hdc3; Kiaa0150	15 D3; 15 34.84 cM	2	No	<i>mTS</i>	TS cell marker	169 bp
<i>Cdx2</i> R	CTGCGGTTCTGAAACC AAAT								-	-	-	-					
<i>CGA</i> F	ATGTTCTCCATTCCGCT CCT	Human	Targets CGA	Chorionic gonadotropin subunit alpha (CGA)	1 and 2	HCG; LHA; FSHA; GPA1; GPHA; TSHA; GPHA1; CG-ALPHA	6q14.3	385	-	-	-	-	-	-	<i>hTS</i>	Human chorionic gonadotropin (hCG)	Designed by AC, spans intron 2, cDNA: 189 bp, gDNA: approx 390 bp
<i>CGA</i> R	AAGTGGACTCTGAGGT GACG								-	-	-	-					
<i>CGB</i> F	CAGCATCCTATCACCT CCTGGT	Human	Targets CGB3, CGB7, CGB8, CGB5, GLCE and LHB	Chorionic gonadotropin subunit beta (CGB)	CGB3, CGB7 v 1 and 2, CGB8, CGB5	CGB; LHB; CGB5; CGB7; CGB8; hCGB	19q13.33	30	Luteinizing hormone subunit beta (LHB)	X1	CGB4; HH23; LSH-B; LSH-beta	19q13.33	0	No	<i>hTS</i>	hCG	Ref: Okae et al, 2018, cDNA: 102 bp
<i>CGB</i> R	CTGGAACATCTCCATC CTTGGT								Glucuronic acid epimerase (GLCE)	X2, X1, X3, X7 and X2	HSEPI	15q23	4	No			
<i>Ctsq</i> F	TGGAACGTCACCTTG GTAG	Mouse	Targets Ctsq	Cathepsin Q (Ctsq)	Standard	1600010J02Rik	13 B2; 13	51	Centriolar coiled coil	-	CP110; cep110;	1	No	<i>Phlda2^{+/+}BACk1</i> (BL6)	Spongiotrophoblast giant cell	cDNA: 196 bp,	

<i>Ctsq</i> R	GTGGGATCAGTTGGC TGTT		and Ccp110				32.65 cM		protein 110 (Ccp110)	3, X1, 1, 2, X2	6330503K22 Rik	7 F2; 7 63.58 cM						gDNA: 1059 bp.	
<i>Dlx3</i> F	CGTTTCCAGAAAGCC AGTA						11 D; 11 59.01 cM	4											
<i>Dlx3</i> R	ACTGTTGTTGGGGCTG TGTT	Mouse	Targets Dlx	Distal-less homeobox 3 (Dlx3)	Standar d				-	-	-	-	-	-	-	-	<i>Phlda2</i> ^{+/+BACk1} (BL6)	Labyrinth	cDNA: 169 bp, gDNA: 1678 bp
<i>Eomes</i> F	GGCAAAGCGGACAATA ACAT						9 70.21 cM; 9 F3	0											2 transcrip ts, Spans 2 introns, cDNA: 192 bp
<i>Eomes</i> R	AGCCTCGGTTGGTATT TGTT	Mouse	Targets Eomes	Eomesodermin (Eomes)	X1, 3, 2 and 1.				-	-	-	-	-	-	-	-	mTS	TS cell marker	
<i>Essrb</i> F	AACAGCCCCTACCTGA ACCT						12 D2; 12 40.49 cM	1	Salt inducible kinase 2 (Sik2)	2, 1, X3, 3	Snf1ik2; G630080D2 ORik	9 A5.3; 9 27.75 cM	1	No			mTS	TS cell marker	Includes all 5 t/c; cDNA: 249 bp
<i>Essrb</i> R	CTCATCTGGTCCCAA GTGT	Mouse	Targets Essrb and Sik2	Estrogen related receptor, beta (Essrb)	X3, X2, X1, 2, 1,														
<i>Flk1</i> F	GGCGGTGGTACAGTA TCTT						5 C3.3; 5 40.23 cM	4	Protein phosphatase 3, regulatory subunit B, alpha isoform (calcineurin B, type I) (Ppp3r1)	Standar d	Cnb1; CaNB1; MCIP1	11 A2; 11 9.71 cM	6	Yes			<i>Phlda2</i> ^{+/+BACk1} (BL6)	Endothelium	cDNA: 163 bp
<i>Flk1</i> R	GTCACCTGACAGAGCG ATGA	Mouse	Targets Kdr (Flk1) and Ppp3r1	Kinase insert domain protein receptor (Kdr) (Flk1)	3,4,5, 2,1														
<i>Gapdh</i> F	CACAGTCAAGGCCGAG AATG						6 F2; 6 59.32 cM	30	Gm29667 predicted gene 29667	Standar d		1 E1.1; 1	Undefin ed	-					
<i>Gapdh</i> R	TCTCGTGGTTCACACC CATC	Mouse	Targets Gapdh, Gm296 67, Cdh23	Glyceraldehyde-3- phosphate dehydrogenase (Gapdh)	6, 4, 1, 7, 3, 8, 5, 2,					X6, 1, X1, X3, 2, X2	v; ahl; bob; bus; ahl1; mdfw; sals; USH1D; nmf112; nmf181; nmf252; 4930542A03 Rik	10 B4; 10 30.11 cM	0	No			<i>Phlda2</i> ^{+/+BACk1} (BL6) and mTS	Reference gene	cDNA: 242 bp, gDNA: 242 bp
<i>Gcm1</i> F	AGCCTGTGTTGAGCAG ACCT						9 E1; 9 43.49 cM	1	Heat shock protein 12A (Hspa12a)	1	DSMgi40; Gm19925; mKIAA0417; 1700063D12 Rik	19 D2; 19 54.51 cM	3	Yes			<i>Phlda2</i> ^{+/+BACk1} (BL6)	Labyrinth	Between exon 1 and exon 2. cDNA: 173 bp, gDNA: 1945 bp.
<i>Gcm1</i> R	TGTCGTCGAGCTGTA GATG	Mouse	Targets Gcm1, Hspa12 a and BMP7	Glial cells missing homolog 1 (Gcm1)	Standar d					Standar d	OP1	2 H3; 2 95.54 cM	2	Yes					
<i>Hand1</i> F	CGCCTGGCTACCAATT ACAT						11 B1.3; 11 35.27 cM	62	Aldo-keto reductase family 1, member C6 (Akr1c6)	1, 2 and 3	Akr1c1; Hsd17b5; 3alpha-HSD	13 A1; 13 2.48 cM	0	No			mTS	Parietal trophoblast giant cells (P- TGC)	Between exon 1 and exon 2. cDNA: 200 bp,
<i>Hand1</i> R	GCGCCCTTAACTCTCT TCT	Mouse	Targets Hand1, Hand2, Akr6	Heart and neural crest derivatives expressed 1 (Hand1)	Standar d														

						6, 18, 9, 15, 7, 13, 10, 30, 21, 16, 1, 3												
<i>Phlda2</i> F	CAGCAAGCACGGGAATATCT	Mouse	Targets Phlda2 and Cnm1	Pleckstrin homology like domain, family A, member 2 (Phlda2)	Standard and X1	Ipl; Tssc3	7 F5; 788.23 cM	163		Cyclin M1 (Cnm1)	X4, X1, X2	Acdp1; CLP-1	19 C3; 1936.67 cM	0	No	mTS	Imprinted gene	Spans exon 1 - exon 2. cDNA: 188 bp
<i>Phlda2</i> R	TCAGCGCTCTGAGTCTGAAA																	
<i>PHLDA2</i> F	GAGAGCTGCTGGAACGCG	Human	Targets PHLDA2	Pleckstrin homology like domain family A member 2 (PHLDA2)	Standard	IPL; BRW1C; HLDA2; TSSC3	11p15.4	44		-	-	-	-	-	-	hTS	Imprinted gene	Ref: Apostolidou, et al, 2007, cDNA: 68 bp
<i>PHLDA2</i> R	CGCACGGGAAGTCTTCTG																	
<i>Pr8a8</i> F	TCAGAGCTGCATCTCACTGC	Mouse	Targets Prl8a8, Zzef1, Ccdc162, Prl8a6 and Islr2 v	Prolactin family 8, subfamily a, member 81 (Prl8a8)	3,2,4 and 1	Ghd14; PLP-C3; Prlpc3; PLP-Cgamma; 1600032B14Rik	13 A3.1; 13 12.49 cM	35		Zinc finger, ZZ-type with EF hand domain 1 (Zzef1)	1, X1, 2	NSPA; mKIAA0399; 8430405D05Rik; C130099L13Rik	11 B4; 1144.56 cM	3	No			
<i>Pr8a8</i> R	GGGACATCTTTCATGGCACT									Coiled-coil domain containing 162 (Ccdc162)	X1, X4, X8 X3, X7, X9, X2, standard	CCDC162; C6orf183; C6orf184; C6orf185	10 B2; 1022.48 cM	0	No			
										Prolactin family 8, subfamily a, member 6 (Prl8a6)	1 and 2	Ghd13; Prlpc; PLP-C1; PLP-Ca; Prlpc1; PLP-calpha	13 A3.1; 13 12.45 cM	6	Shared location/function			<i>Phlda2</i> ^{+/+} <i>BACk1</i> (<i>BL6</i>) Spongiotrophoblast specific cDNA: 173 bp, gDNA: 1206 bp
										Immunoglobulin superfamily containing leucine-rich repeat 2 (Islr2)	3 and X8	Linx; Mbu-3; mKIAA1465; B930052A04Rik	9 B; 931.63 cM	0	No			
<i>Prl2c</i> F	TCCAGAAAAAAGGAA CAAGC	Mouse	Targets Prl2c, Prl2c2, Prl2c4, Prl2c5, Prl2c1, Prl2b1, Nyx, ZZfp33b, Scaf11, Tat1, Cfap211 and	Prolactin family 2, subfamily c, member 2 (Prl2c2)	X1 and X2	Pif; Ghd2; Pif1; MRP-1; PLF-1	13 A1; 13 5.18 cM	2175		Prolactin family 2, subfamily c, member 3 (Prl2c3)	X1 and Standard	Ghd1; Pif2; MRP-2; MRP-3; PLF-2; PLF-3; Prl2c4; Mrpplf3; mrp/plf3	13; 13 A1	2865	Shared location/function			Amplifies from Prl2c2, Prl2c3, Prl2c4, Prl2c5 (proliferin genes). cDNA: 161 bp, gDNA products vary.127
										Prolactin family 2, subfamily c, member 4 (Prl2c4)	Standard	MRP-3; PLF-3; Mrpplf3; mrp/plf3	13; 13 A1	Undefined	-			

<p><i>Prl3d1-3</i> R</p> <p>AGCTCCTGGAAGAGCA GTCA</p>	<p>Ddr1, Paxip1, Bicral, Idnk, Ap2m1, Cdc3711 , Ssbp2, Myt11, UBX, Arhgap 21, Nup160 , Sqstm1 and Atad31.</p>	<p>Prolactin family 3, subfamily d, member 1 (Prl3d1)</p>	<p>12.3 cM</p>	<p>member 1 (Ddr1)</p>	<p>CD167a; 6030432F18</p>	<p>18.7 cM</p>	<p>and Prl3d3, cDNA: 233 bp, gDNA: 3490</p>						
								<p>PAX interacting (with transcription- activation domain) protein 1 (Paxip1)</p>	<p>X6, X1, X5, X3 and X4</p>	<p>PTIP; D5Ert149e</p>	<p>5 B1; 5 13.23 cM</p>	<p>3</p>	<p>No</p>
								<p>BRD4 interacting chromatin remodeling complex associated protein like (Bicral)</p>	<p>X5</p>	<p>Gltscr1; mKIAA0240</p>	<p>17 C; 17 22.9 cM</p>	<p>0</p>	<p>No</p>
		<p>Prolactin family 3, subfamily d, member 2 (Prl3d2)</p>	<p>2</p>	<p>Ghd5; Plib; PL-Ib</p>	<p>13 A3.1; 13 12.28 cM</p>	<p>11</p>	<p>Idnk gluconokinas e homolog (E. coli) (Idnk)</p>	<p>X1</p>	<p>5133401N09 Rik</p>	<p>13 B1; 13 30.95 cM</p>	<p>2</p>	<p>No</p>	
							<p>Adaptor- related protein complex 2, mu 1 subunit (Ap2m1)</p>	<p>1 and 2</p>	<p>mu2; AP50; MRD60; CLAPM1</p>	<p>3q27.1</p>	<p>131</p>	<p>Yes</p>	
							<p>Cell division cycle 37-like 1 (Cdc3711)</p>	<p>4 and 1</p>	<p>Harc; Cdc371; 2700033A15 Rik</p>	<p>19 C1; 19 23.61 cM</p>	<p>2</p>	<p>No</p>	
							<p>Single- stranded DNA binding protein 2 (Ssbp2)</p>	<p>X4</p>	<p>SSDP2; Hspc116; 1500004K09 Rik; 2310079I02 Rik; 9330163K02 Rik; A830008M0 3Rik</p>	<p>13 C3; 13 47.43 cM</p>	<p>0</p>	<p>No</p>	
							<p>Myelin transcription factor 1-like (Myt11)</p>	<p>X40</p>	<p>Nztf1; Pmng1; Png- 1; mKIAA1106; 2900046C06 Rik; 2900093J19 Rik; C630034G21 Rik</p>	<p>12 A2; 12 11.86 cM</p>	<p>0</p>	<p>No</p>	
							<p>Prolactin family 3, subfamily d, member 3 (Prl3d3)</p>	<p>1 and 2</p>	<p>Pl1; Csh1; Ghd4; PL-I; Pl-1; PL-Ia;</p>	<p>13 A3.1; 13</p>	<p>11</p>	<p>UBX domain protein 8 (Ubxn8)</p>	<p>X1</p>

								MC2DN1; NDAXOA											
Syna F	CAGGGACACAAGACC CCTA	Targets Syna, Gm271 79, Synb, Fkbp10 and Strbp	Synctin a (Syna)	X4, X6, X7, X5, X3, X2, X1 and standa rd	Gm52; Gm453; syncytin-A	5 G2; 5 74.67 cM	3	Predicted gene 27179 (Gm27179)	X4, X3, X2, X5, Stand ard	Synb	14 D2; 14	Undefi ned	-	Phlda2 ^{+/+BACk1} (BL6)	Syncytiotropho blast layer I (SynT-I)	cDNA: 180 bp			
								Syncytin b (Synb)	X5, X3, X1, Stand ard, X4, X2	syncytin-B; D930020E02 Rik	14 D2; 14 36.04 cM	4	Shared location/ function						
Syna R	ACCAGAGGAGTTGAGG CAGA	Targets Synb and Gm271 79	Synctin b (Synb)	X5, X4, X2, and standa rd	Syncytin-B; D930020E0 2Rik	14 D2; 14 36.04 cM	4	FK506 binding protein 10 (Fkbp10)	1 and 2	Fkbp6; FKBP65; Fkbprrp; FKBP-10; FKBP-65; Fkbp-rs1; Fkbp1-rs	11 D; 11 63.47 cM	17	Yes				Phlda2 ^{+/+BACk1} (BL6)	Syncytiotropho blast layer I (SynT-I)	cDNA: 180 bp
								Spermatid perinuclear RNA binding protein (Strbp)	X11	Spnr; 6430510M02 Rik; C230082I21 Rik	2 B; 2 24.19 cM	1	No						
Synb F	CTGGCACTTCATTCCC ATTT	Targets Synb and Gm271 79	Synctin b (Synb)	X5, X4, X2, and standa rd	Syncytin-B; D930020E0 2Rik	14 D2; 14 36.04 cM	4	Predicted gene 27179 (Gm27179)	X4, X3, X2, X5, Stand ard	Synb	14 D2; 14	Undefi ned	-	Phlda2 ^{+/+BACk1} (BL6)	Syncytiotropho blast layer I (SynT-I)	cDNA - 163bp			
Synb R	TGGCTGTAGGCTCTCA GGTT	Targets Tpbpa and Lrrc37a	trophoblast specific protein alpha (Tpbpa)	Stand ard	Tb1; Tb-1; Tpbp; b2b1247Clo	13 B2; 13 32.57 cM	2	Leucine rich repeat containing 37A (Lrrc37a)	Stand ard	Gm251	11 E1; 11 67.27 cM	-	-	mTS	Spongiotropho blast specific	Between exon 1 and exon 2. cDNA: 150 bp, gDNA: 1350 bp.			
Tpbpa F	TGAAGAGCTGAACCAC TGGA	Targets YWHAZ	Tyrosine 3- monoxygenase/try ptophan 5- monoxygenase activation protein zeta (YWHAZ)	X4, X3, X5, X1, X2, 3, 5, 6, 4, 1 and 2	HEL4; YWHAD; KCIP-1; HEL-S-3; POPCAS; HEL-S-93; 14-3-3-zeta	8q22.3	92	-	-	-	-	-	-	hTS	Reference gene	cDNA: 211bp, gDNA: 828bp			
YWHAZ F	TTCTTGATCCCCAATGC TTC	Targets YWHAZ	Tyrosine 3- monoxygenase/try ptophan 5- monoxygenase activation protein zeta (YWHAZ)	X4, X3, X5, X1, X2, 3, 5, 6, 4, 1 and 2	HEL4; YWHAD; KCIP-1; HEL-S-3; POPCAS; HEL-S-93; 14-3-3-zeta	8q22.3	92	-	-	-	-	-	-	hTS	Reference gene	cDNA: 211bp, gDNA: 828bp			
YWHAZ R	AGTTAAGGGCCAGACC CAGT	Targets YWHAZ	Tyrosine 3- monoxygenase/try ptophan 5- monoxygenase activation protein zeta (YWHAZ)	X4, X3, X5, X1, X2, 3, 5, 6, 4, 1 and 2	HEL4; YWHAD; KCIP-1; HEL-S-3; POPCAS; HEL-S-93; 14-3-3-zeta	8q22.3	92	-	-	-	-	-	-	hTS	Reference gene	cDNA: 211bp, gDNA: 828bp			

Table 94: qRT-PCR primer blast results and off target details.